UNIVERSITAT DE BARCELONA

Syntheses of Protein Degraders and Compounds for Targeted Drug Release

Craig Donoghue

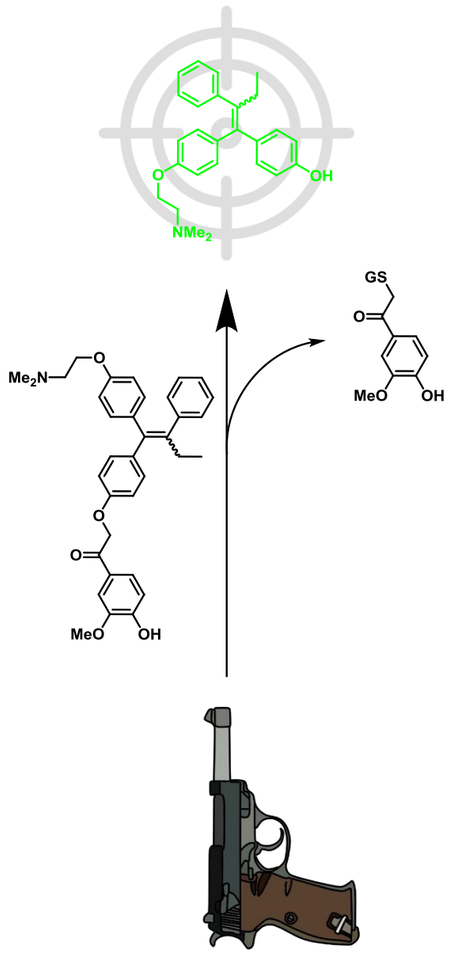

2019

Syntheses of Protein Degraders and Compounds for Targeted Drug Release

Doctoral Thesis

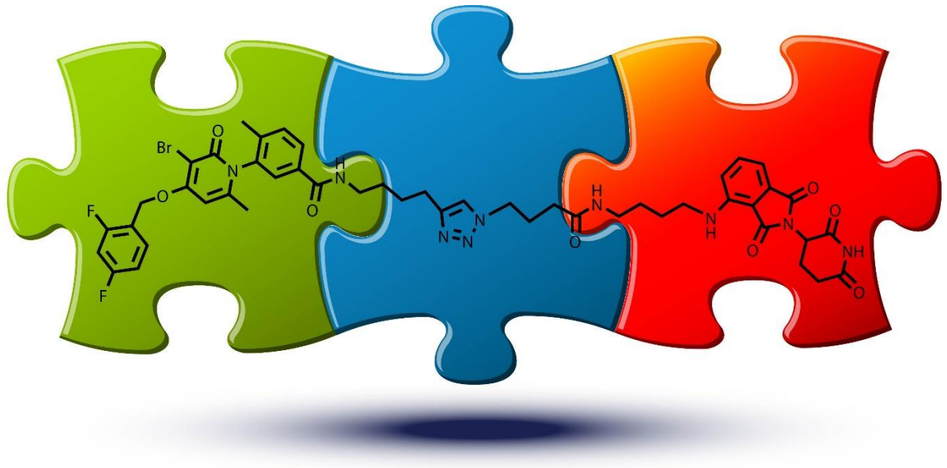

Craig Donoghue

Barcelona 2019

Craig Donoghue

UNIVERSITAT DE BARCELONA

Syntheses of Protein Degraders and Compounds for Targeted Drug Release

Craig Donoghue

Doctoral programme: Química Orgànica

Thesis director: **Antoni Riera Escalé**

Facultat de Química

Departament de Química Orgànica

Universitat de Barcelona

UNIVERSITAT DE BARCELONA

Memoria presentada por Craig Donoghue para optar al grado de doctor por la Universidad de Barcelona

Craig Donoghue

Revisada por

Dr. Antoni Riera Escalé

Barcelona, de junio 2019

Preface

The following doctoral thesis is a summary of the work carried out during four years in the lab of Professor Antoni Riera at the Institute for Research in Biomedicine Barcelona (IRB Barcelona). The work has been carried out with the financial support of the "Ministerio de Economia y Competitividad (MINECO)" (projects CTQ2014-56361-P and CTQ2017-87840-P), the Generalitat de Catalunya (2009SGR 00901), and also the IRB Barcelona. I also acknowledge La Caixa for the Obra Social fellowship, and for the Young BioMedTec funding, which were vital to my doctoral thesis and for which I am very grateful. Without these grants, this doctoral thesis would not have been possible.

This thesis is comprised of two main projects, focussed on the study of further understanding certain cellular mechanisms that lead to cancer and investigating new ways in which to intervene in particular pathways to prevent tumour growth and metastasis. Both projects were designed and performed in close collaboration with oncology groups within IRB Barcelona, the group of Dr. Eduard Batlle and the group of Dr. Ángel Nebreda.

The first main theme is the design, synthesis and preliminary application of a novel method to release a drug at a specific time and place within a model system, to obtain genetic control in a spatiotemporal manner. The drug which was released in our system was 4-hydroxytamoxifen, which we used to activate *Cre* recombinase - a widely used toolkit to invoke specific genetic changes - both *in vitro* and *in vivo*. The chemical experiments were carried out in the lab of Professor Antoni Riera and under his supervision. The biological experiments were carried out by or supervised by Dr. Daniele Tauriello – a postdoctoral researcher in the lab of Dr. Eduard Batlle.

The second part of the thesis was in collaboration with Dr. Ángel Nebreda. Chapter 3 describes our efforts in the optimisation of the p38 inhibitor PH-797804 and its subsequent conjugation to directing groups to enhance tumour selectivity. We designed and synthesised novel p38 degraders (PROTAC) with the aim of overcoming the clinical limitations associated with PH-797804, such as *in vivo* efficacy and therapeutic benefit.

Again, the chemical experiments were carried out under the supervision of Prof. Riera. The biological experiments were carried out by or supervised by Dr. Mónica Cubillos, Dr. Nuria Gutierrez or Dr. Ana Igea – postdoctoral researchers in the lab of Dr. Ángel Nebreda.

Acknowledgements

Maureen and Gordon Donoghue are where my journey began and to whom I owe most gratitude throughout my life. I consider myself extremely lucky for the environments and people they surrounded me with and never once lacked encouragement, inspiration, support nor love. My deepest thanks. Also to my siblings Stephanie and Andrew who inspired me and given me strength on this journey throughout my life and together complete the strong family unit that I have replied on even when we are spread globally! To Margaret and Thomas Donoghue, my amazing grandparents who have supported me throughout everything and take pride in everything I do (except growing my hair!). To the rest of my family, past and present, who have enriched my life and who would be proud to celebrate my doctoral thesis.

I have also been enriched by many friendships, many even made the sacrifice to leave the north to come and visit me here in sunny Barcelona! In particular those who have continued to keep my fire for chemistry lit; Jonno, Natalie, Michael, Ste, Jenny, Liam, Hammy, Joanna, Gayle, Andrew, Etienne, Alex, Lola, and the rest of the teams.

To my teachers who managed to keep a young Craig engaged in science and leniently allowed me to pursue music in parallel; Dr. Laverty, Mr. Cloughley, Dr. Cummings, Dr. Wilkinson, Mr. Simpson.

Many friends with whom I learned and grew with over the years; Phil, Chris B, Chris A, Joe, Mark, Richie, Stu, Craig, Daniel, Connor, Luke “Gee”, Luke “Fletch”, Manus, Rab, Rhuaraidh, Cammy, Chris Dyson, Kirsten, Kyle, Craig Bogle, Sean, Dan, Sheryl, Debbie, Mark, Craig J, Gary, Mike and Liam.

To the many great colleagues here in the Lab and in IRB: Dan “Lord” Byrom, my fellow guiri and guaymoxy teammate, flatmate, beermate, long live Daniel Craig. Anna Escolà, princess peptide and lab manager, thanks for everything especially helping deal with…Ernest, from day 1 we have developed together in the lab and you have been like a

brother to me. Caro, the machine that has churned out so many compounds and helped a great deal with the PROTAC project. To Enric, who has become a close friend and travel companion, and a positive energy in the lab and at home. Many gloved hands have passed through this lab and contributed to my experience or directly to the PhD; Nico, Helèa, Silvia, Alex, Edgar, Marta, Albert, Amparo, Alessandro, Pep, Joan, Guillem, Marina and the "minions" Helena, Maria, Pol, Pedro and of course Prof. Xevi Verdaguer. If the lab has been my family, I guess the collaborating labs are our cousins, special thanks to Nuria, Mónica, Ana and Ángel, Daniele and Eduard, and also to the academic support from my advisory committee along with Prof. Pere Romea and Dr. Jordi Solá.

To our amazing group at the PCB, starting with el nostre president Jordi, Jürgen (guiri number 2), Alejandro (wannabe guiri) , Ricardo, Leyre, Cris, Laura, Gemma, Helena R, Salva "the Peptide Hunter", Helena M, Martí, Adrián, Marina, Adriá, Marcos, Joel, Rosa, Sandra, Adrian, Eric, Andrea, Chico, Milos, Johan, Jesus, Michael, Juan, Marc. The IRBastard football team, and to the rest of you, too many to name! Awesome travels and adventures and unforgettable memories.

Toni has been an outstanding boss, an amazing mentor for my thesis, and a truly inspirational example in research. Many long and interesting discussions in the lab, office and meetings have enriched my experience and his support has been so much more than what is asked for or expected of PIs. I hope to continue to witness his group prosper and his science continue to be shared and applied.

Finally, I can't thank Inés enough for the love, support and scientific motivation. For staying with me in the "busiest" time of my life, for destressing and distracting me then focussing me when I needed it. I promise, in the words of Prof. Brian Cox, "things can only get better."

You can never see the full path. The important thing is to do the next right thing (2015).

Michael Hyatt

At present good work in science pays less well very often than mediocrity in other subjects (1885).

Sir Joseph Norman Lockyer, founder of Nature journal.

This thesis is dedicated to my late chemistry teacher Dr. Theo Laverty,

who always fascinated me with chemistry, believed in my abilities,

and influenced me to pursue a career in chemistry.

4-Hydroxytamoxifen (4OHT)

Acetic acid (AcOH)

Activating transcription factor 2 (ATF2)

Androgen Receptor (AR)

Aqueous (aq.)

Benzyl (Bn)

Benzoyl (Bnz)

Bromodomain and extra terminal domain (BET)

Bromodomain 4 (BRD4)

Catalyst (cat.)

Causes recombination (*Cre*)

Cereblon E3 Ligase (CRBN)

Chronic Obstructive Pulmonary Disease (COPD)

Circa (ca.)

Cytochrome P_{450} (CYP)

Half maximal degradation concentration (DC_{50})

Deoxyribonucleic acid (DNA)

Dibenzylideneacetone (dba)

Dichloromethane (DCM)

Dihydropyran (DHP)

Dimethyl sulfoxide (DMSO)

Dimethylamino pyridine (DMAP)

Dimethylformamide (DMF)

Diphenylphosphoryl azide (DPPA)

Doctor of Philosophy (PhD)

Equivalents (eq.)

Ethanol (EtOH)

Ethyl acetate (EtOAc)

Extracellular matrix (ECM)

Fluorescence-activated cell sorting (FACS)

GlaxoSmithKline (GSK)

Glucose Receptors (GLUTs)

Glutathione (GSH)

Gold nanoparticle (AuNP)

Green fluorescent protein (GFP)

Gram (g)

Growth hormone (GH)

Half maximal inhibitory concentration (IC_{50})

Heat shock protein 27 (Hsp27)

High pressure liquid chromatography (HPLC)

High resolution mass spectroscopy (HRMS)

Interleukin 6/1β (IL-6, IL-1β)

Intraperitoneal (IP)

Isopropanol (iPrOH)

Leaving group (LG)

Ligand binding domain (LBD)

Lithium diisopropyl amine (LDA)

Logarithmic acid dissociation constant (pKa)

Locus of recombination (LoxP)

LY-2228820 (**LY**)

MAPK activated protein kinase 2 (MK2)

Mitogen activated protein kinase (MAPK)

Mass spectroscopy (MS)

Melting point (mp)

Messenger RNA (mRNA)

Mesyl chloride (MsCl)

Methanol (MeOH)

Methoxymethyl acetal (MOM)

4-Methylmorpholine N-oxide (NMO)

Methyl vinyl ketone (MVK)

Michigan Cancer Foundation breat cancer cells (MCF-7)

Mitogen-activated protein kinase (MAPK)

Modified oestrogen receptor (ER^{T2})

Murine sarcoma virus (MuSV)

Nanomolar (nM)

Nanoparticle (NP)

N-bromosuccinamide (NBS)

N-methyl proline (NMP)

Nitroverityl (Nv)

Nuclear magnetic resonance (NMR)

Nucleophilic aromatic substitution (SNAr)

Oestrogen receptor (ER)

Ortho-nitro benzyl (ONB)

p-*substrate* (phosphorylated substrate)

p38 (protein 38 kDa)

Para-methoxy benzyl (PMB)

PH-797804 (**PH**)

Pharmacokinetics (PK)

Phenyl (Ph)

Pivaloyl (Piv)

Proteolysis Targeting Chimera (PROTAC)

p-Toluenesulfonic acid (TsOH or pTSA)

Pyridinium p-toluenesulfonate (PPTS)

Rheumatoid Arthritis (RA)

Relative binding affinity (RBA)

Retention factor (rf)

Ribonucleic acid (RNA)

Argenyl-glycyl-aspartic acid peptide (RGD)

Room temperature (rt)

Selectfluor (F-TEDA-BF_4) (1-(chloromethyl)-4-fluoro-1,4-diazabicyclo[2.2.2]octane-1,4-diium)

Short-hairpin RNA (shRNA)

Small double-stranded interfering RNA (siRNA)

Somatostatin hormone (SST)

Somatostatin receptor (SSTR)

Somatotropin release inhibiting factor (SRIF)

Starting material (SM)

Structure activity relationship (SAR)

Tertiary butyl (t-Bu)

Tetrahydrofuran (THF)

Tetrahydropyran (THP)

Thin-layer chromatography (TLC)

Transforming growth factor beta (TGF-β)

Transforming growth factor-alpha (TGF-α)

Trifluoro acetic acid (TFA)

Trifluoro acetic anhydride (TFAA)

Trimethylsilyl (TMS)

Tumour necrosis factor α (TNF-α)

Ultra-high pressure liquid chromatography (uPLC)

Ultraviolet light (UV)

Visible light (vis)

Chapter 1

Introduction and Objectives

1.1. Cancer

Cancer is one of the leading causes of morbidity worldwide, with an estimated 20 million new cases annually by 2025.[1] A massive global effort and huge amounts of money are spent each year in an attempt to control this advanced disease. In fact, the word "cancer" constitutes a large group of almost 100 diseases, characterised by the development of *abnormal cells that divide uncontrollably and have the ability to infiltrate and destroy normal body tissues* (NCI).[2] Each cancer possesses its own distinct mutational profile (ranging from 10 – 100 000), but in general all display what are known as "the hallmarks of cancer" required for malignant cells to form a tumour.[3,4] The formation of a carcinoma usually proceeds from a benign, well-differentiated localised tumour to an invasive cancer that penetrates and infiltrates adjacent tissue, and ultimately to a metastatic tumour that disseminates to other parts of the body through the lymphatic system or blood vessels. Further improvements to cancer therapy require improved prevention and diagnosis as well as a deeper understanding of tumour biology to develop targeted therapies and prevention of recurrence and resistance. The following projects described herein contribute towards this effort.

1.2. New compounds for spatiotemporal genetic control *via* xenoenzymatic release of 4-hydroxytamoxifen (4OHT)

This project was in continuation of an ambitious project that was first started by Dr. Daniel Byrom during his doctoral thesis, directed by Prof. A. Riera, in collaboration with Dr. Daniele Tauriello - a postdoctoral researcher in the group of Prof. Eduard Batlle. It was devoted to developing a new tool to study communication between a cell and its environment, more specifically between an organoid of metastatic tumour cells and their surrounding stroma.

The suppression or activation of a gene in a given cell and the effect that this has on its neighbouring cells is of great importance in the unravelling of complex cellular interactions that underlie biological processes such as metastasis. A general method to manipulate genes in a truly spatiotemporal manner (at a particular time point and location) would provide a highly advantageous tool in the study of gene function in a wide range of applications.

One of the most widely used methods to delete, activate or otherwise alter a gene is known as *Cre* recombination technology. *Cre* recombination is commonly used in a large number of biological models both *in vitro* and *in vivo,* enabling the insertion or deletion of genes from a specific point in a sequence of DNA.[5,6,7]

Cre recombination technology involves two key components:

1) *Cre*-recombinase – the enzyme which is able to cut the DNA at specific sequences of base-pairs.
2) LoxP sites – which are base-pair sequences at locations either side of the gene, where the recombination takes place.[8]

Depending upon the orientation of the two loxP sites relative to one another, the flanked gene can be either excised, inverted or exchanged for another flanked gene. For example,

by strategically orientating both LoxP sites in the same direction, *Cre* recombinase protein will effectively delete the flanked gene by cutting the double stranded DNA at the loxP sites. Either end is then joined to reform the original DNA sequence minus the flanked gene and without 1 loxP site, preventing further recombination. An inert, circular DNA containing the deleted gene and the deleted loxP site is also produced (figure 1.2.1).

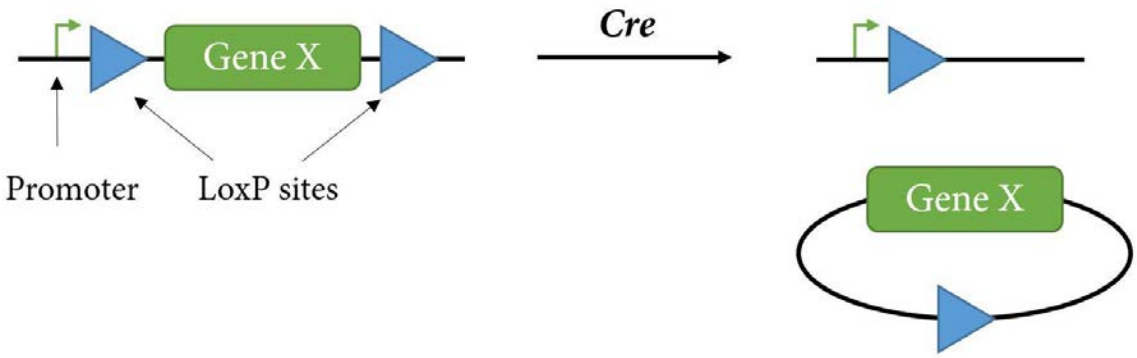

Figure 1.2.1. *An example system showing how Cre recombinase can create a gene knock out. Before recombination, the promoter is upstream of gene X, therefore gene X will be expressed. After Cre recombination, gene X is not found downstream of any promoter, meaning gene X will no longer be expressed.*

Cre-ER^{T2} is a latent complex comprising the *Cre* enzyme fused to a mutant form of the ligand binding domain (LBD) of the oestrogen receptor (ER), which can be activated upon binding of an appropriate ligand.[9] The triple mutation (G400V/M543A/L544A) causes the LBD to lose its affinity for the natural ligand 17β-oestradiol (**1-1**, figure 1.2.2) and enhances affinity for the synthetic inhibitor (4OHT) 4 fold, allowing this technology to be used in mouse models where **1-1** is ubiquitously present. Binding of 4OHT to ER^{T2} causes the dissociation of Cre-ER^{T2} from its complex of associated proteins, allowing it to enter the nucleus (translocation) and perform recombination on DNA at the loxP sites.[10] In summary, administration of 4OHT activates Cre-ER^{T2}, which induces recombination (i.e. deletion of a stop codon, figure 1.2.3).

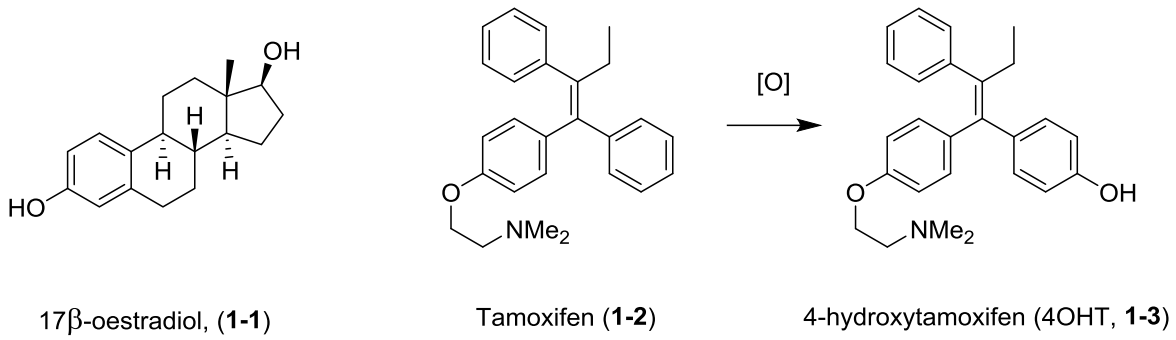

Figure 1.2.2. *17β-Oestradiol, tamoxifen (**1-2**) and its active metabolite 4-hydroxytamoxifen (4OHT).*

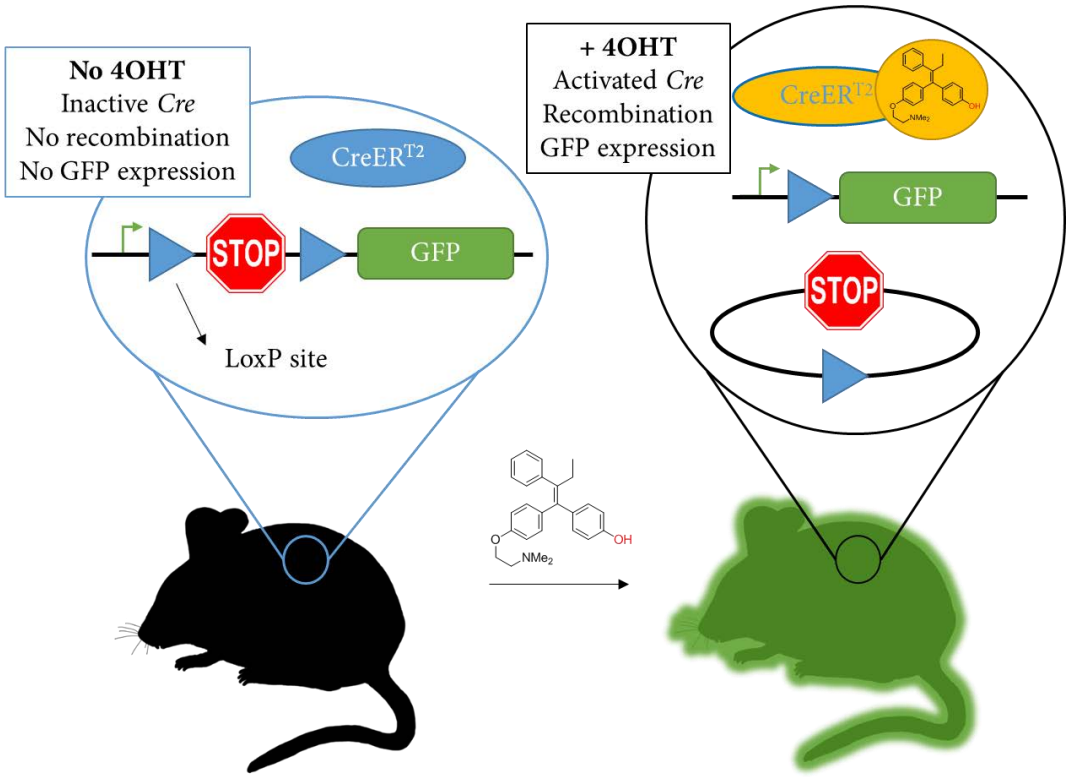

Figure 1.2.3. *Mouse DNA contains a stop codon upstream from the GFP gene, therefore no GFP is translated. CreER in the absence of 4OHT remains in the cytosol and is inactive. In the presence of 4OHT, binding to ER activates CreER (translocation to nucleus) inducing recombination. The stop codon flanked between 2 LoxP sites is deleted, meaning the promoter is now upstream of the gene encoding Green Fluorescent Protein (GFP), causing expression of GFP.*

Chapter 4 and 5 of Dr. Byrom's thesis aimed to add a further level of control to *Cre* technology through release of 4OHT in a spatiotemporally controlled manner, e.g. specific release around metastatic tumour cells. This was to be achieved by designing a masked form

of 4OHT, inactive to Cre-ER^{T2} until cleaved by a xenoenzyme, which liberated 4OHT. Expression of this enzyme solely in tumour cells would control the liberation of 4OHT once these were implanted into a Cre-ER^{T2} mouse model to form metastatic tumours. Liberated 4OHT would then diffuse into the surrounding stromal cells (the tumour microenvironment) and induce *Cre* recombination specifically in the stroma (figure 1.2.4).

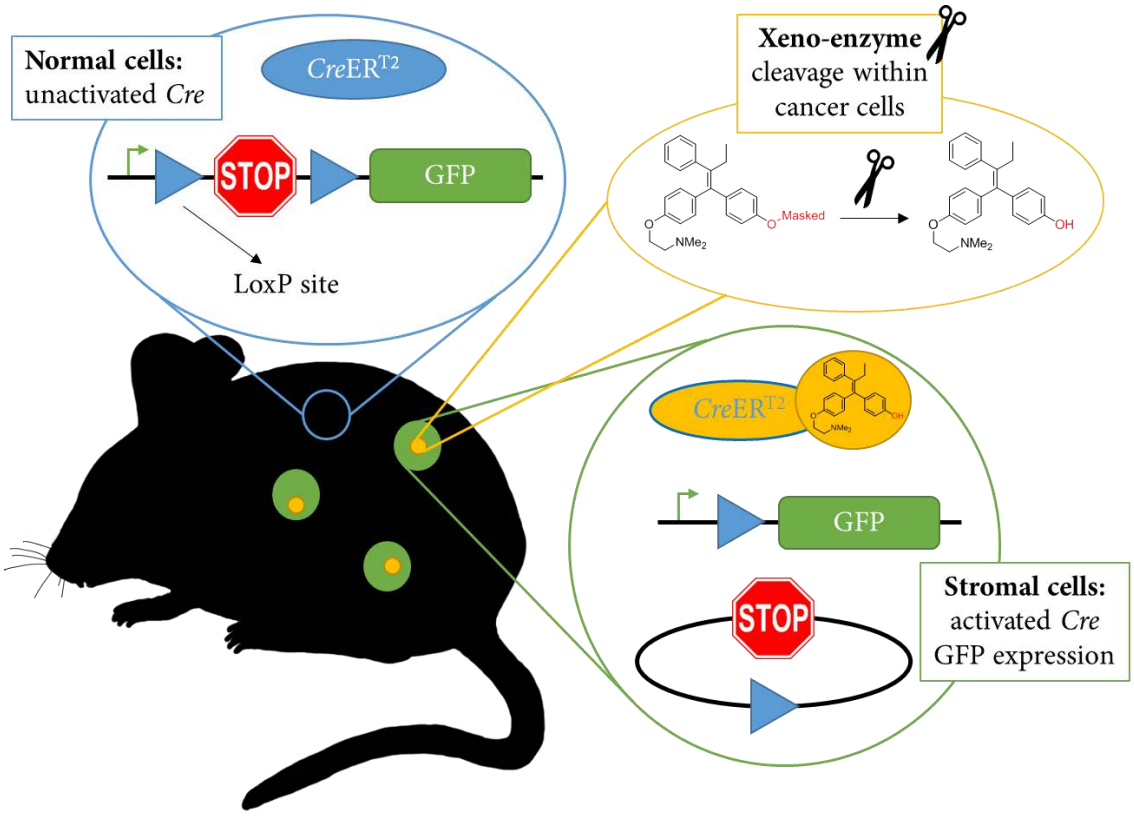

Figure 1.2.4. *Normal mouse cells (blue circle) contain inactive CreER in the presence of masked 4OHT, the stop codon prevents expression of GFP. In tumour sites (yellow) 4OHT is liberated by cleavage of the masked version by the xenoenzyme expressed in these cells. Dissipation of 4OHT into surrounding mouse cells (stroma, green) induces Cre recombination. Subsequent excision of the stop codon causes GFP to be produced locally in these stromal cells.*

The masked form of 4OHT was christened "Guaymoxifen" (**1-4,** scheme 1.2.1), as it consisted of a ta*moxifen* 4OHT substituent (green), covalently linked to a *Guai*acol component (red) *via* a β-ether linkage (similar to that found in lignin). The β-ether bond can be cleaved by LigF enzyme in a glutathione-assisted pathway (scheme 1.2.2), which is only expressed in several fungi and bacteria but not in mammals, such as the Cre-ER^{T2}

mouse model. Therefore by artificially expressing LigF as the xeno-enzyme in the tumour cells to be implanted in the mouse, liberated 4OHT would then diffuse into the surrounding stroma and induce *Cre* recombination specifically in the cells found immediately in this area around the tumour. In other words, spatiotemporal genetic control of the stromal cells would be achieved by the controlled liberation of 4OHT *via* the cleavage of guaymoxifen by LigF within tumour cells. .[11,12]

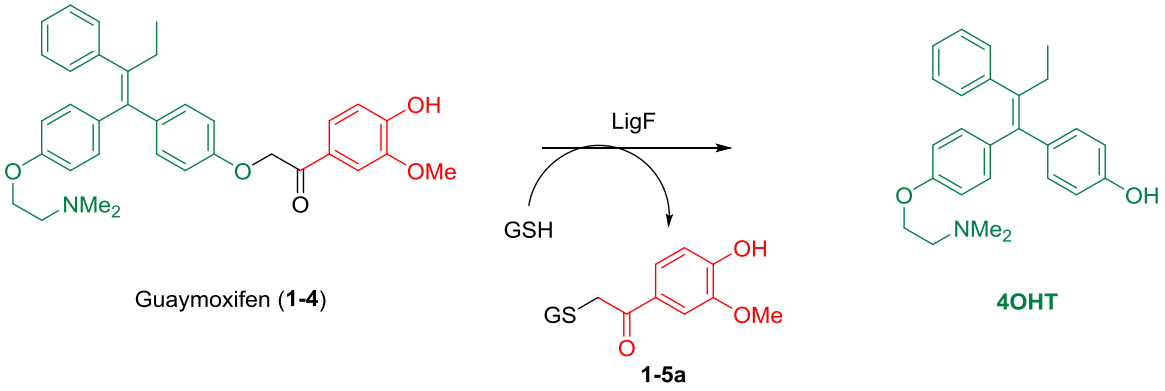

Scheme 1.2.1. *Cleavage of guaymoxifen (**1-4**) by LigF releasing **4OHT**, the activating ligand of CreER for genetic recombination.*

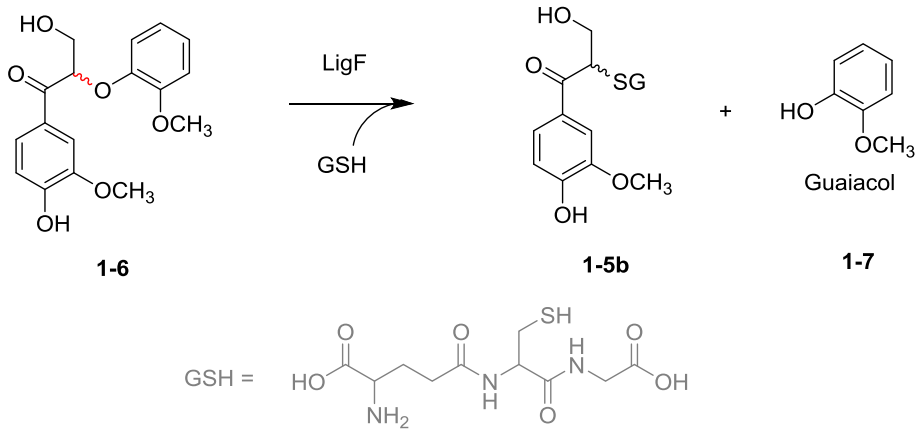

Scheme 1.2.2. *Glutathione-assisted cleavage of a lignin-based compound **1-6** by LigF.*

Work published by Reiter *et al.* demonstrated that the glycerol group alpha to the ketone, which is present in lignin, was not vital for cleavage by LigF.[13] As such, Byrom simplified the target molecule by removing this hydroxymethyl group. Moreover, it has since been

demonstrated that LigF only cleaves the (*S*)-enantiomer of lignin based compounds in possession of this hydroxymethyl, therefore a non-chiral substrate was advantageous for this technology. Byrom also conducted an SAR study using an *in vitro* cleavage assay which revealed no variation was tolerated in the substitution of the aryl ring of the guaiacol moiety, i.e. the 4-hydroxy and 3-methoxy substituents were essential for recognition and cleavage by LigF.

Guaymoxifen was demonstrated to be inactive towards *Cre* in cellular models, until cleavage by LigF, which was proven to occur in both *in vitro* and cellular assays. Therefore this compound was needed in much larger quantities to trial in the transgenic mouse model containing transplanted tumours expressing LigF. **The first objective of this doctoral thesis was to improve and scale up a synthesis to obtain larger quantities of guaymoxifen and test it in mouse models.**

Unfortunately, the metabolic stability of guaymoxifen was not sufficient. 4OHT was released systemically causing recombination (about 5 – 10%) to occur distally from the tumour sites, supposedly *via* β-ether bond cleavage by the liver. CYP (Cytochrome P_{450}) enzymes are concentrated in the liver and are responsible for the oxidation of many drug compounds and their eventual cleavage and clearance from the body.[14] Oxidation of the methylene of the β-ether bridge followed by hydrolytic cleavage was proposed to be the cause of the premature liberation of 4OHT in the mouse model. Our technique would require an analogue of guaymoxifen that was more resistant to this oxidative cleavage, yet retained its susceptibility to cleavage by LigF.

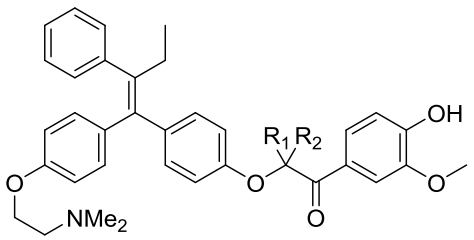

1-8

Scheme 1.2.3. *New guaymoxifen analogues that are more resistant to oxidative cleavage by substitution of R_1 and R_2 about the β-ether bond,* ***1-8****.*

Therefore, the second objective of this doctoral thesis was to conduct an SAR study about the β-ether linkage, to generate a collection of guaymoxifen analogues and identify a new candidate with improved metabolic stability.

Tamoxifen and its corresponding active metabolites and analogues possess a double bond with 4 distinct groups attached. Restricted rotation about the double bond gives rise to 2 distinct isomers. Moreover, *(Z)*-4OHT has between 100-1000 times more affinity for ER than *(E)*-4OHT, therefore it would be highly desirable to synthesise only the corresponding active, proZ version of guaymoxifen.[15] Due to the differing priorities following the Cahn-Ingold Prelog nomenclature,[16] active *Z* OHT is the product of *E* guaymoxifen despite no isomerisation occurring about the double bond. The active *Z* isomer of tamoxifen is sometimes referred to as *trans,* based on the observation that the 2 phenyl groups lay *trans* to one another. However this nomenclature can quickly become confusing when the phenyl rings possess substituents. More details on the relative activities and stereoselectivities will be discussed later in the thesis.

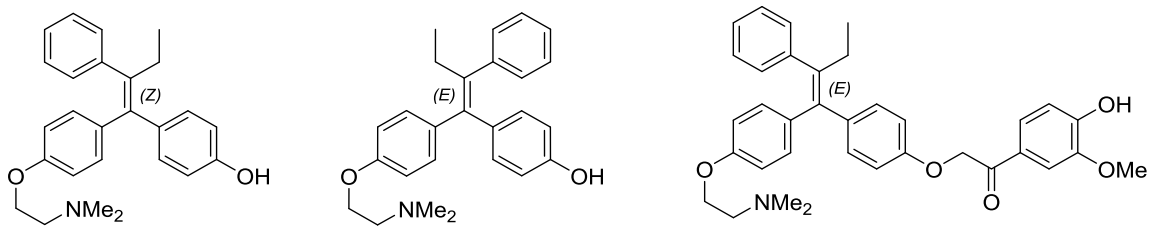

Figure 1.2.5. *(E) and (Z) isomers of 4-hydroxytamoxifen and (Pro-Z)-Guaymoxifen* ***1-4****.*

In chapter 5 of Dr. Byrom's PhD thesis, the large-scale synthesis of guaymoxifen was carried out utilising a McMurry reaction as a key step. This led to an almost 1.2:1 mixture of *E* and *Z* guaymoxifen, which was separated on small amounts into the individual *E* and *Z* isomers by chiral chromatography. Fortunately, it was found that LigF preferentially cleaved the pro-*Z* guaymoxifen over the pro-*E* form, liberating the active isomer *(Z)*-4OHT at a significantly higher rate than (*E).* Chiral separation on a large scale is not practical as 50%

of the starting material is wasted and it is also very expensive and time consuming. Despite the multitude of published routes for the stereo-selective synthesis of tamoxifen, such as sequential palladium catalysed coupling reactions,[17] none of these could be successfully adapted to obtain (pro-*Z*)-guaymoxifen (**(*E*)-1-4**).

Another way to address the problem of isomerisation is to influence the relative equilibrium of the isomers by adding steric groups to disfavour formation of one of the isomers. Various non-isomerisable, fused-ring analogues of tamoxifen and 4OHT were synthesised in the 1980's by McCague and co-workers, however their fused ring conformation extinguished their affinity for ER.[18] On the other hand, addition of a methyl group in the 2-position of the aryl ring bearing the hydroxyl group of 4OHT sufficed to shift the isomerisation equilibrium in favour of the active isomer ((*E*)-**1-9**, scheme 1.2.3), yet retain comparable affinity for ER.[19] Note that Cahn-Ingold Prelog nomenclature now assigns the corresponding active isomer as *E,* because of the additional methyl group. Provided **(*E*)-1-9** analogously maintained its affinity for Cre-ER^{T2}, we reasoned that addition of a methyl group to guaymoxifen in the same position could aid in the synthesis of a new analogue, **1-10** that was enriched in the active *E* isomer.

Therefore, the third objective of the doctoral thesis was to develop a synthesis to generate a guaymoxifen derivative, such as 1-9, that was enriched towards the desiredstereoisomer.

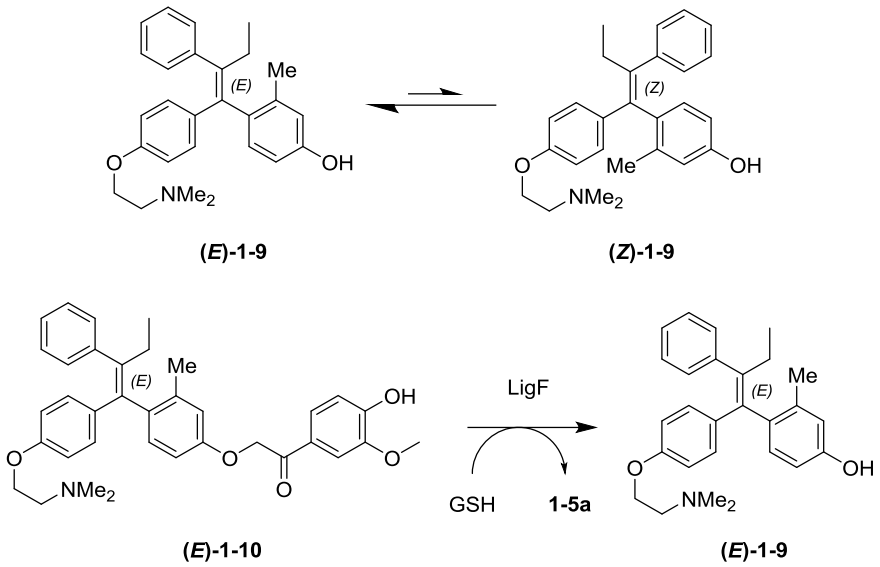

Scheme 1.2.3. *(E) and (Z) isomerisation of methyl derivative* ***1-9****. Guaymoxifen derivative* ***(E)*****-1-10** *and subsequent cleavage by LigF to afford (E)-****1-9****.*

1.3. New compounds to target p38α with improved efficacy and selectivity

In parallel to this work, we embarked upon the development of new tools and therapeutics that target p38α MAPK in collaboration with Prof. Ángel Nebreda. P38α is a ubiquitous protein kinase that has a decisive role in regulating the biosynthesis of a number of proinflammatory cytokines, for example IL-6, IL-1β and TNF-α, through its effect on over 100 substrates. This has made it an extremely attractive target in a number of inflammatory diseases such as rheumatoid arthritis (RA) and chronic obstructive pulmonary disease (COPD) and has also earned it the name *the stress kinase*. A number of p38α inhibitors of varying structures have been developed by several pharmaceutical companies in order to treat these diseases.[20] More recently, p38α related inflammation has also been shown to be involved in many aspects of cancer progression in a range of cancer types. For example, the inhibitor ralimetinib (LY2228820), by Eli Lilly, reduced tumour growth in xenografts of human breast cancer cell lines by up to 72%.[21] This compound advanced to Phase II clinical trials in ovarian cancer and in glioblastoma.[22,23] It has also been used in combined therapy with other inhibitors such as prexasertib (LY2606368) to treat advanced, metastatic, colorectal and non-small cell lung cancers in phase I clinical trials,[24] with evidence that supports its ability to sensitise tumour cells to chemotherapeutics.[25] PH-797804 has also been examined in Phase II clinical trials for COPD and RA.[26,27]

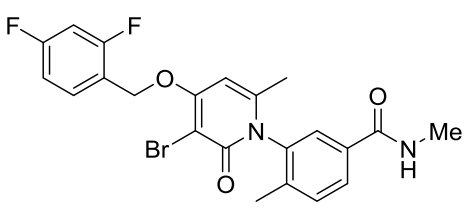

PH-797804 (**PH**)

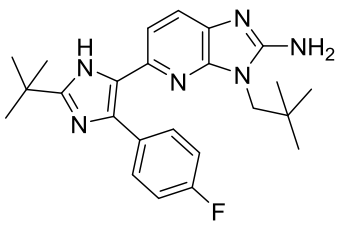

Ralimetinib, LY2228820 (**LY**)

Figure 1.3.1. *Drug candidate compounds that have been through Phase II clinical trials from top pharmaceutical companies Pfizer and Eli Lilly, PH-797804 (**PH**) and Ralimetinib, LY2228820 (**LY**).*

However, a multitude of seemingly contradictory data has been reported whereby p38α appears to have a dual role in tumour formation, metastasis and dormancy.[25] Depending on the tissue type in question and the time point of progression, p38α can have either a suppressive or contributory effect. Care should be taken with some of the *in vitro* data, as it may oversimplify the diversity of the cells found in the tumour microenvironment and could lead to false conclusions.[28]

Nevertheless, these findings clearly demonstrate the therapeutic opportunity in cancer *via* intervention of the p38α MAPK pathway, however a greater understanding of the downstream effects of p38α is needed to obtain maximum therapeutic benefit. For example, whereas attenuation of breast cancer metastasis can be achieved using p38α inhibitors,[29] p38α downregulation can also facilitate the metastatic spread of colon cancer cells from liver to lung.[30]

Currently, none of the existing p38α inhibitors have successfully completed Phase III clinical trials, presumably due to structurally related toxicology, such as off-target effects, and limited efficacy *in vivo,* which leads to a diminished therapeutic benefit for the patient.

In collaboration with the group of Dr. Ángel Nebreda, we aimed to design and synthesise novel compounds in order to overcome these two main drawbacks of the current p38α inhibitors; enhancing the selectivity of the compounds by directly targeting the tumour cells and increasing the efficacy of the compounds towards downregulating the MAPK pathway.

With respect to the first drawback, we aimed to optimise and expand the structure of an existing p38α inhibitor to alter its bio-distribution by conjugation to a tumour-directing group, such as a gold nanoparticle or a peptide sequence that can be recognised by cell surface receptors that are overexpressed in tumour cells. The increase in drug concentration that can be gained in the tumour environment with respect to healthy cells using nanotechnology is known as the EPR (Enhanced Permeability and Retention) effect and is well documented.[31] Likewise, a range of drugs and probes have been conjugated to

peptides such as RGD, which is recognised by integrin receptors on the cell surface and internalised by natural cell uptake mechanisms, liberating the active drug inside the cell upon cleavage by the inherent peptidases.[32] These integrin receptors are overexpressed in a variety of cancer cell types, therefore the drug-RGD conjugate will accumulate in the cancer cells proportionately more than in the healthy cells. These two techniques have even been combined, whereby nanoparticles are coated in RGD recognition fragments in order to further direct and accumulate the nanoparticles within the tumour cells.

Therefore, the fourth objective of the doctoral thesis was to design and synthesise new active analogues of an existing p38α inhibitor that possess groups suitable for conjugation to peptide or nanorod directing groups.

Following on from this, the fifth objective of the doctoral thesis was to synthesise a collection of inhibitor-directing group conjugates and ascertain their biological activity and advantage over systemically distributed inhibitors.

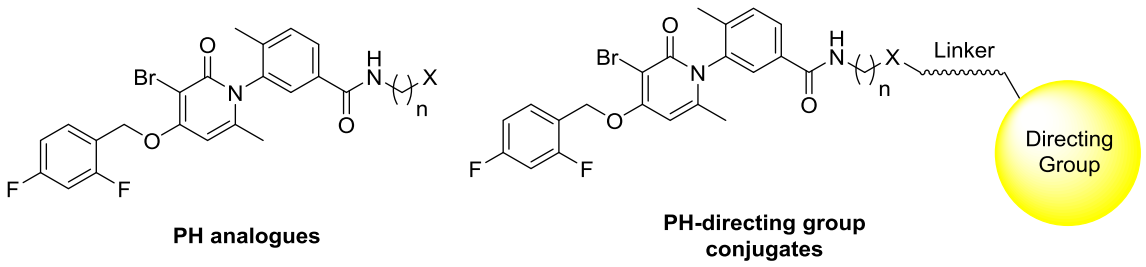

Figure 1.3.2. *Analogues of* ***PH*** *that possess new functionalities attached via different length linkers to the aryl amide moiety. PH-directing group conjugates, whereby these new analogues are conjugated to directing groups such as gold nanoparticles or peptide fragments for receptor recognition.*

We also attempted to control the bio-distribution of our novel inhibitor analogues *via* photo-activation. Nitroverityl (Nv) and *o*-nitro benzyl (ONB) caging groups are photo-sensitive protecting groups that can be cleaved using ultraviolet light. They have found applications in organic synthesis to protect a wide range of functionalities such as phenols, amines and even amides. Futhermore, due to their facile cleavage in aqueous conditions using long wavelength UV light (>400 nm), these protecting groups have been used in a

cellular setting to mask the biological activity of drugs, whereby they can be locally cleaved by UV light to activate the drug without affecting the rest of the cell functions.[33] This leads us to the **sixth objective for this doctoral thesis. To design a caged version of p38α inhibitors that can be activated locally by applying UV light (1-X).**

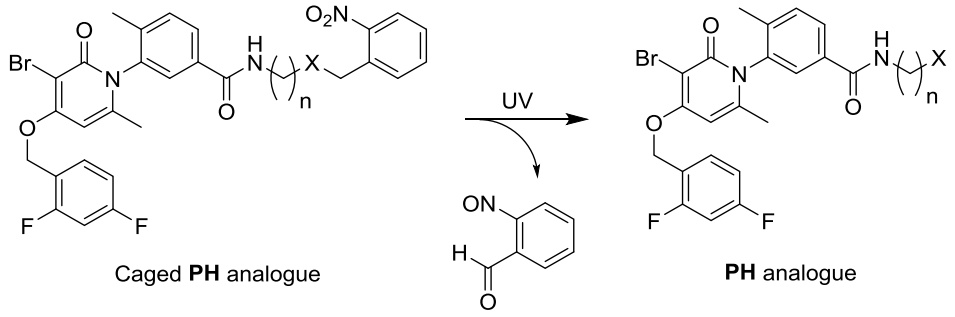

Figure 1.3.2. *Caged analogues of* ***PH****, whose activity has been blocked by an ortho-nitro benzyl group (ONB), which can be cleaved by irradiation of UV light in the site of choice.*

In order to address the latter disadvantage of current p38α MAPK inhibitors, the lack of efficacy in a therapeutic setting, we rationalised that chemically-induced degradation of p38α could overcome the lack of therapeutic effect *in vivo*. This would not only serve as an indispensable tool for the further validation of the p38 MAPK pathway and its involvement in cancer, but could also provide an urgently needed, novel therapy in cancer treatment. PROTAC (PROteolysis TArgeting Chimera) technology is an emerging and revolutionary technique whereby the selective degradation of a specific protein can be achieved using a bifunctional molecule, known as a "PROTAC". The technology has been successfully applied to degrade a range of individual target proteins, such as BRD4,[34] the oestrogen receptor (ER),[35] and the androgen receptor (AR).[36] PROTAC applications range from tool compounds to study the effect of post-translational knock-out or knock-down of certain proteins, to therapeutic applications, with the first protac approved to enter Phase I clinical trials for castration-resistant metastatic prostate cancer, ARV-110.[37]

Thus, the sixth objective for this doctoral thesis was to design a molecule capable of selectively degrading p38α in cells and *in vivo*.

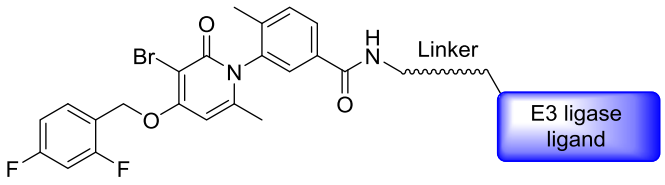

PH-based protac

***Figure 1.3.3. PH**-based protac consisting of **PH** linked via the aryl amide moiety to an E3 ligase ligand with a linker of distinct length. This bifunctional molecule will induce the ubiquitination of p38α and subsequent degradation by the 29S proteasome.*

To summarise, the main objectives of this doctoral thesis were:

i. To improve and scale up a synthesis to obtain larger quantities of guaymoxifen (**1-6**) and test it in Cre-GFP mouse models implanted with tumours expressing LigF
ii. To conduct an SAR study about the β-ether linkage, generating guaymoxifen analogues then identifying a new candidate with improved metabolic stability
iii. To develop a synthesis to generate guaymoxifen analogue **(*E*)-1-9** (enriched in the active E isomer), in sufficient quantities for subsequent biological testing
iv. To design and synthesise new active analogues of an existing p38α inhibitor that possessed groups suitable for conjugation to peptide or nanorod directing groups
v. To then synthesise a collection of p38α inhibitor-directing group conjugates and determine their biological activity compared to currently available p38α inhibitors
vi. To design a PROTAC molecule capable of selectively degrading p38α in cells and *in vivo*
vii. To design and synthesise masked-protacs that could be locally activated upon irradiation with UV light, or through cleavage by a locally expressed xeno-enzyme.

References

(1) Stewart, B.; Wild, C. World Cancer Report 2014. *Int. Agency Res. Cancer* **2014**, *22* (1), 3–4. https://doi.org/9283204298.

(2) Health, N. I. of; Services, U. S. D. of H. and H. NCI Dictionary of Cancer Terms https://www.cancer.gov/publications/dictionaries/cancer-terms/search?contains=false&q=cancer.

(3) Hanahan, D.; Weinberg, R. A. The Hallmarks of Cancer. *Cell* **2000**, *100* (1), 57–70. https://doi.org/10.1016/S0092-8674(00)81683-9.

(4) Hanahan, D.; Weinberg, R. A. Hallmarks of Cancer: The Next Generation. *Cell* **2011**, *144* (5), 646–674. https://doi.org/10.1016/j.cell.2011.02.013.

(5) Sauer, B.; Henderson, N. Site-Specific DNA Recombination in Mammalian Cells by the Cre Recombinase of Bacteriophage P1. *Proc. Natl. Acad. Sci. U. S. A.* **1988**, *85* (14), 5166–5170. https://doi.org/10.1073/pnas.85.14.5166.

(6) Rossant, J.; McMahon, A. 'Cre'-Ating Mouse Mutants---a Meeting Review on Conditional Mouse Genetics. *Genes Dev.* **1999**, *13* (2), 142–145. https://doi.org/10.1101/gad.13.2.142.

(7) Smith, A. J. H.; De Sousa, M. a; Kwabi-Addo, B.; Heppell-Parton, A.; Impey, H.; Rabbitts, P. A Site–Directed Chromosomal Translocation Induced in Embryonic Stem Cells by Cre-LoxP Recombination. *Nat. Genet.* **1995**, *9* (4), 376–385. https://doi.org/10.1038/ng0495-376.

(8) Nagy, A. Cre Recombinase: The Universal Reagent for Genome Tailoring. *Genesis* **2000**, *26* (2), 99–109. https://doi.org/10.1002/(SICI)1526-968X(200002)26:2<99::AID-GENE1>3.0.CO;2-B.

(9) Feil, R.; Wagner, J.; Metzger, D.; Chambon, P. Regulation of Cre Recombinase Activity by Mutated Estrogen Receptor Ligand-Binding Domains. *Biochem. Biophys. Res. Commun.* **1997**, *237* (3), 752–757. https://doi.org/10.1006/bbrc.1997.7124.

(10) Picard, D.; Khursheed, B.; Garabedian, M. J.; Fortin, M. G.; Lindquist, S.; Yamamoto, K. R. Reduced Levels of Hsp90 Compromise Steroid Receptor Action in Vivo. *Nature* **1990**, *348*

(6297), 166–168. https://doi.org/10.1038/348166a0.

(11) Ruiz-Dueñas, F. J.; Martínez, A. T. Microbial Degradation of Lignin: How a Bulky Recalcitrant Polymer Is Efficiently Recycled in Nature and How We Can Take Advantage of This. *Microb. Biotechnol.* **2009**, *2* (2), 164–177. https://doi.org/10.1111/j.1751-7915.2008.00078.x.

(12) Vanholme, R.; Demedts, B.; Morreel, K.; Ralph, J.; Boerjan, W. Lignin Biosynthesis and Structure. *Plant Physiol.* **2010**, *153* (3), 895–905. https://doi.org/10.1104/pp.110.155119.

(13) Reiter, J.; Strittmatter, H.; Wiemann, L. O.; Schieder, D.; Sieber, V. Enzymatic Cleavage of Lignin β-O-4 Aryl Ether Bonds via Net Internal Hydrogen Transfer. *Green Chem.* **2013**, *15* (5), 1373. https://doi.org/10.1039/c3gc40295a.

(14) Muruganandan, S.; Sinal, C. J. Mice as Clinically Relevant Models for the Study of Cytochrome P450-Dependent Metabolism. *Clin. Pharmacol. Ther.* **2008**, *83* (6), 818–828. https://doi.org/10.1038/clpt.2008.50.

(15) Ford, B. M.; Franks, L. N.; Radominska-Pandya, A.; Prather, P. L. Tamoxifen Isomers and Metabolites Exhibit Distinct Affinity and Activity at Cannabinoid Receptors: Potential Scaffold for Drug Development. *PLoS One* **2016**, *11* (12), 1–23. https://doi.org/10.1371/journal.pone.0167240.

(16) Cahn, R. S.; Ingold, C.; Prelog, V. Specification of Molecular Chirality. *Angew. Chemie Int. Ed. English* **1966**, *5* (4), 385–415. https://doi.org/10.1002/anie.196603851.

(17) Shimizu, M.; Nakamaki, C.; Shimono, K.; Schelper, M.; Kurahashi, T.; Hiyama, T. Stereoselective Cross-Coupling Reaction of 1,1-Diboryl-1-Alkenes with Electrophiles: A Highly Stereocontrolled Approach to 1,1,2-Triaryl-1-Alkenes. *J. Am. Chem. Soc.* **2005**, *127* (36), 12506–12507. https://doi.org/10.1021/ja054484g.

(18) McCague, R.; Kuroda, R.; Leclercq, G.; Stoessel, S. Synthesis and Estrogen Receptor Binding of 6,7-Dihydro-8-Phenyl-9-[4-[2-(Dimethylamino)Ethoxy]Phenyl]-5H-Benzocycloheptene, a Nonisomerizable Analog of Tamoxifen. X-Ray Crystallographic Studies. *J. Med. Chem.* **1986**, *29* (10), 2053–2059. https://doi.org/10.1021/jm00160a044.

(19) Foster, A. B.; Jarman, M.; Leung, O. T.; McCague, R.; Leclercq, G.; Devleeschouwer, N.

Hydroxy Derivatives of Tamoxifen. *J. Med. Chem.* **1985**, *28* (10), 1491–1497. https://doi.org/10.1021/jm00148a020.

(20) Bühler, S.; Laufer, S. A. P38 MAPK Inhibitors: A Patent Review (2012 – 2013). *Expert Opin. Ther. Pat.* **2014**, *24* (5), 535–554. https://doi.org/10.1517/13543776.2014.894977.

(21) Campbell, R. M.; Anderson, B. D.; Brooks, N. A.; Brooks, H. B.; Chan, E. M.; De Dios, A.; Gilmour, R.; Graff, J. R.; Jambrina, E.; Mader, M.; et al. Characterization of LY2228820 Dimesylate, a Potent and Selective Inhibitor of P38 MAPK with Antitumor Activity. *Mol. Cancer Ther.* **2014**, *13* (2), 364–374. https://doi.org/10.1158/1535-7163.MCT-13-0513.

(22) COATES, David, A. U.; GILMOUR, R. U.; MARTIN, Jose, A. U.; MARTIN DE LA NAVA, Eva, M. OXAZOLO [5, 4 -B] PYRIDIN- 5 -YL COMPOUNDS AND THEIR USE FOR THE TREATMENT OF CANCER. WO2012074761, 2012.

(23) *Phase II Trial in Ovarian Cancer (NCT01663857)*; 2018.

(24) *A Study of Prexasertib (LY2606368) in Combination With Ralimetinib in Participants With Advanced or Metastatic Cancer (NCT02860780)*; 2016.

(25) Igea, A.; Nebreda, A. R. The Stress Kinase P38α as a Target for Cancer Therapy. *Cancer Res.* **2015**, *75* (19), 3997–4002. https://doi.org/10.1158/0008-5472.CAN-15-0173.

(26) Singh, D.; Siew, L.; Christensen, J.; Plumb, J.; Clarke, G. W.; Greenaway, S.; Perros-Huguet, C.; Clarke, N.; Kilty, I.; Tan, L. Oral and Inhaled P38 MAPK Inhibitors: Effects on Inhaled LPS Challenge in Healthy Subjects. *Eur. J. Clin. Pharmacol.* **2015**, *71* (10), 1175–1184. https://doi.org/10.1007/s00228-015-1920-1.

(27) MacNee, W.; Allan, R. J.; Jones, I.; De Salvo, M. C.; Tan, L. F. Efficacy and Safety of the Oral P38 Inhibitor PH-797804 in Chronic Obstructive Pulmonary Disease: A Randomised Clinical Trial. *Thorax* **2013**, *68* (8), 738–745. https://doi.org/10.1136/thoraxjnl-2012-202744.

(28) Gupta, J.; del Barco Barrantes, I.; Igea, A.; Sakellariou, S.; Pateras, I. S.; Gorgoulis, V. G.; Nebreda, A. R. Dual Function of P38α MAPK in Colon Cancer: Suppression of Colitis-Associated Tumor Initiation but Requirement for Cancer Cell Survival. *Cancer Cell* **2014**, *25* (4), 484–500. https://doi.org/10.1016/j.ccr.2014.02.019.

(29) Wu, X.; Zhang, W.; Font-Burgada, J.; Palmer, T.; Hamil, A. S.; Biswas, S. K.; Poidinger, M.; Borcherding, N.; Xie, Q.; Ellies, L. G.; et al. Ubiquitin-Conjugating Enzyme Ubc13 Controls Breast Cancer Metastasis through a TAK1-P38 MAP Kinase Cascade. *Proc. Natl. Acad. Sci.* **2014**, *111* (38), 13870–13875. https://doi.org/10.1073/pnas.1414358111.

(30) Urosevic, J.; Garcia-Albéniz, X.; Planet, E.; Real, S.; Céspedes, M. V.; Guiu, M.; Fernandez, E.; Bellmunt, A.; Gawrzak, S.; Pavlovic, M.; et al. Colon Cancer Cells Colonize the Lung from Established Liver Metastases through P38 MAPK Signalling and PTHLH. *Nat. Cell Biol.* **2014**, *16* (7), 685–694. https://doi.org/10.1038/ncb2977.

(31) Maeda, H. Tumor-Selective Delivery of Macromolecular Drugs via the EPR Effect: Background and Future Prospects. *Bioconjug. Chem.* **2010**, *21* (5), 797–802. https://doi.org/10.1021/bc100070g.

(32) Danhier, F.; Breton, A. Le; Préat, V. RGD-Based Strategies to Target Alpha(v) Beta(3) Integrin in Cancer Therapy and Diagnosis. *Mol. Pharm.* **2012**, *9* (11), 2961–2973. https://doi.org/10.1021/mp3002733.

(33) Ellis-Davies, G. C. R. Caged Compounds: Photorelease Technology for Control of Cellular Chemistry and Physiology. *Nat. Methods* **2007**, *4* (8), 619–628. https://doi.org/10.1038/nmeth1072.

(34) Winter, G. E.; Buckley, D. L.; Paulk, J.; Roberts, J. M.; Souza, A.; Dhe-Paganon, S.; Bradner, J. E. Phthalimide Conjugation as a Strategy for in Vivo Target Protein Degradation. *Science (80-.).* **2015**, *348* (6241), 1376–1381. https://doi.org/10.1126/science.aab1433.

(35) Bargagna-Mohan, P.; Baek, S. H.; Lee, H.; Kim, K.; Mohan, R. Use of PROTACS as Molecular Probes of Angiogenesis. *Bioorganic Med. Chem. Lett.* **2005**, *15* (11), 2724–2727. https://doi.org/10.1016/j.bmcl.2005.04.008.

(36) Itoh, Y.; Kitaguchi, R.; Ishikawa, M.; Naito, M.; Hashimoto, Y. Design, Synthesis and Biological Evaluation of Nuclear Receptor-Degradation Inducers. *Bioorganic Med. Chem.* **2011**, *19* (22), 6768–6778. https://doi.org/10.1016/j.bmc.2011.09.041.

(37) Guo, J.; Liu, J.; Wei, W. Degrading Proteins in Animals: "PROTAC"Tion Goes in Vivo. *Cell Res.* **2019**, *29* (3), 179–180. https://doi.org/10.1038/s41422-019-0144-9.

Chapter 2

The Synthesis of Compounds for Spatiotemporal Release of 4OHT to Activate *Cre*

2.1. Background and Previous Work

2.1.1. Introduction

The research group of Eduard Batlle is a leading group in the study of colorectal cancer and metastasis.[1,2] A major breakthrough for these studies and many others in the field would be to gain control over specific genes (activate or suppress) in cancer cells in a spatiotemporally controlled manner.

The group´s research focuses on cells in the metastatic tumour microenvironment by control of trans-cellular genetic manipulation.[3] Their main target is the visualisation, isolation, and characterisation of these niche cells in order to dissect their contribution to niche signalling, as well as the alteration of key signalling pathways *in vivo* to directly manipulate cell-cell communication.[4] Conditional gene targeting is challenging, and there are currently many tools under development aiming to achieve it.[5] Our group has a long-term collaboration with Batlle´s group to develop a novel trans-cellular genetic targeting approach. The approach builds on an already established one, involving *Cre* DNA recombinase enzyme, adding an additional level of control by use of a xenoenzymatic reaction.

2.1.2. *Cre* Recombination Methodology

Cre recombination technology involves two key components:

1) *Cre*-recombinase – the enzyme which is able to cut the DNA at specific sequences of base-pairs
2) LoxP sites – which are base-pair sequences at locations either side of the target gene, where the recombination takes place.[6]

The orientation of the two loxP sites can be used to delete, add, invert or swap the flanked gene(s). *Cre* recombinase can delete a flanked gene by cutting the double stranded DNA at the loxP sites, then re-joining either end to reform the original DNA sequence minus the

flanked gene. The new strand is now missing one of the loxP sites, which prevents further recombination. A by-product of circular DNA containing the deleted gene and deleted loxP site is also produced, which is not translated or transcribed in the protein, thus considered inert (figure 2.1.1).

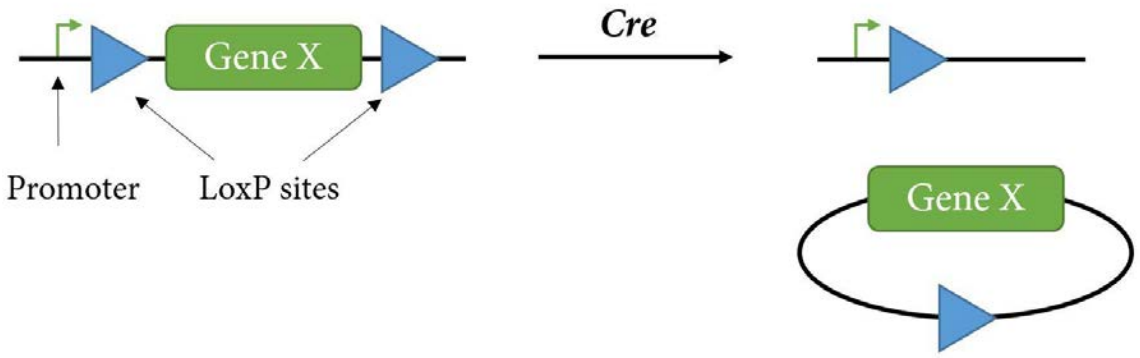

Figure 2.1.1. *An example system of Cre system creating a gene knock out.*

2.1.3. *Cre* Regulation by 4-Hydroxytamoxifen

Cre recombination can be regulated on a principle level by fusion of the *Cre* enzyme to the ligand binding domain (LBD) of hormone receptors, such as oestrogen receptor mutant (ER^{T2}).[7] This ER variant is no longer responsive to the natural ligand 17β-oestradiol (E2), meaning *Cre* will not be active in basal hormone levels when used *in* vivo. *Cre*ER^{T2} can be activated by 4-hydroxytamoxifen **2-2**, which is the active metabolite of the administered prodrug tamoxifen **2-1** (scheme 2.1.1). An example of how **2-2** administration can initiate recombination to delete a stop codon and cause expression of GFP is shown in figure 2.1.2.

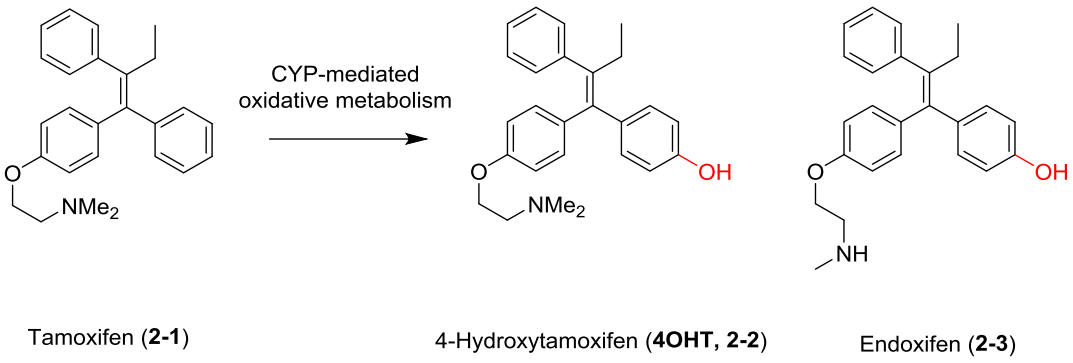

Tamoxifen (**2-1**) 4-Hydroxytamoxifen (**4OHT, 2-2**) Endoxifen (**2-3**)

Scheme 2.1.1. *Tamoxifen* ***2-1****, 4-hydroxytamoxifen* ***2-2****, Endoxifen* ***2-3****.*

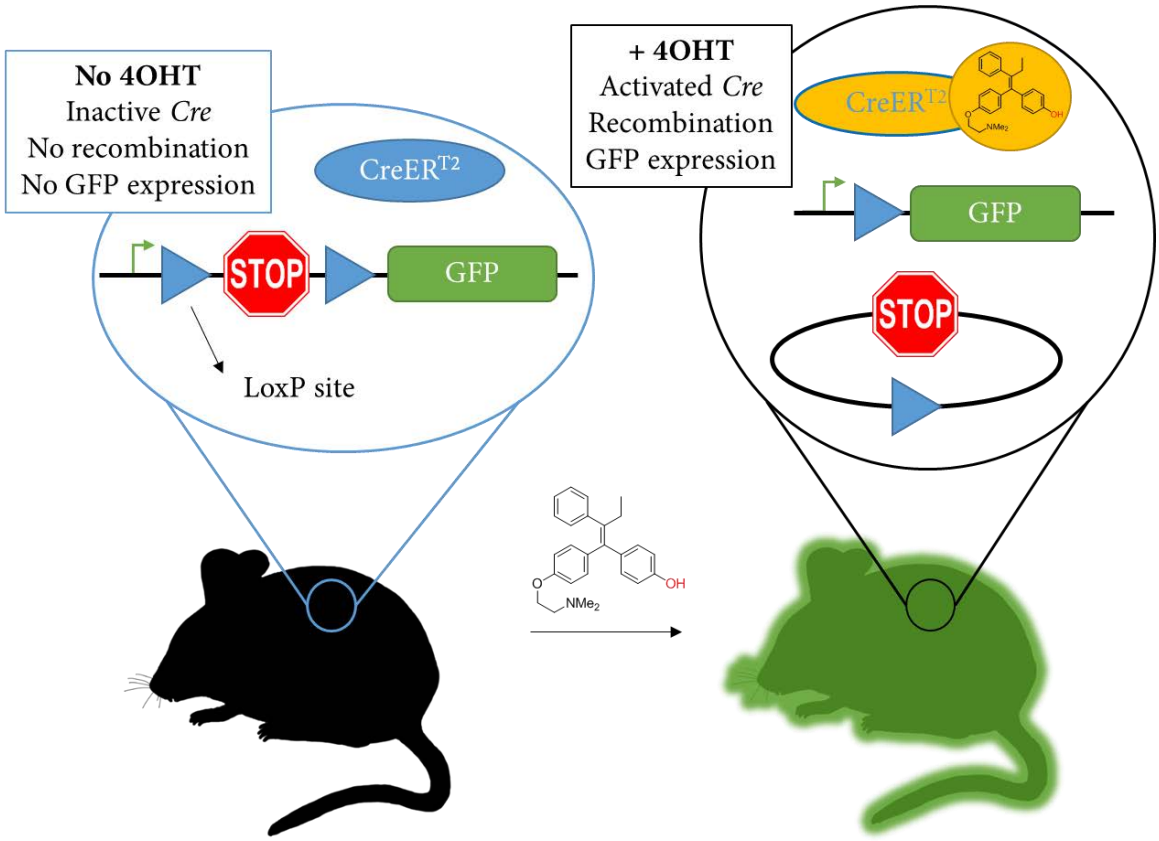

Figure 2.1.2. *Cre-GFP mouse model, containing a stop codon, flanked between LoxP sites, upstream of GFP gene. Left: absence of* ***2-2*** *means no recombination occurs and no GFP is expressed. Right:* ***2-2*** *binds and activates CreER, recombination excises stop codon. The promoter (green arrow) is now upstream of the gene coding GFP, causing GFP to be expressed.*

2.1.4. 4-Hydroxytamoxifen (4OHT, **2-2**)

4-Hydroxytamoxifen (4OHT, **2-2**) is a widely used antagonist of ER to treat patients with ER^+ breast cancer,[8,9] whereby oxidation in the liver (by enzymes including CYP2D6 and CYP3A4) converts **2-1** into the predominant active metabolites **2-2** and Endoxifen **2-3**.[10,11] These metabolites bind around 100x more strongly to ER than the parent molecule **2-1.**[12] The geometry of the double bond is also important, as the *Z* stereoisomer of **2-2** is reported to have over 300x higher affinity than the *E* stereoisomer.[13] Furthermore, isomerisation occurs in many biological systems, converting the active *Z* isomer into the less active *E* conformation.[14]

A variety of non-isomerisable analogues of tamoxifen were designed in an attempt to control the problem of isomerisation (figure 2.1.3). The simple addition of a methyl group in the *ortho*-position of the phenolic ring was sufficient to achieve a 9:1 ratio at equilibrium in favour of the *Z* isomer (**2-4**).[15] The pure isomer was obtained by recrystallisation in methanol and possessed an affinity for ER comparable to that of (*Z*)-4OHT.[16] Structural studies confirmed that the steric hindrance of the methyl group had little effect on the dihedral angles of the aryl groups in the propeller conformation, thus maintaining biological activity.[17]

Fusion of the ethyl moiety of the double bond with the phenolic group to form a 7-membered ring locked the conformation of **2-5** in the active *Z* form and rendered isomerization was impossible.[18] **2-5a** had comparable activity and relative binding affinity (RBA) to **2-1** and oxidation to **2-5b** increased the affinity, but possessed lower RBA and potency in MCF-7 cells than the corresponding oxidised compound **2-2**. The 6-membered ring analogue diminished the RBA and potency, presumably because of unfavourable orientation of the aryl rings. The authors note that this loss was not observed in **2-4**, which maintained the same RBA as **2-2** in these assays.[19]

A series of compounds that were fused on the opposing side *via* the phenolic and phenyl rings was also investigated, **2-6**.[20] Isomerisation was again prevented in these fused ring

structures, however these analogues had much lower affinity for ER. It was concluded that bridging groups (X) in the *ortho*-positions were detrimental to binding affinity, again presumably due to unfavourable orientation of the aryl rings.

Hydrogenation to afford dihydrotamoxifen **2-7** removed the double bond from the molecule and thus prevented isomerisation, since the diastereoisomers cannot interconvert.[21] A downside is that 2 new chiral centres are formed, impeded further by a fivefold lower whole-cell RBA for the most active isomer compared with **2-2.**

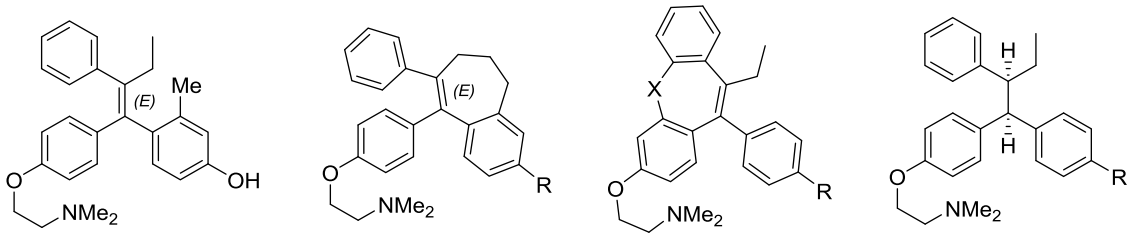

2-4

2-5a, R = H
2-5b, R = OH

2-6a
R = H or OH
X = O, S,
CH_2CH_2 or SCH_2

2-7a, R = H
2-7b, R = OH

Figure 2.1.3. *Non-isomerisable analogues of tamoxifen.*

2-1 and **2-2** have had a massive impact in the treatment of breast cancer and there is a wealth of information available on its activity and mechanisms in patients.[22] **2-1** and **2-2** can also activate *Cre* recombination to trigger the deletion or activation of desired genes and have widespread applications throughout biology labs.[23–25] It is generally assumed that the rules governing the binding affinity and activity of tamoxifen analogues for ER also hold true for their binding affinity to the triple mutated LBD of ER^{T2} and subsequent activation of *Cre* recombinase.

2.1.5. Previous Work from the Group (Guaymoxifen)

Our project aimed to introduce a higher level of regulation than current *Cre* methodology allowed, through spatiotemporal control over **2-2** activity. The approach derived was to liberate **2-2** through cleavage by a specific xenoenzyme expressed only in certain cells. From a chemical point of view, the aim of this project was to design and synthesise a compound

consisting of three components; a recognition site, a cleavable linker and the 4OHT component (scheme 2.1.2).

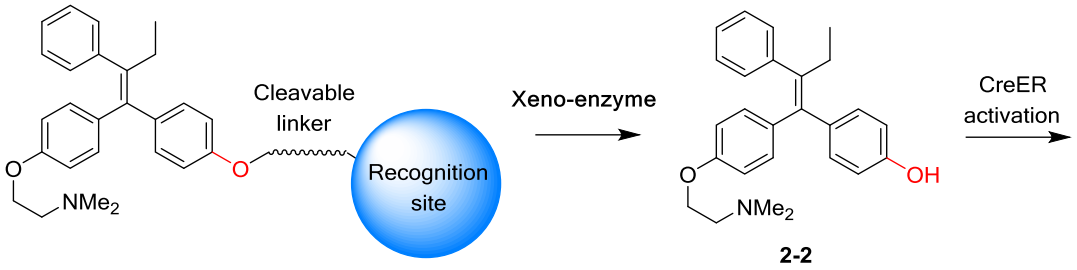

Scheme 2.1.2. *Diagrammatic representation of drug compound.*

Cancer cells (yellow, figure 2.1.4) containing this xeno-enzyme would be transplanted into a *Cre*-ER^{T2} mouse model that carried specific LoxP sites flanking the DNA sequences of choice (e.g. a stop codon). If the masked form of **2-2** is introduced, only the transplanted cancer cells would be able to cleave our inactive compound to liberate active **2-2**. Upon diffusion from the transplanted cancer cells into the local area (stroma, depicted in green), **2-2** would activate *Cre*-mediated gene recombination. The LoxP-flanked stop codon would be removed from these surrounding cells, causing expression of GFP. Niche cells in the stroma could thus be detected, isolated and analysed, e.g. by fluorescence activated cell sorting (FACS).

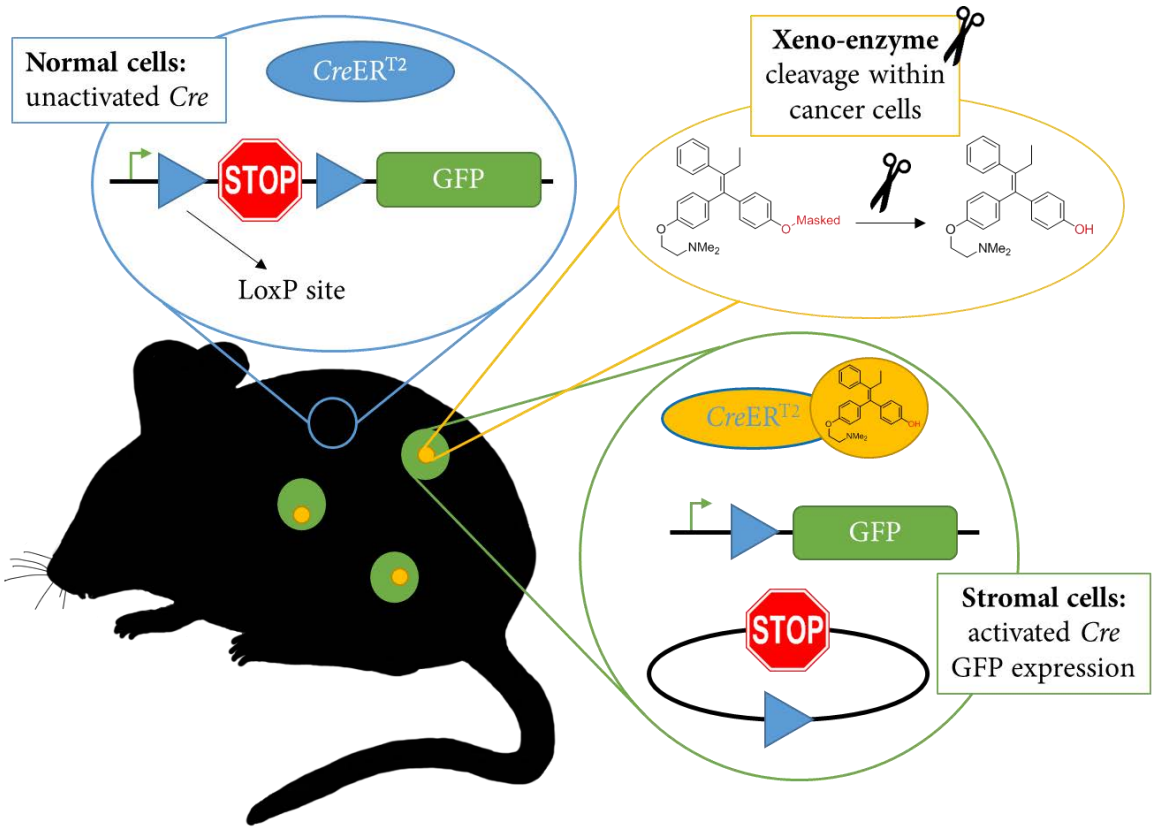

Figure 2.1.4. *Schematic illustration of the Cre-GFP mouse model with a further level of control, via controlled liberation of* ***2-2*** *by a specific xeno-enzyme.*

Similar methodologies have been reported during the course of this investigation such as a caged version of **2-2** which can be activated using UV light, as well as a PCPA-drug conjugate that can liberate **2-2** upon cleavage by LSD1 enzymes, which are overexpressed in tumour cells.[26,27] These compounds show great promise for a wide range of applications, however would have to circumvent many limitations if they are to become universal tools, such as improving metabolic stabilities and how to penetrate UV light into the target without adversely affecting the model. Furthermore, these tools would not be adequate to achieve the level of selectivity required in many cancer research groups, such as the studies carried out within the Batlle lab.

Our group chose to base our pro-drug fragment on lignin as a model structure. Lignin is a polymer found in wood consisting of guaiacol moieties linked *via* β-ether bonds.[28] This structure is resistant to metabolic breakdown in animal organisms as they lack enzymes

that are capable of cleaving the β-ether bonds present, however it can be metabolised by certain bacteria and fungi that contain a set of enzymes including LigF (e.g. *Sphingobium* sp. Strain SYK-6*)*. LigF is a beta etherase which is able to cleave the beta ether bond that is adjacent to the guiacol recognition site releasing guaiacol phenol **2-10** (red, scheme 2.1.3).

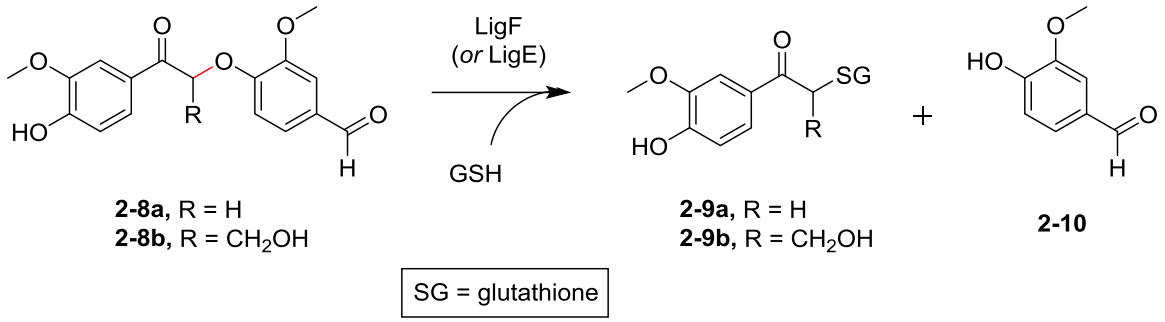

Scheme 2.1.3. *Cleavage of lignin-based compounds* ***2-8****, at the phenolic bond of the β-ether linker (red). Glutathione assists in the cleavage to liberate corresponding guaiacol products* ***2-9*** *and* ***2-10.***

In the thesis of Dan Byrom, the *Cre* activator, **2-2**, was masked by attaching a guaicol moiety *via* a beta ether linkage to create our pro-drug, **2-11**, which was christened "*Guaymoxifen*" (figure 2.1.5). Furthermore, "guay" means "cool" or "super" in Spanish, as we hoped this prodrug will be used as an extremely powerful technique. The methyl hydroxyl substituent of the β-ether linker (shown in grey) was not included in the original prodrug made within our group to omit the chiral centre that would be formed, thus facilitating the synthesis and the biological testing.

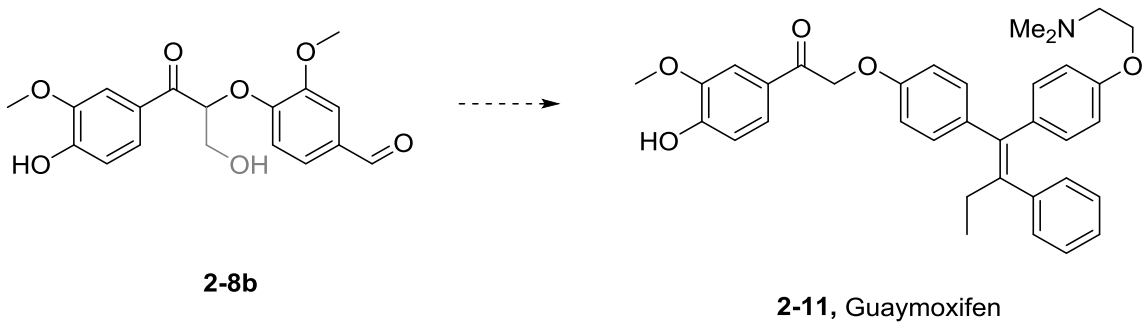

Figure 2.1.5 *Structure of "Guaymoxifen"* ***2-11*** *based on lignin fragment* ***2-8.***

A quick and convenient assay that monitored the cleavage of our compound and subsequent analogues by LigF was designed, where the liberation of a fluorescent compound was monitored. Therefore the 4OHT component was replaced by 4-methylumbeliferone, **2-13,** linked to the guaiacol recognition site to generate **2-12** (scheme 2.1.4).

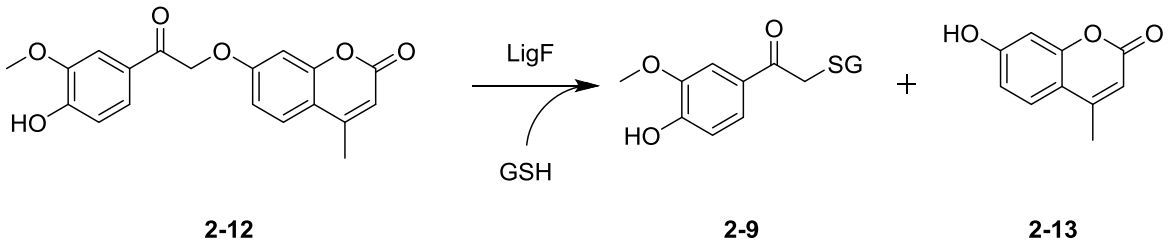

Scheme 2.1.4. *LigF/GSH cleavage of model compound* ***2-12*** *to release* ***2-9*** *and fluorescent compound* ***2-13****.*

2-12 was synthesised by Dr. Byrom using a 4-step route, consisting of the benzyl protection of **2-14a**, followed by bromination to afford **2-15a**. Nucleophilic substitution using **2-15a** with phenol **2-13** generated **2-16a**, before removal of the benzyl protecting group by hydrogenolysis to afford the final compound **2-12** in 44% overall yield (scheme 2.1.5).

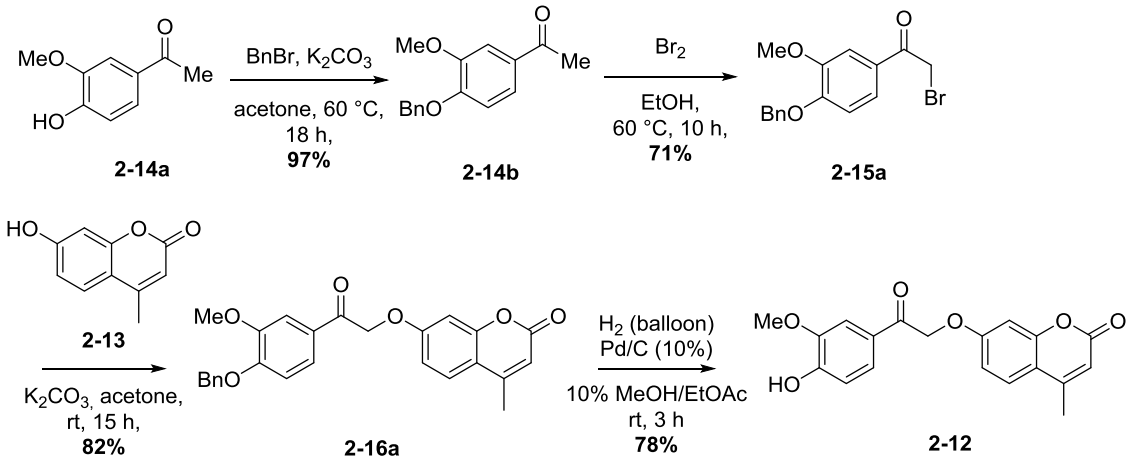

Scheme 2.1.5. *Original synthesis of* ***2-12****.*[29]

2-12 was demonstrated to be cleaved by purified LigF enzyme at a range of concentrations over time *in vitro*. Lower enzymatic loading than that used by Otsuka *et al.*[30] was needed because of rapid production of **2-13** resulting from cleavage of the β-ether bond of **2-12**. Appropriate controls, including wells that contained no GSH, no LigF and no **2-12** ensured that fluorescence was due to LigF enzymatic cleavage of **2-12** and that the ether bond wasn't simply decomposing under the assay conditions. As can be observed in graph 2.1.1A, LigF completed cleavage of **2-12** in approximately 30 min. After 40 minutes the reaction reached a plateau and did not progress further, indicating completion of the reaction. Cleavage of **2-12** was also confirmed in a cellular assay using different concentrations of **2-12** (graph 2.1.1B). These experiments demonstrated that **2-12** was cleaved in mammalian cells expressing LigF and that **2-12** was resistant to cleavage by other enzymes present within cells.

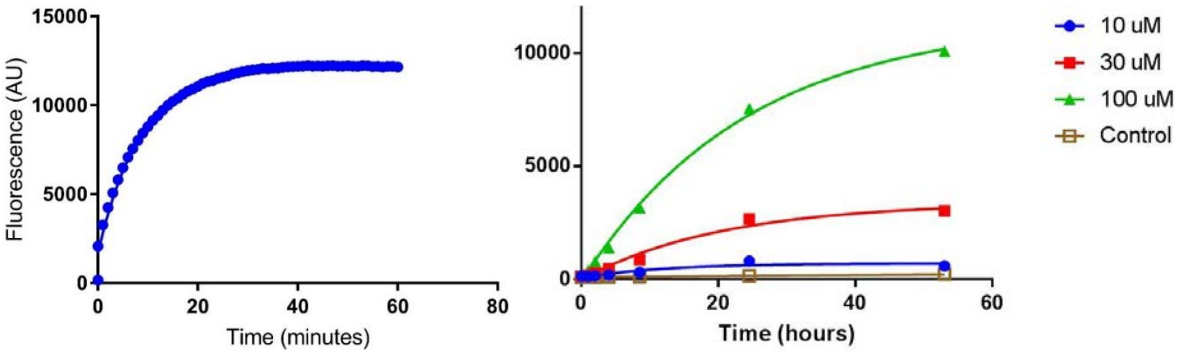

Graph 2.1.1. A) *Cleavage of **2-12** to release **2-13** in a purified LigF in vitro assay monitored by fluorescence.* ***B)*** *Fluorescence monitored cleavage of **2-12** at different concentrations in HEK293T LigF-containing cells.*

Dr. Byrom also generated a collection of analogues of **2-12** to carry out an SAR study about the aryl recognition fragment. However, none of the new analogues were sensitive to cleavage by LigF and the guaiacol moiety was confirmed to be essential for cleavage to occur. With deeper understanding of the cleavage of our fluorescent model compound **2-12**, the real pro-drug **2-11** was required in sufficient scale for further testing. The synthesis of **2-11**(*Z*) proved extremely challenging, further impeded by the massive cost of commercially available **2-2** and the poor nucleophilicity of this phenol group which

prevented nucleophilic addition to the α-bromo ketone **2-15a** (scheme 2.1.6). Instead, various degrees of isomerisation and decomposition of the starting material occurred.

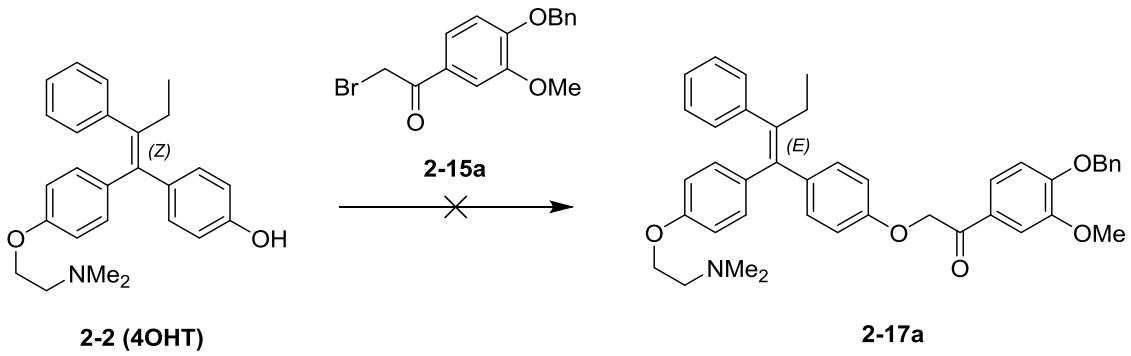

Scheme 2.1.6. *Attempted incorporation of guaicol component (**2-15a**) via nucleophilic displacement with **2-2** to form benzyl-protected guaymoxifen **2-17a.***

There are numerous publications for the syntheses of **2-1** and **2-2**, including routes based on modern palladium coupling reactions such as sequential Stille/Suzuki or sequential Suzuki/Suzuki reactions that can generate **2-2** in high ratios in favour of the more active *Z* isomer.[31,32] Despite this extensive literature, none of these routes could be successfully adapted to obtain **2-11**. Therefore, Byrom opted to utilise a more traditional McMurry reaction as the key step in the C=C double bond formation.[33] He also introduced the dimethyl amine moiety of **2-11** by reductive amination after unsuccessful attempts at direct alkylation of **2-18** using chlorinated dimethyl amino ethane (scheme 2.1.7). The overall synthetic route to afford **2-11** is shown in scheme 2.1.8, with 7% overall yield over 10 steps.

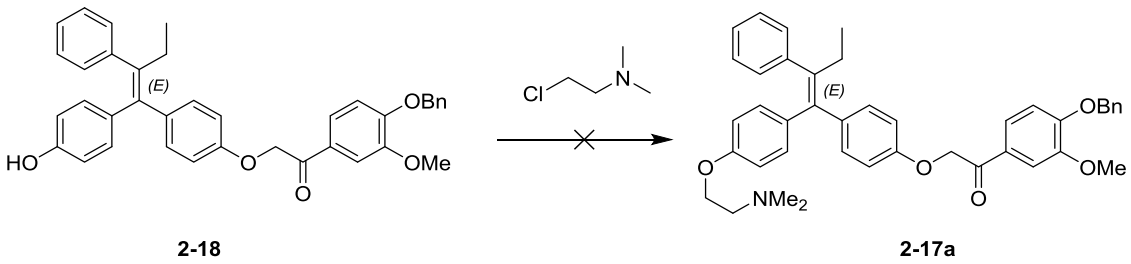

Scheme 2.1.7. *Attempted displacement reaction to incorporate the diamino side-chain as a penultimate step to form intermediate **2-17a**.*

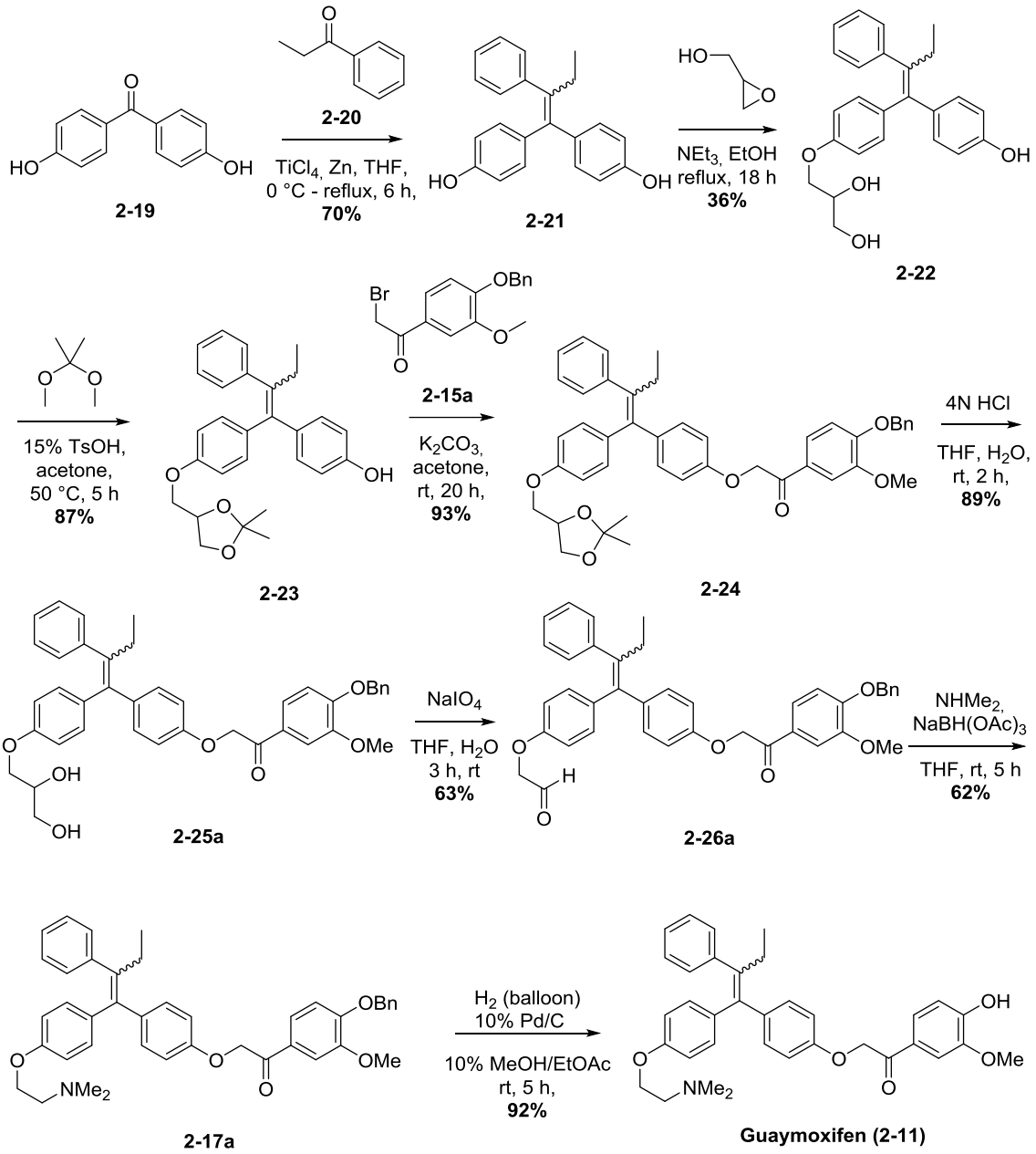

Scheme 2.1.8. *Original synthetic route towards guaymoxifen (**2-11**) in an approximate 1:1.1 Z/E isomeric ratio.*

A small batch of intermediate **2-25a** was separated by chiral HPLC chromatography into the individual *E* and *Z* stereoisomers, then the final reactions were carried out on them separately to obtain small quantities of ***(E)*-2-11** and ***(Z)*-2-11**. It was found that ***(E)*-2-11** & ***(Z)-2-11*** did not undergo isomerisation when dissolved in chloroform-*d*6 and monitored by ^{1}H NMR over one week. 4OHT (**2-2**) on the other hand, isomerised to an approximate

1.2:1 *Z:E* ratio in under 16 hours under the same conditions, which is consistent with examples reported.[34–36]

Dr. Byrom and Dr. Tauriello tested guaymoxifen (**2-11**) in 2 separate assays to demonstrate the expected function of this technology. The first was an *in vitro,* GSH catalysed cleavage assay using LigF (expressed by the protein expression core facility at IRB Barcelona). The reaction was followed by mass spectroscopy and increasing levels of 4OHT (**2-2**) were observed as time progressed. This proved the original hypothesis that LigF could liberate 4OHT (**2-2**) from guaymoxifen (**2-11**). LigF was also expressed in HEK293T cells. These cells were co-cultured with reporter cells that respond to treatment with 4OHT (**2-2**). Upon treatment with guaymoxifen (**2-11**), the reporter cells responded by activation of *Cre* recombination and GFP production. This confirmed that **2-11** was able to penetrate cell walls, that LigF could convert **2-11** into **2-2** inside cells, and that **2-11** was then able to leave LigF cells and enter neighbouring *Cre*-GFP cells to initiate recombination.

Now that **2-11** had shown excellent function in the *in vitro* and cellular assays, we wished to further demonstrate the potential of this technology with *in vivo* experiments. For this, much larger quantities of **2-11** would be needed (objective 1, section 2.2). Further optimisation would require new analogues with improved metabolic stability (objective 2, section 2.3) and to design a synthesis to obtain guaymoxifen enriched in the active pro*Z* stereoisomer (objective 3, section 2.4).

2.2. Optimisation for Large Scale Synthesis of Guaymoxifen and in vivo Results

The original synthesis that was devised to obtain the first batches of guaymoxifen (**2-11**, scheme 2.1.8) had several drawbacks that required optimisation before repeating on a larger scale. Firstly, despite the satisfactory 70% yield from the McMurry step, the reaction was complicated technically to execute and generated large amounts of waste. The subsequent epoxide ring opening of glycidol using diphenol **2-21** gave a statistical mixture of starting material, product and di-alkylated product. Thus, the mixture had to be separated by column chromatography and the low yield of 36% could not be improved (scheme 2.2.1). Secondly, the acetal protection step of diol **2-22** (scheme 2.2.2) and subsequent de-protection of intermediate **2-24** were not quantitative and could potentially be circumvented by reacting the phenol selectively over the unprotected alcohol moieties. By-passing these steps would save time and improve yields. Lastly, the benzyl protecting group was not consistently well removed from the final intermediate **2-17a**, with partial reduction of the carbonyl group present in the β-ether moiety taking place (**2-27a**-b, scheme 2.2.3). Therefore, modifications were made in an attempt to address these key issues and improve the overall synthesis for larger scale synthesis of guaymoxifen (**2-11**).

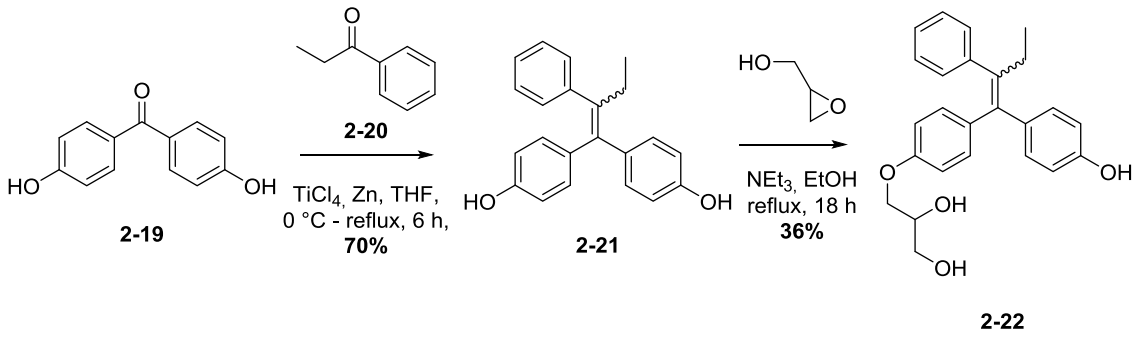

Scheme 2.2.1. *Original synthesis utilised in the thesis of Byrom, comprising a McMurry reaction using* ***2-19*** *and* ***2-20*** *followed by an epoxide ring opening reaction with glycidol and* ***2-21*** *to afford intermediate* ***2-22****.*

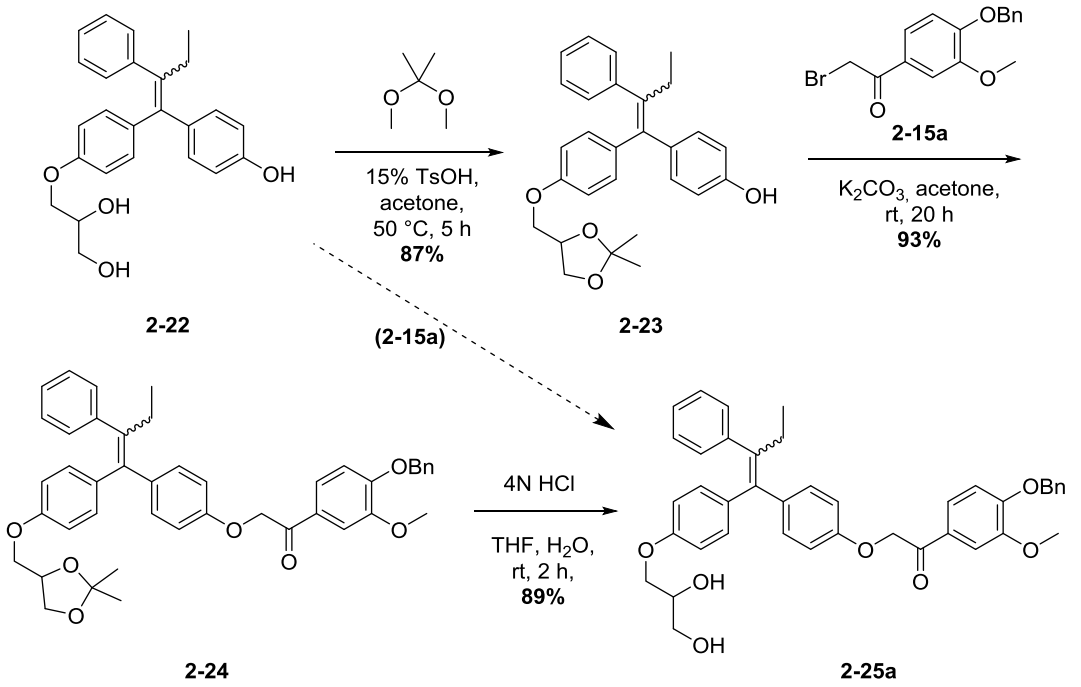

Scheme 2.2.2. *Incorporation of the guaicol fragment using* ***2-15a*** *to afford intermediate* ***2-25****. Showing the original pathway designed by Dan Byrom and the proposed shortcut shown as a dashed arrow.*

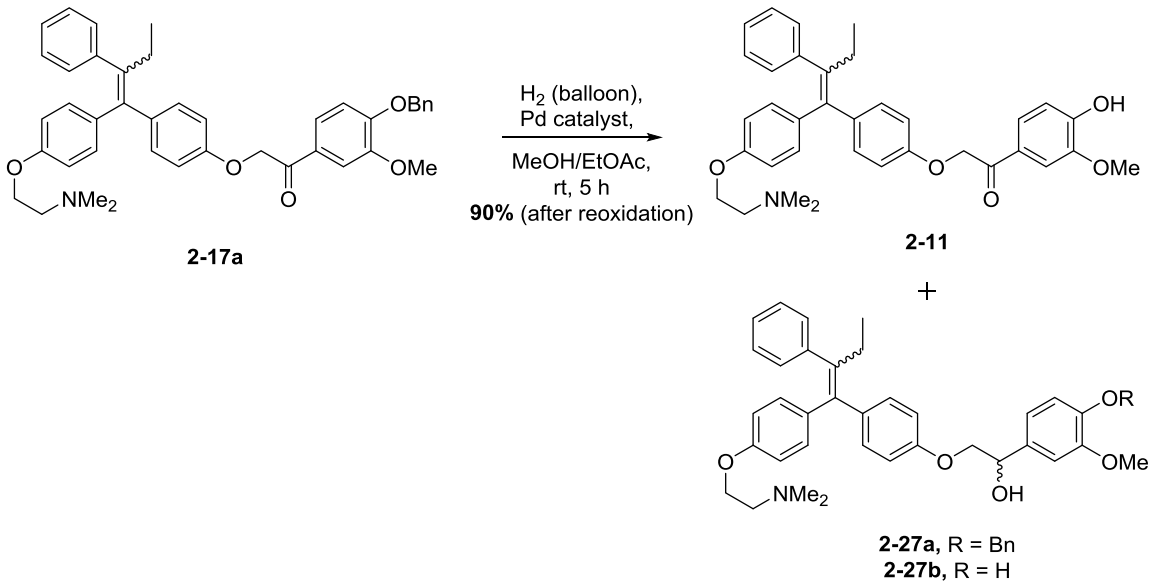

Scheme 2.2.3. *Deprotection of final guaymoxifen intermediate* ***2-17a*** *affording guaymoxifen* ***2-11*** *and carbonyl-reduced starting material and product* ***2-27a-b****.*

2.2.1. Alternative Synthesis of Diol Intermediate **2-22**

We first turned our attention to the initial steps of the synthesis, with an aim of improving the regioselectivity of the reaction forming diol **2-22** and finding a cleaner alternative to the McMurry reaction. Byrom had already experimented with various routes based on palladium couplings without success and we did not pursue these routes further.[29] Therefore, we took inspiration from earlier routes towards tamoxifen whereby the olefin was formed *via* dehydration of a tertiary alcohol intermediate. The tertiary alcohol was prepared by Grignard addition to a ketone intermediate, which in turn was formed by Friedel-Crafts acylation.[35] We devised a similar route towards key diol intermediate **2-22**, the retrosynthetic analysis is shown below in scheme 2.2.4.

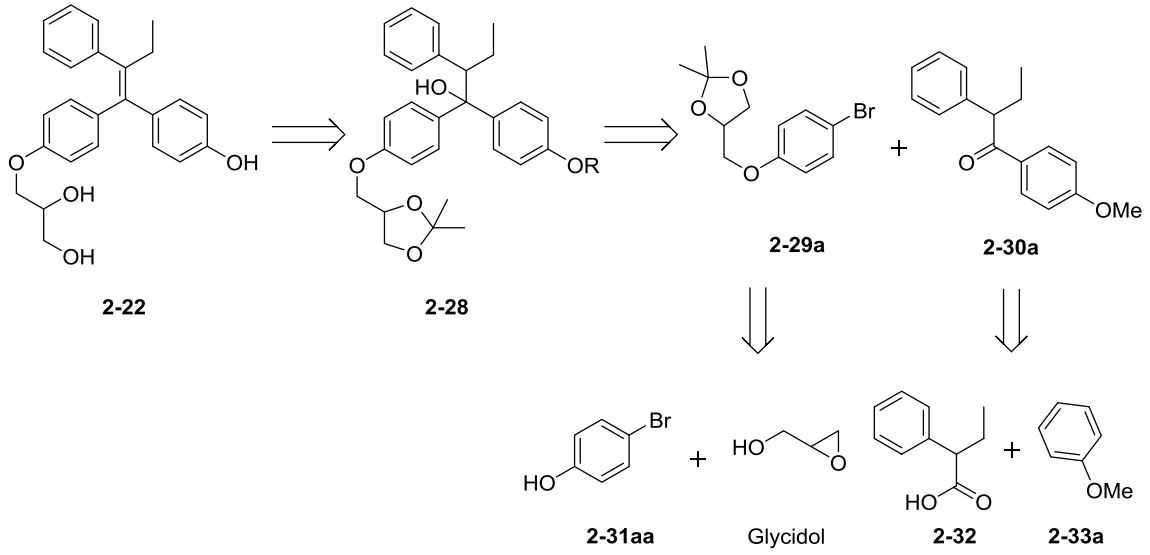

Scheme 2.2.4. *Retrosynthetic analysis of intermediate **2-22**. Formation of an organometallic reagent from **2-29a** (formed by S_N2 of **2-31aa** with glycerol then subsequent acetal protection of the diol), then addition of the organolithium reagent to ketone **2-30a**, formed by the Friedel-Crafts alkylation of **2-32** and **2-33a**.*

The initial Friedel-Crafts reaction afforded **2-30a** in quantitative yield, consistent with literature examples.[15] However, when we tested how labile the methyl protecting group was, we were unable to effectively remove it to afford phenol **2-30b,** despite screening a range of conditions (table 2.2.1).

Table 2.2.1. *Reaction conditions for the deprotection of* ***2-30a.***

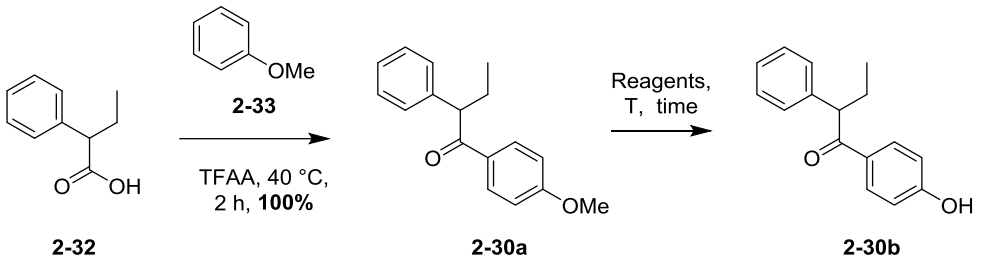

Entry	Conditions	Temperature (°C)	Time (h)	Yield (2-30b)
1	Me_2SiI, $CHCl_3$	50	20	-
2	HBr (48%), AcOH	Reflux (120)	48	Trace
3	HBr (48%), NBu_4Br, AcOH	Reflux (120)	48	Trace
4	$AlCl_3$, DCM	rt	72	-
5	Pyr.HCl, neat.	200	5	15%
5	Pyr.HCl, neat.	150	120	10%
6	$LiSC_{12}H_{23}$, DMF	90	7	decomposition
7	Dodecanethiol, NaOH, NMP	120	1.5	Trace

Therefore, we chose to replace the methyl protecting group with an allyl group (**2-30c**) and found that it could undergo the Friedel-Crafts step with allyl protected **2-33b** in excellent yield and was more easily removed using Pd catalysts in the presence of acid or base (scheme 2.2.5).

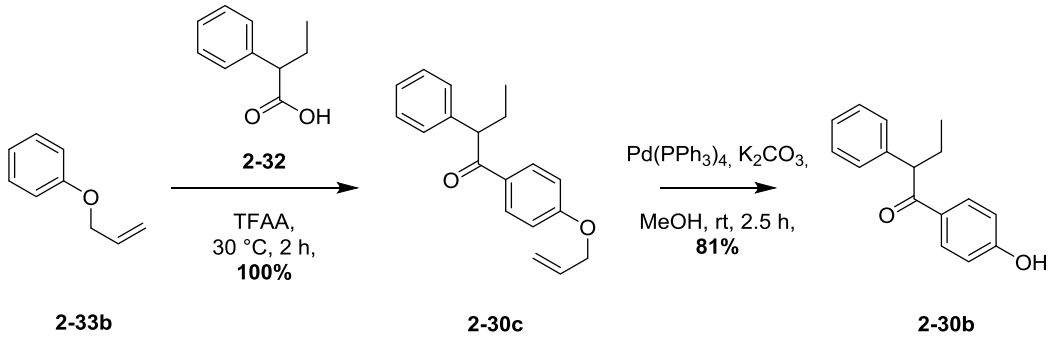

Scheme 2.2.5. *Friedel-Crafts reaction using* ***2-33b*** *and* ***2-32*** *and the subsequent removal of the allyl protecting group from* ***2-30c*** *to afford* ***2-30b.***

The bromo coupling partner **2-29a** was synthesised in moderate yield by reacting *para*-bromo phenol **2-31a** with glycidol to afford **2-32a**, which was then protected as the acetal **2-29a** (scheme 2.2.6). With both coupling partners in hand, we then attempted the coupling of ketone **2-30c** with an organolithium formed by treating **2-29a** with n-BuLi. The iodo analogue **2-29b** was also generated *via* this route

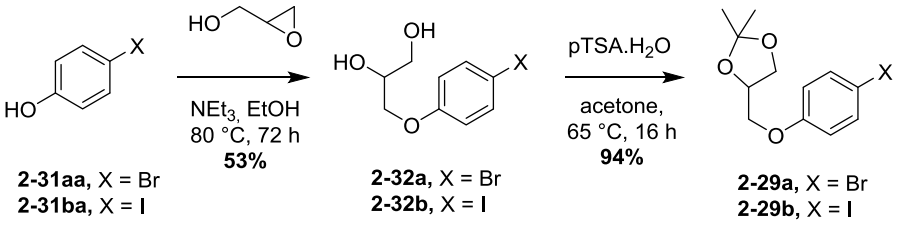

Scheme 2.2.6. *Formation of intermediate* ***2-29a*** *via displacement reaction of* ***2-31aa*** *and glycidol, followed by the acetal protection of diol product* ***2-32a****.*

We rationalised that by forming the Grignard reagent from **2-29a**, this would be less reactive than the organolithium and therefore lead to a more controlled addition to ketone **2-30c**. However, no product was observed and only the starting materials and de-brominated side-products were isolated from the reaction mixture when this was attempted (scheme 2.2.7). When the organolithium or Grignard reaction was performed using the 4-iodo-analogue **2-29b**, the reaction did not form any desired product.

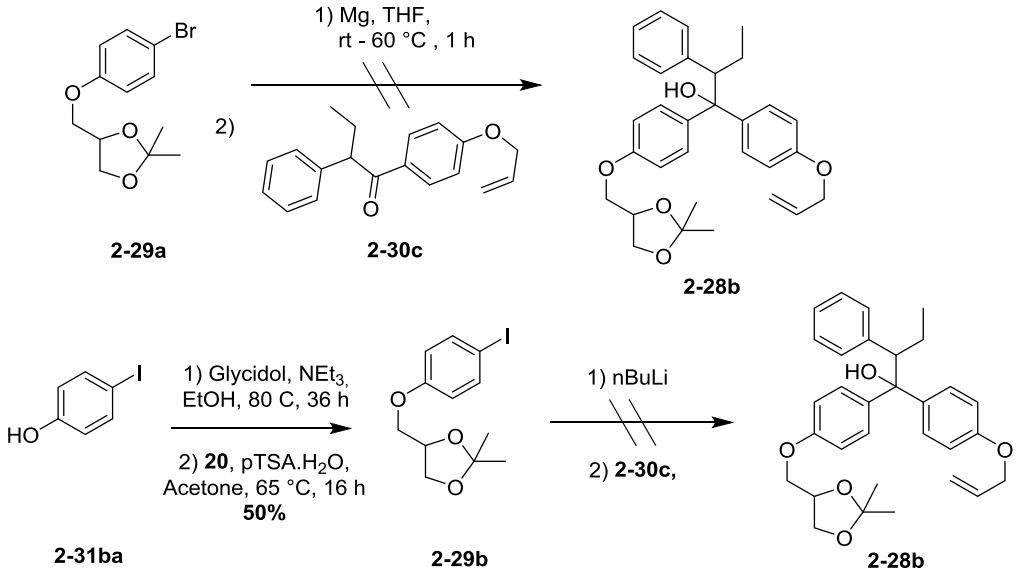

Scheme 2.2.7. *Attempted formation of intermediate* ***2-28b*** *via the Grignard route and using iodo analogue* ***2-29b****.*

Fortunately the reaction using the organolithium generated from bromo intermediate **2-29a** and ketone intermediate **2-30c** was successful and resulted in a moderate yield (76%) of tertiary alcohol product **2-28b** (scheme 2.2.8).

The subsequent de-protection of the acetal and allyl protecting groups occurred simultaneously to the dehydration of the tertiary alcohol to form diol intermediate **2-22** with a yield of 66% (scheme 2.2.8). This new route avoided the difficulties encountered in the messy McMurry reaction and gave a chemoselective alternate route tomonosubstituted product **2-22**, to replace the non-selective glycidol addition to diphenol intermediate **2-21**. It provided a more reproducible route for the scale up of guaymoxifen, despite comprising 3 steps as opposed to 2.

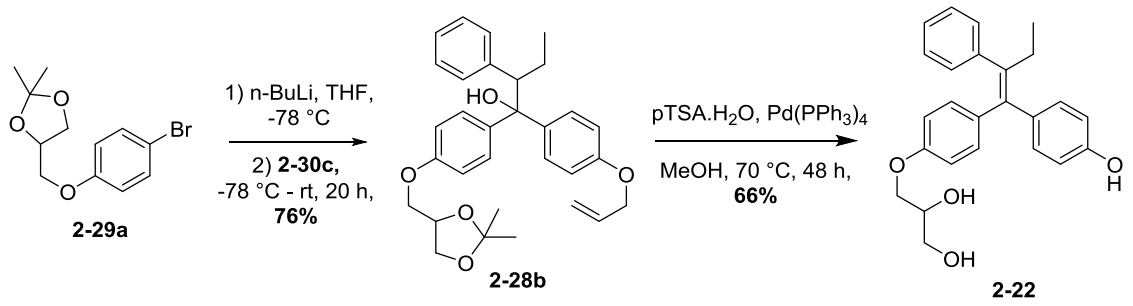

Scheme 2.2.8. *Improved synthesis of* ***2-22*** *via Friedel-Crafts, addition of organolithium reagent (formed from* ***2-29a****), followed by simultaneous deprotection of the allyl and acetal groups as well as dehydration to form the C=C double bond.*

At this stage, we observed that instead of de-protecting the allyl group, we could instead perform a dihydroxylation on the allyl group to directly obtain diol intermediate **2-22** in a more direct manner (scheme 2.2.9). Thus, THP was chosen as the phenol protecting group for the phenol in **2-31ab** due to its prevalence in the literature for similar Grignard reactions.[35,36] The anticipated facile removal of THP in acidic conditions would then be carried out simultaneously to the dehydration reaction forming the double bond of **2-35**. Since this route was much shorter, we began optimisation of the organolithium addition step to improve the yield.

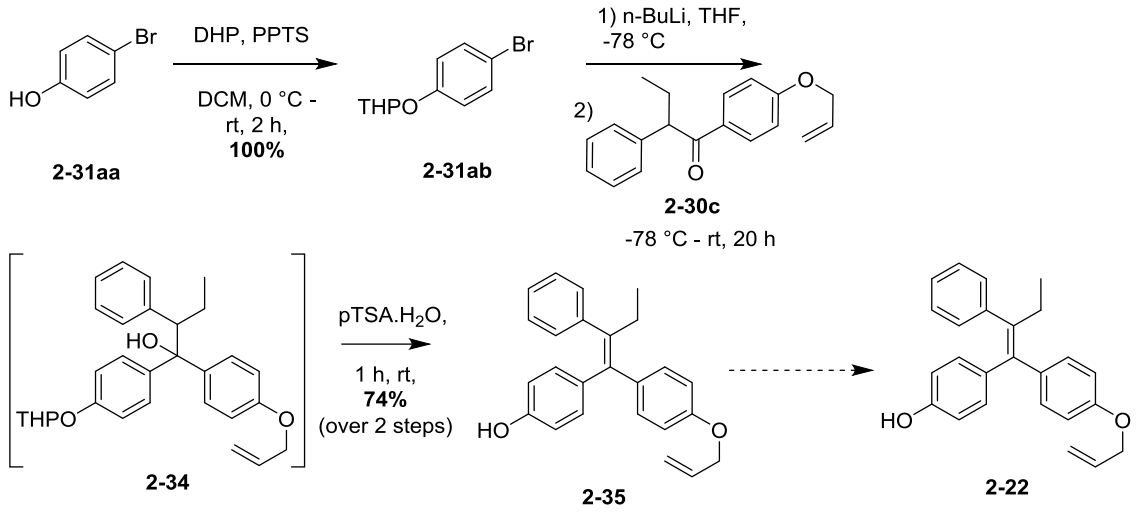

Scheme 2.2.9. *Improved route to* ***2-22*** *using THP-protected intermediate* ***2-31ab*** *to form* ***2-34****, followed by deprotection of the THP group and dehydration of the tertiary alcohol group to form the C=C double bond. Dihydroxylation catalysed by osmate then furnished diol* ***2-22.***

A range of conditions were screened to form organometallic intermediates and subsequent addition to ketone **2-30c**. Table 2.2.2 shows that in general, attack using the organolithium reagent outperformed that of the Grignard and was more consistent overall (entries 7 & 8). The Grignard was more difficult to generate than the organolithium and although the THP-protected Grignard was commercially available, it was not an economically viable route for larger scale syntheses.

Table 2.2.2 *A screening of the formation of organometallic intermediate from* ***2-31ab*** *and subsequent reaction with* ***2-30c*** *to form* ***2-34,*** *followed by simultaneous de-protection and dehydration in acidic conditions to afford* ***2-35****.*

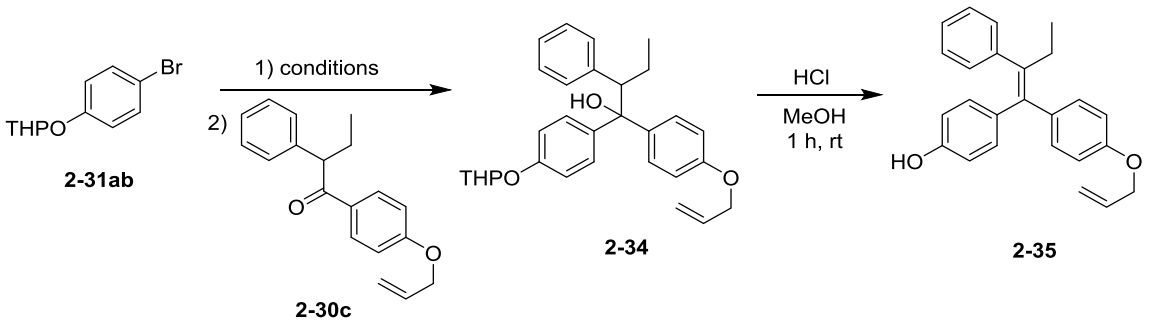

Entry	Conditions	Temperature (°C)	Time (h)	Yield (%)
1	Grignard added to ketone	-78 - rt	48	47
2	Grignard added to ketone	0 (addition), 75	48	60
3	Grignard added to ketone	75	24	46
4	Ketone added to grignard	75	24	40
5	Grignard added to ketone	0 - rt	24	50
6	Grignard added to ketone	0 - 45	24	54
7	1.2 eq nBuLi	-78 - rt	24	66
8	1.5 eq nBuLi	-78 - rt	24	74

We supposed that the origins of the low yields were due to the basic nature of nBuLi and the resulting organometallic compounds formed. It was perhaps also due to the reductive nature of nBuLi, which would have been present in residual amounts (scheme 2.2.10A). Starting material **2-30c** persisted in the reaction mixture as well as minor impurities such as the alcohol product **2-36** in scheme 2.2.10B. Unfortunately no improvement was observed when reversing the order of addition, i.e. forming first the organolithium then adding the ketone dropwise to this solution. Neither did using fewer equivalents of nBuLi result in full conversion of the bromo-starting material.

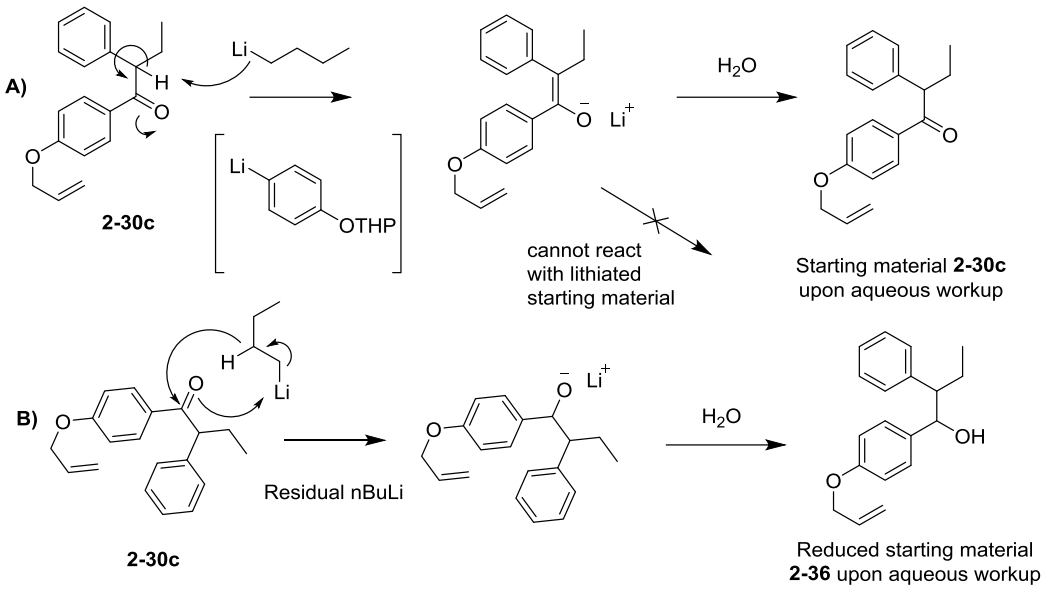

Scheme 2.2.10 A) *α-proton to the carbonyl is removed by organometallic component. The intermediate cannot react and starting material* ***2-30c*** *is re-obtained upon quenching with aqueous workup.* ***B)*** *β-proton of nBuLi reduces the carbonyl of the ketone starting material, which upon aqueous workup yields the reduced starting material as a secondary alcohol,* ***2-36****.*

The acceptable yield of 74% was sufficient for the scale up of diol **2-22**, however the use of column chromatography could not be avoided to obtain pure product, and was necessary to separate the starting material and side products afforded. The dihydroxylation of **2-35** was straightforward and achieved quantitative yields even with larger scale reactions (scheme 2.2.9). OsO_4 is known to be toxic by inhalation therefore we replaced this oxidising agent with less volatile potassium osmate(VI) dehydrate. Although this heavy metal generates toxic waste products, it is used in minuscule catalytic amounts and the Os(VI) by-product can be re-oxidised to the active Os(VIII) *in situ* using NMO, as is OsO_4 in standard Upjohn reaction conditions.[37] The overall yield towards intermediate **2-22** was thereby improved from 25 – 70%.

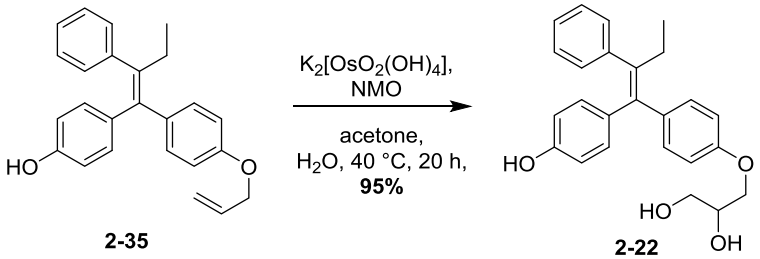

Scheme 2.2.11. *Dihydroxylation of allyl protected intermediate* ***2-35*** *to afford diol* ***2-22****, using osmium catalyst, in high yield.*

2.2.2. Improved Incorporation of Guaiacol Fragment **2-15**

It was observed that the nucleophilic substitution of bromo intermediate **2-15** and phenol **2-22** to afford **2-25** could be performed selectively at the phenol group in the presence of the diol moiety, thus by-passing the 2 extra steps needed for acetal formation and then de-protection (scheme 2.2.11). This reaction was carried out in yields ranging from 86 – 100%, which was even better than that obtained previously using the acetal protected intermediate **2-23**. Furthermore, the steps for acetal formation and subsequent deprotection were no longer required, saving time as well as improving yield. Large amounts of **2-25** were now accessible for the final stages of the synthesis to be trialled and optimised.

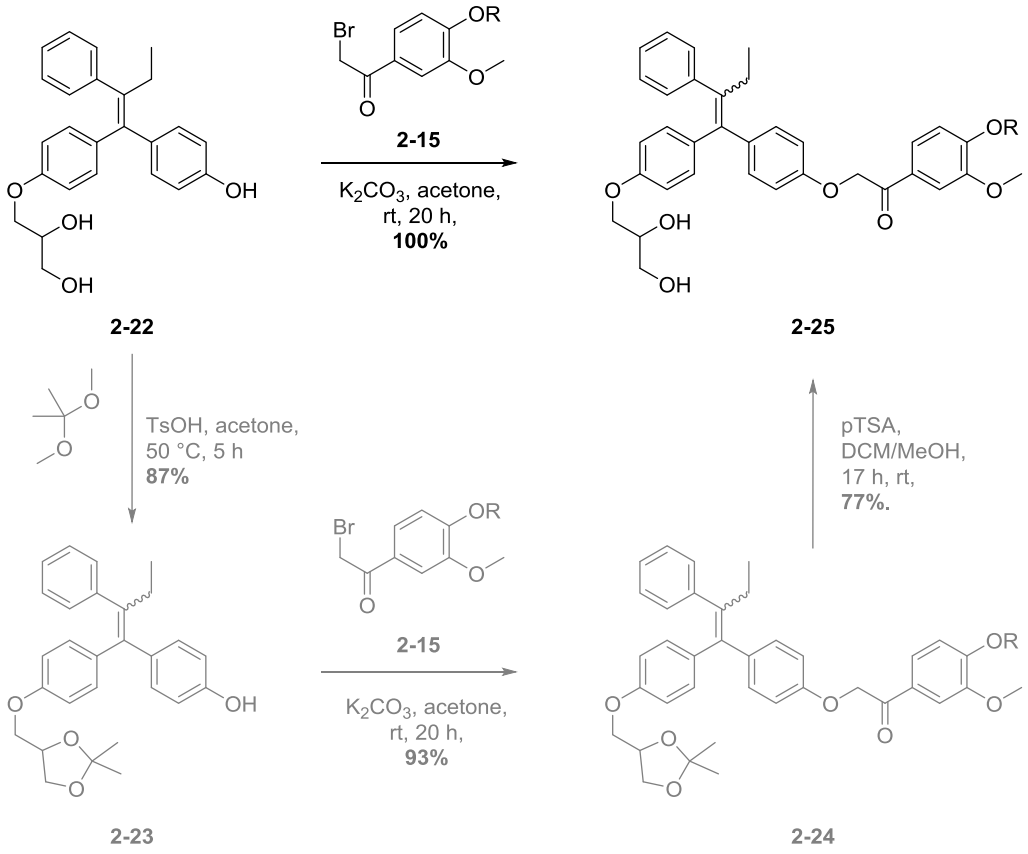

Scheme 2.2.11. *Direct incorporation of guaiacol component and original route via acetal intermediates* ***2-23*** *and* ***2-24****.*

2.2.3. Replacing the Benzyl Protecting Group

Removal of the benzyl protecting group from the phenol moiety of the guaiacol component was not consistent, although a high yield had been achieved on certain reactions. This was probably due to the poor solubilities of starting material and product, further impeded by other reactive functional groups. In particular, reduction of the carbonyl moiety of either starting material or product also led to cleavage of the β-ether linkage (**2-27,** scheme 2.2.12). The alcohol side product **2-27b** could be oxidised using Dess-Martin periodate. Despite screening a range of conditions, including different palladium catalysts, the reaction was not improved. Therefore, we decided to replace the benzyl protecting group.

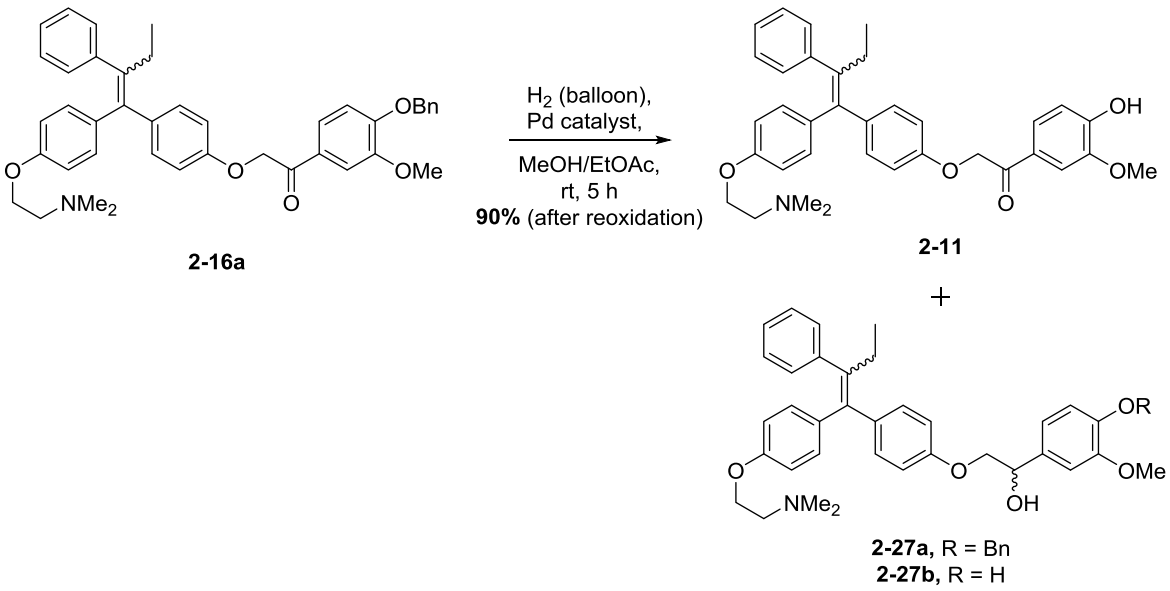

Scheme 2.2.12. *Deprotection of final guaymoxifen intermediate* ***2-16a*** *affording guaymoxifen* ***2-11*** *and carbonyl-reduced starting material and product* ***2-27a-b.***

The new protecting group would have to be resistant to the acidic conditions during the bromination, acetal cleavage, and reductive amination steps. The proposed group should also be easily removed in the final step without reduction of the carbonyl group within the β-ether linker. Additionally, the benzyl group gave rise to a very electron-rich ring, which was problematic during the bromination step, generating side products due to over-bromination and bromination of the aryl ring (**2-37** and **2-38**, scheme 2.2.13). This effect

was even more pronounced when the benzyl group was replaced by a PMB group, with no product and only side products being observed in the reaction.

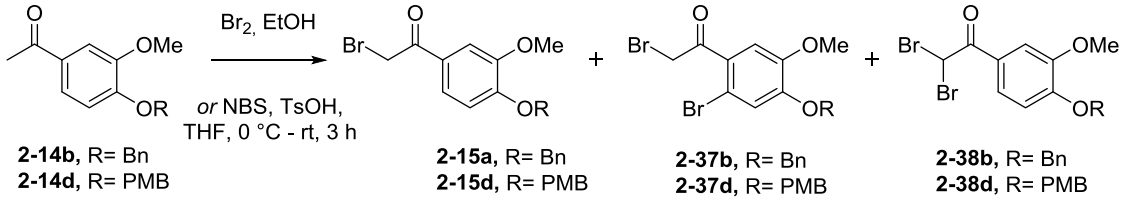

Scheme 2.2.13. *Bromination reaction of* ***2-14b*** *and* ***2-14d*** *using Br_2 in EtOH or NBS, TsOH in THF. Where R = Bn or PMB.*

Other ether groups, such as THP and MOM, were avoided to evade potential cross-reactivity with the β-ether linker moiety, as had been previously experienced in the group. Therefore, benzoate and pivaloate protecting groups were used to trial the subsequent bromination, nucleophilic substitution and deprotection steps. The acetate protecting group used in a previous analogue was not employed because the methyl ketone moiety could also undergo bromination. The displacement reaction was carried out on 4-methylumbeliferone (MU, **2-13**) as it was commercially available, whereas diol intermediate **2-22** had to be synthesised and was therefore more precious (scheme 2.2.14). MU product (**2-12**) that was generated from these optimisations was later used as a control in further fluorescent assays.

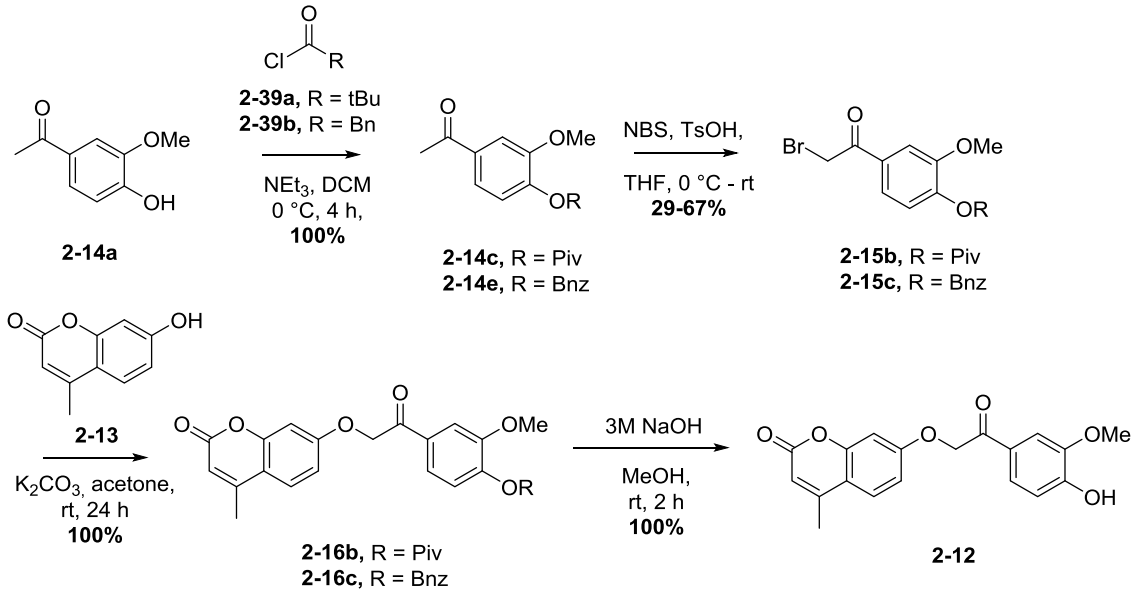

Scheme 2.2.14. *Synthesis of* ***2-12*** *using different protecting groups for the phenol moiety.*

Esterification of phenol **2-14a** using acid chlorides **2-39a** and **b** afforded the aryl pivalate and benzoate intermediates **2-14c** and **2-14e** in quantitative yields. The ester functionality reduced the electron donation into the ring, so that when the bromination step was performed on these intermediates, bromination of the aryl ring was minimised. However, the benzoyl protecting group in **2-14e** was labile in the basic conditions used in the following nucleophilic substitution reaction. When K_2CO_3 was replaced with NEt_3, a bromide salt formed as a result of deprotonation of the bromo starting material and minimal product was isolated from the reaction. However aryl pivaloate **2-14c** proved to be more resistant to K_2CO_3 and the product **2-16b** was then easily deprotected using aqueous NaOH in methanol at room temperature to afford **2-12** without reducing or cleaving the β-ether moiety. Now that a new protecting group had been identified in the synthesis of our MU analogue, the pivaloyl protecting group was utilised to replace the benzyl protecting group in the synthesis of guaymoxifen (**2-11,** scheme 2.2.15).

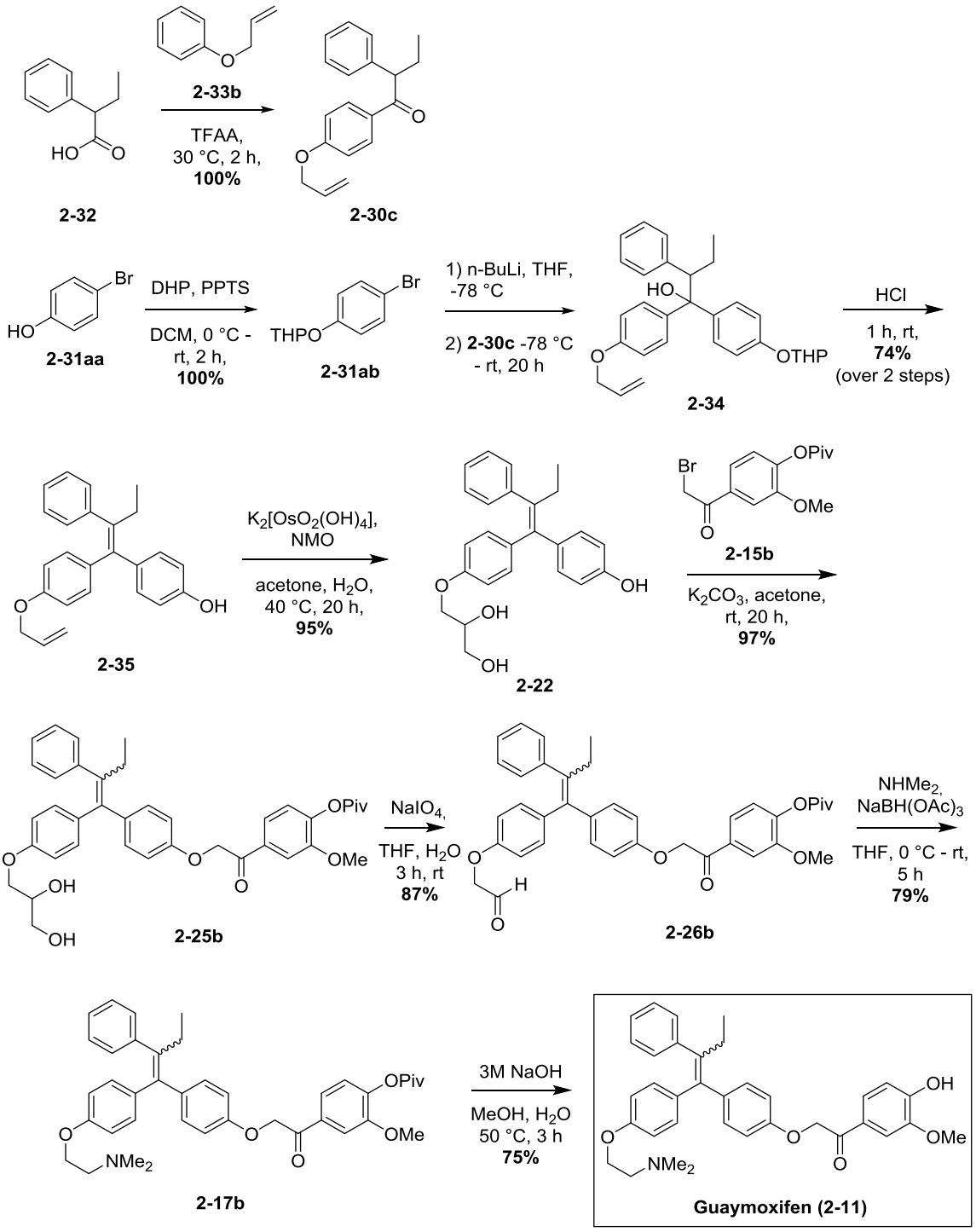

Scheme 2.2.15. *Overall synthetic route towards* ***2-11****, showing the 3 major improvements; 1) organolithium reaction to replace the McMurry step, 2) improved incorporation of the guaiacol component, and 3) replacing the benzyl protecting group with pivaloyl.*

The pivaloyl protecting group proved resistant to the reaction conditions in these remaining 5 steps and the synthesis of **2-11** was achieved in a yield of 39% over the ultimate

5 steps (compared to 30% for these 5 steps using the benzyl protecting group). The increase in yield was thought to be caused by the increase in solubility of some of the pivaloyl protected intermediates in the organic solvents used and of course because no material was lost in the ultimate step due to reduction of the carbonyl on the β-ether linkage. De-protection of the pivaloyl group was much more reproducible than with the benzyl group. It avoided side-products formed by reduction of the carbonyl moiety and gave consistently higher yields.

2.2.4. *In Vivo* Results of Guaymoxifen (**2-11**) Treated *Cre*-GFP Mice possessing LigF Tumours

With large quantities of Guaymoxifen (**2-11**) now in hand, the *in vivo* studies were carried out by Dr. Daniele Tauriello in the Batlle research group. **2-11,** 4OHT (**2-2**) and oil (used as a vehicle to administer compounds) were administered to *Cre* mice that had adequate LigF expressing tumours. After the experiments, analysis of the tumour, liver and other organ tissue (such as lung) was performed. Although *Cre* recombination could be observed in the tumour tissue, in varying amounts, there was also recombination in the liver (5 – 10%, figure 2.2.16) and small amounts in other tissues.

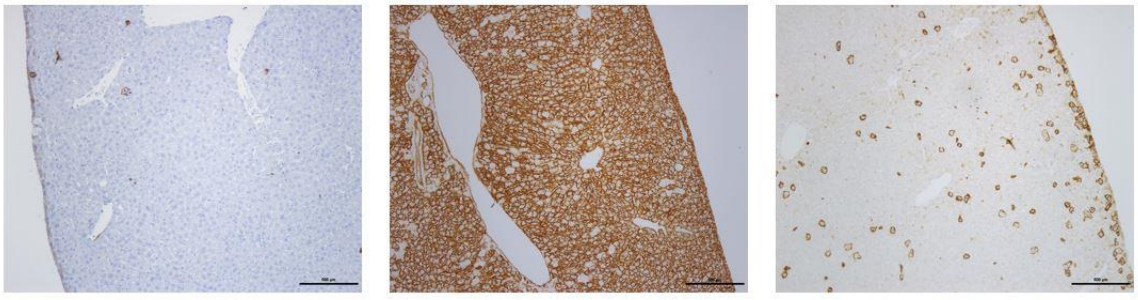

Figure 2.2.16. *Image of the liver cells of the mouse model, showing 5 – 10% recombination occurring in the non-cancer cells of the mouse. Brown stain shows recombination, blue/ yellow normal living cells.*

We predicted that the off-target recombination was due to the cleavage of guaymoxifen (**2-11**), as uncleaved **2-11** did not induce recombination in the cellular assays and proved stable in the absence of LigF enzyme. This cleavage was hypothesised to originate from oxidative metabolism by cytochrome P_{450} (CYP) enzymes, which are concentrated in the liver.

Unfortunately this background recombination could not be prevented by altering the administered dose of **2-11** (5 – 1 μM, at which tamoxifen is still sufficiently active towards *Cre*), nor by shortening the duration of the experiments, at which time *Cre* is not activated. Therefore, we devised a chemical strategy to block the expected oxidation site on the β-ether bond by substitution of this methylene group to obtain more information around the SAR of this moiety (figure 2.2.17).

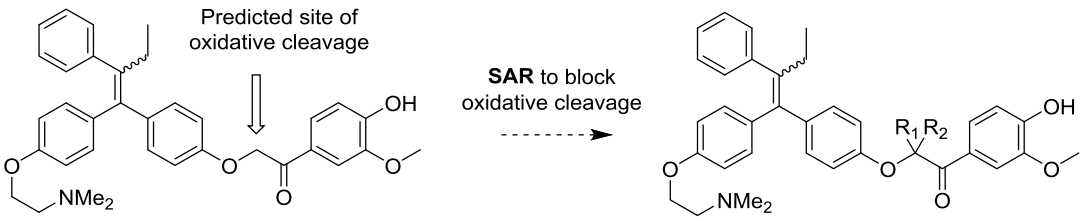

2-11

2-40a $R_1 = CH_3$, $R_2 = H$
2-40b $R_1 = CH_2OH$, $R_2 = H$
2-40c $R_1 = CH_2OH$, $R_2 = CH_3$
2-40d $R_1 = F$, $R_2 = H$
2-40e $R_1 = CH_2OH$, $R_2 = F$
2-40f $R_1 = R_2 = F$

Figure 2.2.17. *The predicted site of oxidative cleavage of* ***2-11*** *and the proposed modifications to the β-ether linker to block oxidative cleavage to afford new analogues* ***2-40a-f****.*

2.3. SAR Study about the β-ether Linker to Prevent Oxidative Metabolism

2.3.1 Syntheses of New Analogues of **2-12** with Substituted β-ether Linkers

Encouraging *in vitro* results from the thesis of Dr Byrom demonstrated that guaymoxifen (**2-11**) and MU-based analogue **2-12** were cleaved by LigF in cells and initiated recombination. However, our *in vivo* experiments revealed that oxidative metabolism of **2-11** by CYP enzymes concentrated in the liver of the mouse caused the liberation of 4OHT (**2-2**) at sites distal from the transplanted metastasis cells, which led to off-target recombination.[38] This meant that GFP expression as a result of *Cre* recombination could not be guaranteed to have been caused by LigF-mediated liberation of **2-2** from within the tumour cells.

In order to diminish this background noise, a SAR study was conducted on the β-ether moiety of the compound and a collection of analogues were generated to increase the ratio of LigF-mediated cleavage over liver metabolism. We first wanted to test that the new analogues remained susceptible to cleavage by LigF *in vitro*. Analogues of **2-12** were synthesised to liberate the fluorescent compound **2-13** instead of **2-2** in order to monitor cleavage by fluorescence (**2-41a-h**, scheme 2.3.1). We chose to include small groups to avoid steric repulsion in the LigF active site and included both electron donating and withdrawing functionalities.

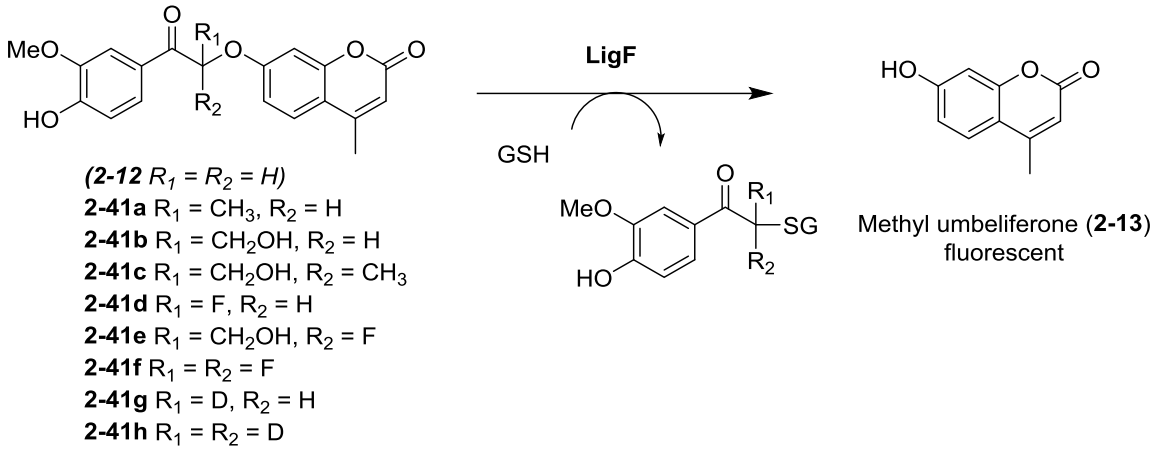

***(2-12** $R_1 = R_2 = H$)*
2-41a $R_1 = CH_3$, $R_2 = H$
2-41b $R_1 = CH_2OH$, $R_2 = H$
2-41c $R_1 = CH_2OH$, $R_2 = CH_3$
2-41d $R_1 = F$, $R_2 = H$
2-41e $R_1 = CH_2OH$, $R_2 = F$
2-41f $R_1 = R_2 = F$
2-41g $R_1 = D$, $R_2 = H$
2-41h $R_1 = R_2 = D$

Scheme 2.3.1. *Initial analogues for the SAR study of cleavage by LigF,* ***2-12*** *and* ***2-41a-h****.*

The preparation of **2-12** was modified from the original route used by Byrom to use the pivaloyl group. This ensured more reproducible reactions and led to a simpler de-protection reaction as the final step (scheme 2.3.2).

Akamanchi and co-workers reported the bromination of α-ketones catalysed by potassium iodide, using hydrogen bromide and sodium nitrate as a reductant. When this procedure was trialled on **2-14c**, no dibrominated side-product was observed, however the reaction could not be pushed to completion. The maximum yield obtained was 60%, which was comparable to that obtained using Br_2, however this method was longer and more technical to execute and perform the work-up, therefore was not pursued further.[39] We therefore used Br_2 in Et_2O as it was much quicker and more straightforward to carry out.

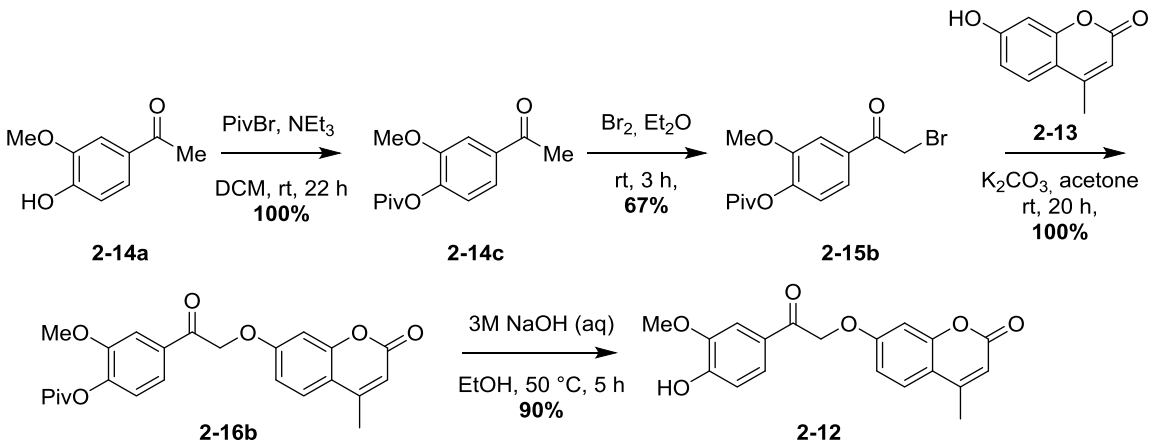

Scheme 2.3.2. *The final synthetic route towards analogue* ***2-12.***

The methyl derivative **2-41a** was synthesised similarly *via* the displacement reaction of bromo intermediate **2-45** (scheme 2.3.2). The selective Grignard addition of ethyl magnesium bromide to the aldehyde moiety of **2-42b** was achieved avoiding the side reaction of the pivaloyl ester by reducing the reaction time and lowering the temperature. This route was also trialled using a benzyl protecting group, the deprotection of which was more complicated for the reasons discussed previously in section 2.2. The oxidation of resultant alcohol **2-43** and then bromination afforded **2-45** in moderate yield (scheme 2.3.3).

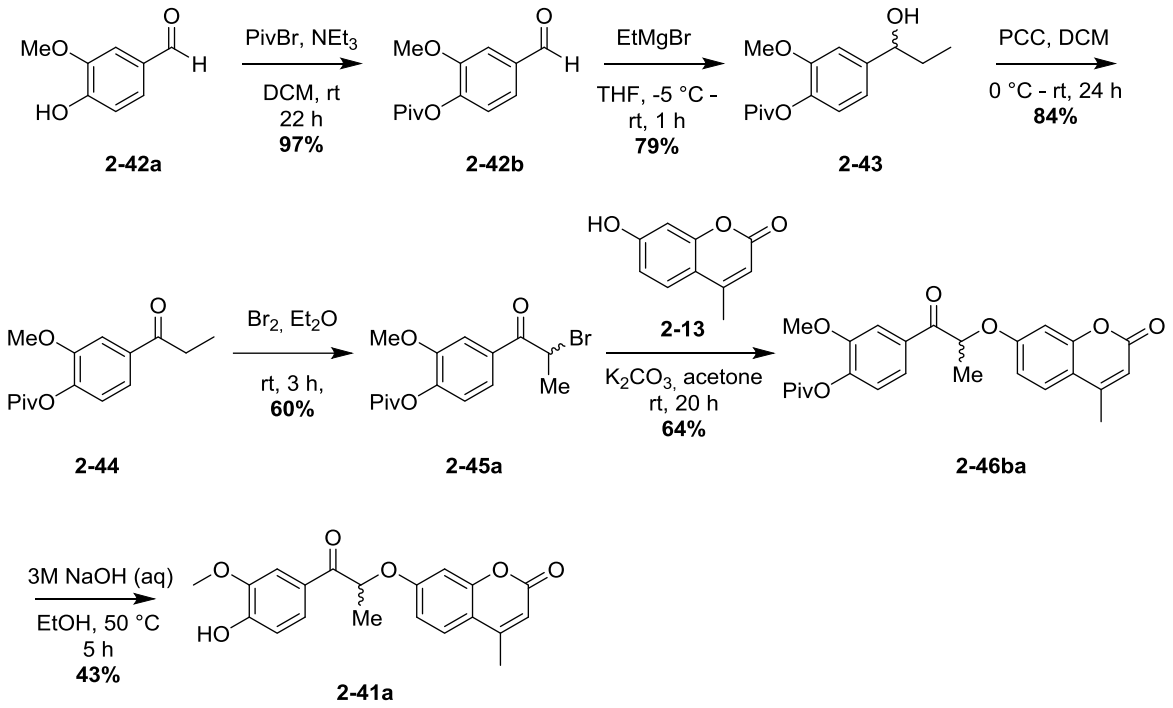

Scheme 2.3.3. *The final synthetic route towards analogue* ***2-41a.***

The methylhydroxylated analogue, **2-41b** was synthesised *via* an aldol alkylation of intermediate **2-16b** (scheme 2.3.3).

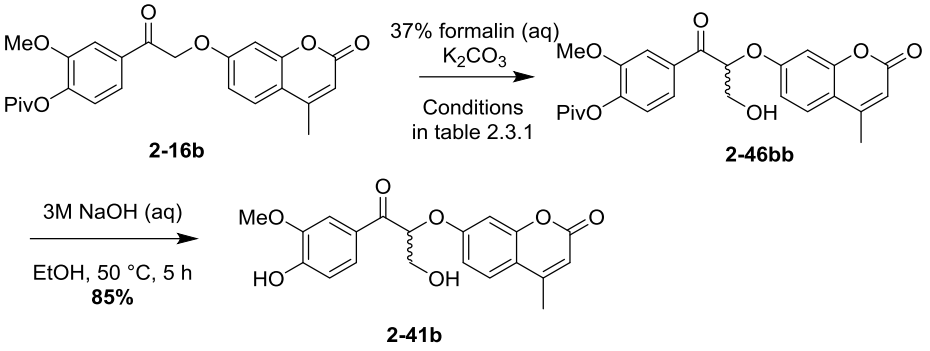

Scheme 2.3.3. *Synthesis of* ***2-41b*** *via an aldol alkylation of the β-ether bond using formaldehyde, followed by removal of the pivaloyl protecting group.*

This reaction was problematic due to the propensity of di-alkylation at the α-carbonyl position (**2-46bi**), owing to the acidic hydrogen of the β-ether bond in the product **2-46bb**. Addition of a single hydroxymethyl group to this class of substrate was not trivial, there are few examples in the literature using complex substrates such as that of guaymoxifen. Most examples use formaldehyde solution, which is aqueous to avoid polymerisation to from the unreactive *para*-formaldehyde form.[40] Various conditions were tried in an attempt to optimise this step, however the more complex structure of our substrate made the β-ether bond less pliable to hydroxymethylation (table 2.3.1).

Table 2.3.1. *Screening of conditions for aldol addition of formaldehyde to* ***2-16b***

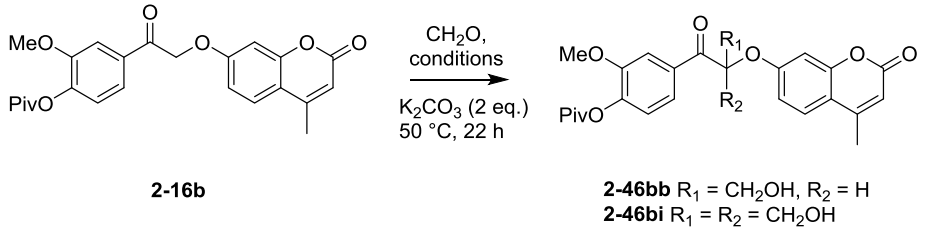

Entry	Formalin	Base	Solvent	2-46b	2-46i	2-16b (SM)
1	1.2 eq.	K_2CO_3 (2 eq.)	Dioxane	45%	36%	<4%
2	1.2 eq.	K_2CO_3 (2 eq.)	THF	64%	32%	<4%
3	1.5 eq.	K_2CO_3 (2 eq.)	THF	48%	30%	<4%
4	1 eq.	K_2CO_3 (2 eq.)	THF	22%	20%	30%
5	1 eq.	NaOH (1 eq)	THF/H_2O	-	-	-Piv, decomp.
6	0.5 eq.	L-threonine, Na_2SO_4	THF	-	-	98%

The optimum conditions were found to be 1.2 equivalents of formalin solution, 2 equivalents of K_2CO_3 in THF affording a yield of 64% hydroxymethyl product (**2-46bb**, entry 2). Altering the equivalents of these reagents adversely affected the product: side-product ratio. Lower temperatures with longer reaction times did not afford significantly more product. We also attempted to form only product **2-46bb** and reobtain the starting material (**2-16b**) for reuse in subsequent reactions, however formation of di-alkylated side product **2-46bi** could not be avoided. Repeating reactions using re-obtained side product would have poor efficiency on a large scale, therefore this was not explored further. Entry 6 was carried out in order to assess the possibility of chiral synthesis of compound **2-41b**, but unfortunately no trace of product was observed.[41] The paper uses cyclohexanone as the model substrate and presumably the substrate scope of these amino acid catalysed reactions is not wide enough to perform on substrates as complex as **2-16b**. We therefore evaluated that the conditions from entry 2 were most suited in the interest of overall yield and time economy.

The aldol alkylation conditions were repeated using methyl intermediate **2-46ba** in order to afford the di-substituted product **2-41c** (scheme 2.3.5). The reaction could be pushed to completion using excess formalin and increased temperature and time, since no over-alkylation was possible because there were no acidic hydrogens on the product formed.

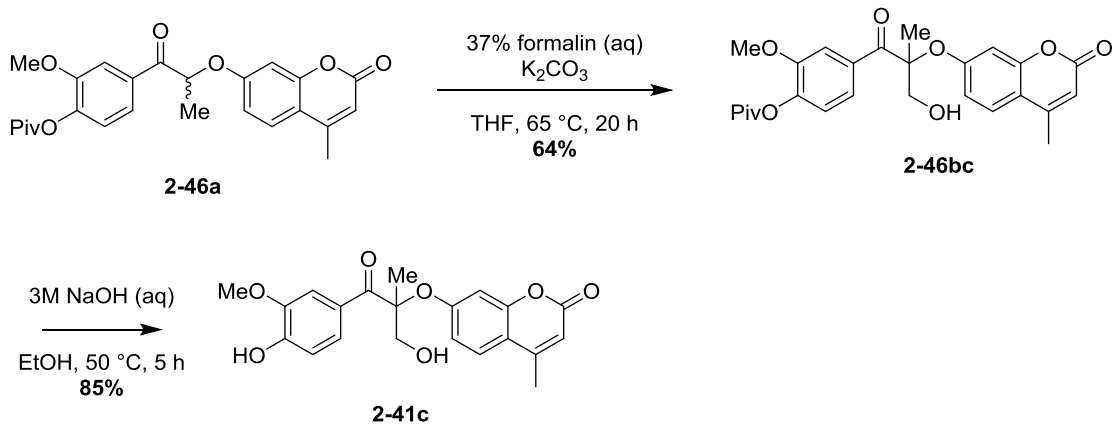

Scheme 2.3.5. *The synthesis of* ***2-41c*** *using a stronger version of the aldol conditions developed previously but using* ***2-46ba*** *as substrate.*

The mono-fluorinated intermediates **2-41d** and **2-41e** were prepared from α-bromoketone intermediate **2-15a**. We initially attempted to form the silyl enol ether intermediate of **2-14b** using LiHMDS and TMSCl, followed by a quench using the nucleophilic fluorine source, selectfluor® (F-TEDA-BF_4), but we were unsuccessful (scheme 2.3.6). LDA and TBDMSCl were also used as reagents but were equally unsuccessful.

Scheme 2.3.6. *Attempted formation of* ***2-47*** *via silyl enol ether formation then reaction with selectfluor® (F-TEDA-BF_4).*

Fluorination chemistry has experienced huge attention in the medicinal chemistry community and a subsequent increase in publications of fluorination procedures.[42,43] When revising the literature, we were convinced that a trans-halogenation would prove most amenable to larger scale synthesis of our substrate class. We began by screening conditions for the optimal trans-halogenation reaction using intermediate **2-15a** or **b**, using reagents that were already available in our lab (table 2.3.2).

Table 2.3.2. *Screening conditions for trans-halogenation reaction to form* ***2-47***

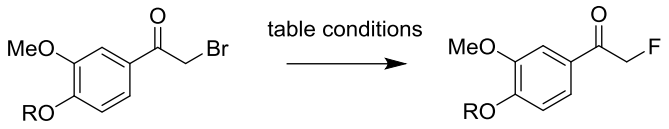

2-15a, R = Bn
2-15b, R = Piv

2-47a, R = Bn
2-47b, R = Piv

Entry	R	Reagents (eq)	Solvent	T (°C)	t (h)	Yield
1	Bn	TBAF (3)	H_2O	100	24	trace
2	Bn	TBAF (0.75), ZnF_2,(1), KF (0.5)	MeCN	85	40	38% (21% SM)
3	Piv	TBAF (0.75), ZnF_2,(1), KF (0.5)	MeCN	85	40	38%
4	Piv	TBAF (0.75), ZnF_2,(1), KF (0.5)	THF	75	24	37%
5	Piv	TBAF (1.5), ZnF_2,(1.5), KF (1.5)	MeCN	85	24	58%

Reactions were first carried out using the ample amount of benzyl protected α-bromo ketone, **2-15a**. Disappointingly, reaction with TBAF in water led to the formation of only trace amounts of product (entry 1). We next moved to using a cocktail of nucleophilic fluoro-containing compounds, following a procedure identified by Zizhan Chen *et al.*[44] The reagents were first heated together to pre-form the active fluorinating species before addition of bromo starting material. A moderate yield of **38%** was achieved and unfortunately the reaction could not be pushed to completion (entry 2). This yield was maintained when changing the benzyl for the pivaloyl protecting group, no significant change was observed using THF as solvent (entries 3 & 4). Increasing the initial equivalents of reagents increased the yield of the reaction to **58%** (entry 5), however there was still starting material present in the mixture and no effect was observed when adding additional reagents during the course of the reaction.

With sufficient fluorinated material in hand, the bromination reaction of **2-47a** and **b** was then optimised (table 2.3.3).

Table 2.3.3. *Screening of bromination conditions to afford* ***2-48.***

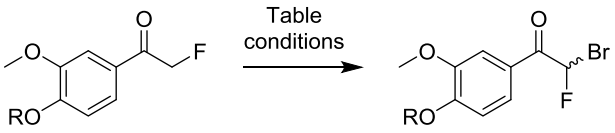

2-47a, R = Bn
2-47b, R = Piv

2-48a, R = Bn
2-48b, R = Piv

Entry	R	Reagents (eq)	Solvent	T (°C)	t (h)	Yield
1	Bn	Br_2 (1.2)	EtOH	50	6	-
2	Bn	Br_2 (1.0)	AcOH	rt	22	-
3	Bn	Br_2 (1.2)	AcOH	50	20	SM*
4	Bn	Br_2 (1.0)	AcOH	40	4	38% (23% SM)
5	Bn	Cu(I)Br	EtOH/$CHCl_3$ (1:4)	70 (μλ)	1	-
6	Piv	Cu(I)Br	EtOH/$CHCl_3$ (1:4)	70 (μλ)	1	-
7	Piv	NBS (1.3), H_2SO_4 (5%)	MeCN	50	3	**SM*** **
8	Piv	Br_2 (1.0)	AcOH	40	4	18%
9	Piv	Br_2 (1.1)	AcOH	0 - rt	48	38%
10	Piv	Br_2 (1.1)	AcOH	50	4	67%

*Deprotection
**Aryl brominated side products

No product formation was observed when repeating the previous bromination conditions, as this position was more electron poor and as a result more difficult to brominate (entry 1). We therefore used acidic conditions to catalyse this step. The reaction was still extremely slow at rt, however heating to 50 °C resulted in the partial de-protection of the phenol moiety (entries 2 & 3). Product was formed when heated to a temperature of 40 °C for a shorter time of 4 hours, however the reaction did not go to completion without formation of over-brominated side products (entry 4). Cu(I)Br was reported to work well for substrates similar to ours,[45] however we were unable to obtain any compound on either Bn or Piv protected intermediate(entries 5 & 6). Maintaining the pivaloyl protecting group, the

desired reaction did not progress well using NBS under acidic catalysis, giving rise to de-pivaloyl-protected starting material and brominated by-products (entry 7).

The best conditions for the benzyl protected **2-47a** (entry 4) were then repeated using the pivaloyl-protected starting material **2-47b**, which experienced a reduced yield of 18% (entry 8). The yield was improved to 38% upon careful addition at 0 °C of 1.1 eq of bromine (2.87M in AcOH), then warming to room temperature and left to stir for 2 days (entry 9). The best yield was achieved by maintaining a slight excess of bromine (1.1 equivalents) and heating to 50 °C for just 4 hours (entry 10). An improved yield of 67% was obtained, with minimum remaining starting material and the main side product being the di-brominated product, which was an insoluble yellow precipitate that could be easily removed by trituration to obtain purified product (**2-48b**). The methyl umbeliferone product **(2-41d)** was then prepared using the standard nucleophilic substitution conditions followed by deprotection of the phenol moiety (scheme 2.3.7).

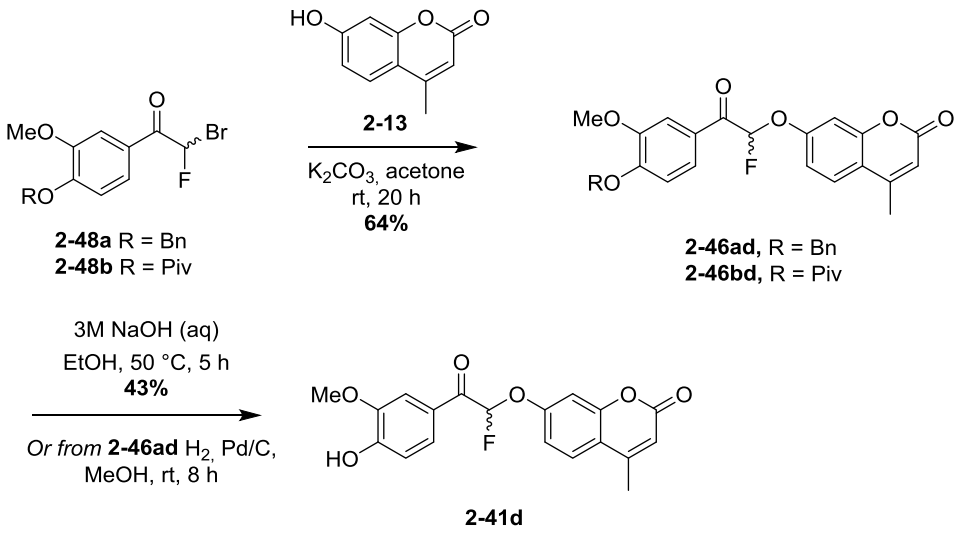

Scheme 2.3.7. *The final steps in the synthesis towards* ***2-41d*** *using bromo, fluoro-intermediate* ***2-48****.*

The methylhydroxy-fluoro, umbeliferone derivative **2-41e** was prepared by performing the aldol alkylation to benzyl protected intermediate **2-46ad**, then deprotecting the resultant product **2-46ae**. These products were made on extremely small scale due to difficulties in

the synthesis, however they were sufficient to perform the *in vitro* cleavage assay as only very small quantities were required and thus not repeated on a larger scale.

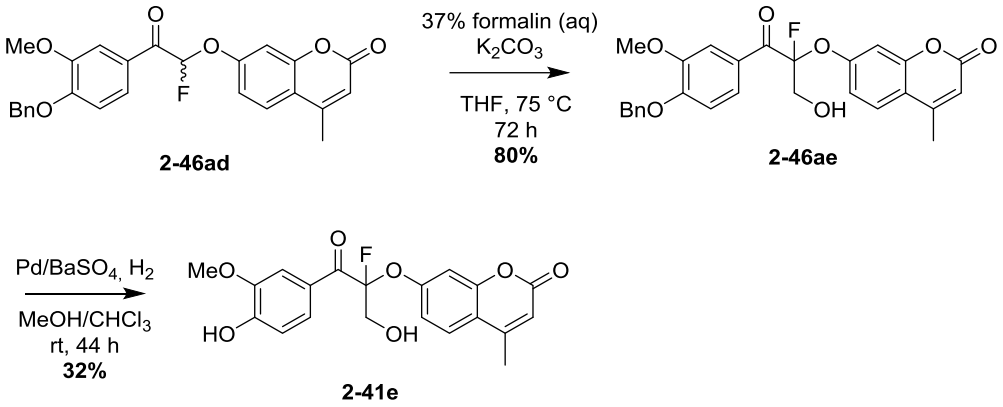

Scheme 2.3.8. *The synthesis of analogue* ***2-41e****.*

The difluoro derivative **2-41f** was accessed *via* an entirely different approach, since the bromination and fluorination steps used to obtain **2-41d** and **e** were long and low yielding. Jinu John and David Colby reported the isolation of difluoro-iodo and difluoro-bromo α-ketones *via* the release of trifluoroacetate from α-fluorinated gem-diols (scheme 2.3.9).[46]

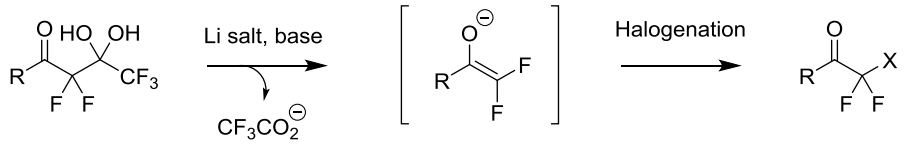

Scheme 2.3.9. *General scheme showing the formation of α-difluoro, halo ketone compounds using a lithium salt in the presence of base.*

Intermediate **2-49** was synthesised using NaH in THF after initial attempts using K_2CO_3 in MeCN were unsuccessful (scheme 2.3.10). Difluorination using selectfluor® to afford **2-50** was straightforward and high yielding. We next carried out the displacement reaction using **2-13** to obtain **2-46af** without isolating iodo intermediate **2-51,** as these compounds were reported to have low stability. This key step was successful however low in yield. Although the bromo intermediate may have been more stable, we predicted it may have had less reactivity towards **2-13**, which was a very poor nucleophile. The final debenzylation step

provided **2-41f** in low yield but with sufficient quantity for characterisation and for testing the kinetics of cleavage by LigF.

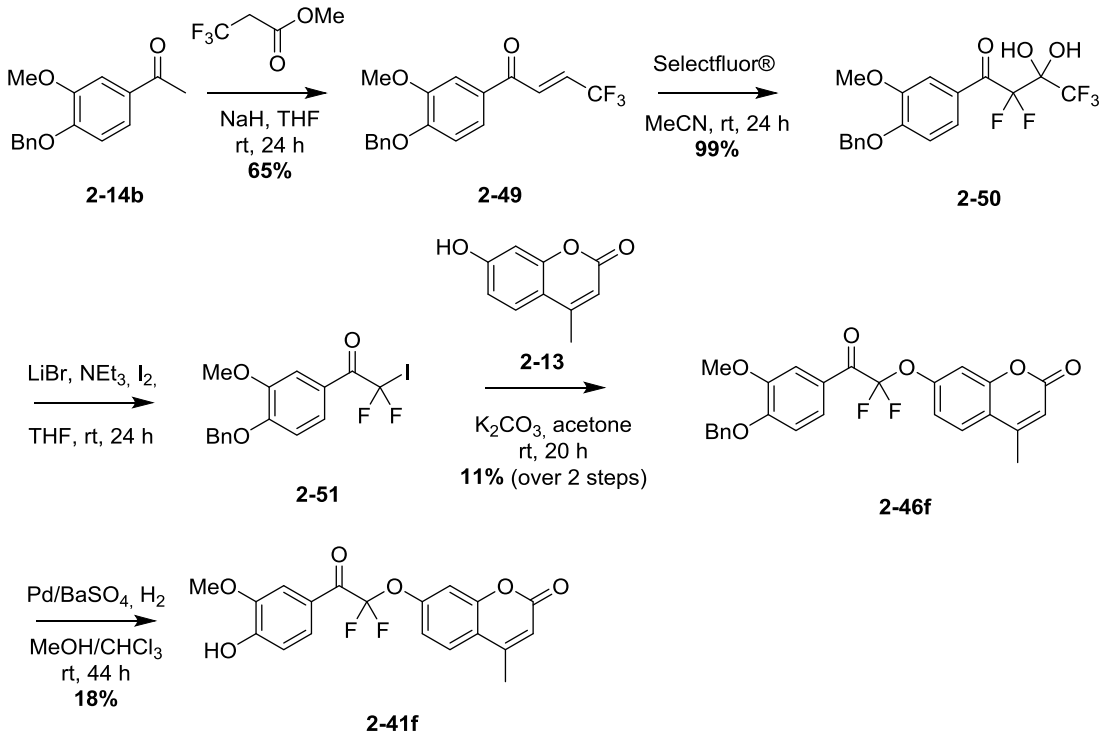

Scheme 2.3.10. *The overall synthetic route towards difluorinated analogue* ***2-41f****.*

The di-substituted analogues were anticipated to be most resistant to metabolism by CYP enzymes, however they were also less likely to undergo cleavage by the GSH assisted LigF pathway due to the absence of a proton leaving group (**2-41c, e** and **f**). Similar conclusions about the restricted active site of LigF were made by Helmich *et al.*[47] Further compounds of this type that were also attempted (dimethyl and methyl fluoro) were very difficult to synthesise and so these compounds were abandoned to prioritise other areas of the projects.

Deuteration of drug compounds by D_2O and D_2 is well documented.[48] The first deuterated drug compound successfully completed clinical trials in 2016, and with many more currently under clinical trials we were encouraged to introduce a deuterium to the β-ether bridge of our molecule.[49] Deuterium is a bioisostere of hydrogen and the bond it forms with carbon is stronger than that of C-H, which slows down the kinetics of its reactions. This trait has been exploited in a number of drug molecules to overcome metabolic sensitivity

and could slow or block oxidative metabolism in our drug compound. The deuteration of phenyl β-ether bonds was not well precedented in the literature and initial attempts to directly deuterate the methylene moiety using weak bases, such as K_2CO_3, were unsuccessful. The route was not attempted using the pivaloyl protecting group, as the acidic conditions needed to de-protect the phenol were expected to displace the deuterium with a proton. The reaction was trialled using the benzyl protected intermediate **2-16**, to afford **2-46g** and **h,** however deprotection was not achievable and we anticipated further difficulties with the synthesis of the tamoxifen version and then metabolism *in vivo*.

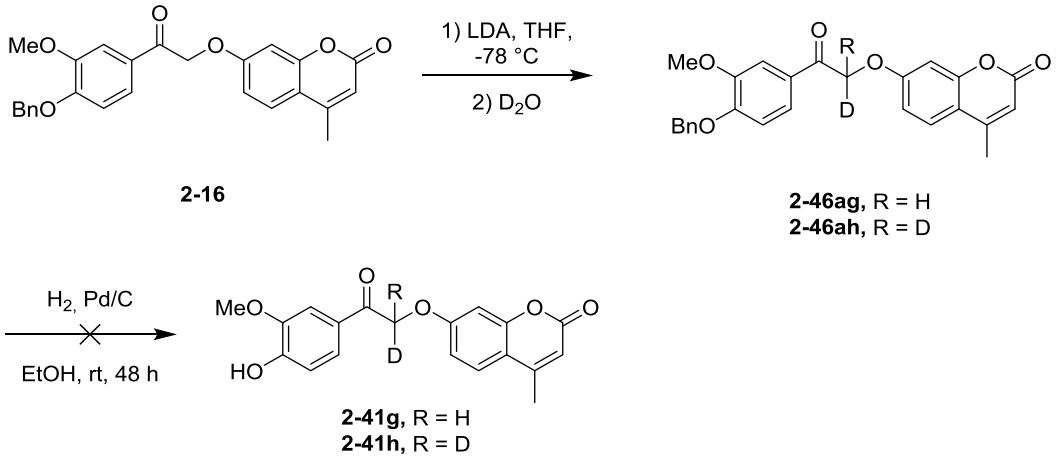

Scheme 2.3.11. *Route towards a deuterated analogue of* ***2-12,*** *terminated at* ***2-46ah.***

Compounds **2-52a** & **2-52b** were synthesised and tested because lignin-based compounds featuring a dimethoxy recognition site were reported to be cleaved by LigF *in vitro*.[40] However, **2-52a** and **b** experienced negligible cleavage compared to **2-12** in our hands, perhaps due to a difference in the strain of LigF we were using. Compound **2-53** was designed to examine the effect of a double-guay constituent on the cleavage and liberation of **2-13**. We rationalised that this might slow down the kinetics of cleavage, as cleavage of the first guaicol linker would first have to release **2-12**, which would still remain non-fluorescent until a further cleavage event took place to release **2-13**. However, this compound was not stable and decomposition occurred during the final de-protection step and purification, therefore we decided to concentrate our efforts on the mono-guay compounds.

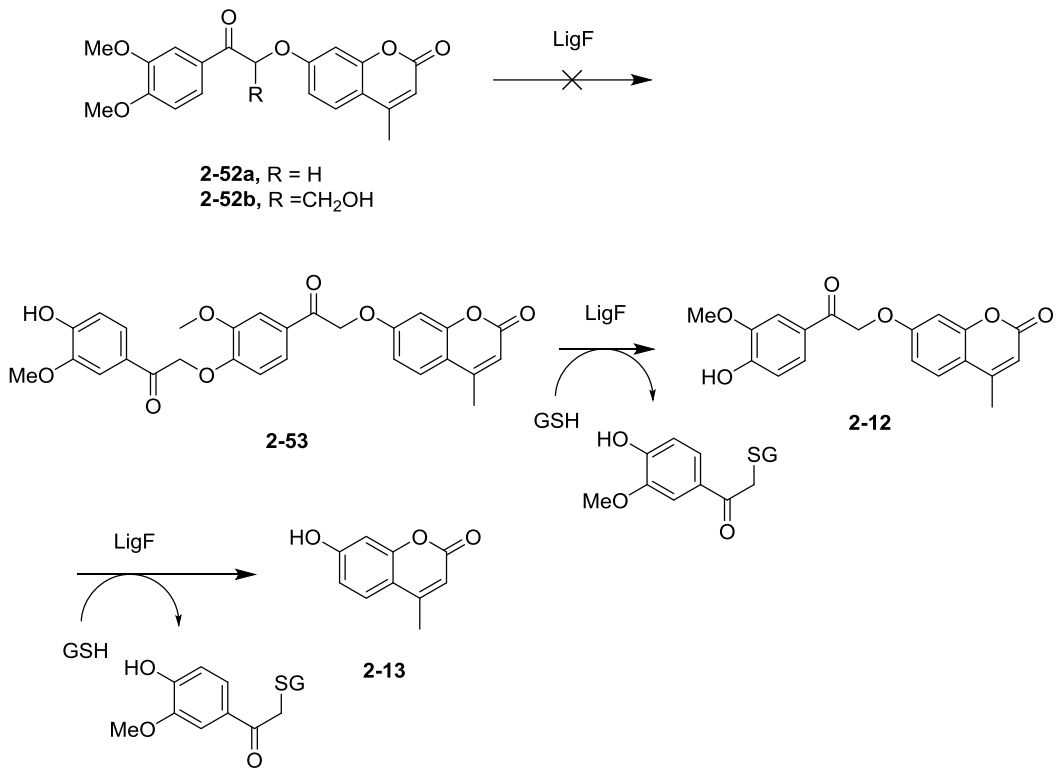

Scheme 2.3.12 *Dimethoxy analogues* ***2-52a and 2-52b****, which were not cleaved by LigF. Theorised cleavage pathway of diguaymoxifen* ***2-53*** *by LigF and glutathione to eventually liberate* ***2-13****.*

2.3.2 *In vitro* Testing of **2-41a,b,d** in a LigF Cleavage Assay

The cleavage of these new analogues **2-41a,b,d** were assessed using the same assay used by Dr Byrom during his thesis and using the same strain of LigF enzyme, using **2-12** and **2-13** as controls. The fluorescence results of **2-12**, **2-41a, b** and **d** are shown in graph 2.3.1.

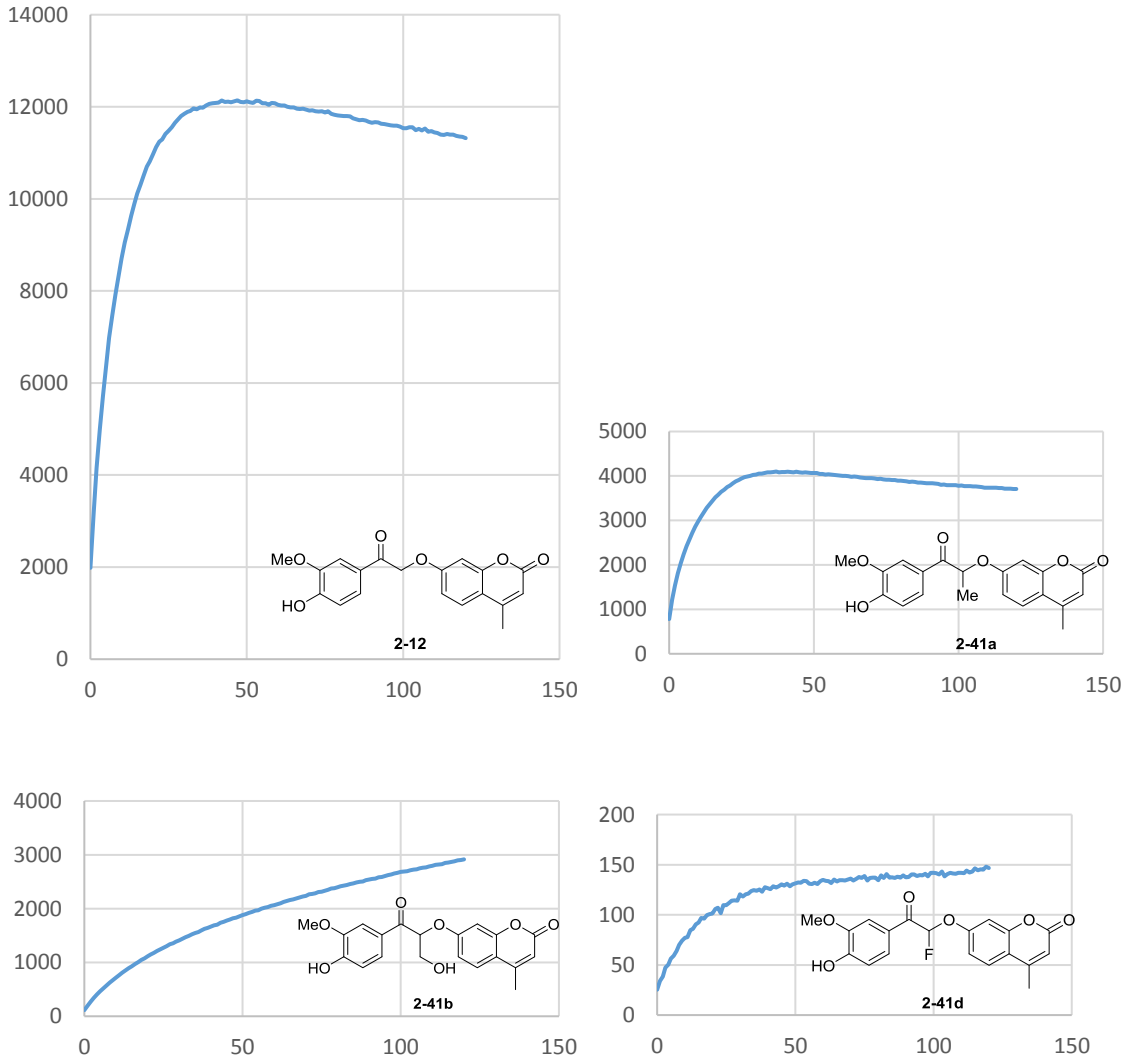

Graph 2.3.1. *Showing the release of* ***2-13*** *over time, monitored by fluorescence, as a result of the cleavage of analogues* ***2-12*** *and* ***2-41a, b*** *and* ***d*** *by LigF enzyme assisted by GSH. Try to put in same graph.*

These results show that original analogue **2-12** was cleaved most effectively by LigF and that addition of methyl and methylhydroxy substituents (**2-41a** and **b**) slow down the rate of cleavage and reduce the maximum intensity reached. We rationalised that this was due to a preference for cleavage of one enantiomer over the other, as seen in other lignin based

compounds which show that LigF preferentially cleaves the (*S*) isomer, and that LigE preferentially cleaves the (*R*) isomer.[40,47] The mono-fluorinated analogue **2-41d** showed very little cleavage (i.e. lower maximum), suggesting that the electronics of this bond play an extremely important role in the susceptibility to cleavage by LigF. Quaternary compounds **2-41c, e** and **f** were not cleaved by LigF and indeed **2-41c** proved to be unstable and decomposed even in the control experiment with no LigF present, therefore these compounds were omitted from further studies. Analogues **2-12**, **2-41a** and **b** were identified as most cleaved by LigF *in vitro*. Fluoro derivative **2-41d** was also chosen for further study as it showed partial cleavage by LigF, and possessed distinct electronic properties about the β–ether bond.

2.3.3 Stereospecificity of LigE and LigF

It was recently shown that LigF was stereospecific, in that it could only cleave the (*S*) enantiomer of lignin based compound **2-8b** (scheme 2.1.13).[40] Cleavage of the other enantiomer **(*R*)-2-8b** was carried out by a related enzyme, LigE. Structural studies revealed the differences in the active site responsible for these selectivities and revealed more insight into glutathione (GSH) assisted S_N2 reactions was gained. LigE cleavage of fluoro-analogue **(*S*)-2-54**, which lacked a hydrogen on the β-ether bond, provided further evidence of this mechanism.[47] Interestingly LigF did not cleave the corresponding enantiomer (**(*R*)-2-13**), perhaps due to a more restrictive active site as suggested by the authors (scheme 2.1.14).

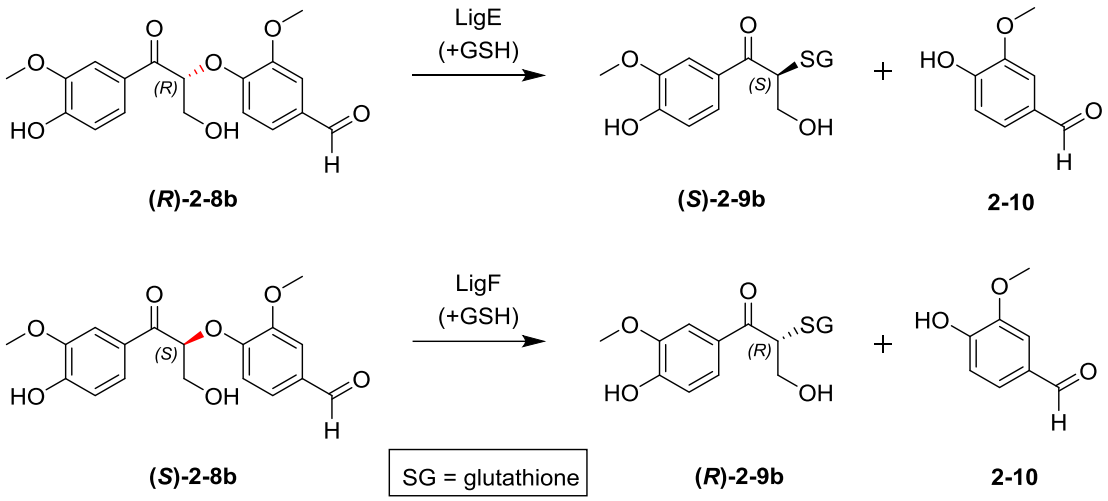

Scheme 2.1.13. *Key step of the lignin decomposition pathway depicting the cleavage by LigE and LigF of lignin derivatives* ***2-8b,*** *liberating* ***2-9b*** *and* ***2-10*** *respectively.*

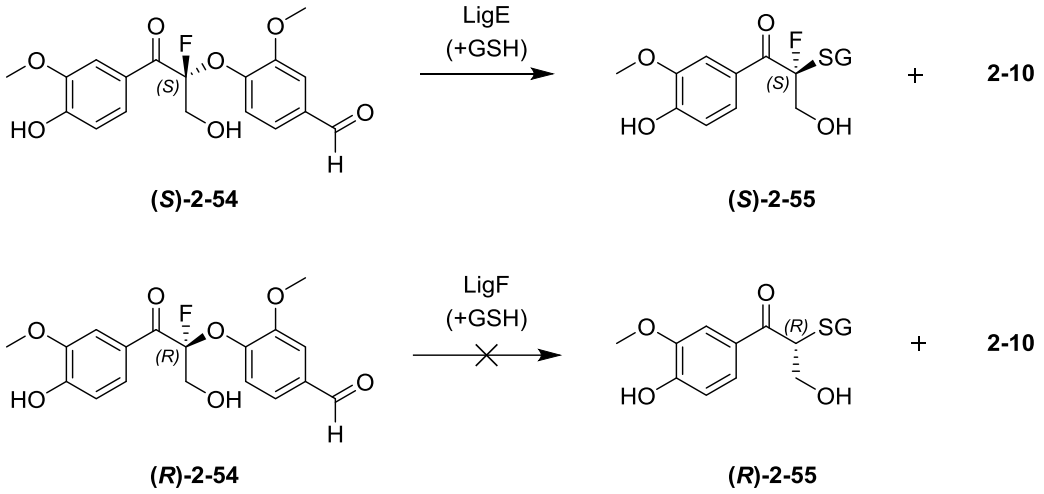

Scheme 2.1.14. *LigE and LigF cleavage of fluorinated analogues* ***2-54*** *to release* ***2-55*** *and* ***2-10.***

These findings are in accordance with our original cleavage data for our own analogues and the structural information revealed here is informative for future work on our project. It appears that LigE has a more sterically accessible active site than LigF and the wider scope of substrates may indeed provide more opportunities in future guaymoxifen analogues. This would require rising the tumour cell lines from zero and re-validating the entire biological models, therefore the original xeno-enzyme (LigF) was maintained throughout this project.

2.3.4 Syntheses of Guaymoxifen Analogues **2-40a, b** and **d**

We wanted to examine the 3 new analogues that were cleaved by LigF *in vivo*, in order to compare their relative liver cleavage to that of **2-11**. Therefore large scale syntheses were performed based on the original routes to the **2-40a,b** and **d** analogues, but using **2-22** instead of **2-13**.

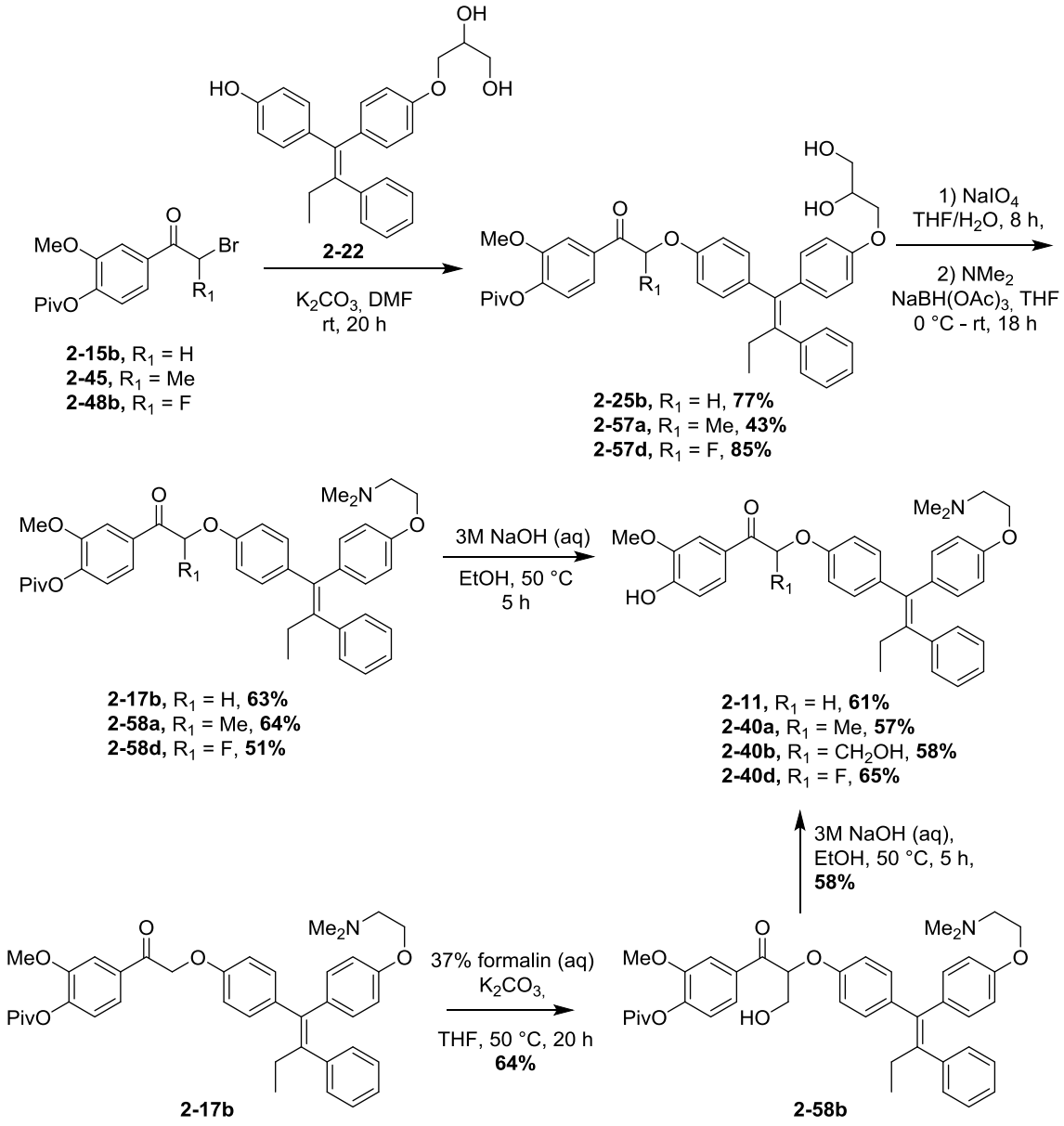

Scheme 2.3.15. *General nucleophilic substitution reaction to afford corresponding tamoxifen analogues* ***2-11*** *and* ***2-40a,b*** *and* ***d*** *on a large scale.*

The penultimate step in the synthesis towards **2-40d** was an aldol reaction, which was useful for late stage functionalisation for a convergent synthesis, but the yield low meaning loss of advanced intermediate. To avoid this loss of material in the penultimate step of the synthesis, we tested the performing the aldol step at an earlier stage in the synthesis to the less precious intermediate **2-14**. (Table 2.3.4). Various conditions have been reported for this modification to similar substrates, although most are substituted with alkyl substituents in the α-position.[50]

Table 2.3.4. *Screening of aldol conditions using starting material* ***2-15****.*

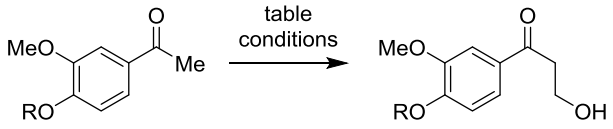

2-14 **2-56**

Entry	R	Formalin	Base	Solvent	T (°C)	t (h)	Outcome
1	Piv	1 eq.	NaOH (1 eq.)	-	rt	24	SM*
2	Bn	1.5 eq.	NaOH 1.5 eq.)	-	50	48	SM
3	H	1.5 eq.	NaOH (2 eq.)	-	50	48	Trace
4	Piv	1.5 eq.	K_2CO_3 (1.1 eq.)	THF/H_2O	rt	48	SM
5	Piv	1.5 eq.	K_2CO_3 (1.1 eq.) +Na_2SO_4	THF	50	48	SM

Other routes tpwards intermediate **2-56** were also expolred, such as expoxide formation and selective opening. However, we finally opted to maintain late stage addition of the hydroxymethyl functionality using formalin, such as in scheme 2.3.15.

2.3.5 *In vivo* Monitoring of the Liver Cleavage of Guaymoxifen **2-11** and Analogues **2-40a, b** and **d**

These compounds were administered individually to separate mutant mice, ubiquitously expressing *Cre*-ER^{T2} GFP, in order to assess the background levels of recombination resulting from liver metabolism and release of 4OHT (**2-2**). There were no tumour cells introduced to these mice models and therefore no LigF enzyme present. Therefore any cleavage that occurred would be due to decomposition or metabolism of the administered inactive guaymoxifen analogue. 1 μmol of guaymoxifen was administered to the mice, then after 5 days they were sacrificed and histology samples were examined by microscope. Higher recombination was observed in the peripheral cells of the organs monitored, especially in the liver (hepatocytes). Figure 2.3.17 demonstrates a typical histology sample showing the higher recombination levels in the peripheral hepatocytes after exposure to guaymoxifen **2-11** (left) and after injection of the inert vehicle oil (right).

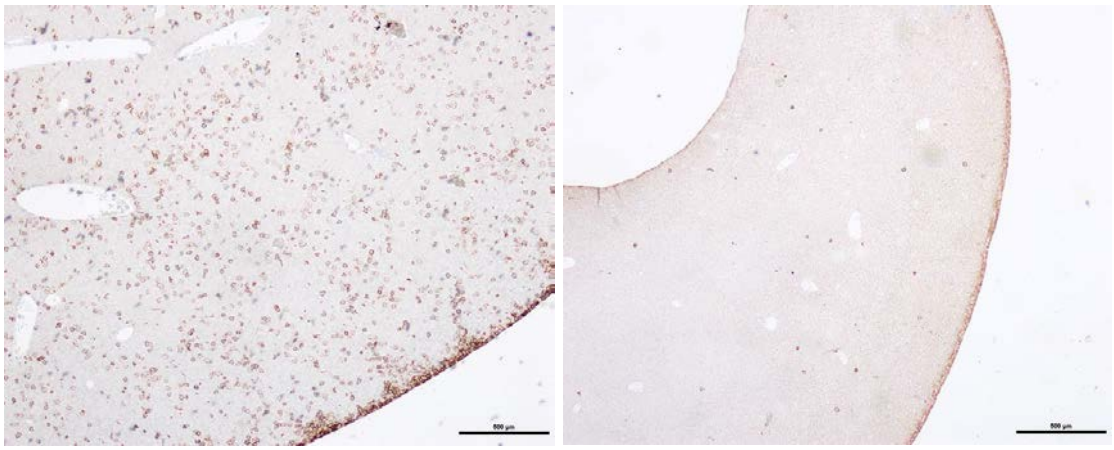

Figure 3.2.17. Left: *Low magnification image of a section of liver, stained for GFP, from a mouse treated with 1 μmol guaymoxifen (**2-11**). Recombined cells can be seen as small rings/bubbles amongst an otherwise peach/grey tissue (white spaces are blood vessels). Border shows ~90% recombination as opposed to ~5-10% in the interior.*
Right: *As previous but mouse was treated with oil as a control. Border and interior show <1% recombination.*

The observation that peripheral organ cells experience higher recombination than inner cells may be explained by the higher exposed dose of guaymoxifen that peripheral cells experience after intraperitoneal injection. These cells may also possess a higher concentration of CYP enzymes

leading to higher enzymatic activity, liberating active 4OHT (**2-2**). The following guaymoxifen analogues were treated in the same manner, and the comparative results are given below in graph 2.3.2.

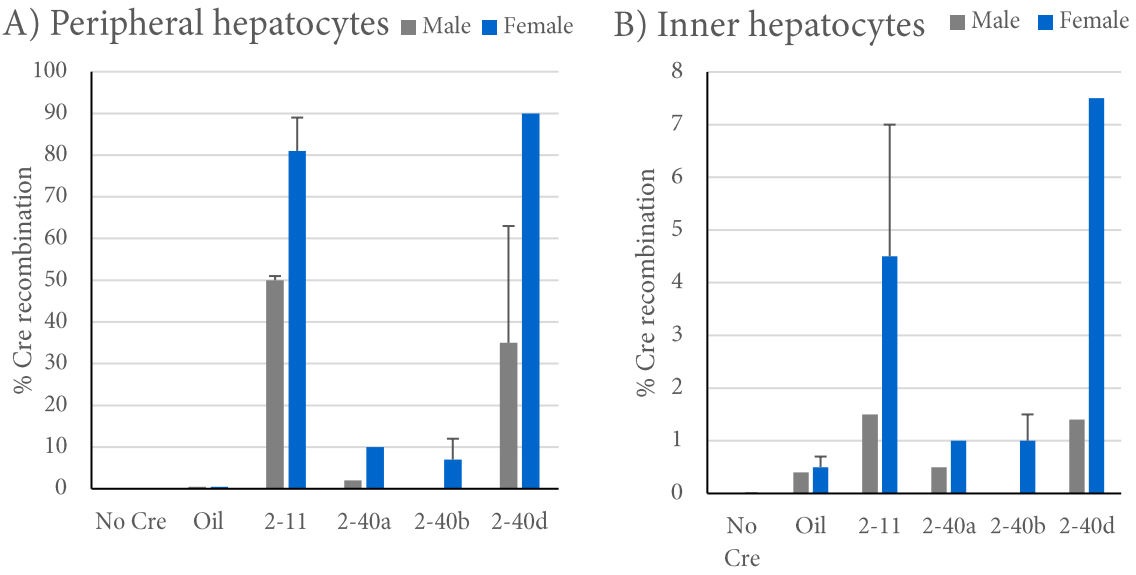

Graph 2.3.2. *Graphs show the approximate recombination levels in male and female mice in the peripheral and inner hepatocytes after administration of guaymoxifen* ***2-11, 2-40a, 2-40b, 2-40d*** *or vehicle oil.* ***2-11*** *was also administered to non-GFP mice as a further control and calibration.*

As can be observed in the graphs, females have higher recombination levels than males and we subsequently monitored these populations separately. **2-40a** and **b** resulted in less background recombination relative to the original guaymoxifen analogue **2-11**. Fluorinated analogue **2-40d** resulted in more recombination, despite the methyl umbeliferone derivative **2-41d** barely being cleaved by LigF in the *in vitro* assay. Addition of the fluorine substituent seemed to increase the rate of metabolic oxidation and cleavage of the β-ether linker, liberating 4OHT (**2-2**). This observation provided evidence that CYP enzymes and LigF have distinct cleavage mechanisms and suggested a potential window for exploiting this difference to do exactly the opposite, to gain preference for LigF cleavage over oxidative metabolism. Therefore, the monofluoro analogue **2-40d** possesses worsened or similar metabolic stability compared to original guaymoxifen and analogues **2-41a** and **b** were identified as having a more stable profile in male and female mice. Recombination within lung tissue was similar (~5% less) than in inner hepatocytes, suggesting systemic levels of

4OHT (**2-2**) were present, further supporting our hypothesis. By using only males in further experiments, we would keep background recombination to a minimum. Furthermore, we might improve the biodistribution by altering the administration of these compounds to the mice and avoiding overexposure to the liver, e.g. subcutaneous injection or directly into the tumours.

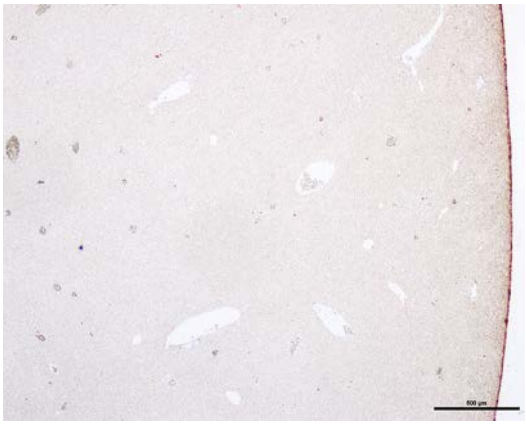

Figure 2.3.18. *Low magnification image of a section of lung, stained for GFP, from a female mouse treated with 1 μmol guaymoxifen (**2-11**). Recombined cells can be seen as small rings/bubbles amongst an otherwise peach/grey tissue (white spaces are blood vessels). Border and inner cells show <2% recombination.*

Although methyl and methylhydroxy derivatives **2-40a** and **2-40b** showed a reduced susceptibility to liver cleavage, corresponding analogues **2-41a** and **b** did not liberate quantitative values of **2-13** in the LigF cleavage assay compared with **2-12** (presumably due to the presence of an inactive isomer that could not be cleaved). These results provide evidence that they could be administered to female mice up to 1 μmol, (higher in males). But the relative gain in resistance to liver metabolism may be compromised by a drop in activity towards LigF. Adequate levels of recombination from LigF cleavage in the tumour would possibly require higher doses of **2-40a** and **b**, which would subsequently generate background liver cleavage. Therefore we wished to examine this cleavage in more detail before going *in vivo* with the transplanted tumours in the full model system.

2.3.6 Cleavage Assay of **2-11** and **2-40b** by LigF Monitored by Mass Spectrometry

The cleavage of these new analogues to liberate the active compound **2-2** was performed in an *in vitro* LigF cleavage experiment followed by mass spectroscopy. In order to economise the experiment, we chose to compare just **2-11** and **2-40b. 2-40a** and **b** had comparable liver cleavage in mice and the corresponding fluorescent analogues were similarly cleaved in the LigF *in vitro* assay. **2-40b** was chosen as the methoxy substituted β-ether linker was most similar to the natural substrate *lignin* and had slightly increased aqueous solubility (however these compounds, like tamoxifen itself, have extremely low aqueous solubility).

The following fragments were identified by mass spectrometry analysis to follow the disappearance of starting material **2-11** and **2-40b**, and also the rise in concentration of **2-2**, figure 2.3.2.

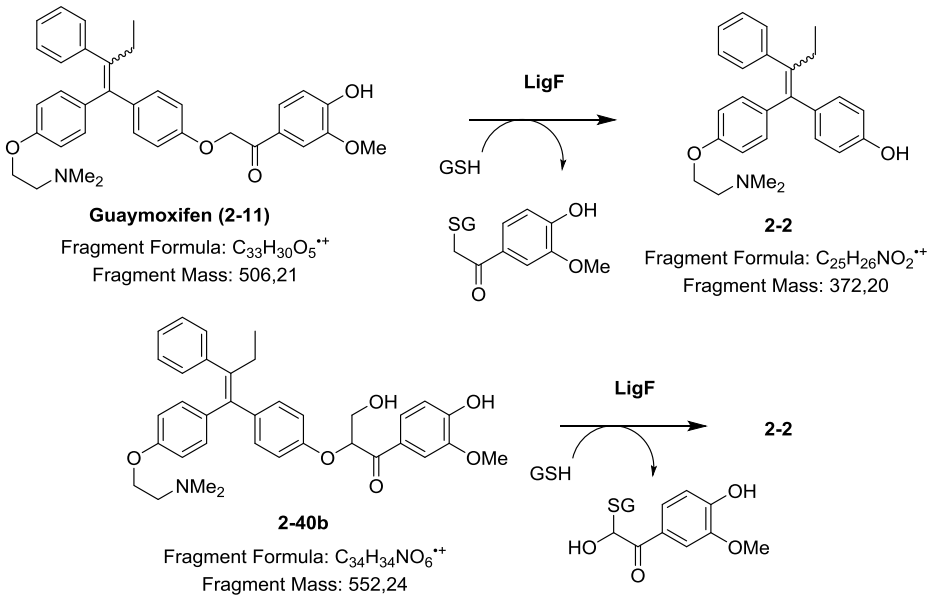

Figure 2.3.2. *Identified fragments for the detection of guaymoxifen* ***2-11****,* ***2-40b*** *and* ***2-2****. Individual isomers were detected by separate peaks in the HPLC column run, and relative absorbances of the isomers were assumed to be comparable.*

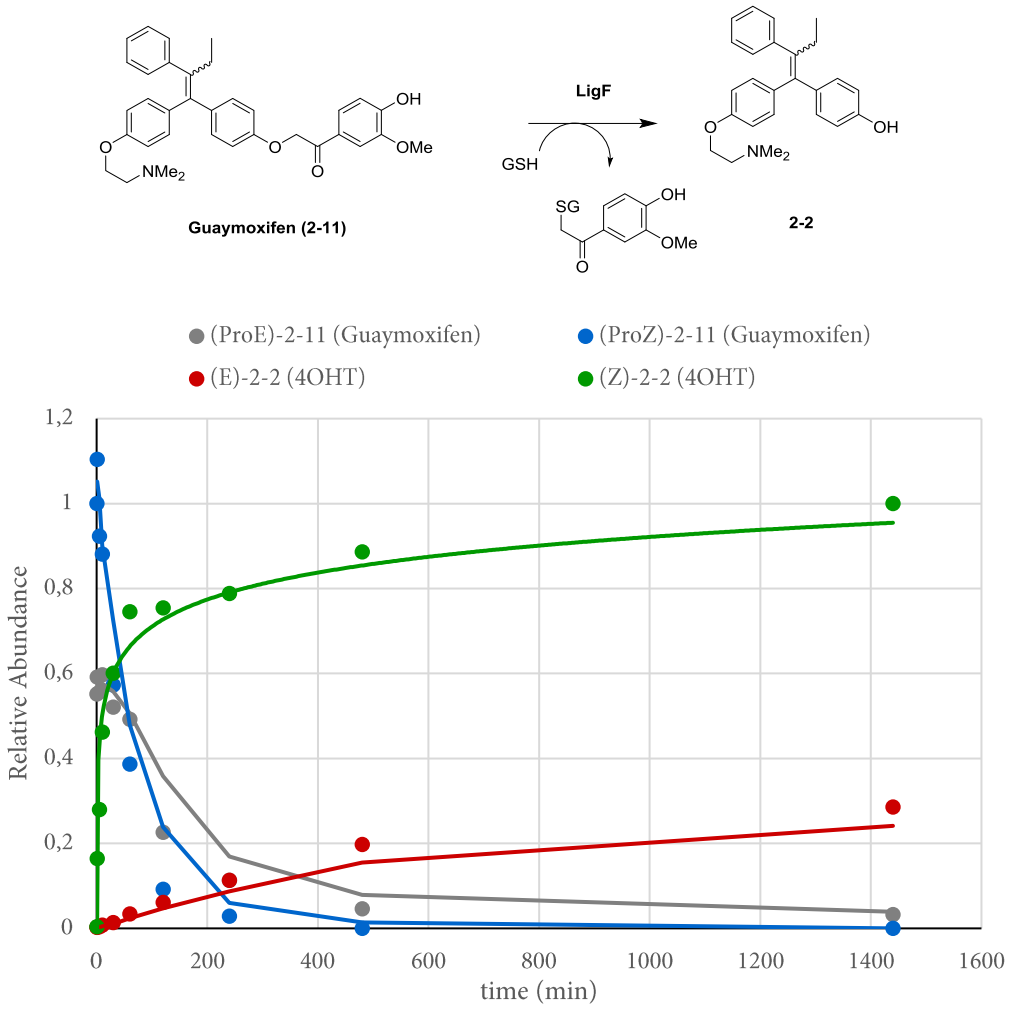

Graph 2.3.3. *Plot of the decrease in relative abundance of guaymoxifen isomers (**2-11**) (proE in gray, proZ in blue) as a result of cleavage by LigF and the resultant increase in 4OHT (**2-2**) (E in red, Z in green) over a 24 hour period.*

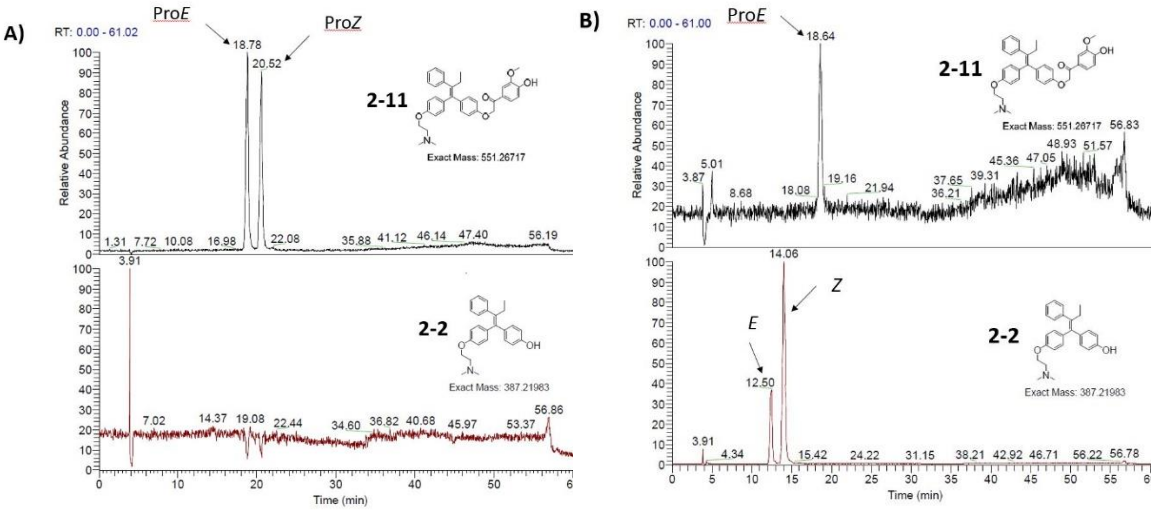

Figure 2.3.3. A) *At time = 0, showing an approximate 1.1:1 proE/Z ratio of **2-11** and no **2-2** cleavage product yet in the mixture.* ***B)*** *At time = 24 h, no (proZ)-**2-11** remained, (Z)-**2-2** cleavage product was in excess. Some (proE)-**2-11** remained, and less (E)-**2-2** had been liberated.*

As can be observed in figure 2.3.1, at time = 0 there is an approximate 1.1:1 ratio of (*proE*):(*proZ*)-**2-11**, which was consistent with the NMR spectra. However, in graph 2.3.3, the initial 4 readings over 25 minutes gave misleadingly low values for (*proE)*-**2-11**, which then seemed to decrease at a similar rate to (*proZ)*-**2-11**. This was potentially due to inconsistent ionisation or detection of the fragment which was traced in the experiment. Before contact with LigF, there was no 4OHT (**2-2**) present in the mixture. Disappearance (and therefore cleavage) of (*proZ*)-**2-11** appeared to occur to a greater extent than (*proE*)-**2-11,** which remained partially present even after 24 hours, observed in figure 2.3.3B. The rate and extent of liberation of (*Z*)-**2-2** was far greater than that of (*E*)-**2-2**, despite the misleading values for the disappearance of (*proE*)-**2-11.** This observation was consistent with what was initially observed in the thesis of Byrom. LigF began cleaving the *E* isomer even in the presence of remaining (*proZ*), (e.g. t = 60 min), however at a much slower rate. An apparent increase in the rate of cleavage of (*proE*) is observed as the concentration of (*proZ*) disappears. This trait is consistent with enzymatic resolution of compounds in general.[51]

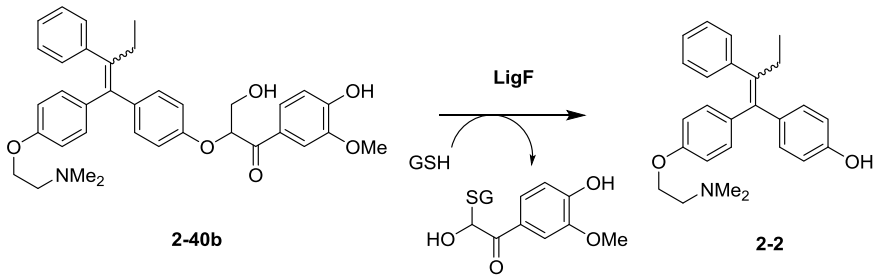

2-40b **2-2**

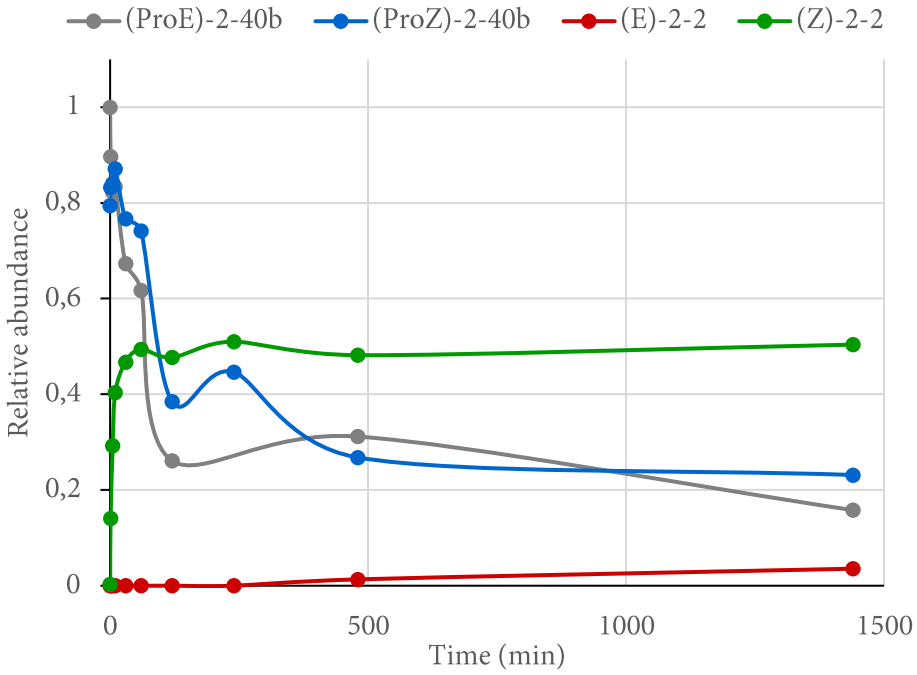

Graph 2.3.4. *Plot of the decrease in relative abundance of guaymoxifen isomers (**2-40b**) as a result of cleavage by LigF and the resultant increase in 4OHT (**2-2**) over a 24 hour period.*

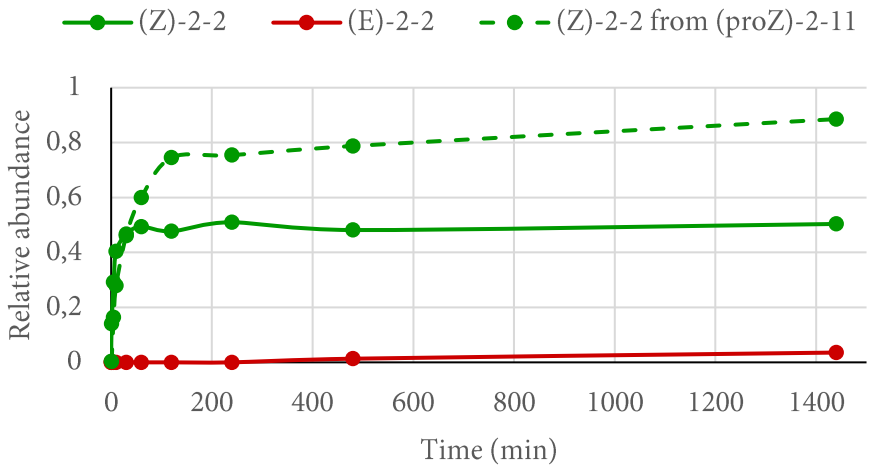

Graph 2.3.5. *Plot of the increase in 4OHT (**2-2**) over a 24 hour period from cleavage of guaymoxifen derivative **2-40b** and from guaymoxifen **2-11** (in dashed green line).*

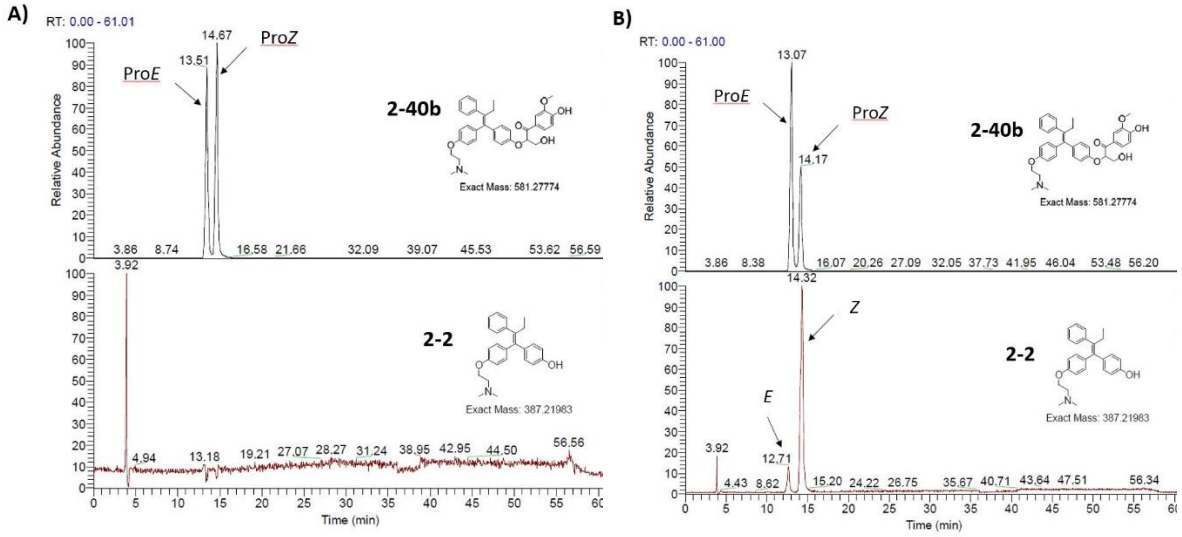

Figure 2.3.4. A) *At time = 0, showing an approximate 1:1.0 proE/Z ratio of* ***2-40b*** *and no* ***2-2*** *in the mixture.* ***B)*** *At time = 24 h, less (proZ)****2-40b*** *remains than (proE)****2-40b****, (Z)****2-2*** *is in excess of (E)****2-2****.*

From graphs 2.3.4 and 2.3.5 showing LigF cleavage of **2-40b**, there are several striking differences from the cleavage of original guaymoxifen, (**2-11** in graph 2.3.3). As expected, LigF was not able to cleave one of the enantiomeric configurations about the β-ether bond as well as the other, therefore approximately half of the material (two of the diastereomers) was inactive and unable to produce any 4OHT product. Analogously to guaymoxifen, the enzyme again seemed to show a preference for the (*proZ*) isomer of **2-40b** and cleaved the (*proE*) isomer at a much slower rate. Curiously, the graphs seem to suggest that (*proE*)-**2-40b** begins to be cleaved immediately and is >75% consumed by minute 480, without forming any (*E*)-**2-2** product. It is highly improbable that the cleavage of (*proE*)-**2-40b** would give rise to (*Z*)-**2-2**, so this unusual result must be due to abnormalities in the ionisation and detection of (*proE*)-**2-40b** (or indeed that a reaction took place to form an adduct that is not (*E*)-**2-2**). An important outcome is that the graph of the liberation of (*Z*)-**2-2** *via* cleavage of the administered **2-40b** (mixture containing all isomers) is about half of that liberated by the cleavage of guaymoxifen (**2-11**). This observation was consistent with the hypothesis that only one enantiomer would be susceptible to cleavage by LigF. Our proposed rational to explain these observations is summarized below in scheme 2.3.16.

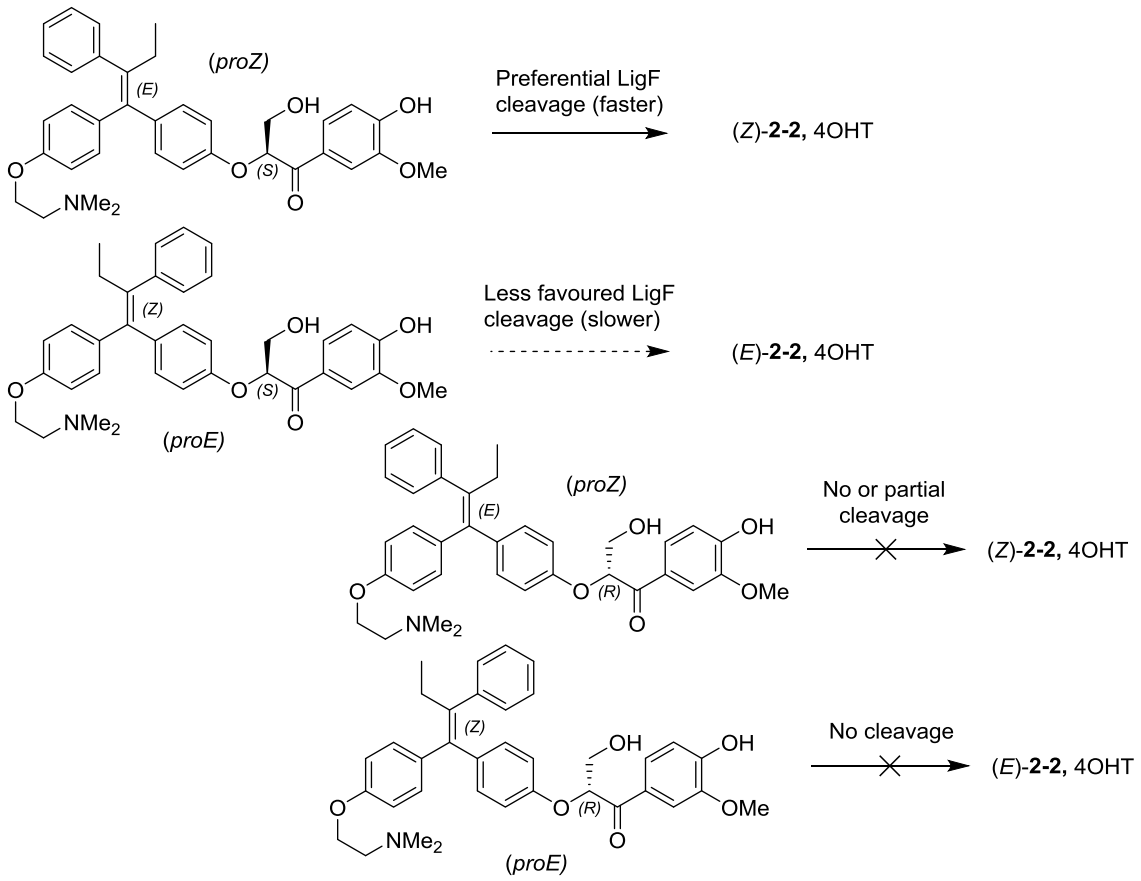

Scheme 2.3.16. *The 4 diastereoisomers of* ***2-40b*** *and their hypothesised GSH-assisted cleavage by LigF enzyme. Showing E-(S) to have the fastest rate, followed by slower cleavage of Z-(S), whereas neither (R) isomer is thought to be cleaved by LigF.*

Now with a more in-depth understanding of the kinetic properties of new analogue **2-40b**, we decided to examine these 2 compounds in the complete *Cre*-GFP mouse model with tumours expressing LigF.

2.3.7 *In vivo* Experiments Using **2-11** & **2-40a,b,d** in a *Cre*-GFP Mouse Model with metastatic tumours Expressing LigF HA tag

Below are images of the *in vivo* experiments using the four analogues and tamoxifen at both 5 and 1 μM concentrations, showing recombination in liver tissue *via* coomassie GFP staining to visualise GFP expression.

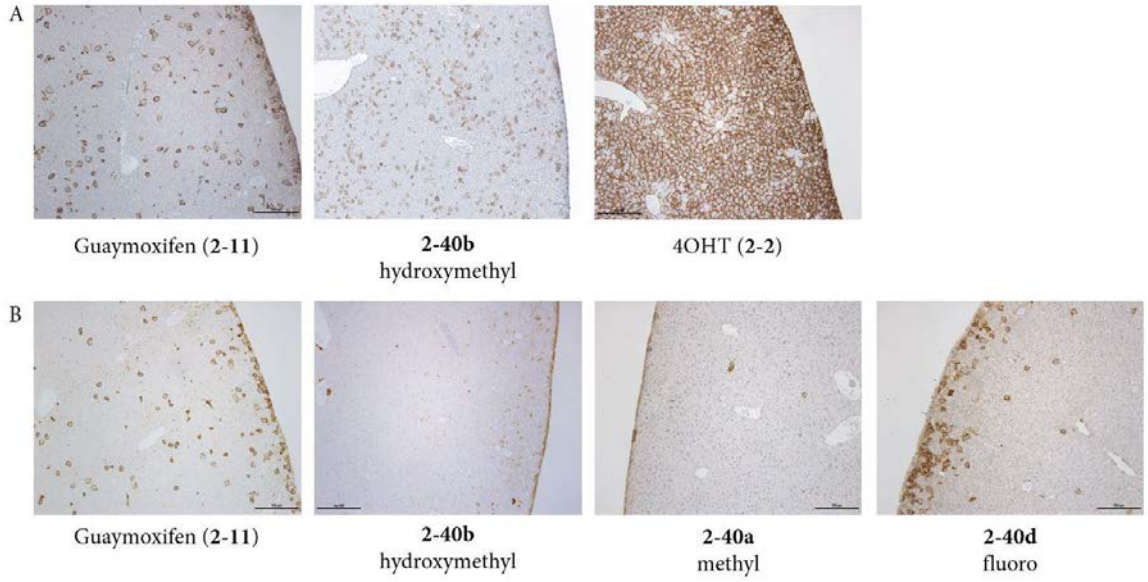

Figure 2.3.5.A. *Liver tissue from Cre-GFP mice treated with 5 μM of appropriate compound, stained with coomassie to visualise GFP expression as brown.* ***B.*** *using only 1 μM of appropriate compound.*

We see a clear difference in liver metabolism, as described in section 2.3.5. at 1 μM, whereby the methyl and hydroxyl methyl guaymoxifen analogues **2-40a-b** gave rise to less GFP expression than original guaymoxifen (**2-11**) or the fluoro substituted analogue **2-40d.** However at higher concentrations this difference was not maintained. A further problem was that we were not witnessing the expected levels of recombination at the tumour sites after guaymoxifen administration, when compared to 4OHT levels. This may be due to many technical reasons of the system, therefore we began investigating first whether LigF was being expressed in sufficient levels in the tumour sites. An HA tag had been incorporated to the LigF enzyme enabling it to be traced by staining for HA.

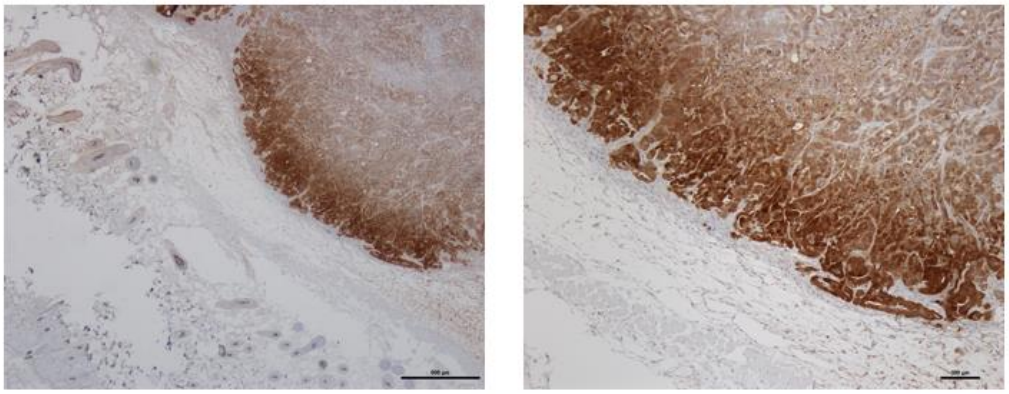

Scheme 2.3.6. *Subcutaneous tumour tissue histological sample having been stained for HA, to visualise presence of LigF within tumour sites as brown. At 2 levels of zoom.*

As can be observed in the above figure, LigF is indeed present in the tumour tissue to a high level. LigF cleaves our compound *in vitro* to initiate recombination and GFP expression, LigF is expressed in metastatic tumour cells *in vivo*, but does not cleave our compound to liberate active 4OHT and induce *Cre* recombination locally around the tumour site. Work is ongoing to determine how we can improve this system and investigating exactly what is happening with more biological data.

2.4. The Synthesis of 2nd Generation Guaymoxifen, Enriched in the Active *E*-Stereoisomer

2.4.1 Synthesis of Methyl Substituted Hydroxytamoxifen Analogue **2-4**

Although further understanding was gained of the β-ether linkage and small improvements were made to the metabolic stability of guaymoxifen analogues, the fact remained that only one of the stereoisomers was able to be cleaved rapidly by LigF. Moreover, any (*E*)-OHT that was liberated was unlikely to have affinity for ERT2 in order to activate *Cre*, as discussed in section 2.1. Additionally, we had been unable to synthesise any analogue stereoselectively, meaning that half of the administered compound was inactive thus requiring unnecessarily high doses.

Owing to the lower activity of fused ring analogues such as **2-5b**, we turned our attention to the minor modification made to obtain 2-Me, 4-OH Tamoxifen, **2-4**.[15,19]

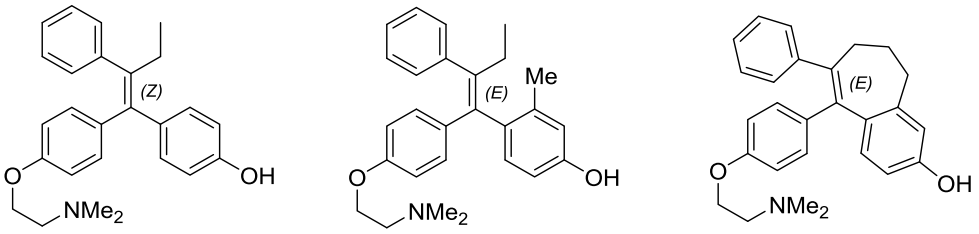

2-2 **2-4** **2-5a**

Figure 2.4.1. *(Z)-4OHT,* ***2-2****, and non-isomerisable tamoxifen analogues from the literature* ***2-4*** *and* ***2-5a****.*

The presence of the methyl group in the 2-position of the phenol ring generates sufficient steric repulsion towards the ethyl and aryl substituents on the opposite end of the double bond to enrich the *E*-isomer in a 9:1 ratio. Note that due to a change in priorities following Cahn-Ingold prelog nomenclature, *E* is now the active isomer, which corresponds to active

(*Z*)**2-2**. The affinity of **2-4** for the oestrogen receptor (ER) was comparable to that of (*Z*)**2-2** and maintained a similar antiproliferative effect on MCF-2 cancer cell assays. There did not seem to be any examples of this compound's ability to activate *Cre*-ER^{T2}. Therefore our first step was to synthesise **2-4** and verify its activity towards *Cre*-ER^{T2} (scheme 2.4.1).

In the original route designed by McCague in 1984 to obtain **2-4**, the (*E*) stereoisomer was isolated in high purity by recrystallisation using methanol, by reacting ketone intermediate **2-61** with the organolithium species formed from bromo intermediate **2-62b**.

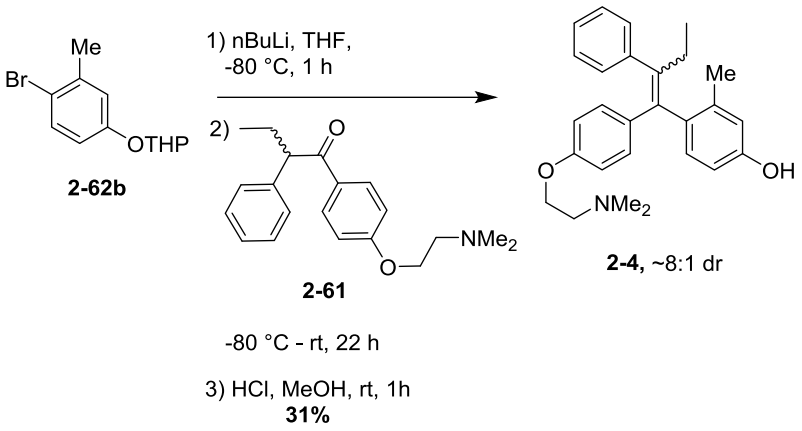

Scheme 2.4.1. *Final step in the synthesis of derivative* ***2-4*** *as performed by McCague, isolated in an approximate 8:1 dr. Recrystallisation using methanol gave a small quantity of the pure E isomer.*

We adapted our own improved synthesis of guaymoxifen to afford ketone intermediate **2-61**, which we then used to furnish **2-4** as an approximate 5:1 ratio in favour of the *E* isomer in the same manner as McCagues final step. We then recrystallized the afforded compound using methanol to obtain a small amount of pure *E* stereoisomer for the cellular assay (scheme 2.4.2).

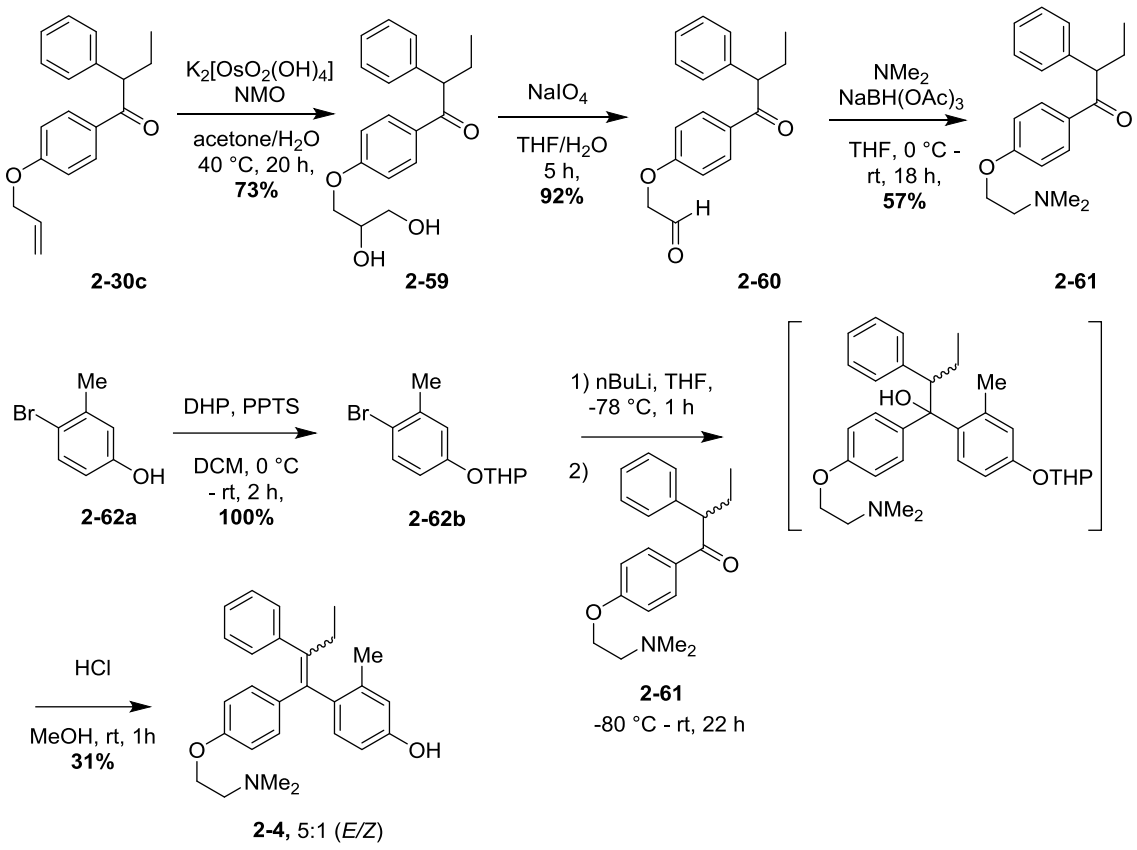

Scheme 2.4.1. *Synthesis of* ***2-4*** *analogue based on our previous routes to guaymoxifen analogues, isolated in an approximate 5:1 (E:Z). Recrystallisation using methanol gave a small quantity of the pure E isomer to use in the cellular assay.*

2-4 was also accessed *via* deprotection of **2-30a** followed by a displacement reaction using 2-chloro-*N,N*-dimethylethan-1-amine. However, this last step was challenging and the low yield could not be improved upon (scheme 2.4.2).

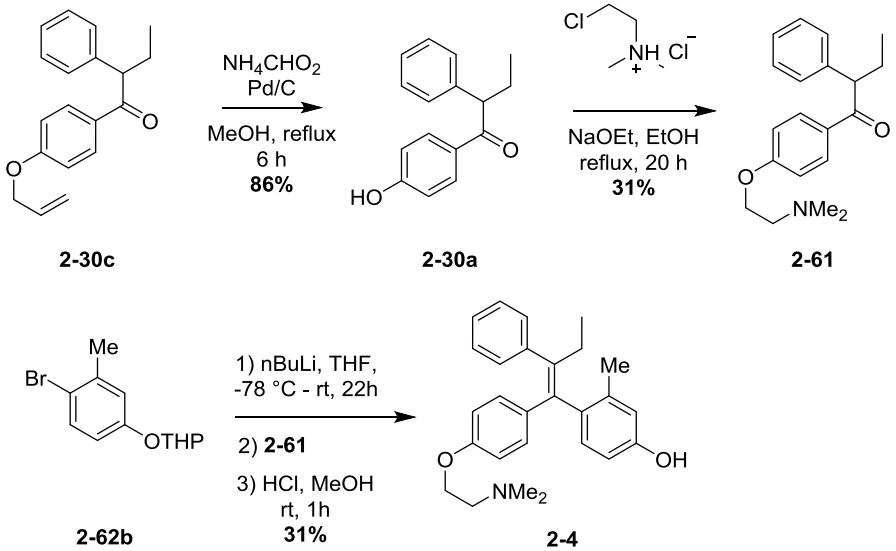

Scheme 2.4.2. *Alternative synthesis of* ***2-4****.*

We utilised a *Cre*^{T2}-p38α model that had been developed within the thesis of Dr Begoña Cánovas, whereupon p38α MAP kinase was expressed as a direct result of OHT-induced recombination.[52] The p38α levels were identified by relevant fluorescent antibodies and quantified, which directly related to *Cre* activity. This is analogous to the *Cre*-GFP model, but replacing the gene encoding GFP for p38α (figure 2.4.2).

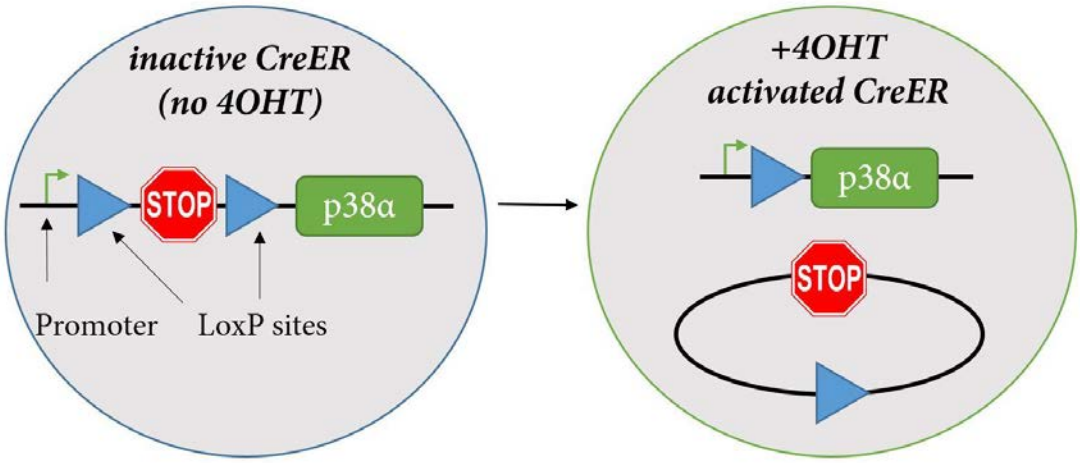

***Figure 2.4.2. Cre-p38α assay**. Cells in normal conditions (blue circle), a LoxP-flanked stop codon is located between the promoter and the gene encoding p38α, so no p38α will be expressed. In the presence of 4OHT, CreER^{T2} is activated, which removes the stop codon from the DNA sequence. The promoter is now directly upstream of the gene encoding p38α, therefore p38α will be expressed in cells.*

The results from this assay are shown below in graph 2.4.1, comparing *Cre* induction by commercial diastereomerically pure (*Z*)-**2-2** and diastereomerically pure **(***E***)-2-4**. It is important to note that p38α expression was only used as a marker for *Cre* activity and that we did not plan to incorporate the expression of p38α into the guaymoxifen system at any point.

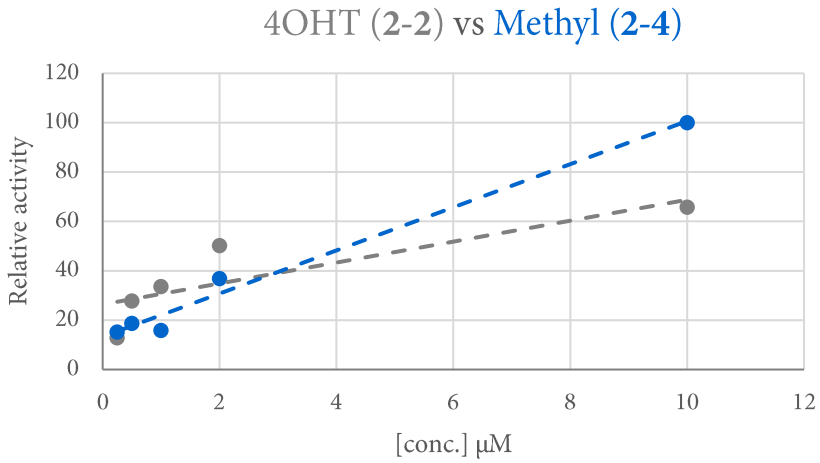

Graph 1. *The relative activity of (**Z**)-**2-2** (grey) compared with (**E**)-**2-4** (blue), where the activity of **2-2** at 10 µM is qualified to be 100%.*

The graph shows that the activity of (***E***)-**2-4** is comparable to that of (***Z***)-**2-2** within the concentration range used in standard cellular assays. The data may suggest that (***E***)-**2-4** is slightly less potent at 10 µM than (***Z***)-**2-2,** however the activity between 0.5 and 2 µM suggests (***E***)-**2-4** is the most potent analogue within this range. It is likely that the accuracy of this assay is not sufficient to reveal specific details of this activity, but sufficed as confirmation of the relative activity (***E***)-**2-4**, which closely matched that of (***Z***)-**2-2.**

A further analogue of interest was the dimethyl analogue **2-65** (scheme 2.4.4). We wished to observe the steric effect of a second methyl group on the isomeric ratio, however the organolithium reaction was difficult to achieve. No organolithium was formed when using n-BuLi and reaction using s-BuLi was also troublesome. The THP protecting group was much more labile than the mono methyl analogue **2-62b**, aided by the hyperconjugation from the additional methyl group (scheme 2.4.4). The THP group of **2-63b** deprotected after 1 week on the bench, and would need to replaced by an alternative protecting group.

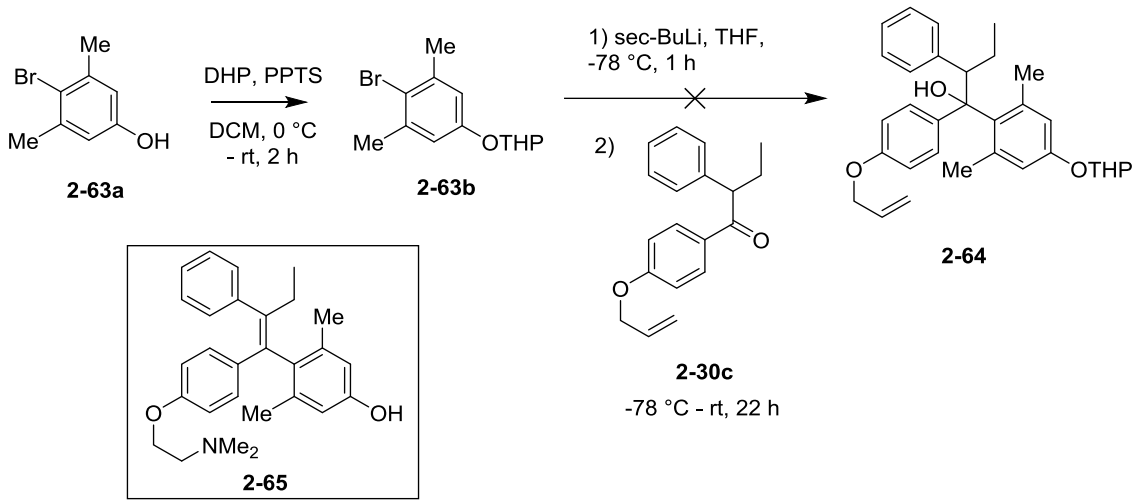

Scheme 2.4.4. *Attempted synthesis of a di-ortho-methyl analogue of hydroxytamoxifen.*

Therefore further work was abandoned in attempting to reach analogue **2-65** and we focussed our efforts on the mono-methyl series. A larger batch of **2-4** was synthesised, obtained as an approximate 6:1 ratio for the activity to be confirmed *in vivo* in a *Cre*ER^{T2} mouse model. The results confirmed that at 5 μM, **2-4** was able to activate *Cre* and induce recombination to cause expression of GFP, with comparable activity to (***Z***)-**2-2**.

2.4.2 Synthesis of Methyl Substituted Guaymoxifen Analogue **2-66**

Now that we had proven that the relative activity of diastereomerically pure (***E***)-**2-4** was close to that of (***Z***)-**2-2** in *in vitro* assays, and *in vivo* as a ~5:1 mixture of diastereoisomers, we began the synthesis of second generation guyamoxifen featuring this *ortho-* methyl group, which would liberate **2-4** upon cleavage by LigF enzyme (**2-66**, scheme 2.4.5).

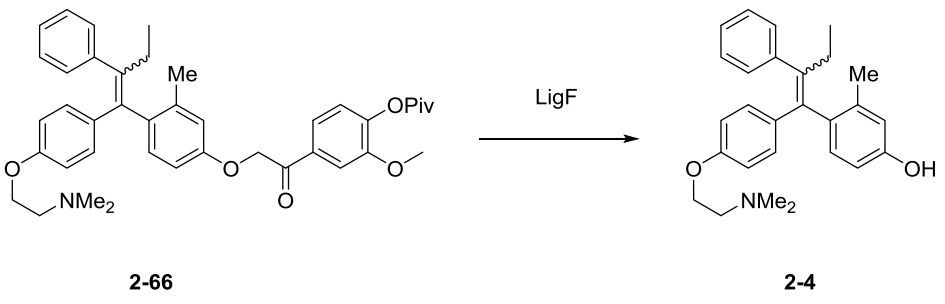

2-66 **2-4**

Scheme 2.4.5. *2nd Generation guaymoxifen **2-66**, which upon cleavage by LigF liberates **2-4**.*

In order to function, the new compound **2-66** would have to be inactive towards *Cre*ER^{T2} and also be susceptible to cleavage by LigF, analogously to **2-11** and **2-40b**. It should be noted that the fluorescence assay was no longer of use because the additional methyl is featured on the tamoxifen component of the molecule, which is replaced by the fluorescent methyl umbeliferone component (**2-13**) in the fluorescent analogues.

Exploration of an alternative synthesis guaymoxifen analogues was carried out, which could have offered a more convergent route to **2-66**, provided the key organolithium addition had worked in sufficient yield. The route is summarised below (scheme 2.4.6).

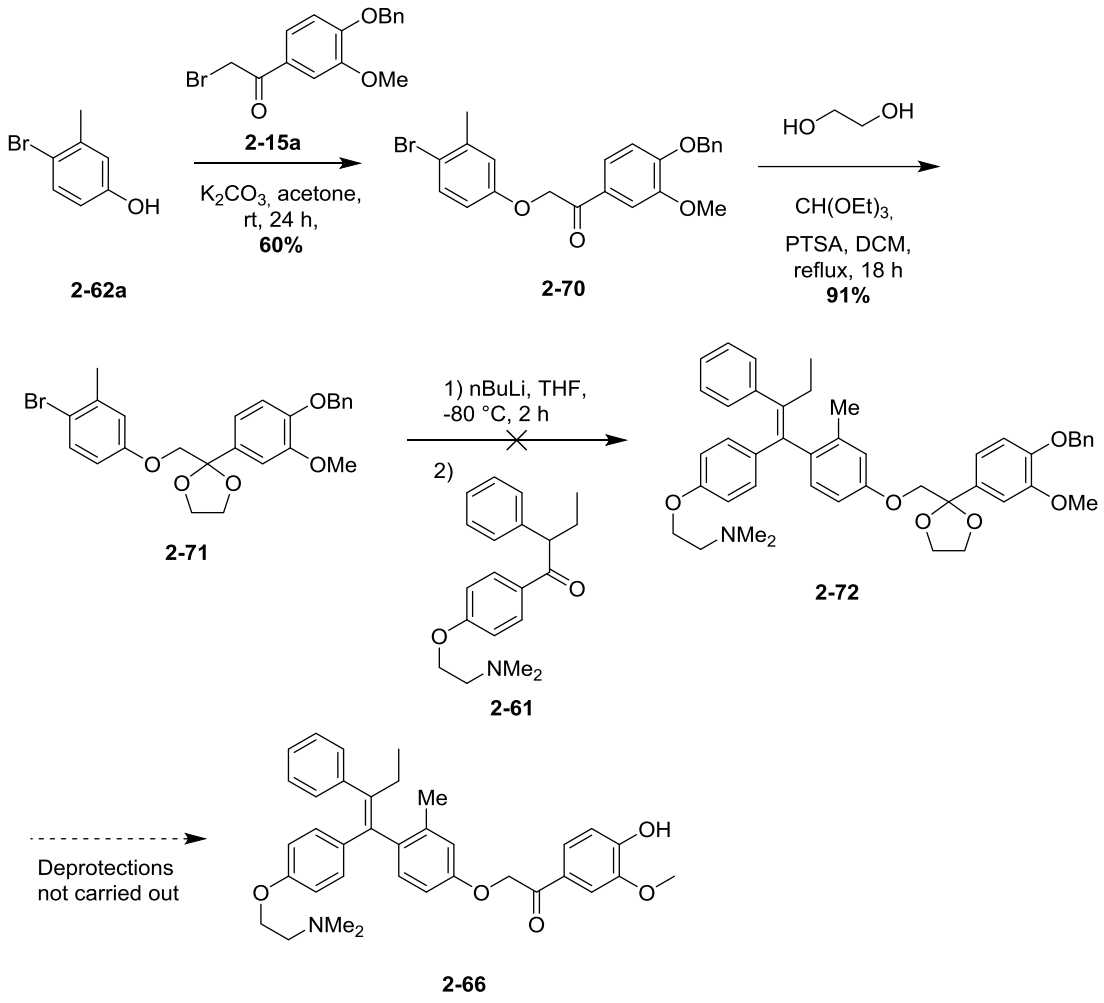

Scheme 2.4.6. *Towards an alternative synthesis of* ***2-66.*** *The organolithium reaction was unsuccessful and the Grignard could also not be formed.*

Unfortunately, no reaction was observed in the organolithium step, only the starting materials were recovered. The route was also repeated with *p*-iodo phenol, to ensure that

steric repulsion of the *ortho*-methyl group was not the culprit for the lack of reaction and to increase the lability of the halo-leaving group (scheme 2.4.7). A TIPS protecting group was used to afford intermediate **2-76**, as described by Dr. Byrom in his attempted synthesis of guaymoxifen. However, this step also failed to produce any product.

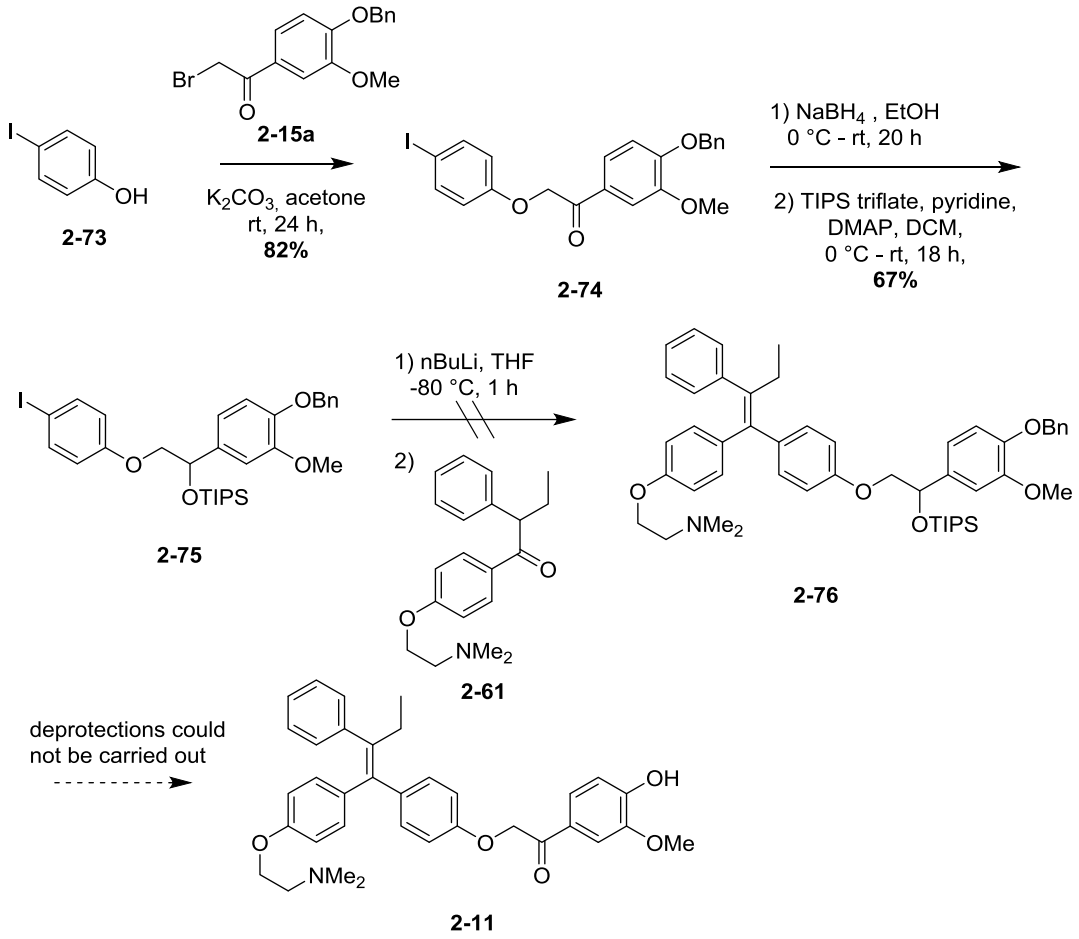

Scheme 2.4.7. *Trial of a convergent route leading to guaymoxifen, via a key organometallic formation and addition to ketone* ***2-61****. This key step could not be achieved and the final steps could not be carried out to reach product* ***2-11****.*

It was concluded that the formation of organolithiums and grignards were too difficult in the presence of so many functionalities and that it was preferable to carry out this step earlier on the synthesis, as with our original 1st generation guaymoxifen analogues. In the interest of time, further optimisation of the route was postponed until the identification of a single target analogue was identified.

The synthesis was therefore carried out following the route used to afford **2-11** but using intermediate **2-59** instead of **2-22**. The guaymoxifen derivative **2-66** was furnished in 25% overall yield from commercial starting materials (scheme 2.4.8).

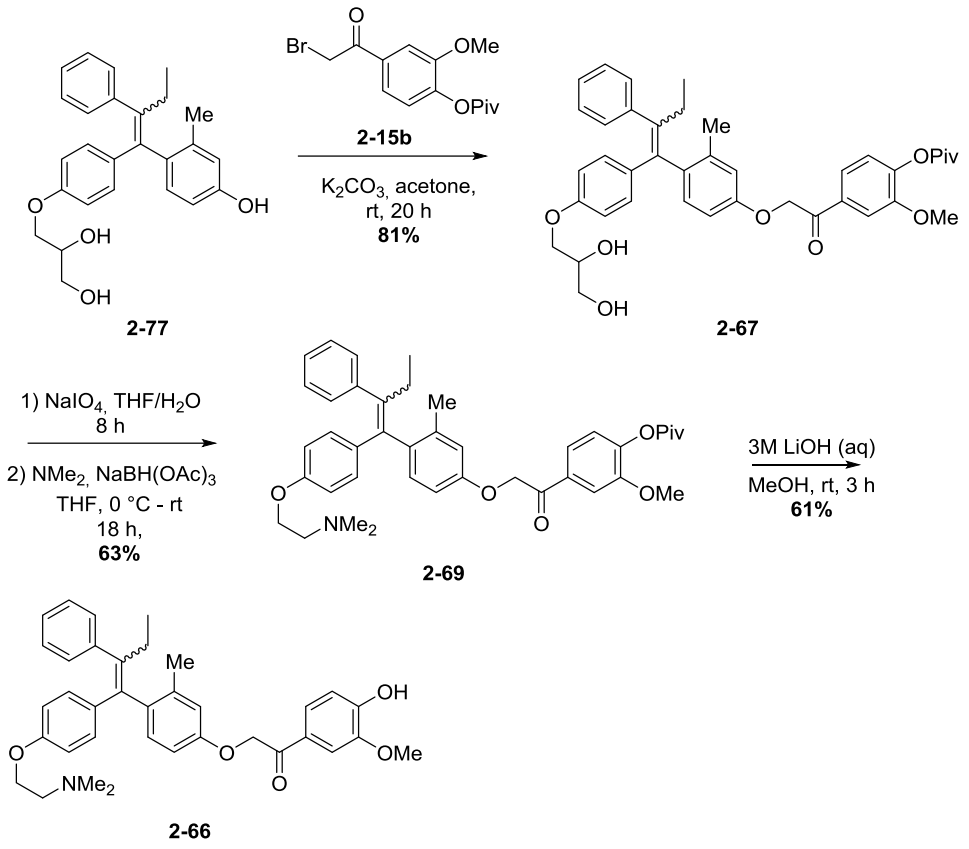

Scheme 2.4.8. *The synthesis of 2nd generation guaymoxifen analogue* ***2-66.***

Because the methylhydroxy analogue **2-40b** showed very promising initial results (i.e. lower metabolic cleavage in the liver), we synthesised analogue **2-78** from intermediate **2-69** *via* the aldol reaction conditions identified previously with **2-40b**, then deprotection of the pivaloyl group (scheme 2.4.8).

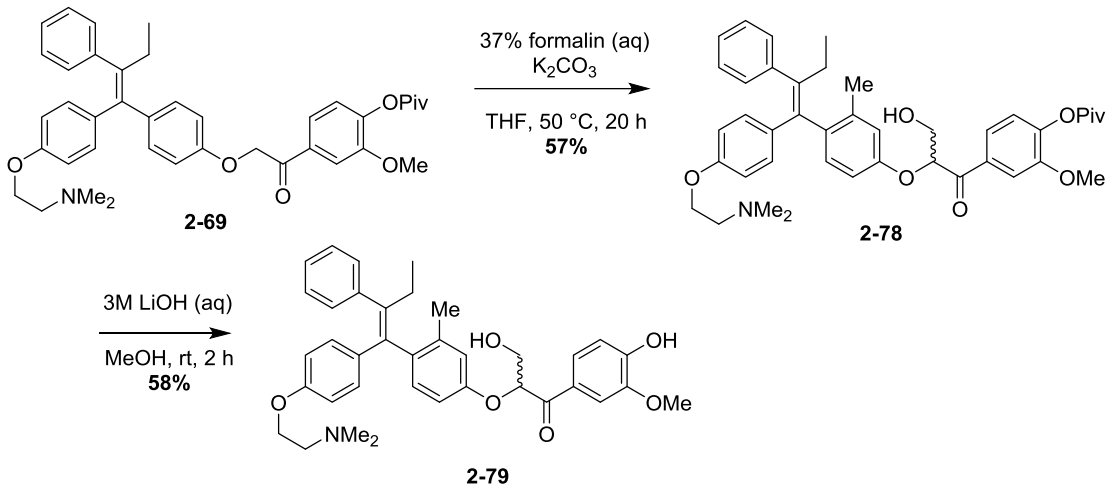

Scheme 2.4.8. *Synthesis of hydroxymethyl substituted 2nd generation guaymoxifen,* ***2-78.***

2.4.3 Cleavage Assay of **2-66** and **2-78** by LigF Monitored by Mass Spectrometry

Before progressing to the LigF tumour implanted-*Cre*ER-GFP *in vivo* model with the new 2nd generation guaymoxifen analogues, we wanted to ensure that they could be cleaved by LigF enzyme *in vitro.* The enzymatic cleavage had thus far proven to be selective for just one stereoisomer, and the addition of a methyl group on the ring may well have diminished activity *via* steric hindrance. Therefore compounds were administered to solutions of LigF and GSH as previously, and aliquots were taken over 24 hours. The aliquots were analysed by mass spectrometry to identify the quantities of **2-4** generated from each separate analogue. The results are shown in graphs 2.4.1 and 2.4.2.

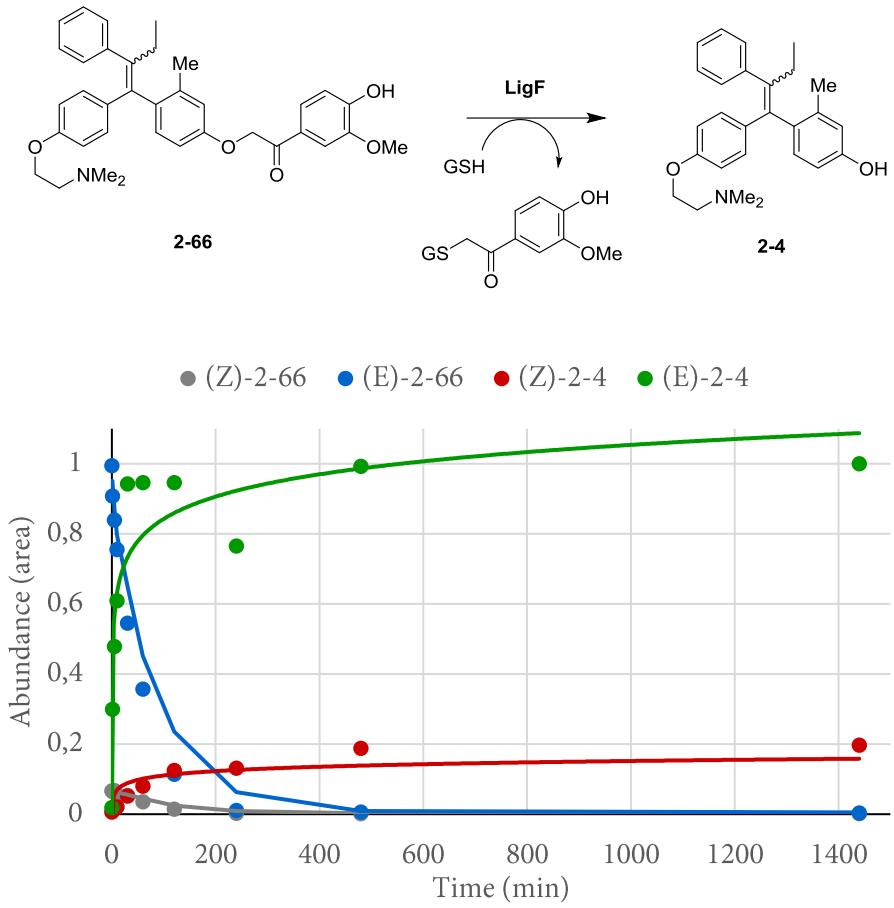

Graph 2.4.1. *The GSH-assisted cleavage of* ***2-66*** *by LigF over a 24 hour period and liberation of* ***2-4****. Relative abundance calculated by the average area of the mass peak by mass spectrometry corresponding to the characteristic degradation fragment. Active E isomers shown in blue and green, less active Z isomers shown in grey and red.*

As can be observed from cleavage graph 2.4.1; at t = 0, the starting ratio of *E*/*Z*-**2-66** is around 10:1, which is higher than the ratio assigned by NMR spectroscopy (6:1). We witness rapid cleavage of the more abundant *E* isomer and a reflected increase in formation of the active *E* product (**2-4**) in graph 2.4.1. The rate of cleavage of the *Z* isomer is slightly slower, suggesting the enzyme has a small preference in cleavage of the active *E* isomer. The rate of formation of *E* product also reflects this observation, and is analogous to what was witnessed previously with the preferred cleavage of the *E* isomers of **2-11** and **2-40b.**

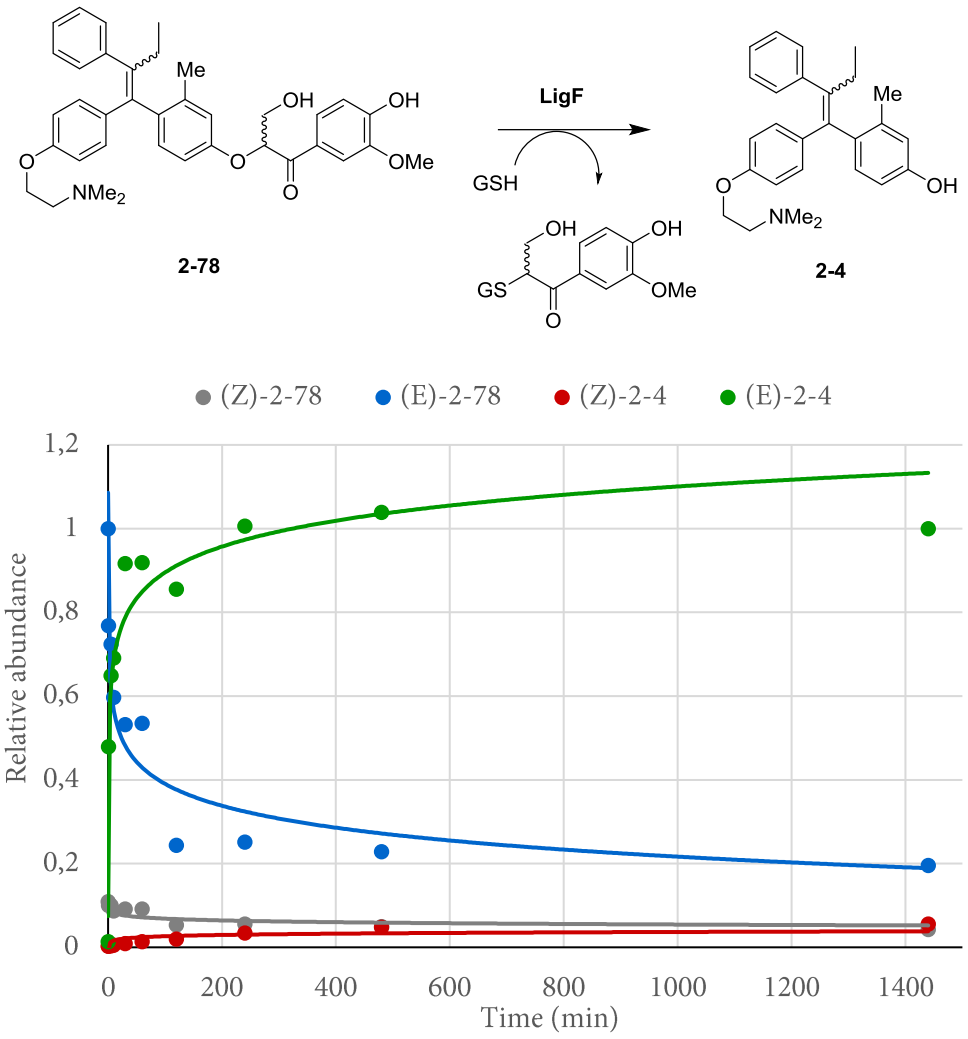

Graph 2.4.2. *GSH-assisted cleavage of* ***2-78*** *by LigF and resultant release of* ***2-4*** *over 24 hours. Relative abundance calculated using the average area of the peak by mass spectrometry corresponding to the characteristic degradation fragment for respective isomers.*

2-78 at t = 0 again displays an enriched ratio (10:1) of the active E isomer, again higher than that observed by NMR spectroscopy. Cleavage of (*E*)-**2-78** does not appear to reach completion even after 24 hours of enzyme digestion yet seems to reach a plateau minimum at 120 min and barely decreases from this time point. This might suggest that the enzyme is saturated with a by-product or more likely an error in ionisation and fragment detection, revealing a caveat of this detection method.

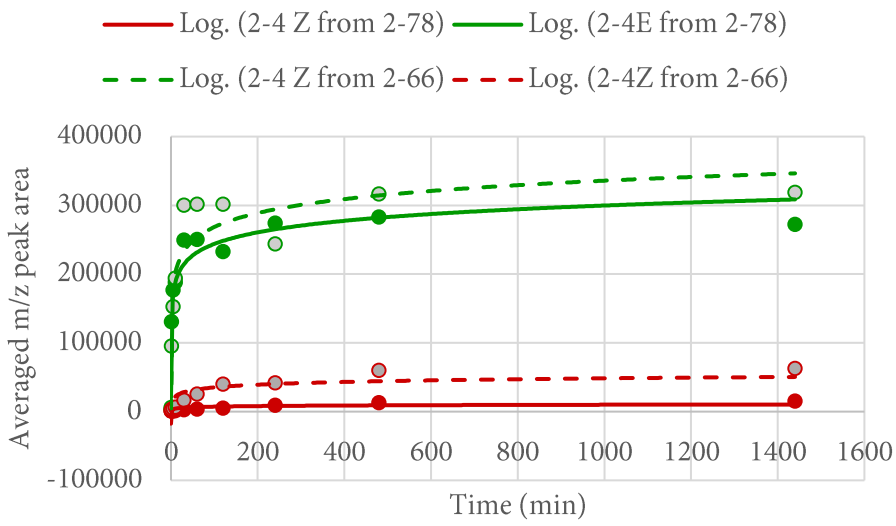

Graph 2.4.3. *Graph showing the release of (E/Z)-**2-4** from the same GSH-assisted cleavage of **2-66** and **2-78** by LigF. Green line shows (**E**)-**2-4** released from (**E**)-**2-78** cleavage, red line shows (**Z**)-**2-4** released from (**Z**)-**2-78.** The dotted lines correspond to **(E)-2-4** and **(Z)-2-4** liberated by cleavage of **2-66 E** and **Z** isomers, as in graph 2.4.1.*

Interestingly, graph 2.4.3 shows that the liberation of the active stereoisomer (*E*)-**2-4** from **2-78(*E*)** is comparable to that liberated from cleavage of (*E*)-**2-66**. This was unexpected, as the presence of a hydroxymethyl group to the β-ether bridge in analogue **2-40b** gave rise to a chiral centre, and LigF was seemingly unable to cleave one of the enantiomers. This resulted in a liberation of (*Z*)-**2-2** that was approximately half of that liberated by the cleavage of **2-11**, which lacked the hydroxymethyl group. Therefore, this result may suggest that the liberation of (*E*)-**2-4** from non-hydroxymethylated derivative **2-66** is only half of what would be expected, or perhaps that liberation of (*E*)-**2-4** by **2-78** is higher because LigF does not distinguish between the *E* and *Z* isomers of **2-78**. We were not able to compare the relative abundances of liberated **2-4** to liberated **2-2**, as they are different mass fragments monitored by mass spectroscopy and unfortunately we did not run any experiments with internal standards of known concentration of corresponding compound.

The overall conclusions that were made by these experiments were that both analogues **2-66** and **2-78** were rapidly cleaved by LigF to release active *E*-**2-4** in higher ratio than the inactive *Z* stereoisomer. These two new analogues had the advantage of being enriched in

the active *E* isomer, meaning much less useless *Z* material needed to be administered to the mouse subjects. These compounds are therefore expected to provide a larger therapeutic window, to generate genetic recombination in the tumour environment but minimising background recombination as a result of liver metabolism. They may also have different metabolic profiles in the liver, or possess a small change in pharmacokinetic properties, as the solubilities seemed slightly increased in the organic solvents used in the synthesis. The methyl group may affect metabolism of the groups about the phenol ring.

2.4.4 *In vivo* Testing of 2nd Generation Guaymoxifen Analogues **2-66** and **2-78**

The 2 new 2nd generation guaymoxifen analogues are currently going under *in vivo* testing in the full mouse model. Further optimisation needs to be made to improve the expression of LigF in the tumour cells, and also to improve the implanted metastasis in the mouse models. **2-66** and **2-78** will be compared to original guaymoxifen analogues **2-11** and the improved **2-40b** in order to identify a best candidate for spatiotemporal activation of *Cre*. Once we have proof of concept of this novel methodology, further validation of the model and assessment of its scope will be carried out using the surplus material already synthesised of each analogue.

Conclusions

A more amenable route towards guaymoxifen (**2-11**) was developed and used to obtain larger quantities of **2-11** for *in vivo* testing.

Initial trials demonstrated that **2-11** could be cleaved *in vivo* to release 4OHT (**2-2**) and induce recombination in the stroma surrounding metastatic tumour sites. It was discovered that the liver of the mouse could also cleave and release **2-2,** to cause recombination in cells around the liver, thus guaymoxifen (**2-11**) could not be used to identify new metastasis sites *in vivo.*

An SAR study about the β-ether bond identified 3 new analogues of guaymoxifen that could be cleaved by LigF enzyme *in vitro.* 2 of these analogues (methyl substituted **2-40a,** and hydroxymethyl substituted **2-40b**) generally showed less metabolic liver cleavage *in vivo.* However, initial studies with LigF expressing tumours have not been able to reproduce earlier results, where significant recombination in the stromal cells around tumour sites was observed.

HA-tagged LigF was shown to be expressed in sufficient concentration in the tumour tissue, therefore we have not identified the exact problem with this system.

Compound (**2-40b**) was synthesised on a large scale and ongoing *in vivo* experiments aim to identify the problem with the guaymoxifen system, then find conditions where it can be used in as a tool for genetic control of the stroma around metastatic tumours.

Finally, 2nd generation guaymoxifen analogues **2-66** and **2-78** were synthesised, which were enriched in the active *E*-isomer due to an additional methyl substituent on the guai-phenol ring.

2-66 and **2-78** were both cleaved by LigF *in vitro,* and showed metabolic cleavage in the liver when administered *in vivo,* compared to the corresponding 1st generation analogues **2-11** and **2-40b**.

References

(1) Tauriello, D. V. F.; Palomo-Ponce, S.; Stork, D.; Berenguer-Llergo, A.; Badia-Ramentol, J.; Iglesias, M.; Sevillano, M.; Ibiza, S.; Cañellas, A.; Hernando-Momblona, X.; et al. TGFβ Drives Immune Evasion in Genetically Reconstituted Colon Cancer Metastasis. *Nature* **2018**, *554* (7693), 538–543. https://doi.org/10.1038/nature25492.

(2) Calon, A.; Lonardo, E.; Berenguer-Llergo, A.; Espinet, E.; Hernando-Momblona, X.; Iglesias, M.; Sevillano, M.; Palomo-Ponce, S.; Tauriello, D. V. F.; Byrom, D.; et al. Stromal Gene Expression Defines Poor-Prognosis Subtypes in Colorectal Cancer. *Nat. Genet.* **2015**, *47* (4), 320–329. https://doi.org/10.1038/ng.3225.

(3) Cortina, C.; Turon, G.; Stork, D.; Hernando-Momblona, X.; Sevillano, M.; Aguilera, M.; Tosi, S.; Merlos-Suárez, A.; Stephan-Otto Attolini, C.; Sancho, E.; et al. A Genome Editing Approach to Study Cancer Stem Cells in Human Tumors. *EMBO Mol. Med.* **2017**, *9* (7), 869–879. https://doi.org/10.15252/emmm.201707550.

(4) Oskarsson, T.; Batlle, E.; Massagué, J. Metastatic Stem Cells: Sources, Niches, and Vital Pathways. *Cell Stem Cell* **2014**, *14* (3), 306–321. https://doi.org/10.1016/j.stem.2014.02.002.

(5) Rajewsky, K.; Gu, H.; Kühn, R.; Betz, U. A. K.; Müller, W.; Roes, J.; Schwenk, F. Conditional Gene Targeting. *J. Clin. Invest.* **1996**, *98* (3), 600–603. https://doi.org/10.1172/JCI118828.

(6) Nagy, A. Cre Recombinase: The Universal Reagent for Genome Tailoring. *Genesis* **2000**, *26* (2), 99–109.

(7) Feil, R.; Wagner, J.; Metzger, D.; Chambon, P. Regulation of Cre Recombinase Activity by Mutated Estrogen Receptor Ligand-Binding Domains. *Biochem. Biophys. Res. Commun.* **1997**, *237* (3), 752–757. https://doi.org/10.1006/bbrc.1997.7124.

(8) Horwitz, K. B.; McGuire, W. L. Antiestrogens: Mechanism of Action and Effects in Breast Cancer. In *Breast Cancer:Advances in Research and Treatment, Vol. 2: Experimental Biology*; Springer US: Boston, MA, 1978; pp 155–204. https://doi.org/10.1007/978-1-4757-4673-0_5.

(9) Fabian, C.; Sternson, L.; El-serafi, M.; Cain, L.; Hearne, E. Clinical Pharmacology of Tamoxifen in Patients with Breast Cancer: Correlation with Clinical Data. *Cancer* **1981**, *48* (4), 876–882.

(10) Lim, C. K.; Yuan, Z.-X.; Lamb, J. H.; White, I. N. H.; De Matteis, F.; Smith, L. L. A Comparative Study of Tamoxifen Metabolism in Female Rat, Mouse and Human Liver Microsomes.

Carcinogenesis **1994**, *15* (4), 589–593. https://doi.org/10.1093/carcin/15.4.589.

(11) Osborne, C. K.; Jarman, M.; McCague, R.; Coronado, E. B.; Hilsenbeck, S. G.; Wakeling, a. E. The Importance of Tamoxifen Metabolism in Tamoxifen-Stimulated Breast Tumor Growth. *Cancer Chemother. Pharmacol.* **1994**, *34* (2), 89–95. https://doi.org/10.1007/s002800050111.

(12) JORDAN, V. C.; KOCH, R.; LANGAN, S.; McCAGUE, R. Ligand Interaction at the Estrogen Receptor to Program Antiestrogen Action: A Study With Nonsteroidal Compounds in Vitro *. *Endocrinology* **1988**, *122* (4), 1449–1454. https://doi.org/10.1210/endo-122-4-1449.

(13) Katzenellenbogen, B. S.; Norman, M. J.; Eckert, R. L.; Peltz, S. W.; Mangel, W. F. Bioactivities , Estrogen Receptor Interactions , and Plasminogen Activator-Inducing Activities of Tamoxifen and Hydroxytamoxifen Isomers in MCF-7 Human Breast Cancer Cells Bioactivities , Estrogen Receptor Interactions , and Plasminogen Tamoxifen Isomers. *Cancer Res.* **1984**, *44*, 112–119. https://doi.org/0008-5472.

(14) Katzenellenbogen, J. A.; Carlson, K. E.; Katzenellenbogen, B. S. Facile Geometric Isomerization of Phenolic Non-Steroidal Estrogens and Antiestrogens: Limitations to the Interpretation of Experiments Characterizing the Activity of Individual Isomers. *J. Steroid Biochem.* **1985**, *22* (5), 589–596. https://doi.org/10.1016/0022-4731(85)90210-9.

(15) Foster, A. B.; Jarman, M.; Leung, O. T.; McCague, R.; Leclercq, G.; Devleeschouwer, N. Hydroxy Derivatives of Tamoxifen. *J. Med. Chem.* **1985**, *28* (10), 1491–1497. https://doi.org/10.1021/jm00148a020.

(16) McCague, R.; Leung, O.-T.; Jarman, M.; Kuroda, R.; Neidle, S.; Webster, G. The Role of the 2-Methyl Substituent in Governing Stereoselective Formation of the E Isomer in the Synthesis of 4-Hydroxy-2-Methyltamoxifen (1-{4-[2-(Di-Methylamino)Ethoxy]Phenyl}-1-(4-Hydroxy-2-Methylphenyl)-Phenylbut-1-Ene). *J. Chem. Soc. Perkin Trans. 2* **1988**, No. 7, 1201. https://doi.org/10.1039/p29880001201.

(17) Kuroda, R.; Cutbush, S.; Neidle, S.; Lueng, O. T. Structural Studies on Some Tamoxifen Derivatives. *J. Med. Chem.* **1985**, *28* (10), 1497–1503. https://doi.org/10.1021/jm00148a021.

(18) McCague, R.; Kuroda, R.; Leclercq, G.; Stoessel, S. Synthesis and Estrogen Receptor Binding of 6,7-Dihydro-8-Phenyl-9-[4-[2-(Dimethylamino)Ethoxy]Phenyl]-5H-Benzocycloheptene, a Nonisomerizable Analog of Tamoxifen. X-Ray Crystallographic Studies. *J. Med. Chem.* **1986**, *29* (10), 2053–2059. https://doi.org/10.1021/jm00160a044.

(19) McCague, R.; Leclercq, G.; Jordan, V. C. Nonisomerizable Analogs of (Z)- and (E)-4-

Hydroxytamoxifen. Synthesis and Endocrinological Properties of Substituted Diphenylbenzocycloheptenes. *J. Med. Chem.* **1988**, *31* (7), 1285–1290. https://doi.org/10.1021/jm00402a005.

(20) Acton, D.; Hill, G.; Tait, B. S. Tricyclic Triarylethylene Antiestrogens: Dibenz[b,f]Oxepins, Dibenzo[b,f]Thiepins, Dibenzo[a,e]Cyclooctenes, and Dibenzo[b,f]Thiocins. *J. Med. Chem.* **1983**, *26* (8), 1131–1137. https://doi.org/10.1021/jm00362a009.

(21) McCague, R.; Leclercq, G. Synthesis, Conformational Considerations, and Estrogen Receptor Binding of Diastereoisomers and Enantiomers of 1-[4-[2-(Dimethylamino)Ethoxy]Phenyl]-1,2-Diphenylbutane (Dihydrotamoxifen). *J. Med. Chem.* **1987**, *30* (10), 1761–1767. https://doi.org/10.1021/jm00393a014.

(22) MacGregor, J. I.; Jordan, V. C. Basic Guide to the Mechanisms of Antiestrogen Action. *Pharmacol. Rev.* **1998**, *50* (2), 151–196.

(23) Rossant, J.; McMahon, A. 'Cre'-Ating Mouse Mutants---a Meeting Review on Conditional Mouse Genetics. *Genes Dev.* **1999**, *13* (2), 142–145. https://doi.org/10.1101/gad.13.2.142.

(24) Tsien, J. Z. Cre-Lox Neurogenetics: 20 Years of Versatile Applications in Brain Research and Counting…. *Front. Genet.* **2016**, *7*. https://doi.org/10.3389/fgene.2016.00019.

(25) Henderson, C. J.; McLaughlin, L. A.; Osuna-Cabello, M.; Taylor, M.; Gilbert, I.; McLaren, A. W.; Wolf, C. R. Application of a Novel Regulatable Cre Recombinase System to Define the Role of Liver and Gut Metabolism in Drug Oral Bioavailability. *Biochem. J.* **2015**, *465* (3), 479–488. https://doi.org/10.1042/BJ20140582.

(26) Faal, T.; Wong, P. T.; Tang, S.; Coulter, A.; Chen, Y.; Tu, C. H.; Baker, J. R.; Choi, S. K.; Inlay, M. A. 4-Hydroxytamoxifen Probes for Light-Dependent Spatiotemporal Control of Cre-ER Mediated Reporter Gene Expression. *Mol. Biosyst.* **2015**, *11* (3), 783–790. https://doi.org/10.1039/C4MB00581C.

(27) Ota, Y.; Itoh, Y.; Kaise, A.; Ohta, K.; Endo, Y.; Masuda, M.; Sowa, Y.; Sakai, T.; Suzuki, T. Targeting Cancer with PCPA-Drug Conjugates: LSD1 Inhibition-Triggered Release of 4-Hydroxytamoxifen. *Angew. Chemie Int. Ed.* **2016**, *55* (52), 16115–16118. https://doi.org/10.1002/anie.201608711.

(28) Akiyama, T.; Magara, K.; Matsumoto, Y.; Meshitsuka, G.; Ishizu, A.; Lundquist, K. Proof of the Presence of Racemic Forms of Arylglycerol-B-Aryl Ether Structure in Lignin: Studies on the Stereo Structure of Lignin by Ozonation. *J. Wood Sci.* **2000**, *46* (5), 414–415.

https://doi.org/10.1007/BF00776407.

(29) Byrom, D. Synthesis of TGF-Beta Inhibitors and Compounds for Spatiotemporal Drug Release Daniel Byrom, Universitat de Barcelona, 2018.

(30) Otsuka, Y.; Sonoki, T.; Ikeda, S.; Kajita, S.; Nakamura, M.; Katayama, Y. Detection and Characterization of a Novel Extracellular Fungal Enzyme That Catalyzes the Specific and Hydrolytic Cleavage of Lignin Guaiacylglycerol Beta-Aryl Ether Linkages. *Eur. J. Biochem.* **2003**, *270* (11), 2353–2362. https://doi.org/10.1046/j.1432-1033.2003.03545.x.

(31) Takemoto, Y.; Yoshida, H.; Takaki, K. Copper-Catalyzed Three-Component Borylstannylation of Alkynes. *Chem. - A Eur. J.* **2012**, *18* (46), 14841–14844. https://doi.org/10.1002/chem.201202435.

(32) Shimizu, M.; Nakamaki, C.; Shimono, K.; Schelper, M.; Kurahashi, T.; Hiyama, T. Stereoselective Cross-Coupling Reaction of 1,1-Diboryl-1-Alkenes with Electrophiles: A Highly Stereocontrolled Approach to 1,1,2-Triaryl-1-Alkenes. *J. Am. Chem. Soc.* **2005**, *127* (36), 12506–12507. https://doi.org/10.1021/ja054484g.

(33) Gauthier, S.; Mailhot, J.; Labrie, F. New Highly Stereoselective Synthesis of (Z)-4-Hydroxytamoxifen and (Z)-4-Hydroxytoremifene via McMurry Reaction. *J. Org. Chem.* **1996**, *61* (11), 3890–3893. https://doi.org/10.1021/jo952279l.

(34) Osborne, C. K.; Wiebe, V. J.; McGuire, W. L.; Ciocca, D. R.; DeGregorio, M. W. Tamoxifen and the Isomers of 4-Hydroxytamoxifen in Tamoxifen-Resistant Tumors from Breast Cancer Patients. *J. Clin. Oncol.* **1992**, *10* (2), 304–310. https://doi.org/10.1200/JCO.1992.10.2.304.

(35) Robertson, D. W.; Katzenellenbogen, J. A. Synthesis of the (E) and (Z) Isomers of the Antiestrogen Tamoxifen and Its Metabolite, Hydroxytamoxifen, in Tritium-Labeled Form. *J. Org. Chem.* **1982**, *47* (12), 2387–2393. https://doi.org/10.1021/jo00133a030.

(36) Ruenitz, P. C.; Bagley, J. R.; Mokier, C. M. Estrogenic and Antiestrogenic Activity of Monophenolic Analogues of Tamoxifen, (Z)-2-[p-(1,2-Diphenyl-1-Butenyl)Phenoxy]-N,N-Dimethylethylamine. *J. Med. Chem.* **1982**, *25* (9), 1056–1060. https://doi.org/10.1021/jm00351a010.

(37) VanRheenen, V.; Kelly, R. C.; Cha, D. Y. An Improved Catalytic OsO4 Oxidation of Olefins to -1,2-Glycols Using Tertiary Amine Oxides as the Oxidant. *Tetrahedron Lett.* **1976**, *17* (23), 1973–1976. https://doi.org/10.1016/S0040-4039(00)78093-2.

(38) Slaughter, R. L.; Edwards, D. J. Recent Advances: The Cytochrome P450 Enzymes. *Ann. Pharmacother.* **1995**, *29* (6), 619–624. https://doi.org/10.1177/106002809502900612.

(39) Ghorpade, A. K.; Huddar, S. N.; Akamanchi, K. G. Aq HBr–NaNO2–KI/Air: A New Catalytic System for α-Monobromination of Ketones. *Tetrahedron Lett.* **2016**, *57* (44), 4918–4921. https://doi.org/10.1016/j.tetlet.2016.09.073.

(40) Gall, D. L.; Kim, H.; Lu, F.; Donohue, T. J.; Noguera, D. R.; Ralph, J. Stereochemical Features of Glutathione-Dependent Enzymes in the Sphingobium Sp. Strain SYK-6 β-Aryl Etherase Pathway. *J. Biol. Chem.* **2014**, *289* (12), 8656–8667. https://doi.org/10.1074/jbc.M113.536250.

(41) Chen, A.; Xu, J.; Chiang, W.; Chai, C. L. L. L-Threonine-Catalysed Asymmetric α-Hydroxymethylation of Cyclohexanone: Application to the Synthesis of Pharmaceutical Compounds and Natural Products. *Tetrahedron* **2010**, *66* (7), 1489–1495. https://doi.org/10.1016/j.tet.2009.11.100.

(42) Gouverneur, V.; Seppelt, K. Introduction: Fluorine Chemistry. *Chem. Rev.* **2015**, *115* (2), 563–565. https://doi.org/10.1021/cr500686k.

(43) Wang, J.; Sánchez-Roselló, M.; Aceña, J. L.; del Pozo, C.; Sorochinsky, A. E.; Fustero, S.; Soloshonok, V. A.; Liu, H. Fluorine in Pharmaceutical Industry: Fluorine-Containing Drugs Introduced to the Market in the Last Decade (2001–2011). *Chem. Rev.* **2014**, *114* (4), 2432–2506. https://doi.org/10.1021/cr4002879.

(44) Chen, Z.; Zhu, W.; Zheng, Z.; Zou, X. One-Pot α-Nucleophilic Fluorination of Acetophenones in a Deep Eutectic Solvent. *J. Fluor. Chem.* **2010**, *131* (3), 340–344. https://doi.org/10.1016/j.jfluchem.2009.11.008.

(45) Ouyang, X. P.; Liu, C. L.; Pang, Y. X.; Qiu, X. Q. Synthesis of a Trimeric Lignin Model Compound Composed of α-O-4 and β-O-4 Linkages under Microwave Irradiation. *Chinese Chem. Lett.* **2013**, *24* (12), 1091–1094. https://doi.org/10.1016/j.cclet.2013.09.001.

(46) John, J. P.; Colby, D. A. Synthesis of α-Halo-α,α-Difluoromethyl Ketones by a Trifluoroacetate Release/Halogenation Protocol. *J. Org. Chem.* **2011**, *76* (21), 9163–9168. https://doi.org/10.1021/jo2017179.

(47) Helmich, K. E.; Pereira, J. H.; Gall, D. L.; Heins, R. A.; McAndrew, R. P.; Bingman, C.; Deng, K.; Holland, K. C.; Noguera, D. R.; Simmons, B. A.; et al. Structural Basis of Stereospecificity in the Bacterial Enzymatic Cleavage of β-Aryl Ether Bonds in Lignin. *J. Biol. Chem.* **2016**, *291* (10), 5234–5246. https://doi.org/10.1074/jbc.M115.694307.

(48) Harbeson, S. L.; Tung, R. D. Deuterium Medicinal Chemistry: A New Approach to Drug Descovery

and Development. *Medchem news* **2014**, No. 2, 8–22.

(49) Schmidt, C. First Deuterated Drug Approved. *Nat. Biotechnol.* **2017**, *35* (6), 493–494. https://doi.org/10.1038/nbt0617-493.

(50) Kumar, R.; Azim, a.; Kumar, V.; Sharma, S. K.; Prasad, a. K.; Howarth, O. W.; Olsen, C. E.; Jain, S. C.; Parmar, V. S. Lipase-Catalyzed Chemo- and Enantioselective Acetylation of 2-Alkyl/Aryl-3-Hydroxypropiophenones. *Bioorganic Med. Chem.* **2001**, *9* (10), 2643–2652. https://doi.org/10.1016/S0968-0896(01)00184-5.

(51) Chen, C. S.; Fujimoto, Y.; Girdaukas, G.; Sih, C. J. Quantitative Analyses of Biochemical Kinetic Resolutions of Enantiomers. *J. Am. Chem. Soc.* **1982**, *104* (25), 7294–7299. https://doi.org/10.1021/ja00389a064.

(52) Cánovas Bilbao, B. Role of P38 MAPK in Breast Cancer, Universitat de Barcelona, 2017.

Chapter 3

Introduction and Background to Compounds Targeting p38α

3.1. p38α MAPK

One pathway that plays an important role in the development of tumours is the p38 MAPK pathway. The Nebreda lab has focussed their efforts on the study of this protein's role in cancer progression and new treatments that prevent cancer by blocking this protein to regulate the pathway.

3.1.1. The Mitogen-Activated Protein Kinase (MAPK) Activation

The mitogen-activated protein kinase (MAPK) signalling pathways can be activated by a broad variety of stimuli to regulate many cellular responses, such as cell differentiation, proliferation and survival.[1] Canonical MAPKs comprise the p38 family members (α, β, χ, δ) as well as the ERK and JNK kinase families. They share specific regulatory features and are expressed in all eukaryotic cells. P38 MAPKs have almost no catalytic activity in basal conditions, but become rapidly activated *via* a phosphorylation cascade.[2] A 3-part core signalling module comprising a MAPK kinase kinase (MKKK), a MAPK kinase (MKK), and a MAPK sequentially phosphorylate and activate the three components (figure 3.1.1). Upon stimulation, MKKKs are phosphorylated on the serine or threonine residues and are activated through interaction with other proteins. The activated MKKKs trigger the sequential phosphorylation and activation of MKKs and MAPKs. More specifically, MAPKs are doubly phosphorylated on a conserved motif (Thr-X-Tyr) located within the activation loop of the kinase domain. This causes a conformational change in the protein which allows ATP and the substrate to bind.[3]

Depending on the stimuli, different MAPKs are activated. Generally, p38 (and JNK) kinases are responsive to stress stimuli, such as cytokine stimulation, osmotic shock, and ionizing radiation.[4] Activation is highly dependent upon the cell type and the biological context. Inactivation by phosphatases (MKPs) is regulated by complex interactions of JNK, ERK, p38 and the MKPs.[5] These events are summarised in figure 3.1.1.

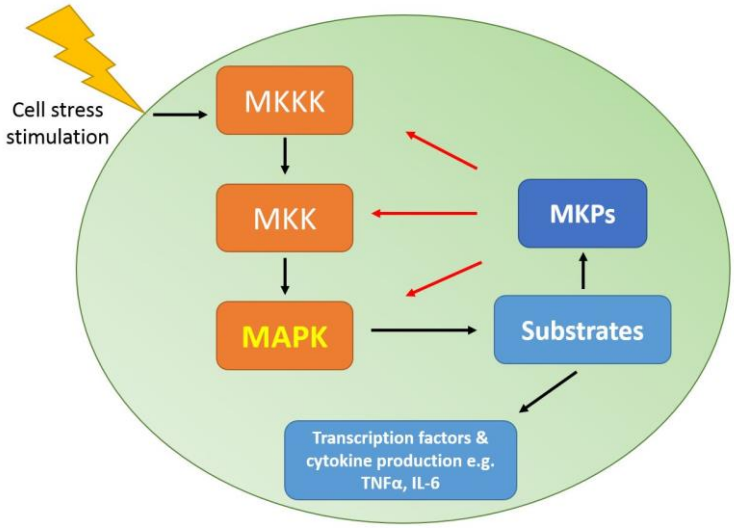

Figure 3.1.1. *Highly simplified representation of the general activation pathway of MAPKs, involving stress activation of the 3-tier core signalling module, sequential phosphorylation of MKKK, MKK, MAPK. Phosphorylation of downstream substrates leads to effects in the cell. Activation of phosphatases (MKPs) also causes negative feedback through deactivation/degradation of MAPKs.*

3.1.2. p38 MAPK and its Signalling Pathway

The mammalian p38 MAPK family comprises four members: p38α, p38β, p38χ and p38δ. They are encoded by four genes and share approximately 60% of identity in their overall amino acid sequence and more than 90% within their kinase domain. However, the members have notable differences in tissue localisation, upstream activators and downstream effectors, as well as in their sensitivity to chemical inhibitors.[6] The most abundant family member, p38α, is highly expressed in many tissues, whereas p38β is usually found at low levels, except in brain tissue. In contrast, p38χ is expressed at high levels only in skeletal muscle, and p38δ is found mainly in pancreas, kidney and small intestine tissues.[3]

In particular, p38α and p38β are able to phosphorylate a wide range of substrates, whereas p38χ and p38δ seem to target a lower number.[7] p38α is by far the target that has been most studied in inflammatory and other disease types and has been most targeted by inhibition, although most inhibitors also possess affinity for the β isoform.

3.1.3. MAPK Substrate Phosphorylation

MAPKs regulate a wide range of functions by phosphorylating downstream partners, including transcription factors, regulatory and structural proteins, several protein kinases, as well as some phosphatases.[8] The p38 family members are estimated to have from 200 – 300 substrates each and usually phosphorylate on serine or threonine residues, which is usually followed by a proline (SP/TP) to activate their substrate.[9] Some of the main protein kinase substrates and transcription factors include MK2/3, MNK1/2 and MSK1/2, which are involved in the intracellular amplification of stress signals. p38α activation in particular leads to expression of various inflammatory mediators including TNFα, IL-1β, IL-6 and CXCl2.[10] Further downstream targets that are affected include HSP27 (heat shock protein 27) and ATF1/2/6 (activating transcription factor), all of which are highly associated with inflammatory response.

As demonstrated, the activation and downstream activity of p38α contribute to a range of processes that are important for normal tissue functioning and that are frequently deregulated in many pathologies. Its decisive role in regulating the biosynthesis of a number of proinflammatory cytokines (IL-6, IL-1β and TNF-α) has made it an extremely attractive target in a number of stress-related inflammatory diseases such as rheumatoid arthritis (RA) and chronic obstructive pulmonary disease (COPD) and has also earned it the name *the stress kinase*. A number of p38α inhibitors of varying structures have been developed by several pharmaceutical companies in order to treat these diseases.[11] More recently, p38α related inflammation has also been shown to be involved in many aspects of cancer progression in a range of cancer types. p38 can impact on cancer cell homeostasis at different levels, e.g. p38α promoted tumour cell proliferation and survivial,[12] and facilitating cancer cell survival in response to chemotherapy treatments.[13,14] For example, the inhibitor ralimetinib (LY2228820), by Eli Lilly, reduces tumour growth in xenografts of human breast cancer cell lines by up to 72%.[15] This compound advanced to Phase II clinical trials in ovarian cancer, and in glioblastoma.[16,17] It has also been used in combined therapy with other inhibitors such as prexasertib (LY2606368) to treat advanced, metastatic,

colorectal and non-small cell lung cancers in phase I clinical trials,[18] with evidence that supports its ability to sensitise tumour cells to chemotherapeutics.[19]

However, there also exists a multitude of seemingly contradictory data whereby p38α appears to have a dual role in tumour formation, metastasis and dormancy.[19] Depending on the tissue type in question and the time point of progression, p38α can have either a suppressive or contributory effect. For example, whereas attenuation of breast cancer metastasis can be achieved using p38α inhibitors,[20] p38α downregulation can also facilitate the metastatic spread of colon cancer cells from liver to lung.[21] Care should be taken with some of the *in vitro* data, as it may oversimplify the diversity of cells found in the tumour microenvironment and could lead to false conclusions.[12]

Nevertheless, these findings clearly demonstrate that there is a therapeutic opportunity in cancer *via* the intervention of the p38α MAPK pathway and that a greater understanding of the downstream effects of p38α is needed to obtain maximum therapeutic benefit.

3.1.4. p38α Chemical Inhibitors

There were a range of chemical inhibitors with distinct cores that had already been reported in the literature and in patents, several already having gone through clinical trials in humans up to phase II. Pfizer's PH797804 (**PH**) and Eli Lilly's LY2228820 (**LY**) were the main inhibitors used in the study of p38α in Angel Nebreda's research group. Both inhibitors demonstrated extremely promising profiles in their respective companies pre-clinical testing, however they were not continued past Phase II clinical trials in humans due to limited efficacy against the disease type, and side-effects such as skin rash and liver toxicity at higher dosis.[11,22]

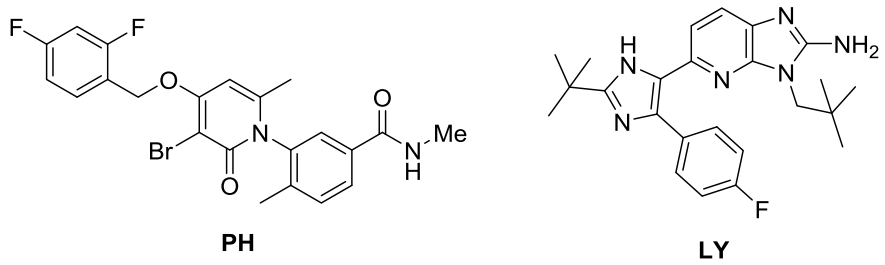

Figure 3.1.2. *Inhibitor compounds developed by big pharma companies Pfizer (**PH**) and Eli Lilly (**LY**), which have been trialled in Phase II clinical trials for several diseases, e.g. COPD and RA.*

The overall goal of this project was to optimise an existing p38α inhibitor to overcome these hurdles and improve their therapeutic index, examined in the current models used within the Nebreda lab. This would be done by designing a small collection of new analogues that could be conjugated to tumour-directing groups to accumulate the active compound in the tumours. Targeted delivery of the inhibitor would increase the effective dose, giving rise to higher concentrations within the tumour cells for improved efficacy, whilst reducing potential damage to normal cells which would diminish off-target side effects. In parallel, we would design small molecule degraders (Protacs) based on the original inhibitor core structure for an anticipated stronger downregulation of the pathway and therefore improved efficacy.

3.1.5. Background and Synthesis of **PH** Inhibitor

PH was initially selected for its chemical structure: it possessed a terminal amide which could easily be diversified to include functional groups for conjugation to directing groups and could be easily synthesised *via* a 5-step synthesis (scheme 3.1.1). The route commenced with the nucleophilic ring-opening of lactone **3-1** by aniline **3-2**. The phenol group of the resulting product, **3-3**, then attacked difluorobenzyl bromide (**3-5)** to afford **3-6**. Selective bromination at the alkene position adjacent to the carbonyl, followed by cleavage of the methyl ester under basic conditions afforded **3-7**. The final compound **PH** was furnished by *in situ* formation of the acyl chloride then coupling to methyl amine. This final step provided an excellent diversification point to generate many analogues in possession of

extended alkyl chains and terminal functional groups to act as handles for further functionalisation, by varying the amine coupling partner (described further in section 3.2).

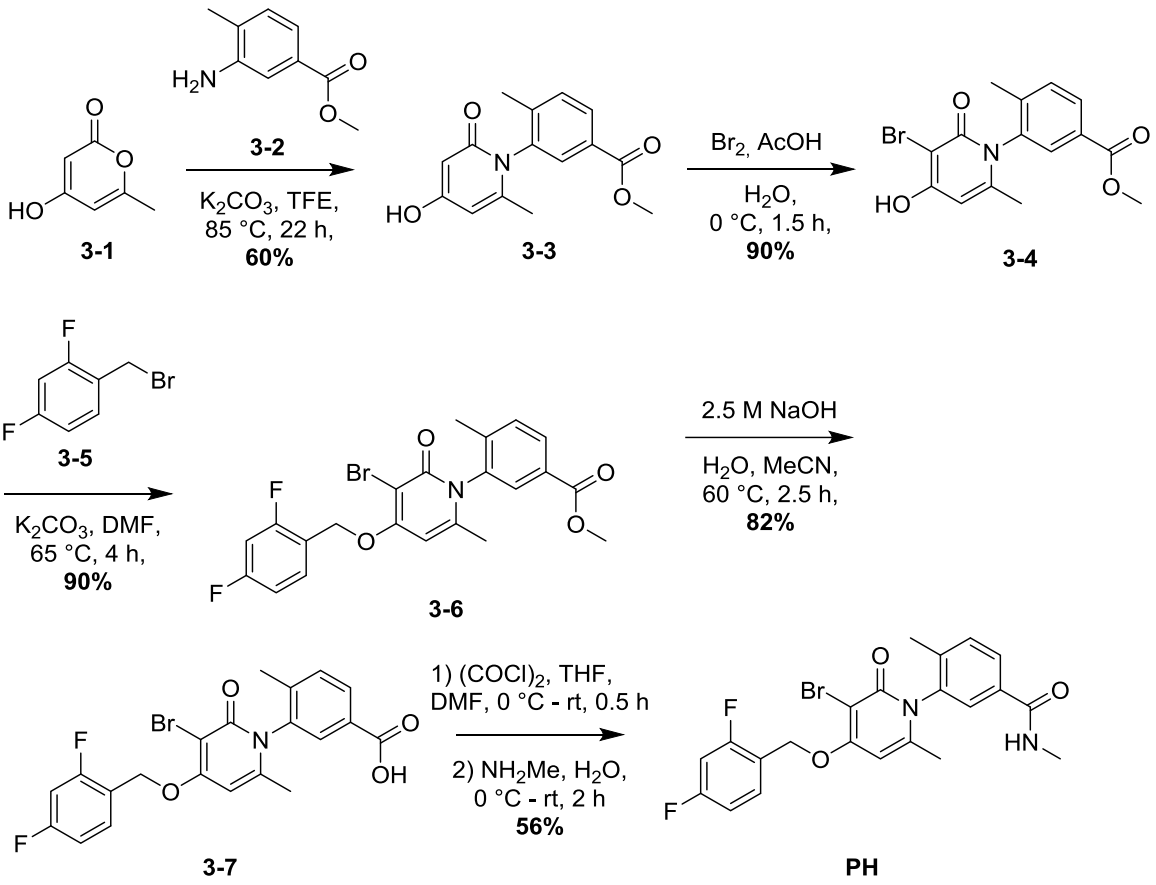

Scheme 3.1.1. *Synthetic route towards* ***PH****, p38α inhibitor.*

PH was developed from compound **SC-25028**, originally identified from a Pfizer high throughput screening assay. This was optimised to **3-8** to improve inhibition potency for p38α and also metabolic stability. 2,4-Difluoro substitution prevented *O*-debenzylation and converting the *N*-benzyl group to an *N*-phenyl prevented *N*-debenzylation and improved clearance in mouse and rat models.[23]

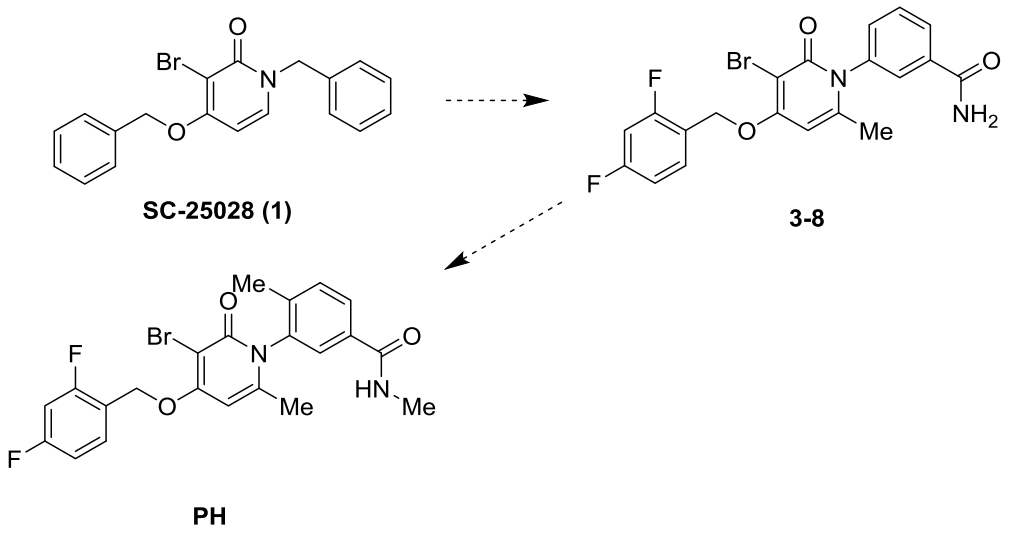

Scheme 3.1.2. *Lead optimisation by Pfizer® towards p38α inhibitor PH, from HTS hit SC-25028.*

2, 5-substitution of the *N*-aryl ring by the methyl and amide substituents was favoured to achieve high potency of **PH**, however hindered rotation resulting from the steric interference of the pyridinone carbonyl and methyl groups gave rise to 2 atropoisomers.[24] (diagram) A rotational barrier of 25 kcal/mol was observed and minimal interconversion occurred under 110 °C in a range of solvents. Furthermore, it was found that (-)**PH** was 2 orders of magnitude more potent than (+)**PH**, but the mixture of isomers was roughly equipotent in the kinase assay and slightly less potent in cells.

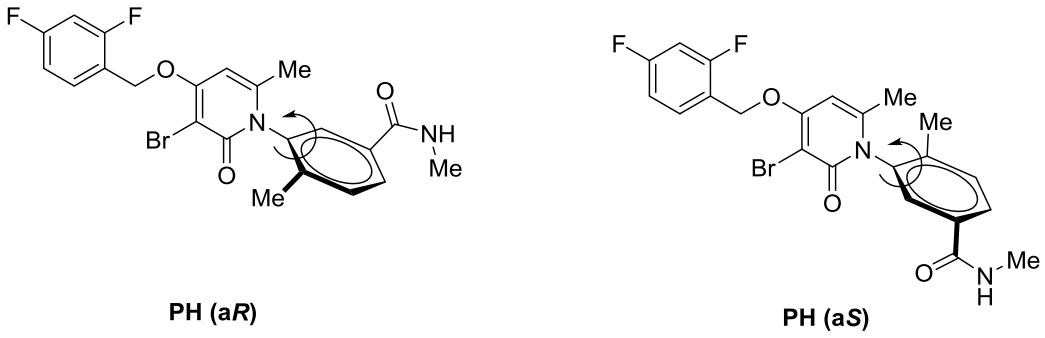

Figure 3.1.3. *Showing the atropoisomers (aS) and (aR) of* ***PH****, as described by Monahan and coworkers.*

Table 3.1.1. *IC_{50} of **PH** as a mixture of atropoisomers and as separate (-) and (+) atropoisomers in a p38/MK-2 cascade assay and a human peripheral blood monocyte assay (hPBMC). Nd = not determined.*

	(+/-)PH	(-)PH	(+)PH
p38α enzyme cascade, IC_{50} (nM)	2.5	2.3	247
hPBMC TNFα in cells, IC_{50} (nM)	15	3.4	nd

The 3D structure elucidated from co-crystal X-ray studies of **PH**-p38α reveal that the drop in potency of the (a*R*) isomer is due to steric repulsion of the *N*-methyl on the pyridinone ring with residues Asp112 and Asn115 of the p38α active site.[25]

PH exhibits high specificity for p38α over 65 other kinases tested, due to 3 key interactions with the active site of its protein target, exemplified in figure 3.1.4.

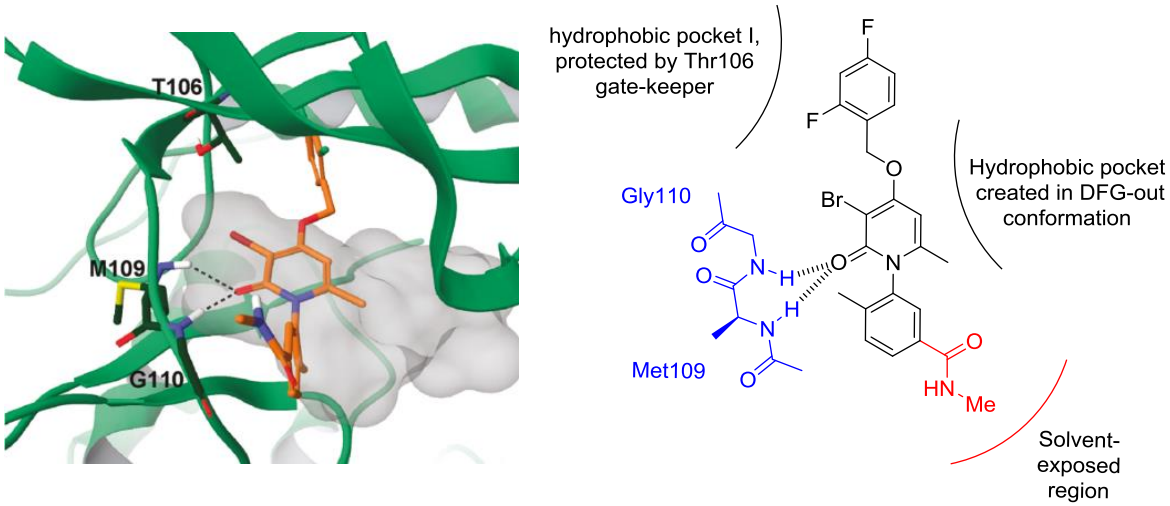

Figure 3.1.4. A) *Crystal co-structure of **PH-797804** bound to the p38α kinase domain.[25]* ***B)*** *Planar diagrammatic representation of the key interactions of **PH-797804** within the ATP active site of p38α.*

1) The threonine gatekeeper (Thr368), which blocks large groups from entering hydrophobic pocket I which lies deep inside the protein core. This Thr residue is only found in ~40 other kinases and is therefore exploited in the design of inhibitor structures to gain selectivity for p38α over other kinases. The *O*-difluorobenzyl

group of **PH** was optimal for occupation of this pocket. Because of the small size of this hydrophobic pocket, only small substituents like fluorine were well tolerated.

2) A second hydrophobic pocket is located further down, which is occupied by the methyl substituent of the pyridinone ring. Functionalisation of this moiety with larger or highly polar groups diminished potency against the kinase.
3) As with all kinases, binding to the ATP hinge region is crucial for gaining binding affinity *via* hydrogen bond formation between polar groups of the inhibitor and the amino acid residues of this hinge region.[26] The carbonyl moiety of PH forms a dual hydrogen bond with the amide nitrogen of Met109 and with the backbone NH group of Gy110, which undergoes a 180° rotational flip in order to achieve this geometry (known as a glycine flip).

These traits are responsible for the exceptional potency and high specificity of **PH** for p38α over other kinases. The compound also shows affinity for p38β (which has an amino acid sequence that is 75% identical to p38α), also confirmed by experiments performed in the Nebreda lab. **PH** has a stability profile that is compatible with oral delivery and showed excellent anti-inflammatory properties in pre-clinical studies, i.e. reduction of pro-inflammatory mediators such as prostaglandin E_2, cytokines TNFα and IL-6.[27] Rapid on and off-rates were found for this inhibitor (K_{on}) 1.53 x 10^7 M^{-1} s^{-1} and (K_{off}) 0.058 s^{-1}, and strong binding affinity for p38 both in its active and non-active states. In human clinical trials, **PH** was generally well tolerated in several Phase I studies and demonstrated efficacy in Phase II clinical trials for patients with chronic obstructive pulmonary disease (COPD, NCT00559910) and in rheumatoid arthritis patients (RA, NCT00620685), however this was not sustained after 2 weeks.

PH also suffered from poor solubility. Further analogues were developed to improve the solubility, by replacing the bromo-substituted pyridinone core with a chloro-substituted pyrimidinone core and addition of a short alcohol bearing chain to the amide.[28] A 20-fold increase in dissolution rate was observed, improved bioavailability and clearance, whilst maintaining efficacy *in vivo*.

Table 3.1.2. PH *PK data and analogue* ***3-9*** *with improved solubility and clearance profile.*

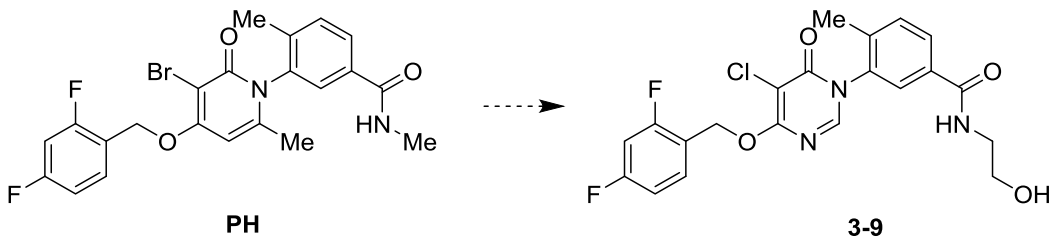

	PH	**3-9**
Solubility (μg/mL)	10.00	23.00
Intrinsic dissolution rate (μg/min/cm^2)	0.30	6.10
logP	3.35	1.65
Cell permeability (10^{-6} cm/s)	15.90	8.00

Further development of either of these series seems to have been abandoned by Pfizer, which one can speculate to be because of limited efficacy in Phase II clinical trials, associated side effects such as skin rash and elevated hepatic enzymes, and also perhaps financial and marketing reasons. One of the strategies we used to overcome the hurdles associated with this series by targeted delivery of the inhibitor through conjugation to directing groups, such as peptide recognition fragments and functionalisation of gold nanorods. This would increase accumulation of our active inhibitors within tumour cells for more efficacy and reduced side effects.

3.2. Controlling Biological Activity with Caging Groups and UV Light

Caging groups, or photolabile protecting groups (PPG) such as *ortho*-nitro benzyl compounds can be incorporated to biologically active compounds to mask their activity. These groups can be cleaved by ultraviolet (UV) or visible (vis) light to liberate the active compound, thus gaining control over biological activity through use of light (scheme 3.2.1).

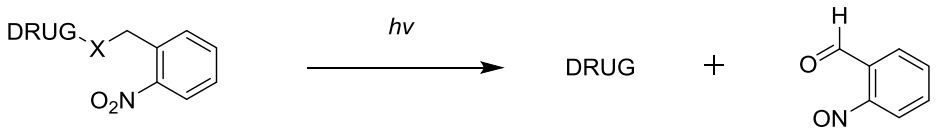

3-10 **3-11**

Scheme 3.2.1. *General reaction scheme showing the liberation of an active drug molecule by application of UV light to a caged intermediate of the drug compound (**3-10**).*

As can be seen from the scheme above, the term "caged" may be confusing as the compound is not encapsulated or trapped, but instead a protecting group is used to modify or block a key functionality "X" of the drug molecule *via* steric and/or electronic interaction.

There are a wide number of PPGs that have found use in organic synthesis, however the most popular are *ortho*-nitro benzyl, (veratryl)-derivatives, as shown in the example (scheme 3.2.1). First communicated in 1970 by Woodward and co-workers,[29] this PPG has been used to protect a wide range of functional groups, such as alcohols and amines.[30] PPGs can provide a high level of orthogonality as they do not require addition of reagents to be removed, only application of UV light, to which most other substrates are inert. A wide range of these protecting groups have also been used to control and examine biological processes, (figure 3.2.1).

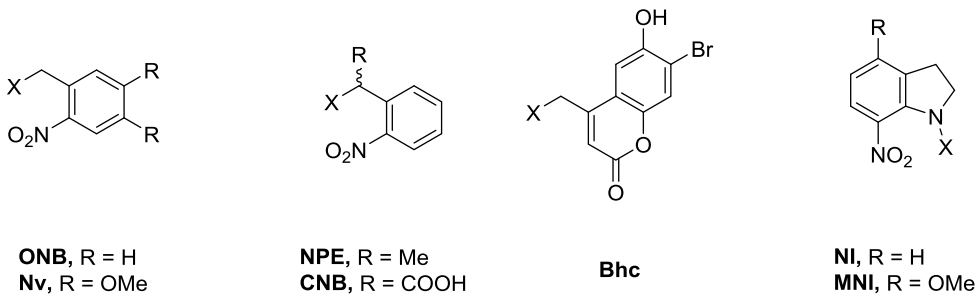

Figure 3.2.1. *Some examples of most common photolabile protecting groups that can be used to protect a range of functional groups, such as alcohols, amines and thiols.*

The mechanism of this reaction has been widely studied and this information has aided the modifications to improve photolytic cleavage conditions and increase the reaction rate. The generally accepted mechanism is summarised in scheme 3.2.2., as proposed by Wirz and coworkers.[31] The process is initiated by the excited nitro group, which receives a hydrogen atom via intramolecular transfer from the benzyl methylene (**3-12** → **3-13**). Decay of bicyclic intermediate **3-14** then leads to liberation of the free functionality "X" and nitroso side product **3-15**. This by-product may be toxic in high concentrations in certain biological contexts, and is highly UV-absorbing, which can also perturb its function. Modifications to the α-position (such as **CNB**, **figure 3.2.1**) can circumvent these shortcomings and even enhance the quantum yield and rate of the uncaging reaction.[32]

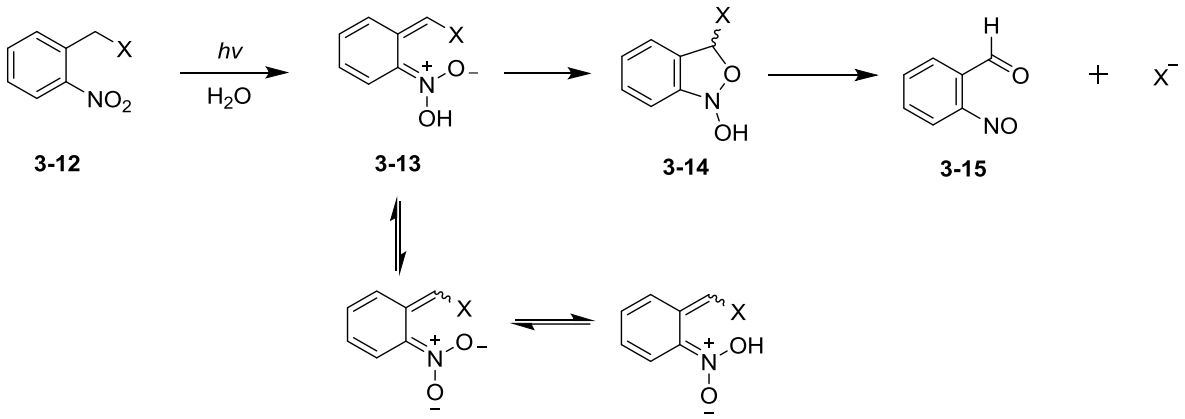

Scheme 3.2.2. *The reaction mechanism for the decay of nitrobenzyl leaving group from substrate* ***3-12*** *after exposure to UV light (hν).*

One of the first examples of the application of caged molecules in biological systems was caged adensine triphosphate (ATP), published by Hoffmann and co-workers.[33] Caged ATP could not be hydrolysed by its natural enzyme, purified Na,K-ATPase. The rapid release of ATP was achieved, 70% yield in under 30 seconds of UV light (340 nm) in aqueous solution. These findings established that release of ATP within the cell was possible and has since been used to gain control over the many ATP-controlled biological effects in a range of applications. Caged ATP is now commercially available and opened the door to further caged molecules for many types of biological applications.

Caged variants of glutamate (an excitatory neurotransmitter) have also had an enormous impact in the study of neurological processes, enabling highly localised release of glutamate at specific time points in brain tissue.[34] With continuing technological advances in the field of photo-pharmacology, two-photon excitation is now possible which provides three-dimensional, spatially resolved uncaging of effector molecules.[35] This also allows much longer wavelengths (650 – 900 nm) to be used which aids in light penetration through tissue (haemoglobin < 650 nm, water > 900 nm) and causes even less damage to cells. MNI-caged glutamate can undergo two-photon uncaging at wavelengths of 700 – 735 nm for use in neural circuit imaging.[36]

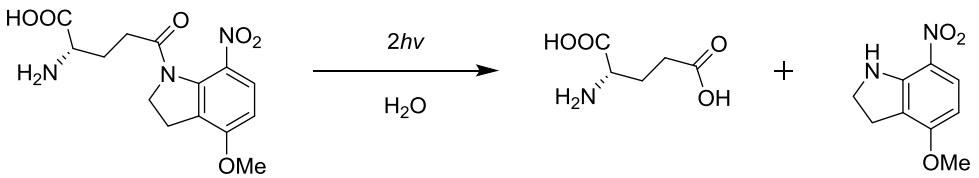

3-16 **Glutamate** **3-17**

Scheme 3.2.3. *Caged glutamate is released after two-photon stimulation using light (~720 nm).*

Use of this wider range of wavelengths also enables wavelength-selective uncaging, as described by Ellis-Davies and coworkers.[37] They synthesised photolabile coumarin derivatives of γ-aminobutyric acid (GABA, an inhibitory neurotransmitter), which would liberate free GABA upon excitation of 450 nm light and two-photon at 900 nm, but was

inert to two-photon excitation at 720 nm. Therefore this neurotransmitter could be used simultaneously with caged glutamates to selectively liberate either GABA (irradiate at 900 nm) for inhibition or glutamate (720 nm) for excitation in a highly accurate and resolved manner.

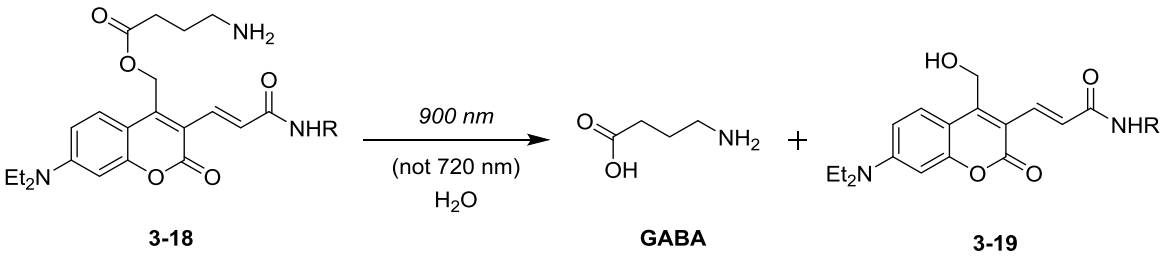

Scheme 3.2.4. *Caged GABA is released after two-photon stimulation using light (900 nm).*

A wide scope of biologically active molecules have been caged to impact a great range of biological functions, including hormone receptors (ER), secondary messengers for cellular signalling (Ca^{2+} ions or NO), nucleic acids and the active sites of proteins.[38–40]

Many of these applications have had huge impacts in imaging and probes *x-vivo*, however many examples of photo-pharmacology being used as a therapy have been reported and are under investigation to eventually go into humans. One of the major hurdles of the field is of course how to penetrate the skin and deliver UV light to the zone of interest in a non-invasive manner. Lerch *et al.*[41]recently proposed a ranking order of organ/tissue based on ease of penetration. Class 1 tissue such as eyes and skin are easily accessed by light, whereas class 2 such as gastro intestinal tracts would require endoscopy and class 4 tissue such as the liver and pancreas would require minor incision.

The aforementioned examples of light-sensitive compounds are all irreversibly activated after application of light uncages them. Another class of light activated molecules are known as reversible photo-switches. They offer an enhanced level of control using UV light, as they may be isomerised to the active form after application of a particular wavelength of light and then slowly relax back to the inactive form or ideally stay active until induced by

a distinct wavelength of UV light. 3 exemplary structures are shown below in both conformations (figure 3.2.2).

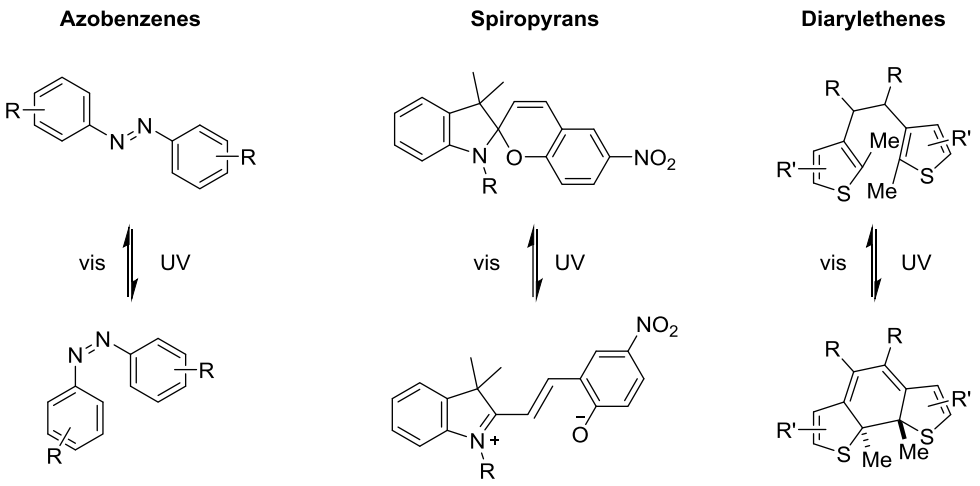

Figure 3.2.2. *The structures and conformations of the most prevalent reversible switch compound structures: azobenzenes, spiropyrans and diarylethenes.*

The most prevalent of the 3 described above are the azobenzenes. This is probably the most versatile in terms of structure and ease of incorporation into bioactive molecules. The advantage of reversibility comes at a price, as there is a more restricted chemical space in which to identify a compound that can be biologically active in the UV-activated form (ideally the *cis* form), and then inactive in the relaxed state (*trans*). Balancing biological activity with UV absorption properties along with pharmacokinetics begins to be more challenging when further structural limitations are introduced, such as including spiropyran cores. Nevertheless, reversible switches have been utilised in an enormous range of applications, enhancing small molecule drugs, proteins and probes with reversible switches.[42]

Rapid development and a heightened interest in photopharmacology continues to drive research of photosensitive and photolabile medicines and indeed other fields.

3.3. Directing Groups for Tumour-Targeted Drug Accumulation

3.3.1. Overview of Directing Group Methodology

Targeted drug delivery has become a massive focus especially within the realm of oncology. There is an extremely vast array of drug delivery systems available, utilising many different moieties to conjugate or encapsulate cytotoxic compounds or diagnostic agents, which cause accumulation at a target cell type or tissue, before releasing their cargo for a targeted effect.[43] Active targeting methods include using ligands which have an affinity for receptors that are overexpressed on tumour cells, such as peptide recognition fragments, antibodies and carbohydrates. Nanoparticle-drug conjugates, such as metallic, liposomes, etc. also lead to accumulation in tumour cells but by passive accumulation. Although related in their overall function, each are very different in structure from one another and have distinct mechanisms for targeting the cells of interest. Many examples of these strategies are used in FDA approved marketed medicines, each method having its own advantages and disadvantages for a given target cell-type and disease. The following section contains an overview of some commonly used drug-delivery techniques, focussing on peptide recognition fragments that were utilised in the thesis and drug-functionalised nanoparticles.

3.3.2. Nanoparticle technology

Another way to influence the biodistribution of a drug compound is through conjugation to nanoparticles. Nanoparticles have received an enormous amount of attention over the past 15 years, including biomedical applications such as oncology.[44] Micelles, liposomes and metallic nanoparticles of a dimension between 10^{-9} – 10^{-8} m possess many theoretical size advantages over traditional small-molecule medicines and over other drug delivery systems, such as large loading capacities and distinct biodistribution. There were over 51

FDA-approved nanomedicines before 2016 identified by Corrie and co-workers, and a further 77 such products in clinical development.[45] As shown in the below graphs, the results are weighted towards micelle, liposomal and nanocrystal materials, but a significant amount of metallic compounds have been approved and are under development (graph 3.3.1).

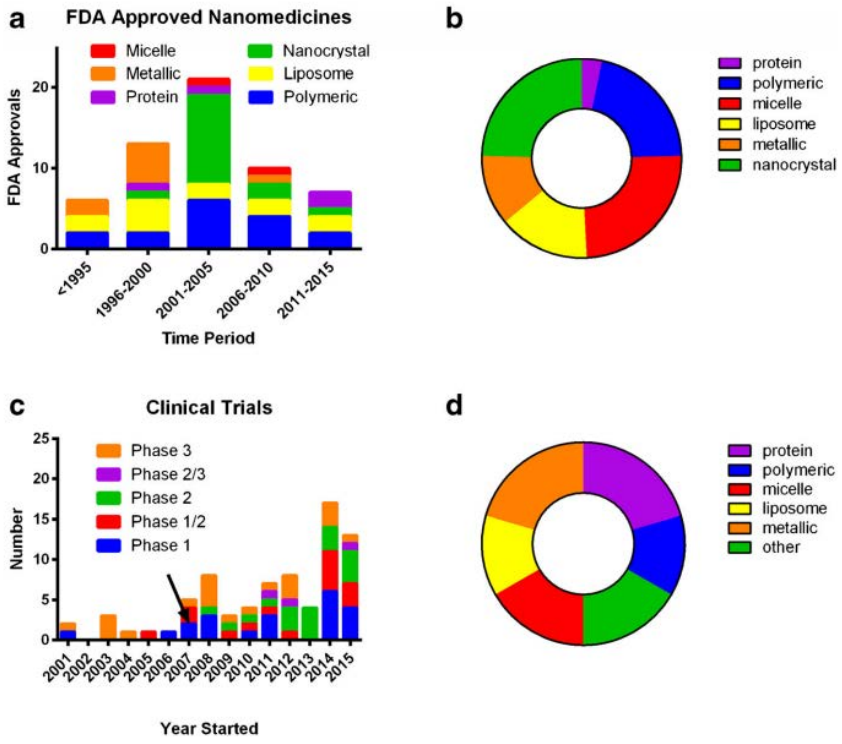

Graph 3.3.1. *Development trends in nanomedicines showing the FDA approved medicines per given year (**a** and **b**) stratified by nano-category, and likewise those currently under clinical trials (**c** and **d**).*[45]

Gold nanoparticles have had a particular focus as multifunctional platforms due to their unique physical, chemical, optical and electronic properties. Their surface can be easily functionalised with therapeutic agents or directing ligands with strong non covalent or dative bonds (Au-S bond, around 40 kcal mol^{-1}).[46] Avidity of these functionalised particles has been reported, whereby the simultaneous recruitment of multiple targets (e.g. receptors) is possible, dependent on particle size.[47] Synthesis is straightforward by colloidal methods, usually involving chemical reduction of an Au salt (e.g. $AuCl_3$) solution in the presence of surface stabilisers.[48]

Passive accumulation of nanoparticles in tumour cells and in inflamed tissue occurs because of enhanced permeation retention (EPR), first reported by Matsumura and Maeda.[49] Nanoparticles leak slowly in normal capillary beds due to their large size (with respect to small molecules). Tumours have a distinct vasculature, whereby blood vessels are enlarged and more in number making them more permeable in order to supply the growing tumour with nutrients and oxygen, a hallmark of cancer known as angiogenesis.[50] Nanoparticles can therefore extravasate into the tumour space and then remain there due to poor lymphatic drainage of tumours.

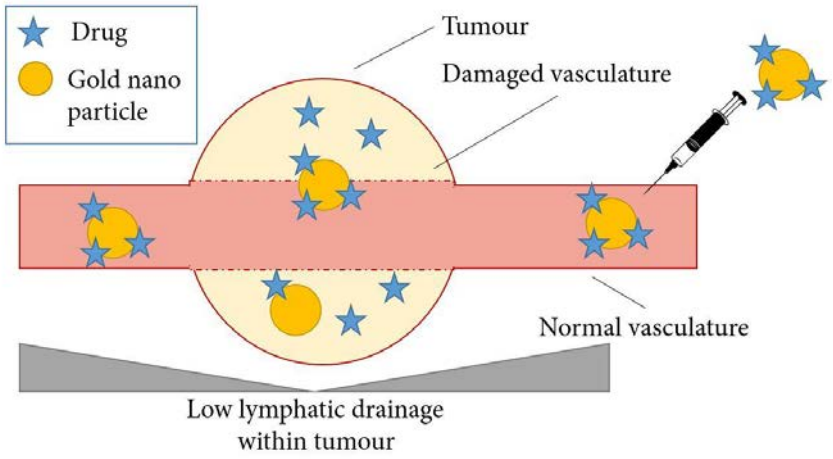

Figure 3.3.1. *Representation of the EPR effect. After intravenous injection of nano-drug conjugates, and systemic circulation, drugs are unable to pass through healthy vasculature. Nano-drug conjugates pass more readily through the damaged vasculature of the tumour, and accumulate here due to poor lymphatic drainage of the tumour tissue. Liberation of drug occurs due to the slightly more acidic environment of the tumour and through metabolic processes.*

This effect is reportedly slow and modest, around 2-fold in respect to other organs, in particular the liver, spleen and blood plasma.[51] Moreover, the attached drug is often detached, excreted or metabolised before therapeutic concentrations are reached within the tumours. Large molecules of this size are normally recognised and trapped by the reticuloendothelial system (RES), causing accumulation in these organs, whereas smaller particles are normally filtered and/or excreted by the kidney.[52] Therefore, the size of nanoparticles must be fine-tuned to obtain adequate biodistribution. Nanoparticles may

also be functionalised with PEG groups, to avoid non-specific adsorption of biomaterials and evade recognition by macrophages and RES.[53] They may be functionalised with active targeting groups, such as antibodies (e.g. EGFR receptors, which are over-expressed on a variety of cancer cell types),[54] peptides such as RGD to target integrin receptors,[55] or small molecules such as folic acid (folic acid receptors are upregulated in many cancer types).[56]

The unique optical absorption properties of gold nanorods (AuNRs), enable absorption of near infrared (IR) light and conversion into thermal energy. This property has been exploited for thermal degradation (hyperthermia treatment) of tumour cells, for example by Prof. Romain Quidant, ICFO (Casteldefells). They have optimised the morphology of AuNRs to be used *in vivo,* whereby the accumulation of nanorods in the tumour cells was achieved, then irradiation using IR light induced thermal destruction of the tumour cells *via* light to heat transfer of the nanorods.[57]

Initial work has also been carried out between the Nebreda and Quidant groups using NP-drug conjugates of p38α inhibitor **LY (LY-NP,** figure 3.3.2)**.** Large accumulation of gold was observed in the liver and spleen when nanrods functionalised with **LY** inhibitor were administered to mice, due to RES.[58] These results were a measure of where the NPs were located, irrespective of whether **LY** was still bound to the NP or had already dissociated. It was also suspected that inhibitor was dissociating from the nanorod during and after administration, which would cause dispersion throughout the body in a more or less equilibrated manner, and therefore losing any advantages offered by nanoparticle conjugation. This was not proven directly, as it could not be easily monitored without significantly altering the inhibitor structure to include a probe. The inhibitory effect on tumour growth was also monitored and the gold NPs showed good correlation with free **LY** inhibitor of similar concentrations. However, it should be noted that the quantification of **LY** that was initially bound to the NP before injection was an inaccurate approximation and could indeed misrepresent the true value of **LY** present, leading to erroneous results.

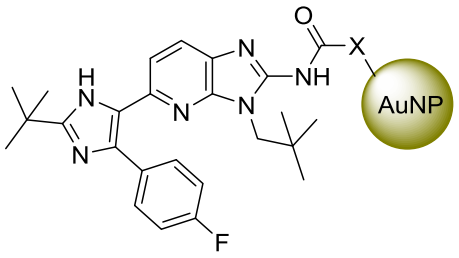

LY-NP

Figure 3.3.2. *General structural representation of* ***LY-NP*** *drug conjugate.*

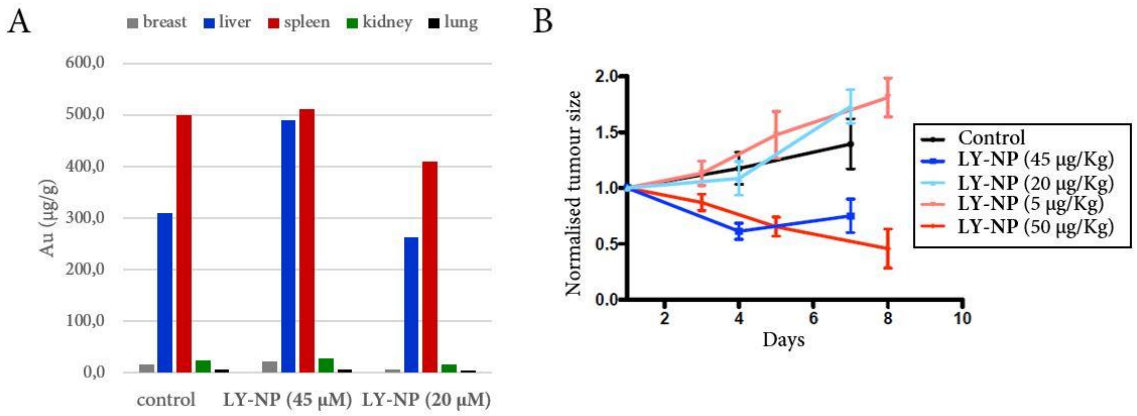

Graph 3.3.2. A) *Concentration of gold found in tissues of mouse after nanoparticle administration.* ***B)*** *Inhibitory effect on tumour growth of* ***LY*** *at 5 and 50 µg/Kg and gold nanorods functionalised with differing amounts of* ***LY****, (****LY-NP*** *20 and 45 µg/Kg). BBL PyMT TG/+ mice.*

Translation of nano-technologies into the clinic still has many hurdles, such as further improvements to biodistribution and improving the stability and effectiveness of the nano-drug conjugates, not to mention the uncertainties surrounding long term toxicology. Nevertheless, nano-drug conjugation remains an interesting field of research and can bring particular advantages over traditional inhibitors in certain cases.

3.3.3. Cell Surface Receptor Recognition

An increased demand in energy and nutrients by tumour cells lead to an upregulation of many different receptors on the cell surface, which is the main way in which these cells can be distinguished from physiologically normal cells. For example, certain integrin receptors are upregulated in endothelial tumours.[59] This has been exploited in the design of drug-peptide conjugates, which bind to the overexpressed receptors, are internalised and release their active cargo (e.g. in figure 3.3.1).

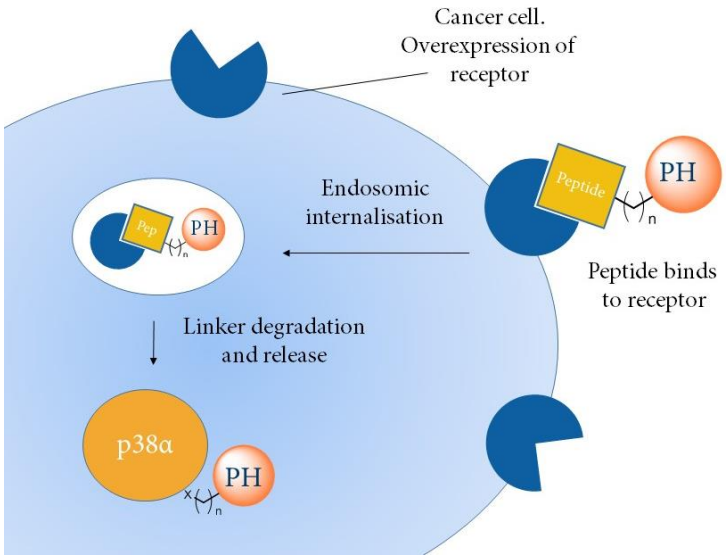

Scheme 3.3.1. *Proposed mechanism of action for peptide-drug conjugate binds to specific receptors over-expressed on cancer cells. Endosomic internalisation of complex followed by degradation of conjugate then releases the drug into the cytosol of the cell.*

3.3.3.1. Integrins and RGD

Integrins are transmembrane glycoproteins consisting of an α subunit and a β subunit, various combinations of these subunits give rise to more than 20 different heterodimeric combinations. They are involved in interactions at the extra cellular matrix (ECM), in response to various ECM proteins such as fibronectin and collagen through recognition of a common tripeptide motif (Arg-Gly-Asp, or RGD).[60] This sequence was identified in 1984 by Pierschaber & Ruoslahti and has led to the development of many analogues that can bind and antagonise the integrin family of receptors.[61] The simplest recognition sequence

that can be recognised by the integrin family is the tripeptide RGD sequence itself. This sequence cannot be varied, but amino acids can be added at either end and cyclic versions can give extra stability and gain selectivity for a certain integrin subtype.

$\alpha_v\beta_3$ integrin has a major role in angiogenesis, the process in which tumour cells acquire their own heightened blood supply, altering their vasculature to receive more nutrients needed for growth. It is expressed at heightened levels on the cell surface of endothelial tumours and has become a common target in cancer therapy *via* antagonism by RGD analogues that inhibit angiogenesis, and has also been exploited to direct drug-conjugates to the tumour environment to selectively kill tumour cells. Iodinated cRGD has been used for diagnosis and imaging of osteosarcoma tumours, which selectively accumulates in these tumours in less than 60 min.[62] Zitzmann *et al.*[63] showed FITC labelled RGD peptide bound to both tumour and tumour-endothelial cells of human xenograft mouse models after intravenous injection. Only background presence was observed in other organs, making this an excellent system for imaging and therapy. Dox-RGD conjugate was administered to mice with human breast cancer xenografts.[64] These mice outlived those that were administered with doxorubicin alone, having less primary tumour growth and metastases. It was also found to be less toxic to the heart and liver in these models. There are many more examples of integrin antagonists, imaging agents and drug-conjugates under investigation and being used in therapy.

3.3.3.2. Somatostatin Hormone (SST) and Somatostatin Receptors (SSTRs)

Another family of receptors that has been targeted in this way is known as the somatostatin receptor (SSTR) family. It is found in a wide range of tissues including the pancreas, intestine and central nervous system out with the hypothalamus.[65] Somatostatin (SST) is an endogenous hormone, also known as somatotropin release inhibiting factor (SRIF). It inhibits the secretion of growth hormone (GH) in somatotropin cells. Many analogues have been designed to inhibit SSTRs or individual members of the family sub members. SST is a 14 amino acid cyclic peptide, which suffers from a halflife of under 3 minutes in human and lacks selectivity within the family members of SST receptors.[66] Commercial analogues

include octreotide (Sandostatin®), an 8 amino acid cyclic peptide which possesses an improved affinity for SSTR-2 and has a much longer halflife (60 – 90 min in human).[67] These properties arise from strategic replacements of non-natural amino acid residues within the structure (figure 3.1.6). It is currently marketed as a treatment for a range of intestinal diseases and diabetes as well as the clinical visualisation and treatment of tumours.[68]

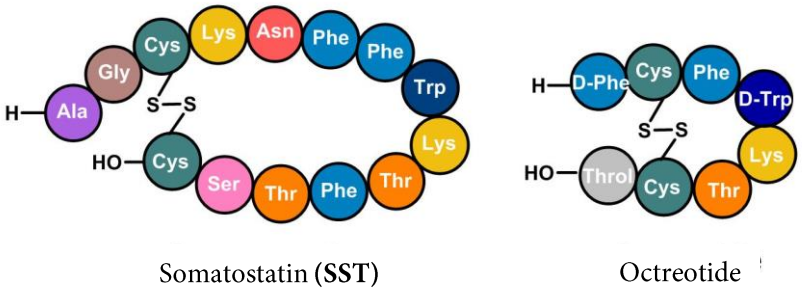

Somatostatin **(SST)** Octreotide

Figure 3.3.2. *The structures of the natural somatostatin hormone and octreotide derivative, amino acids are represented by coloured circles.*

Within the Riera group, many new analogues of SST have been designed to have higher stability or selectivity within the families. These are the same size as the natural ligand, 14 amino acid residues, and have a more rigid structure to allow better understanding of receptor binding and conformations.[69] During the thesis of Dr. Escola, she successfully used certain analogues to bind fluorescent cargos to monitor release into the targeted tissues, and also drug conjugates with **PH**.[70]

3.3.3.3. Antibody Directing Groups

Antibodies could be considered similar, as much larger, more complex and more specific versions of the peptide recognition fragments. Antibody-drug conjugates (ADCs) usually consist of potent cytotoxic compounds linked *via* biodegradable linkers to an antibody, usually by site directed mutagenesis to a cysteine or lysine residue or by genetically engineering the DNA sequence to be transcribed. The antibody has an affinity for specific antigens or receptors that are expressed on the surface of the cancer cells. The whole

antibody-drug conjugate is then internalised within the cancer cell by the endosome-lysosome pathway, where the linker is degraded by proteases and the mildly acidic environment, which releases the cytotoxic drug (figure 3.1.5). The first fully human monoclonal antibody (Mab) was approved in 2004, called Adalimumab (D2E7), for the treatment of rheumatoid arthritis (RA).[71] Since then more than 60 MAbs and ADCs have been FDA approved to treat a range of diseases, especially in cancer.[72,73]

There are also examples of bispecific antibodies that target 2 separate epitopes with each arm. For example, "Trim-away" antibodies target TRIM21 enzyme simultaneous to their target protein, causing the ubiquitination and degradation of the target protein.[74]

Major limitations of this technology include inefficient and expensive generation of these conjugates, identification and isolation usually involves a large screening array and phage display methods, a lack of efficacy in clinical models (lack of cytotoxicity), poor PK properties, a massive cost of administration, e.g. Alemtuzumab costs £37 000 annually to treat leukaemia patients.[75]

3.3.3.4. Glucose (GLUTs)

An increase in the uptake of glucose and other sugars by tumour cells compared to normal cells is one of the key differentiating factors for malignant cells.[76] This is a result of overexpression of glucose transporter (GLUT) proteins expressed on the tumour cell surface due to oncogenic mutations and changes in the tumour microenvironment.[77] The increased energy needed by cancer cells to grow and multiply causes a change from normal oxidative phosphorylation of glucose to aerobic glycolysis, a phenomenon known as the "Warburg Effect".[78,79] It has been exploited for clinical diagnosis of cancer, e.g. positron emission tomography (PET), using glucose labelled with a radioactive fluorine atom. Glycoconjugates have also been implemented to target cytotoxic drugs more specifically to the tumour cells.[80] Larger polymers of glycan particles can also be used to transport cargos with improved metabolic stability and tumour directed effect with minimal off-target reactions. These tend to have more favourable PK properties, such as better biodistribution and higher biostabilities.

3.4. Protein Degradation

3.4.1. Chemically Induced Degradation of Target Proteins

In parallel to our work in conjugating **PH** analogues to drug delivery systems, we also designed and synthesised small molecule degraders of p38α (protacs). Degradation of p38α was expected to possess several advantages over inhibition. Firstly, p38α genetic knock-out mice are embryonically lethal due to placental defects.[81] Moreover, conditional deletion of p38α in mouse embryos also leads to lethality shortly after birth as result of developmental problems in the lungs.[82] Therefore a tool compound that could induce late stage knock out would enable study of p38 and the pathway´s role in cancer therapy to a deeper level. Furthermore, there are many non-catalytic functions associated with MAPKs. Kinases that use their kinase domain in a catalytically independent manner are known as pseudokinases e.g. by allosteric regulation of other proteins, by acting as scaffolds or by direct interaction with DNA.[83] Therefore, we hypothesised that degradation of p38α would prevent any additional functions that may be leading to cell proliferation that would not be blocked by chemical inhibitors.

Protein degradation further has several immediate benefits over conventional inhibition of a target protein. For example, it does not depend on occupation of the active site of the target protein, requiring only a transient binding effect in order to initiate degradation, therefore enabling sub-stoichiometric quantities of protac to be used.[84] Furthermore, the degraded protein's function is subdued until the subsequent regeneration of the protein has taken place, which is generally much longer than in inhibition where it is limited by the off-rate of the inhibitor. A superior level of selectivity is normally observed with protein degradation, as ubiquitination is dependent upon formation of a stable ternary complex and highly sensitive to linker distance and geometries. Therefore, not all off-target interactions would result in degradation and the affinity and inhibition of the protac are significantly reduced compared to the parent inhibitor used.[85]

There are a range of methods currently employed to induce degradation of target proteins. Selective oestrogen receptor degrader (SERD), for example the drug Fulvestrant (figure 2.6.7), functions by binding to ER *via* the portion that mimics the receptor natural hormone.[86] The hydrophobicity of the long alkyl chain, fluorinated at the terminal part, disrupts the ER causing misfolding, which is then recognised by the cells repair machinery and subsequently degraded. This drug is now the standard care treatment for women with HER2 negative advanced or metastatic breast cancer (in combination with palbociclib, which targets CDK4/6 kinases). Likewise SARDs target the androgen receptor (AR) and are used to treat metastatic prostate cancer, such as UT-155.[87] Degradation of the receptor provides a greater inhibitory potency than the corresponding inhibitors approved for ER or AR.

Similarly, hydrophobic tagging (HyT) aims to mimic a partially unfolded protein state, to initiate the machinery that degrades unfolded proteins in normal functioning cells. These bifunctional molecules typically display a warhead to target the protein, linked a large hydrophobic group such as adamantine or triple boc-protected argenine, for example **Fur-Boc3Arg**.[88]

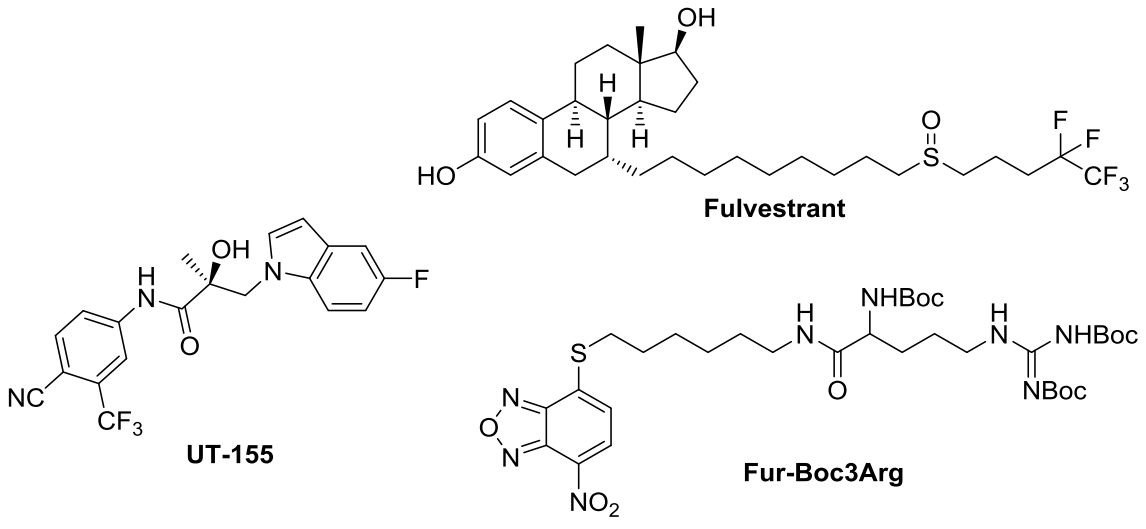

Figure 3.4.1. *Examples of protein degraders that disrupt the protein structure via hydrophobic interaction.* ***Fulvestrant*** *(SERD),* ***UT-155*** *(SARD) and Fur-Boc3Arg (HyT).*

Recently, examples of a much more robust and powerful tool to degrade proteins has generated huge interest in the medicinal chemistry and wider communities, known as protein targeting chimera, or protac.

3.4.2. Protac Technology

Proteolysis targeting chimera (Protacs) are bifunctional compounds that induce the specific degradation of a target protein using the Ubiquitin Proteasome System (UPS), hijacking enzymes that are inherent in mammalian cells. Structurally, protacs consist of a warhead on one end that specifically binds to the target protein (e.g. a small molecule inhibitor) covalently linked to an E3 ubiquitin ligase ligand (most commonly peptide recognition fragments or a thalidomide analogue). The length and composition of the covalent linkage is not trivial, as it must bring the protein and ligase in close proximity to each other and with the correct orientation to initiate a protein-protein interaction, forming a ternary complex and ultimately inducing ubiquitination of the target protein.[89] The poly-ubiquitinated protein is then degraded by the 26S proteasome. The pathway of this event-driven pharmacological process is depicted in figure 3.1.8.

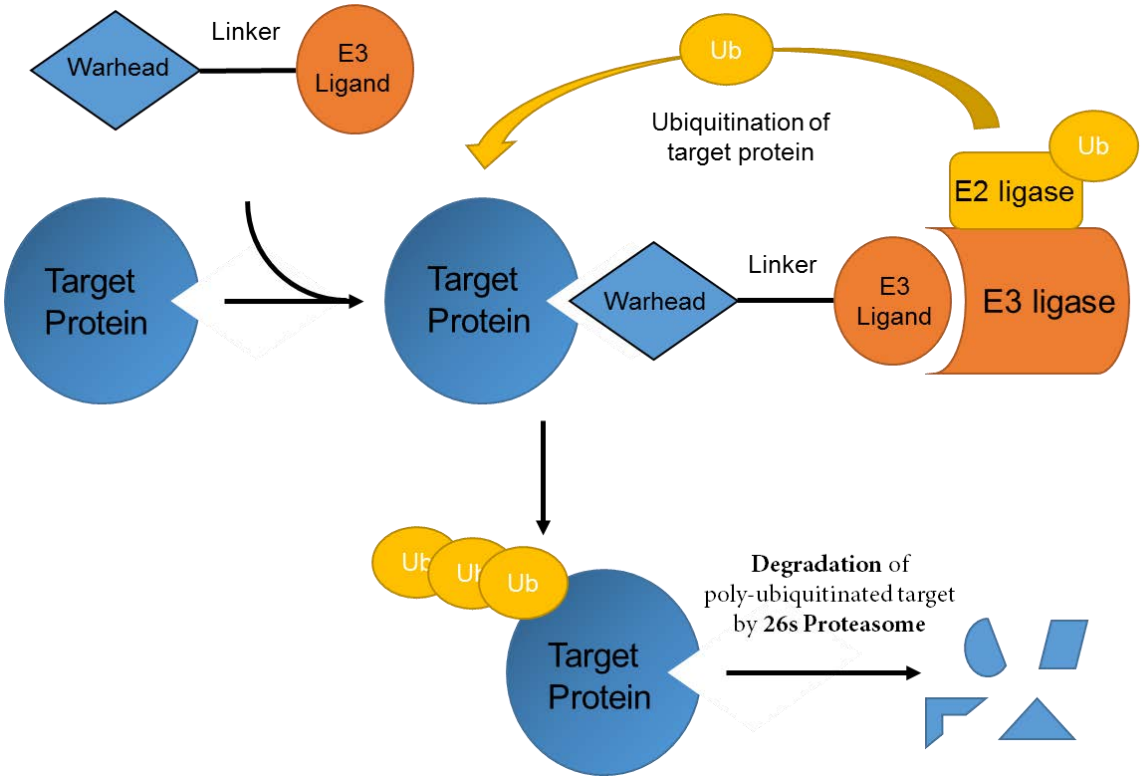

Figure 3.4.2. *Simplified cartoon of protac-induced degradation of a target protein showing poly-ubiquitination of target protein, followed by degradation of the protein by the 26S proteasome.*

There are 4 main groups of small molecule-like ligands that have been reported to initiate E3 ligases and cause the polyubiquitination of target proteins (figure 3.1.9).[84] Pomalidomide is an analogue of thalidomide, which is a ligand of CRBN E3 ligase, and has a dominating presence in recent publications. There are also detailed examples of syntheses of protacs possessing a pomalidomide functionality from commercially available starting materials. Resultant protacs have a higher likelihood of possessing drug-like properties than protacs using the larger peptide-based E3 ligase ligands.

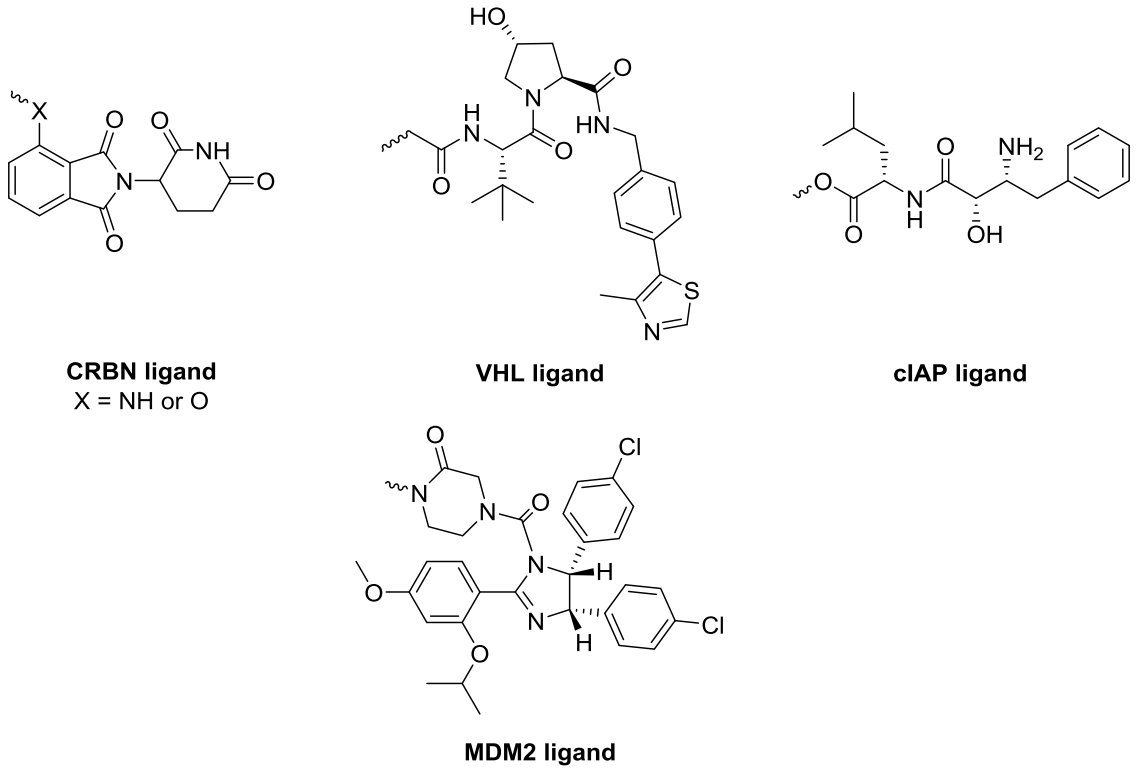

Figure 3.4.3. *The most commonly used E3 ligase-recruiting ligands. The squiggly line represents the linker attachment point. (From top left: Pomalidomide (CRBN ligand), hydroxyproline binding motif (VHL ligand), betastatin (cIAP ligand), nutlin-3a (MDM2 ligand).*

There are currently a number of protacs under development for a range of target proteins.[84] Winter reported one of the first examples of *in vivo* protein degradation, using a protac to degrade BET proteins (80%), which resulted in a reduction of tumour volume in a mouse xenograft model after 14 days.[90] Although much of the reports of protein degradation targets are predominantly *in vitro*, there are increasing examples of *in vivo* examples in the literature. A great many more unpublished information held by large pharma companies is likely to be known, as many have protac research lines such as GSK and Merck, who collaborate with academic investigators worldwide. Arvinas, (founded by Craig Crews), is set to launch 2 protac clinical trials this year.[91] Protacs will be administered to humans for the first time and the field will anticipate the first results reported of how well they are tolerated in humans. There is certainly already a lot of unpublished information about the

in vivo behaviour held confidentially by this company and others in the field, in a range of animal models.

Recent *in vivo* examples were recently reviewed by Watt *et al.* many of which target BET, but also include BTK, MDM2, ERα and ALK.[92] Reduction of the target protein varied from 39 – 80% depending on the model and dosing regimen, with up to 14 days of dosing. Reduction in tumour size was also monitored in certain cases and found to be efficacious, leading to longer survival times.[93] Tissue discrepancies were also reported, for example Zorba *et al.* reported degradation of BTK in the rat spleen but was not detected in the lung, despite comparable compound concentrations (2 – 3 μg/mL).[94] This observation reflects the differences in degradation *in vitro* between cell lines, indicating that further research is needed to better understand the action of PROTACs *in vivo.*

After the work on this project was already complete, 2 PROTAC molecules (**SJFα** and **SJFδ,** figure 2.3.10) were reported by Smith *et al.* based on a single warhead (foretinib) and recruited E3 ligase (von Hippel-Lindau).[95] By variation of the linker length and attachment to the E3 ligase, they could control the ternary complex formed during the ubiquitination to influence selectivity for either p38α or p38δ degradation. However, in a previous publication, this same family of PROTACs also efficiently degrade c-Met kinase, as well as 8 other kinase targets.[85]

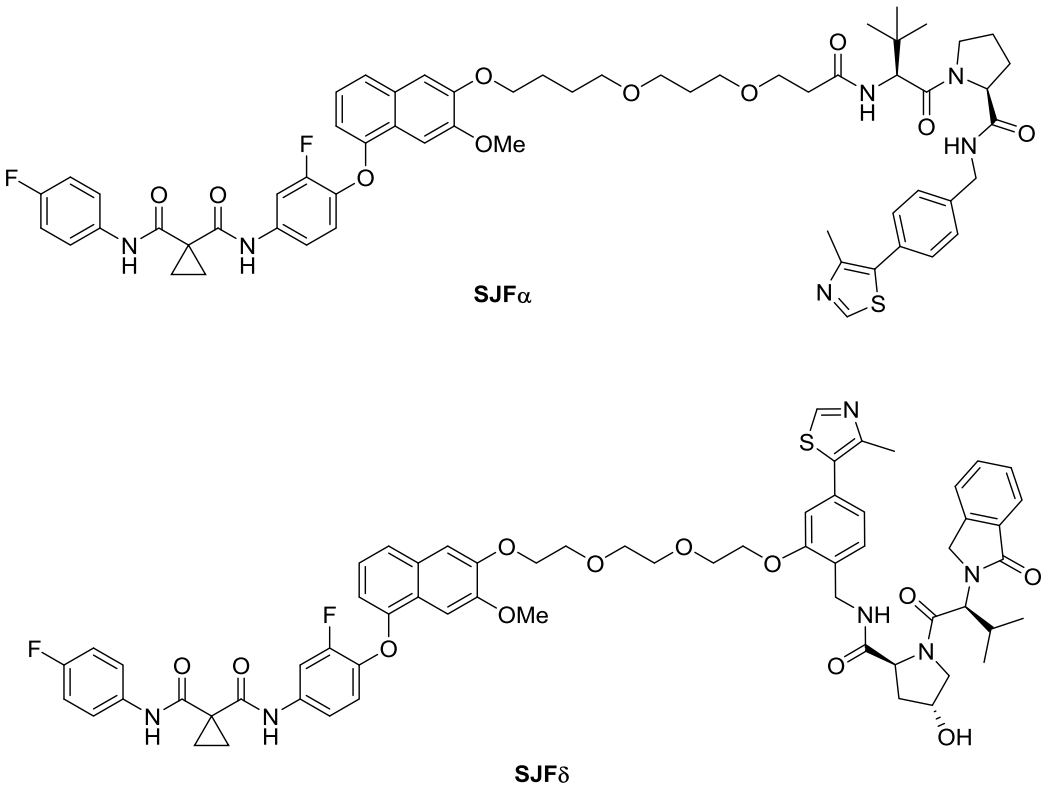

Figure 3.4.4. *Protac molecules recently published for the selective degradation of p38α (**SJFα**) and p38δ (**SJFδ**).*

The increasing number of PROTACs reported for various applications and protein targets demonstrate the enormous impact that this technology is having over several fields, and also illustrate the need for further investigation. This particular paper also highlights the importance of degradation of p38α, and a need for further biological evaluation using degradation technology to firmly establish a role in cancer or inflammatory therapy.

References

(1) Lewis, T. S.; Shapiro, P. S.; Ahn, N. G. Signal Transduction through MAP Kinase Cascades; 1998; pp 49–139. https://doi.org/10.1016/S0065-230X(08)60765-4.

(2) Coulombe, P.; Meloche, S. Atypical Mitogen-Activated Protein Kinases: Structure, Regulation and Functions. *Biochim. Biophys. Acta - Mol. Cell Res.* **2007**, *1773* (8), 1376–1387. https://doi.org/10.1016/j.bbamcr.2006.11.001.

(3) Cuenda, A.; Rousseau, S. P38 MAP-Kinases Pathway Regulation, Function and Role in Human Diseases. *Biochim. Biophys. Acta - Mol. Cell Res.* **2007**, *1773* (8), 1358–1375. https://doi.org/10.1016/j.bbamcr.2007.03.010.

(4) Pearson, G.; Robinson, F.; Beers Gibson, T.; Xu, B.; Karandikar, M.; Berman, K.; Cobb, M. H. Mitogen-Activated Protein (MAP) Kinase Pathways: Regulation and Physiological Functions 1. *Endocr. Rev.* **2001**, *22* (2), 153–183. https://doi.org/10.1210/edrv.22.2.0428.

(5) Owens, D. M.; Keyse, S. M. Differential Regulation of MAP Kinase Signalling by Dual-Specificity Protein Phosphatases. *Oncogene* **2007**, *26* (22), 3203–3213. https://doi.org/10.1038/sj.onc.1210412.

(6) Gum, R. J.; McLaughlin, M. M.; Kumar, S.; Wang, Z.; Bower, M. J.; Lee, J. C.; Adams, J. L.; Livi, G. P.; Goldsmith, E. J.; Young, P. R. Acquisition of Sensitivity of Stress-Activated Protein Kinases to the P38 Inhibitor, SB 203580, by Alteration of One or More Amino Acids within the ATP Binding Pocket. *J. Biol. Chem.* **1998**, *273* (25), 15605–15610. https://doi.org/10.1074/jbc.273.25.15605.

(7) Shi, Y.; Gaestel, M. In the Cellular Garden of Forking Paths: How P38 MAPKs Signal for Downstream Assistance. *Biol. Chem.* **2002**, *383* (10). https://doi.org/10.1515/BC.2002.173.

(8) Kyriakis, J. M.; Avruch, J. Mammalian MAPK Signal Transduction Pathways Activated by Stress and Inflammation: A 10-Year Update. *Physiol. Rev.* **2012**, *92* (2), 689–737. https://doi.org/10.1152/physrev.00028.2011.

(9) Roux, P. P.; Blenis, J. ERK and P38 MAPK-Activated Protein Kinases: A Family of Protein Kinases with Diverse Biological Functions. *Microbiol. Mol. Biol. Rev.* **2004**, *68* (2), 320–344. https://doi.org/10.1128/MMBR.68.2.320-344.2004.

(10) Böttcher, C.; Lassowskat, I.; Scheel, D.; Lee, J.; Eschen-Lippold, L. Cellular Reprogramming through Mitogen-Activated Protein Kinases. *Front. Plant Sci.* **2015**, *6* (October), 1–11. https://doi.org/10.3389/fpls.2015.00940.

(11) Bühler, S.; Laufer, S. A. P38 MAPK Inhibitors: A Patent Review (2012 – 2013). *Expert Opin. Ther. Pat.* **2014**, *24* (5), 535–554. https://doi.org/10.1517/13543776.2014.894977.

(12) Gupta, J.; del Barco Barrantes, I.; Igea, A.; Sakellariou, S.; Pateras, I. S.; Gorgoulis, V. G.; Nebreda, A. R. Dual Function of P38α MAPK in Colon Cancer: Suppression of Colitis-Associated Tumor Initiation but Requirement for Cancer Cell Survival. *Cancer Cell* **2014**, *25* (4), 484–500. https://doi.org/10.1016/j.ccr.2014.02.019.

(13) Canovas, B.; Nebreda, A. R.; Dolado, I.; Pereira, L.; Igea, A. Inhibition of P38 MAPK Sensitizes Tumour Cells to Cisplatin-Induced Apoptosis Mediated by Reactive Oxygen Species and JNK. *EMBO Mol. Med.* **2013**, *5* (11), 1759–1774. https://doi.org/10.1002/emmm.201302732.

(14) Rudalska, R.; Dauch, D.; Longerich, T.; McJunkin, K.; Wuestefeld, T.; Kang, T.-W.; Hohmeyer, A.; Pesic, M.; Leibold, J.; von Thun, A.; et al. In Vivo RNAi Screening Identifies a Mechanism of Sorafenib Resistance in Liver Cancer. *Nat. Med.* **2014**, *20* (10), 1138–1146. https://doi.org/10.1038/nm.3679.

(15) Campbell, R. M.; Anderson, B. D.; Brooks, N. A.; Brooks, H. B.; Chan, E. M.; De Dios, A.; Gilmour, R.; Graff, J. R.; Jambrina, E.; Mader, M.; et al. Characterization of LY2228820 Dimesylate, a Potent and Selective Inhibitor of P38 MAPK with Antitumor Activity. *Mol. Cancer Ther.* **2014**, *13* (2), 364–374. https://doi.org/10.1158/1535-7163.MCT-13-0513.

(16) COATES, David, A. U.; GILMOUR, R. U.; MARTIN, Jose, A. U.; MARTIN DE LA NAVA, Eva, M. OXAZOLO [5, 4 -B] PYRIDIN- 5 -YL COMPOUNDS AND THEIR USE FOR THE TREATMENT OF CANCER. WO2012074761, 2012.

(17) *Phase II Trial in Ovarian Cancer (NCT01663857)*; 2018.

(18) *A Study of Prexasertib (LY2606368) in Combination With Ralimetinib in Participants With Advanced or Metastatic Cancer (NCT02860780)*; 2016.

(19) Igea, A.; Nebreda, A. R. The Stress Kinase P38α as a Target for Cancer Therapy. *Cancer Res.* **2015**, *75* (19), 3997–4002. https://doi.org/10.1158/0008-5472.CAN-15-0173.

(20) Wu, X.; Zhang, W.; Font-Burgada, J.; Palmer, T.; Hamil, A. S.; Biswas, S. K.; Poidinger, M.; Borcherding, N.; Xie, Q.; Ellies, L. G.; et al. Ubiquitin-Conjugating Enzyme Ubc13 Controls Breast Cancer Metastasis through a TAK1-P38 MAP Kinase Cascade. *Proc. Natl. Acad. Sci.* **2014**, *111* (38), 13870–13875. https://doi.org/10.1073/pnas.1414358111.

(21) Urosevic, J.; Garcia-Albéniz, X.; Planet, E.; Real, S.; Céspedes, M. V.; Guiu, M.; Fernandez, E.; Bellmunt, A.; Gawrzak, S.; Pavlovic, M.; et al. Colon Cancer Cells Colonize the Lung from Established

Liver Metastases through P38 MAPK Signalling and PTHLH. *Nat. Cell Biol.* **2014**, *16* (7), 685–694. https://doi.org/10.1038/ncb2977.

(22) Lee, M.; Dominguez, C. MAP Kinase P38Inhibitors: Clinical Results and an Intimate Look at Their Interactions with P38a Protein. *Curr. Med. Chem.* **2005**, *12* (25), 2979–2994. https://doi.org/10.2174/092986705774462914.

(23) Selness, S. R.; Boehm, T. L.; Walker, J. K.; Devadas, B.; Durley, R. C.; Kurumbail, R.; Shieh, H.; Xing, L.; Hepperle, M.; Rucker, P. V.; et al. Design, Synthesis and Activity of a Potent, Selective Series of N-Aryl Pyridinone Inhibitors of P38 Kinase. *Bioorganic Med. Chem. Lett.* **2011**, *21* (13), 4059–4065. https://doi.org/10.1016/j.bmcl.2011.04.120.

(24) Selness, S. R.; Devraj, R. V.; Devadas, B.; Walker, J. K.; Boehm, T. L.; Durley, R. C.; Shieh, H.; Xing, L.; Rucker, P. V.; Jerome, K. D.; et al. Discovery of PH-797804, a Highly Selective and Potent Inhibitor of P38 MAP Kinase. *Bioorganic Med. Chem. Lett.* **2011**, *21* (13), 4066–4071. https://doi.org/10.1016/j.bmcl.2011.04.121.

(25) Xing, L.; Shieh, H. S.; Selness, S. R.; Devraj, R. V.; Walker, J. K.; Devadas, B.; Hope, H. R.; Compton, R. P.; Schindler, J. F.; Hirsch, J. L.; et al. Structural Bioinformatics-Based Prediction of Exceptional Selectivity of P38 MAP Kinase Inhibitor PH-797804. *Biochemistry* **2009**, *48* (27), 6402–6411. https://doi.org/10.1021/bi900655f.

(26) Xing, L.; Klug-Mcleod, J.; Rai, B.; Lunney, E. A. Kinase Hinge Binding Scaffolds and Their Hydrogen Bond Patterns. *Bioorg. Med. Chem.* **2015**, *23* (19), 6520–6527. https://doi.org/10.1016/j.bmc.2015.08.006.

(27) Hope, H. R.; Anderson, G. D.; Burnette, B. L.; Compton, R. P.; Devraj, R. V; Hirsch, J. L.; Keith, R. H.; Li, X.; Mbalaviele, G.; Messing, D. M.; et al. Anti-Inflammatory Properties of a Novel N -Phenyl Pyridinone Inhibitor of P38 Mitogen-Activated Protein Kinase : Preclinical-to-Clinical Translation. *J. Pharmacol. Exp. Ther.* **2009**, *331* (3), 882–895. https://doi.org/10.1124/jpet.109.158329.Rheumatoid.

(28) Devadas, B.; Selness, S. R.; Xing, L.; Madsen, H. M.; Marrufo, L. D.; Shieh, H.; Messing, D. M.; Yang, J. Z.; Morgan, H. M.; Anderson, G. D.; et al. Substituted N-Aryl-6-Pyrimidinones: A New Class of Potent, Selective, and Orally Active P38 MAP Kinase Inhibitors. *Bioorganic Med. Chem. Lett.* **2011**, *21* (13), 3856–3860. https://doi.org/10.1016/j.bmcl.2011.05.006.

(29) Patchornik, A.; Amit, B.; Woodward, R. B. Photosensitive Protecting Groups. *J. Am. Chem. Soc.* **1970**, *92* (21), 6333–6335. https://doi.org/10.1021/ja00724a041.

(30) Bochet, C. G. Photolabile Protecting Groups and Linkers. *J. Chem. Soc. Perkin Trans. 1* **2002**, No. 2, 125–142. https://doi.org/10.1039/b009522m.

(31) Il'ichev, Y. V.; Schwörer, M. A.; Wirz, J. Photochemical Reaction Mechanisms of 2-Nitrobenzyl Compounds: Methyl Ethers and Caged ATP. *J. Am. Chem. Soc.* **2004**, *126* (14), 4581–4595. https://doi.org/10.1021/ja039071z.

(32) Pelliccioli, A. P.; Wirz, J. Photoremovable Protecting Groups: Reaction Mechanisms and Applications. *Photochem. Photobiol. Sci.* **2002**, *1* (7), 441–458. https://doi.org/10.1039/b200777k.

(33) Kaplan, J. H.; Forbush, B.; Hoffman, J. F. Rapid Photolytic Release of Adenosine 5′-Triphosphate from a Protected Analogue: Utilization by the Na:K Pump of Human Red Blood Cell Ghosts. *Biochemistry* **1978**, *17* (10), 1929–1935. https://doi.org/10.1021/bi00603a020.

(34) Callaway, E. M.; Yuste, R. Stimulating Neurons with Light. *Curr. Opin. Neurobiol.* **2002**, *12* (5), 587–592. https://doi.org/10.1016/S0959-4388(02)00364-1.

(35) Denk, W.; Strickler, J.; Webb, W. Two-Photon Laser Scanning Fluorescence Microscopy. *Science (80-.).* **1990**, *248* (4951), 73–76. https://doi.org/10.1126/science.2321027.

(36) Nikolenko, V.; Poskanzer, K. E.; Yuste, R. Two-Photon Photostimulation and Imaging of Neural Circuits. *Nat. Methods* **2007**, *4* (11), 943–950. https://doi.org/10.1038/nmeth1105.

(37) Amatrudo, J. M.; Olson, J. P.; Lur, G.; Chiu, C. Q.; Higley, M. J.; Ellis-Davies, G. C. R. Wavelength-Selective One- and Two-Photon Uncaging of Gaba. *ACS Chem. Neurosci.* **2014**, *5* (1), 64–70. https://doi.org/10.1021/cn400185r.

(38) Shi, Y.; Koh, J. T. Light-Activated Transcription and Repression by Using Photocaged SERMs. *ChemBioChem* **2004**, *5* (6), 788–796. https://doi.org/10.1002/cbic.200300823.

(39) Ellis-Davies, G. C. R. Caged Compounds: Photorelease Technology for Control of Cellular Chemistry and Physiology. *Nat. Methods* **2007**, *4* (8), 619–628. https://doi.org/10.1038/nmeth1072.

(40) Mayer, G.; Heckel, A. Biologically Active Molecules with a "Light Switch". *Angew. Chemie Int. Ed.* **2006**, *45* (30), 4900–4921. https://doi.org/10.1002/anie.200600387.

(41) Lerch, M. M.; Hansen, M. J.; van Dam, G. M.; Szymanski, W.; Feringa, B. L. Emerging Targets in Photopharmacology. *Angew. Chemie Int. Ed.* **2016**, *55* (37), 10978–10999. https://doi.org/10.1002/anie.201601931.

(42) Szymański, W.; Beierle, J. M.; Kistemaker, H. A. V.; Velema, W. A.; Feringa, B. L. Reversible

Photocontrol of Biological Systems by the Incorporation of Molecular Photoswitches. *Chem. Rev.* **2013**, *113* (8), 6114–6178. https://doi.org/10.1021/cr300179f.

(43) Vasir, J. K.; Labhasetwar, V. Targeted Drug Delivery in Cancer Therapy. *Technol. Cancer Res. Treat.* **2005**, *4* (4), 363–374. https://doi.org/10.1177/153303460500400405.

(44) D'Mello, S. R.; Cruz, C. N.; Chen, M.-L.; Kapoor, M.; Lee, S. L.; Tyner, K. M. The Evolving Landscape of Drug Products Containing Nanomaterials in the United States. *Nat. Nanotechnol.* **2017**, *12* (6), 523–529. https://doi.org/10.1038/nnano.2017.67.

(45) Bobo, D.; Robinson, K. J.; Islam, J.; Thurecht, K. J.; Corrie, S. R. Nanoparticle-Based Medicines: A Review of FDA-Approved Materials and Clinical Trials to Date. *Pharm. Res.* **2016**, *33* (10), 2373–2387. https://doi.org/10.1007/s11095-016-1958-5.

(46) Nel, A. E.; Mädler, L.; Velegol, D.; Xia, T.; Hoek, E. M. V; Somasundaran, P.; Klaessig, F.; Castranova, V.; Thompson, M. Understanding Biophysicochemical Interactions at the Nano-Bio Interface. *Nat. Mater.* **2009**, *8* (7), 543–557. https://doi.org/10.1038/nmat2442.

(47) Jiang, W.; Kim, B. Y. S.; Rutka, J. T.; Chan, W. C. W. Nanoparticle-Mediated Cellular Response Is Size-Dependent. *Nat. Nanotechnol.* **2008**, *3* (3), 145–150. https://doi.org/10.1038/nnano.2008.30.

(48) Rodríguez-González, B.; Mulvaney, P.; Liz-Marzán, L. M. An Electrochemical Model for Gold Colloid Formation via Citrate Reduction. *Zeitschrift fur Phys. Chemie* **2007**, *221* (3), 415–426. https://doi.org/10.1524/zpch.2007.221.3.415.

(49) Maeda, H.; Matsumura, Y. A New Concept for Macromolecular Therapeutics in Cancer Chemotherapy: Mechanism of Tumoritropic Accumulation of Proteins and the Antitumor Agent Smancs. *Cancer Res.* **1986**, *46* (12 Pt 1), 6387–6392. https://doi.org/10.1021/bc100070g.

(50) Hanahan, D.; Weinberg, R. A. The Hallmarks of Cancer. *Cell* **2000**, *100* (1), 57–70. https://doi.org/10.1016/S0092-8674(00)81683-9.

(51) Nakamura, Y.; Mochida, A.; Choyke, P. L.; Kobayashi, H. Nanodrug Delivery: Is the Enhanced Permeability and Retention Effect Sufficient for Curing Cancer? *Bioconjug. Chem.* **2016**, *27* (10), 2225–2238. https://doi.org/10.1021/acs.bioconjchem.6b00437.

(52) Kobayashi, H.; Brechbiel, M. W. Nano-Sized MRI Contrast Agents with Dendrimer Cores. *Adv. Drug Deliv. Rev.* **2005**, *57* (15), 2271–2286. https://doi.org/10.1016/j.addr.2005.09.016.

(53) Niidome, T.; Yamagata, M.; Okamoto, Y.; Akiyama, Y.; Takahashi, H.; Kawano, T.; Katayama, Y.; Niidome, Y. PEG-Modified Gold Nanorods with a Stealth Character for in Vivo Applications. *J.*

Control. Release **2006**, *114* (3), 343–347. https://doi.org/10.1016/j.jconrel.2006.06.017.

(54) El-Sayed, I. H.; Huang, X.; El-Sayed, M. A. Selective Laser Photo-Thermal Therapy of Epithelial Carcinoma Using Anti-EGFR Antibody Conjugated Gold Nanoparticles. *Cancer Lett.* **2006**, *239* (1), 129–135. https://doi.org/10.1016/j.canlet.2005.07.035.

(55) Wu, P. H.; Onodera, Y.; Ichikawa, Y.; Rankin, E. B.; Giaccia, A. J.; Watanabe, Y.; Qian, W.; Hashimoto, T.; Shirato, H.; Nam, J. M. Targeting Integrins with RGD-Conjugated Gold Nanoparticles in Radiotherapy Decreases the Invasive Activity of Breast Cancer Cells. *Int. J. Nanomedicine* **2017**, *12*, 5069–5085. https://doi.org/10.2147/IJN.S137833.

(56) Dixit, V.; Van Den Bossche, J.; Sherman, D. M.; Thompson, D. H.; Andres, R. P. Synthesis and Grafting of Thioctic Acid-PEG-Folate Conjugates onto Au Nanoparticles for Selective Targeting of Folate Receptor-Positive Tumor Cells. *Bioconjug. Chem.* **2006**, *17* (3), 603–609. https://doi.org/10.1021/bc050335b.

(57) Morales-Dalmau, J.; Vilches, C.; De Miguel, I.; Sanz, V.; Quidant, R. Optimum Morphology of Gold Nanorods for Light-Induced Hyperthermia. *Nanoscale* **2018**, *10* (5), 2632–2638. https://doi.org/10.1039/c7nr06825e.

(58) Maeda, H. Tumor-Selective Delivery of Macromolecular Drugs via the EPR Effect: Background and Future Prospects. *Bioconjug. Chem.* **2010**, *21* (5), 797–802. https://doi.org/10.1021/bc100070g.

(59) Avraamides, C. J.; Garmy-Susini, B.; Varner, J. A. Integrins in Angiogenesis and Lymphangiogenesis. *Nat. Rev. Cancer* **2008**, *8* (8), 604–617. https://doi.org/10.1038/nrc2353.

(60) Ruoslahti, E. Rgd and Other Recognition Sequences for Integrins. *Annu. Rev. Cell Dev. Biol.* **2002**, *12* (1), 697–715. https://doi.org/10.1146/annurev.cellbio.12.1.697.

(61) Pierschbacher, M. D.; Ruoslahti, E. Cell Attachment Activity of Fibronectin Can Be Duplicated by Small Synthetic Fragments of the Molecule. *Nature* **1984**, *309* (5963), 30–33. https://doi.org/10.1038/309030a0.

(62) Haubner, R.; Wester, H.-J.; Reuning, U.; Senekowitsch-Schmidtke, R.; Diefenbach, B.; Kessler, H.; Stöcklin, G.; Schwaiger, M. Radiolabeled Avβ3 Integrin Antagonists: A New Class of Tracers for Tumor Targeting. *J. Nucl. Med.* **1999**, *40* (6), 1061–1071.

(63) Zitzmann, S.; Ehemann, V.; Schwab, M. Arginine-Glycine-Aspartic Acid (RGD)-Peptide Binds to Both Tumor and Tumor-Endothelial Cells in Vivo. *Cancer Res.* **2002**, *62* (18), 5139–5143.

(64) Arap, W.; Pasqualini, R.; Ruoslahti, E. Cancer Treatment by Targeted Drug Delivery to Tumor

Vasculature in a Mouse Model Cancer Treatment by Targeted Drug Delivery to Tumor Vasculature in a Mouse Model. *Science (80-.).* **2012**, *377* (1998), 377–380. https://doi.org/10.1126/science.279.5349.377.

(65) Tousson, E.; Abou-easa, K. Increase in Somatostatin Immunoreactivity in the Organotypic Slice Culture of Mouse Hypothalamic Suprachiasmatic Nucleus. **2010**, *6* (1), 91–98.

(66) Reubi, J. C. Peptide Receptors as Molecular Targets for Cancer Diagnosis and Therapy. *Endocr. Rev.* **2003**, *24* (4), 389–427. https://doi.org/10.1210/er.2002-0007.

(67) Hsieh, H. P.; Wu, Y. T.; Chen, S. T.; Wang, K. T. Direct Solid-Phase Synthesis of Octreotide Conjugates: Precursors for Use as Tumor-Targeted Radiopharmaceuticals. *Bioorganic Med. Chem.* **1999**, *7* (9), 1797–1803. https://doi.org/10.1016/S0968-0896(99)00125-X.

(68) Weckbecker, G.; Liu, R.; Tolcsvai, L.; Brans, C. Antiproliferative Effects of the Somatostatin Analogue Octreotide (SMS 201-995) on ZR-75-1 Human Breast Cancer Cells in Vivo and in Vitro. *Cancer Res.* **1992**, *52* (18), 4973–4978.

(69) Martín-gago, P.; Ramón, R.; Aragón, E.; Fernández-carneado, J.; Martin-malpartida, P.; Verdaguer, X.; López-ruiz, P.; Colás, B.; Alicia, M.; Ponsati, B.; et al. Bioorganic & Medicinal Chemistry Letters A Tetradecapeptide Somatostatin Dicarba-Analog : Synthesis , Structural Impact and Biological Activity. **2014**, *24*, 103–107. https://doi.org/10.1016/j.bmcl.2013.11.065.

(70) Escolà Jané, A. Somatostatin Analogues as Drug Delivery Systems for Receptor-Targeted Cancer Therapy, Universitat de Barcelona, 2018.

(71) Kempeni, J. Preliminary Results of Early Clinical Trials with the Fully Human Anti-TNFalpha Monoclonal Antibody D2E7. *Ann. Rheum. Dis.* **2008**, *58* (Supplement 1), i70–i72. https://doi.org/10.1136/ard.58.2008.i70.

(72) S., S.; N.K., T.; P., D.; J., C.; R., K.; P., S.; V.K., C. Monoclonal Antibodies: A Review. *Curr. Clin. Pharmacol.* **2018**, *13* (2), 85–99. https://doi.org/10.2174/1574884712666170809124728.

(73) Sievers, E. L.; Senter, P. D. Antibody-Drug Conjugates in Cancer Therapy. *Annu. Rev. Med.* **2013**, *64* (1), 15–29. https://doi.org/10.1146/annurev-med-050311-201823.

(74) Clift, D.; McEwan, W. A.; Labzin, L. I.; Konieczny, V.; Mogessie, B.; James, L. C.; Schuh, M. A Method for the Acute and Rapid Degradation of Endogenous Proteins. *Cell* **2017**, *171* (7), 1692-1706.e18. https://doi.org/10.1016/j.cell.2017.10.033.

(75) A.F., S. Monoclonal Antibodies: Magic Bullets with a Hefty Price Tag. *BMJ* **2012**, *345* (7887), 10–12.

https://doi.org/10.1136/bmj.e8346.

(76) Airley, R. E.; Mobasheri, A. Hypoxic Regulation of Glucose Transport, Anaerobic Metabolism and Angiogenesis in Cancer: Novel Pathways and Targets for Anticancer Therapeutics. *Chemotherapy* **2007**, *53* (4), 233–256. https://doi.org/10.1159/000104457.

(77) Chen, Z.; Lu, W.; Garcia-Prieto, C.; Huang, P. The Warburg Effect and Its Cancer Therapeutic Implications. *J. Bioenerg. Biomembr.* **2007**, *39* (3), 267–274. https://doi.org/10.1007/s10863-007-9086-x.

(78) Warburg, O. On the Origin of Cancer Cells. *Science (80-.).* **1956**, *123* (3191), 309–314. https://doi.org/10.1126/science.123.3191.309.

(79) Vander Heiden, M. G.; Cantley, L. C.; Thompson, C. B. Understanding the Warburg Effect: The Metabolic Requirements of Cell Proliferation. *Science (80-.).* **2009**, *324* (5930), 1029–1033. https://doi.org/10.1126/science.1160809.

(80) Monsigny, M.; Roche, A.-C.; Kieda, C.; Midoux, P.; Obrénovitch, A. Characterization and Biological Implications of Membrane Lectins in Tumor, Lymphoid and Myeloid Cells. *Biochimie* **1988**, *70* (11), 1633–1649. https://doi.org/10.1016/0300-9084(88)90299-4.

(81) Adams, R. H.; Porras, A.; Alonso, G.; Jones, M.; Vintersten, K.; Panelli, S.; Valladares, A.; Perez, L.; Klein, R.; Nebreda, A. R. Essential Role of P38α MAP Kinase in Placental but Not Embryonic Cardiovascular Development. *Mol. Cell* **2000**, *6* (1), 109–116. https://doi.org/10.1016/S1097-2765(05)00014-6.

(82) Hui, L.; Bakiri, L.; Mairhorfer, A.; Schweifer, N.; Haslinger, C.; Kenner, L.; Komnenovic, V.; Scheuch, H.; Beug, H.; Wagner, E. F. P38α Suppresses Normal and Cancer Cell Proliferation by Antagonizing the JNK-c-Jun Pathway. *Nat. Genet.* **2007**, *39* (6), 741–749. https://doi.org/10.1038/ng2033.

(83) Jacobsen, A. V.; Murphy, J. M. The Secret Life of Kinases: Insights into Non-Catalytic Signalling Functions from Pseudokinases. *Biochem. Soc. Trans.* **2017**, *45* (3), 665–681. https://doi.org/10.1042/BST20160331.

(84) Lai, A. C.; Crews, C. M. Induced Protein Degradation: An Emerging Drug Discovery Paradigm. *Nat. Rev. Drug Discov.* **2017**, *16* (2), 101–114. https://doi.org/10.1038/nrd.2016.211.

(85) Bondeson, D. P.; Smith, B. E.; Burslem, G. M.; Buhimschi, A. D.; Hines, J.; Jaime-Figueroa, S.; Wang, J.; Hamman, B. D.; Ishchenko, A.; Crews, C. M. Lessons in PROTAC Design from Selective Degradation with a Promiscuous Warhead. *Cell Chem. Biol.* **2018**, *25* (1), 78-87.e5.

https://doi.org/10.1016/j.chembiol.2017.09.010.

(86) Boér, K. Fulvestrant in Advanced Breast Cancer: Evidence to Date and Place in Therapy. *Ther. Adv. Med. Oncol.* **2017**, *9* (7), 465–479. https://doi.org/10.1177/1758834017711097.

(87) Ponnusamy, S.; Coss, C. C.; Thiyagarajan, T.; Watts, K.; Hwang, D.; He, Y.; Selth, L. A.; McEwan, I. J.; Duke, C. B.; Pagadala, J.; et al. Novel Selective Agents for the Degradation of Androgen Receptor Variants to Treat Castration-Resistant Prostate Cancer. *Cancer Res.* **2017**, *77* (22), 6282–6298. https://doi.org/10.1158/0008-5472.CAN-17-0976.

(88) Long, M. J. C.; Gollapalli, D. R.; Hedstrom, L. Inhibitor Mediated Protein Degradation. *Chem. Biol.* **2012**, *19* (5), 629–637. https://doi.org/10.1016/j.chembiol.2012.04.008.

(89) Cyrus, K.; Wehenkel, M.; Choi, E.-Y.; Han, H.-J.; Lee, H.; Swanson, H.; Kim, K.-B. Impact of Linker Length on the Activity of PROTACs. *Mol. BioSyst.* **2011**, *7* (2), 359–364. https://doi.org/10.1039/C0MB00074D.

(90) Winter, G. E.; Buckley, D. L.; Paulk, J.; Roberts, J. M.; Souza, A.; Dhe-Paganon, S.; Bradner, J. E. Phthalimide Conjugation as a Strategy for in Vivo Target Protein Degradation. *Science (80-.).* **2015**, *348* (6241), 1376–1381. https://doi.org/10.1126/science.aab1433.

(91) Guo, J.; Liu, J.; Wei, W. Degrading Proteins in Animals: "PROTAC"Tion Goes in Vivo. *Cell Res.* **2019**, *29* (3), 179–180. https://doi.org/10.1038/s41422-019-0144-9.

(92) Watt, G. F.; Scott-Stevens, P.; Gaohua, L. Targeted Protein Degradation in Vivo with Proteolysis Targeting Chimeras: Current Status and Future Considerations. *Drug Discov. Today Technol.* **2019**, *xxx* (xx). https://doi.org/10.1016/j.ddtec.2019.02.005.

(93) Zhang, X.; Lee, H. C.; Shirazi, F.; Baladandayuthapani, V.; Lin, H.; Kuiatse, I.; Wang, H.; Jones, R. J.; Berkova, Z.; Singh, R. K.; et al. Protein Targeting Chimeric Molecules Specific for Bromodomain and Extra-Terminal Motif Family Proteins Are Active against Pre-Clinical Models of Multiple Myeloma. *Leukemia* **2018**, *32* (10), 2224–2239. https://doi.org/10.1038/s41375-018-0044-x.

(94) Garcia-Irrizary, C. N.; Chang, J. S.; Xu, Y.; Luthra, S.; Zorba, A.; Zhu, H.; Niosi, M.; Shah, J. C.; Nguyen, C.; Czabaniuk, L.; et al. Delineating the Role of Cooperativity in the Design of Potent PROTACs for BTK. *Proc. Natl. Acad. Sci.* **2018**, *115* (31), E7285–E7292. https://doi.org/10.1073/pnas.1803662115.

(95) Smith, B. E.; Wang, S. L.; Jaime-Figueroa, S.; Harbin, A.; Wang, J.; Hamman, B. D.; Crews, C. M. Differential PROTAC Substrate Specificity Dictated by Orientation of Recruited E3 Ligase. *Nat.*

Commun. **2019**, *10* (1), 1–13. https://doi.org/10.1038/s41467-018-08027-7.

Chapter 4

Synthesis and Biological Evaluation of Compounds Targeting p38α

4.1. Synthesis and Biological Activity of Novel Analogues of PH

As described in section 3.1, **PH** is a highly useful p38 inhibitor developed by Pfizer with proven activity in a number of functional assays, *in vivo* models and phase II clinical trials in humans. Speculative reasons as to why this drug (and many others) were not continued into the clinical market are its low efficacy in humans against inflammatory diseases and side-effects including skin rash and liver toxicity.[1] In collaboration with the Nebreda research group, our aim was to further optimise this compound for selective delivery to tumour tissue to target cancer. Targeted delivery would liberate a higher concentration of the active drug into the tumours to increase efficacy, and less drug would be present in surrounding tissues to reduce side-effects. After identification of suitable analogues, they would be conjugated to appropriate directing groups, such as gold nanorods and peptide recognition fragments. The resulting drug-conjugates would then be tested in cellular assays and the most active of these would also be tested in *in vivo* models to assess their therapeutic value.

4.1.1. Design and Synthesis of New **PH** Analogues

The key interactions and SAR studies outlined in section 3.1.5 guided the identification of the methyl amide moiety as a starting point for substitution. This moiety was not only amenable for extension and further functionalisation, but also resided in the solvent exposed region of the ATP binding site of p38 when the inhibitor is bound. Therefore, conjugation of a large directing group to this moiety was least likely to interfere with the affinity of the PH-based analogue.

We therefore designed a small collection of compounds based on **PH** to carry out a SAR study about the methyl amide functionality. We investigated extensions of the methyl

group to short alkyl chains and additional functionalities that were tractable to conjugation of directing groups (figure 4.1.1).

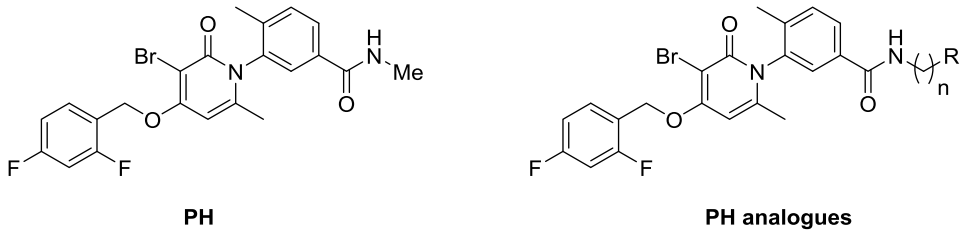

***Figure 4.1.1. PH** and proposed new analogues with longer chain amides (n = 2 – 5) and extra functional handles (R = OH, NH_2, COOH, etc.).*

PH is a well-studied compound and there existed a range of syntheses for its preparation. A patent procedure reported by Dukeshereer *et al.*[2] obtained **PH** in a high yield (35%) in 5 straightforward steps. The procedure had been optimised to be carried out on kilogram scale, therefore avoided the use of column chromatography or other such limiting techniques. We prepared an initial batch of **PH** by modifying this route to obtain a 10 g of final compound, and 40 g of acid intermediate **4-7** (scheme 4.1.1). The two atropoisomers were not separated by chiral chromatography as the mixture of the 2 is biologically active (despite one atropoisomer being less potent). Furthermore, separation is costly and time-consuming and the interconversion may take place during the final reaction steps of our derivatives or after administration *in vivo*. The activity of our newly synthesised sample exactly matched that of the commercial sample when tested in the standard cellular and kinase assays used in the Nebreda lab.

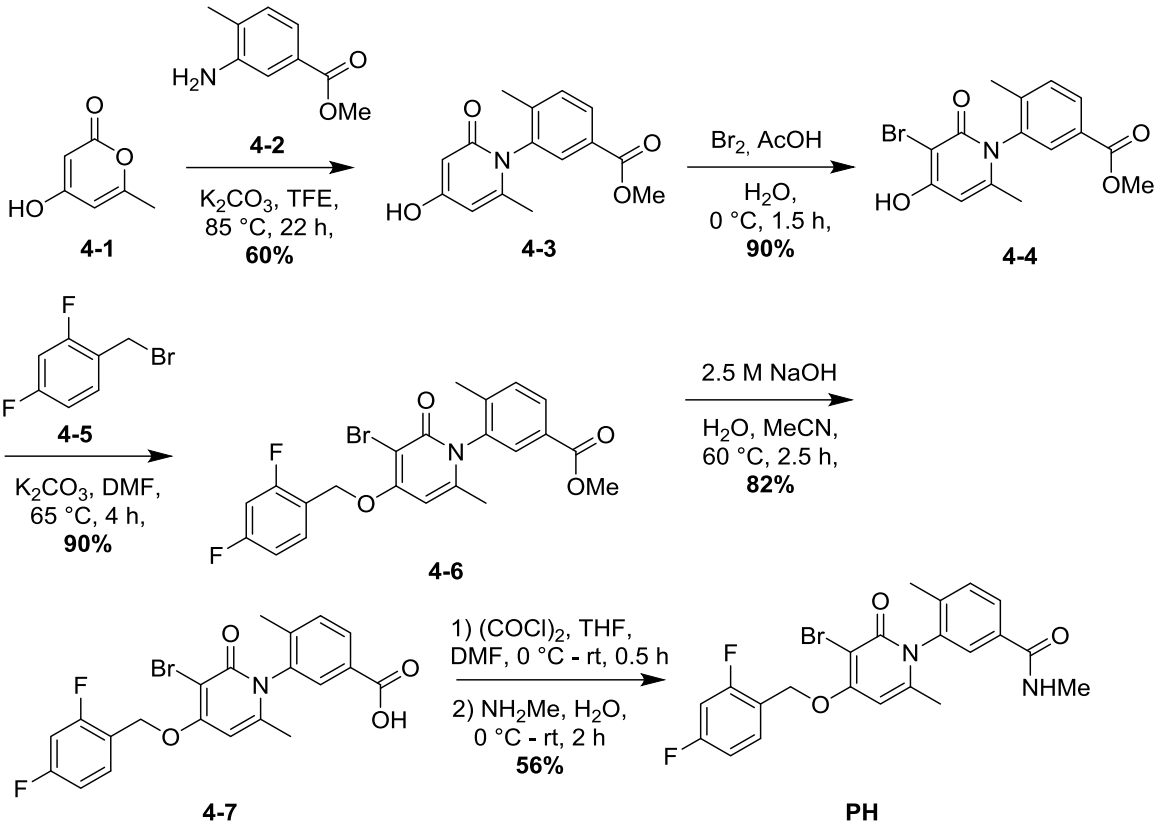

Scheme 4.1.1. *Synthetic route towards* ***PH****, optimised for large scale synthesis.*

The acid intermediate **4-7** provided a crucial diversification point for the synthesis of further analogues. The activity of **4-7** was also examined in cellular and *in vitro* kinase assays (figure 4.1.2).

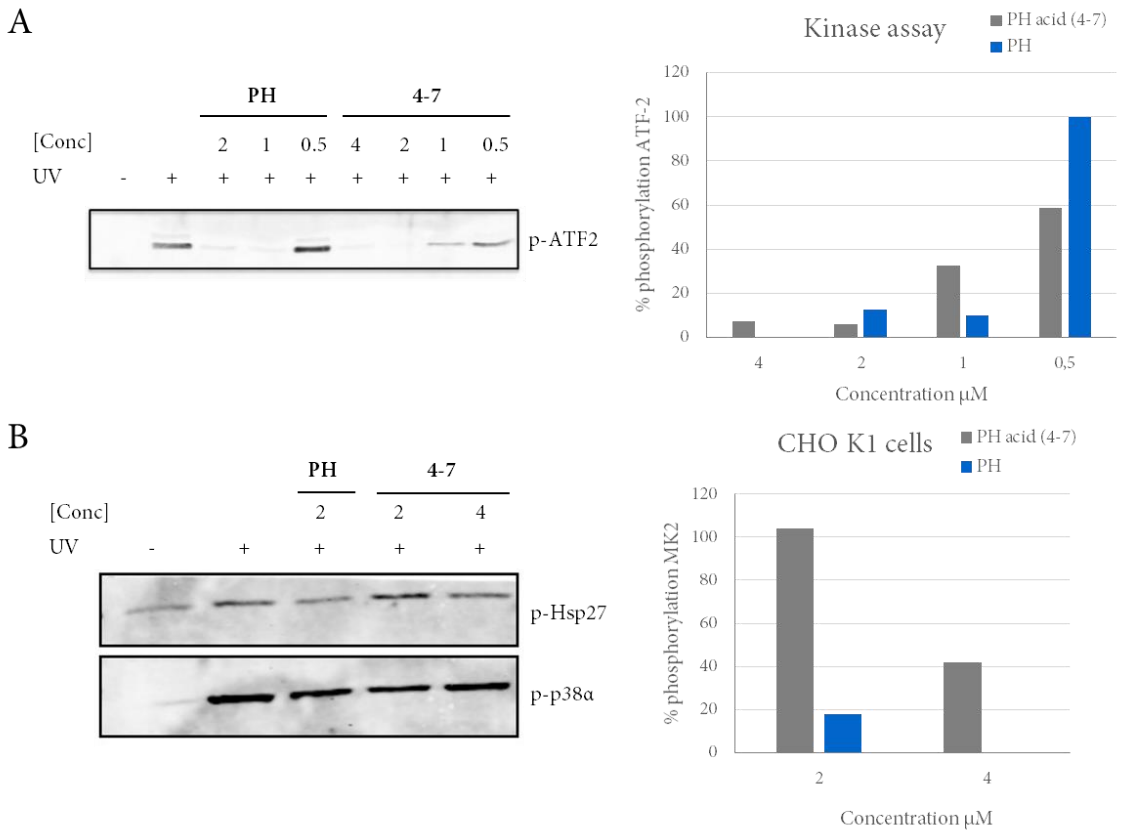

Figure 4.1.2. *PH vs PHacid* ***4-7****. P38 MAPK, ATF2 activation assay, and p-Hsp27 activation in chinese hamster ovary (CHO) cells.*

As can be seen in figure 4.1.2, the affinity for p38α of carboxylic acid **4-7** was found to be ~2 fold less than **PH** in the *in vitro* kinase assay, and much less inhibition was observed in the cellular assay (about 5x less). There is probably some affinity loss due to the polar carboxylic acid group, which is amplified in the cellular assay because of reduced cellular penetration of the inhibitor. This highlighted the importance of the amide group as the acid moiety was not well tolerated in this position, therefore our resulting analogues all featured an amide moiety.

We next began optimising this amide moiety by extending the methyl substituent into longer alkyl chains, and also decorating this substituent with a variety of functional groups, such as ester, acid, amino acid, amine and alcohol moieties (figure 4.1.3).

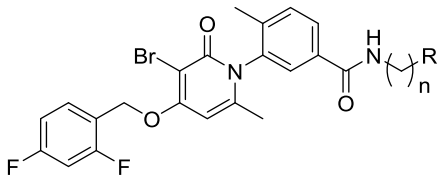

PH analogues

n	R	Name	n	R	Name
0	H	**4-8**	**3**	NH_2	**4-13a**
1	COOMe	**4-9a**	**3**	N_3	**4-14**
1	COOH	**4-9b**	**4**	OH	**4-15**
1	2,2-dimethyl-1,3-dioxolane	**4-10**	**4**	NH_2	**4-16**
2	OH	**4-11**	**4**	C(NHBoc)COOMe	**4-17a**
3	OH	**4-12a**	**4**	$C(NH_2)COOH$	**4-17b**

Figure 4.1.3. *Synthesis of **PH** and the collection of subsequent analogues synthesised, **4-8** – **4-17**.*

Compounds were synthesised from acid intermediate **4-7** by forming the acid chloride then substitution reaction with the appropriate amine, akin to the synthesis of **PH** (scheme 4.1.2).

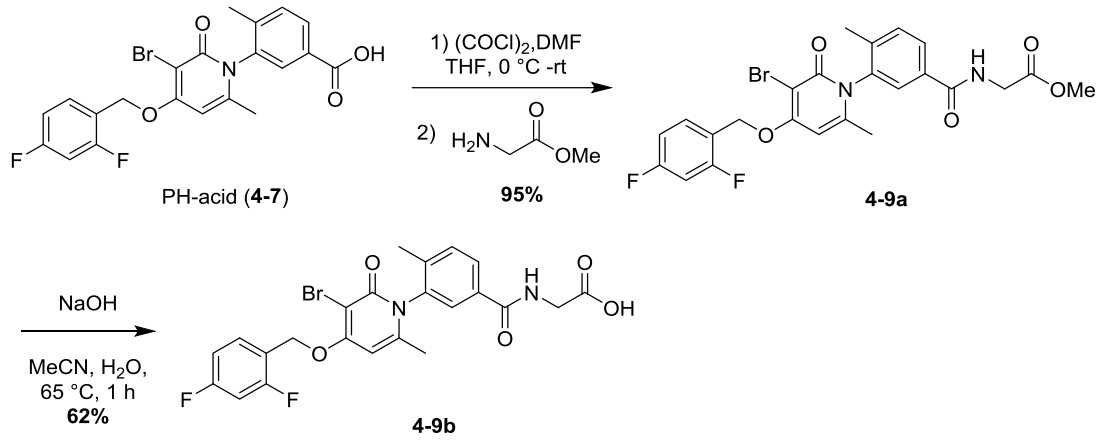
1) (COCl)2,DMF
THF, 0 °C -rt
2)
95%
PH-acid (4-7)
4-9a
NaOH
MeCN, H2O,
65 °C, 1 h
62%
4-9b

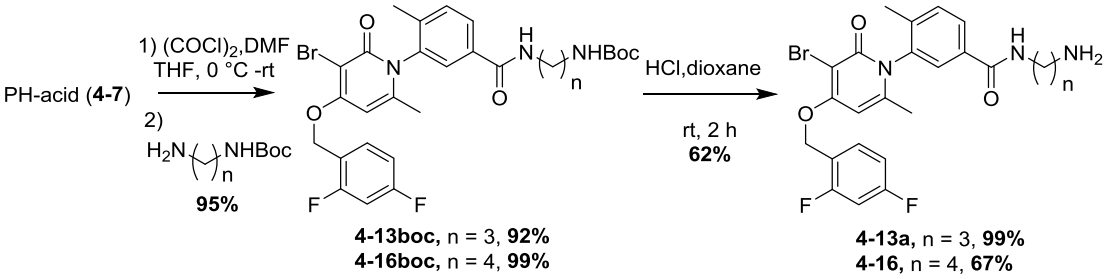
PH-acid (4-7)
1) (COCl)2,DMF
THF, 0 °C -rt
2)
95%
HCl,dioxane
rt, 2 h
62%
4-13boc, n = 3, 92%
4-16boc, n = 4, 99%
4-13a, n = 3, 99%
4-16, n = 4, 67%

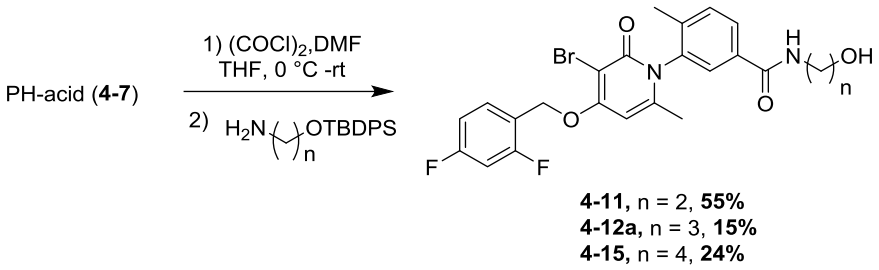
PH-acid (4-7)
1) (COCl)2,DMF
THF, 0 °C -rt
2)
4-11, n = 2, 55%
4-12a, n = 3, 15%
4-15, n = 4, 24%

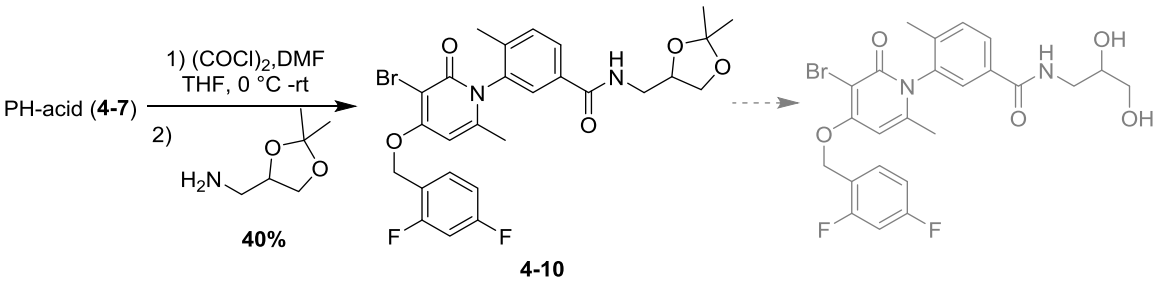
PH-acid (4-7)
1) (COCl)2,DMF
THF, 0 °C -rt
2)
40%
4-10

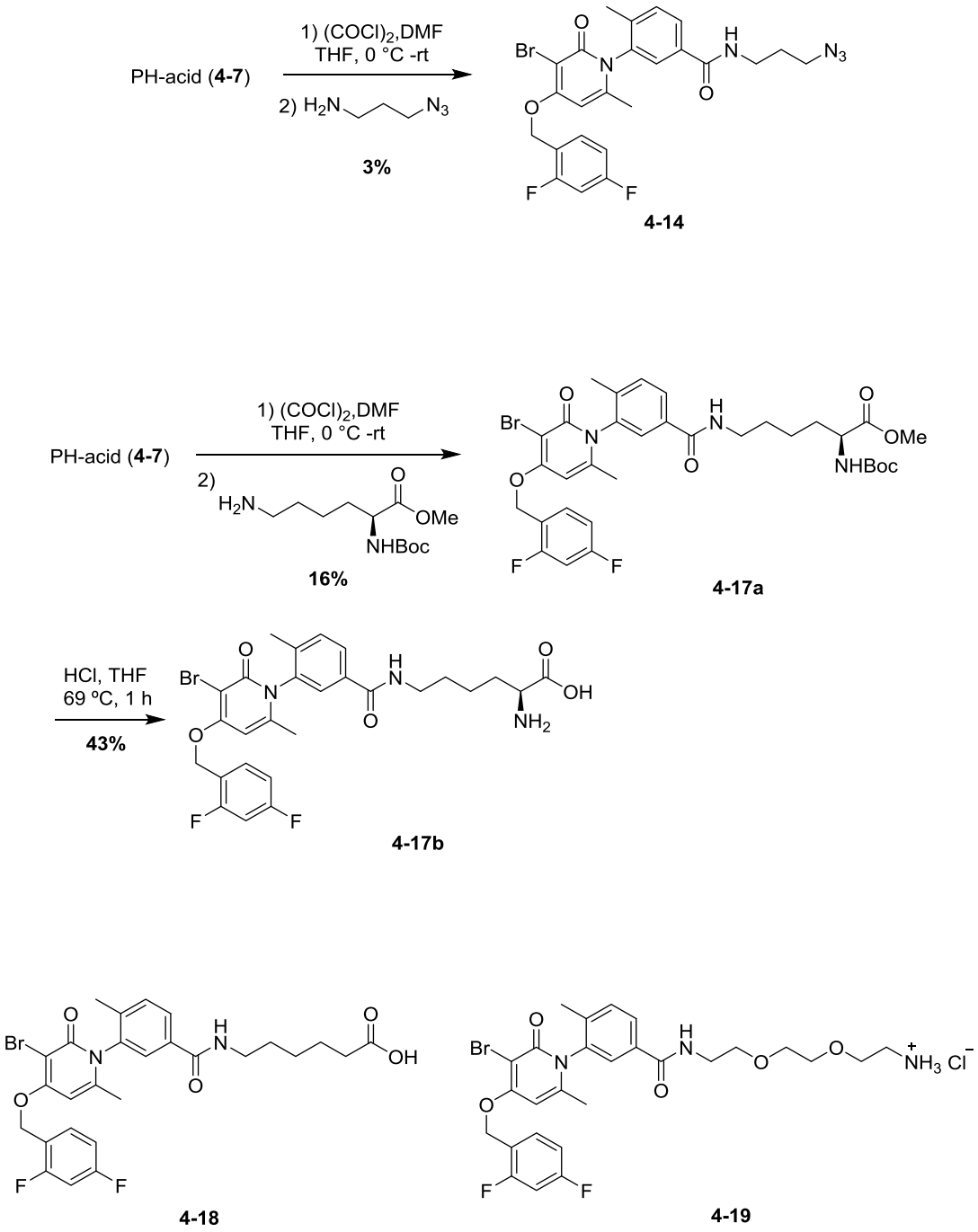

Scheme 4.1.2. *Syntheses of novel p38α inhibitors based on the core structure of* ***PH****, starting from acid intermediate* ***4-7.***

Isolation of **PH** on a large scale was straightforward by precipitation and filtration, however, low yields were obtained when these reaction conditions were repeated using longer amines to synthesise new analogues **4-8 – 4-19** on a much smaller scale. It was assumed that competitive nucleophilic attack by water and the presence of additional functional groups

were to blame for the lower yields, combined with a more challenging isolation of the product. Differing solubilities of these new analogues led to the formation of a gum upon quenching with water, which meant products had to be extracted using organic solvents and then purified by column chromatography. Therefore, we added the amine in anhydrous THF to the reaction instead of in aqueous solution, then carefully added the reaction mixture to water or aqueous $KHCO_3$ to quench the reaction upon completion. These anhydrous conditions improved the execution and workup of the reaction and also the yields, although in general these yields were low.

Analogues **4-9 – 4-17** were tested using a range of concentrations, in both cellular and kinase assays to compare the relative activities (figure 4.1.4). Analogues **4-8, 4-14, 4-18** and **4-19** have yet to be tested but were no longer a priority of this project and were also used as intermediates in subsequent reactions.

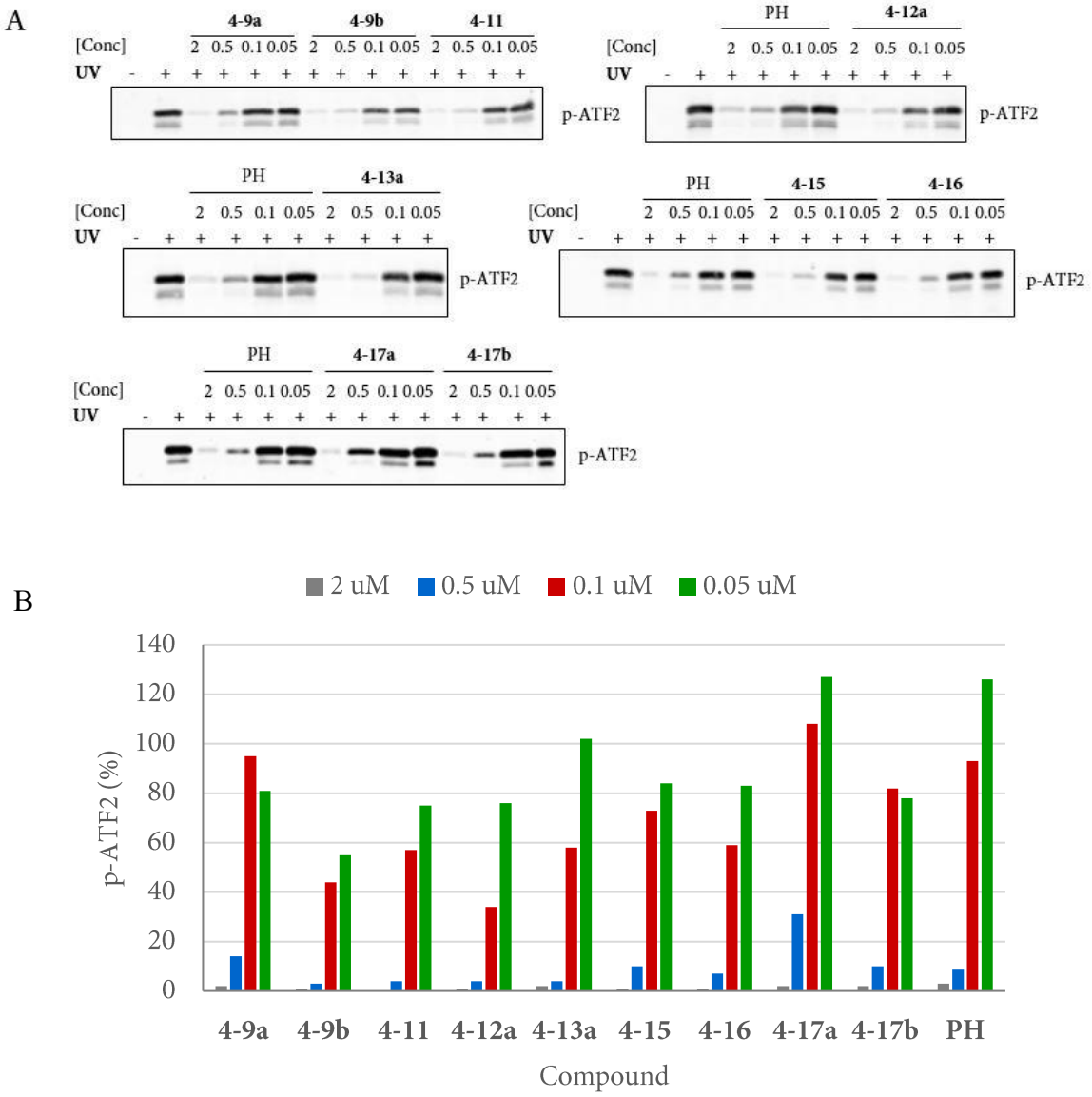

Figure 4.1.4. A) *Inhibition of the phosphorylation of ATF2 (downstream substrate) by p38α at a range of concentrations for PH-based analogues analogues* ***4-9 – 4-17****. Purified p38α was activated using ATP, and then incubated with appropriate inhibitor, ATF2 and ATP. Protein levels were revealed using selective antibodies and fluorescent antibodies.* ***B)*** *Graphical representation of the above western blots.*

The activity of these compounds was also verified in cellular assays using BBL 358 cells. Some example western blot results are shown below in figure 4.1.5.

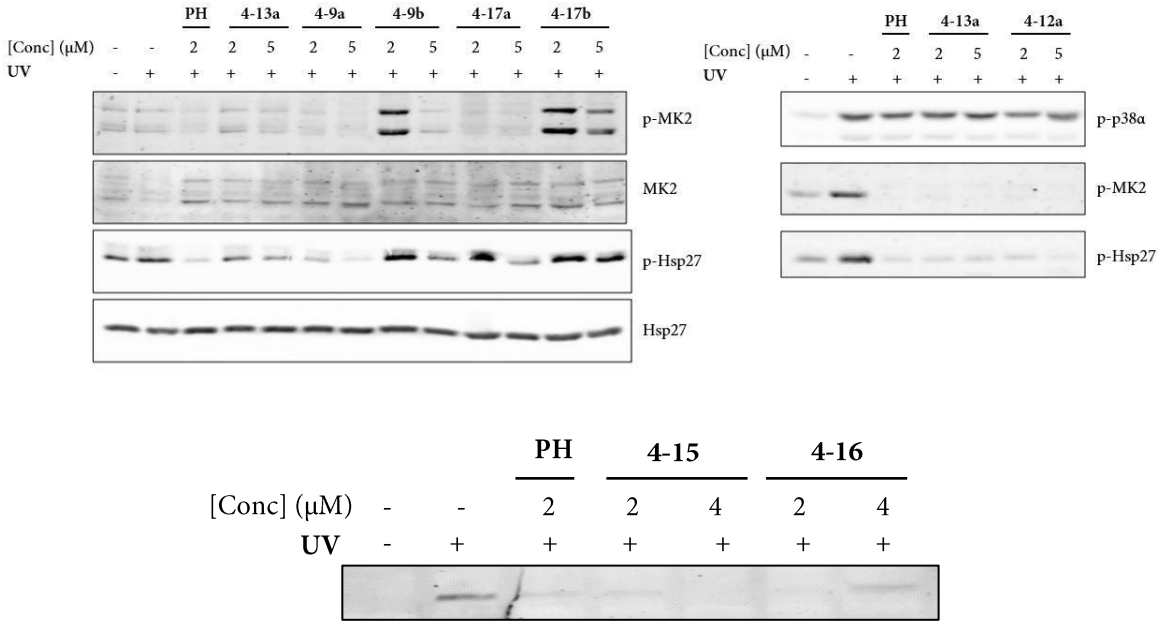

Figure 4.1.5. *Inhibition of p38α-mediated phosphorylation of downstream targets MK2 and Hsp27 at a range of concentrations for* ***PH*** *analogues* ***1 – 13.*** *BBL 358IM cells were incubated with appropriate inhibitor before irradiation by UV light (80 J)to activate the p38 MAPK pathway. Protein levels were revealed using the corresponding selective antibodies and fluorescent antibodies.*

As can be observed from the cellular assay western blot (figure 4.1.5), compounds **4-13a**, **4-9a** and **4-17a** were most active of the series, confirming that amine, ester and carbamate groups were tolerated in this position and resulted in active inhibitors. Alkyl acids **4-9b** and amino acid groups **4-17b** were not active probably due to poor cell permeability as opposed to unfavourable interactions with p38α´s active site. This is supported by the observation that the corresponding ester **4-9a** and boc protected amino acid **4-17a** analogues retain their activity despite being much bulkier. The reverse is true for the activity of these analogues in the kinase assays (figure 4.1.4). This assay takes place in aqueous buffer solution and therefore does not involve any cell permeation, explaining why these polar groups diminish activity mainly in cellular assays. It was also evident that the longer bulkier amino acid chains, such as **4-17a** and **b** diminished p38α affinity by the most, whereas small, simple chains were best tolerated, such as **4-11** and **4-13a.** Alcohol groups were very active, as demonstrated by compounds **4-11, 4-12a** and **4-15.** Interestingly, the affinity of the 4

carbon chain alcohol (**4-15**) was less than the 2 or 3 carbon chain (figure 4.1.4, **4-11** and **4-12a**). 4 carbon chain analogues **4-15** and **4-16** effectively inhibited p38α MAPK pathway in cells at concentrations of 2 and 5 μM concentrations, however the blot was not clear enough to provide conclusive evidence.

In summary, we selected analogues **4-11, 4-12a** and **4-13a** to take forward for *in vivo* experiments, as they were most active and featured appropriate handles for conjugation to directing groups.

4.1.2. *In vivo* Testing of Most Active Analogues

The most active compounds of the series were analogues **4-11**, **4-12a** and **4-13a**, which performed well both *in vitro* and in cellular assays. These compounds were synthesised on a larger scale to be tested *in vivo*. Doses were used as for **PH** and performed very well compared with this inhibitor (graph 4.1.1A and B). The tests using **4-12a** and **4-13a** were continued to be monitored until day 22 despite ceasing administration of inhibitor at day 14. In the case of **4-13a**, we observed a continued effect of the compound, with tumour size diminishing to minute levels before a recession in growth commenced.

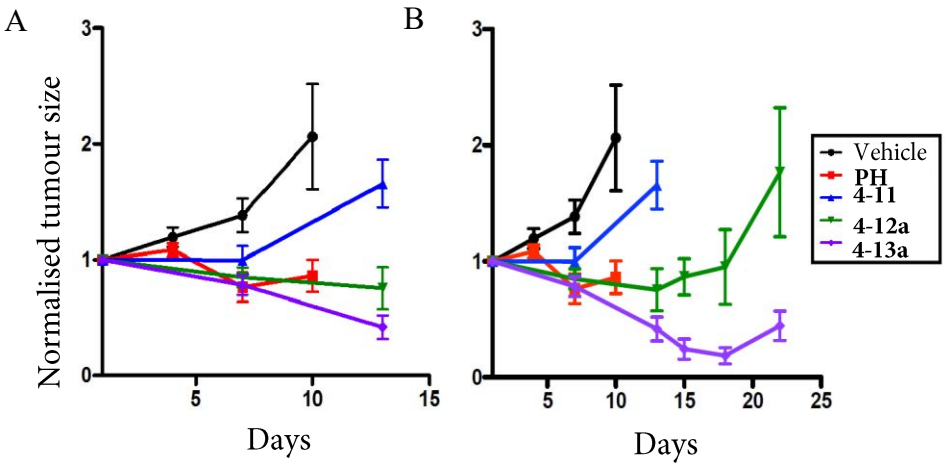

Graph 4.1.1. *PyMT mice administered with inhibitors daily (10 mg/Kg) until day 14. Normalised tumour size was monitored of two separate tumours on two different mouse subjects.* ***A)*** *15 day treatment and monitoring.* ***B)*** *continued monitoring of the lasting effect up to 22 days, without further treatment.*

The improved *in vivo* activity of **4-13a** was not expected based on the *in vitro* data, perhaps resulting from improved bioavailability and cellular uptake, or perhaps due to the establishment of an extra hydrogen bond as was observed with inhibitor L-Skepinone, which is another p38α inhibitor of the same class as **PH** (figure 4.1.6).[3]

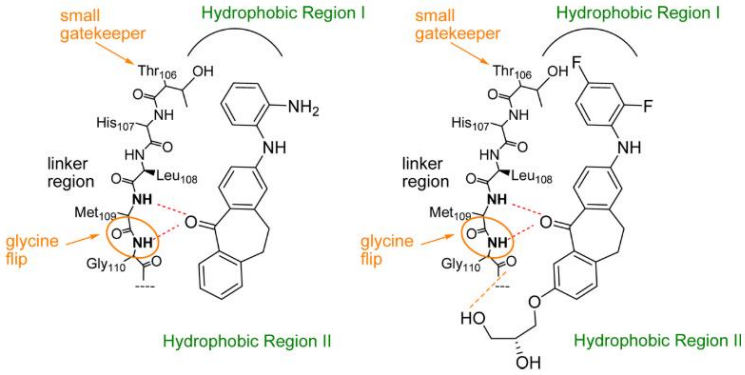

Figure 4.1.6. *L-Skepinone p38α inhibitor (right) bound to active site of p38α, showing the key interactions responsible for affinity, interaction with hydrophobic region I, passing Thr106 gatekeeper, and hydrogen bonding induced glycine flip. Initial hit (left) lacks the terminal alcohol group, therefore does not display the extra H-bond.*[4]

When the experiment was repeated using **4-13a** compared to a more potent drug **LY** and increasing the dose of **PH**, it was evident that the compound did not excel over more active compounds or doses.

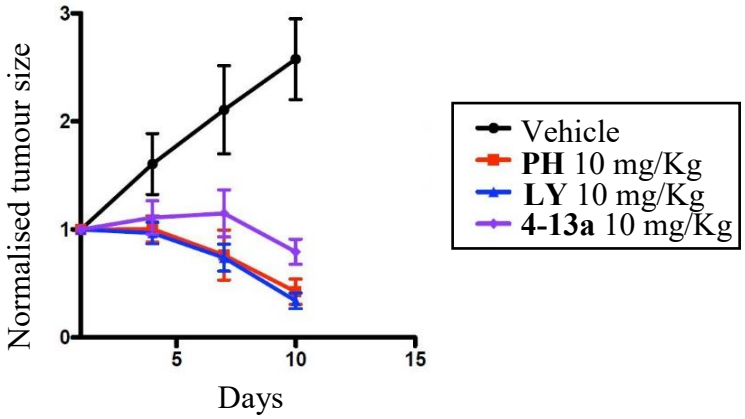

Graph 4.1.2. *Repeat of in vivo study of **4-13a** against **LY** and higher dose of **PH** (15 mg/Kg).*

Active analogues **4-12a** and **4-13a** were also administered to mouse models bearing human breast cancer tumour xenografts to assess the activity in a more human-related model of cancer. It can be observed that the treatment of tumours of this type is more challenging, but their growth can be decelerated or decreased by inhibition of p38α, reflecting limitations of the model and of the more challenging cell types in human disease. It is again observed that **4-13a** is more potent than **PH** at this concentration. Furthermore, **PH** lacks an appropriate handle for conjugation to a directing group, whereas **4-13a** possesses a terminal amine that can be easily conjugated to nanoparticles or undergo peptide coupling to a peptide recognition fragment. **4-13a** performed consistently well in the range of experiments that were carried out and was therefore selected as our lead analogue for conjugation to directing groups.

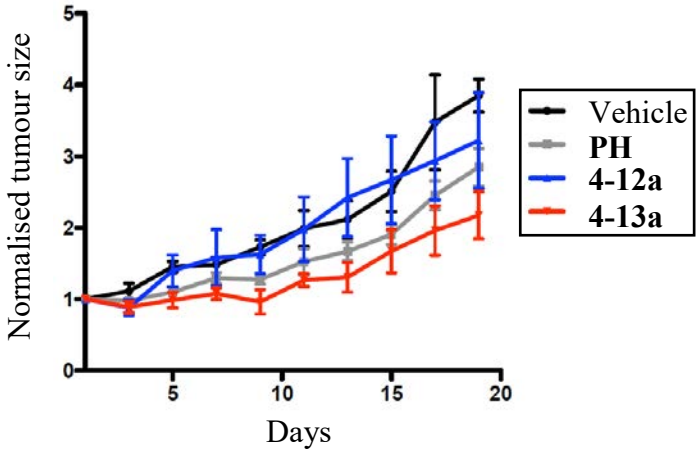

Graph 4.1.3. *In vivo experiment using compounds* ***4-12a*** *and* ***4-13a, PH*** *and control, mice grafted with human skin cancer tumour implants.*

4.2. Caged Analogues of 4-12a and 4-13a

Two of our most active compounds, **4-12a** and **4-13a**, were chosen to make caged analogues, *i.e.* the alcohol and amine functional groups would be protected with a nitroveratryl group (Nv). Compounds **4-12b** and **4-13b** were therefore synthesised in order to further explore the steric limitations at this end of the molecule and determine whether the inhibition activity could be blocked *via* substitution at this part of the molecule (scheme 4.2.1). This work is based on caging methodology described in section 3.2.

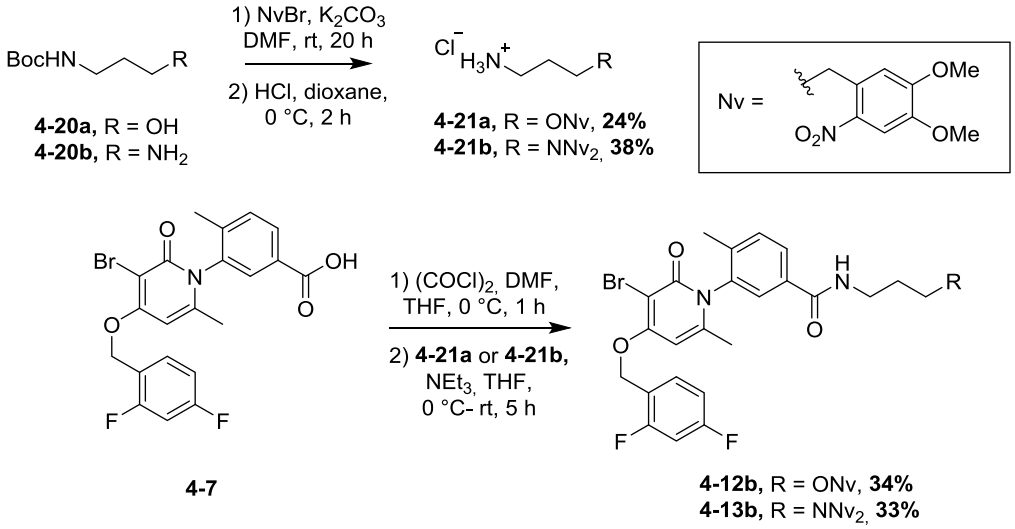

Scheme 4.2.1. *Preparation of caged analogues* ***4-12b*** *and* ***4-13b.***

We hypothesised that a large aryl caging group, such as nitroveratryl, blocking the terminal amine or alcohol of the analogue would diminish inhibition activity of the original inhibitors **4-12a** and **4-13a** due to steric repulsion. This caging group was easily removed by irradiation with long-wave UV light (ca. 380 nm) in under 30 minutes in *d6*-methanol, and in aqueous solvent (scheme 4.2.2). Caging of inhibitors and other active compounds in this way has had a wide success in many applications, as summarised in section 3.2. Our goal was to prevent p38α inhibition activity until activated by UV light, which would be applied specifically to tumour sites, thereby controlling the activity of the inhibitor and improving selectivity. This technique would be especially useful in the treatment of surface

tumours, as the UV light does not penetrate more than a few millimetres below the skin surface. New technologies have been developed to deliver light inside mice and humans, selectively to the target tissues. We aimed to demonstrate the proof of concept of these caged analogues for further development and applications, and hopefully utilise available techniques to gain proof of concept in mouse models.

The addition of a bulky nitroverityl (Nv) group to alcohol **4-12a** (forming **4-12b**) was not sufficient to block inhibition of p38α, having little effect on activity. **4-13b** possessed two Nv groups and indeed reduced the affinity for p38α by a more significant amount (at 0.1, 0.5 and 1 μM) compared to **4-13a**, however did not diminish affinity entirely.

In cellular assays, activation of the p38α pathway within cells was carried out using anisomycin, a known chemical inducer of the pathway. This avoided the use of UV light to activate the pathway which would have risked cleavage of our caging Nv group. The longer wavelength used for the cleavage of the caging group (ca. 380 nm) would not induce phosphorylation of p38α and activate the pathway, as indicated by the control experiments, as activation only occurs under shorter wavelengths of higher energy (ca. 254 nm). Compound **4-13b** had much lower activity than its parent compound **4-13a** or **PH** at 2 μM, but unfortunately at higher concentration (5 μM), it remained comparably inhibitive of the p38α pathway. This was a very encouraging result, however the difference in activity may not have been large enough for *in vivo* applications. Indeed, we believed the inhibition activity could be blocked entirely by caging an alternative part of the inhibitor structure, therefore caging of this position was not investigated further.

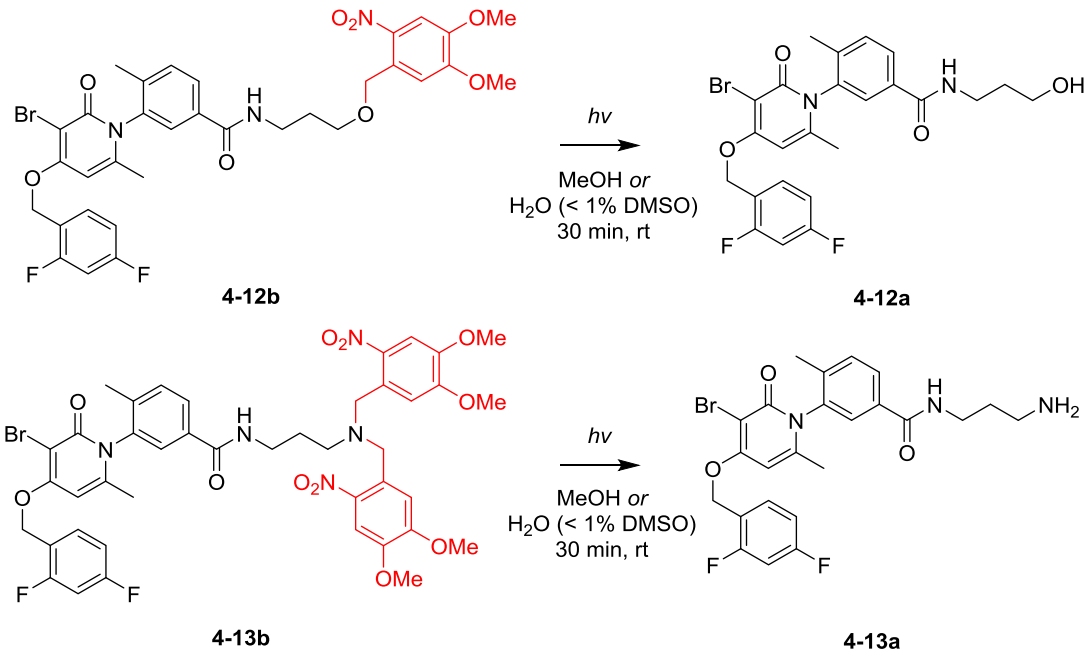

Scheme 4.2.2. *UV light stimulated uncaging of compounds* ***4-12b*** *and* ***4-13b*** *to afford active inhibitors* ***4-12a*** *and* ***4-13a.***

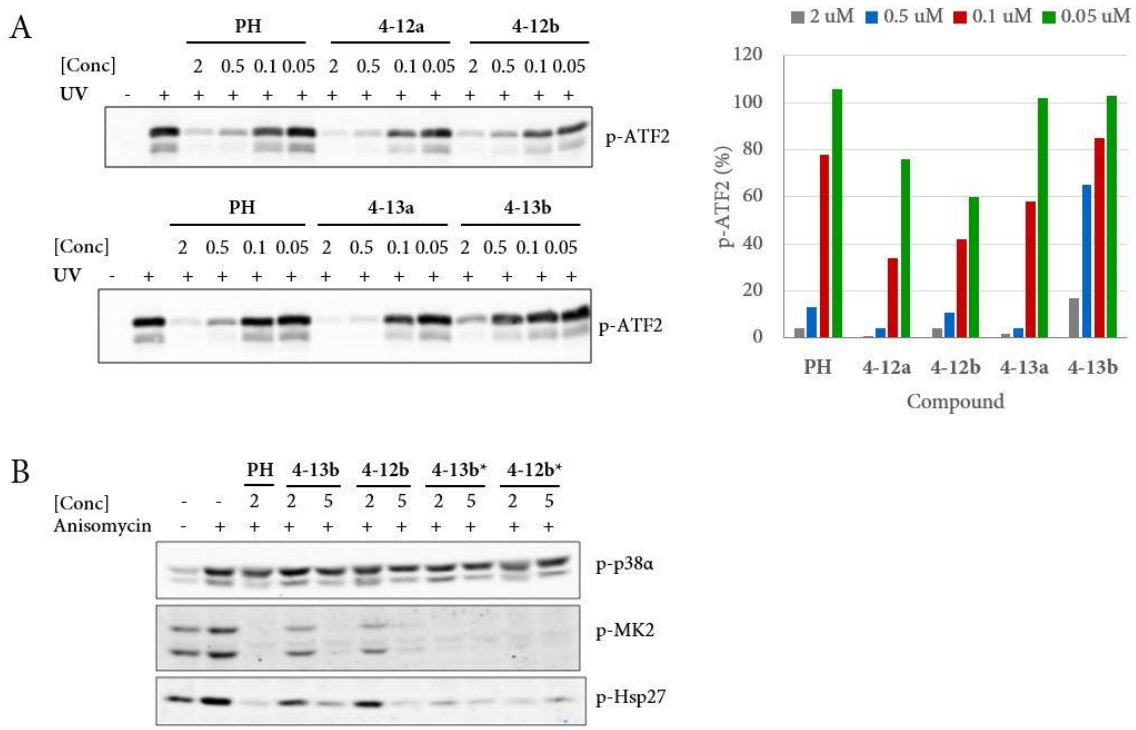

Figure 4.2.1. A) Kinase assay: *Showing the inhibitory effect of compounds* ***4-12b*** *and* ***4-13b*** *compared with free inhibitors* ***4-12a*** *and* ***4-13a****, by % phosphorylation of downstream substrate ATF2.* ***B) Cellular assay:*** *Showing the inhibitory effect of compounds* ***4-12b*** *and* ***4-13b*** *and UV irradiated samples* ***4-***

13b and **4-12b*** (360nm, 30 min, aq) on downstream substrates MK2 and Hsp27. Compounds were irradiated first before addition to cells to show effect in this assay. Inhibitor, followed by anisomycin were added to 358 cells.*

In continuation, de-activation of **PH** (and our analogues) was sought by caging other parts of the molecule that had more likelihood of interfering with key interactions between the active site and the inhibitor. In metabolic studies of **PH**, metabolite **4-23** was shown to maintain inhibitory activity, however larger or polar groups (e.g. COOH) were not tolerated in this position.[5] This extra alcohol would serve as an appropriate handle for caging. We attempted to reproduce the synthesis reported by Selness *et al.* and then cage the resulting product to test the activity in our hands in cellular assays. However the reported synthesis of **4-23** could not be reproduced, giving low yields in the first steps towards **4-26,** which then could not be easily brominated nor purified to obtain bromo-product **4-27** (scheme 4.2.3). Therefore this target was abandoned since the synthesis of large amounts of inhibitor would not be straightforward.

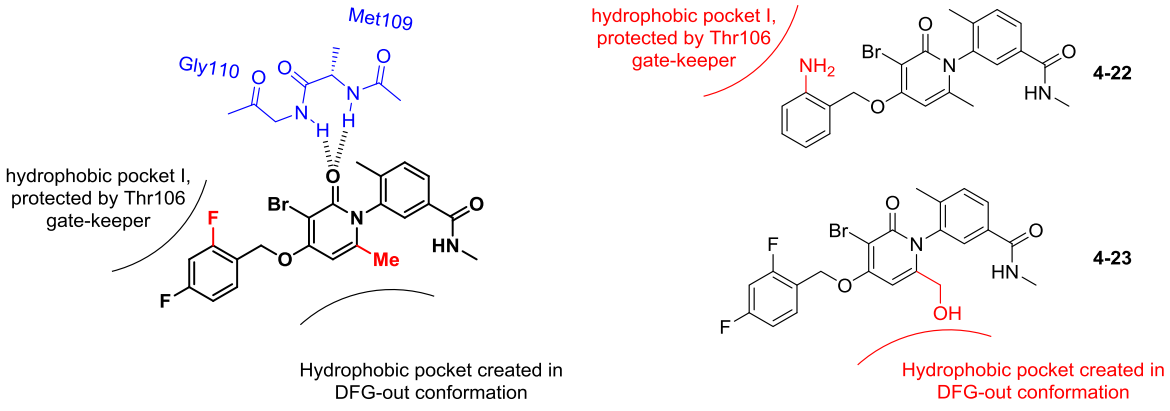

***Figure 4.2.2. Left:** Schematic representation of **PH** bound to its active site, highlighting key interactions. **Right:** Proposed analogues **4-22** and **4-23** with changes shown in red, with predicted steric interactions with p38α active site shown in red*

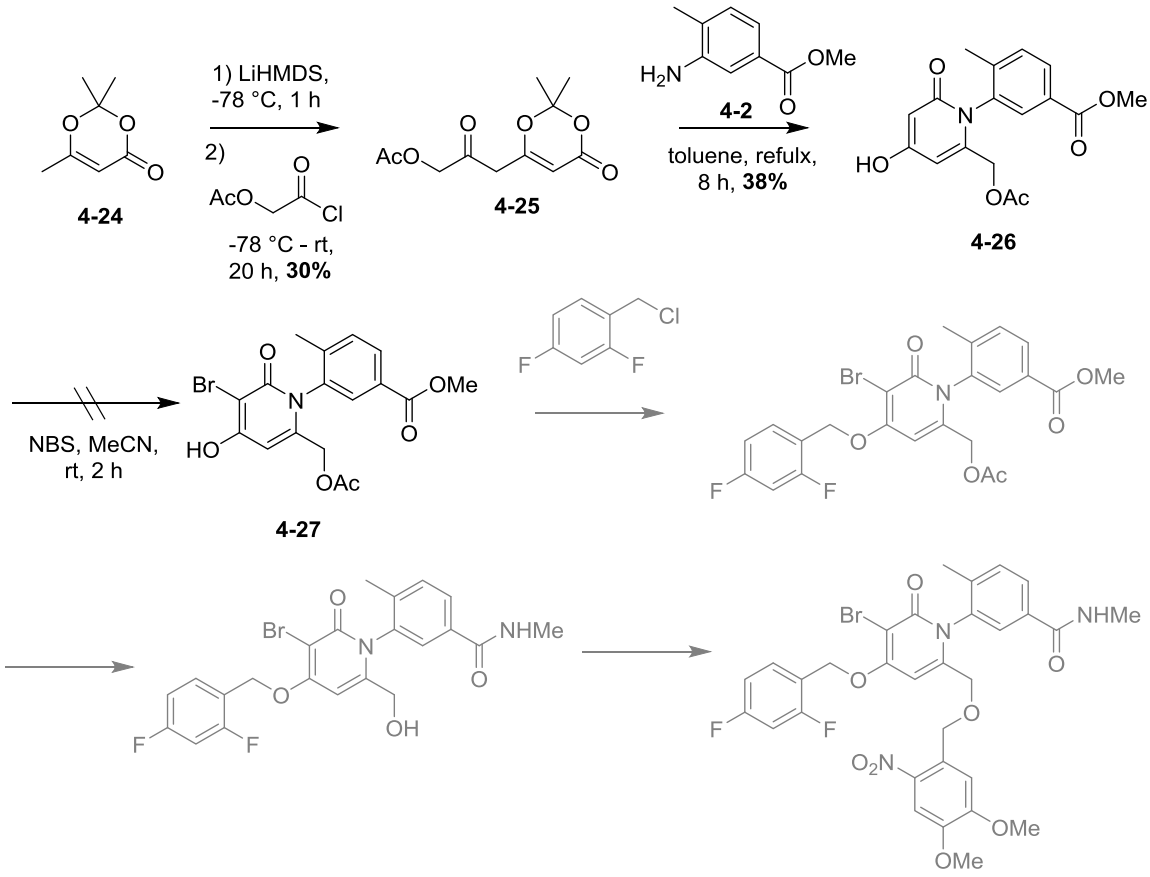

Scheme 4.2.3. *Unsuccessful synthetic route towards caged-version of inhibitor* ***4-23****.*

Skepinone is another inhibitor of p38α of the same binding class, but has a distinct core structure, long and rigid fused ring struture.[4] It binds similar to **PH**, utilising the same 3 traits to gain affinity and selectivity (summarisied in figure 4.2.2).

Laufer and coworkers identified an initial hit compound from a screening library, which possessed an aniline in the *ortho*-position, before replacement with a 2, 4 difluoro-aryl group (discussed in section 3.1.5). Assuming that this head group bound and behaved exactly as the head group of **PH,** we could then replace the difluoro benzyl moiety of our **PH** analogues with an *ortho*-aniline group (e.g. **4-21**) and retain affinity for p38α. We would then be able to cage this aniline handle and have a high chance of blocking activity due to the steric restrictions of the threonine gate-keeper and hydrophobic region I (scheme 4.2.4).

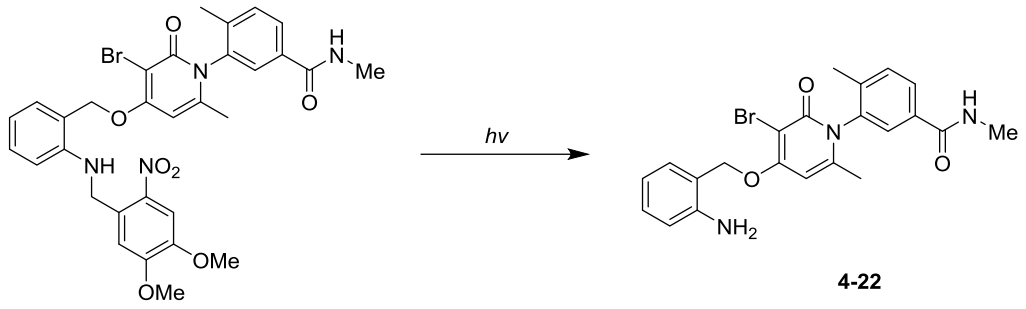

4-28 **4-22**

Scheme 4.2.4. *Scheme showing analogue **4-28** which was theorised to be inactive due to the Nv group positioned on the aniline head group of **4-22**. **4-22** was predicted to retain inhibition activity for p38α, based on SAR studies of similar inhibitors in the literature.*

The synthesis of **PH** would have had to be adapted again to incorporate this group, as proposed in scheme 4.2.5. Hydrogenation of the aryl nitro to an aniline could not be performed selectively over the reduction of other moieties in the compound. Various conditions were trialled to improve this reductive step, including platinum, palladium, iron, tin and zinc catalysts. The direct reduction of the *o*-nitro bromo benzyl intermediate was also challenging, and therefore routes towards caged p38α inhibitors were abandoned in order to prioritise other areas of the project.

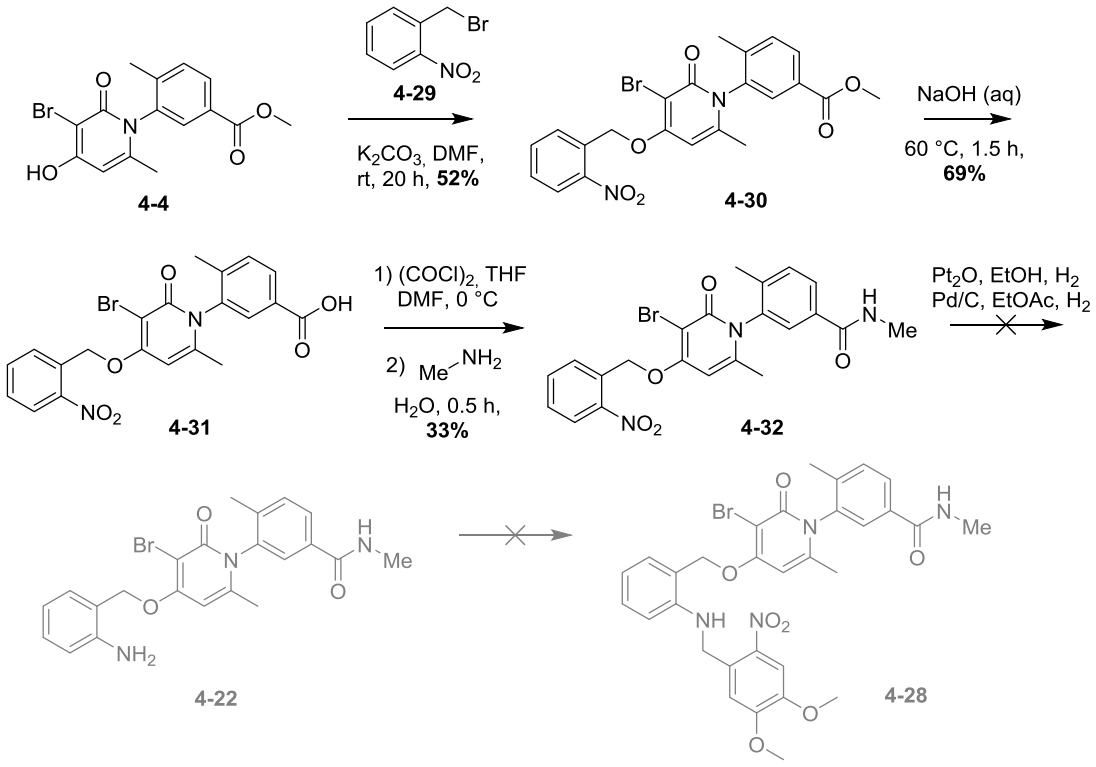

4-4 **4-30** **4-31** **4-32** **4-22** **4-28**

Scheme 4.2.5. *Towards the synthesis of caged p38α inhibitor **2-28**.*

4.3. Conjugation of PH Derivatives to Gold Nanoparticles (ICFO)

After exploration of caging our novel analogues of **PH**, we next turned our attention to the direction of inhibitors to accumulate selectively at tumour sites. Gold nanorods were initially functionalised with **LY**, in collaboration with the Plasmon Nano-optics (Prof. Quidant) group at the Institute of Photonic Sciences (ICFO) as discussed in section 3.2.2. The enhanced permeation and retention (EPR) effect was expected to cause an approximate 2-fold higher accumulation of nanoparticles (NPs) in the tumour tissue compared to other tissues. However, large accumulations in the liver and spleen could not be avoided.

4-13a was chosen from our analogues for conjugation to gold NPs, as it performed best in the *in vivo* experiments and also possessed an amine group, which allowed facile conjugation to the nanoparticle using the same methodology as for **LY**. NPs were functionalised with pegalyl chains terminating in a carboxylic acid group, which were coupled to the amine moiety of **4-13a.** The resulting conjugates (**4-13aNP**) were tested in the standard cellular assay conditions to directly compare with free **PH** inhibitor**,** un-functionalised NP controls, and control cells (figure 4.3.1).

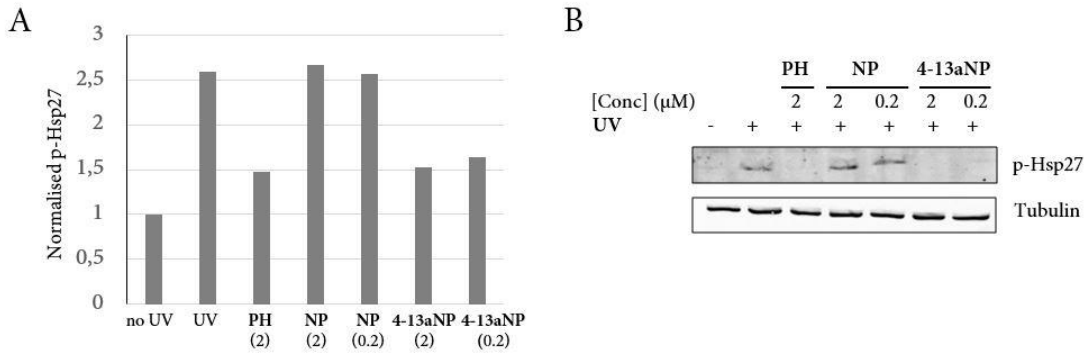

Figure 4.3.1. *Showing the inhibitory activity against phosphorylation of Hsp27, downstream substrate of p38α, of* ***PH, NP*** *(at 0.2 and 2 μM), and* ***4-13aNP*** *(at 0.2 and 2 μM), with tubulin measured as a calibrative control.* ***A)*** *Basal level of p-Hsp27 is normalised to "1" in graph.* ***B)*** *western blot.*

As with **LY**-NPs, it was not possible to accurately measure the amount of inhibitor (**4-13a**) bound to the nanoparticles, nor to monitor **4-13a** dissociation from the nanoparticle. Therefore the activity observed in cells could be due to free **4-13a** that had already dissociated from its NP carrier. Furthermore, discrepancies were observed in the cellular activity of samples that were stored for longer periods, which was further evidence of the instability of these nano-drug conjugates. We observed little difference in activity despite a 10x concentration increase of 0.2 – 2 μM **4-13aNP**. Initial testing of these conjugates *in vivo* led to surprising results, where the **4-13aNP** conjugate suppressed tumour growth and reduced tumour size over a 42 day period (graph 4.3.1). However, the NP-control, which did not possess any inhibitor led to a retention of tumour growth when compared to the control. This was not verified by further experiments therefore we cannot conclude that the nanoparticles have an anti-tumoral effect on their own, based upon these isolated experiments with few mice.

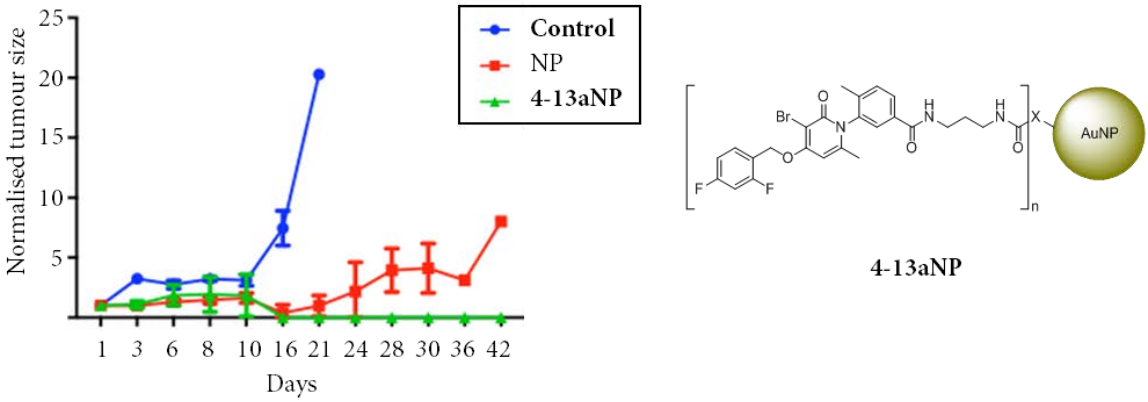

Graph 4.3.1. *In vivo experiments of nanoparticles and nanoparticle* ***4-13a*** *conjugate compared to control mouse. BBL PyMT TG/+ mice were administered with 4 injections via tail vein of 100 μl of either 45 nM NP-aminoethanol or* ***4-13aNP*** *on Mondays, Wednesdays and Fridays.*

As discussed in section 3.3.2, gold NPs can be conjugated with RGD recognition fragments or PEG chains to mask the surface of the NP in a way that disguises it from recognition by macrophages, which diminishes accumulation in RES organs (e.g. liver and spleen).[6,7] Futhermore, NPs can be dually functionalised with an inhibitor and also with PEG or RGD. A range of NPs were synthesised, functionalised with different ratios of **4-13a:**RGD in order

to identify an effective ratio for inhibitory activity and selective accumulation in the tumour sites figure 4.3.2.

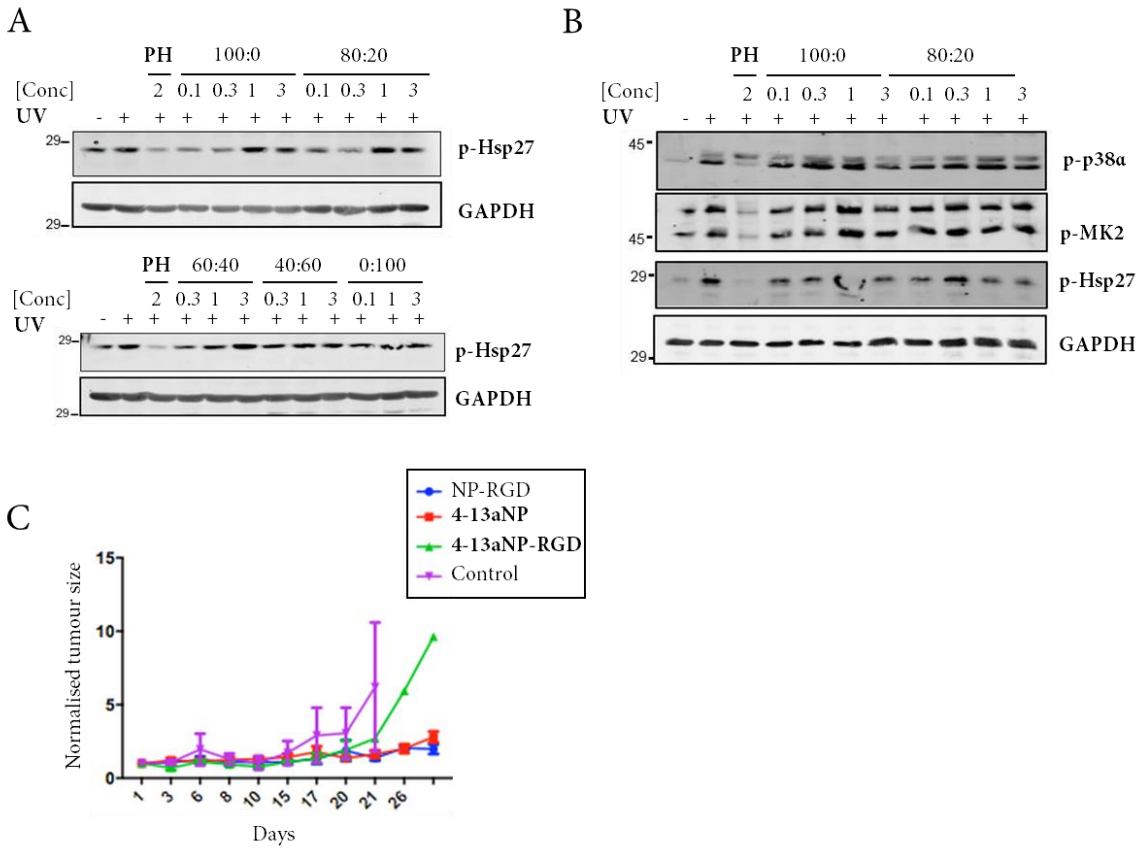

Figure 4.3.2. A) *Western blots showing the activity of* ***4-13a****-RGD-NP conjugates with differing ratios of* ***4-13a****:RGD, monitored by phosphorylation of Hsp27 in 358 cells.* ***B)*** *Repeated blot using the ratios with highest inhibitory activity (100:0 and 80:20) after storing for >14 days at -20 °C.* ***C)*** *In vivo testing of* ***4-13a:****RGD-NP conjugates compared with NP-RGD and* ***4-13aNP****. BBL PyMT TG/+ mice were administered with 4 injections via tail vein of 100 µl of NP solution on Mondays, Wednesdays and Fridays.*

Further experiments were not carried out due to the many complications and high cost of these complicated *in vivo* studies. Misleading quantifications of bound inhibitor and the instability of NP-conjugates meant that it was too difficult to conclude anything from these experiments. It can also be observed in figure 4.3.2B that the stability of these nanoparticles could indeed be lower than required for this application.

Azide **4-14** was synthesised more easily *via* a click reaction to NPs that had been functionalised with strained alkyne moieties (scheme 4.3.1). This bond was expected to bind tightly and resist metabolism, reducing dissociation of inhibitor from the nanorods. It may also have enabled controlled release of this analogue, based on initial experiments at ICFO, which showed that light-induced thermal release of the free analogue could be achieved *in vitro*. However no further experiments were carried out using this methodology after the collaboration was ceased.

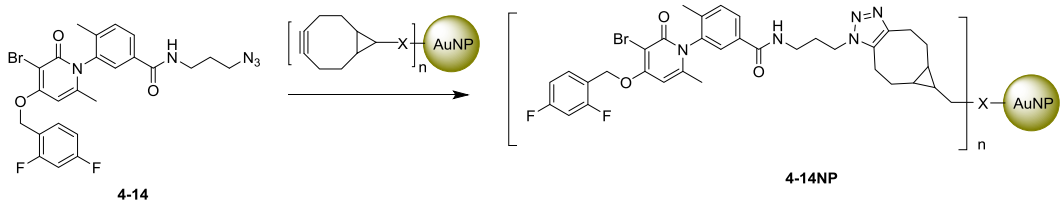

Scheme 4.3.1. *Synthesis of* ***4-14NP*** *nanoparticle-drug conjugates via a click reaction, using a strained alkyne and the terminal azide of analogue* ***4-14.***

4.4. Conjugation of Active Inhibitors to Peptide Recognition Fragments

Peptide recognition fragments have had many successful applications in the literature. Peptides are favoured for their low toxicity, can be easily synthesised using resin support technologies, and may be recognised by a range of receptors located on cell surfaces as they are common natural ligands of these receptors. Many such receptors are overexpressed in tumour cells as the tumour rapidly grows and consumes energy, requiring higher uptake of nutrients. For example, $\alpha_v\beta_3$ integrin receptors are overexpressed in a range of cancer cell types (such as MCF-2) and many RGD analogues have been used to selectively target receptors on tumour surfaces for diagnosis and treatment of various cancer types, as outlined in section 3.3.3.

We began by synthesising the simplest form of **PH-RGD** (**4-35**) by coupling carboxylic acid intermediate **4-7** directly to a linear RGD sequence bound to resin (**4-33**), which was synthesised by Dr. Escolà (scheme 4.4.1).

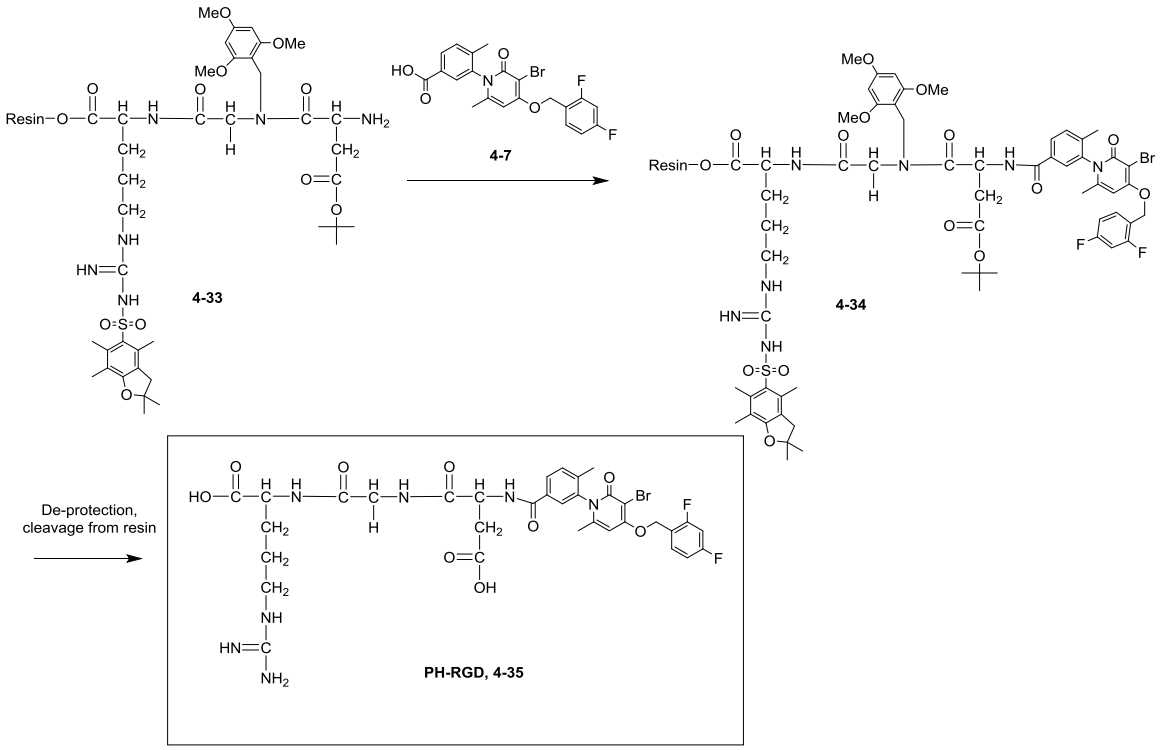

Scheme 4.4.1. *Synthesis of* ***PH-RGD*** *drug conjugate* ***4-35a.***

PH-RGD (**4-35**) was tested in cellular assays to compare its activity relative to **PH** (graph 4.4.1). As was predicted from the low affinities of analogues **4-17a** and **4-17b**, which possessed amino acid moieties directly bound to the amide of **PH**, **PH-RGD**'s affinity for p38α and inhibition of ATF-2 phosphorylation was much lower than for free **PH.** It was also administered to mice to compare its anti-tumoural activity with free **PH**, (graph 4.4.2).

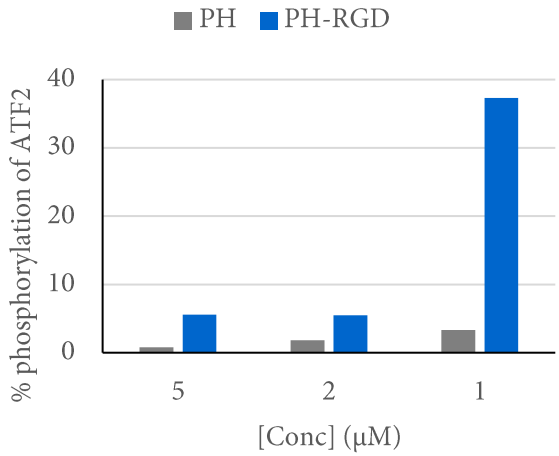

Graph 4.4.1. *Kinase assay showing the activity of* ***PH-RGD (4-35)*** *compared to* ***PH*** *at different concentrations of inhibitor*

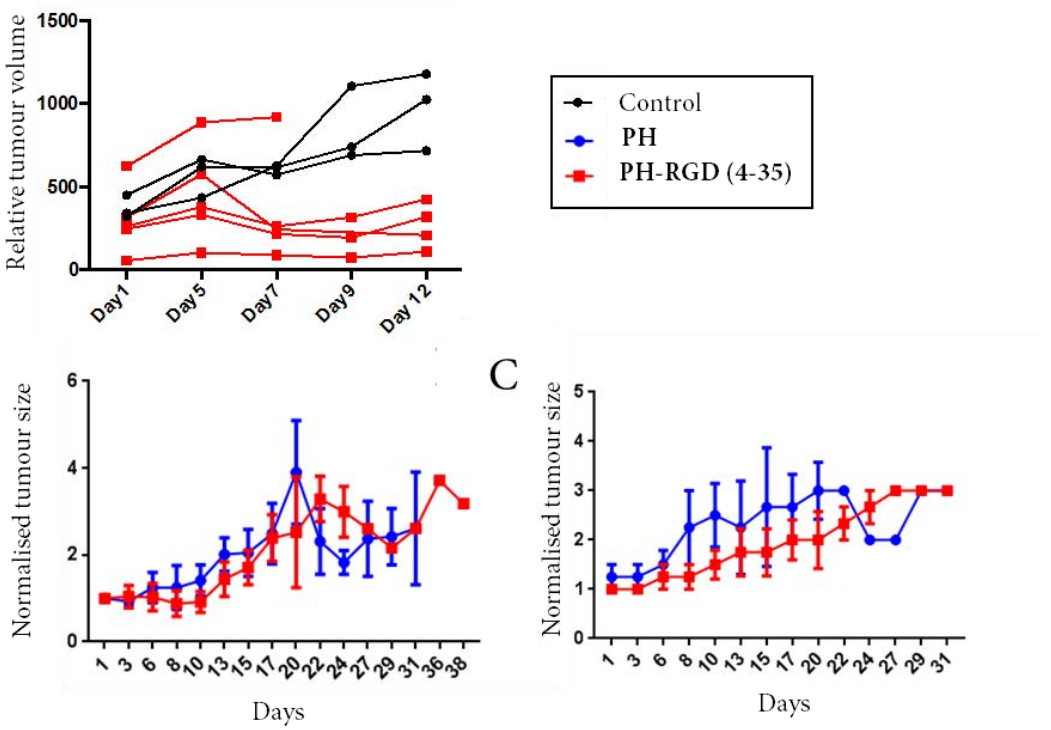

Graph 4.4.2. *In vivo testing of* ***PH-RGD*** *compared with vehicle (black) and* ***PH*** *(blue). BBL PyMT TG/+ mice were administered by oral gavage using 250 µl of 1.66 mg/mL (**PH-RGD, 4-35a**) or 1 mg/mL (**PH**). NP solution was administered every working day after tumours reached >200 mm³ in volume.*

As is observed from the *in vivo* data shown in graph 4.4.2, **PH-RGD (4-35a)** conjugate retains tumour growth compared to the control experiments, and closely matches that exhibited by free **PH**, at the same molar concentration. Note, that dosing was increased to 1.66 mg/mL concentration, as **PH-RGD** weighs 1.66x more than **PH**. The metabolic stability of **PH-RGD** is unknown in mice, therefore the antitumoral activity could be due to liberated **PH** or **4-7**. There was not any obvious benefit observed by conjugating **PH** to **RGD** and we were not able to quantify the relative drug concentrations within different tissues of the mice.

In chapter 7 of her doctoral thesis, Escolà describes how somatostatin analogues (overview in section 3.3.3.2) can be conjugated to **4-7** in the same way as for **PH-RGD** (**4-35**). This was another receptor, and another peptide ligand, but demonstrated the potential for use as targeted delivery of **PH** analogues to endocrinal cells, which over express SSTR2.[8] She observed that higher inhibition of p38α occurred in cells expressing SSTR2 compared to

wild type cells lacking the receptor, when treated with equal concentrations of the **PH-SST** conjugate. Two of these drug conjugates were included as references in the kinase assay as well as free **PH** to assess the affinity of the new **PH-RGD** conjugate (graph 4.4.3). **PH-RGD** was much less potent than either of the 2 **PH-SST** analogues, despite the enormous size of SST compared to RGD, and bound to the same position. We suspected the unusually high activity of **PH-SSTa** and **PH-SSTb** arose from liberated **PHacid** (or related fragments) resulting from the hydrolysis of these analogues during the assay. In fact, when a more stable analogue of somatostatin was conjugated to **PH**, which featured a D-alanine linked to **4-7**, the potency was much lower, which further supported this hypothesis. Note, a general caveat of this assay and using too high a concentration mean passive diffusion will dominate conjugate or cleaved inhibitor entry into the cell. Lower concentrations may lead to a system where passive diffusion does not take place to such an extent, in order to monitor the active diffusion responsible by receptor recognition and internalisation.

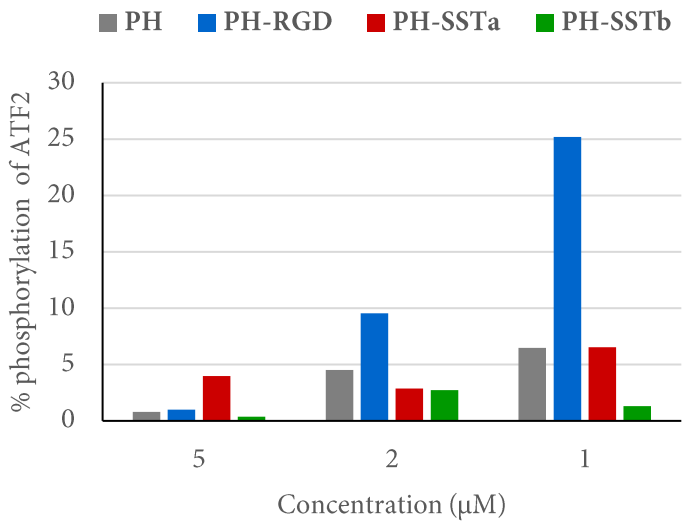

Graph 4.4.3. *Kinase assay showing the % phosphorylation of ATF2 in a p38α kinase assay as described, using stated concentrations of inhibitor or conjugate:* ***PH, PH-RGD, 4-7SSTa*** *and* ***4-7SSTb.***

We hypothesised that the addition of an extra amino acid or pegalyl linker would create more space between the peptide recognition fragment and the active drug component, thereby increasing the affinity of the drug conjugate. We also wished to balance the overall

charge of the compound by adding additional amino acid residues, because negatively charged analogues were least active in cellular assays due to poor cell permeability. Therefore, compounds **D-RGD-PH (4-35b)**, **RGD-linker-PH (4.35c)** and **RGD-R-PH (4-35d)** were synthesised in order to improve affinity and activity. These are awaiting testing in cellular assays. **D*-RGD-PH (4-35e)** and **D*-PH (4-36)** contained a fluorescent amino acid, which was not expected to interfere significantly with the activity of the analogues, but would allow the visualisation of cell internalisation of analogues within assays (figure 4.4.1).

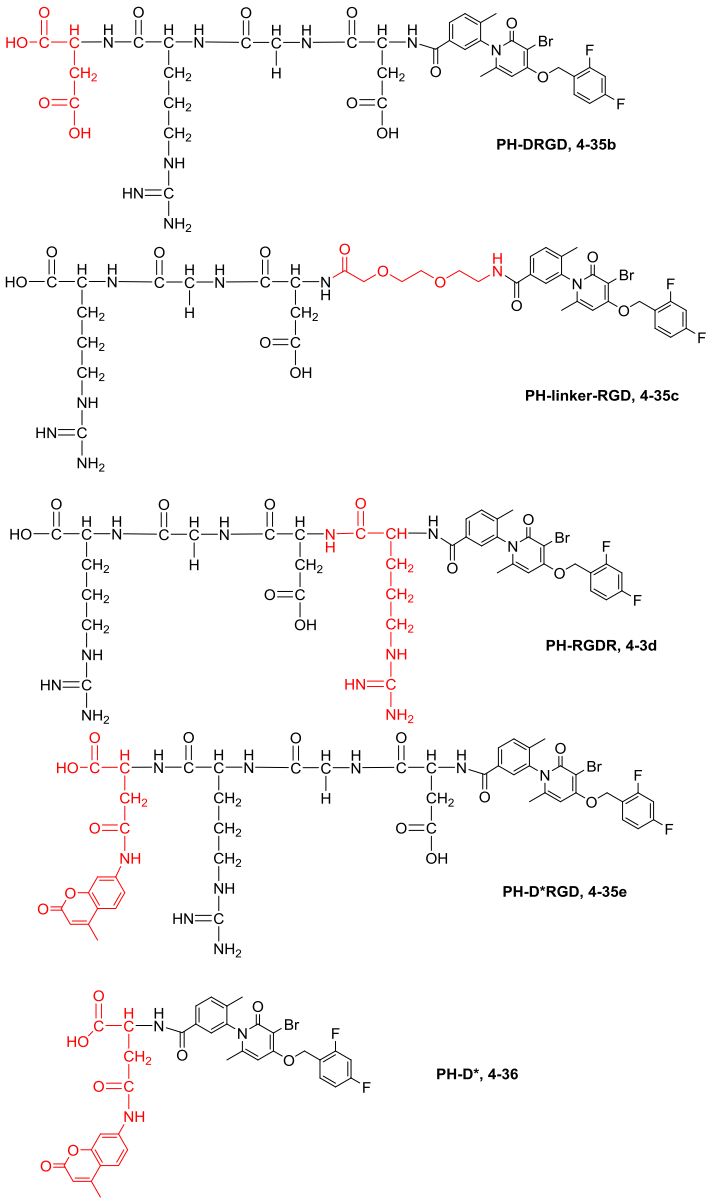

***Figure 4.4.1. PH-RGD** analogues containing extra amino acids and fluorescent amino acids*

Cyclic versions of RGD have been reported to add metabolic stability and the locked conformation can provide more affinity and selectivity within the integrin receptor family. We did not pursue the design and synthesis of such cyclic RGD analogues, instead choosing to study **PH** with other cyclic peptides with which the group had more experience, such as octreotide, a stable and potent ligand of SSTR. There is already detailed clinical knowledge on this peptide as it is administered as a treatment for a range of intestinal diseases, diabetes as well as clinical visualisation and treatment of tumours, under the name Sandostatin®.[9] A batch of **PH-PEG-Oct** (**4-41**) was synthesised Joan Matarín in order to test the inhibitory activity towards p38α. We would then compare the activity in cells compared to the wild type cells, as was done for RGD and SST-PH analogues previously. Lower concentrations would be used where passive diffusion was not dominating cell permeation, in order to see more clearly the differing effect of the SST receptor-assisted absorption by the cells.

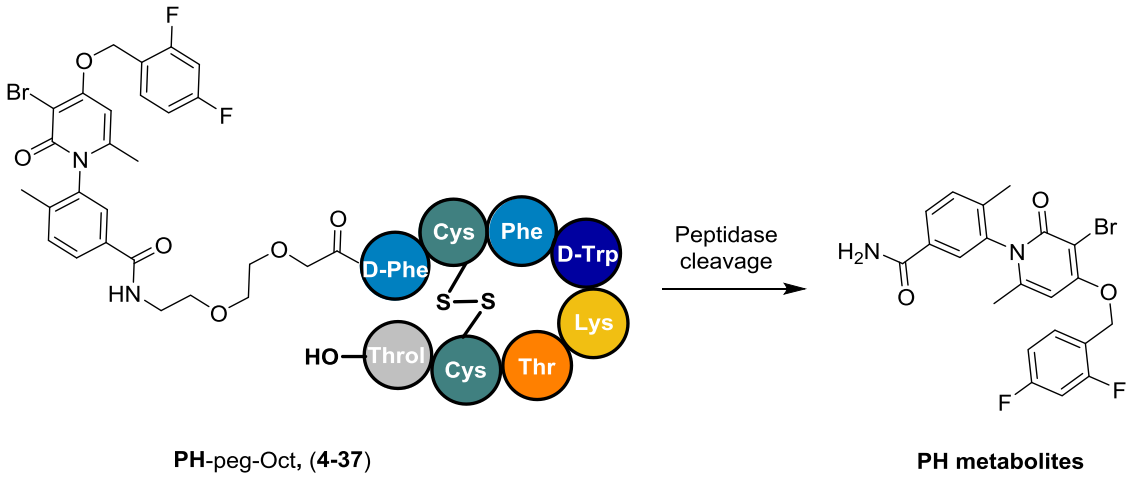

Figure 4.4.2. PH-peg-Oct (4-37), *Peptide drug conjugate featuring* ***4-7*** *linked via a PEG2 linker to Octreotide. The octreotide portion has a strong affinity for SSTR2, overexpressed in endocrine tumour cells, to cause accumulation of the drug conjugate. Internalisation followed by cleavage by proteases is expected to eventually liberate* ***4-7*** *and similar active metabolites within the tumour cells.*

The cleavage of this peptide bond to liberate free **4-7** (or similar derivatives) is predicted to occur once inside the cell, after internalisation along with bound SSTR. The metabolic stability of the new analogue has not been studied. It may be very slow and imprecise, resulting in many metabolites which would limit activity. In order to gain further control

over the release of more active analogues, we designed a photo-labile linker to join **4-13a** to octreotide (figure 4.4.3). We hoped to obtain an inhibitor that gained selectivity from the octreotide directing group, causing accumulation in cancer cells expressing SSTRs. The accumulated compound could then be cleaved by UV light to liberate our most active analogue, solely in the cells that have been UV irradiated. We would thereby achieve selectivity, through the accumulation of our conjugate due to the strong affinity for SSTR, thus avoiding off-target interactions to reduce side effects. We would also gain more directional and temporal control *via* controlled liberation of **4-13a**, only where UV light had been applied, to potentially achieve higher localised efficacy. **4-38** can be thought of as a caged version of **4-13a**, but the ONB caging group has additional tumour-directing functionality. Validation of this light assisted cleavage and biological testing of these analogues is ongoing.

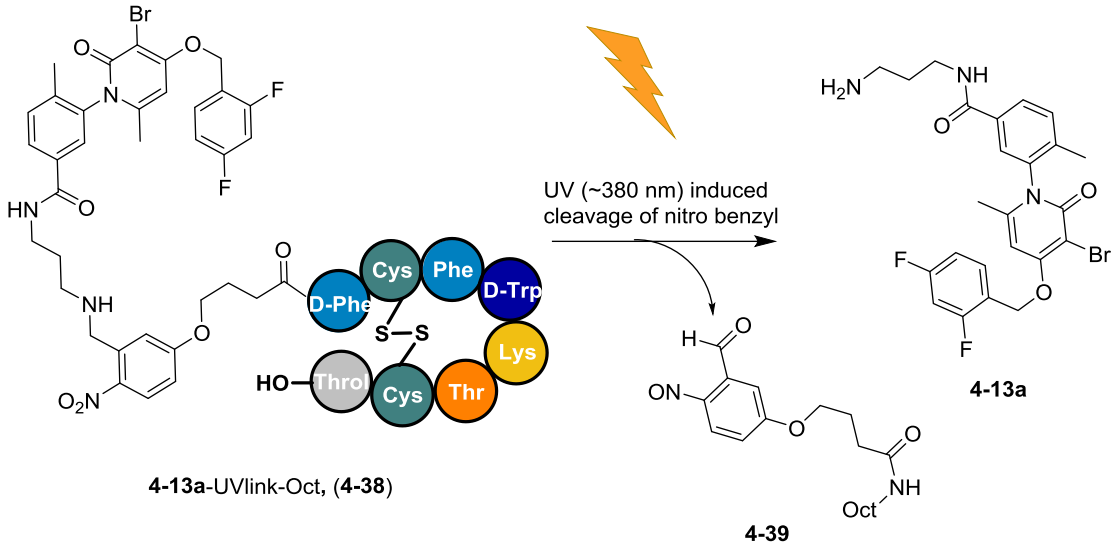

***Scheme 4.4.3. 4-38**, a UV-cleavable derivative of of octreotide bound to **4-13a**, drug conjugate, showing cleavage after exposure to UV light of 380 nm. The ONB linker acts as a caging group which can direct the drug conjugate to tumour cells, then be cleaved upon irradiation using UV light to release active **4-13a** locally in the tumour cells.*

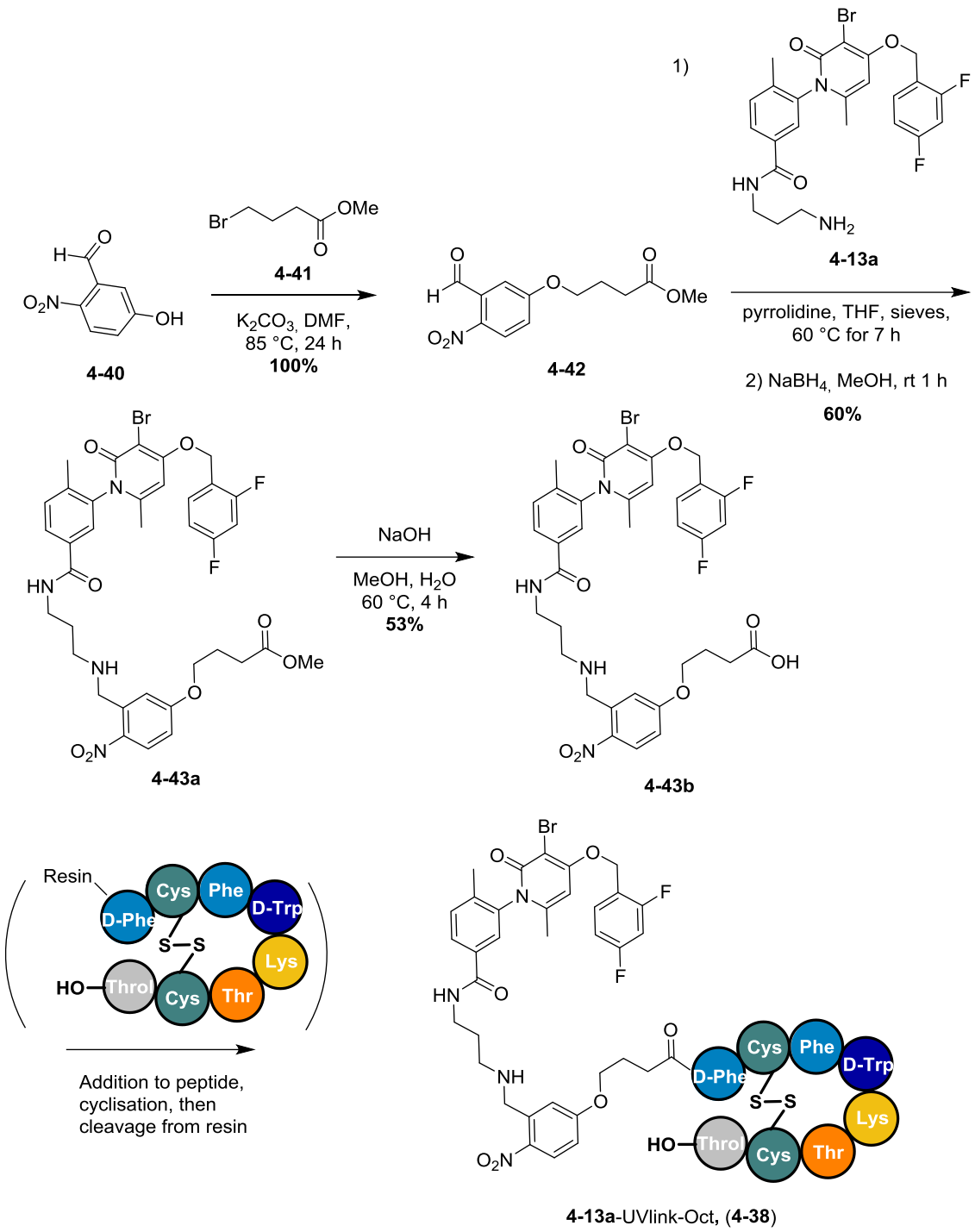

Scheme 4.4.4. *Synthesis of peptide-drug conjugate* ***4-13a****-UVlinker-Oct (****4-42****). Analogue* ***4-43b*** *was synthesised, before attachment to a resin-bound Octreotide (that had not yet been cyclised), then oxidised to form the cycle and cleaved from the resin to afford* ***4-42****, similar to the preparations described by Hsieh et al.*[10] *Final steps carried out by Joan Matarin.*

.

4.5. Design and Synthesis of PROTACs for the Degradation of p38α

We rationalised that the chemically-induced degradation of p38α would not only be an indispensable tool in the further validation of the p38 MAPK pathway and its involvement in cancer progression, but could also lead to novel therapeutic treatments in cancer. Targeted degradation of p38α could overcome the short-comings associated with existing p38α inhibitors, such as the lack of efficacy in clinical trials and off-target effects.

Proteolysis targeting chimera (Protac) are bifunctional compounds that induce the specific degradation of a target protein using the Ubiquitin Proteasome System (UPS), hijacking enzymes that are inherent in mammalian cells. Structurally, protacs consist of one end that specifically binds to the target protein, such as an inhibitor, covalently linked to an E3 ubiquitin ligase ligand (figure 4.5.1). The length and composition of the linker must bring the target protein and E3 ligase in close proximity to each other and with the correct orientation to initiate a protein-protein interaction. A ternary complex is formed and ultimately induces ubiquitination of the target protein.[11] The poly-ubiquitinated protein will then be degraded by the proteasome, inherent in cells. The pathway of this event-driven pharmacological process was depicted in figure 3.4.2.

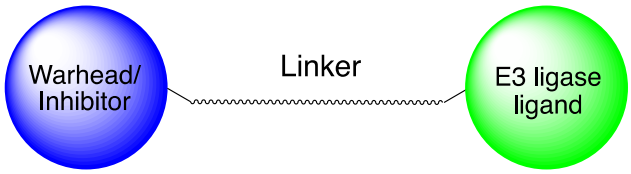

Figure 4.5.1. *A diagrammatic representation of a general protac structure, consisting of a warhead (blue) that has an affinity for the target protein, such as an inhibitor. This component is covalently bound via a linker to an E3 ubiquitin ligase ligand (green), which initiates the ubiquitin ligase and forms the ubiquitination complex of associated proteins.*

4.5.1. Selection of an E3 Ligase Ligand to Design **PH**-Based Protacs for Degradation of p38α

Modifying the amide position of **PH** was unlikely to interfere with the key interactions from which the inhibitor gains its activity and selectivity (figure 3.1.4).[12] Based on the rationale described in section 3.4 and the previous analogues synthesised and tested in this chapter, we reasoned that attachment of a linker in this location would also be best for the correct positioning of a linker and ligase initiator, directing them away from p38α's active site to allow heterodimerisation of p38α and the E3 ubiquitin ligase complex. This gave us our starting point for the **PH**-based warhead of the protac molecule. For the other side, we looked to the literature to select a ligand for the E3 ligase.

There are 4 main groups of small molecule-like ligands that have been reported to initiate E3 ligases and cause the polyubiquitination of target proteins (figure 3.4.3).[13] We commenced our initial screening using analogues of thalidomide, which include known recruitment ligands of CRBN E3 ligase already featured in published protac examples (figure 4.5.2). They can be synthesised with relative ease from commercially available starting materials. We also anticipated that resultant protacs would possess more drug-like properties such as metabolic stability and bioavailability than protacs based upon peptide-like ligands, such as VHL recruiting ligand.[14,15]

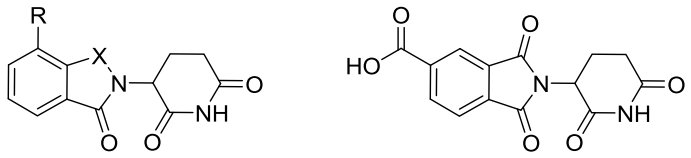

4-44a, R = H, X = CO
4-44b, R = OH, X = CO
4-44c, R = NH_2, X = CO Pomalidomide
4-44d, R = NH_2, X = CH_2 Lenalidomide

5' carboxylic acid thalidomide analogue, **4-45**

Figure 4.5.2. *Thalidomide (**4-44a**), phenol thalidomide analogue **4-44b**, marketed drugs Pomalidomide (**4-44c**) and Lenalidomide (**4-44d**)), and carboxylic acid analogue (**4-45**).*

With the identification of structural starting points for either side of the p38α protacs, we began optimisation of the linker. Thus, we embarked upon the synthesis of a collection of compounds with varying linker lengths to be tested in cellular assays to assess their degradation activity by monitoring total p38α in cells.

4.5.2. Synthesis of p38α PROTACs with Short, Simple Linkers

Early literature examples of protacs used phenolic thalidomide analogues, accessed *via* S_N2 reaction with a chloro-alkyl linker. We first tried to use this reaction starting from the commercially available anhydride **4-48**, but unfortunately without success (scheme 4.5.1).

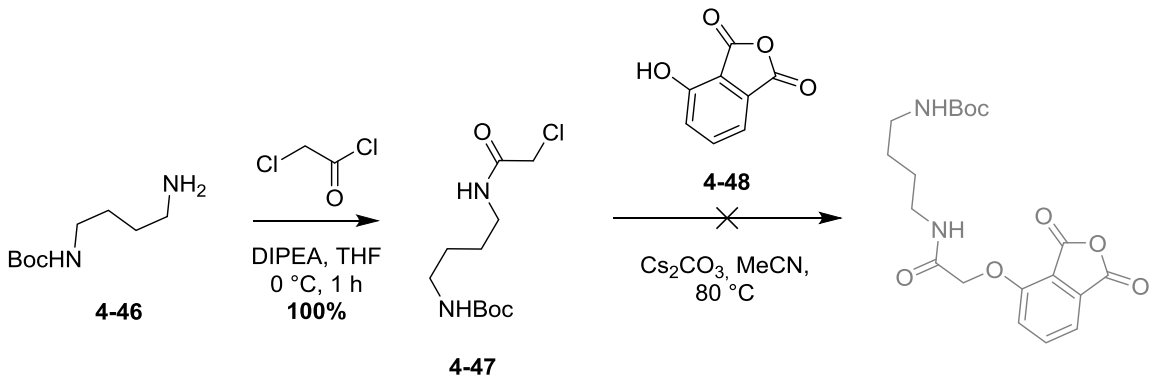

Scheme 4.5.1. *Reaction of phenol anhydride* ***4-48*** *with chloro linker* ***4-47****.*

The anhydride moiety was also susceptible to nucleophilic attack causing side reactions such as dimerisation to take place. We therefore attempted this step after protection of the anhydride as the di-methyl ester (**4-49,** scheme 4.5.2), which gave a successful outcome, affording the protected amine **4-50** in moderate yield. Hydrolysis of the diester allowed the recovery of the anhydride functionality in low yield (30%). The subsequent incorporation of the pthalimide component to anhydride **4-51**, and the deprotection of the terminal Boc group of the linker were also carried out successfully affording **4-54** as a TFA salt. Unfortunately, the final coupling reaction to incorporate the **PH** component using **4-7** did not yield any product, and there was very little material salvaged from the reaction mixture.

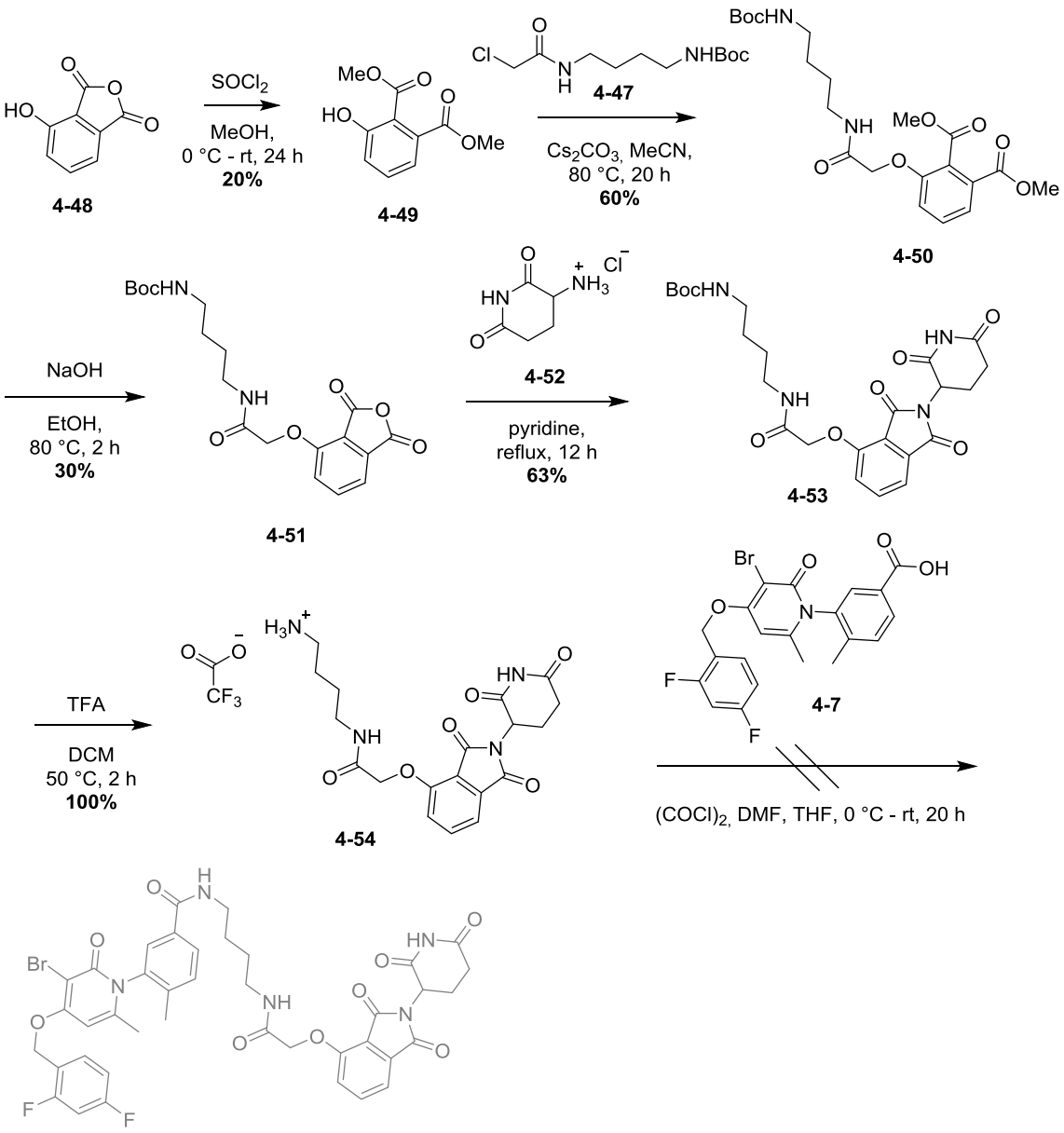

Scheme 4.5.2. *Reaction of ester-protected intermediate phenol* ***4-49*** *with chloro-substituted linker* ***4-47****.*

Due to the difficulties encountered following this route, we turned our attention away from the *O*-linked thalidomide structures to the *N*-linked structures, resembling pomalidomide. This route was therefore abandoned in favour of more direct routes to aniline-based protacs.

Initial routes using the commercially available compound, pomalidomide (**4-44c**) were unsuccessful due to the poor nucleophilicity of the aniline moiety, and the acidity of the NH proton of the 2,6-dioxopiperidine. Attempted reactions are depicted in scheme 4.5.3.

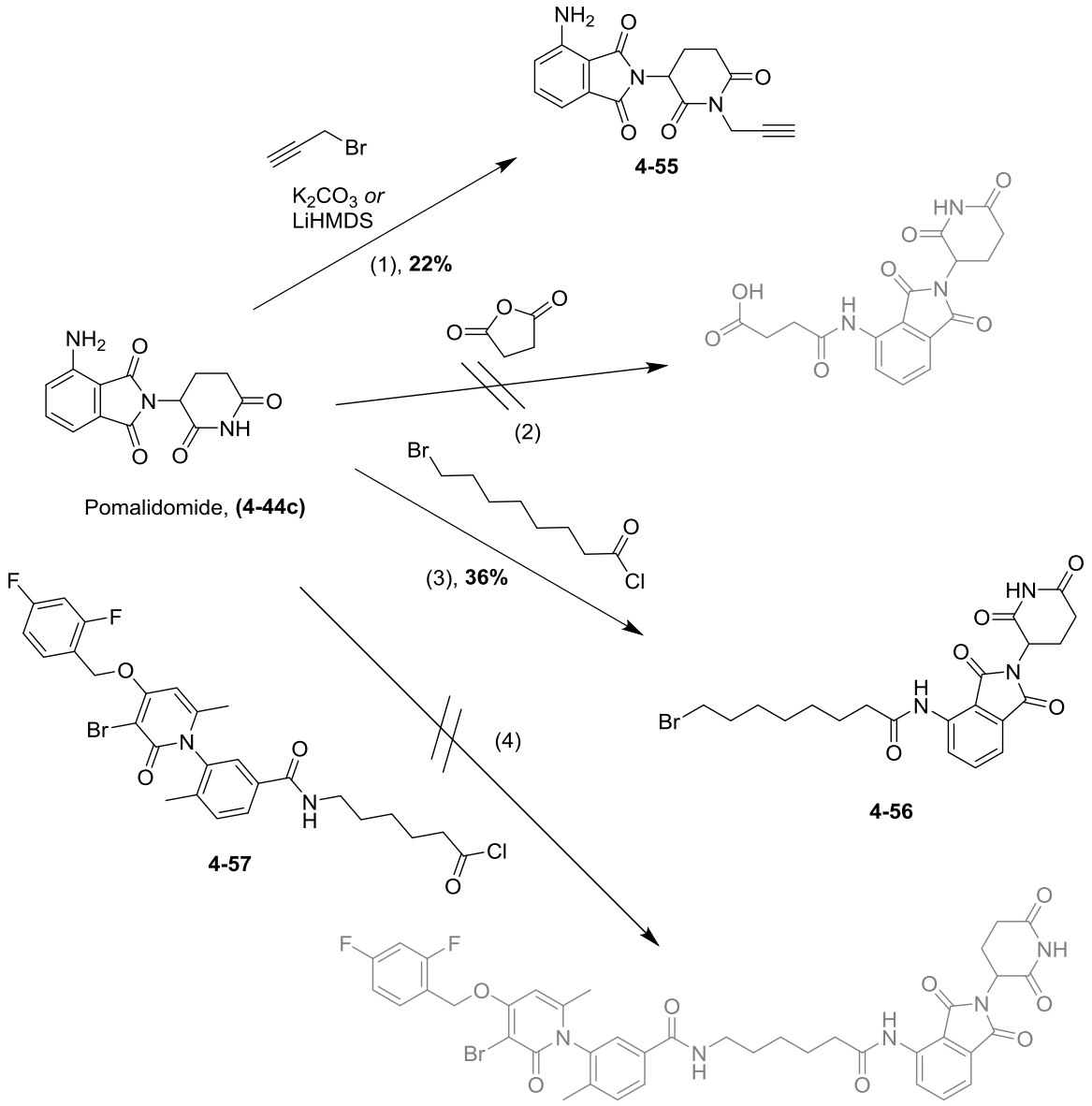

Scheme 4.5.3. *Initial reactions attempted using pomalidomide (**4-44c**) as a starting material.*

Despite increasing the temperature and reaction time of reactions, variation of the base and increasing equivalents, reaction of the aniline moiety of pomalidomide was not possible with bromo-alkyl substrates, anhydrides, or other electrophiles. S_N2 reaction of the NH of the 2,6-dioxopiperidine was preferred over that of the aniline when attempted using propargyl bromide (reaction 1), forming **4-55**. No S_N2 reaction took place with succinamide (reaction 2). Reaction with acid chloride to form **4-56** was possible in low yield (reaction

3), however when this reaction was repeated with the more complex acid chloride (**4-57**), the reaction did not yield any expected product (reaction 4).

With the subsequent appearance of more patented and published literature on protacs, it became evident that *N*-linked thalidomide analogues could be accessed *via* S_NAr reactions with fluoro-substituted anhydride precursors (**3-59**). This led us to begin the synthesis of an initial series of short *N*-linked protacs based on the key S_NAr step (scheme 4.5.4).

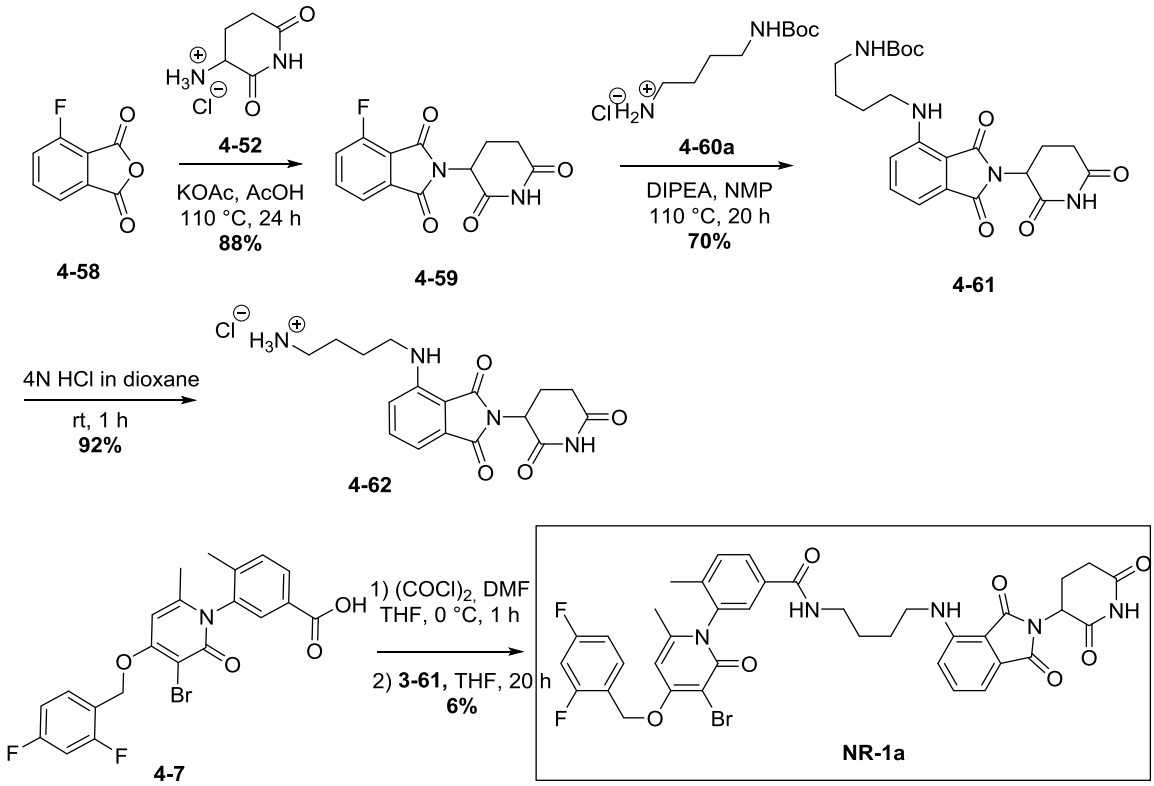

Scheme 4.5.4. *Route to protac* ***NR-1a*** *from commercially available fluoro-anhydride*

NR-1a was isolated in poor yield and had to be isolated by preparative TLC to obtain sufficient quantity for characterisation and cellular testing. **NR-1b** was made analogously using a mono-boc-protected diamino pegalyl linker (**4-63a** and **b**). The final step of the linker had to be modified to use the peptide coupling reaction conditions shown in the final

step to achieve the longer linker compound **NR-2c** in sufficient quantity for characterisation and cellular testing.

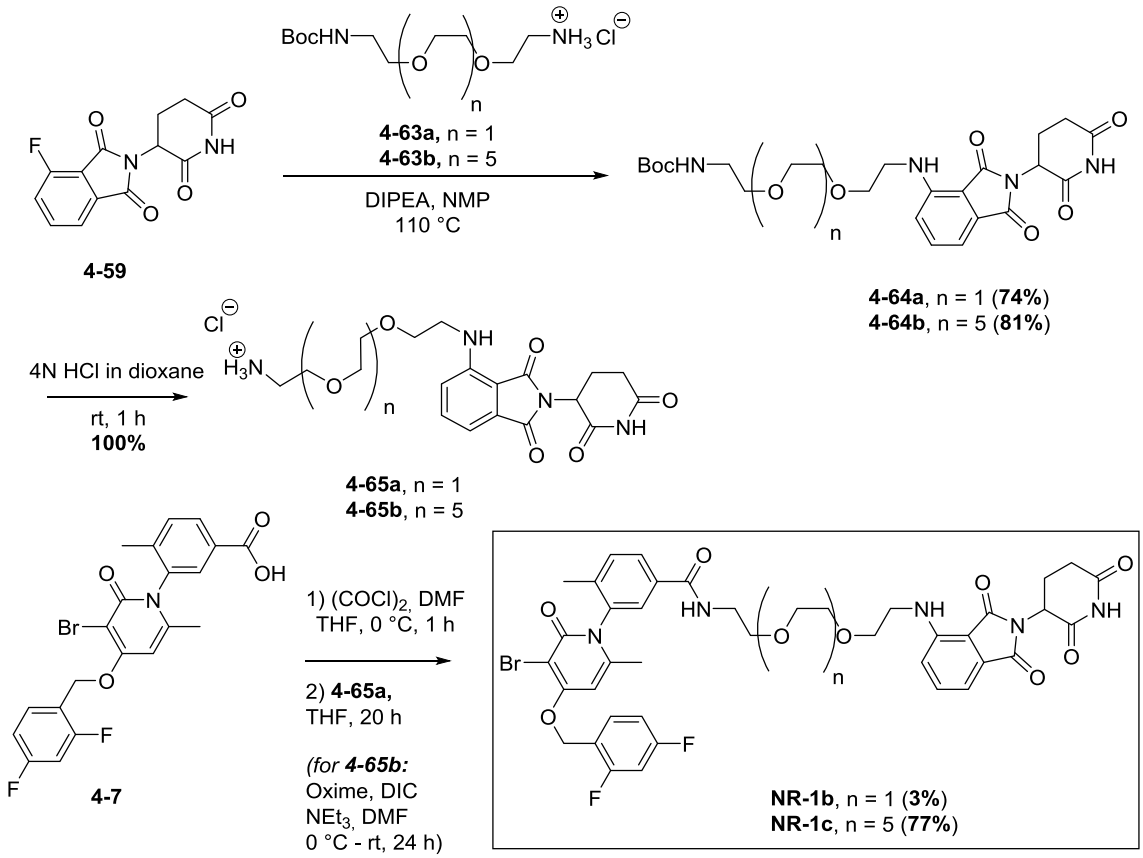

Scheme 4.5.5. *Analogously,* ***NR-1b*** *and* ***NR-1c*** *were synthesised from the fluoro anhydride starting material* ***4-59.***

Note that the yields to furnish C4 and 2PEG PROTACs **NR-1a** and **b** were so low due to the very messy acid chloride coupling step, which meant that products had to be separated from by-products using preparative-TLC. We therefore wanted to replace this acid chloride coupling step, to improve installation of future linkers, and which was subsequently used to afford **NR-1c** in improved yield (77%). Although this step was useful for generating **PH** on a large scale, and indeed isolation of **PH** was straightforward by precipitation and filtration. However, lower yields were obtained when these reaction conditions were repeated using larger amines for the synthesis of new analogues with more difficult isolation of the product due to varying solubilities of the new analogues, some of which formed a gum upon quenching with water. Therefore, a screening of different conditions

using anhydrous conditions and using various amide coupling reagents was carried out, table 4.5.1.

Table 4.5.1. *Screening of peptide coupling conditions for acid* ***4-7*** *to form* ***4-16b****.*

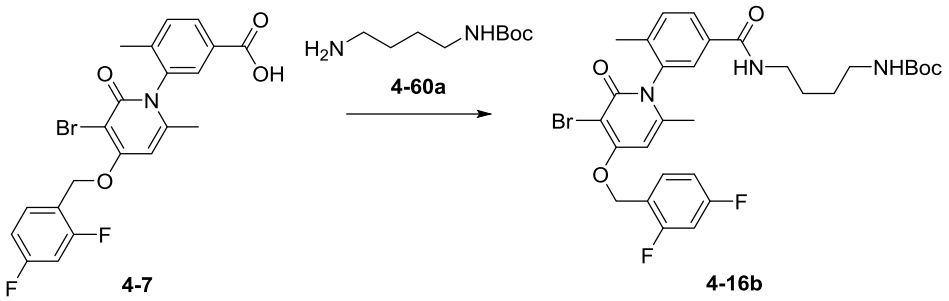

Entry	Conditions	T	T (h)	Yield
1	$(COCl)_2$, DMF, THF (*in situ* acyl chloride)	0-rt	20 h	12%
2	ByBOP, DIPEA, HOAt, DMF	0-rt	50	32%
3	T3P, DIPEA, DMF	rt	50	2%
4	DIC, oxime, NEt_3, DMF	0-rt	50	38%

It can be observed from table 4.5.1 that **PH** acid derivative **4-7** is a challenging substrate to perform amide coupling reactions with, which is reflected by a range of low yields for similar reactions in literature and patents. A low yield was obtained using triphosphorous anhydride (T3P), entry 3. This is a useful system as the phosphoric acid by-product is water soluble and can be removed by washing with water in the workup, however was not useful for this particular substrate, although would be utilised with other substrates. Higher yields were obtained using HOAt/ByBOP or oxime and DIC systems (entries 2 and 4), which were further optimised using other substrates to obtain much higher yields. The main urea side-product could not be removed by aqueous workup and required column chromatography to obtain pure product. The alternative reagent EDC is commonly used in larger scale operations, as the additional amine moiety provides more aqueous solubility in order for its by-product to be washed out in the aqueous workup phase. However, our cellular assays required only very small amounts of product, and our conditions were already optimised

for the more organic-soluble DIC. Therefore we continued to use DIC coupling reagent and left further optimisation of EDC conditions to be continued after a single active protac candidate had been identified and needed in larger scale.

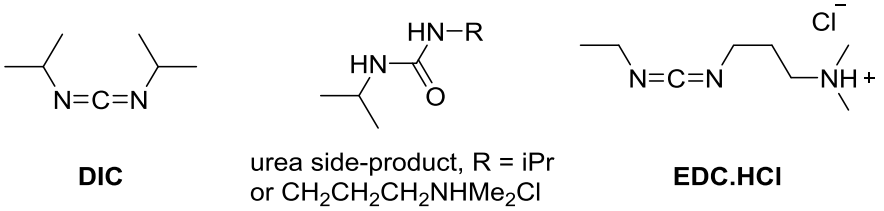

Figure 4.5.3. *The structures of DIC and EDC coupling reagents along with their corresponding urea side product.*

We also synthesised amide-linked PROTACs to investigate the activity of the 5′*meta*-postion, using a carboxylic acid anhydride that was a commercially available (**4-66**, scheme 4.5.6).

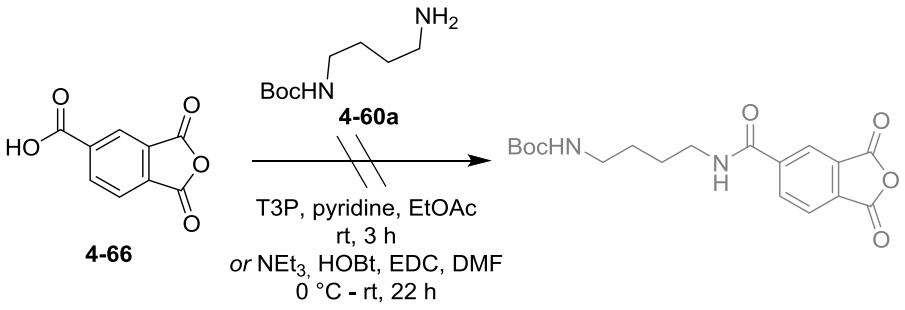

Scheme 4.5.6. *Unsuccessful amide coupling reaction using commercially available, acid-substituted anhydride* ***4-66****.*

After unsuccessful attempts to form the peptide starting from **4-66** using the coupling conditions from the table, we decided to first react the anhydride portion with the dioxopiperidine (**4-52**) to form the thalidomide core (**4-45**) then subsequently couple this with the boc-protected diaminocompound **4-60a**.

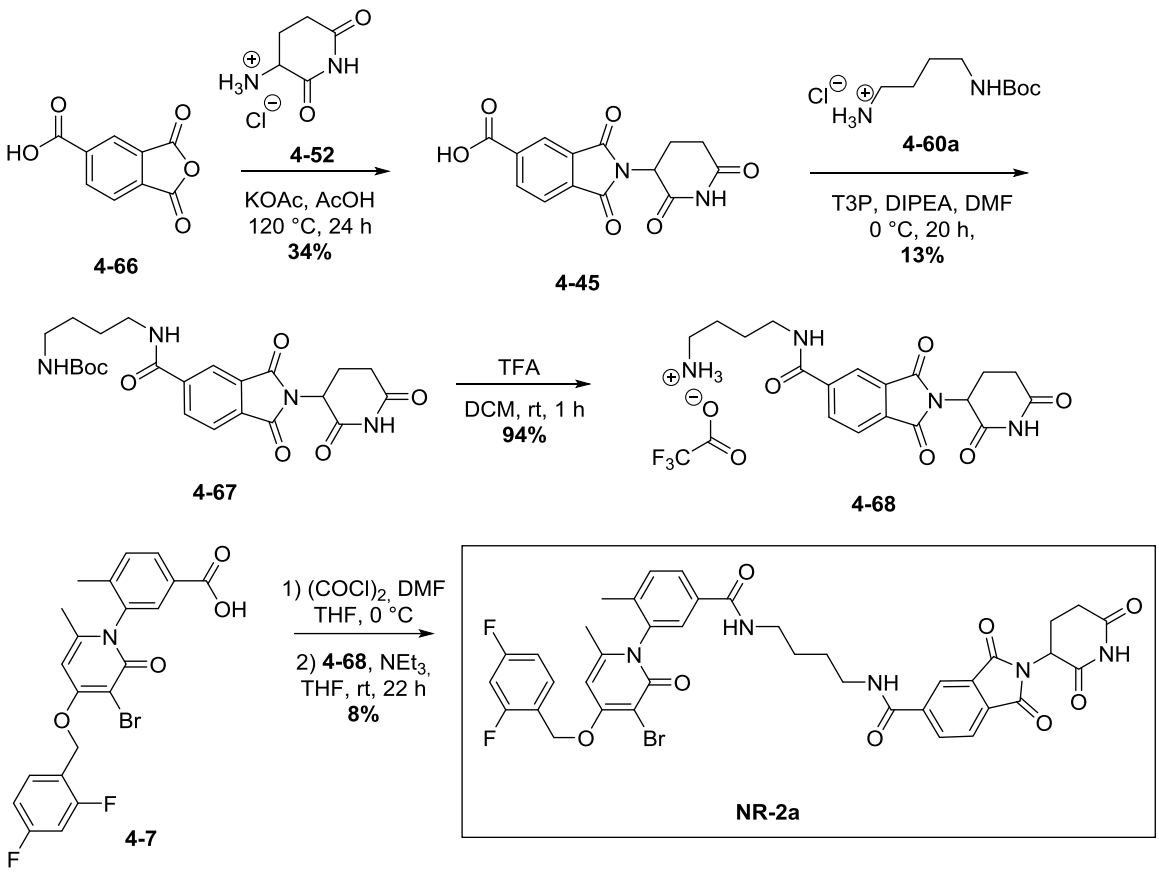

Scheme 4.5.7. *Synthetic route towards protac* ***NR-2a.***

This route was adequate to generate sufficient small amounts of protac **NR-2a** for cellular assays. The low yield of the final step was expected to have been improved by using the improved coupling conditions using DIC and oxime, however was not carried after the identification of these conditions. The same route was also used to generate analogue **NR-2b** using pegalyl chain **4-63a**, analogous to the *N*-linked protac **NR-1b** in order to compare linker connectors with the same linker (scheme 4.5.8).

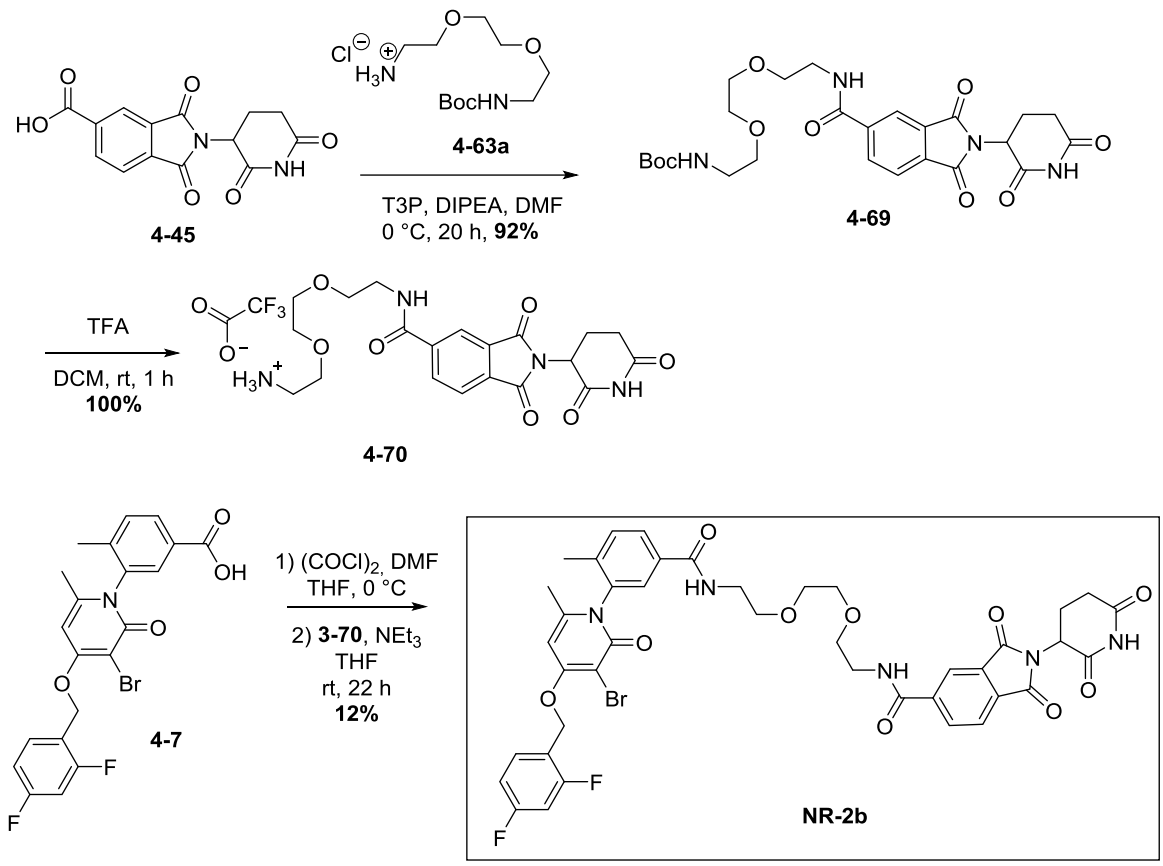

Scheme 4.5.8. *Synthesis of PROTAC* ***NR-2b.***

4.5.3. Biological Activity of PROTACS **NR-1a-c** and **NR-2a-b**

These five protac analogues were tested in cellular assays at concentrations of 10 μM, and the levels of total p38α were monitored 24 hours after addition of protac analogue. Specific fluorescent antibodies were used to detect the total p38α in the cell, regardless of whether it was phosphorylated or not (immunofluorescence).

Table 4.5.2. *PROTAC structures indicating their ability to induce p38α degradation after treating BBL358 or T47D cells for 24 h with a 10 μM solution (Yes >75%; Partial 25-75%; No <25% degradation).* ***1a-c*** *and* ***2a-b****.*

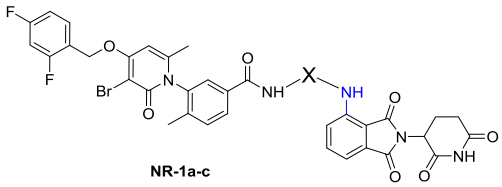

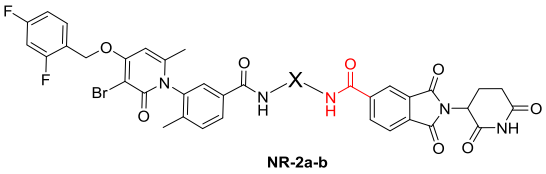

Compound	X (Linker)	Linker length (atoms)	Linker connection	Degradation	
				358	T47D
NR-1a	-$(CH_2)_4$-	4	4' –NH-	No	No
NR-2a	-$(CH_2)_4$-	4	5' –NHC(O)-	No	No
NR-1b	-CH_2-$(CH_2$-O-$CH_2)_2$-CH_2-	8	4' –NH-	No	No
NR-2b	-CH_2-$(CH_2$-O-$CH_2)_2$-CH_2-	8	5' –NHC(O)-	No	No
NR-1c	-CH_2-$(CH_2$-O-$CH_2)_6$-CH_2-	20	4' –NH-	Yes	No

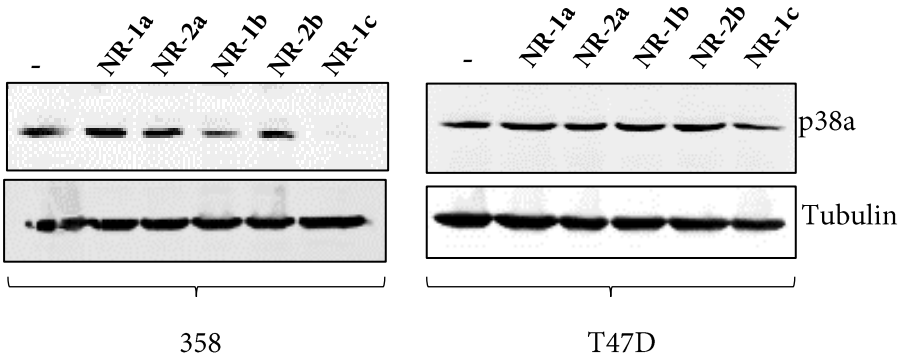

Figure 4.5.4. *The cell lines BBL358 (left) and T47D cells (right) were treated with 10 μM of the indicated PROTAC for 24 h and p38α expression was analysed by immunoblotting. Western-blots of the degradation of p38α in 358 and T47D cell lines after 24 h treatment of 10 μM solution of compounds* ***NR-1a-c*** *and* ***NR-2a-b****.*

It was found that protacs that possessed linkers of 4 or 8 atoms in length did not induce degradation of p38α in any cell line tested (table 4.5.2, compounds **NR-1a,b** and **NR-2a,b**). This was presumably because the protacs were too short to bind to both p38α and CRBN at the same time, preventing a favourable interaction between E3 ligase and target protein.

This would prevent the assembly of the ternary complex and impede ubiquitination. Gratifyingly, degradation activity was observed for the much longer linker length of 21 atoms in compound **NR-1c** within 358 cell lines. However, activity was not consistent throughout the cell lines tested, for example no activity was observed in T47D cells. This could perhaps be explained by the varying levels of E3 ligase present in different cell lines. However, when CRBN levels were revealed using specific antibodies in these two cell lines, we did not observe significantly lower expression in T47D cells.

4.5.4. Synthesis of p38α PROTACs with Longer Linkers

In order to further improve the scope of cell lines that could undergo degradation of p38α, longer protac analogues were synthesised to explore the effect of different linker lengths and compositions. We utilised a click chemistry platform to facilitate the synthesis of new protacs in possession of longer linkers, as depicted in the retrosynthesis in scheme 4.5.9. A similar approach was subsequently published by Wurz *et al.*[16] during the course of our investigation to synthesise unrelated PROTACS that target BET protein.

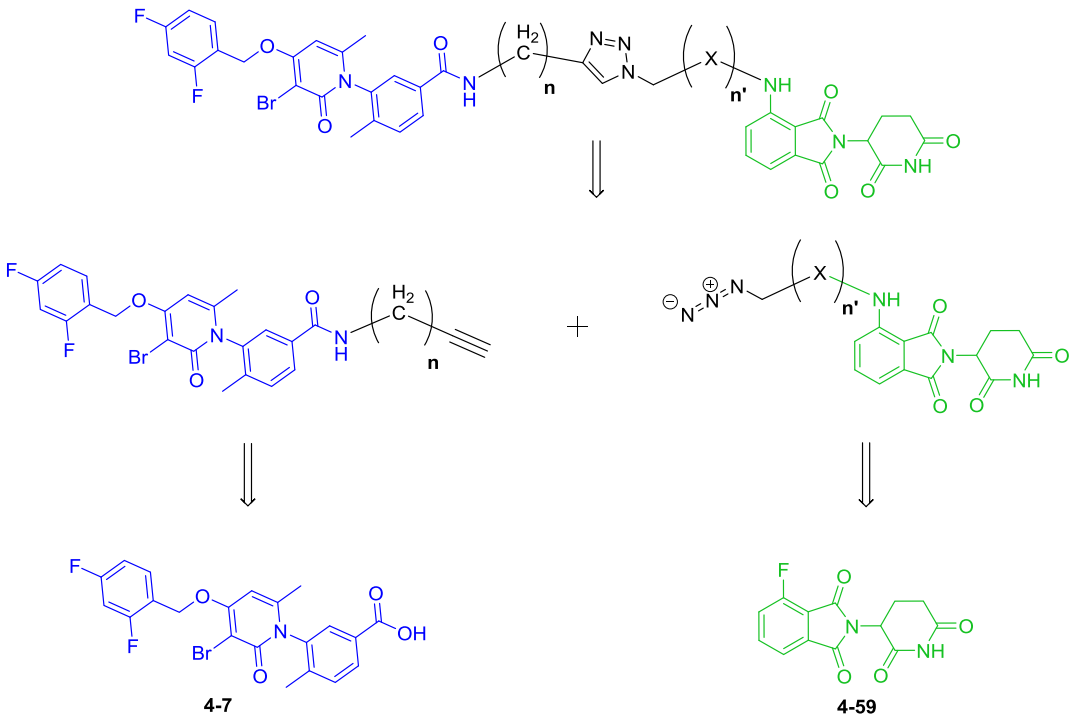

Scheme 4.5.9. *Retrosynthetic analysis of protacs in possession of longer linkers with amide and triazole moieties based on a key click reaction of the alkyne and azide components.*

By introducing a terminal alkyne to the **PH** side of the protac, we could then build up the thalidomide-linker side to possess a terminal azide and then "click" them together in a highly selective final reaction step.[17]

The triazole and amide moieties resulting from this route were expected reduce the flexibility of these linkers to some extent, and we anticipated a potential gain in potency through the positive interaction of these functionalities with the protein surfaces, as had been observed using other protacs in the literature.[18]

When we used the improved peptide coupling conditions from table 4.5.1 to synthesise compound **4-72a**, the yield was improved to 77% (scheme 4.5.10). This intermediate was synthesised on a larger scale for subsequent click reactions with the corresponding azides of the thalidomide end.

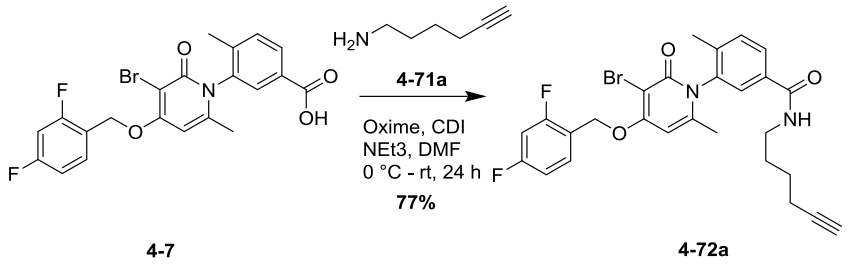

Scheme 4.5.10. *Synthesis of key* ***PH*** *alkyne intermediate* ***4-72a.***

Protacs **NR-3a** and **3b** were then generated utilising the previously identified S_NAr methodology to construct the azide thalidomide fragment (described in scheme 4.5.5) then perform the click reaction with alkyne **4-72a**. These protac analogues were then synthesised using the following synthetic routes shown in schemes 4.5.11.

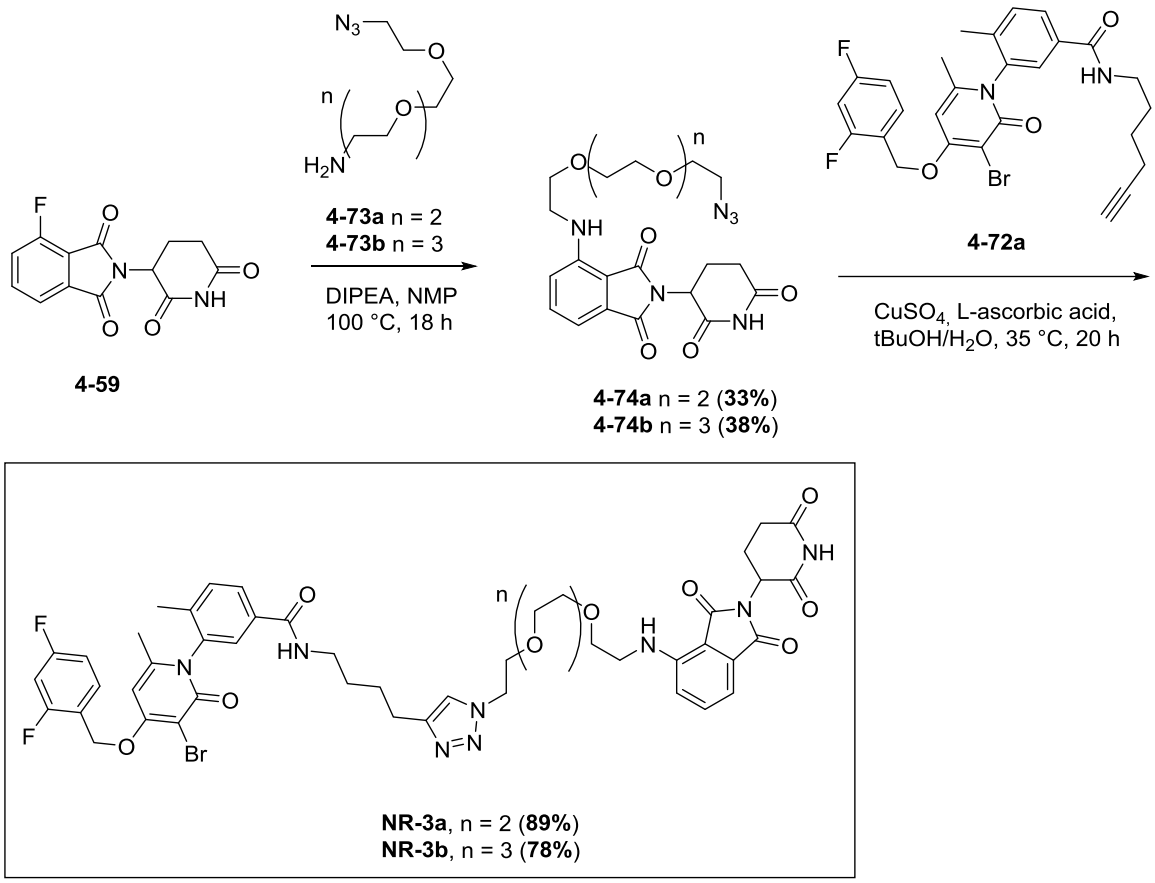

Scheme 4.5.11. *Reaction conditions for the synthesis of protac analogues* ***NR-3a*** *and* ***3b*** *featuring long pegalyl linkers and triazole moieties.*

The high cost of the longer PEG linkers **4-73a** and **b,** featuring a terminal azide and amine, combined with the poor yield of the S_NAr to install them to the thalidomide fragment were 2 large drawbacks of this route. Therefore compound **4-77** was used to install the azide moiety onto terminal amines of future thalidomide fragments, which can be easily synthesised in a 2 step, 1-pot process (scheme 4.5.12).

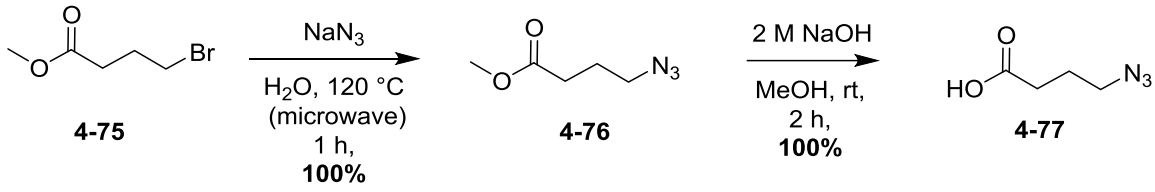

Scheme 4.5.12. *2-step, 1-pot process towards intermediate* ***4-76,*** *for the facile installation of terminal azides to thalidomide fragments.*

Compounds **NR-3c** and **NR-4** were synthesised by coupling the previously made PEG2 linker thalidomide fragments (**4-65a** and **4-70)** with azide **4-77** to afford **4-78** and **4-79**. These were then reacted with alkyne **4-72a** in a final click reaction as for PROTACs **NR-3a-b** (scheme 4.5.13).

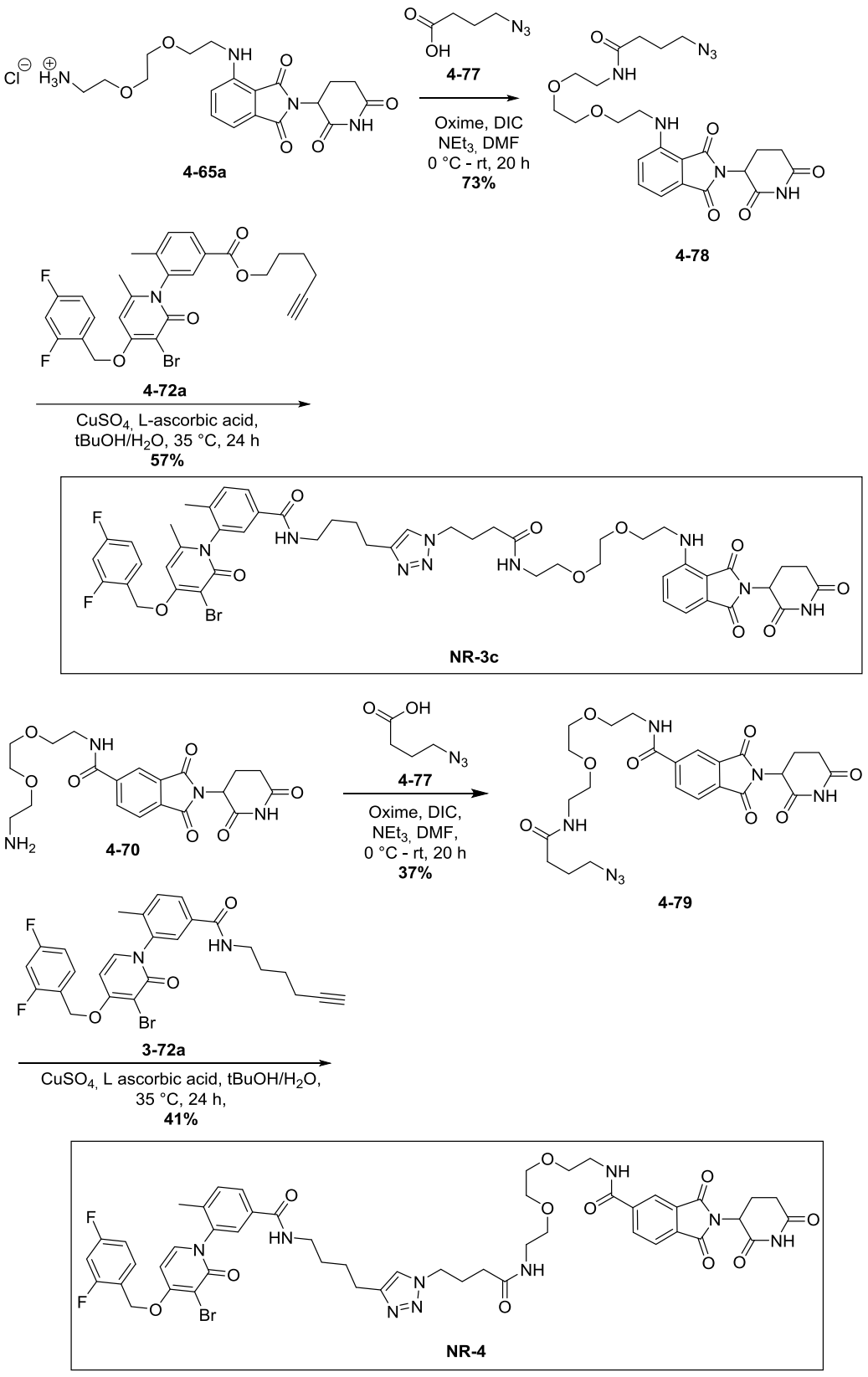

Scheme 4.5.13. *Synthetic route towards* ***NR-3c*** *and* ***NR-4****.*

This route achieved a higher yield in the S_NAr step (70-81% over 33-38%) as the amine nucleophile did not possess an azide, but rather a Boc-protected amine moiety on the opposite end, which proved more resistant to the high reaction temperature of this step. This reagent was also less expensive, and could then easily be deprotected and coupled with aza-acid intermediate **4-77** to afford a terminal azide linker in a more cost-effective manner. The corresponding analogue **NR-4** was also prepared by this route to give 2 PROTACs with the same linker, but differing only in their connection to the thalidomide fragment. This would determine whether the linkage to the thalidomide analogue has an effect on PROTAC activity, (i.e. 5'amide compared to 4'-aniline), shown in scheme 4.5.13. These compounds were then tested in the cellular assay as described previously, the results are shown in table 4.5.3.

Compound **NR-8** was also synthesised to examine the effect of a reverse-amide in the 4'-position, encouraged by literature precedents featuring this linkage to thalidomide in PROTACs targeting other proteins. For this PROTAC we used the intermediate **4-56** from our previous screening of reaction conditions to functionalise pomalidomide (scheme 4.5.3). Although this intermediate was not useful using our non-click methodology, it could now be subjected to azide formation and click reaction with alkyne **4-72a** (scheme 3.3.14)**.** This gave rise to a protac with a shorter linker than active analogue **NR-3c** (17 as opposed to 20 atoms long), which is not a direct comparison in linker length or composition, but would be useful to see if this type of linker would indeed induce degradation of p38α.

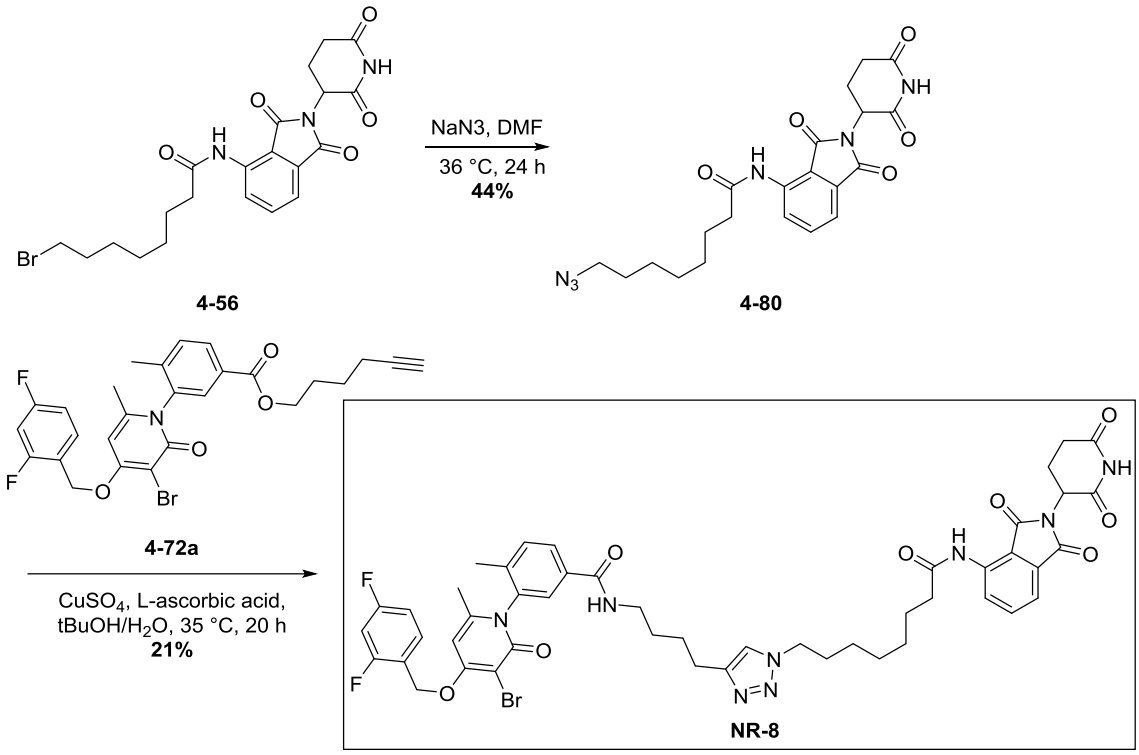

Scheme 4.5.14. *Synthesis of protac* ***NR-8*** *transforming bromo intermediate* ***4-56*** *into azide intermediate* ***4-80,*** *then performing a click reaction with alkyne* ***4-72a.***

Lastly, it is known that the NH moiety of thalidomide is essential for binding the E3 ligase CRBN. PROTACs featuring a methyl or a benzyl group in this position do not induce degradation, as there is no affinity to E3 ligase and the compound therefore cannot induce the ubiquitination and degradation of the target protein. PROTACs of this type are normally generated to use as control compounds in PROTAC development programmes. We therefore added an ONB group to the NH moiety of PROTAC **NR-3c,** (with the same linker length as active PROTAC **NR-1c**) to have a negative control PROTAC to trial alongside the others in the standard cellular assays.

4.5.5. Biological evaluation of PROTACs **NR-3a-d, NR-4** and **NR-8**

Table 4.5.3. *Degradation of p38a after 24 h treatment of 10 μM solution of compounds* ***3a-d, NR-4, NR-8****.*

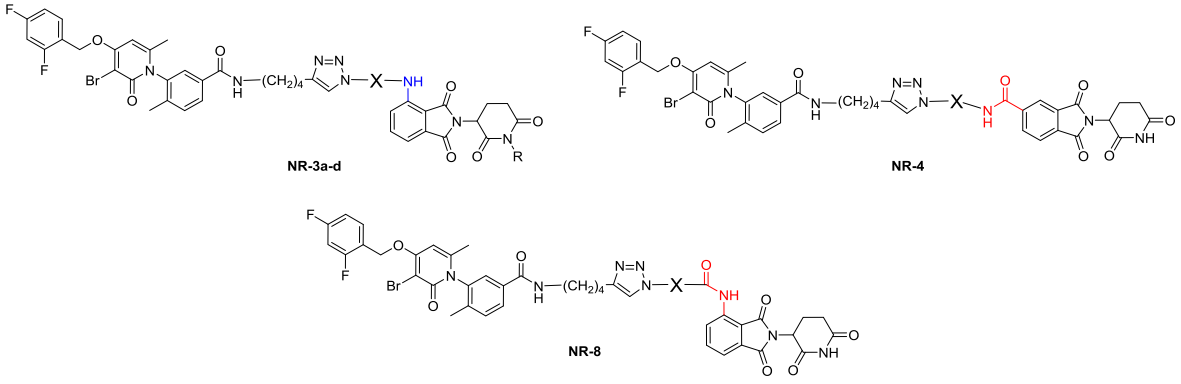

Cmpd	Fragment X	R	Linker length (atoms)	Linker connection	p38α degradation	
					358	T47D
NR-3a	-CH_2-(CH_2-O-CH_2)$_3$-CH_2-	H	18	4' -NH-	Partial	No
NR-3b	-CH_2-(CH_2-O-CH_2)$_4$-CH_2-	H	21	4' -NH-	Yes	No
NR-3c	-(CH_2)$_3$-CO-NH-CH_2-(CH_2-O-CH_2)$_2$-CH_2-	H	20	4' -NH-	Yes	Partial
NR-3d	-(CH_2)$_3$-CO-NH-CH_2-(CH_2-O-CH_2)$_2$-CH_2-	ONB	20	4' –NH-	No	No
NR-4	-(CH_2)$_3$-CO-NH-CH_2-(CH_2-O-CH_2)$_2$-CH_2-	H	20	5' -CONH-	No	No
NR-8	-(CH_2)$_7$-	H	17	4'-NHCO-	No	No

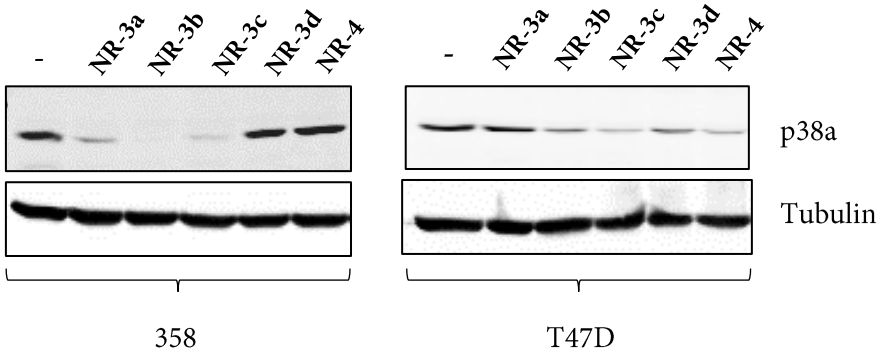

Figure 4.5.5. *Western-blots of the degradation of p38α in 358 and T47D cell lines after 24 h treatment of 10 μM solution of compounds* ***NR-3a-d, NR-4*** *&* ***8****.*

The results shown in the above western blot and table confirm that protacs in possession of linkers 18 to 21 atoms in length were also active (**NR-3a-c**) apart from control PROTAC **NR-3d**, blocked by an ONB group**,** which was observed to be inactive. Interestingly, **NR-4**, which has the exact same linker as **NR-3c**, but differs only in its connection to thalidomide *via* an amide bond in the 5' position, as opposed to a 4' aniline connection, did not degrade p38α in any cell line tested (perhaps partially in T47D cells). This emphasises the importance of the orientation of the thalidomide fragment relative to the linker. .**NR-8** did not induce p38α degradation in any of the cell lines tested, although this compound was not included when testing this series.

Also interestingly, **NR-3c** is more potent than **NR-3a-b** in T47D cells and has comparable potency in 358 cells. **NR-1c,** (figure 4.5.3), which is the same length as **NR-3c**, but lacks triazole or amide moieties, does not degrade p38α in T47D cells, which suggests that the triazole and amide moieties play a role in activating the E3 ligase complex, at least in certain cell lines.

As mentioned, the N-H of thalidomide is crucial for ligase affinity and by replacing this hydrogen with a nitro-benzyl group (ONB, **NR-3d**) we were able to diminish affinity for CRBN ligase, thus blocking the degradation activity demonstrated in NH compound **NR-3c**. Furthermore, this group can be removed by ultra violet irradiation (as discussed in section 4.2) to reform the active protac analogue **NR-3c** (scheme 4.5.15).

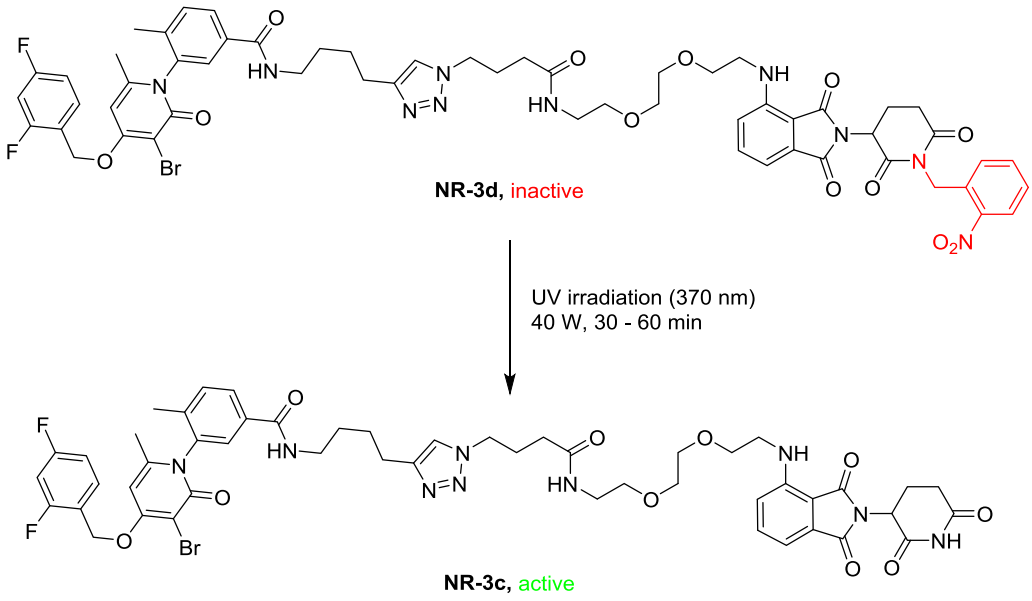

Scheme 4.5.15. *Liberation of active protac* ***NR-3c*** *by irradiation using UV light to inactive (caged) protac* ***NR-3d****.*

The cleavage of **NR-3d** using UV light (uncaging) was successfully performed *in vitro* using solvents that closely represented conditions of the cellular assays (10 μM DMSO in water). Disappearance of **NR-3d** was monitored by uHPLC and was >80% complete in under 30 mins. Substantial compound had disappeared after 10 min, which is more compatible with cellular exposure times for caged compounds (figure 4.5.6). However, when the initial trial was carried out in the cellular assays to perform the reaction within cells, the inactive compound was also active (*ie* degraded p38α), potentially due to a mix up of samples or an unintended exposure to UV light. Further testing and optimisation of a photo-cleavable protac is ongoing.

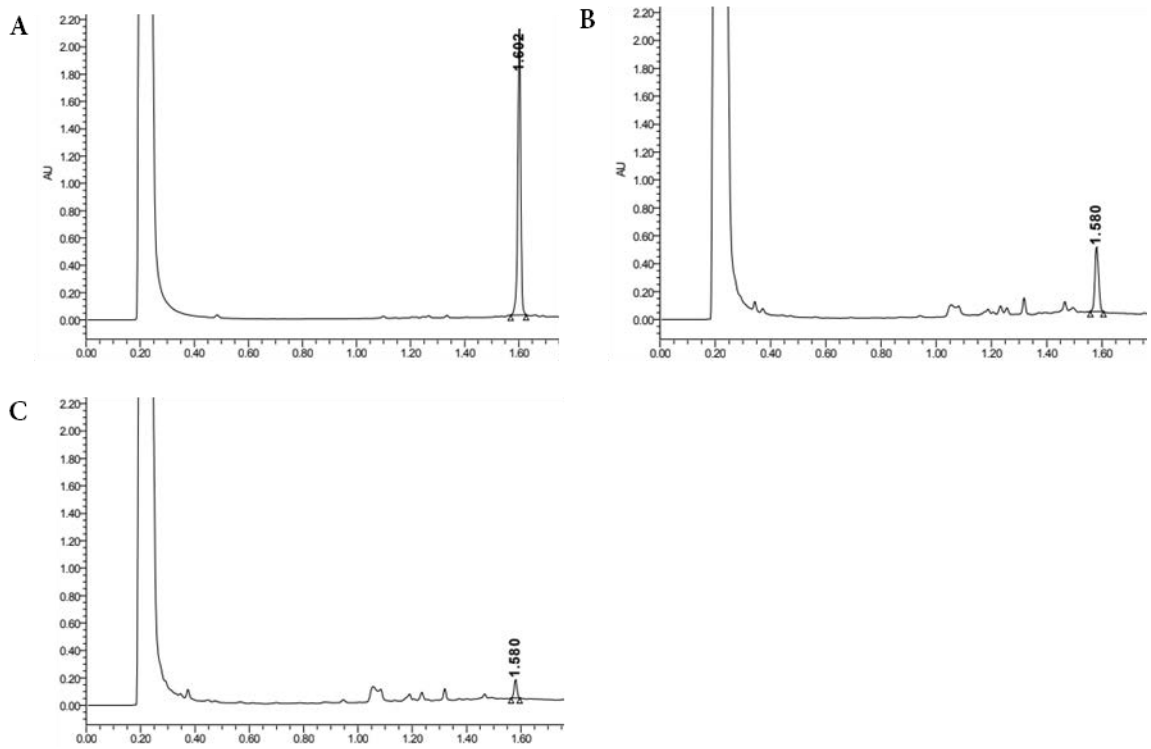

Figure 4.5.6. *Disappearance of* ***NR-3d*** *(RT = 1.58 – 1.60min), by application of UV light (~380 nm) by a radleys lamp at room temperature in aqueous solution (<1% DMSO). A = 0 min, B = 10 min, C = 30 min*

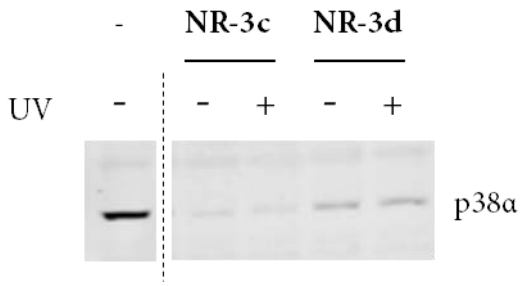

Figure 4.5.7. *Western blot result from the experiment using* ***NR-3c*** *and* ***NR-3d*** *PROTACs to degrade p38α, as previously. + cells were treated with UV light from a 40 Watt UV lamp, 15-20 cm distance from the cell plate (lid removed) for 5 minutes, then after 5 mintues resting, another 5 minutes of UV radiation.*

4.5.6. Replacing the Aniline Linker Connection with a Methylene to Obtain *C*-Linked PROTACs (**NR-5a,b** and **NR-6a,b**)

Shaomeng Wang *et al.,* described the replacement of the 4' NH group connecting thalidomide with a 4' methylene group and removal of one of the carbonyls from the indoline moiety (resembling *Lenalidomide*) resulted in a BET degrader with 2 – 3 times more potency than the initial pomalidomide-based protac of the same length.[19] They suggested that this was due to improved pharmacokinetic profiles as opposed to an improvement in the affinity for the CRBN. Fischer *et al.* observed that a thalidomide analogue with a 4' methyl substituent, which lacked one carbonyl from the indoline moiety had higher relative binding affinity for CRBN than lenalidomide, pomalidomide or thalidomide (note, not PROTACs here, but free thalidomide analogues binding and inhibiting CRBN target).[20] We thus designed compounds **5a-b** and **6a-b** to examine the effect of medium length methylene linkers on degradation of p38α with and without the pthalimide carbonyl.

Compounds of this methylene linker type were synthesised based on our previous routes and also incorporating steps towards new thalidomide fragments (**4-85a-b, 4-91a-b**) based on those used and developed in the Shaomeng group (schemes 4.5.16 and 4.5.17). Bromo substituted anhydride intermediate **4-82** was commercially available and was subjected to ring opening using **4-52** to form the thalidomide core as was performed previously, in good yield (81%, scheme 4.5.16). Alkyne analogues **4-71a-b** were boc protected using boc2 anhydride, then coupled to the bromo-thalidomide analogue **4-83** *via* a Sonagashira reaction to form **4-84a-b**. Subsequent reduction of the alkyne moiety using hydrogen over palladium on carbon catalyst followed by removal of the boc protecting group afforded primary amine intermediates **4-85a-b** as the trifluoroacetate salts. These intermediates could then be reacted as previously with aza-acid intermediate **4-77** to achieve azide intermediates **4-86a-b** in moderate yield (49 – 68%), which then underwent click reaction with **PH**-alkyne intermediate **4-71a** to furnish PROTACs **NR-5a-b** in moderate to low yield

(26 – 59%). Note that the lower yields of these analogues may have been because of coordination of the many functionalities present in these complex molecules. This was later overcome by preforming active copper species from CuI using acetic acid and ascorbic acid, more rigorous degassing of the mixture using N_2 at this stage before adding the reagents.

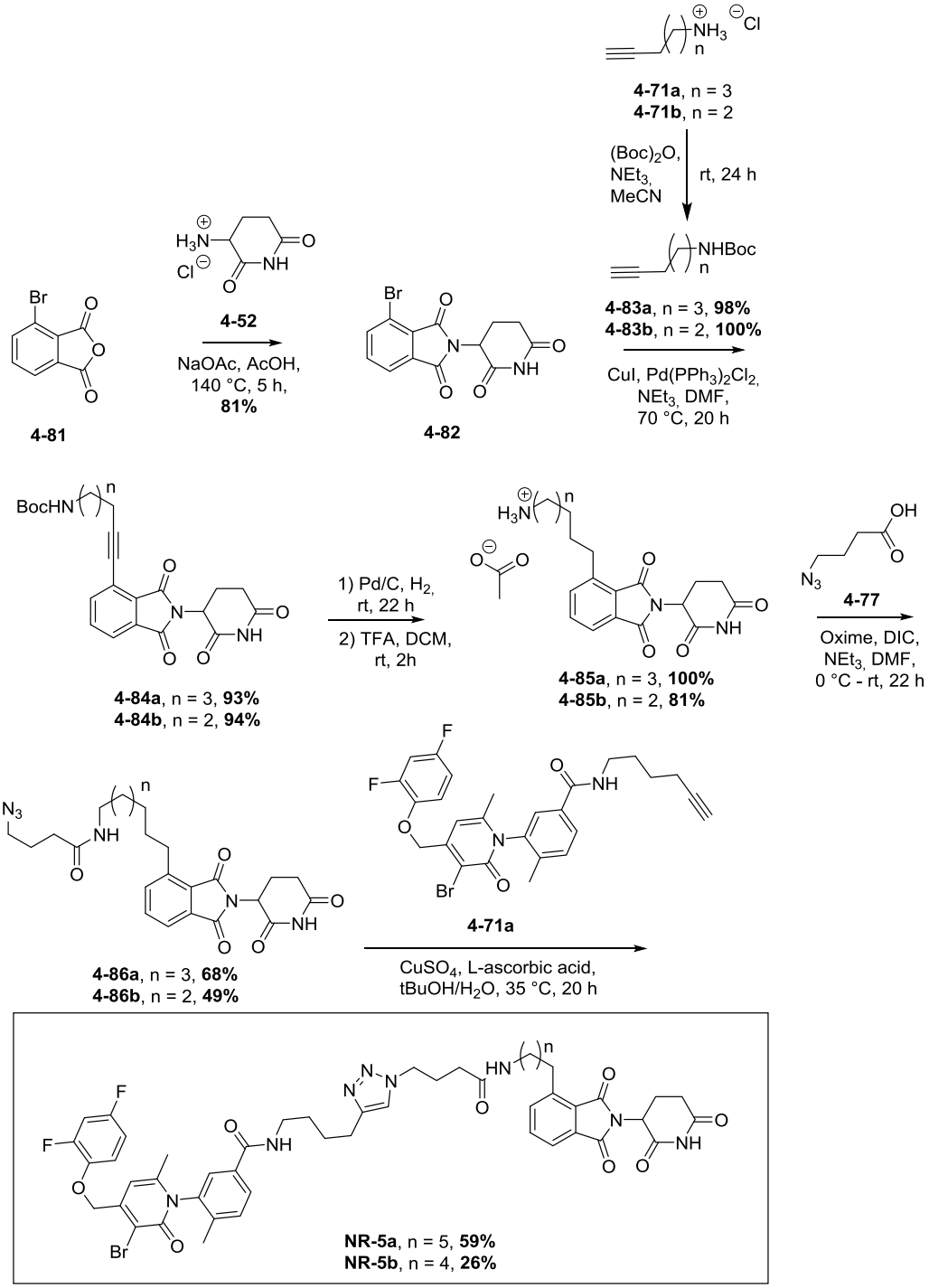

Scheme 4.5.16. *Protacs* ***NR-5a*** *and* ***b.*** *The route based on our previous work and methodology described by the Shaomeng group.*

PROTACs **NR-6a-b** were synthesised analogously but starting from bromo intermediate **4-87**. The lack of the carbonyl meant that **4-87** could not be prepared from anhydride **4-80,** Therefore, the radical induced bromination of aryl methyl compound **4-85** was carried out, to form **4-86,** which was then subjected to S_N2 reaction and ring formation with piperidinone intermediate **4-52**. Aryl bromo intermediate **4-87** was then used in the subsequent Sonogashira coupling, hydrogenation and Boc deprotection, peptide coupling with azide **4-76** and then click reaction with **4-71a** steps to afford the PROTAC products in moderate yields (scheme 4.5.17).

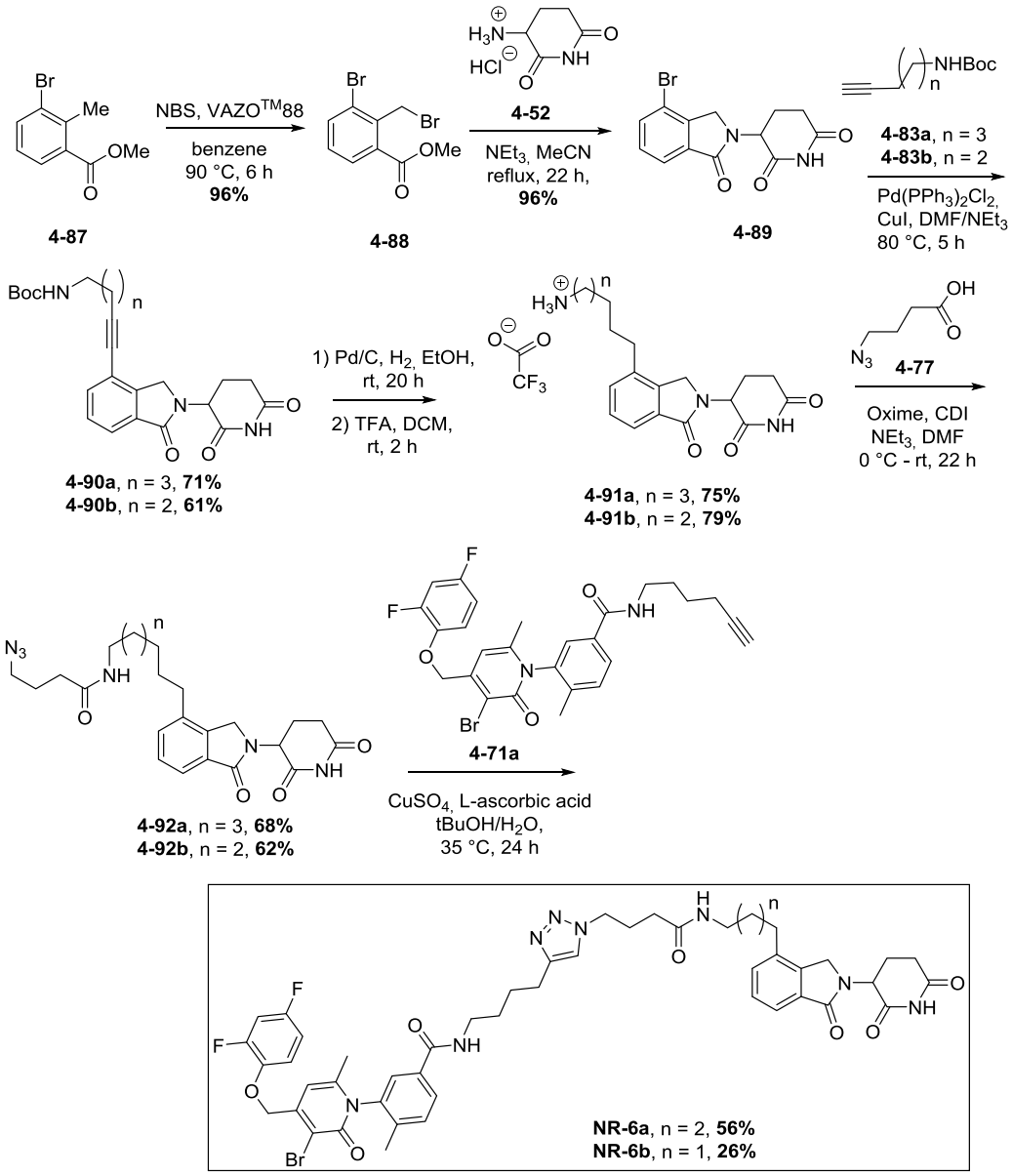

Scheme 4.5.17. *Synthetic route towards protacs* ***NR-6a*** *and* ***b,*** *involving the radical bromination of the aryl methyl group of compound* ***4-87,*** *then*

*cyclisation of the ring to form the thalidomide-type core of **4-89.** This then underwent the same conditions as **5a-b** from scheme 4.5.17.*

We also attempted the synthesis of a lenalidomide version of **NR-6a,** where one of the carbonyl groups of the thalidomide fragment was removed. However, the aldehyde intermediates required for these analogues (**4-94)** were highly unstable, difficult to isolate and we could not successfully perform the reductive amination step with lenalidomide (**4-44c**) to obtain PROTAC product **NR-9**. We did not pursue this target further (scheme 4.5.18).

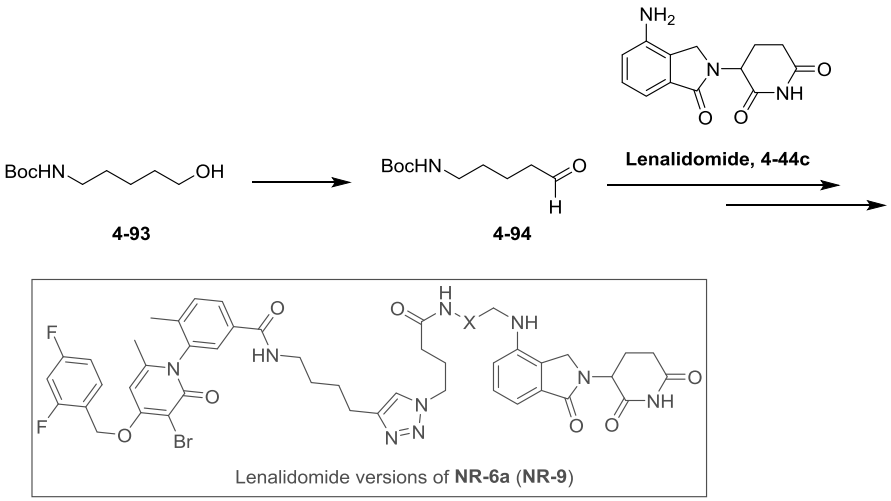

Scheme 4.5.18.** Attempted synthesis of the lenalidomide versions of PROTACs **NR-3c** and **NR-6a.

4.5.7. Biological Assessment of PROTACs **NR-5-6a-b**

Table 4.5.4. *PROTACs **NR-5a-b** and **NR-6a-b** indicating their ability to induce p38α degradation after treating BBL358 ot T47D cells for 24 h with a 10 μM solution (Yes >75%; Partial 25-75%; No <25% degradation).*

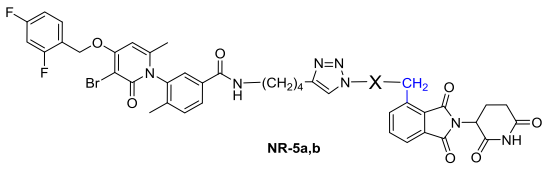

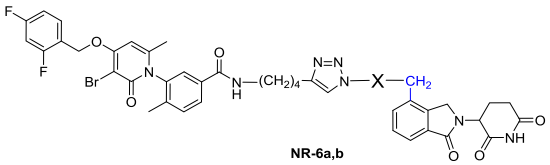

Cmpd	Linker "X"	Length (atoms)	Linker Connection	P38α degradation 358	P38α degradation T47D
NR-5a	-$(CH_2)_3$-C(O)-NH-$(CH_2)_5$-	17	4'-CH_2-	No	Yes
NR-5b	-$(CH_2)_3$-C(O)-NH--$CH_2)_4$-	16	4'-CH_2-	Partial	Yes
NR-6a	-$(CH_2)_3$-C(O)-NH-$(CH_2)_5$-	17	4'-CH_2-	Yes	Yes
NR-6b	-$(CH_2)_3$-C(O)-NH-$(CH_2)_4$-	16	4''-CH_2-	Partial	No

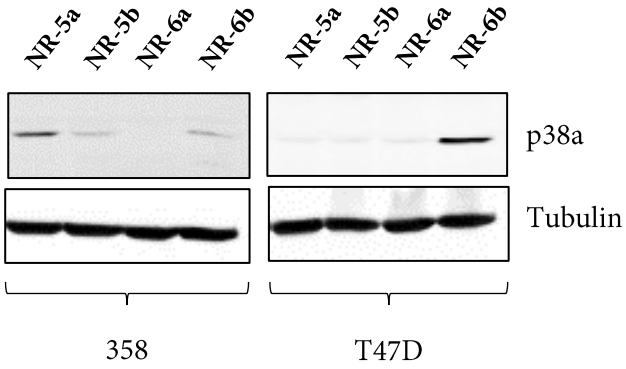

Figure 4.5.8. *Western-blots of the degradation of p38α in 358 and T47D cell lines after 24 h treatment of 10 μM solution of compounds **NR-5a-b** and **NR-6a-b**.*

Protac **NR-6a** showed a very high level of p38 degradation in both 358 and in T47D cells, making it the most active compound of the series. Interestingly, protac **NR-6b,** which is just 1 carbon shorter than **NR-6a,** did not degrade p38α in T47D cells at all and only partially induced degradation in 358 cells. **NR-5a** also resembles **NR-6a** but maintains both

carbonyls of the isoindole moiety, however almost no degradation was observed in 358 cells. This raises interest as to the exact role linker length and thalidomide composition play in protein degradation, and whether general rules can be established for the SAR. From our initial and few results it is hard to draw clear comparisons, but it appears that lenalidomide and pomalidomide based protacs do not follow the same rules for an optimal linker length. Indeed one might wonder if the same E3 ubiquitin ligase complex is being initiated and formed in each case, and also if p38α is being ubiquitinated on the same lysine residue every time for degradation to occur. We postulated this could explain why changes to linker length and connection to thalidomide affected degradation activity so drastically. As this was not the aim of the thesis and without resources to begin investigating these questions, we unfortunately await more data being published in this field.

Compounds **NR-5a** and **6a**, which possessed linkers of 17 atoms long, also provided a fair comparison with **NR-8,** whose linker was also 17 atoms in length, but possessed an amide connection to thalidomide. As mentioned, there are examples of PROTACs active against other targets with this type of connection to thalidomide in the literature, therefore the inactivity could be due to a change in orientation, as opposed to electron or steric changes, and again challenges any general rules we attempted to form for the SAR of this series of PROTACs.

4.5.8. Fine-Tuning the Linker Length in the *N*-Linked PROTAC Series

Since the most active protac in our series so far (**NR-6a**) had a linker of 17 atoms, we returned to the aniline series to closely examine the effect that small changes to linker length made to the protac activity. A collection of protac analogues (**NR-7a-h**) was synthesised, decreasing the length either side of the triazole and amide moieties using alkyl linkers of 2

– 4 carbons in length, using the methodology as before with analogue **NR-3c** (scheme 4.5.19 and 4.5.20).

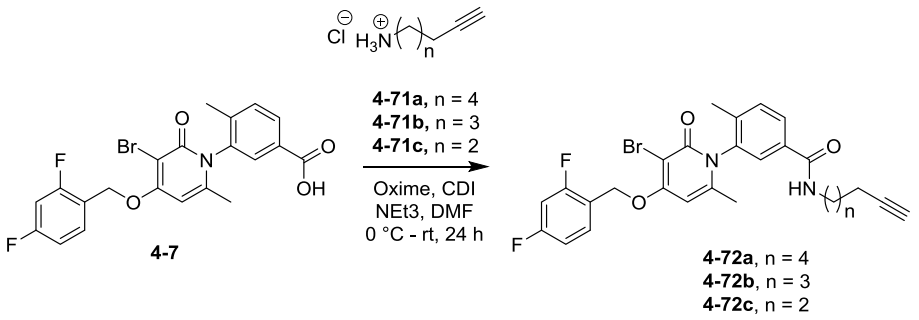

Scheme 4.5.19. *Synthesis of different* ***PH*** *alkyne intermediates, for synthesis of a variety of protacs with shorter lengths via click chemistry.*

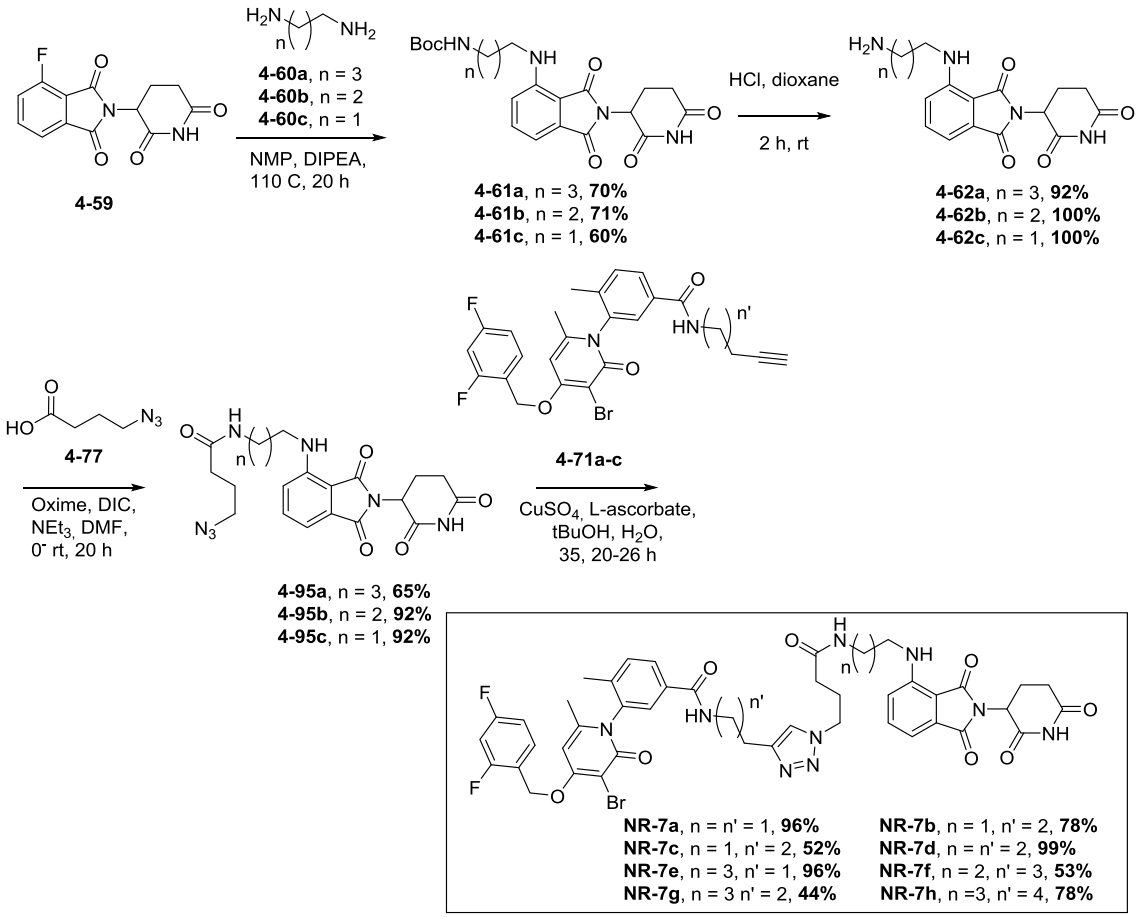

Scheme 4.5.20. *Protacs* ***NR-7a-h.*** *The route based on our previous analogue* ***NR-3c.***

4.5.9. Biological Evaluation of PROTACs **NR-7a-h**

Table 4.5.5. *Degradation of p38α after 24 h treatment of 10 μM solution of compounds* ***7a-h****.*

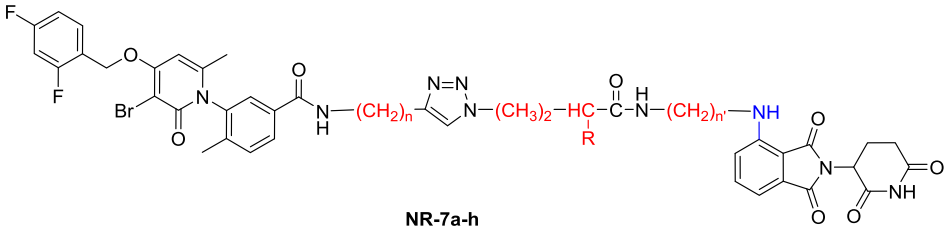

NR-7a-h

Compound	n	n'	R	Total length (atoms)	P38α Degradation 358	T47D
7a	2	2	H	12	No	No
7b	2	3	H	13	Partial	No
7c	3	3	H	14	Partial	No
7d	2	4	H	14	Partial	No
7e	4	2	H	14	No	No
7f	3	4	H	15	Yes	Yes
7g	4	3	H	15	Yes	Yes
7h	4	4	H	16	Yes	Yes

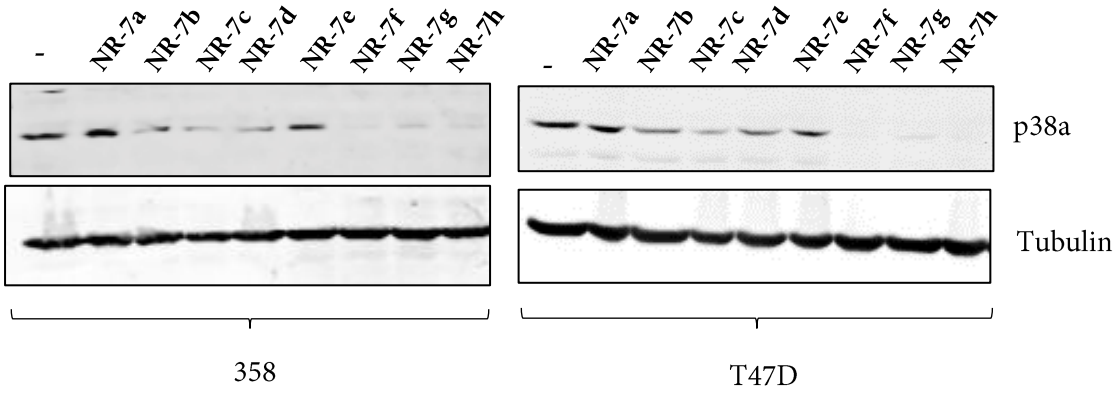

Figure 4.5.9. *Western-blots of the degradation of p38 in 358 and T47D cell lines after 24 h treatment of 10 μM solution of compounds* ***NR-7a-h****.*

A clear threshold was identified where linkers that were 15 atoms or shorter did not degrade p38, suggesting that this was the minimum length of linker required to establish the ternary

complex needed to initiate ubiquitination. A length of 15 – 17 atoms was observed to be optimum for degradation to occur, as complete degradation of p38α was observed using compounds **NR-7f, 7g, 7h** in both cell lines. Interestingly compounds **NR-5b** and **6b**, which also possessed linkers that were16 atoms in length, and differed only in their connection to thalidomide, did not degrade p38α in both cell lines. A more accurate approximation of linker length could have been acquired *via* simulation of the total atoms and bonds in angstroms of low energy states. However there is evidence that PROTAC linkers for other targets adopt folded and kinked conformations, as the linkers have enormous rotational freedom, meaning exploration and fine-tuning of PROTAC linker length and the connection to thalidomide should be carried out on a case by case basis for each target.

Compound **NR-7h**, which is one of the most active PROTACs of this series, is also a fluorescent molecule, which absorbs light at a maximum of 413 nm and emits light of 513 nm. The large shift of 100 nm can be used to track this compound in cells and *in vivo*. The absorption and emission spectra are shown below (graph 4.5.1). The fluorescence intensity was not particularly strong, as at concentrations of 1 uM difficult to visualise, but at 10 uM it was possible. However this higher concentration is already perhaps much more than needed for effective degradation of p38α, shown later with the DC_{50} values.

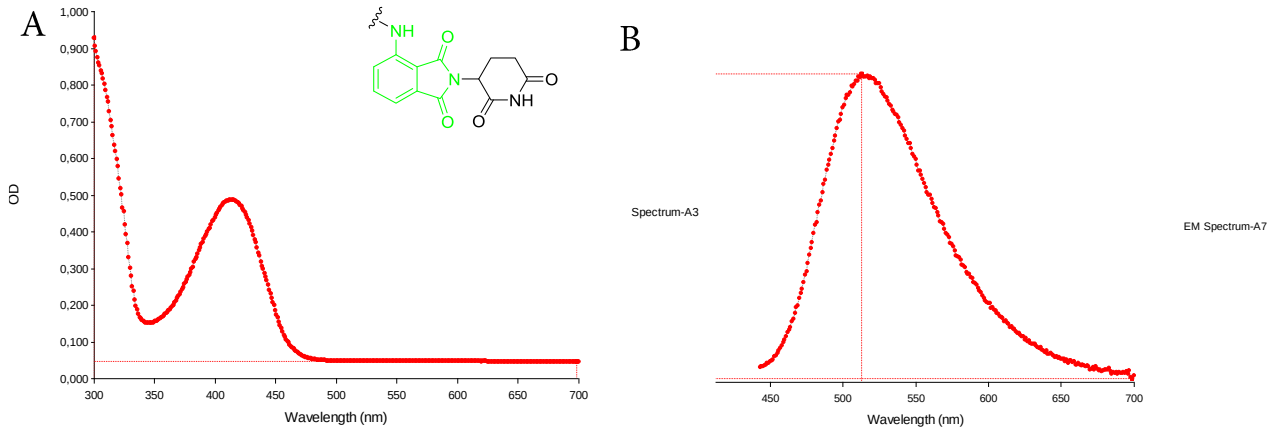

Graph 4.5.1. A) *Absorption spectrum of* ***NR-7a*** *[0.1 μM] in methanol, showing a maximal absorption at 413 nm. The fluorophore of the molecule is depicted in green.* ***Right:*** *Emission spectrum when irradiated at 413nm showing an emission maximal of 513 nm.*

The *N*-linked PROTACs have these advantages over the carbon linked compounds: they are bright yellow allowing for easy tracking during their synthesis and administration to cells (and mice), they are also traceable in cells which allows the visualisation of internalisation, half-life and other biological processes (figure 4.5.10).

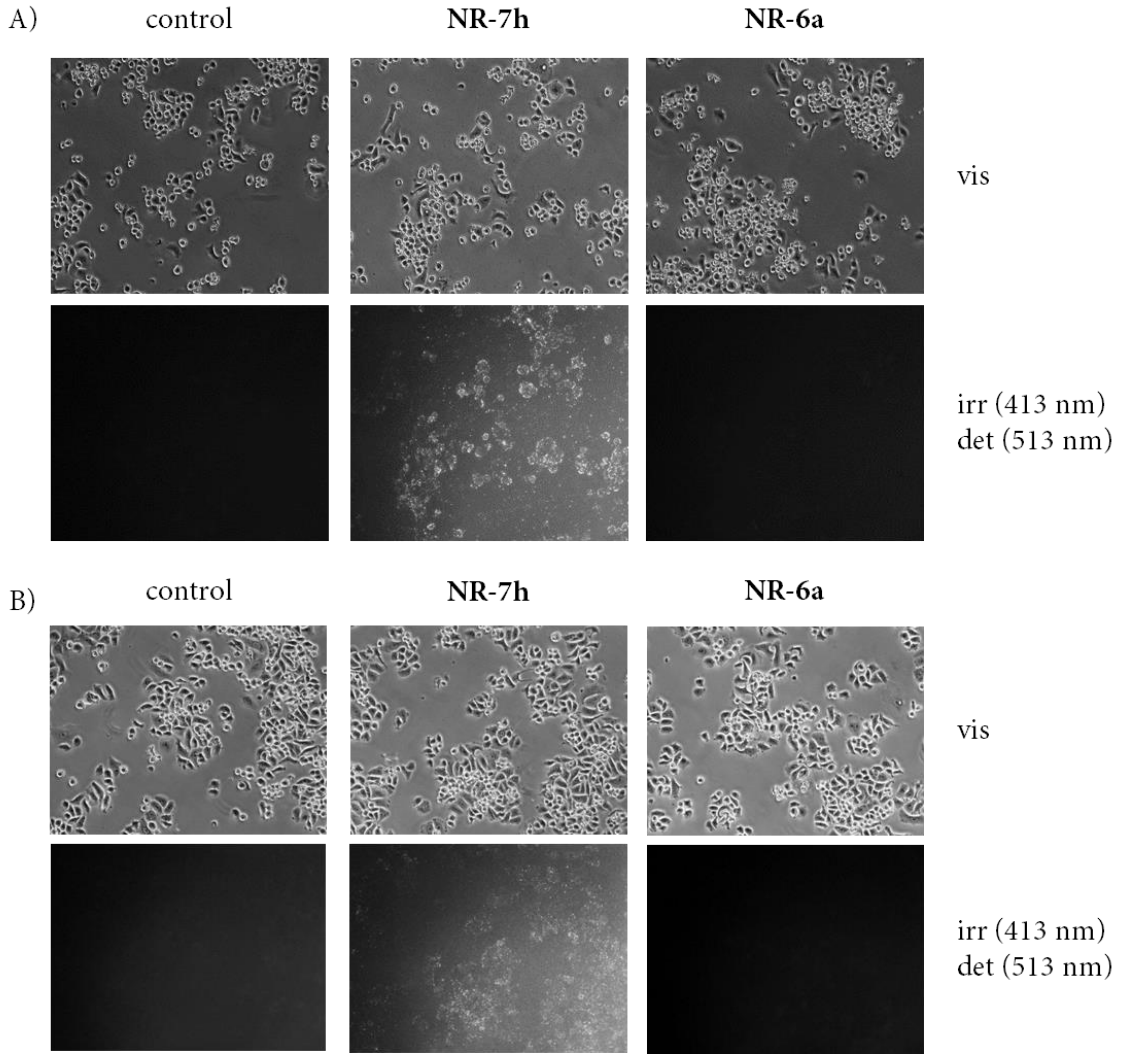

Scheme 4.5.10. *Control is shown in upper pannels of* ***A*** *and* ***B*** *using visible wavelength to visualise healthy cells during experiment.PROTACs* ***NR-7h*** *and* ***6a*** *were administered to T47D cells then fluoresence was monitored after 4 h (****A****) and after 24 h (****B****) by irradiating at 413 nm wavelength then scanning for 513 nm wavelength.* ***NR-7h*** *can be visualised by fluorescence at this wavelength, whereas no fluorescence is observed in the control or with* ***NR-6a.***

These images reveal that **NR-7h** and all other *N*-linked PROTACs can be tracked using fluorescence at 10 μM concentrations. Lower concentrations are more difficult to visualise, therefore a stronger fluorophore would be needed for *in vivo* applications.

High lipophilicity made these compounds poorly soluble in aqueous media, which would limit their application *in vivo* and the pharmacokinetics in a therapeutic setting. Therefore compounds **NR-7i** and **7j** were synthesised to probe the inter-protein space when bound to p38α and the ubiquitin ligase complex. This would also validate the potential for expansion of the linker in this direction. **NR-7i** and **j** were synthesised by route similar to **NR-7a-h**, but incorporating azide fragment **4-96b** instead of **4-74,** which featured a boc amine (scheme4.5.21).

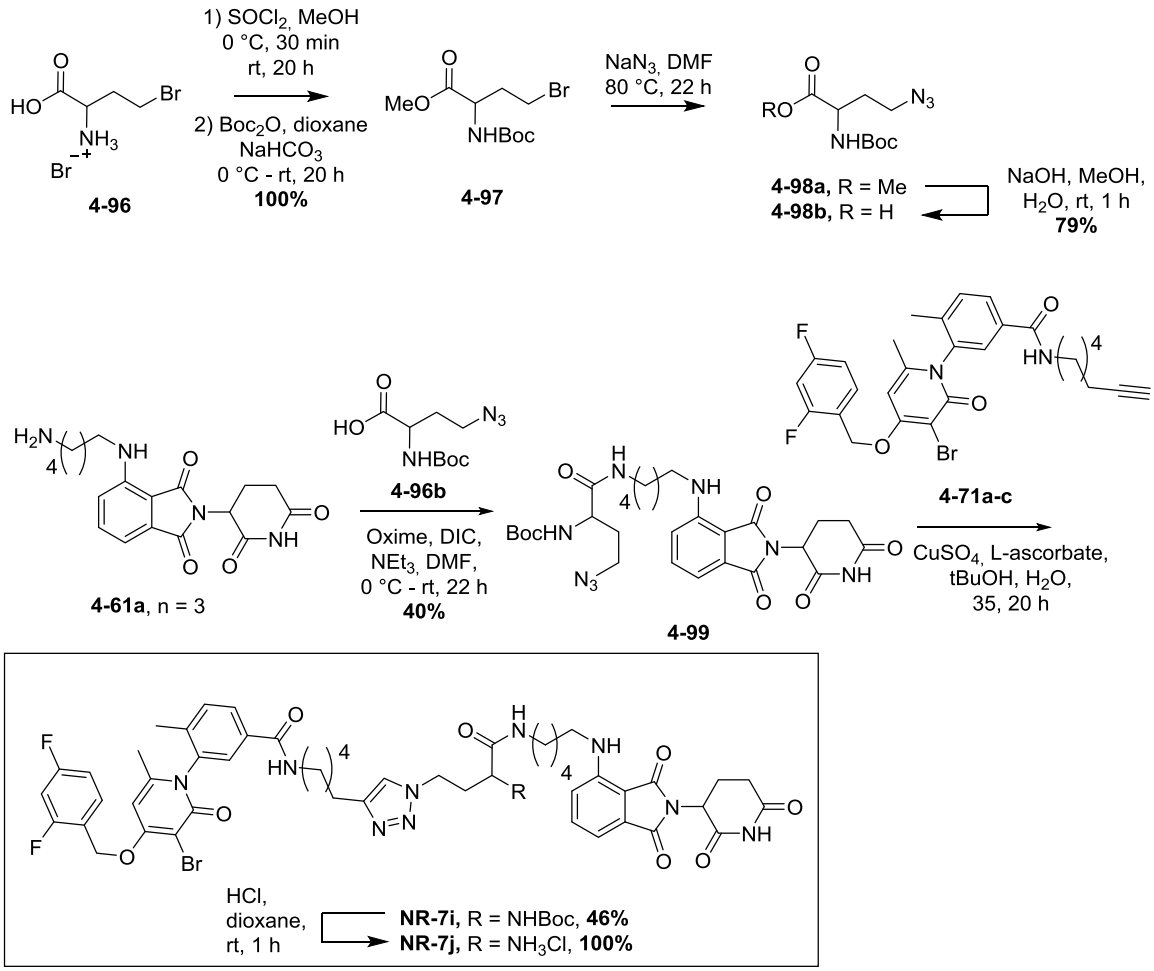

Scheme 4.5.21. *Synthesis of protacs* ***NR-7i*** *and* ***j****, using azide intermediate* ***4-98b****.*

These PROTACs were then tested as previously in 358 and T47D cell lines at 10 μM concentration compared with parent compound **NR-7h** (figure 4.5.11).

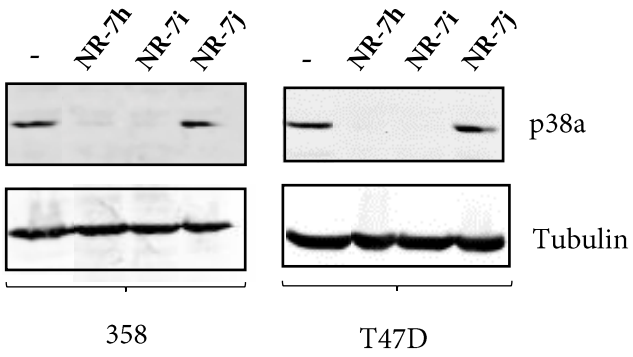

Figure 4.5.11. *Western-blots of the degradation of p38α in 358 and T47D cell lines after 24 h treatment of 10 μM solution of compounds* ***NR-7h-j.***

NR-7j possessed an amine hydrochloric salt which would boost polarity and consequently aqueous solubility for improved administration. However, as observed in figure 4.5.7, this PROTACS had no degradative activity against p38α. The ionic functionality may have prevented the compound from entering the cell or might have disrupted interaction of the ligase ternary complex, thus diminishing activity. Ongoing fluorescent studies should hopefully answer these hypotheses. **NR-7j** features a bulky t-butyl carbamate in the same position, demonstrating that steric hindrance of this position does not affect activity and it is indeed due to the presence of a positive charge. This opens the possibility for further substitution in this location and may enable further functionalisation of PROTACs to selectively direct them to tumour sites, although no further work has been carried out in this area so far.

We next wished to verify the relative activities of the 5 most active PROTACs of the series, **NR-6a** and **NR-7f-i**. These compounds were applied to T47D cells at lower concentrations (figure 4.5.12).

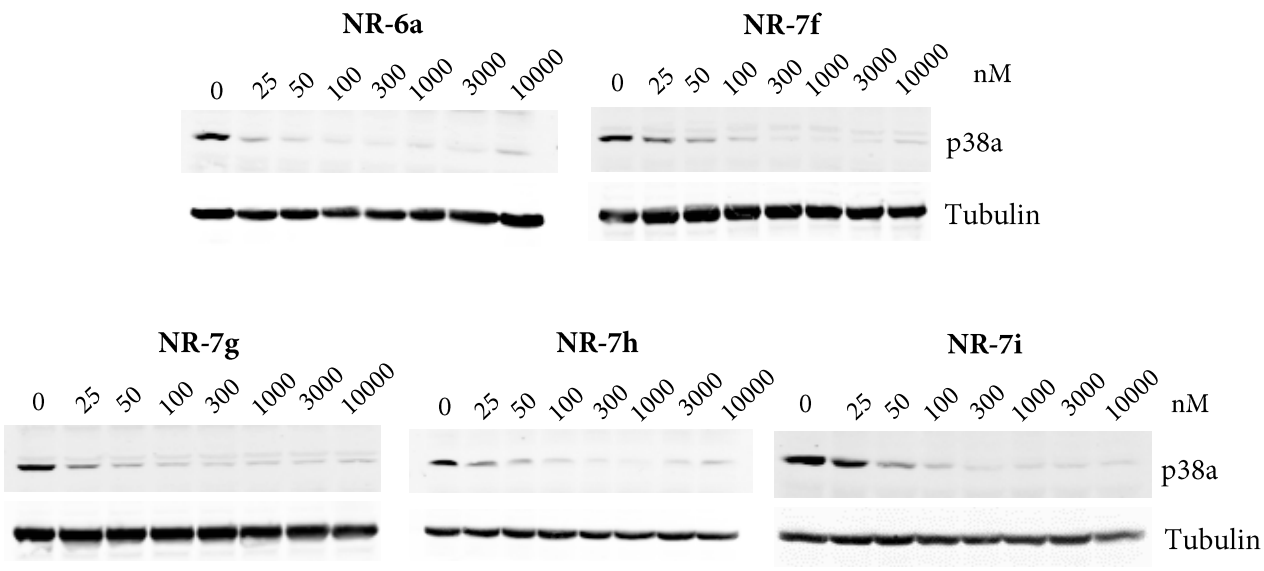

Figure 4.5.12. *T47D cells were treated with the indicated concentrations of the PROTACs* ***NR-6a, NR-7f-i*** *for 24 h and p38α expression was analyzed by immunoblotting.*

It should be noted that PROTACs display what is known as a hook effect at high concentrations, experienced by many 3-component systems. Until the degradation maximum concentration, degradation of the target protein steadily increases with increasing PROTAC concentration. However after this concentration, individual PROTAC molecules bind target protein, and other PROTAC molecules bind E3 ligase, which disfavours the binding of both by one PROTAC molecule and formation of the protein-ligase complex (graph 4.5.2).

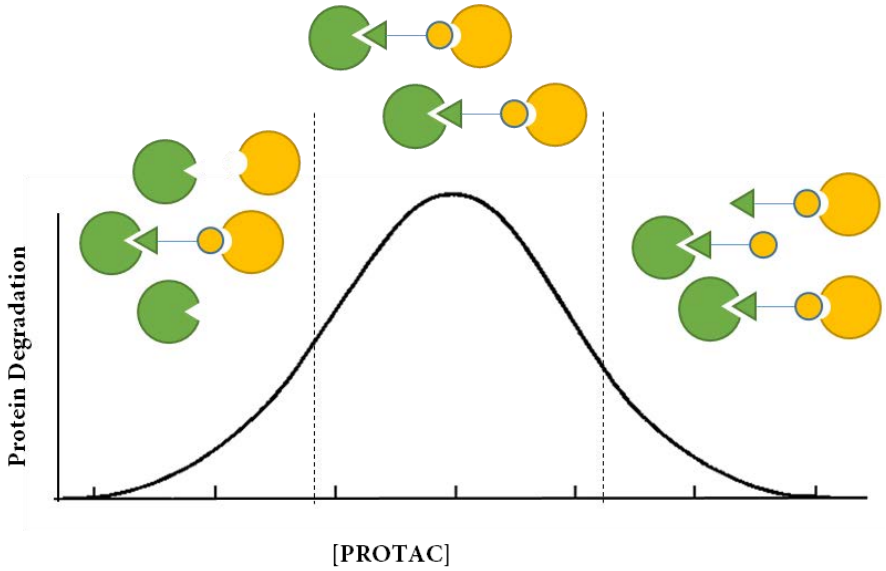

Graph 4.5.2. *General graph showing the "hook effect" of increasing PROTAC concentration against protein degradation. The first half of the graph behaves as normal 2-component inhibitor-protein systems, then after the maximum begins to decrease as PROTAC outnumbers available target protein and ligase, therefore does not bind both at the same time.*

This explains why at 10 μM some PROTACs show poorer degradation activity than at lower concentrations in the previous studies. This assay reveals that **NR-6a** and **NR-7h** are most active, as they degrade p38α at lower concentrations. We therefore chose to study and quantify their degradation ability in more detail and calculated the concentrations needed for 50% protein degradation (DC_{50}), shown in figure 4.5.13.

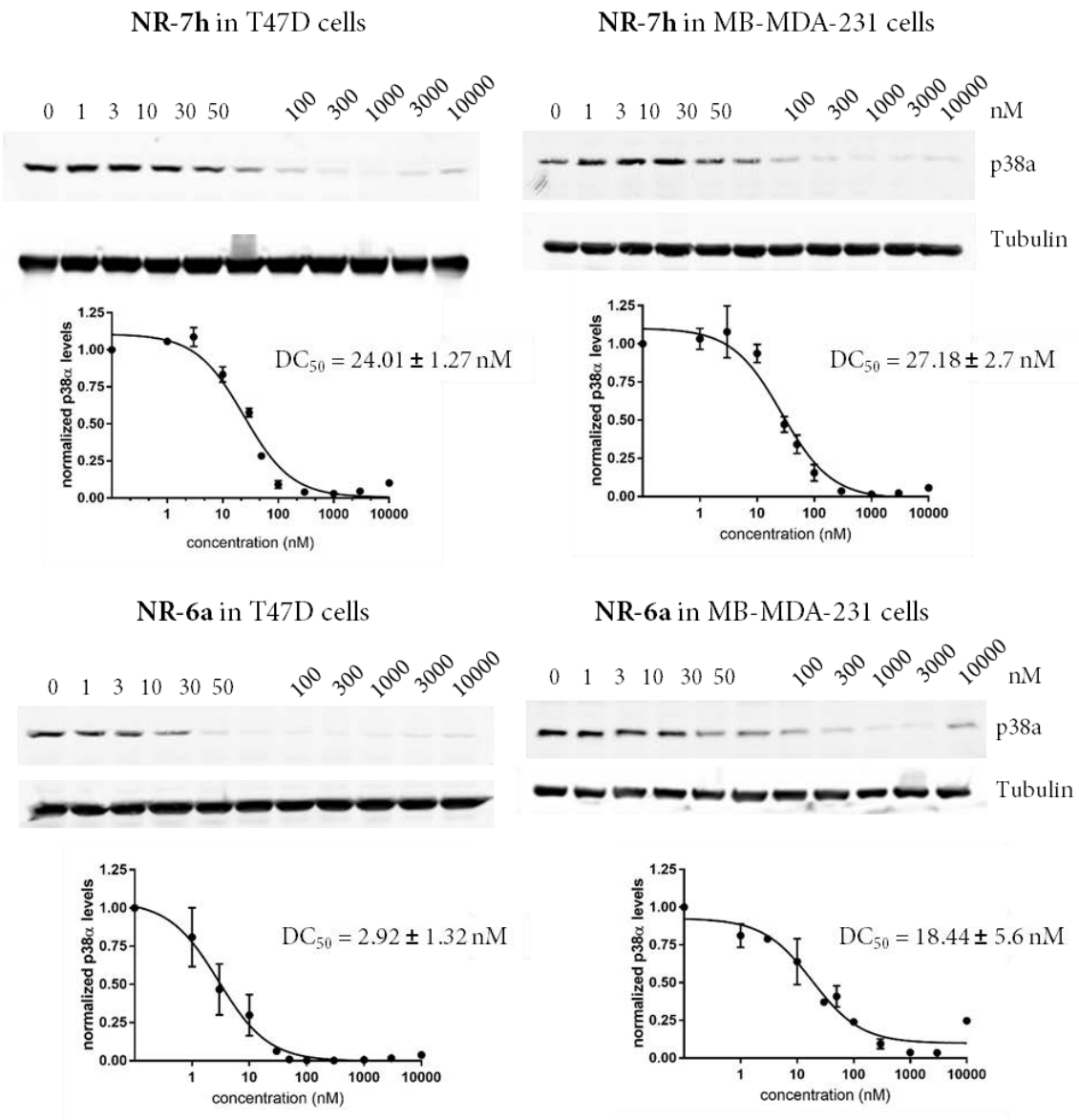

Figure 4.5.13. Determination of the DC_{50} for p38α degradation. *T47D cells (left) or MB-MDA-231 cells (right) were treated for 24 h with the indicated concentrations of the PROTACs **NR-6a** or **NR-7h** for 24 h, and p38α expression was analyzed by immunoblotting. The p38α levels were quantified in biological duplicates and values were used to determine the DC_{50}.*

NR-7h and **6a** both display DC_{50} values which are extremely low compared with other PROTACs for other protein targets and would translate very well for clinical use. We next compared our PROTACs with a genetic knockout model and were pleased to observe an identical effect in cells (figure 4.5.14).

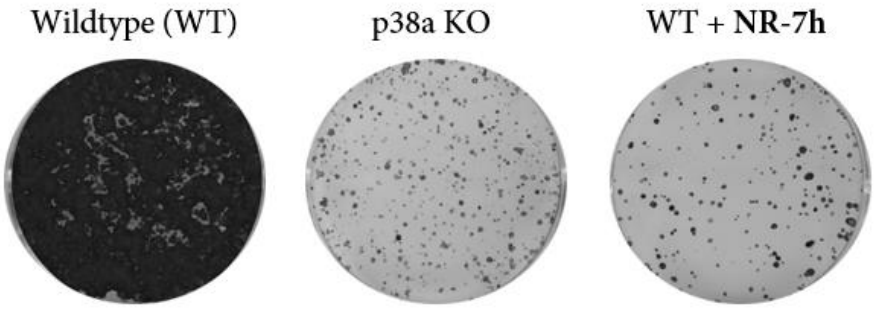

Scheme 4.5.14. *BBL358 cells were treated with 0.5 μM Tamoxifen to induce deletion of the p38α encoding gene (p38α KO) or with 10 μM of the PROTAC* ***NR-7h*** *for 2 days, and then were reseeded at low confluence for 7 days to allow then to form colonies*

Of course, PROTACs offer many advantages over genetic knockout techniques, such as the tamoxifen induced *Cre* technique discussed in chapter 2. They are more laborious, generally depend on viral infection or breeding, and generally do not offer control over the time of gene deletion, i.e. in organisms, the gene is knocked out from intitial development. Whereas with PROTACs the knockout can be applied to genetically unaltered subjects at any time of development. We also monitored the RNA levels after administration of PROTACs and observed that these were unaffected, unlike genetic knockout techniques or by siRNA techniques (figure 4.5.11).

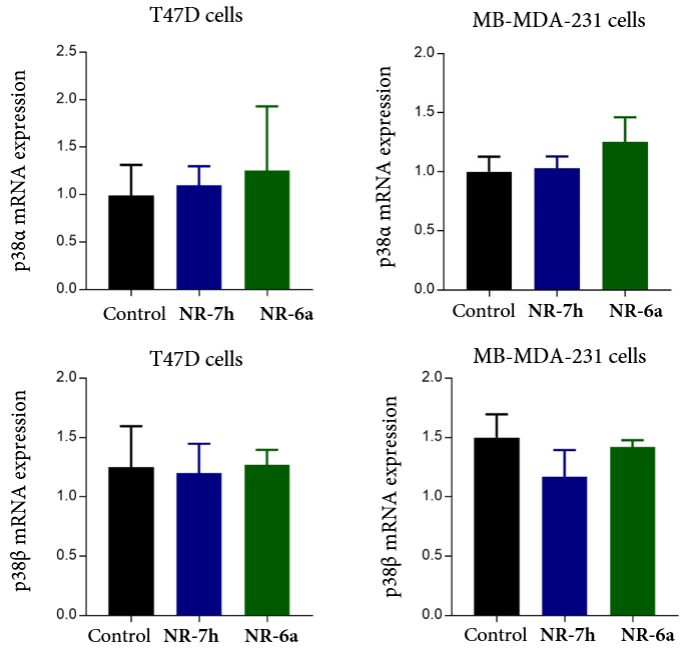

Figure 4.5.15. *T47D cells or MB-MDA-231 cells were treated with 1 μM of PROTACs* ***NR-6a*** *and* ***7h*** *for 24 h, and mRNA levels were analyzed by RT-PCR.*

Now convinced that degradation of p38α by PROTACs **NR-6a** and **7h** was occurring to a high level at low concentrations, and also control compound **NR-3d** did not induce degradation, we wished to further confirm the process was occurring by ubiquitination then degradation by the 26S proteasome. Therefore performed a rescue experiment by inhibiting the 26S proteasome with inhibitor Bortezomib then treating with PROTAC, observing no degradation of p38α, which confirmed the role of 26S proteasome (figure 4.5.15).

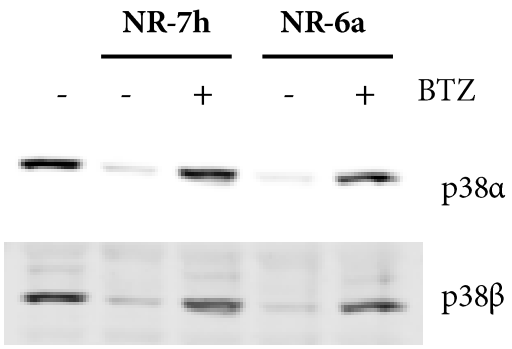

Figure 4.5.16. *MDA-MB-231 cells were pre-treated with 100 nM of the proteasome inhibitor Bortezomib (BTZ) for 30 min and then were treated with 1 μM of the PROTACs **NR-6a** and **NR-7h** for 8 h. Total p38α and p38β levels were analyzed by immunoblotting.*

4.5.10. Downstream Effect of PROTACs **NR-7h** and **6a** on the p38 MAPK Pathway Compared to Inhibitor **PH**

We had confirmed that our most active PROTACs **NR-7h** and **6a** effectively degraded p38α in a range of cell lines at nanomolar concentrations and confirmed it was *via* the ubiquitination/proteasome pathway. Therefore, we were convinced that these analogues would display some of the advantages associated with degraders over inhibitors, i.e. a more efficacious effect on the downstream targets, or lower doses required as it is an event driven process compared to stoichiometric inhibition. Indeed a level of selectivity was expected to be gained using PROTACs with respect to their parent inhibitor compounds, as reported by Crews and coworkers.[21]

As **PH** is known to inhibit both p38α and p38β at high concentrations, but not other related MAPKs such as JNK or ERK, we therefore tested the selectivity of our PROTAC molecules in a range of cell lines against these kinases (figure 4.5.17).

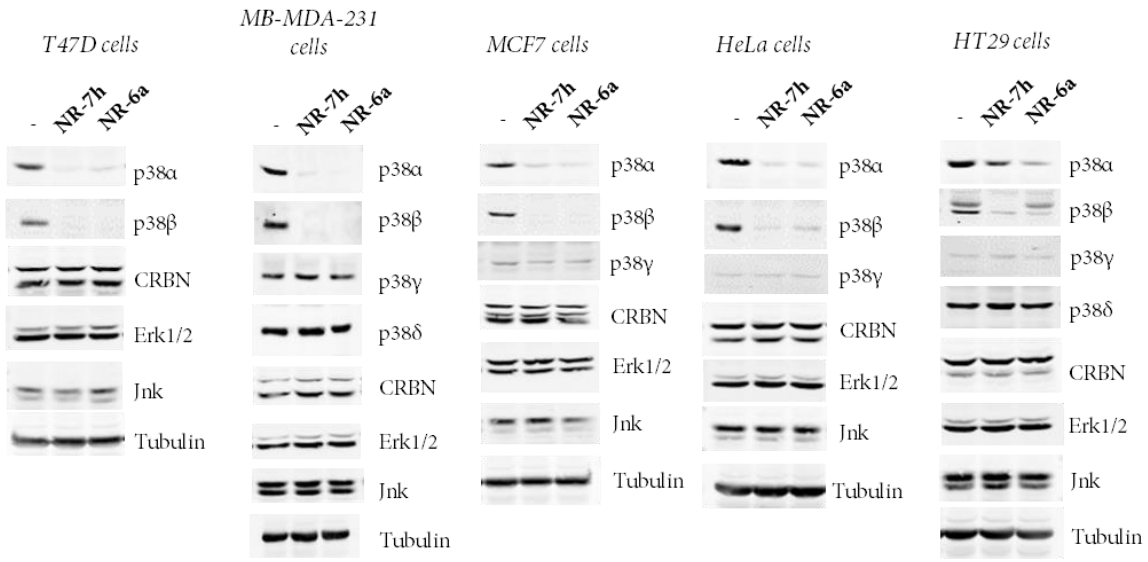

Figure 4.5.17. *The indicated cell lines were incubated with 1 μM of the PROTACs* ***NR-6a*** *and* ***NR-7h*** *for 24 h, and then cells lysates were analysed by immunoblotting using the indicated antibodies.*

PROTACs **NR-7h** and **6a** displayed degradation activity towards p38α and β but not other related kinases, apparently showing the same selectivity profile as **PH.** The experimental DC_{50} values for degradation of p38β were 10x higher than that of p38α for both PROTACs, therefore there is a slight increase when compared to the IC_{50} values of **PH** inhibition. It should also be noted that p38β has a much lower expression in humans and targeting p38β may also provide clinical benefit in cancer and inflammatory disease models.

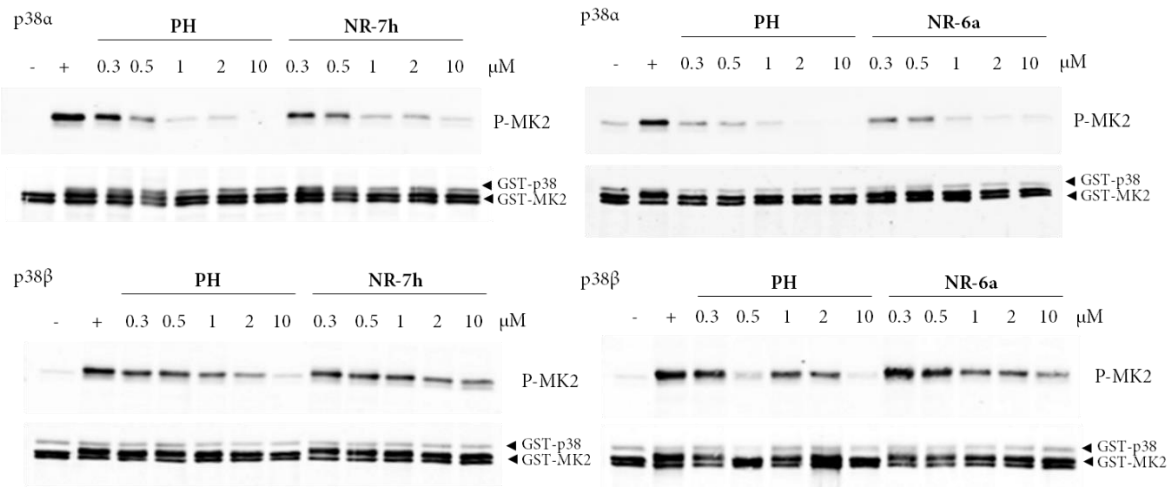

Figure 4.5.18. Kinase assay: inhibition of p38α and p38β kinase activity by PROTACs. *Active recombinant p38α and p38β proteins were pre-incubated for 10 min with the indicated concentrations of* ***PH*** *or the PROTACs* ***NR-6a*** *and* ***NR-7h*** *and then the kinase activity was assayed using GST-MK2 as a substrate. Samples were analyzed by immunoblotting with antibodies for GST and phospho-MK2.*

The above assay demonstrates that there is no significant difference in the downstream kinase phosphorylation levels when targeting p38α or β by inhibition or by degradation in a kinase assay (*i.e.* not within cells) *via* the most prevalent downstream kinase targets. However, until a clinically relevant assay is utilised, we may not see a difference in the efficacy against a given disease model.

It should be noted that we obtain a distinct selectivity profile from that of SFJα, the other reported p38α inhibitor by Crews and coworkers.[22] This PROTAC possesses affinity for p38δ, and indeed for c-Met kinase, the protein target for which the Foretinib warhead was originally designed to inhibit.

We next tested the time of action that PROTAC molecules would have an effect over the MAPK pathway. Therefore **PH** and PROTACs were used to treat cells, which were then monitored over 24 and 48 h intervals (figure 4.5.19).

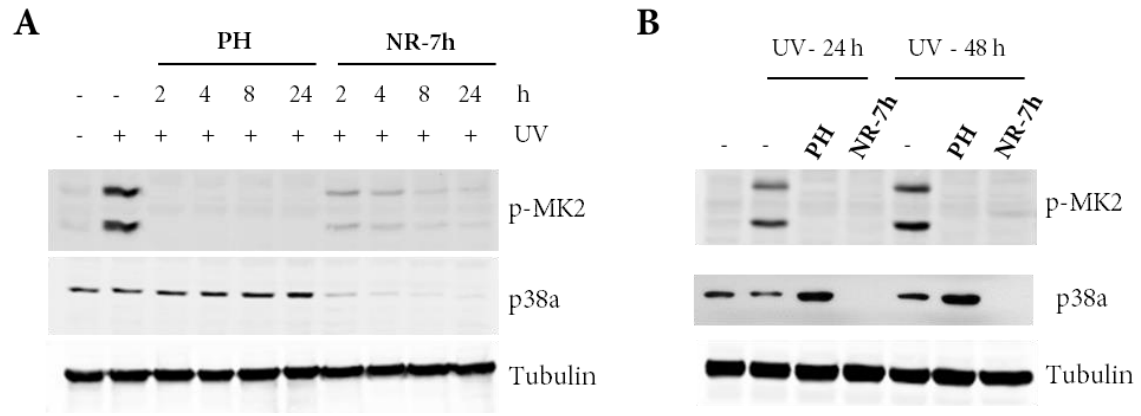

Figure 4.5.19. *BBL358 cells were treated with 2 μM* ***PH*** *or 1 μM of* ***NR-7h*** *for the indicated times prior to irradiation with UV (30 J/m^2). After 1 h, cells were lysed and analysed by immunoblotting with the indicated antibodies*

As can be seen from the above experiments, there is a delay in degradation of p38α of ~4 hours and a corresponding 4 – 8 h delay in inhibition of MK2 phosphorylation. After 48 h of UV stimulation in figure 4.5.19B, it is observed that both **PH** and **NR-7h** maintain strong inhibition of the pathway, and in the case of **NR-7h**, that this is due to degradation of p38α/β. Importantly, the kinetics of p38 regeneration is not a limiting factor in these treatments, and we may postulate that at much longer timepoints, the effects of the PROTAC may still be active once **PH** inhibitor has begun to be broken down excreted and can no longer inhibit p38. Further experiments would be needed to verify this hypothesis as it cannot yet be concluded from our current data.

4.5.11. *In vivo* testing of **NR-7h**

With a wealth of cellular information about our protac molecules, we next aimed to treat mice with PROTAC **NR-7h** to examine *in vivo* degradation of p38α.

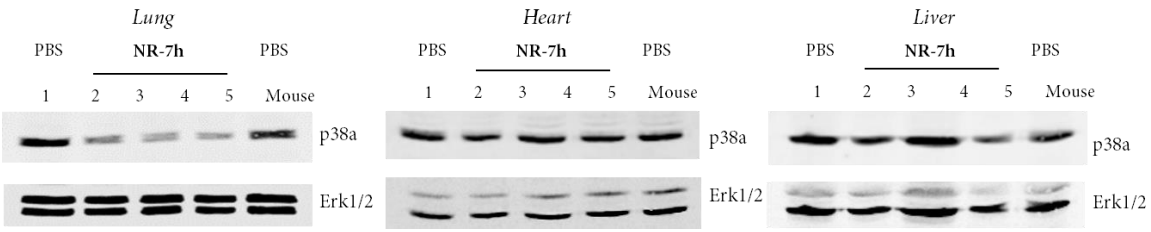

Figure 3.5.20. *Mice were administered intratracheally with vehicle (PBS) or* ***NR-7h*** *(30 mg/Kg), then 16 h later tissues were removed and analysed by immunoblotting with the indicated antibodies.*

The above data demonstrates that **NR-7h** can effectively degrade p38α in lung tissue and not in neighbouring heart of lung tissues, and with no effect of structurally related ERK kinases. It is important to note that PROTAC was administered specifically to the lung *via* intratracheal administration, therefore our PROTAC is not selective for lunch tissue, and longer running experiments will be needed to determine biodistribution of this PROTAC. Experiments are also being carried out to determine the effect of our PROTACs in clinically relevant tumour models, and these may then be compared with **PH** treated, and genetic knock-out models, to determine any advantages presented by degradation over inhibition of p38α.

Conclusions and Future Work

The above work represents a variety of optimisations of the inhibitor **PH.**

We have developed a range of active inhibitors that possess functional handles that are amenable to conjugation to tumour-directing groups.

We have conjugated the most active inhibitors to nanoparticles and showed preliminary data which indicates potential for tumour-directed delivery of these analogues.

Active analogues were also conjugated to peptide recognition fragments such as RGD, somatostatin and octreotide. Initial cellular data suggests that these compounds can inhibit p38α, which is supported by initial *in vivo* results, which compare well with free **PH** inhibitor. More data is needed to determine the benefits of conjugating inhibitors to these analogues and further testing of new analogues is ongoing.

A drug conjugate of octreotide linked to analogue **4-13a** *via* a photo-labile linker was synthesised in order to gain more control of the release of active analogues to the site of interest (**4-42**). The UV-assisted cleavage and biological evaluation of this drug conjugate is currently underway.

Finally, PROTACs to degrade p38α and p38β were designed and synthesised, verified in a range of biological models. We showed that linker length and also the connection to the thalidomide fragment was crucial for degradation activity. Our PROTACs possess a selectivity profile that is distinct from the only other published example of a p38 degrader (SFJα). A publication is currently under revision for this part of the thesis.

A photosensitive PROTAC molecule was also designed and shown to be cleaved upon radiation with UV light (380 nm) in under 30 minutes. Demonstration of the application of this PROTAC molecule in cellular assays is ongoing.

Finally, design of a more soluble PROTAC is ongoing to enable facile administration to mice and acquire more favourable PK properties for therapeutic use. **NR-7j** showed that it may be possible to further functionalise PROTACs of this series in the centre of the linker. Conjugation to directing groups or solubilising components is currently under investigation to obtain a more potent PROTAC molecule.

References

(1) Bühler, S.; Laufer, S. A. P38 MAPK Inhibitors: A Patent Review (2012 – 2013). *Expert Opin. Ther. Pat.* **2014**, *24* (5), 535–554. https://doi.org/10.1517/13543776.2014.894977.

(2) Dukeshereer, D.; Mao, M.; Vonderembse, R.; Yalamanchili, G.; Vaidyanathan, R.; Chekal, B.; Klemm, G.; Van Derrost, R.; Geurink, R. Processes for the Preparation of 3-(4-(2,4-Difluorobenzyloxy)-3-Bromo-6-Methyl-2-Oxopyridin- 1(2H)-Yl)-N,4-Dimethylbenzamide. WO2008072079A2, 2008.

(3) Borst, O.; Walker, B.; Münzer, P.; Russo, A.; Schmid, E.; Faggio, C.; Bigalke, B.; Laufer, S.; Gawaz, M.; Lang, F. Skepinone-L, a Novel Potent and Highly Selective Inhibitor of P38 MAP Kinase, Effectively Impairs Platelet Activation and Thrombus Formation. *Cell. Physiol. Biochem.* **2013**, *31* (6), 914–924. https://doi.org/10.1159/000350110.

(4) Koeberle, S. C.; Fischer, S.; Schollmeyer, D.; Schattel, V.; Grütter, C.; Rauh, D.; Laufer, S. a. Design, Synthesis, and Biological Evaluation of Novel Disubstituted Dibenzosuberones as Highly Potent and Selective Inhibitors of P38 Mitogen Activated Protein Kinase. *J. Med. Chem.* **2012**, *55* (12), 5868–5877. https://doi.org/10.1021/jm300327h.

(5) Selness, S. R.; Devraj, R. V.; Devadas, B.; Walker, J. K.; Boehm, T. L.; Durley, R. C.; Shieh, H.; Xing, L.; Rucker, P. V.; Jerome, K. D.; et al. Discovery of PH-797804, a Highly Selective and Potent Inhibitor of P38 MAP Kinase. *Bioorganic Med. Chem. Lett.* **2011**, *21* (13), 4066–4071. https://doi.org/10.1016/j.bmcl.2011.04.121.

(6) Niidome, T.; Yamagata, M.; Okamoto, Y.; Akiyama, Y.; Takahashi, H.; Kawano, T.; Katayama, Y.; Niidome, Y. PEG-Modified Gold Nanorods with a Stealth Character for in Vivo Applications. *J. Control. Release* **2006**, *114* (3), 343–347. https://doi.org/10.1016/j.jconrel.2006.06.017.

(7) Wu, P. H.; Onodera, Y.; Ichikawa, Y.; Rankin, E. B.; Giaccia, A. J.; Watanabe, Y.; Qian, W.; Hashimoto, T.; Shirato, H.; Nam, J. M. Targeting Integrins with RGD-Conjugated Gold Nanoparticles in Radiotherapy Decreases the Invasive Activity of Breast Cancer Cells. *Int. J. Nanomedicine* **2017**, *12*, 5069–5085. https://doi.org/10.2147/IJN.S137833.

(8) Escolà Jané, A. Somatostatin Analogues as Drug Delivery Systems for Receptor-Targeted Cancer Therapy, Universitat de Barcelona, 2018.

(9) Weckbecker, G.; Liu, R.; Tolcsvai, L.; Brans, C. Antiproliferative Effects of the Somatostatin Analogue

Octreotide (SMS 201-995) on ZR-75-1 Human Breast Cancer Cells in Vivo and in Vitro. *Cancer Res.* **1992**, *52* (18), 4973–4978.

(10) Hsieh, H. P.; Wu, Y. T.; Chen, S. T.; Wang, K. T. Direct Solid-Phase Synthesis of Octreotide Conjugates: Precursors for Use as Tumor-Targeted Radiopharmaceuticals. *Bioorganic Med. Chem.* **1999**, *7* (9), 1797–1803. https://doi.org/10.1016/S0968-0896(99)00125-X.

(11) Cyrus, K.; Wehenkel, M.; Choi, E.-Y.; Han, H.-J.; Lee, H.; Swanson, H.; Kim, K.-B. Impact of Linker Length on the Activity of PROTACs. *Mol. BioSyst.* **2011**, *7* (2), 359–364. https://doi.org/10.1039/C0MB00074D.

(12) Xing, L.; Shieh, H. S.; Selness, S. R.; Devraj, R. V.; Walker, J. K.; Devadas, B.; Hope, H. R.; Compton, R. P.; Schindler, J. F.; Hirsch, J. L.; et al. Structural Bioinformatics-Based Prediction of Exceptional Selectivity of P38 MAP Kinase Inhibitor PH-797804. *Biochemistry* **2009**, *48* (27), 6402–6411. https://doi.org/10.1021/bi900655f.

(13) Lai, A. C.; Crews, C. M. Induced Protein Degradation: An Emerging Drug Discovery Paradigm. *Nat. Rev. Drug Discov.* **2017**, *16* (2), 101–114. https://doi.org/10.1038/nrd.2016.211.

(14) Hon, W. C.; Wilson, M. I.; Harlos, K.; Claridge, T. D. W.; Schofield, C. J.; Pugh, C. W.; Maxwell, P. H.; Ratcliffe, P. J.; Stuart, D. I.; Jones, E. Y. Structural Basis for the Recognition of Hydroxyproline in HIF-1α by PVHL. *Nature* **2002**, *417* (6892), 975–978. https://doi.org/10.1038/nature00767.

(15) Schneekloth, J. S.; Sakamoto, K.; Deshaies, R.; Koldobskiy, M.; Fonseca, F. N.; Crews, C. M.; Mandal, A. Chemical Genetic Control of Protein Levels: Selective in Vivo Targeted Degradation. *J. Am. Chem. Soc.* **2004**, *126* (12), 3748–3754. https://doi.org/10.1021/ja039025z.

(16) Wurz, R. P.; Dellamaggiore, K.; Dou, H.; Javier, N.; Lo, M. C.; McCarter, J. D.; Mohl, D.; Sastri, C.; Lipford, J. R.; Cee, V. J. A 'Click Chemistry Platform' for the Rapid Synthesis of Bispecific Molecules for Inducing Protein Degradation. *J. Med. Chem.* **2018**, *61* (2), 453–461. https://doi.org/10.1021/acs.jmedchem.6b01781.

(17) Kolb, H. C.; Finn, M. G.; Sharpless, K. B. Click Chemistry: Diverse Chemical Function from a Few Good Reactions. *Angew. Chemie Int. Ed.* **2001**, *40* (11), 2004–2021. https://doi.org/10.1002/1521-3773(20010601)40:11<2004::AID-ANIE2004>3.0.CO;2-5.

(18) Gadd, M. S.; Testa, A.; Lucas, X.; Chan, K.-H.; Chen, W.; Lamont, D. J.; Zengerle, M.; Ciulli, A. Structural Basis of PROTAC Cooperative Recognition for Selective Protein Degradation. *Nat. Chem.*

Biol. **2017**, *13* (5), 514–521. https://doi.org/10.1038/nchembio.2329.

(19) Zhou, B.; Hu, J.; Xu, F.; Chen, Z.; Bai, L.; Fernandez-Salas, E.; Lin, M.; Liu, L.; Yang, C. Y.; Zhao, Y.; et al. Discovery of a Small-Molecule Degrader of Bromodomain and Extra-Terminal (BET) Proteins with Picomolar Cellular Potencies and Capable of Achieving Tumor Regression. *J. Med. Chem.* **2018**, *61* (2), 462–481. https://doi.org/10.1021/acs.jmedchem.6b01816.

(20) Fischer, E. S.; Böhm, K.; Lydeard, J. R.; Yang, H.; Stadler, M. B.; Cavadini, S.; Nagel, J.; Serluca, F.; Acker, V.; Lingaraju, G. M.; et al. Structure of the DDB1–CRBN E3 Ubiquitin Ligase in Complex with Thalidomide. *Nature* **2014**, *512* (7512), 49–53. https://doi.org/10.1038/nature13527.

(21) Bondeson, D. P.; Smith, B. E.; Burslem, G. M.; Buhimschi, A. D.; Hines, J.; Jaime-Figueroa, S.; Wang, J.; Hamman, B. D.; Ishchenko, A.; Crews, C. M. Lessons in PROTAC Design from Selective Degradation with a Promiscuous Warhead. *Cell Chem. Biol.* **2018**, *25* (1), 78-87.e5. https://doi.org/10.1016/j.chembiol.2017.09.010.

(22) Smith, B. E.; Wang, S. L.; Jaime-Figueroa, S.; Harbin, A.; Wang, J.; Hamman, B. D.; Crews, C. M. Differential PROTAC Substrate Specificity Dictated by Orientation of Recruited E3 Ligase. *Nat. Commun.* **2019**, *10* (1), 1–13. https://doi.org/10.1038/s41467-018-08027-7.

Chapter 5

Conclusions

An improved route towards guaymoxifen (**2-11**) was developed and proved more amenable to obtain larger quantities of **2-11** for *in vivo* testing.

Initial *in vivo* experiments demonstrated that **2-11** was cleaved *in vivo* releasing 4OHT (**2-2**) and inducing recombination in the stroma surrounding metastatic tumour sites. It was discovered that the liver of the mouse also cleaved and released **2-2,** causing recombination in cells around the liver, thus guaymoxifen (**2-11**) was not suitable for the identification of new metastasis sites in this *in vivo* model.

An SAR study about the β-ether bond identified 3 new analogues of guaymoxifen that could be cleaved by LigF enzyme *in vitro*. Two of these analogues (methyl substituted **2-40a** and hydroxymethyl substituted **2-40b**) generally showed less metabolic liver cleavage *in vivo* than original **2-11**.

2-11 and **2-40b** were demonstrated to be cleaved by LigF *in vitro*, where the enzyme apparently showed a preference for the active *pro-Z* isomer, and also for one of the enantiomers of **2-40b**.

However, initial studies with LigF expressing tumours have not been able to reproduce earlier results, where significant recombination in the stromal cells around tumour sites was observed.

HA-tagged LigF was shown to be expressed in sufficient concentration in tumour tissue, therefore further research is needed to identify the problem with this system.

Compound (**2-40b**) was synthesised on a large scale and ongoing *in vivo* experiments aim to identify problems with the guaymoxifen system, then find conditions where it can be used as a tool for genetic control of the stroma around metastatic tumours.

Finally, 2nd generation guaymoxifen analogues **2-66** and **2-78** were synthesised, which were enriched in the active *E*-isomer due to an additional methyl substituent on the guai-phenol ring.

2-66 and **2-78** were both cleaved by LigF *in vitro*, and showed metabolic cleavage in the liver when administered *in vivo*, compared to the corresponding 1st generation analogues **2-11** and **2-40b**.

We have developed a range of active inhibitors based on the inhibitor **PH,** which possess functional handles that are amenable to conjugation to tumour-directing groups.

We have conjugated the most active inhibitor (**4-13a**) to nanoparticles. Preliminary cellular and *in vivo* data indicates a potential for tumour-directed delivery of these analogues, provided accumulation in RES tissue and premature detatchment of inhibitor from the NP can be overcome.

Active analogues (**4-7, 4-13a**) were also conjugated to peptide recognition fragments such as RGD, somatostatin and octreotide. Initial cellular data suggests that these compounds can inhibit p38α, which is supported by initial *in vivo* results. These conjugates compared well with free **PH** inhibitor. More data is needed to determine the benefits of conjugating inhibitors to these analogues and further testing of new drug-conjugates is ongoing.

A drug-conjugate of octreotide linked to analogue **4-13a** *via* a photo-labile linker was synthesised in order to gain a further level of control over the release of **4-13a** at the site of interest (**4-42**). The UV-assisted cleavage and biological evaluation of this drug conjugate is currently underway, compared with a control drug-conjugate (**4-41**), which relied on endosomic internalisation and liberation of active metabolites *via* protease action.

Finally, PROTACs to degrade p38α and p38β were designed and synthesised, then verified in a range of biological models. We showed that linker length and also the connection to the thalidomide fragment was crucial for degradation activity. A publication is currently under revision for this part of the thesis.

A photosensitive PROTAC molecule was also designed and shown to be cleaved upon radiation with UV light (380 nm) in under 30 minutes. Demonstration of the application

of this PROTAC molecule in cellular assays is ongoing. Further analogues have also been synthesised to improve this function.

Finally, design of a more soluble PROTAC is ongoing to enable facile administration to mice and acquire more favourable PK properties for therapeutic use. **NR-7j** showed that it may be possible to further functionalise PROTACs of this series in the centre of the linker. Conjugation to directing groups or solubilising components is currently under investigation to obtain a more potent, trivalent PROTAC molecule.

Chapter 6

Experimental section

6.1. General methods and instrumentation

Non-aqueous reactions were carried out under nitrogen atmosphere using nitrogen gas passed through a Drierite® column. Anhydrous THF, Et_2O and DCM/CH_2Cl_2 were obtained from a Solvent Purification System (SPS PS-MD-3). Reagents and solvents were purchased from Sigma-Aldrich (Merck), Fluorochem, Apollo Scientific, Acros, TCI, Alfa Aesar and Tebu Bio (Broad Pharm) and were used without further purification. Thin layer chromatography was carried out using TLC-aluminium sheets with silica gel (Merck 60 F_{254}). Preparative thin layer chromatography was carried out when necessary using TLC-glass plates (RediSep F_{254}). Silica gel chromatography was performed using 35-70 mm silica or an automated chromatography system (Combiflash®, Teledyne Isco) utilising hexanes, ethyl acetate, dichloromethane, methanol (triethylamine or ammonia solution as additive) as eluents.

Reaction temperature was controlled using baths of ice plus water or brine, dry ice plus acetone, or heating mantels with silica oil baths. Microwave radiation was applied to reactions where stated using a CEM Discover microwave unit.

NMR spectra were recorded at 23 °C on a Varian Mercury 400 or Varian 500 apparatus. ^{1}H NMR and ^{13}C NMR spectra were referenced either to relative internal TMS or to residual solvent peaks. ^{19}F NMR spectra were referenced by the spectrometer without any external pattern. Signal multiplicities in the ^{13}C NMR spectra were assigned by HSQC or DEPT experiments. Optical rotations were measured at room temperature (25 °C) using a Jasco P-2000 iRM-800 polarimeter. Concentration is expressed in g/100 mL. The cell was 10 cm in length and had 1 mL capacity. The measured wavelength (λ) was 589 nm, which corresponds to a sodium lamp. Melting points were determined using a Büchi M-540 apparatus without recrystallization of the final solids and were not corrected. Differential scanning calorimetry (DSC) performed by the CCiTUB Polymorphism and Calorimetry unit on a Mettler-Toledo DSC-822e calorimeter, from 30 – 300 °C (10 °C min^{-1}) under N_2. IR spectra were recorded in a Thermo Nicolet Nexus FT-IR apparatus by depositing a film of the product on a sodium chloride disk. HRMS were recorded in a LTQ-FT Ultra (Thermo Scientific) using Nanoelectrospray technique. HPLC chromatography was performed on Hewlett-Packard 1050 equipment with UV detection using a Kinetix EVO C18 50x 4.6 mm, 2.6 μm column (Standard gradient: 10 mM NH_4CO_3 / MeCN (95:5) – (0:100)).

6.2. Preparation and characterisation of guaymoxifen compounds (from chapter 2)

4-Acetyl-2-methoxyphenyl pivalate (2-14c)

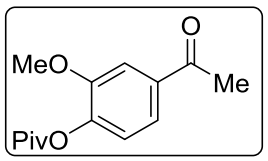

1-(4-hydroxy-3-methoxyphenyl)ethan-1-one (5.0 g, 30.1 mmol), pivaloyl bromide (3.8 mL, 33.1 mmol) and NEt_3 (4.7 mL, 36.1 mmol) were mixed in DCM (60 mL) and stirred at rt for 22 h. The mixture was removed from the oil bath and allowed to cool before addition of $NaHCO_3$. The aqueous were extracted with further DCM, the combined organics were washed with H_2O, brine, dried over $MgSO_4$, then concentrated under reduced pressure to afford **1** as an off-white solid (7.8 g, 30.1 mmol, **100%**).

^{1}H NMR (400 MHz, Chloroform-*d*) δ 7.58 (d, *J* = 2 Hz, 1H), 7.55 (dd, *J* = 8, 2 Hz, 1H), 7.09 (d, *J* = 8 Hz, 1H), 3.87 (s, 3H), 2.60 (s, 3H), 1.38 (s, 9H) ppm.

^{13}C NMR (101 MHz, Chloroform-*d*) δ 197.0 (C), 176.2 (C), 151.5 (C), 144.5 (C), 135.7 (C), 122.7 (CH), 122.0 (CH), 111.4 (CH), 56.0 (CH_3), 39.2 (C), 27.2 (3 x CH_3), 26.5 (CH_3) ppm.

IR (Film): 2968, 2916, 1749, 1684, 1505, 1279, 1096 cm^{-1}.

HRMS (ESI): calc. for $[C_{14}H_{19}O_4]^+$: 251.12779; found: 251.12773.

4-(2-bromoacetyl)-2-methoxyphenyl pivalate (2-15b)

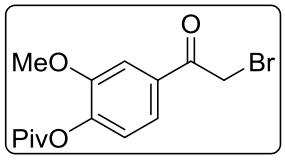

To a solution of **2-14c** (4.0 g, 16.0 mmol) in Et_2O (30 mL) was added dropwise Br_2 (0.86 mL, 16.8 mmol) then stirred at rt for 2.5 h. $Na_2S_2O_3$ (sat.) solution was then added to the mixture then extracted with EtOAc (x2), washed with $NaHCO_3$, H_2O, then brine. The organics were dried over $MgSO_4$, then concentrated under reduced pressure to afford a cream-pink solid. Trituration was performed using DCM, leaving a yellow precipitate (tri-brominated product). The mother liquors were evaporated to dryness, then the resulting solid was dissolved in hexanes and recrystallised (heating to 76 °C) to afford product as a white solid (3.7 g, 10.8 mmol, **67%**).

^{1}H NMR (400 MHz, Chloroform-*d*) δ 7.60 (d, *J* = 2, 1 Hz, 1H), 7.57 (dd, *J* = 8, 2 Hz, 1H), 7.11 (d, *J* = 8, 1 Hz, 1H), 4.43 (s, 2H), 3.87 (s, 3H), 1.37 (s, 9H) ppm.

^{13}C NMR (101 MHz, Chloroform-*d*) δ 190.3 (C), 176.1 (C), 151.8 (C), 145.2 (C), 132.4 (C), 123.0 (CH), 122.3 (CH), 112.2 (CH), 56.1 (CH_2), 39.2 (C), 30.5 (CH_3), 27.1 (3 x CH_3) ppm.

IR (Film): 2964, 2924, 1754, 1501, 1271, 1096 cm^{-1}.

HRMS (ESI): calc. for $[C_{14}H_{18}O_4Br]^+$: 329.03830; found: 329.03786.

M_P: 73.8 – 74.7 °C.

2-Methoxy-4-(2-((4-methyl-2-oxo-2*H*-chromen-7-yl)oxy)acetyl)phenyl pivalate (2-16b)

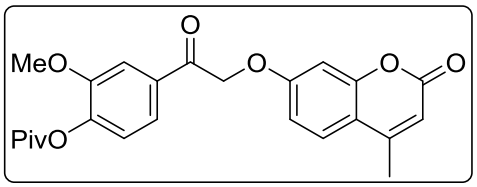

7-hydroxy-4-methyl-2*H*-chromen-2-one (112 mg, 0.64 mmol), **2-15b** (220 mg, 0.67 mmol) and K_2CO_3 (105 mg, 0.76 mmol) were dissolved in acetone (5 mL) and stirred at rt for 21 h. The reaction mixture was diluted with K_2CO_3 (sat) then extracted with 10% MeOH/DCM (x3). The organics were washed with H_2O, then brine, dried over $MgSO_4$, then concentrated under reduced pressure to afford an off-white solid (270 mg, 0.64 mmol, **100%**).

^{1}H NMR (400 MHz, Chloroform-*d*) δ 7.62 – 7.56 (m, 2H), 7.52 (d, *J* = 9 Hz, 1H), 7.14 (d, *J* = 8 Hz, 1H), 6.93 (dd, *J* = 9, 3 Hz, 1H), 6.82 (d, *J* = 3 Hz, 1H), 6.15 (d, *J* = 1 Hz, 1H), 5.35 (s, 2H), 3.88 (s, 3H), 2.40 (d, *J* = 1 Hz, 3H), 1.38 (s, 9H) ppm.

^{13}C NMR (101 MHz, Chloroform-*d*) δ 192.2 (C), 176.1 (C), 161.0 (C), 160.8 (C), 155.1 (C), 152.3 (C), 152.0 (C), 145.4 (C), 132.6 (C), 125.8 (CH), 123.1 (CH), 121.2 (CH), 114.4 (CH), 112.5 (CH), 111.5 (CH), 102.0 (CH), 70.6 (CH_2), 56.1 (CH_3), 39.2 (C), 27.1 (3 x CH_3), 18.7 (CH_3) ppm.

IR (Film): 2977, 2912, 1702, 1601, 1262, 1105 cm^{-1}.

HRMS (ESI): calc. for $[C_{14}H_{18}O_4Br]^+$: 329.03830; found: 329.03786.

M_P: 171.1 – 171.9 °C.

7-(2-(4-Hydroxy-3-methoxyphenyl)-2-oxoethoxy)-4-methyl-2*H*-chromen-2-one (2-12)

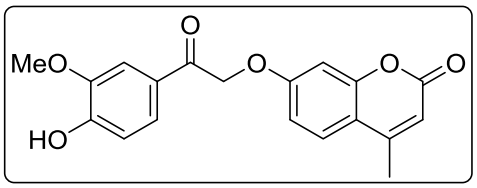

To a solution of **2-16b** (250 mg, 0.59 mmol) in MeOH (1 mL) and dioxane (1 mL) was added 10% NaOH (1 mL) and stirred at rt for 45 min. 1M HCl (3 mL) was then added

until pH 2, at which point precipitation occurred. The solid was collected by filtration, washed with H_2O to afford a white solid (200 mg, 0.59 mmol, **100%**).

The NMR spectra were consistent with that reported in the literature.[1]

^{1}H NMR (400 MHz, Chloroform-*d*) δ 7.57 (dq, *J* = 11, 2, 1 Hz, 2H), 7.52 (d, *J* = 9 Hz, 1H), 7.00 (d, *J* = 8 Hz, 1H), 6.95 (dd, *J* = 9, 3 Hz, 1H), 6.79 (d, *J* = 2 Hz, 1H), 6.20 – 6.13 (m, 2H), 5.33 (d, *J* = 1 Hz, 2H), 3.97 (s, 2H), 2.40 (s, 3H) ppm.

1-(4-(Benzyloxy)-3-methoxyphenyl)ethan-1-one (2-14b)

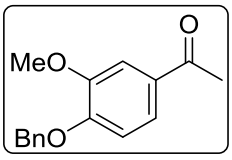

(Bromomethyl)benzene (3.9 mL, 33.1 mmol) was added dropwise to a solution of 1-(4-hydroxy-3-methoxyphenyl)ethan-1-one (5.0 g, 30.1 mmol) and K_2CO_3 (5.0 g, 36.1 mmol) in DMF (20 mL) at rt. The reaction mixture was then heated at 40 °C for 18 h. H_2O was added and the organics were extracted using EtOAc (x3), then washed with brine (x3), dried over $MgSO_4$, then concentrated under reduced pressure to afford an light yellow solid (7.6 g, 29.7 mmol, **99%**).

The NMR spectra were consistent with that reported in the group.[2]

^{1}H NMR (400 MHz, Chloroform-*d*) δ 7.55 (d, *J* = 2 Hz, 1H), 7.50 (dd, *J* = 8, 2 Hz, 1H), 7.46 – 7.28 (m, 5H), 6.89 (d, *J* = 8 Hz, 1H), 5.24 (s, 2H), 3.95 (d, *J* = 0.5 Hz, 3H), 2.55 (s, 3H) ppm.

1-(4-(Benzyloxy)-3-methoxyphenyl)-2-bromoethan-1-one (2-15a)

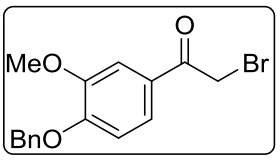

To a solution of **2-14b** (7.6 g, 29.7 mmol) in EtOH (100 mL) was added dropwise Br_2 (1.52 mL, 29.7 mmol) then stirred at 55 °C for 19 h in dark conditions. The mixture was slowly cooled to rt, then to 0 °C for 1 h, whereupon formation of a yellow precipitate formed. The solid was collected by filtration and washed with cold to afford the product as a cream-white solid (8.0 g, 24.0 mmol, **81%**).

The NMR spectra were consistent with that reported in the group.[2]

^{1}H NMR (400 MHz, Chloroform-*d*) δ 7.56 (d, *J* = 2 Hz, 1H), 7.54 (dd, *J* = 8, 2 Hz, 1H), 7.46 – 7.31 (m, 5H), 6.92 (d, *J* = 8 Hz, 1H), 5.25 (s, 2H), 4.39 (s, 2H), 3.95 (s, 3H) ppm.

7-(2-(4-(Benzyloxy)-3-methoxyphenyl)-2-oxoethoxy)-4-methyl-2*H*-chromen-2-one (2-16a)

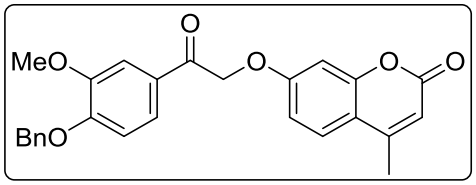

Product was prepared as for **2-16b** using **2-15a** as starting material. Product was afforded as a white solid (489 mg, **99%**).

The NMR spectra were consistent with that reported in the group.[2]

^{1}H NMR (400 MHz, Chloroform-*d*) δ 7.58 – 7.52 (m, 2H), 7.50 (d, *J* = 9 Hz, 1H), 7.46 – 7.29 (m, 5H), 6.96 – 6.90 (m, 2H), 6.77 (d, *J* = 3 Hz, 1H), 6.13 (q, *J* = 1 Hz, 1H), 5.31 (s, 2H), 5.25 (s, 2H), 3.95 (s, 3H), 2.38 (d, *J* = 1 Hz, 3H) ppm.

7-(2-(4-(Benzyloxy)-3-methoxyphenyl)-2-oxoethoxy-1-*d*)-4-methyl-2*H*-chromen-2-one (2-46g)

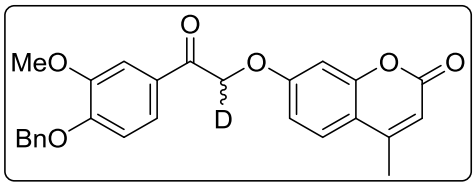

To a solution of **2-16a** (100 mg, 0.23 mmol) in THF (2 mL) at -78 °C was added dropwise 2 M LDA (0.13 mL, 0.26 mmol). After 40 min the reaction was quenched with D_2O (0.1 mL, 6.44 mmol) then diluted further with H_2O. The organics were extracted using EtOAc (x3), then washed with brine, dried over $MgSO_4$, then concentrated under reduced pressure to afford a beige oil (100 mg, 0.32 mmol, **100%**).

^{1}H NMR (400 MHz, Chloroform-*d*) δ 7.57 – 7.52 (m, 2H), 7.51 (d, *J* = 9 Hz, 1H), 7.46 – 7.30 (m, 5H), 6.96 – 6.90 (m, 2H), 6.78 (dd, *J* = 3, 2 Hz, 1H), 6.14 (q, *J* = 1 Hz, 1H), 5.31 (s, 1H), 5.26 (s, 2H), 3.95 (s, 3H), 2.39 (d, *J* = 1 Hz, 3H) ppm.

^{13}C NMR (101 MHz, Chloroform-*d*) δ 191.7 (C), 161.1 (C), 161.0 (C), 155.1 (C), 153.3 (C), 152.4 (C), 149.9 (C), 136.0 (C), 128.7 (CH), 128.2 (CH), 127.5 (CH), 127.2 (CH), 125.7 (CH), 122.4 (2 x CH), 114.2 (C), 112.7 (CH), 112.3 (d, 2 x CH), 110.6 (CH), 101.9 (CH), 70.9 (CH_2), 70.4 (CH*D*), 56.1 (CH_3), 18.7 (CH_3) ppm.

IR (Film): 2977, 2912, 1702, 1601, 1262, 1105 cm^{-1}.

HRMS (ESI): calc. for $[C_{26}H_{23}DO_6]^+$: 433.1630; found: 433.1620.

4-(3-Hydroxy-2-((4-methyl-2-oxo-2*H*-chromen-7-yl)oxy)propanoyl)-2-methoxyphenyl pivalate (2-46b)

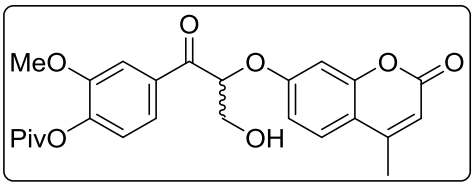

To a solution of **2-16b** (73 mg, 0.17 mmol) in THF (2 mL) at rt was added K_2CO_3 (48 mg, 0.34 mmol) then 37% formalin solution (17 µL, 0.21 mmol). The reaction mixture was heated at 50 °C for 20 h then acidified using 1M HCl (pH 5). The organics were extracted using EtOAc (x3), then washed with brine, dried over $MgSO_4$, then concentrated under reduced pressure to afford a foamy beige solid. The crude was purified by flash column chromatography, whereby the product eluted at 50% EtOAc/hexanes as an off white foamy solid (50 mg, 0.11 mmol, **64%**).

^{1}H NMR (400 MHz, Chloroform-*d*) δ 7.68 (dd, *J* = 8, 2 Hz, 1H), 7.61 (d, *J* = 2 Hz, 1H), 7.48 (d, *J* = 9 Hz, 1H), 7.13 (d, *J* = 8 Hz, 1H), 6.89 – 6.84 (m, 1H), 6.78 (d, *J* = 3 Hz, 1H), 6.14 (d, *J* = 1 Hz, 1H), 5.64 (dd, *J* = 6, 4 Hz, 1H), 4.27 – 4.10 (m, 2H), 3.85 (s, 3H), 2.37 (dd, *J* = 1, 0.5 Hz, 3H), 2.30 (t, *J* = 7 Hz, 1H), 1.37 (d, *J* = 0.5 Hz, 9H) ppm.

^{13}C NMR (101 MHz, Chloroform-*d*) δ 194.1 (C), 176.0 (C), 161.0 (C), 160.0 (C), 155.0 (C), 152.3 (C), 152.0 (C), 145.6 (C), 132.7 (C), 126.0 (CH), 123.2 (CH), 121.8 (CH), 114.6 (C), 112.6 (CH), 112.4 (CH), 112.1 (CH), 102.7 (CH), 81.4 (CH), 63.4 (CH_2), 56.1 (CH_3), 39.2 (C), 27.1 (3 x CH_3), 18.6 (CH_3) ppm.

IR (Film): 3456, 2968, 1719, 1606, 1274, 1101, 735 cm^{-1}.

HRMS (ESI): calc. for $[C_{25}H_{27}O_8]^+$: 455.17004; found: 455.17055.

4-(3-Hydroxy-2-(hydroxymethyl)-2-((4-methyl-2-oxo-2*H*-chromen-7-yl)oxy)propanoyl)-2-methoxyphenyl pivalate.

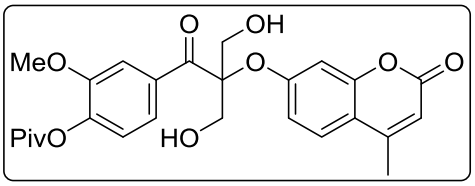

From reaction **2-46b**, a second product was eluted from the column at 80% EtOAc/hexanes as an off white foamy solid (20 mg, **19%**).

^{1}H NMR (400 MHz, Chloroform-*d*) δ 7.93 (ddd, *J* = 8.4, 2.0, 0.7 Hz, 1H), 7.78 (dd, *J* = 2.0, 0.7 Hz, 1H), 7.39 (d, *J* = 8.6 Hz, 1H), 7.00 (dd, *J* = 8.3, 0.7 Hz, 1H), 6.86 – 6.74 (m, 2H), 6.11 (q, *J* = 1.1 Hz, 1H),

4.32 (ddd, *J* = 66.0, 12.0, 6.6 Hz, 4H), 3.83 (s, 3H), 2.80 (t, *J* = 6.9 Hz, 2H), 2.32 (s, 3H), 1.32 (s, 9H) ppm.

^{13}C NMR (101 MHz, Chloroform-*d*) δ 199.5 (C), 176.0 (C), 160.8 (C), 157.7 (C), 154.7 (C), 152.1 (C), 151.5 (C), 145.3 (C), 132.6 (C), 125.9 (CH), 123.2 (CH), 123.0 (CH), 115.1 (C), 114.3 (CH), 113.1 (CH), 112.9 (CH), 105.6 (CH), 88.1 (C), 65.0 (2 x CH_2), 56.0 (CH_3), 39.2 (C), 27.1 (3 x CH_3), 18.5 (CH_3) ppm.

IR (Film): 3443 (br), 2973, 1723, 1606, 1501, 1101, 731 cm^{-1}.

HRMS (ESI): calc. for $[C_{26}H_{29}O_9]^+$: 485.18061; found: 485.18170.

7-((3-Hydroxy-1-(4-hydroxy-3-methoxyphenyl)-1-oxopropan-2-yl)oxy)-4-methyl-2*H*-chromen-2-one (2-41b)

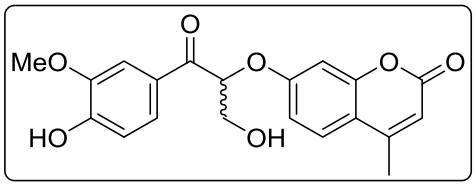

The product was prepared as for **2-12** using **2-46b** as starting material. The crude was purified by flash column chromatography, whereby the product eluted at 4% MeOH/DCM as an off white foamy solid (91 mg, **85%**).

^{1}H NMR (400 MHz, Chloroform-*d*) δ 7.69 (dd, *J* = 8, 2 Hz, 1H), 7.56 (d, *J* = 2 Hz, 1H), 7.49 (d, *J* = 9 Hz, 1H), 6.99 (d, *J* = 8 Hz, 1H), 6.90 (dd, *J* = 9, 3 Hz, 1H), 6.72 (d, *J* = 3 Hz, 1H), 6.13 (d, *J* = 1 Hz, 1H), 5.65 (dd, *J* = 6, 4 Hz, 1H), 4.25 – 4.10 (m, 2H), 3.94 (s, 3H), 2.37 (d, *J* = 1 Hz, 3H) ppm.

^{13}C NMR (101 MHz, Chloroform-*d*) δ 193.2 (C), 161.0 (C), 160.2 (C), 155.0 (C), 152.3 (C), 151.7 (C), 147.1 (C), 127.1 (C), 125.9 (CH), 123.9 (CH), 114.5 (C), 114.3 (CH), 112.8 (CH), 112.5 (CH), 110.5 (CH), 102.4 (CH), 81.0 (CH), 63.6 (CH_2), 56.2 (CH_3), 18.7 (CH_3) ppm.

IR (Film): 3447 (br), 2916, 1719, 1610, 1510, 1266 cm^{-1}.

HRMS (ESI): calc. for $[C_{21}H_{21}O_7]^+$: 385.12818; found: 385.12855.

2-bromo-1-(3,4-dimethoxyphenyl)ethan-1-one (2-15c)

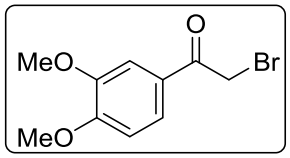

To 1-(3,4-dimethoxyphenyl)ethan-1-one (4.00 g, 22.2 mmol) in EtOAc (100 mL) at rt was added pyridinium tribromide (7.45 g, 23.3 mmol). After 30 min the reaction mixture was washed with Na_2CO_3 (sat, x3), H_2O then brine, dried over $MgSO_4$, then concentrated under reduced pressure to afford a yellow solid. This was then recrystallized using MeOH to obtain the product as a cream/white solid (4.2 g, 16.2 mmol, **73%**).

The NMR spectra were consistent with that reported in the literature.[3]

^{1}H NMR (400 MHz, Chloroform-*d*) δ 7.61 (dd, *J* = 8, 2 Hz, 1H), 7.54 (d, *J* = 2 Hz, 1H), 6.91 (d, *J* = 8 Hz, 1H), 4.41 (s, 2H), 3.97 (s, 3H), 3.94 (s, 3H) ppm.

7-(2-(3,4-dimethoxyphenyl)-2-oxoethoxy)-4-methyl-2*H*-chromen-2-one(2-52a)

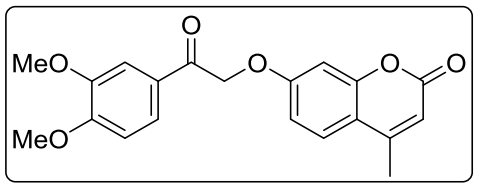

The product was prepared as for **2-16b** but starting from **2-15c**. Product eluted from the column at 65% EtOAc/hexanes as a white solid (100 mg, **15%**).

The NMR spectra were consistent with that reported in the literature.[3]

^{1}H NMR (400 MHz, Chloroform-*d*) δ 7.63 (dd, *J* = 8, 2 Hz, 1H), 7.57 – 7.49 (m, 2H), 6.99 – 6.90 (m, 2H), 6.80 (d, *J* = 3 Hz, 1H), 6.14 (q, *J* = 1 Hz, 1H), 5.34 (s, 2H), 3.98 (s, 3H), 3.95 (s, 3H), 2.39 (d, *J* = 1 Hz, 3H) ppm.

7-((1-(3,4-Dimethoxyphenyl)-3-hydroxy-1-oxopropan-2-yl)oxy)-4-methyl-2*H*-chromen-2-one (2-52b)

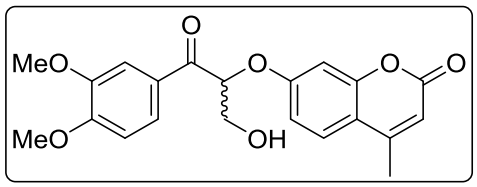

The product was prepared as for **2-46b** but starting from **2-52a**. The product eluted from the column at 78% EtOAc/hexanes as a white solid (21 mg, **26%**).

^{1}H NMR (400 MHz, Chloroform-*d*) δ 7.74 (dd, *J* = 9, 2 Hz, 1H), 7.54 (d, *J* = 2 Hz, 1H), 7.48 (d, *J* = 9 Hz, 1H), 6.95 – 6.87 (m, 2H), 6.72 (d, *J* = 3 Hz, 1H), 6.12 (q, *J* = 1 Hz, 1H), 5.66 (dd, *J* = 6, 4 Hz, 1H), 4.26 – 4.13 (m, 2H), 3.97 (s, 3H), 3.91 (s, 3H), 2.36 (d, *J* = 1 Hz, 3H) ppm.

^{13}C NMR (101 MHz, Chloroform-*d*) δ 193.3 (C), 161.0 (C), 160.1 (C), 155.0 (C), 154.5 (C), 152.3 (C), 149.6 (C), 127.4 (C), 125.9 (CH), 123.3 (CH), 114.4 (C), 112.8 (CH), 112.4 (CH), 110.7 (CH), 110.3 (CH), 102.3 (CH), 81.0 (CH), 63.6 (CH_2), 56.2 (CH_3), 56.0 (CH_3), 18.6 (CH_3) ppm.

IR (Film): 3447 (br), 2916, 1719, 1610, 1510, 1266 cm^{-1}.

HRMS (ESI): calc. for $[C_{21}H_{21}O_7]^+$: 385.12818; found: 385.12855.

4-Formyl-2-methoxyphenyl pivalate (2-42b)

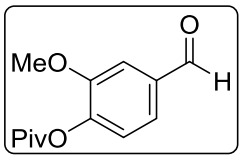

The product was prepared as for **2-14c** using 4-hydroxy-3-methoxybenzaldehyde (**2-42a**) as starting material. This was then recrystallised using MeOH to obtain the product as a colourless oil (9.8 g, **97%**).

The NMR spectra were consistent with that reported in the literature.[4]

^{1}H NMR (400 MHz, Chloroform-*d*) δ 9.94 (s, 1H), 7.49 – 7.45 (m, 2H), 7.19 (d, *J* = 8 Hz, 1H), 3.88 (s, 3H), 1.38 (s, 9H) ppm.

4-(1-hydroxypropyl)-2-methoxyphenyl pivalate (2-43)

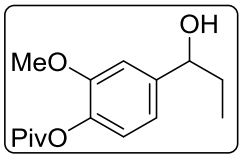

To a solution of **2-42b** (4.4 g, 18.7 mmol) in THF (35 mL) at ca. -5 °C was added 40% ethyl magnesium bromide (6.86 mL, 20.6 mmol). After 1 h the reaction was quenched with NH_4Cl (sat) then extracted using EtOAc (x2). The combined organics were washed with H_2O, brine, dried over $MgSO_4$, then concentrated under reduced pressure to afford a pale yellow oil (9.8 g, **79%**).

^{1}H NMR (400 MHz, Chloroform-*d*) δ 6.98 (bd, *J* = 2 Hz, 1H), 6.96 (bd, *J* = 8 Hz, 1H), 6.88 (ddd, *J* = 8, 2, 0.6 Hz, 1H), 4.59 (t, *J* = 7 Hz, 1H), 3.81 (s, 3H), 1.85 – 1.69 (m, 2H), 1.36 (s, 9H), 0.92 (t, *J* = 7 Hz, 3H) ppm.

^{13}C NMR (101 MHz, Chloroform-*d*) δ 176.8 (C), 151.2 (C), 143.3 (C), 139.4 (C), 122.4 (CH), 118.1 (CH), 110.0 (CH), 75.7 (CH), 55.9 (CH_3), 39.0 (C), 31.9 (CH_2), 27.2 (3 x CH_3), 10.1 (CH_3) ppm.

IR (Film): 2973, 1750, 1670, 1506, 1112, 883 cm^{-1}.

HRMS (ESI): calc. for $[C_{15}H_{22}O_4]^+$: 266.15126; found: 266.14957.

2-methoxy-4-propionylphenyl pivalate (2-44)

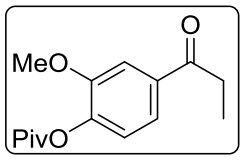

To a solution of **2-43** (660 mg, 2.48 mmol) in DCM (15 mL) at 0 °C was added portionwise pyridinium chlorochromate (882 mg, 4.09 mmol). The reaction mixture was allowed to reach rt then left for 24 h. The mixture was filtered through a silica plug, washing with DCM, then concentrated under reduced pressure to afford an oil which solidified upon standing (550 mg, 2.09 mmol, **84%**).

^{1}H NMR (400 MHz, Chloroform-*d*) δ 7.52 (d, *J* = 2 Hz, 1H), 7.49 (dd, *J* = 8, 2 Hz, 1H), 7.01 (d, *J* = 8 Hz, 1H), 3.80 (s, 3H), 2.92 (q, *J* = 7 Hz, 2H), 1.30 (s, 9H), 1.16 (t, *J* = 7 Hz, 3H) ppm.

^{13}C NMR (101 MHz, Chloroform-*d*) δ 199.7 (C), 176.2 (C), 151.5 (C), 144.2 (C), 135.5 (C), 122.6 (CH), 121.3 (CH), 111.4 (CH), 56.0 (CH_3), 39.2 (C), 31.7 (CH_2), 27.2 (3 x CH_3), 8.3 (CH_3) ppm.

IR (Film): 2960, 1749, 1675, 1506, 1266, 1105, 883 cm^{-1}.

HRMS (ESI): calc. for $[C_{15}H_{21}O_4]^+$: 265.14344; found: 265.14343.

M_P: 91.0 – 91.7 °C.

4-(2-Bromopropanoyl)-2-methoxyphenyl pivalate (2-45)

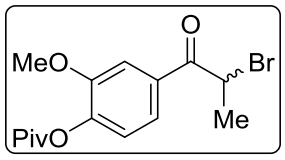

The product was prepared as for **2-15b** using **2-44** as starting material. The crude was purified by flash column chromatography, whereby the product eluted at 11% EtOAc/hexanes as a cream/white solid (628 mg, **60%**).

^{1}H NMR (400 MHz, Chloroform-*d*) δ 7.66 – 7.60 (m, 3H), 7.11 (d, *J* = 8 Hz, 1H), 5.27 (q, *J* = 7 Hz, 2H), 3.88 (s, 3H), 1.90 (d, *J* = 7 Hz, 3H), 1.38 (s, 11H) ppm.

^{13}C NMR (101 MHz, Chloroform-*d*) δ 192.3 (C), 176.1 (C), 151.7 (C), 144.9 (C), *132.5 (C), 125.0 (C),* 122.8 (C), 122.1 (CH), 122.1 (CH), 115.3 (C), 112.6 (CH), 56.1 (CH_3), 41.2 (CH), 39.2 (C), *37.8 (CH),* 27.1 (3 x CH_3), 20.2 (CH_3) ppm.

IR (Film): 2912, 1758, 1680, 1593, 1262, 1105 cm^{-1}.

HRMS (ESI): calc. for $[C_{15}H_{20}O_4Br]^+$: 343.05395; found: 343.05419.

M_P: 59.8 – 61.5 °C.

2-Methoxy-4-(2-((4-methyl-2-oxo-2*H*-chromen-7-yl)oxy)propanoyl)phenyl pivalate (2-46a)

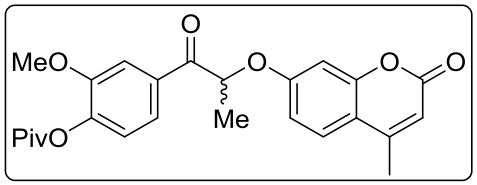

The product was prepared as for **2-16b**. White solid (160 mg, **64%**).

^{1}H NMR (400 MHz, Chloroform-*d*) δ 7.69 (dd, *J* = 8, 2 Hz, 1H), 7.63 (d, *J* = 2 Hz, 1H), 7.46 (d, *J* = 9 Hz, 1H), 7.11 (d, *J* = 8 Hz, 1H), 6.84 (dd, *J* = 9, 3 Hz, 1H), 6.74 (d, *J* = 3 Hz, 1H), 6.11 (q, *J* = 1 Hz, 1H), 5.54 (q, *J* = 7 Hz, 1H), 3.85 (s, 3H), 2.36 (d, *J* = 1 Hz, 3H), 1.76 (d, *J* = 7 Hz, 3H), 1.37 (s, 9H) ppm.

^{13}C NMR (101 MHz, Chloroform-*d*) δ 196.6 (C), 176.1 (C), 161.0 (C), 160.2 (C), 155.1 (C), 152.3 (C), 151.9 (C), 145.3 (C), 132.0 (C), 125.9 (CH), 123.0 (CH), 121.9 (CH), 114.2 (C), 112.5 (CH), 112.3 (2 x CH), 102.4 (CH), 76.9 (CH), 56.1 (CH_3), 39.2 (C), 27.1 (3 x CH_3), 18.9 (CH_3), 18.6 (CH_3) ppm.

IR (Film): 2976, 1754, 1612, 1265, 1109, 849 cm^{-1}.

HRMS (ESI): calc. for $[C_{25}H_{27}O_7Br]^+$: 439.17513; found: 439.17500.

M_P: 151.2 – 151.6 °C.

7-((1-(4-Hydroxy-3-methoxyphenyl)-1-oxopropan-2-yl)oxy)-4-methyl-2*H*-chromen-2-one (2-41a)

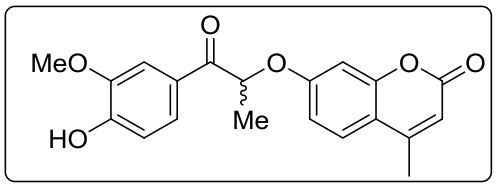

The product was prepared as for **2-12** starting from **2-46a**. White solid (52 mg, **43%**).

^{1}H NMR (400 MHz, Chloroform-*d*) δ 7.69 (dd, *J* = 8, 2 Hz, 1H), 7.58 (d, *J* = 2 Hz, 1H), 7.46 (d, *J* = 9 Hz, 1H), 6.97 (d, *J* = 8 Hz, 1H), 6.88 (dd, *J* = 9, 3 Hz, 1H), 6.69 (d, *J* = 3 Hz, 1H), 6.12 – 6.10 (m, 1H), 5.56 (q, *J* = 7 Hz, 1H), 3.95 (s, 3H), 2.36 (d, *J* = 1 Hz, 3H), 1.75 (d, *J* = 7 Hz, 3H) ppm.

^{13}C NMR (101 MHz, Chloroform-*d*) δ 196.0 (C), 161.1 (C), 160.4 (C), 155.0 (C), 152.4 (C), 151.3 (C), 147.0 (C), 126.5 (C), 125.8 (CH), 123.8 (CH), 114.1 (CH), 114.1 (C), 112.9 (CH), 112.2 (CH), 110.6 (CH), 102.1 (CH), 76.4 (CH), 56.1 (CH_3), 19.2 (CH_3), 18.6 (CH_3) ppm.

IR (Film): 2972, 1758, 1600, 1262, 1105, 861 cm^{-1}.

HRMS (ESI): calc. for $[C_{20}H_{19}O_6]^+$: 355.11761; found: 355.11743.

M_P: 159.8 – 161.5 °C.

The product was separated into the respective enantiomers by chiral HPLC with the following retention times: 14.29 and 18.39 min (Chiralpak ADH 250x 4.6 mm, 5u (50% heptane/EtOAc).

4-(2-Fluoroacetyl)-2-methoxyphenyl pivalate (2-47b)

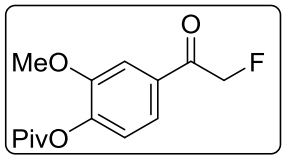

A solution of 1 M TBAF (10 mL, 10.0 mmol), ZnF (1.04 g, 10.0 mmol), and KF (364 mg, 6.3 mmol) in MeCN (10 mL) was heated at 85 °C for 1 h then added **2-15b** (2.75 g, 8.4 mmol), heating was continued for 20 h. The reaction mixture was cooled, filtered, and then concentrated under reduced pressure. The resulting residue was then separated between EtOAc and H_2O, then re-extracted using EtOAc (x2). The combined organics were washed with 0.5 M HCl, brine, then dried over $MgSO_4$ and concentrated under reduced pressure to afford a brown oil. The crude was purified by flash column chromatography, whereby the product eluted at 7% EtOAc/hexanes as a beige solid (1.02 g, 3.80 mmol, **45%**).

^{1}H NMR (400 MHz, Chloroform-*d*) δ 7.57 (d, *J* = 2 Hz, 1H), 7.43 (dd, *J* = 8, 2 Hz, 1H), 7.11 (d, *J* = 8 Hz, 1H), 5.51 (d, *J* = 47 Hz, 2H), 3.87 (s, 3H), 1.37 (s, 9H) ppm.

^{13}C NMR (101 MHz, Chloroform-*d*) δ 192.3 (d, J_F = 15 Hz, C), 176.1 (C), 152.0 (C), 145.3 (C), 132.2 (C), 123.1 (CH), ***122.9*** (d, J_F = 3 Hz, CH), 111.4 (d, J_F = 3 Hz CH), 83.5 (d, J_F = 183 Hz, CH_2), 56.1 (CH_3), 39.2 (C), 27.1 (3 x CH_3) ppm.

^{19}F NMR (376 MHz, Chloroform-*d*) δ 0.87 (t, *J* = 47 Hz) ppm.

IR (Film): 2912, 1754, 1706, 1258, 1101, 757 cm^{-1}.

HRMS (ESI): calc. for $[C_{14}H_{18}O_4F]^+$: 269.11836; found: 269.11846.

M_P: 79.4 – 79.8 °C.

4-(2-Bromo-2-fluoroacetyl)-2-methoxyphenyl pivalate (2-48b)

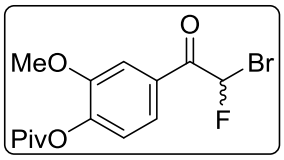

To a solution of **2-47b** (688 mg, 2.56 mmol) in AcOH (10 mL) was added dropwise Br_2 (0.98 mL, 2.82 mmol) then heated at 50 °C for 48 h. $Na_2S_2O_3$ (sat.) solution was then added to the mixture, before extracted with EtOAc (x2), washed with $KHCO_3$, then H_2O, dried over $MgSO_4$, then concentrated under reduced pressure to afford a beige solid. The crude was purified by flash column chromatography, whereby the product eluted at 10% EtOAc/hexanes as a white solid (460 mg, 1.33 mmol, **51%**).

^{1}H NMR (400 MHz, Chloroform-*d*) δ 7.62 – 7.58 (m, 2H), 7.10 (d, J_F = 51 Hz, 1H), 7.06 (dd, J = 9, 0.5 Hz, 1H), 3.82 (s, 3H), 1.31 (s, 9H) ppm.

^{13}C NMR (101 MHz, Chloroform-*d*) δ 186.6 (C), 173.6 (C), 151.9 (C), 145.8 (C), 129.3 (C), 123.1 (CH), 122.9 (d, J_F = 3 Hz, CH), 113.0 (d, J_F = 2 Hz, CH), 86.0 (d, J_F = 268 Hz, CH), 56.1 (CH_3), 39.2 (C), 27.1 (3 x CH_3) ppm.

^{19}F NMR (376 MHz, Chloroform-*d*) δ -151.46 (d, J = 51 Hz) ppm.

IR (Film): 2970, 2932, 1751, 1696, 1265, 1100 cm^{-1}.

HRMS (ESI): calc. for $[C_{14}H_{17}O_4BrF]^+$: 347.02888; found: 347.02889.

M_P: 69.4 – 69.9 °C.

1-(4-(benzyloxy)-3-methoxyphenyl)-2-fluoroethan-1-one (2-47a)

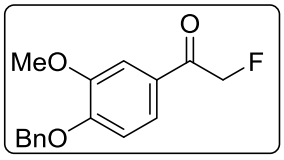

The product was prepared as for **2-15a**. The crude was purified by flash column chromatography, whereby the product eluted at 7% EtOAc/hexanes as a beige solid (1.02 g, 3.80 mmol, **45%**).

^{1}H NMR (400 MHz, Chloroform-*d*) δ 7.57 (d, J = 2 Hz, 1H), 7.43 (dd, J = 8, 2 Hz, 1H), 7.11 (d, J = 8 Hz, 1H), 5.51 (d, J = 47 Hz, 2H), 3.87 (s, 3H), 1.37 (s, 9H) ppm.

^{13}C NMR (101 MHz, Chloroform-*d*) δ 192.3 (d, J_F = 15 Hz, C), 176.1 (C), 152.0 (C), 145.3 (C), 132.2 (C), 123.1 (CH), 122.9 (d, J_F = 3 Hz, CH), 111.4 (d, J_F = 3 Hz CH), 83.5 (d, J_F = 183 Hz, CH_2), 56.1 (CH_3), 39.2 (C), 27.1 (3 x CH_3) ppm.

^{19}F NMR (376 MHz, Chloroform-*d*) δ 0.87 (t, *J* = 47 Hz) ppm.

IR (Film): 2912, 1754, 1706, 1258, 1101, 757 cm^{-1}.

HRMS (ESI): calc. for $[C_{14}H_{18}O_4F]^+$: 269.11836; found: 269.11846.

M_P: 76.4 – 77.0 °C.

1-(4-(Benzyloxy)-3-methoxyphenyl)-2-bromo-2-fluoroethan-1-one (2-48a)

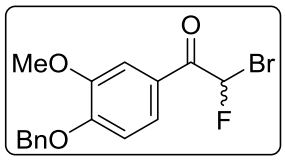

To a solution of **2-47a** (314 mg, 1.15 mmol) in AcOH (5 mL) was added dropwise Br_2 (0.06 mL, 1.15 mmol) then heated at 40 °C for 4 h. $Na_2S_2O_3$ (sat.) solution was then added to the mixture, before extraction with EtOAc (x2), washed with $KHCO_3$, then H_2O, dried over $MgSO_4$, then concentrated under reduced pressure to afford a beige solid. The crude was purified by flash column chromatography, whereby the product eluted at 45% EtOAc/hexanes as a colourless oil (154 mg, **38%**).

^{1}H NMR (400 MHz, Chloroform-*d*) δ 7.64 (ddd, *J* = 8, 2, 1 Hz, 1H), 7.60 (d, *J* = 2 Hz, 1H), 7.46 – 7.30 (m, 5H), 7.15 (d, *J* = 51 Hz, 1H), 6.93 (d, *J* = 9 Hz, 1H), 5.25 (s, 2H), 3.95 (s, 3H) ppm.

^{13}C NMR (101 MHz, Chloroform-*d*) δ 186.2 (d, J_F = 21 Hz, C), 153.8 (C), 149.8 (C), 135.8 (C), 128.7 (CH), 128.3 (2 x CH), 127.2 (2 x CH), 124.2 (d, J_F = 4 Hz, CH), 112.1 (CH), 111.9 (d, J_F = 2 Hz, CH), 86.2 (d, J_F = 268 Hz, CH), 70.9 (CH_2), 56.1 (CH_3) ppm.

^{19}F NMR (376 MHz, Chloroform-*d*) δ -150.68 (d, *J* = 51 Hz) ppm.

IR (Film): 2938, 1689, 1588, 1506, 1266, 1144 cm^{-1}.

HRMS (ESI): calc. for $[C_{16}H_{15}O_3BrF]^+$: 353.01831; found: 353.01870.

M_P: 70.4 – 70.0 °C.

7-(2-(4-(Benzyloxy)-3-methoxyphenyl)-1-fluoro-2-oxoethoxy)-4-methyl-2*H*-chromen-2-one (2-46ad)

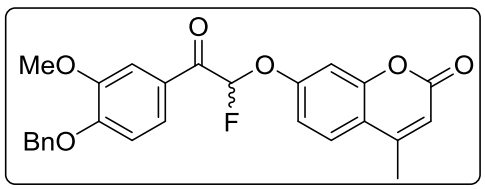

2-48a (30 mg, 0.085 mmol), 7-hydroxy-4-methyl-2*H*-chromen-2-one (15 mg, 0.085 mmol) and K_2CO_3 (23 mg, 0.170 mmol) were dissolved in acetone (1 mL) and stirred at rt for 20 h. Na_2CO_3 was then added to the

mixture, before extraction with 10% MeOH/$CHCl_3$ (x3). The combined organic layers were washed with brine, dried over $MgSO_4$, then concentrated under reduced pressure to afford a beige solid. The crude was purified by flash column chromatography, whereby the product eluted at 30% EtOAc/hexanes as a colourless oil (30 mg, 0.067 mmol, **79%**).

^{1}H NMR (400 MHz, Chloroform-*d*) δ 7.73 (ddd, *J* = 9, 2, 1 Hz, 1H), 7.65 (d, *J* = 2 Hz, 1H), 7.60 (d, *J* = 9 Hz, 1H), 7.45 – 7.30 (m, 4H), 7.25 (dd, *J* = 8, 7 Hz, 1H), 7.20 – 7.08 (m, 3H), 6.95 (d, *J* = 9 Hz, 1H), 6.40 (d, *J* = 60 Hz, 1H), 6.24 (q, *J* = 1 Hz, 1H), 5.26 (s, 2H), 3.95 (s, 3H), 2.43 (d, *J* = 1 Hz, 3H) ppm.

^{13}C NMR (101 MHz, Chloroform-*d*) δ 186.4 (d, J_F = 27 Hz, C), 171.2 (C), 160.5 (C), 158.2 (d, J_F = 3 Hz, C), 154.8 (C), 153.8 (C), 151.9 (C), 149.8 (C), 135.9 (C), 128.7 (2 x CH), 128.2 (CH), 127.2 (2 x CH), 126.1 (CH), 125.0 (d, J_F = 4 Hz, CH), 116.5 (C), 113.8 (CH), 113.5 (d, J_F = 2 Hz, CH), 112.2 (CH), 111.8 (d, *J* = 1 Hz, CH), 106.4 (d, J_F = 238 Hz, CH), 105.2 (d, J_F = 2 Hz, CH) 70.9 (CH_2), 56.1 (CH_3), 18.7 (CH_3) ppm.

^{19}F NMR (376 MHz, Chloroform-*d*) δ -127.12 (d, *J* = 60 Hz) ppm.

IR (Film): 2938, 1689, 1588, 1506, 1266, 1144 cm^{-1}.

HRMS (ESI): calc. for $[C_{16}H_{15}O_3BrF]^+$: 353.01831; found: 353.01870.

7-(1-fluoro-2-(4-hydroxy-3-methoxyphenyl)-2-oxoethoxy)-4-methyl-2H-chromen-2-one (2-41d)

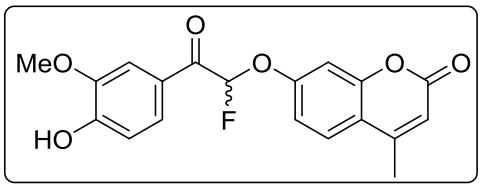

2-46ad (50 mg, 0.112 mmol) was dissolved in 25% MeOH/$CHCl_3$ (1 mL), degassed, then added 10% Pd/$BaSO_4$ (5 mg), then degassed and purged using N_2 then H_2. The mixture was stirred at rt for 20 h. Na_2CO_3 (aq) was then added to the mixture, before extraction with 10% MeOH/$CHCl_3$ (x3). The combined organic layers were washed with brine, dried over $MgSO_4$, and then concentrated under reduced pressure to afford a beige solid. The crude was purified by flash column chromatography, whereby the product eluted at 30% EtOAc/hexanes as a colourless oil (15 mg, 0.042 mmol, **38%**).

^{1}H NMR (400 MHz, Chloroform-*d*) δ 7.77 (ddd, *J* = 8, 2, 1 Hz, 1H), 7.66 (d, *J* = 2 Hz, 1H), 7.61 (d, *J* = 9 Hz, 1H), 7.15 (d, *J* = 2 Hz, 1H), 7.12 (dd, *J* = 9, 3 Hz, 1H), 7.01 (d, *J* = 8 Hz, 1H), 6.41 (d, *J* = 60 Hz, 1H), 6.25 (q, *J* = 1 Hz, 1H), 6.23 (s, 1H), 3.98 (s, 3H), 2.44 (d, *J* = 1 Hz, 3H) ppm.

^{13}C NMR (101 MHz, Chloroform-*d*) δ 186.4 (d, J_F = 27 Hz, C), 160.5 (C), 158.1 (C), 154.8 (C), 151.9 (C), 146.9 (C), 126.1 (CH), 125.8 (d, J_F = 3 Hz, CH), 116.5 (C), 114.2 (CH), 113.9 (CH), 113.6 (d, J_F = 2 Hz, CH), 111.2 (CH), 107.6 (CH), 105.3 (d, J_F = 2 Hz, CH), 56.2 (CH_3), 18.7 (CH_3) ppm.

^{19}F NMR (376 MHz, Chloroform-*d*) δ -127.1 (d, J = 60 Hz) ppm.

IR (Film): 3343, 2920, 1732, 1615, 1275, 1144 cm^{-1}.

HRMS (ESI): calc. for $[C_{19}H_{16}O_6F]^+$: 359.09254; found: 359.09255.

7-((1-(4-(Benzyloxy)-3-methoxyphenyl)-2-fluoro-3-hydroxy-1-oxopropan-2-yl)oxy)-4-methyl-2*H*-chromen-2-one (2-46e)

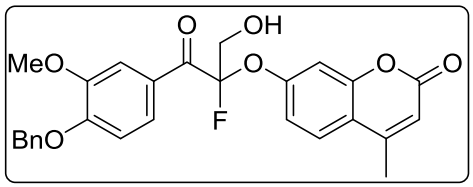

2-46ad (20 mg, 0.045 mmol) in THF (2 mL) at rt was added K_2CO_3 (46 mg, 0.34 mmol) then 37% formalin solution (11 μL, 0.34 mmol). The reaction mixture was heated at 75 °C for 72 h then acidified using 1M HCl (pH 5). The organics were extracted using EtOAc (x3), then washed with brine, dried over $MgSO_4$, then concentrated under reduced pressure to afford a foamy beige solid. The crude was purified by flash column chromatography, whereby the product eluted at 55% EtOAc/hexanes as an off white waxy solid (17 mg, 0.036 mmol, **80%**).

^{1}H NMR (400 MHz, Chloroform-*d*) δ 7.80 – 7.77 (m, 1H), 7.57 (d, J = 2 Hz, 1H), 7.44 – 7.40 (m, 1H), 7.38 – 7.25 (m, 5H), 7.06 – 7.01 (m, 2H), 6.84 (d, J = 9 Hz, 1H), 6.13 (d, J = 1 Hz, 1H), 5.17 (s, 2H), 4.18 – 3.96 (m, 2H), 3.85 (s, 3H), 2.31 (d, J = 1 Hz, 3H) ppm.

^{13}C NMR (101 MHz, Chloroform-*d*) δ 181.0 (C), 175.3 (C), 160.6 (C), 153.8 (C), 151.9 (C), 149.5 (C), 145.5 (C), 141.1 (C), 135.9 (C), 135.9 (C), 128.7 (CH), 128.2 (CH), 127.2 (CH), 125.7 (CH), 116.6 (CH), 114.5 (CH), 113.8 (CH), 112.5 (CH), 112.1 (CH), 108.1 (CH), 70.9 (CH_2), 64.7 (d, J_F = 32 Hz, CH_2), 56.1 (CH_3), 18.6 (CH_3) ppm.
(Not all expected J_{CF} couplings were observed.)

IR (Film): 3417, 2920, 1723, 1619, 1266, 1127, 731 cm^{-1}.

HRMS (ESI): calc. for $[C_{27}H_{24}O_7F]^+$: 479.15006; found: 479.15049.

HPLC: RT: 5.02 min, m/z: 479.1

7-((2-fluoro-3-hydroxy-1-(4-hydroxy-3-methoxyphenyl)-1-oxopropan-2-yl)oxy)-4-methyl-2*H*-chromen-2-one (2-41e)

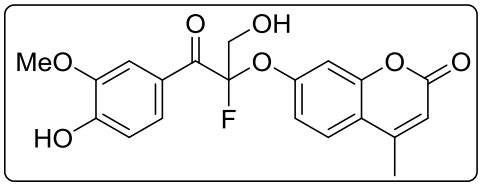

2-46e (17 mg, 0.36 mmol) was dissolved in 10% MeOH/$CHCl_3$ (1 mL), degassed, then added 10% Pd/$BaSO_4$ (4 mg), then degassed and purged using N_2 then H_2. The mixture was stirred at rt for 44 h. Na_2CO_3 was then added to the mixture, before extraction with 10% MeOH/$CHCl_3$ (x3). The combined organic layers were washed with brine, dried over $MgSO_4$, and then concentrated under reduced pressure to afford a beige solid. The crude was purified by flash column chromatography, whereby the product eluted at 30% EtOAc/hexanes as a colourless wax (4 mg, 0.012 mmol, **32%**).

^{1}H NMR (400 MHz, Chloroform-*d*) δ 7.84 – 7.79 (m, 1H), 7.57 (d, *J* = 2 Hz, 1H), 7.43 (d, *J* = 10 Hz, 1H), 7.06 – 7.01 (m, 2H), 6.91 – 6.86 (m, 1H), 6.15 – 6.11 (m, 1H), 4.18 – 4.06 (m, 2H), 3.88 (s, 3H), 2.31 (d, *J* = 1 Hz, 3H) ppm.

^{13}C NMR (101 MHz, 5:1 Chloroform:Methanol-*d*) δ *194.3* (C), 165.6 (C), 160.5 (C), 158.1 (C), 157.1 (C), 156.8 (C), 151.5 (C), 129.8 (C), 129.2 (C), 119.9 (CH), 119.1 (CH), 118.6 (CH), 116.9 (CH), 116.4 (CH), 110.5 (d, J_F = 3 Hz, CH), 69.8 (C), 69.3 (d, J_F = 28 Hz, CH_2), 59.6 (CH_3), 18.7 (CH_3) ppm. *(Compound was insoluble in available deuterated solvents; methanol-d added to aid solubility)*

IR (Film): 3373, 2920, 1710, 1615, 1261, 1079, 796 cm^{-1}.

HRMS (ESI): calc. for $[C_{20}H_{18}O_7F]^+$: 389.10464; found: 389.10434.

HPLC: RT: 3.24 min, m/z: 389.0

(*E*)-1-(4-(Benzyloxy)-3-methoxyphenyl)-4,4,4-trifluorobut-2-en-1-one (2-49)

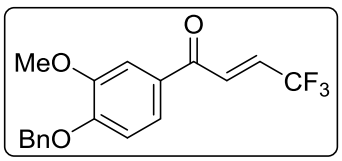

NaH (74 mg, 3.1 mmol) was added to **2-14b** (450 mg, 1.76 mmol) dissolved in THF (10 mL), degassed, then added ethyl 2,2,2-trifluoroacetate (262 mg, 1.85 mmol) and stirred for 24 h. NH_3Cl (sat.) solution was then added to the mixture, before extraction with EtOAc (x2). The organics were

washed with H_2O, then brine, dried over $MgSO_4$, then concentrated under reduced pressure. The crude was purified by flash column chromatography, whereby the product eluted at 25% EtOAc/hexanes as a colourless oil (450 mg, **65%**).

^{1}H NMR (400 MHz, Chloroform-*d*) δ 7.54 – 7.49 (m, 2H), 7.45 – 7.30 (m, 5H), 6.95 (d, *J* = 8 Hz, 1H), 6.50 (s, 1H), 5.25 (s, 2H), 3.97 (s, 3H) ppm.

^{13}C NMR (101 MHz, Chloroform-*d*) δ 186.7 (C), 174.8 (d, J_F = 36 Hz, C), 153.5 (C), 149.8 (C), 135.9 (C), 128.7 (CH), 128.3 (CH), 127.2 (CH), 126.0 (C), 122.3 (CH), *118.9 , 116.1 (C),* 112.7 (CH), 110.2 (CH), 92.2 – 91.6 (m, CH), 70.9 (CH_2), 56.2 (CH_3) ppm.

IR (Film): 2921, 1592, 1514, 1213, 1150, 788 cm^{-1}.

HRMS (ESI): calc. for $[C_{18}H_{16}O_4F_3]^+$: 353.09952; found: 353.09952.

1-(4-(Benzyloxy)-3-methoxyphenyl)-2,2,4,4,4-pentafluoro-3,3-dihydroxybutan-1-one (2-50)

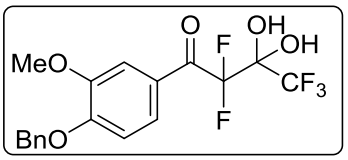

Selectfluor® (754 mg, 2.1 mmol) was added to **2-49** (300 mg, 1.76 mmol) dissolved in MeCN (10 mL), then stirred for 24 h. $NaHCO_3$ (sat.) solution was then added to the mixture before extraction with DCM (x2). The organics were washed with brine, dried over $MgSO_4$, and then concentrated under reduced pressure to afford a yellow solid (400 mg, **99%**).

^{1}H NMR (400 MHz, Chloroform-*d*) δ 7.81 (dq, *J* = 8.6, 1.7 Hz, 1H), 7.59 (d, *J* = 2.1 Hz, 1H), 7.45 – 7.32 (m, 5H), 6.96 (d, *J* = 8.7 Hz, 1H), 5.27 (s, 2H), 4.75 (s, 2H), 3.95 (s, 3H) ppm.

^{13}C NMR (101 MHz, Chloroform-*d*) δ 155.0 (C), 149.6 (C), 135.6 (C), 128.8 (CH), 128.4 (CH), 127.2 (CH), 126.5 (t, J_F = 6 Hz, CH), 112.4 (CH), 112.2 (CH), 71.0 (CH_2), 56.1 (CH_3) ppm.

^{19}F NMR (376 MHz, Chloroform-*d*) δ -81.1 (t, *J* = 11 Hz), -110.92 (q, *J* = 11 Hz) ppm.

IR (Film): 3407, 2926, 1676, 1592, 1511, 1202, 715 cm^{-1}.

HRMS (ESI): calc. for $[C_{18}H_{16}O_5F_5]^+$: 407.09124; found: 407.09110.

1-(4-(Benzyloxy)-3-methoxyphenyl)-2,2-difluoro-2-iodoethan-1-one (2-51)

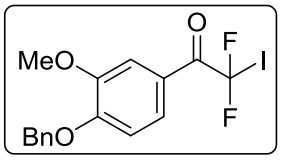

To a solution of **2-50** (119 mg, 0.29 mmol) in THF (3 mL) was added LiBr (161 mg, 1.86 mmol), NEt_3 (0.08 mL, 0.59 mmol) and I_2 (156 mg, 0.62 mmol) then stirred for 24 hr at rt, followed by 1 hr at 40 °C. The reaction mixture was quenched using $Na_2S_2O_3$ then $NaHCO_3$ and extracted using EtOAc (x3). The organics were washed with brine, dried over $MgSO_4$, and then concentrated under reduced pressure to afford the crude product as a beige solid. The material was used directly in the next reaction due to the reported instability of these α-difluoro, iodo compounds:

7-(2-(4-(Benzyloxy)-3-methoxyphenyl)-1,1-difluoro-2-oxoethoxy)-4-methyl-2*H*-chromen-2-one (2-46f)

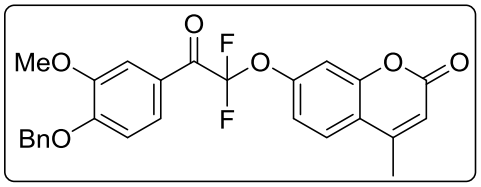

The compound was prepared following the procedure for **2-16** using **2-51**. Product obtained as a brown oil (15 mg, **11% over two steps)**

^{1}H NMR (400 MHz, Chloroform-*d*) δ 7.80 (ddt, *J* = 9, 2, 1 Hz, 1H), 7.65 (d, *J* = 2 Hz, 1H), 7.59 (d, *J* = 9 Hz, 1H), 7.46 – 7.30 (m, 5H), 7.24 – 7.16 (m, 2H), 6.97 (d, *J* = 9 Hz, 1H), 6.27 (q, *J* = 1 Hz, 1H), 5.27 (s, 2H), 3.95 (s, 3H), 2.42 (d, *J* = 1 Hz, 3H) ppm.

^{13}C NMR (101 MHz, Chloroform-*d*) δ 180.8 (t, *J* = 34 Hz, C), 160.3 (C), 154.2 (d, J_F = 5 Hz, C), 152.1 (t, J_F = 2 Hz, C), 151.7 (C), 149.7 (C), 135.7 (C), 128.8 (2 x CH), 128.3 (CH), 127.2 (2 x CH), 125.8 (CH), 125.7 (t, J_F = 3 Hz, CH), 123.6 (C), 118.7 (C), 117.9 (C), 116.9 (CH), 115.9 (C), 114.6 (CH), 112.3 (CH), 112.2 (CH), 109.4 (d, J_F = 1.2 Hz, CH), 70.9 (CH_2), 56.1 (CH_3), 18.7 (CH_3) ppm.

IR (film): 3061, 2933, 1732, 1588, 1510, 1258, 1131 cm^{-1}.

HRMS (ESI): calc. for $[C_{26}H_{21}O_6F_2]^+$: 467.13007; found: 467.12970.

7-(1,1-Difluoro-2-(4-hydroxy-3-methoxyphenyl)-2-oxoethoxy)-4-methyl-2*H*-chromen-2-one (2-41f)

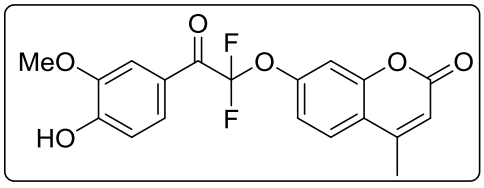

The compound was prepared as for **2-41d** using **2-46f** as starting material. Solid wax (6 mg, **18%**).

^{1}H NMR (400 MHz, Chloroform-*d*) δ 7.86 – 7.80 (m, 1H), 7.65 (d, *J* = 2.0 Hz, 1H), 7.60 (d, *J* = 8.6 Hz, 1H), 7.25 – 7.18 (m, 2H), 7.02 (d, *J* = 8.5 Hz, 1H), 6.31 (s, 1H), 6.28 (q, *J* = 1.3 Hz, 1H), 3.98 (s, 3H), 2.43 (d, *J* = 1.3 Hz, 3H) ppm.

^{19}F NMR (376 MHz, Chloroform-*d*) δ -72.96 (s) ppm.

^{13}C NMR (101 MHz, Chloroform-*d*) δ 181.1 (C), 160.3 (C), 154.2 (C), 152.3 (C), 152.1 (C), 151.7 (C), 146.8 (C), 126.6 – 126.3 (m, CH), 125.8 (CH), 123.3 (C), 117.9 (C), 116.9 (CH), 114.6 (CH), 114.4 (CH), 111.8 (CH), 109.4 (CH), 56.2 (CH_3), 18.7 (CH_3) ppm. (1 *quaternary signal not observed due to weak signal strength*).

IR (film): 3061, 2933, 1732, 1588, 1510, 1258, 1131 cm^{-1}.

HRMS (ESI): calc. for $[C_{19}H_{15}O_6F_2]^+$: 377.08312; found: 377.08309.

2-(4-bromophenoxy)tetrahydro-2*H*-pyran (2-31ab)

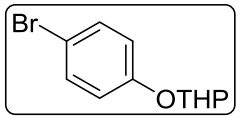

To a flask charged with 2-(4-bromophenoxy)tetrahydro-2H-pyran **2-31aa** (10 g, 60.9 mmol) dissolved in DCM (25 mL) at 0 °C was added DHP (mL, mmol) then PPTS (g, mmol). The mixture was stirred for 25 h warming to rt before separation between DCM and H_2O. The organic layer was then washed with brine, dried over $MgSO_4$, then concentrated under reduced pressure to afford a colourless oil, which solidified upon standing (16 g, **94%**).

The NMR spectra were consistent with that reported in the literature.[5]

^{1}H NMR (400 MHz, Chloroform-*d*) δ 7.99 – 7.89 (m, 2H), 7.33 – 7.26 (m, 4H), 7.23 – 7.15 (m, 1H), 6.91 – 6.84 (m, 2H), 6.01 (ddt, *J* = 17, 11, 5 Hz, 1H), 5.39 (dq, *J* = 17, 2 Hz, 1H), 5.29 (dq, *J* = 11, 1 Hz, 1H), 4.55 (dt, *J* = 5, 2 Hz, 2H), 4.39 (t, *J* = 7 Hz, 1H), 2.19 (dt, *J* = 14, 7 Hz, 1H), 1.84 (dt, *J* = 14, 7 Hz, 1H), 0.89 (t, *J* = 7 Hz, 3H) ppm.

2-(4-Bromo-3-methylphenoxy)tetrahydro-2*H*-pyran (2-62b)

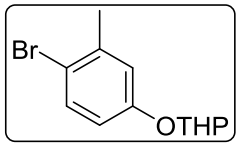

To a flask charged with 4-bromo-3-methylphenol **2-62a** (2.0 g, 10.69 mmol) dissolved in DCM (25 mL) at 0 °C was added DHP (2.9 mL, 32.1 mmol) then PPTS (0.27 g, 1.07 mmol). The mixture was stirred for 25 h warming to rt

before separation between DCM and H_2O. The organic layer was then washed with brine, dried over $MgSO_4$, then concentrated under reduced pressure to afford a colourless oil (2.8 g, **97%**).

The NMR spectra were consistent with that reported in the literature.[6]

^{1}H NMR (400 MHz, Chloroform-*d*) δ 7.39 (d, *J* = 9 Hz, 1H), 6.95 (dd, *J* = 3, 1 Hz, 1H), 6.77 (ddd, *J* = 9, 3, 1 Hz, 1H), 5.37 (t, *J* = 3 Hz, 1H), 3.91 – 3.84 (m, 1H), 3.59 (dtd, *J* = 11, 4, 2 Hz, 1H), 2.36 (s, 3H), 2.03 – 1.93 (m, 1H), 1.90 – 1.80 (m, 2H), 1.76 – 1.50 (m, 3H) ppm.

1-(4-(Allyloxy)phenyl)-2-phenylbutan-1-one (2-30c)

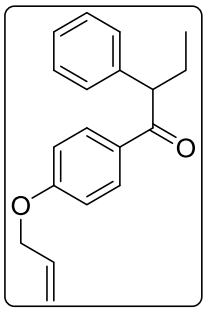

To a flask charged with 2-phenylbutanoic acid **2-32** (10 g, 60.9 mmol) was added (allyloxy)benzene (8.3 mL, 60.9 mmol) then TFAA (9.5 mL, 67.0 mmol). The mixture was stirred for 2.5 h at 30 °C, then added dropwise to $KHCO_3$ (sat), washing with DCM. The combined organic layers were then washed with brine, dried over $MgSO_4$, then concentrated under reduced pressure to afford a colourless oil, which solidified upon standing (16 g, **94%**).

^{1}H NMR (400 MHz, Chloroform-*d*) δ 7.99 – 7.89 (m, 2H), 7.33 – 7.26 (m, 4H), 7.23 – 7.15 (m, 1H), 6.91 – 6.84 (m, 2H), 6.01 (ddt, *J* = 17, 11, 5 Hz, 1H), 5.39 (dq, *J* = 17, 2 Hz, 1H), 5.29 (dq, *J* = 11, 1 Hz, 1H), 4.55 (dt, *J* = 5, 2 Hz, 2H), 4.39 (t, *J* = 7 Hz, 1H), 2.19 (dt, *J* = 14, 7 Hz, 1H), 1.84 (dt, *J* = 14, 7 Hz, 1H), 0.89 (t, *J* = 7 Hz, 3H) ppm.

^{13}C NMR (101 MHz, Chloroform-*d*) δ 198.6 (C), 162.2 (C), 140.0 (C), 132.5 (CH), 130.9 (CH), 130.1 (C), 128.8 (CH), 128.2 (CH), 126.8 (CH), 118.1 (CH_2), 114.3 (CH), 68.8 (CH_2), 55.1 (CH), 27.1 (CH_2), 12.3 (CH_3) ppm.

IR (Film): 3026, 1666, 1597, 1258, 1020, 744 cm^{-1}.

HRMS (ESI): calc. for $[C_{19}H_{21}O_2]^+$: 281.15361; found: 281.15354.

4-(1-(4-(allyloxy)phenyl)-2-phenylbut-1-en-1-yl)phenol (2-35)

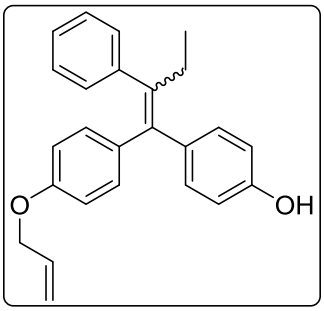

To a flask charged with 2-(4-bromophenoxy)tetrahydro-2*H*-pyran (**2-31ab**) (6.9 g, 26.8 mmol) dissolved in THF (15 mL) at -78 °C was added dropwise 2.5 M n-BuLi (10.7 mL, 26.8 mmol). The mixture was maintained between -72 – -68 °C for 45 min before the dropwise addition of **2-30c** (5.0 g, 18.0 mmol) dissolved in THF (15 mL). The mixture was stirred for 22 h warming to rt then separated between H_2O and EtOAc. The organic layer was then washed with brine, dried over $MgSO_4$, then concentrated under reduced pressure to afford the tertiary alcohol intermediate as a brown oil, 11.7 g. The crude intermediate was dissolved in MeOH (40 mL), then conc. HCl (2.0 mL, 26 mmol) was added dropwise to the mixture at rt. After 1 h, 1 M NaOH (20 mL) was added until pH 9, dilution with H_2O and then extracted using EtOAc (x3). The combined organic layers were washed with brine, dried over $MgSO_4$, then concentrated under reduced pressure to afford a brown oil. The residue was purified by flash column chromatography, whereby the product eluted at 7% EtOAc/hexanes as an off-white waxy solid, as an approximate 1:1 mixture of both stereoisomers (6.12 g, **66%**).

^{1}H NMR (400 MHz, Chloroform-*d*) δ 7.12 – 7.00 (m, 7H), 6.84 – 6.80 (m, 2H), 6.67 – 6.63 (m, 2H), 6.42 – 6.37 (m, 2H), 6.01 (ddt, *J* = 17, 11, 5 Hz, 1H), 5.36 (dq, *J* = 17, 2 Hz, 1H), 5.23 (dq, *J* = 11, 1 Hz, 1H), 4.48 (dt, *J* = 5, 2 Hz, 2H), 2.41 (q, *J* = 7 Hz, 2H), 0.85 (t, *J* = 7 Hz, 3H) ppm.

^{13}C NMR (101 MHz, Chloroform-*d*) δ 157.3* , 156.5 (C), 154.2* , 153.3 (C), 142.6* , 142.6 (C), 141.1* , 141.1 (C), 137.7* , 137.7 (C), 136.4* , 136.4 (C), 136.0* , 135.9 (C), 133.4* , 133.3 (CH), 132.1* , 131.9 (2 x CH), 130.8* , 130.5 (CH), 129.7 (2 x CH), 127.8 (2 x CH), 125.9 (2 x CH), 117.7* , 117.5 (CH_2), 114.9* , 114.2 (2 x CH), 114.2* , 113.5 (2 x CH), 68.8* , 68.6 (CH_2), 29.0* , 29.0 (CH_2), 13.6 (CH_3) ppm. (Asterisks* denote extra signals belonging to the other isomer)

IR (Film): 3395, 2964, 1606, 1506, 1231, 844 cm^{-1}.

HRMS (ESI): calc. for $[C_{25}H_{25}O_2]^+$: 357.18491; found: 357.18526.

4-(1-(4-(Allyloxy)phenyl)-2-phenylbut-1-en-1-yl)-3-methylphenol (2-35Me)

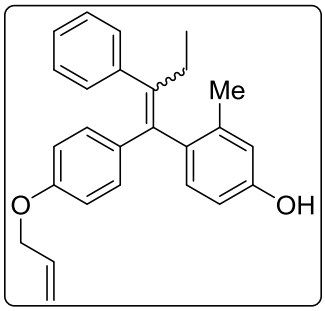

The product was prepared following the procedure for **2-35** using **2-62b** as starting material. The product eluted at 8% EtOAc/hexanes as an off-white waxy solid, as an approximate 4:1 mixture of *Z/E* isomers (2.8 g, **97%**).

^{1}H NMR (400 MHz, Chloroform-*d*) δ 7.23 – 7.00 (m, 5H), 6.90 – 6.82* (m), 6.82 – 6.66 (m, 4H), 6.57 – 6.48 (m, 2H), 6.44 – 6.33 (m, 1H), 6.12 – 6.01* (m), 6.06 – 5.90 (m, 1H), 5.42* (dq, *J* = 17, 2 Hz), 5.37 – 5.29 (m, 1H), 5.29 – 5.26* (m), 5.22 (dq, *J* = 11, 1 Hz, 1H), 4.53* (dt, *J* = 5, 2 Hz), 4.38 (dt, *J* = 5, 2 Hz, 2H), 2.39 – 2.20 (m, 2H), 2.09 (s, 3H), 1.97* (s), 1.00* (t, *J* = 7 Hz), 0.82 (t, *J* = 8 Hz, 3H) ppm.

^{13}C NMR (101 MHz, Chloroform-*d*) δ 157.1* , 156.4 (C), 154.3 (C), 153.7* , 142.6* , 142.3 (C), 141.5 (C), 137.9 (C), 137.8* , 137.3* , 136.6 (C), 135.8* , 135.5 (C), 135.4* , 134.3 (C), 133.3* , 133.3 (CH), 132.6 (C), 131.4 (2 x CH), 130.7* , 130.2* , 129.7 (2 x CH), 128.9* , 127.9 (CH), 127.5* , 126.0 (2 x CH), 125.9* , 117.7* , 117.5 (CH_2), 117.0 (2 x CH), 116.4* , 114.1* , 113.4 (2 x CH), 112.3 (CH), 112.0* , 68.8* , 68.6 (CH_2), 29.2 (CH_2), 27.9* , 20.3* , 19.9 (CH_3), 13.9* , 12.9 (CH_3) ppm. (Asterisks* denote extra signals belonging to the other isomer)

IR (Film): 3421, 2964, 1597, 1501, 1227, 705 cm^{-1}.

HRMS (ESI): calc. for $[C_{26}H_{27}O_2]^+$: 371.20056; found: 371.20089.

3-(4-(1-(4-Hydroxyphenyl)-2-phenylbut-1-en-1-yl)phenoxy)propane-1,2-diol (2-22)

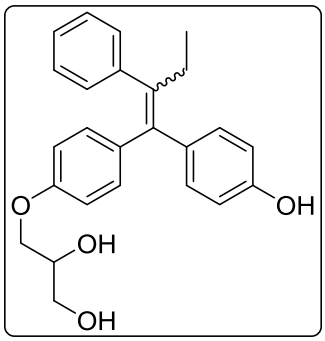

To a solution of **2-35** (6.9 g, 26.8 mmol) dissolved in acetone (35 mL) and H_2O (10 mL) was added NMO (1.3 g, 3.64 mmol) and $K_2[OsO_2(OH)_4]$ (30 mg, 0.08 mmol) then heated to 40 °C for 20 h. The reaction was quenched via addition of sat. Na_2SO_4 (aq.) then filtered, washing with EtOAc. The organics were extracted using EtOAc then washed with 10% sulfuric acid (50 mL). The acidic aqueous layer was further extracted with EtOAc, then the combined organic layers were washed with $NaHCO_3$ (x3), H_2O (x2), brine (x2), dried over $MgSO_4$, then concentrated under reduced

pressure to afford the product as an amber oil, as an approximate 1:1 mixture of both stereoisomers (1.35 g, **95%**).

The spectra were consistent with that previously reported within our group.[2]

^{1}H NMR (400 MHz, Acetone-d_6) δ 8.33* (s, 1H), 8.08 (s, 1H), 7.22 – 7.06 (m, 7H), 6.98 – 6.92 (m, 1H), 6.88 – 6.83* (m, 1H), 6.81 – 6.76* (m, 1H), 6.73 – 6.67 (m, 1H), 6.61 – 6.55* (m, 1H), 6.52 – 6.46 (m, 1H), 4.14 – 3.53 (m, 7H), 2.49 (qd, *J* = 7, 6 Hz, 2H), 0.91 (t, *J* = 7 Hz, 3H) ppm.

3-(4-(1-(4-hydroxy-2-methylphenyl)-2-phenylbut-1-en-1-yl)phenoxy)propane-1,2-diol (2-77)

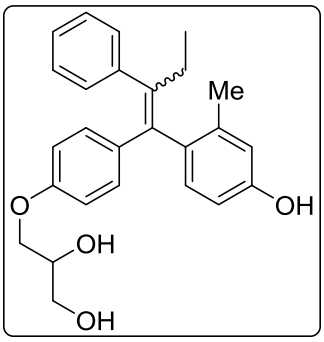

The product was prepared following the procedure for **2-22** using **2-35Me** as starting material. The product was isolated as an off-white foamy solid, as an approximate 4:1 mixture of *Z*/*E* isomers (1.35 g, **95%**).

^{1}H NMR (400 MHz, Chloroform-*d*) δ 7.22 – 7.00 (m, 5H), 6.88 – 6.64 (m, 4H), 6.51 (d, *J* = 8.9 Hz, 2H), 6.42 – 6.33 (m, 1H), 4.17 – 3.59 (m, 5H), 2.58 (bs, 1H), 2.35 – 2.23 (m, 2H), 2.06 (s, 3H), 1.95* (s), 0.99* (td, *J* = 7, 1 Hz), 0.82 (td, *J* = 8, 1 Hz, 3H) ppm.

^{13}C NMR (101 MHz, Chloroform-*d*) δ 156.8* , 156.0 (C), 154.5 (C), 153.8* , 142.5* , 142.4* , 142.2 (C), 141.8 (C), 137.8 (C), 137.7* , 137.1* , 136.5 (C), 136.0* , 135.6* , 135.2 (C), 134.9 (C), 133.0* , 132.6 (CH), 131.5 (2 x CH), 130.7* , 130.3* , 129.7 (2 x CH), 128.8* , 127.9 (CH), 127.5* , 126.1 (2 x CH), 125.9* , 117.0 (2 x CH), 116.5* , 113.9* , 113.2 (2 x CH), 112.4 (CH), 112.1* , 70.4* , 70.4 (CH), 69.1* , 68.8 (CH_2), 63.6* , 63.6 (CH_2), 29.2 (CH_2), 27.9* , 20.4* , 19.9 (CH_3), 13.9* , 12.9 (CH_3) ppm. (Asterisks* denote extra signals belonging to the other isomer).

IR (film): 3395, 2925, 1600, 1505, 1233, 1042, 909 cm^{-1}.

HRMS (ESI): calc. for $[C_{26}H_{29}O_4]^+$: 405.20604; found: 405.20639.

4-(1-(4-((2,2-dimethyl-1,3-dioxolan-4-yl)methoxy)phenyl)-2-phenylbut-1-en-1-yl)phenol (2-23)

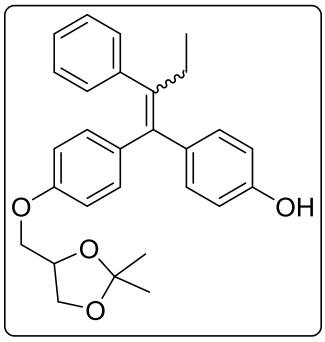

To a solution of **2-22** (1.4 g, 3.66 mmol) dissolved in acetone (8 mL) was added 2,2-dimethoxypropane (0.90 mL, 7.32 mmol) and pTSA.H_2O (105 mg, 0.55 mmol) then sealed and heated to 65 °C for 21 h. The reaction was separated between sat. $NaHCO_4$ (aq.) and EtOAc. The organics were extracted using EtOAc then washed with H_2O (x2), brine (x2), dried over $MgSO_4$, then concentrated under reduced pressure to afford beige solid crude. The residue was purified by flash column chromatography, whereby the product eluted at 1.5% MeOH/DCM as an off-white foamy solid, as an approximate 1:1 mixture of both stereoisomers (579 mg, **37%**). Unreacted starting material was re-obtained and re-used in subsequent reactions (586 mg, **41%**)

The spectra were consistent with that previously reported within our group.[2]

^{1}H NMR (400 MHz, Chloroform-*d*) δ 7.20 – 7.05 (m, 7H), 6.91 – 6.87 (m, 1H), 6.83 – 6.78 (m, 1H), 6.78 – 6.74 (m, 1H), 6.74 – 6.70 (m, 1H), 6.56 – 6.52 (m, 1H), 6.49 – 6.44 (m, 1H), 4.54 – 4.33 (m, 1H), 4.21 – 3.77 (m, 4H), 2.47 (qd, *J* = 8, 3 Hz, 2H), 1.49 – 1.36 (m, 6H), 0.92 (t, *J* = 7 Hz, 3H) ppm. (Note, additional multiplicities and extra signals* are due to the presence of the other stereoisomer).

4-(2-(4-(1-(4-((2,2-dimethyl-1,3-dioxolan-4-yl)methoxy)phenyl)-2-phenylbut-1-en-1-yl)phenoxy)acetyl)-2-methoxyphenyl pivalate (2-24b)

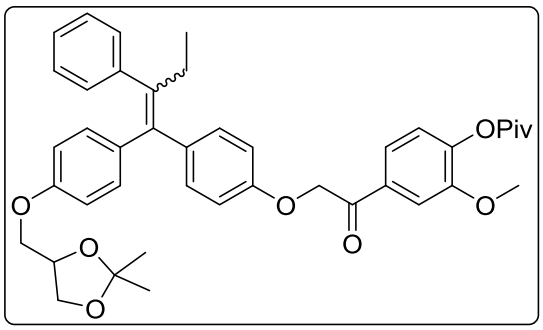

2-23 (579 mg, 1.35 mmol), **2-15b** (463 mg, 1.41 mmol) and K_2CO_3 (278 mg, 2.02 mmol) were dissolved in acetone (10 mL) stirred at rt for 18 h. The reaction was separated between sat. NH_4Cl (aq.) and EtOAc. The organics were extracted using EtOAc then washed with H_2O (x2), brine (x2), dried over $MgSO_4$, then concentrated under reduced pressure to afford the product as a foamy yellow solid, as an approximate 1:1 mixture of both stereoisomers (831 mg, **97%**).

^{1}H NMR (400 MHz, Chloroform-*d*) δ 7.66 – 7.51 (m, 2H), 7.19 – 7.06 (m, 8H), 6.90 (t, *J* = 8 Hz, 2H), 6.78 – 6.73 (m, 2H), 6.59 – 6.52 (m, 2H), 5.26 (s, 1H), 5.10 (s, 1H), 4.54 – 4.35 (m, 1H), 4.20 – 3.74 (m, 7H), 2.51 – 2.41 (m, 2H), 1.48 – 1.35 (m, 15H), 0.91 (t, *J* = 7 Hz, 3H) ppm.

^{13}C NMR (101 MHz, Chloroform-d) δ 193.6* , 193.5 (C), 176.1* , 176.1 (C), 157.3* , 157.2 (C), 156.7* , 156.4 (C), 156.1* , 155.9 (C), 151.8* , 151.7 (C), 145.1* , 145.0 (C), 142.5* , 142.4 (C), 141.5* , 141.4 (C), 137.5* , 137.5 (C), 137.3* (C), 136.8 (C), 136.5* , 136.1 (C), 133.1* , 133.0 (CH), 132.0*, 131.9 (2 x CH), 130.7* , 130.6 (CH), 129.7*, 129.7 (2 x CH), 127.8* , 127.8 (2 x CH), 126.0* , 125.9 (2 x CH), 123.0* , 122.9 (CH), 121.4* , 121.4 (CH), 114.4* , 114.1 (2 x CH), 113.6* , 113.3 (2 x CH), 111.7* , 111.7 (CH), 109.7* , 109.6 (CH), 74.0* , 74.0 (CH), 71.0* , 70.8 (CH_2), 68.7* , 68.4 (CH_2), 66.9* , 66.8 (CH_2), 56.1* , 56.1 (CH_3), 39.2* , 39.2 (C), 29.0* , 29.0 (CH_2), 27.1* , 27.1 (3 x CH_3), 26.8* , 26.7 (CH_3), 25.4* , 25.3 (CH_3), 13.6* , 13.6 (CH_3) ppm. (Additional multiplicities and extra signals* are due to the presence of the other stereoisomer).

IR (film): 3447, 2930, 1601, 1504, 1234, 909 cm^{-1}.

HRMS (ESI): calc. for $[C_{42}H_{47}O_8]^+$: 679.32654; found: 679.32666.

4-(2-(4-(1-(4-(2,3-dihydroxypropoxy)phenyl)-2-phenylbut-1-en-1-yl)phenoxy)acetyl)-2-methoxyphenyl pivalate (2-25b)

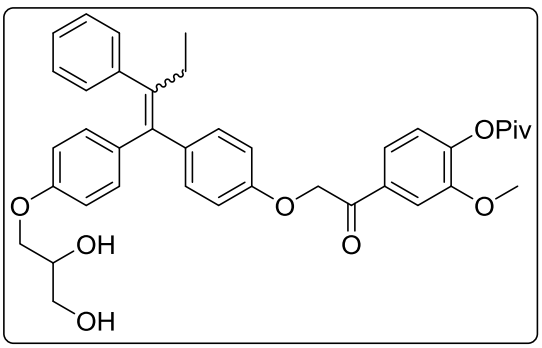

A solution of **2-24b** (730 mg, 1.07 mmol) and TsOH (30 mg, 0.17 mmol) in DCM (3 mL) and MeOH (6 mL) was stirred for 17 h at rt. $KHCO_3$ (sat.) was then added to the reaction mixture and organics were extracted using 10% MeOH/$CHCl_3$ (x3). The combined organics were dried over $MgSO_4$, then concentrated under reduced pressure to afford foamy yellow solid. The residue was purified by flash column chromatography, whereby the product eluted at 9% MeOH/DCM as an off-white foamy solid, as an approximate 1:1 mixture of both stereoisomers (604 mg, **77%**).

The product was also prepared as for CDO166 using CDO486 as starting material. (408 mg, **94%**).

^{1}H NMR (400 MHz, Acetone-d_6) δ 7.78 – 7.65 (m, 2H), 7.27 – 7.07 (m, 8H), 7.03 – 6.98 (m, 1H), 6.98 – 6.93 (m, 1H), 6.84 – 6.77 (m, 2H), 6.68 – 6.63 (m, 1H), 6.62 – 6.57 (m, 1H), 5.55 (s, 1H), 5.37

(s, 1H), 4.13 – 3.82 (m, 7H), 3.76 – 3.54 (m, 3H), 2.78 – 2.77 (m, 2H), 2.48 (qd, *J* = 7, 2 Hz, 2H), 1.35 (d, *J* = 5 Hz, 8H), 0.91 (t, *J* = 7 Hz, 3H) ppm.

^{13}C NMR (101 MHz, Acetone-*d*$_6$) δ 193.0* , 193.0 (C), 175.3* , 175.3 (C), 157.3* , 157.1 (C), 156.6* , 156.4 (C), 151.8* , 151.8 (C), 144.9* , 144.8 (C), 142.6* , 142.6 (C), 141.0* , 140.9 (C), 138.1* , 138.1 (C), 136.6* , 136.3 (C), 136.0* , 135.7 (C), 133.5* , 133.5 (C), 131.7* , 131.6 (2 x CH), 130.3* , 130.3 (2 x CH), 129.6 (2 x CH), 127.8* , 127.8 **(CH),** 126.0* , 125.9 (2 x CH), 123.1* , 123.0 **(CH)**, 121.2* , 121.1 **(CH),** 114.3* , 114.1 (2 x CH), 113.5* , 113.3 (2 x CH), 111.6* , 111.6 **(CH),** 70.5* , 70.4 (CH), 70.3* , 70.2 (CH_2), 69.4* , 69.2 (CH_2), 63.2* , 63.2 (CH_2), 55.7* , 55.6 (CH_3), 38.8* , 38.8 (C), (*CH_2 hidden under acetone solvent peak, visible in HSQC experiment*), 26.5 (3 x CH_3), 12.9* , 12.9 (CH_3) ppm. (Additional multiplicities and extra signals* are due to the presence of the other stereoisomer).

IR (film): 3447, 2973, 1758, 1501, 1235, 1118 cm^{-1}.

HRMS (ESI): calc. for $[C_{26}H_{29}O_4]^+$: 639.29525; found: 639.29551.

2-methoxy-4-(2-(4-(1-(4-(2-oxoethoxy)phenyl)-2-phenylbut-1-en-1-yl)phenoxy)acetyl)phenyl pivalate (2-26b)

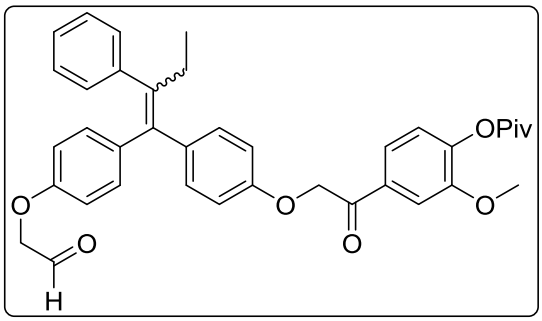

To a solution of **2-25b** (764 mg, 1.20 mmol) in THF (6 mL) and H_2O (1 mL) was added $NaIO_4$ (448 mg, 2.10 mmol) at 0 °C then stirred for 17 h warming to rt. H_2O was then added to the reaction mixture and organics were extracted using EtOAc (x3). The combined organics were dried over $MgSO_4$, then concentrated under reduced pressure to afford foamy beige solid (700 mg, **96%**).

^{1}H NMR (400 MHz, Chloroform-*d*) δ 9.84 (dt, *J* = 45, 1 Hz, 1H), 7.66 – 7.52 (m, 2H), 7.20 – 7.06 (m, 7H), 6.94 – 6.86 (m, 2H), 6.82 – 6.74 (m, 2H), 6.60 – 6.52 (m, 2H), 5.18 (d, *J* = 65 Hz, 2H), 4.51 (dd, *J* = 65, 1 Hz, 2H), 3.86 (d, *J* = 15 Hz, 3H), 2.47 (qd, *J* = 7, 4 Hz, 2H), 1.38 (d, *J* = 5 Hz, 9H), 0.92 (t, *J* = 7 Hz, 3H) ppm.

^{13}C NMR (101 MHz, Chloroform-*d*) δ 199.6* , 199.5 (C=O), 193.5* , 193.5 (C), 176.1* , 176.1 (C), 156.8* , 156.3 (C), 155.9* , 155.5 (C), 151.9* , 151.8 (C), 145.1* , 145.0 (C), 142.3* , 142.3 (C), 141.8*

, 141.7 (C), 137.4 (C), 137.2* , 137.2 (C), 137.0* , 136.6 (C), 133.1* , 133.0 (C), 132.2* , 132.0 (2 x CH), 130.9* , 130.7 (2 x CH), 129.6* , 129.6 (2 x CH), 127.9* , 127.9 (2 x CH), 126.1 (CH), 123.0* , 122.9 (CH), 121.4* , 121.4 (CH), 114.5* , 114.2 (2 x CH), 113.7* , 113.4 (2 x CH), 111.7* , 111.7 (CH), 72.7* , 72.5 (CH_2), 70.9* , 70.8 (CH_2), 56.1* , 56.1 (CH_3), 39.2* , 39.2 (C), 29.0 (CH_2), 27.2* , 27.1 (3 x CH_3), 13.6 (CH_3) ppm. (Additional multiplicities and extra signals* are due to the presence of the other stereoisomer).

IR (film): 3460, 2968, 1749, 1506, 1266, 1100 cm^{-1}.

HRMS (ESI): calc. for $[C_{38}H_{39}O_7]^+$: 607.26903; found: 607.26866.

4-(2-(4-(1-(4-(2-(dimethylamino)ethoxy)phenyl)-2-phenylbut-1-en-1-yl)phenoxy)acetyl)-2-methoxyphenyl pivalate (2-17b)

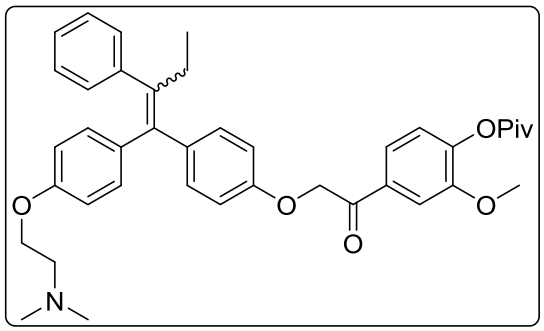

A solution of **2-26b** (700 mg, 1.13 mmol) and 2M $NHMe_2$ in THF (0.56 mL, 1.13 mmol) in THF (6 mL) was stirred for 30 min, then cooled to 0 °C before addition of $NaBH(OAc)_3$ (359 mg, 1.69 mmol) then stirred for 18 h warming to rt. $KHCO_3$ was added to the reaction mixture and the organics were extracted using EtOAc (x3). The combined organics were washed with H_2O, brine, dried over $MgSO_4$, then concentrated under reduced pressure to afford foamy beige solid. The residue was purified by flash column chromatography, whereby the product eluted at 7% MeOH/DCM as a yellow foamy solid (452 mg, **63%**).

^{1}H NMR (400 MHz, Chloroform-*d*) δ 7.65 – 7.50 (m, 2H), 7.17 – 7.05 (m, 7H), 6.94 – 6.85 (m, 3H), 6.79 – 6.72 (m, 2H), 6.56 (ddd, *J* = 12, 9, 1 Hz, 2H), 5.17 (d, *J* = 65 Hz, 2H), 4.04 (dt, *J* = 63, 6 Hz, 2H), 3.86 (dd, *J* = 15, 1 Hz, 3H), 2.76 (dt, *J* = 39, 6 Hz, 2H), 2.47 (qd, *J* = 7, 2 Hz, 2H), 2.37 (d, *J* = 25 Hz, 6H), 1.37 (dd, *J* = 5, 1 Hz, 9H), 0.91 (td, *J* = 7, 2 Hz, 3H) ppm.

^{13}C NMR (101 MHz, Chloroform-*d*) δ 193.6* , 193.5 (C), 176.1* , 176.1 (C), 157.4* , 156.7 (C), 156.6* , 155.9 (C), 151.8* , 151.7 (C), 145.1* , 145.0 (C), 142.5* , 142.5 (C), 141.4* , 141.3 (C), 137.6* , 137.5 (C), 137.3* , 136.8 (C), 136.3* , 135.8 (C), 133.1* , 133.1 (C), 132.0* , 131.9 (CH), 130.7* , 130.6 (CH), 129.7 (CH), 127.8* , 127.8 (CH), 125.9* , 125.9 (CH), 123.0* , 122.9 (CH),

121.4* , 121.4 (CH), 114.4* , 114.1 (CH), 113.6* , 113.3 (CH), 111.7* , 111.7 (CH), 71.0* , 70.8 (CH_2), 65.6* , 65.3 (CH_2), 58.2* , 58.1 (CH_2), 56.1* , 56.1 (CH_3), 45.7* , 45.6 (2 x CH_3), 39.2* , 39.2 (C), 29.0* , 29.0 (CH_2), 27.2* , 27.1 (3 x CH_3), 13.6* , 13.6 (CH_3) ppm.
(Additional multiplicities and extra signals* are due to the presence of the other stereoisomer).

IR (film): 2973, 1749, 1601, 1501, 1231, 1096 cm^{-1}.

HRMS (ESI): calc. for $[C_{40}H_{46}O_6N]^+$: 636.33197; found: 636.33111.

Guaymoxifen:

2-(4-(1-(4-(2-(dimethylamino)ethoxy)phenyl)-2-phenylbut-1-en-1-yl)phenoxy)-1-(4-hydroxy-3-methoxyphenyl)ethan-1-one (2-11)

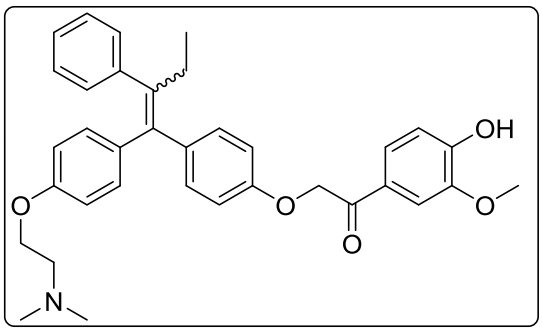

To a solution of **2-17b** (291 mg, 0.46 mmol) in MeOH (3 mL) at 0 °C was added 3 M LiOH (0.75 mL, 2.25 mmol) then stirred for 2 h warming to rt. Conc. HCl was added until the mixture reached pH 4 and then the organics were extracted using 10% MeOH/$CHCl_3$ (x3). The combined organics were washed with H_2O, brine, dried over $MgSO_4$, then concentrated under reduced pressure to afford foamy beige solid. The residue was purified by flash column chromatography, whereby the product eluted at 8% MeOH/DCM (+2% NEt_3) as a yellow foamy solid (155 mg, **61%**).

The spectra were consistent with that previously reported within our group.[2]

^{1}H NMR (400 MHz, Chloroform-*d*) δ 7.62 – 7.48 (m, 2H), 7.18 – 7.04 (m, 7H), 6.97 – 6.84 (m, 3H), 6.79 – 6.71 (m, 2H), 6.61 – 6.48 (m, 2H), 5.15 (d, *J* = 65 Hz, 2H), 4.05 (dt, *J* = 62, 6 Hz, 2H), 3.92 (d, *J* = 14 Hz, 3H), 2.78 (dt, *J* = 39, 6 Hz, 2H), 2.46 (q, *J* = 7 Hz, 2H), 2.38 (d, *J* = 25 Hz, 6H), 0.91 (td, *J* = 7, 2 Hz, 3H) ppm.

4-(2-(4-(1-(4-(2-(dimethylamino)ethoxy)phenyl)-2-phenylbut-1-en-1-yl)phenoxy)-3-hydroxypropanoyl)-2-methoxyphenyl pivalate (2-46b)

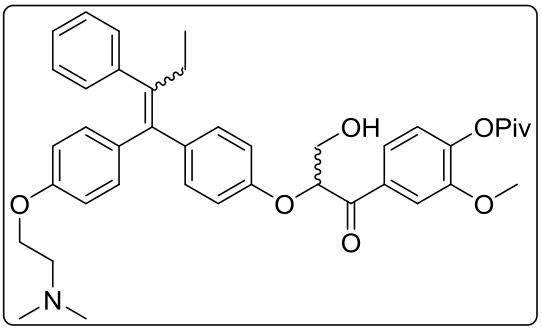

To a solution of **2-17b** (100 mg, 0.16 mmol) and K_2CO_3 (44 mg, 0.32 mmol) in dioxane (3 mL) was added molecular sieves, followed by 36% formalin solution (0.14 mL, 0.17 mmol) then stirred for 20 h at 50 °C. NH_4Cl (aq) was added to the reaction mixture and the organics were extracted using EtOAc (x3). The combined organics were washed with H_2O, brine, dried over $MgSO_4$, then concentrated under reduced pressure to afford a grey gum. The residue was purified by flash column chromatography, whereby the product eluted at 6% MeOH/DCM as a crunchy foam solid (60 mg, **57%**).

^{1}H NMR (400 MHz, Chloroform-*d*) δ 7.76 – 7.54 (m, 2H), 7.17 – 7.03 (m, 8H), 6.89 – 6.84 (m, 2H), 6.75 – 6.70 (m, 2H), 6.57 – 6.49 (m, 2H), 5.45 (ddd, *J* = 75.6, 6.1, 4.1 Hz, 1H), 4.22 – 3.99 (m, 4H), 3.80 (dd, *J* = 17.9, 0.7 Hz, 3H), 2.85 (d, *J* = 34.4 Hz, 2H), 2.45 (d, *J* = 21.4 Hz, 8H), 1.37 (d, *J* = 1.8 Hz, 9H), 0.90 (td, *J* = 7.4, 2.1 Hz, 3H) ppm.

^{13}C NMR (101 MHz, Chloroform-*d*) δ 195.6* , 195.4 (C), 176.1 (C), 155.9* , 155.1 (C), 151.8* , 151.7 (C), 145.3* , 145.1 (C), 142.4* , 142.3 (C), 141.6* , 141.5 (C), 137.6* , 137.4 (C), 137.3* , 137.1 (C), 133.1* , 133.0 (C), 132.1* , 131.9 (2 x CH), 130.8* , 130.6 (2 x CH), 129.6 (2 x CH), 127.8* , 127.8 (2 x CH), 126.0* , 126.0 (CH), 123.0* , 122.9 (CH), 122.0* , 122.0 (CH), 114.8* , 114.1 (2 x CH), 113.3 (2 x CH), 112.3* , 112.3 (CH), 81.1* , 81.0 (CH), 63.3* , 63.2 (CH_2), 57.9* , 57.8 (CH_2), 56.0* , 56.0 (CH_3), 45.4* , 45.3 (2 x CH_3), 39.2 (C), 29.0* , 29.0 (CH_2), 27.1 (3 x CH_3), 13.6 (CH_3) ppm. (Higher order multiplicities and extra signals* are due to the presence of the other stereoisomer).

IR (film): 2967, 1751, 1601, 1505, 1236, 1106, 736 cm^{-1}.

HRMS (ESI): calc. for $[C_{41}H_{48}O_7N]^+$: 666.34253; found: 666.34148.

2-(4-(1-(4-(2-(Dimethylamino)ethoxy)phenyl)-2-phenylbut-1-en-1-yl)phenoxy)-3-hydroxy-1-(4-hydroxy-3-methoxyphenyl)propan-1-one (2-41b)

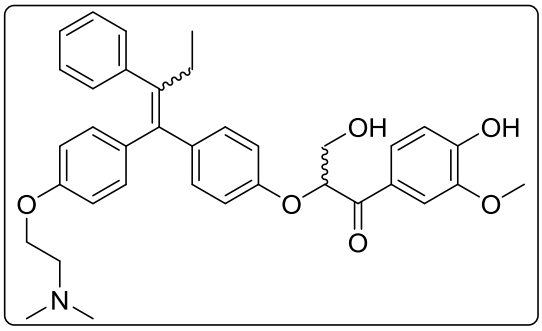

The compound was prepared following the procedure for Guaymoxifen (**2-12**) using **2-46b** as starting material. The product eluted from the column at 8% MeOH/DCM as a crunchy foam solid (90 mg, **58%**).

^{1}H NMR (400 MHz, Chloroform-*d*) δ 7.65 (ddd, *J* = 44, 8, 2 Hz, 1H), 7.53 (dd, *J* = 32, 2 Hz, 1H), 7.17 – 7.00 (m, 7H), 6.92 (dd, *J* = 22, 8 Hz, 1H), 6.88 – 6.83 (m, 2H), 6.74 – 6.67 (m, 2H), 6.54 – 6.48 (m, 2H), 5.45 (ddd, *J* = 73, 6, 4 Hz, 1H), 4.20 – 3.92 (m, 4H), 3.87 (d, *J* = 15 Hz, 3H), 2.74 (dt, *J* = 39, 6 Hz, 2H), 2.48 – 2.40 (m, 2H), 2.35 (d, *J* = 24 Hz, 6H), 0.89 (td, *J* = 7, 4 Hz, 3H) ppm.

^{13}C NMR (101 MHz, Chloroform-*d*) δ 194.8* , 194.7 (C), 157.4* , 156.5 (C), 156.0* , 155.2 (C), 151.7* , 151.5 (C), 147.1* , 146.9 (C), 142.4* , 142.4 (C), 141.4* , 141.3 (C), 137.5 (C), 137.4* , *137.0 (C)*, 136.2* , 135.7 (C), 132.1* , 131.8 (2 x CH), 130.8* , 130.5 (2 x CH), 129.6* , 127.8 (CH), 127.3* , 127.3 (CH), 125.9* , 125.9 (2 x CH), 124.1* , 124.0 (CH), 114.9* , 114.3 (2 x CH), 114.2* , 114.1 (2 x CH), 114.0* , 113.3 (2 x CH), 110.7* , 110.7 (CH), 80.8* , 80.7 (CH), 65.6* , 65.4 (CH_2), 63.6* , 63.5 (CH_2), 58.2* , 58.1 (CH_2), 56.0* , 56.0 (2 x CH_3), 45.7* , 45.7 (CH_3), 29.0* , 28.9 (CH_2), 13.6* , 13.6 (CH_3) ppm. (Higher order multiplicities and extra signals* are due to the presence of the other stereoisomer).

IR (film): 3436, 2958, 1601, 1500, 1231, 727 cm^{-1}.

HRMS (ESI): calc. for $[C_{36}H_{40}O_6N]^+$: 582.28501; found: 582.28415.

4-(2-(4-(1-(4-(2,3-Dihydroxypropoxy)phenyl)-2-phenylbut-1-en-1-yl)phenoxy)propanoyl)-2-methoxyphenyl pivalate (2-57a)

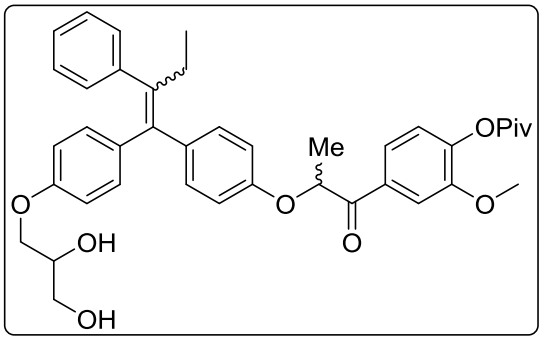

The product was prepared following the procedure for **2-25b** but using **2-45a** as starting material. The residue was purified by flash column chromatography, whereby the product eluted at 8% MeOH/DCM as a yellow foamy solid (495 mg, **43%**).

^{1}H NMR (400 MHz, Acetone-d_6) δ 7.86 – 7.63 (m, 2H), 7.25 – 7.08 (m, 8H), 6.96 – 6.90 (m, 2H), 6.79 – 6.74 (m, 2H), 6.61 – 6.54 (m, 2H), 5.75 (dq, *J* = 83, 7 Hz, 1H), 4.12 – 3.53 (m, 10H), 2.79 – 2.76 (m, 1H), 2.46 (qd, *J* = 7, 2 Hz, 2H), 1.61 (dd, *J* = 42, 7 Hz, 3H), 1.35 (d, *J* = 2 Hz, 9H), 0.89 (td, *J* = 7, 2 Hz, 3H) ppm.

^{13}C NMR (101 MHz, Acetone-d_6) δ 196.7* , 196.7 , 175.3 , 158.2 – 157.7 (m), 157.1 , 156.4* , 155.6 , 151.8* , 151.7 , 146.6 , 144.8 , 142.5* , 142.5 , 141.1* , 141.0 , 138.0 , 136.7* , 136.4 , 136.0* , 135.7 , 133.1* , 133.0 , 131.7* , 131.6 , 130.4* , 130.3 , 129.6* , 129.6 , 127.8 , 126.0* , 125.9 , 123.1* , 123.1 , 121.8* , 121.7 , 114.7* , 114.1 , 113.9* , 113.3 , 112.2* , 112.2 , 75.2* , 75.2 , 70.6 – 70.2 (m), 69.4* , 69.2 , 63.2* , 63.1 , 55.6 , 38.8 , 26.5 , 17.9* , 17.8 , 12.9 ppm.

IR (film): 3436, 2958, 1601, 1500, 1231, 727 cm^{-1}.

HRMS (ESI): calc. for $[C_{40}H_{45}O_8]^+$: 653.30468; found: 653.30222.

4-(2-(4-(1-(4-(2,3-dihydroxypropoxy)phenyl)-2-phenylbut-1-en-1-yl)phenoxy)propanoyl)-2-methoxyphenyl pivalate

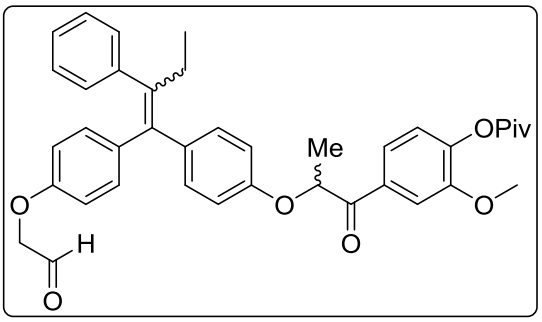

The product was prepared following the procedure for **2-26b** but using **2-57a** as starting material. the product as a yellow foamy solid (450 mg, **96%**). The product was used directly in the subsequent reaction:

4-(2-(4-(1-(4-(2-(dimethylamino)ethoxy)phenyl)-2-phenylbut-1-en-1-yl)phenoxy)propanoyl)-2-methoxyphenyl pivalate (2-58a)

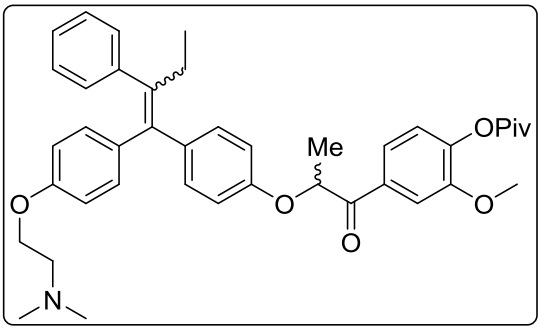

The product was prepared following the procedure for **2-17b** but using **4-(2-(4-(1-(4-(2,3-dihydroxypropoxy)phenyl)-2-phenylbut-1-en-1-yl)phenoxy)propanoyl)-2-methoxyphenyl pivalate** as starting material. The residue was purified by flash column chromatography,

whereby the product eluted at 7% MeOH/DCM as a yellow foamy solid (302 mg, **64%**). (**26%** over 3 steps)

^{1}H NMR (400 MHz, Acetone-d_6) δ 7.86 – 7.63 (m, 2H), 7.25 – 7.09 (m, 8H), 6.96 – 6.89 (m, 2H), 6.79 – 6.73 (m, 2H), 6.60 – 6.53 (m, 2H), 5.76 (dq, *J* = 83, 7 Hz, 1H), 4.01 (dt, *J* = 67, 6 Hz, 2H), 3.85 (d, *J* = 17 Hz, 3H), 2.63 (dt, *J* = 41, 6 Hz, 2H), 2.46 (qd, *J* = 7, 3 Hz, 2H), 2.24 (d, *J* = 26 Hz, 6H), 1.61 (dd, *J* = 42, 7 Hz, 3H), 1.35 (d, *J* = 2 Hz, 9H), 0.89 (td, *J* = 7, 3 Hz, 3H) ppm.

^{13}C NMR (101 MHz, acetone) δ 197.6*, 197.6 (C), 176.2*, 176.1 (C), 158.8*, 157.9 (C), 157.3*, 156.5 (C), 152.7*, 152.6 (C), 145.8*, 145.7 (C), 143.4*, 143.4 (C), 141.9*, 141.8 (C), 138.9 (C), 137.6*, 137.3 (C), 136.8*, 136.5 (C), 134.0*, 133.9 (C), 132.6*, 132.5 (2 x CH), 131.3*, 131.2 (2 x CH), 130.5*, 130.5 (2 x CH), 128.7*, 128.7 (2 x CH), 126.9*, 126.8 (CH), 124.0*, 124.0 (CH), 122.7*, 122.6 (CH), 115.6*, 115.0 (2 x CH), 114.8*, 114.2 (2 x CH), 113.1*, 113.1 (CH), 76.1*, 76.1 (CH), 67.2*, 66.9 (CH_2), 59.0*, 58.9 (CH_2), 56.5*, 56.4 (CH_3), 46.2*, 46.1 (2 x CH_3), 39.7 (C), 27.4 (3 x CH_3), 18.8*, 18.7 (CH_3), 13.8 (CH_3) ppm. (Note, additional multiplicities and extra signals are due to the presence of the other diastereomer).

IR (film): 2970, 1754, 1696, 1595, 1508, 1239, 1106 cm^{-1}.

HRMS (ESI): calc. for $[C_{41}H_{48}O_6N]^+$: 650.34762; found: 650.34646.

2-(4-(1-(4-(2-(dimethylamino)ethoxy)phenyl)-2-phenylbut-1-en-1-yl)phenoxy)-1-(4-hydroxy-3-methoxyphenyl)propan-1-one (2-41a)

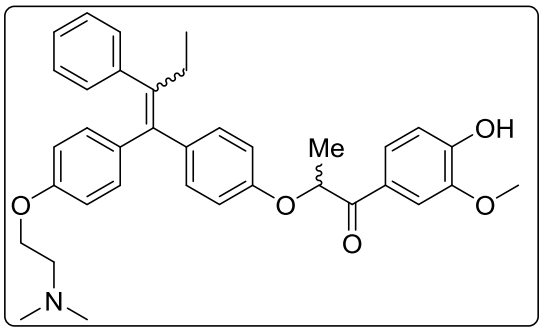

The product was prepared following the procedure for **2-11** but using **2-46a** as starting material. The residue was purified by flash column chromatography, whereby the product eluted at 7% MeOH/DCM as a yellow foamy solid (151 mg, **57%**).

^{1}H NMR (400 MHz, Chloroform-*d*) δ 7.77 – 7.51 (m, 2H), 7.18 – 7.01 (m, 8H), 6.91 (dd, *J* = 22, 8 Hz, 1H), 6.85 – 6.80 (m, 2H), 6.73 – 6.67 (m, 2H), 6.54 – 6.46 (m, 2H), 5.36 (dq, *J* = 71, 7 Hz, 1H), 4.03 (dt, *J* = 61, 6 Hz, 2H), 3.89 (d, *J* = 16 Hz, 2H), 2.75 (dt, *J* = 39, 6 Hz, 2H), 2.44 (qd, *J* = 7, 3 Hz, 2H), 2.36 (d, *J* = 24 Hz, 6H), 1.65 (dd, *J* = 41, 7 Hz, 3H), 0.89 (td, *J* = 7, 3 Hz, 3H) ppm.

^{13}C NMR (101 MHz, Chloroform-*d*) δ 197.4* , 197.4 (C), 157.3* , 156.5 (C), 156.2* , 155.4 (C), 151.3* , 151.1 (C), 147.0* , 146.8 (C), 142.5* , 142.4 (C), 141.2* , 141.1 (C), 137.6* , 137.6 (C), 136.9* , 136.4 (C), 136.3* , 135.9 (C), 132.0* , 131.9 (CH), 130.6* , 130.5 (CH), 129.6* , 129.6 (CH), 127.8* , 127.8 (CH), 126.7* , 126.7 (C), 125.9* , 125.9 (CH), 124.1* , 124.0 (CH), 114.7* , 114.2 (CH), 114.1* , 114.0 (CH), 113.9* , 113.3 (CH), 110.9* , 110.9 (CH), 76.4* , 76.4 (CH), 65.6* , 65.3 (CH_2), 58.1* , 58.0 (CH_2), 56.0* , 56.0 (CH_3), 45.7* , 45.6 (2 x CH_3), 29.0* , 28.9 (CH_2), 19.3* , 19.1 (CH_3), 13.6 (CH_3) ppm. (Note, additional multiplicities and extra signals* are due to the presence of the other diastereomer).

IR (film): 2958, 1592, 1505, 1236, 727 cm^{-1}.

HRMS (ESI): calc. for $[C_{36}H_{40}O_5N]^+$: 566.29010; found: 566.28920.

4-(2-(4-(1-(4-(2,3-dihydroxypropoxy)phenyl)-2-phenylbut-1-en-1-yl)phenoxy)-2-fluoroacetyl)-2-methoxyphenyl pivalate (2-57d)

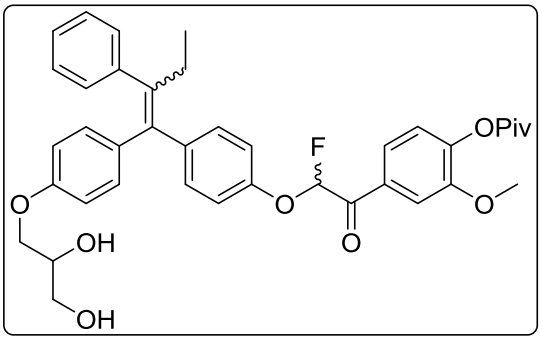

The product was prepared following the procedure for **2-25b** but using **2-48b** as starting material. The residue was purified by flash column chromatography, whereby the product eluted at 95% EtOAc/hexanes as a colourless oil (41 mg, **85%**).

^{1}H NMR (400 MHz, Chloroform-*d*) δ 7.87 – 7.64 (m, 2H), 7.24 – 7.07 (m, 9H), 6.94 – 6.75 (m, 4H), 6.61 – 6.52 (m, 1H), 6.28 (dd, J_F = 70, 61 Hz, 1H), 4.07 – 3.63 (m, 8H), 2.53 – 2.43 (m, 2H), 1.38 (d, J = 6 Hz, 9H), 0.94 (t, J = 7 Hz, 3H) ppm.

^{13}C NMR (101 MHz, Chloroform-*d*) δ 187.8* , 187.6 (C), 176.1* , 176.0 (C), 157.2* , 156.4 (C), 154.6* (d), 153.8 (d, J_F = 3 Hz, C), 151.7* , 151.6 (C), 145.6* , 145.5 (C), 142.4* , 142.1* , 142.1 (C), 142.0 (C), 140.0* , 139.6 (C), 137.1* , 137.0 (C), 136.4* , 135.9 (C), 132.2* , 131.9 (CH), 131.0* , 130.7 (CH), 129.6 (CH), 128.0* , 127.9 (2 x CH), 126.2*, 126.2 (CH), 123.8* , 123.8 (CH), 123.7 (2 x CH), 123.0* , 122.9 (2 x CH), 116.8* , 116.0 (2 x CH), 114.2* , 113.4 (2 x CH), 113.1* , 113.1 (CH), 108.6* (d), 106.3 (d, J_F = 7 Hz, CH), 70.4* , 70.3 (CH), 69.1* , 68.9 (CH_2), 63.7* , 63.6 (CH_2), 56.1* , 56.1

(CH_3), 39.2* , 39.2 (C), 29.1* , 29.0 (CH_2), 27.1* , 27.1 (3 x CH_3), 13.6* , 13.5 (CH_3) ppm. (Additional multiplicities and extra signals* are due to the presence of the other diastereomer).

^{19}F NMR (376 MHz, Chloroform-*d*) δ -124.97 (d, *J* = 61 Hz), -125.06 (d, *J* = 61 Hz) ppm.

IR (film): 3417, 2977, 1762, 1510, 1100, 735 cm^{-1}.

HRMS (ESI): calc. for $[C_{39}H_{42}O_8F]^+$: 657.28582; found: 657.28683.

4-(2-fluoro-2-(4-(1-(4-(2-oxoethoxy)phenyl)-2-phenylbut-1-en-1-yl)phenoxy)acetyl)-2-methoxyphenyl pivalate

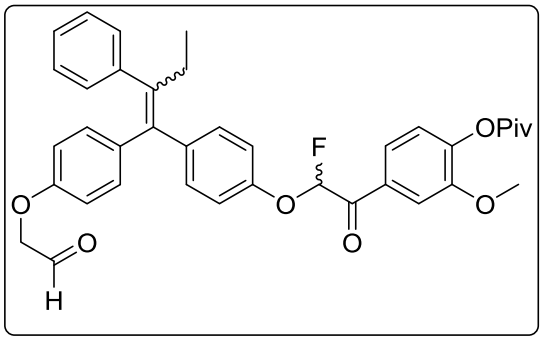

The product was prepared following the procedure for CDO but using CDO696 as starting material. The product was afforded as a colourless oil and was taken directly on to subsequent reaction (CDO698) without further purification to avoid further degradation and due to the low quantity of material.

^{1}H NMR (400 MHz, Chloroform-*d*) δ 9.76 (dt, *J* = 45, 1 Hz, 1H), 7.78 – 7.58 (m, 2H), 7.17 – 6.99 (m, 9H), 6.85 – 6.76 (m, 1H), 6.76 – 6.66 (m, 2H), 6.52 – 6.46 (m, 1H), 6.20 (dd, *J* = 70, 61 Hz, 1H), 4.44 (dd, *J* = 65, 1 Hz, 2H), 3.79 (d, *J* = 19 Hz, 2H), 2.46 – 2.36 (m, 2H), 1.30 (d, *J* = 6 Hz, 9H), 0.91 – 0.82 (m, 3H) ppm. (Additional multiplicities and extra signals are due to the presence of the other stereoisomer).

^{19}F NMR (376 MHz, Chloroform-*d*) δ -124.9 (d, *J* = 61 Hz), -125.0 (d, *J* = 61 Hz) ppm.

4-(2-(4-(1-(4-(2-(dimethylamino)ethoxy)phenyl)-2-phenylbut-1-en-1-yl)phenoxy)-2-fluoroacetyl)-2-methoxyphenyl pivalate (2-58d)

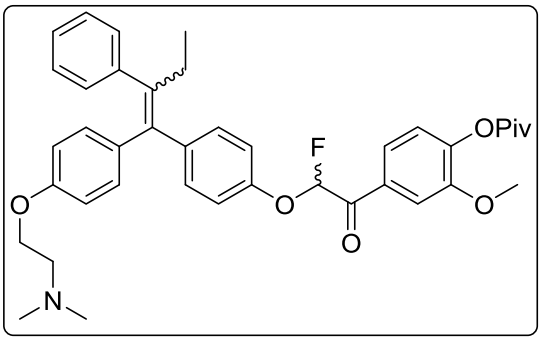

The product was prepared following the procedure for **2-17b** but using **4-(2-fluoro-2-(4-(1-(4-(2-oxoethoxy)phenyl)-2-phenylbut-1-en-1-yl)phenoxy)acetyl)-2-methoxyphenyl pivalate** as starting material. The residue was purified by flash column chromatography, whereby the product eluted at 95% EtOAc/hexanes as a colourless oil (19 mg, **51%**).

^{1}H NMR (400 MHz, Chloroform-*d*) δ 7.77 – 7.65 (m, 2H), 7.26 – 7.07 (m, 9H), 6.93 – 6.84 (m, 2H), 6.82 – 6.73 (m, 2H), 6.58 – 6.54 (m, 1H), 6.27 (dd, *J* = 70, 61 Hz, 1H), 4.09 (t, *J* = 6 Hz, 1H), 3.97 (t, *J* = 6 Hz, 1H), 3.86 (d, *J* = 19 Hz, 3H), 2.76 (dt, *J* = 39, 6 Hz, 2H), 2.48 (dq, *J* = 11, 8 Hz, 2H), 2.37 (d, *J* = 25 Hz, 6H), 1.37 (dd, *J* = 6, 0.5 Hz, 9H), 0.93 (td, *J* = 7, 2 Hz, 3H) ppm.

^{13}C NMR (101 MHz, Chloroform-*d*) δ 187.7 (C), 176.2 (C), 157.7* , 156.9 (C), 154.8* , 154.0 (C), 151.8* , 151.7 (C), 147.7 (C), 145.7* , 145.7 (C), 142.4* , 142.4 (C), 142.3* , 142.0 (C), 140.3* , 139.9 (C), 137.4* , 137.3 (C), 136.1* , 135.6 (C), 132.4* , 132.0 (2 x CH), 131.2* , 130.7 (CH), 129.8* , 129.8 (2 x CH), 128.1* , 128.0 (2 x CH), 126.3* , 126.3 (2 x CH), 124.0 – 123.9 (m, CH), 123.1* , 123.1 (CH), 117.0* , 116.2 (2 x CH), 114.3* , 113.6 (2 x CH), 113.3* , 113.2 (CH), 108.8* , 106.5 (CH), 65.8* , 65.5 (CH_2), 58.3* , 58.2 (CH_2), 56.3* , 56.2 (CH_3), 45.8* , 45.7 (2 x CH_3), 39.4* , 39.4 (C), *29.8* , 29.2* , 29.2 (CH_2), 27.3* , 27.3 (3 x CH_3), 13.7* , 13.7 (CH_3) ppm. (Note, additional multiplicities and extra signals* are due to the presence of the other diastereomer).

IR (film): 3417, 2977, 1762, 1510, 1100, 735 cm^{-1}.

HRMS (ESI): calc. for $[C_{40}H_{45}O_6NF]^+$: 654.32254; found: 654.32287.

2-(4-(1-(4-(2-(Dimethylamino)ethoxy)phenyl)-2-phenylbut-1-en-1-yl)phenoxy)-2-fluoro-1-(4-hydroxy-3-methoxyphenyl)ethan-1-one (2-41d)

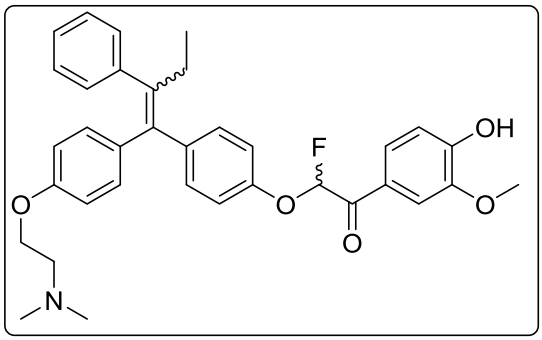

The product was prepared following the procedure for **2-11** but using **2-58d** as starting material. The residue was purified by flash column chromatography, whereby the product eluted at 95% EtOAc/hexanes as a colourless oil (4 mg, **65%**).

^{1}H NMR (400 MHz, Chloroform-*d*) δ 7.72 (dd, *J* = 33, 9 Hz, 1H), 7.58 (dd, *J* = 30, 2 Hz, 1H), 7.18 – 7.00 (m, 8H), 6.95 – 6.66 (m, 5H), 6.49 (d, *J* = 9 Hz, 1H), 6.19 (dd, *J* = 71, 61 Hz, 1H), 4.09 – 3.84 (m, 5H), 2.70 (d, *J* = 39 Hz, 2H), 2.48 – 2.34 (m, 2H), 2.33 (s, 3H), 2.27 (s, 3H), 0.86 (td, *J* = 7, 2 Hz, 3H) ppm.

^{19}F NMR (376 MHz, Chloroform-*d*) δ -124.6 (d, *J* = 61 Hz), -124.8 (d, *J* = 61 Hz) ppm.

^{13}C NMR (126 MHz, Chloroform-*d*) δ 187.3 (d, *J* = 27 Hz, C), 157.0 (d, *J* = 107 Hz, C), 154.3 (d, *J* = 98 Hz, C), 151.6 (d, *J* = 12 Hz, C), 146.7 (d, *J* = 11 Hz, C), 142.4 – 141.5 (m, 2 x C), 139.8 (d, *J* = 54 Hz, C), 137.2 (d, *J* = 8 Hz, C), 135.8 (d, *J* = 58 Hz, C), 132.0 (d, *J* = 47 Hz, CH), 130.8 (d, *J* = 47 Hz, CH), 129.6 (d, *J* = 2 Hz, CH), 127.9 (d, *J* = 3 Hz, CH), 126.1 (d, *J* = 9 Hz, CH), 125.9 (CH), 125.0 (d, *J* = 8 Hz, CH), 116.5 (d, *J* = 102 Hz, CH), 114.2 – 113.4 (m, CH), 111.4 (d, *J* = 7 Hz, CH), 107.6 (d, *J* = 234 Hz, CHF), 65.3 (d, *J* = 37 Hz, CH_2), 57.9 (d, *J* = 13 Hz, CH_2), 56.1 (d, *J* = 4 Hz, CH_3), 45.5 (d, *J* = 11 Hz, 2 x CH_3), 29.0 (d, *J* = 8 Hz, CH_2), 13.5 (d, *J* = 4 Hz, CH_3) ppm.

IR (film): 3417, 2977, 1762, 1510, 1100, 735 cm^{-1}.

HRMS (ESI): calc. for $[C_{35}H_{37}O_5NF]^+$: 570.26503; found: 570.26447.

4-(2-(4-(1-(4-(2,3-Dihydroxypropoxy)phenyl)-2-phenylbut-1-en-1-yl)-3-methylphenoxy)acetyl)-2-methoxyphenyl pivalate (2-67)

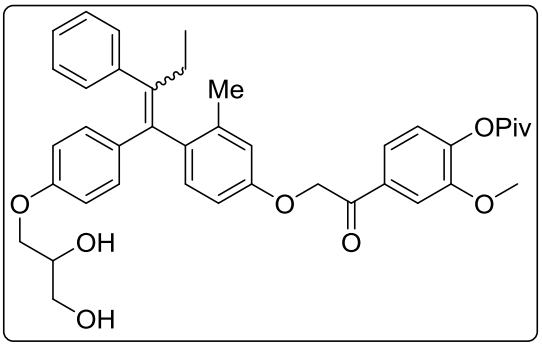

The compound was prepared as for **2-25b** using **2-15b** and **2-77** as starting materials. The residue was purified by flash column chromatography, whereby the product eluted at 8% MeOH/DCM as an off-white foamy solid, as an approximate 4:1 *E/Z* mixture of stereoisomers (211 mg, **81%**).

^{1}H NMR (400 MHz, Chloroform-*d*) δ 7.3 (d, *J* = 8 Hz, 1H), 7.2 – 7.0 (m, 6H), 7.0 – 6.9 (m, 2H), 6.8 (d, *J* = 9 Hz, 1H), 6.8 – 6.7 (m, 2H), 6.7 – 6.6 (m, 1H), 6.6 – 6.5 (m, 2H), 4.2 – 3.6 (m, 8H), 2.5 (d, *J* = 32 Hz, 2H), 2.3 (qd, *J* = 14, 7 Hz, 2H), 2.1 (d, *J* = 44 Hz, 3H), 1.3 (d, *J* = 33 Hz, 9H), 0.9 (dt, *J* = 75, 7 Hz, 3H) ppm.

^{13}C NMR (101 MHz, Chloroform-*d*) δ 193.7 (C), 193.6* , 176.2 (C), 176.1* , 171.2 , 156.9 (C), 156.3* , 156.1 (C), 151.8 (C), 151.7* , 145.0 (C), 144.9* , 142.6* , 142.3* , 142.1 (C), 141.8 (C), 137.8 (C), 137.7* , 137.0* , 136.6* , 136.4 (C), 136.2 (C), 135.7* , 134.6* , 133.1 (C), 132.5* , 131.5 (CH), 130.6 (CH), 130.3* , 129.7 (CH), 128.8* , 127.9 (CH), 127.5* , 126.1 (CH), 126.0* , 123.0 (CH), 122.9* , 121.4 (CH), 121.4* , 116.7 (CH), 116.1* , 113.9* , 113.3 (CH), 111.7 (CH), 111.7* , 111.7 (CH), 111.3* , 70.9 (CH_2), 70.8* , 70.4* , 70.3 (CH), 69.1* , 68.9 (CH_2), 63.6* , 63.6 (CH_2), 56.1 (CH_3), 39.2 (C), 31.6* , 29.1 (CH_2), 27.2 (3 x CH_3), 22.6* , 20.1 (CH_3), 14.2* , 12.9 (CH_3) ppm.
(Note, additional multiplicities and extra signals are due to the presence of the other stereoisomer).

IR (film): 3459, 2970, 1760, 1595, 1505, 1100 cm^{-1}.

HRMS (ESI): calc. for $[C_{40}H_{45}O_8]^+$: 653.31090; found: 653.31226.

4-(2-(4-(1-(4-(2-(Dimethylamino)ethoxy)phenyl)-2-phenylbut-1-en-1-yl)-3-methylphenoxy)acetyl)-2-methoxyphenyl pivalate (2-66)

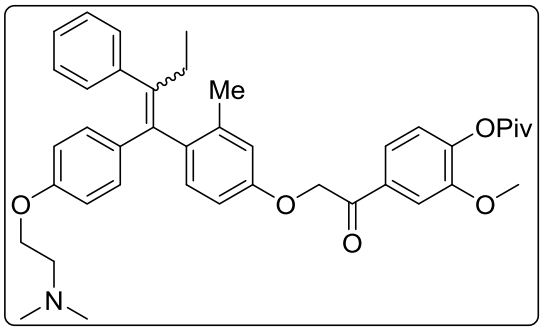

The compound was prepared as for **2-17b** using **2-67** as starting material. The residue was purified by flash column chromatography, whereby the product eluted at 7% MeOH/DCM as a yellow foamy solid (452 mg, **63%**).

^{1}H NMR (400 MHz, Chloroform-*d*) δ 7.65 – 7.50 (m, 2H), 7.17 – 7.05 (m, 7H), 6.94 – 6.85 (m, 3H), 6.79 – 6.72 (m, 2H), 6.56 (ddd, *J* = 12, 9, 1 Hz, 2H), 5.17 (d, *J* = 65 Hz, 2H), 4.04 (dt, *J* = 63, 6 Hz, 2H), 3.86 (dd, *J* = 15, 1 Hz, 3H), 2.76 (dt, *J* = 39, 6 Hz, 2H), 2.47 (qd, *J* = 7, 2 Hz, 2H), 2.37 (d, *J* = 25 Hz, 6H), 1.37 (dd, *J* = 5, 1 Hz, 9H), 0.91 (td, *J* = 7, 2 Hz, 3H) ppm.

^{13}C NMR (101 MHz, Chloroform-*d*) δ 193.6*, 193.5 (C), 176.1*, 176.1 (C), 157.4*, 156.7 (C), 156.6*, 155.9 (C), 151.8*, 151.7 (C), 145.1*, 145.0 (C), 142.5*, 142.5 (C), 141.4*, 141.3 (C), 137.6*, 137.5 (C), 137.3*, 136.8 (C), 136.3*, 135.8 (C), 133.1*, 133.1 (C), 132.0*, 131.9 (CH), 130.7*, 130.6 (CH), 129.7 (CH), 127.8*, 127.8 (CH), 125.9*, 125.9 (CH), 123.0*, 122.9 (CH), 121.4*, 121.4 (CH), 114.4*, 114.1 (CH), 113.6*, 113.3 (CH), 111.7*, 111.7 (CH), 71.0*, 70.8 (CH_2), 65.6*, 65.3 (CH_2), 58.2*, 58.1 (CH_2), 56.1*, 56.1 (CH_3), 45.7*, 45.6 (2 x CH_3), 39.2*, 39.2 (C), 29.0*, 29.0 (CH_2), 27.2*, 27.1 (3 x CH_3), 13.6*, 13.6 (CH_3) ppm.
(Note, additional multiplicities and extra signals are due to the presence of the other stereoisomer).

IR (film): 2973, 1749, 1601, 1501, 1231, 1096 cm^{-1}.

HRMS (ESI): calc. for $[C_{40}H_{46}O_6N]^+$: 636.33197; found: 636.33111.

2-(4-(1-(4-(2-(Dimethylamino)ethoxy)phenyl)-2-phenylbut-1-en-1-yl)-3-methylphenoxy)-1-(4-hydroxy-3-methoxyphenyl)ethan-1-one (2-69)

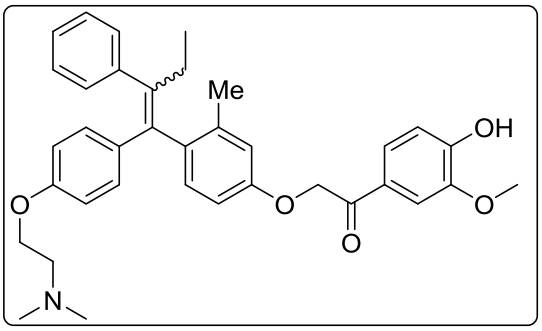

The compound was prepared as for **2-11** using **2-66** as starting material. The residue was purified by flash column chromatography, whereby the product eluted at 8% MeOH/DCM (+2% NEt_3) as a yellow foamy solid (155 mg, **61%**).

^{1}H NMR (400 MHz, Chloroform-*d*) δ 7.62 – 7.59 (m, 2H), 7.52 (m)*, 7.22 – 7.09 (m, 5H), 7.09 – 6.99 (m)*, 6.97 – 6.93 (m, 1H), 6.90 (d)*, 6.85 – 6.78 (m, 3H), 6.76 – 6.71 (m, 2H), 6.55 – 6.47 (m, 2H), 5.22 (s, 2H), 5.06 (s)*, 4.08 (t)*, 3.96 – 3.89 (m, 5H), 2.76 (t)*, 2.67 (t, *J* = 6 Hz, 2H), 2.36 (s)*, 2.33 – 2.22 (m, 8H), 2.09 (s, 3H), 1.98 (s)*, 0.98 (t)*, 0.81 (t, *J* = 7 Hz, 3H) ppm.

^{13}C NMR (101 MHz, Chloroform-*d*) δ 193.1 (C), 157.0 (C), 156.5 (C), 151.5 (C), 147.1 (C), 142.2 (C), 141.5 (C), 137.7 (C), 136.5 (C), 136.2 (C), 134.1 (C), 131.4 (CH), 130.5 (CH), 129.7 (CH), 127.9 (CH), 127.3 (CH), 126.0 (CH), 123.4 (CH), 116.6 (CH), 114.3 (CH), 113.2 (CH), 111.6 (CH), 110.2 (CH), 70.7 (CH_2), 65.4 (CH_2), 58.1 (CH_2), 56.1 (CH_3), 45.7 (2 x CH_3), 29.1 (CH_2), 20.1 (CH_3), 12.9 (CH_3) ppm.

IR (film): 2964, 1684, 1601, 1510, 1223, 727 cm^{-1}.

HRMS (ESI): calc. for $[C_{36}H_{40}O_5N]^+$: 566.29010; found: 566.29075.

4-(2-(4-(1-(4-(2-(Dimethylamino)ethoxy)phenyl)-2-phenylbut-1-en-1-yl)-3-methylphenoxy)-3-hydroxypropanoyl)-2-methoxyphenyl pivalate (2-78)

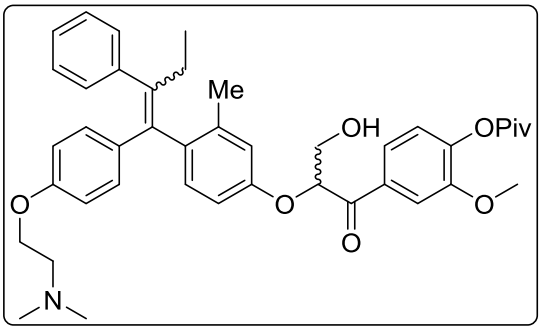

To a solution of **2-69** (100 mg, 0.16 mmol) and K_2CO_3 (44 mg, 0.32 mmol) in dioxane (3 mL) was added molecular sieves, followed by 36% formalin solution (0.14 mL, 0.17 mmol) then stirred for 20 h at 50 °C. NH_4Cl (aq) was added to the reaction mixture and the organics were extracted using EtOAc (x3). The combined organics were washed with H_2O, brine, dried over $MgSO_4$, then concentrated under reduced pressure to afford a grey gum. The residue was purified by flash

column chromatography, whereby the product eluted at 6% MeOH/DCM as a crunchy foam solid (60 mg, **57%**).

^{1}H NMR (400 MHz, Chloroform-*d*) δ 7.76 – 7.54 (m, 2H), 7.17 – 7.03 (m, 8H), 6.89 – 6.84 (m, 2H), 6.75 – 6.70 (m, 2H), 6.57 – 6.49 (m, 2H), 5.45 (ddd, *J* = 75.6, 6.1, 4.1 Hz, 1H), 4.22 – 3.99 (m, 4H), 3.80 (dd, *J* = 17.9, 0.7 Hz, 3H), 2.85 (d, *J* = 34.4 Hz, 2H), 2.45 (d, *J* = 21.4 Hz, 8H), 1.37 (d, *J* = 1.8 Hz, 9H), 0.90 (td, *J* = 7.4, 2.1 Hz, 3H) ppm.

^{13}C NMR (101 MHz, Chloroform-*d*) δ 195.6* , 195.4 (C), 176.1 (C), 155.9* , 155.1 (C), 151.8* , 151.7 (C), 145.3* , 145.1 (C), 142.4* , 142.3 (C), 141.6* , 141.5 (C), 137.6* , 137.4 (C), 137.3* , 137.1 (C), 133.1* , 133.0 (C), 132.1* , 131.9 (2 x CH), 130.8* , 130.6 (2 x CH), 129.6 (2 x CH), 127.8* , 127.8 (2 x CH), 126.0* , 126.0 (CH), 123.0* , 122.9 (CH), 122.0* , 122.0 (CH), 114.8* , 114.1 (2 x CH), 113.3 (2 x CH), 112.3* , 112.3 (CH), 81.1* , 81.0 (CH), 63.3* , 63.2 (CH_2), 57.9* , 57.8 (CH_2), 56.0* , 56.0 (CH_3), 45.4* , 45.3 (2 x CH_3), 39.2 (C), 29.0* , 29.0 (CH_2), 27.1 (3 x CH_3), 13.6 (CH_3) ppm. (Higher order multiplicities and extra signals* are due to the presence of the other stereoisomer).

IR (film): 2967, 1751, 1601, 1505, 1236, 1106, 736 cm^{-1}.

HRMS (ESI): calc. for $[C_{41}H_{48}O_7N]^+$: 666.34253; found: 666.34148.

2-(4-(1-(4-(2-(dimethylamino)ethoxy)phenyl)-2-phenylbut-1-en-1-yl)-3-methylphenoxy)-3-hydroxy-1-(4-hydroxy-3-methoxyphenyl)propan-1-one (2-79)

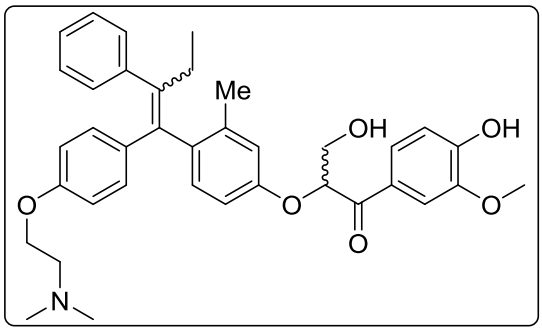

The compound was prepared following the procedure for Guaymoxifen (**2-11**) using **2-78** as starting material. The product eluted from the column at 8% MeOH/DCM as a crunchy foam solid (90 mg, **58%**).

^{1}H NMR (400 MHz, Chloroform-*d*) δ 7.65 (ddd, *J* = 44, 8, 2 Hz, 1H), 7.53 (dd, *J* = 32, 2 Hz, 1H), 7.17 – 7.00 (m, 7H), 6.92 (dd, *J* = 22, 8 Hz, 1H), 6.88 – 6.83 (m, 2H), 6.74 – 6.67 (m, 2H), 6.54 – 6.48 (m, 2H), 5.45 (ddd, *J* = 73, 6, 4 Hz, 1H), 4.20 – 3.92 (m, 4H), 3.87 (d, *J* = 15 Hz, 3H), 2.74 (dt, *J* = 39, 6 Hz, 2H), 2.48 – 2.40 (m, 2H), 2.35 (d, *J* = 24 Hz, 6H), 0.89 (td, *J* = 7, 4 Hz, 3H) ppm.

^{13}C NMR (101 MHz, Chloroform-*d*) δ 194.8* , 194.7 (C), 157.4* , 156.5 (C), 156.0* , 155.2 (C), 151.7* , 151.5 (C), 147.1* , 146.9 (C), 142.4* , 142.4 (C), 141.4* , 141.3 (C), 137.5 (C), 137.4* , *137.0 (C)*, 136.2* , 135.7 (C), 132.1* , 131.8 (2 x CH), 130.8* , 130.5 (2 x CH), 129.6* , 127.8 (CH), 127.3* , 127.3 (CH), 125.9* , 125.9 (2 x CH), 124.1* , 124.0 (CH), 114.9* , 114.3 (2 x CH), 114.2* , 114.1 (2 x CH), 114.0* , 113.3 (2 x CH), 110.7* , 110.7 (CH), 80.8* , 80.7 (CH), 65.6* , 65.4 (CH_2), 63.6* , 63.5 (CH_2), 58.2* , 58.1 (CH_2), 56.0* , 56.0 (2 x CH_3), 45.7* , 45.7 (CH_3), 29.0* , 28.9 (CH_2), 13.6* , 13.6 (CH_3) ppm. (Higher order multiplicities and extra signals* are due to the presence of the other stereoisomer).

IR (film): 3436, 2958, 1601, 1500, 1231, 727 cm^{-1}.

HRMS (ESI): calc. for $[C_{36}H_{40}O_6N]^+$: 582.28501; found: 582.28415.

LigF was expressed by the Protein Expression Core Facility within the IRB Barcelona by inserting the His-tagged LigF DNA into a pOPINF vector and expressed in E. coli BL21 (DE3) Rosetta lysS cells. After expression and lysis, the protein was purified by using a nickel column followed by gel filtration. Noteworthy, the His tags were not removed from the protein after purification.

Mass spectroscopy was carried out on our analogues to determine the distinct ionic degradations of each analogue and identify unique fragments which could be screened to identify the presence of each analogue remaining at certain time points during cleavage by LigF.

The following figures are the more detailed data of the LigF *in vitro* experiment detected by mass spectrometry:

CDO609 MS/MS Mass spectrum m/z 582; iso width 10, CID 45 **H_2O:ACN (50:50) + 1%FA**

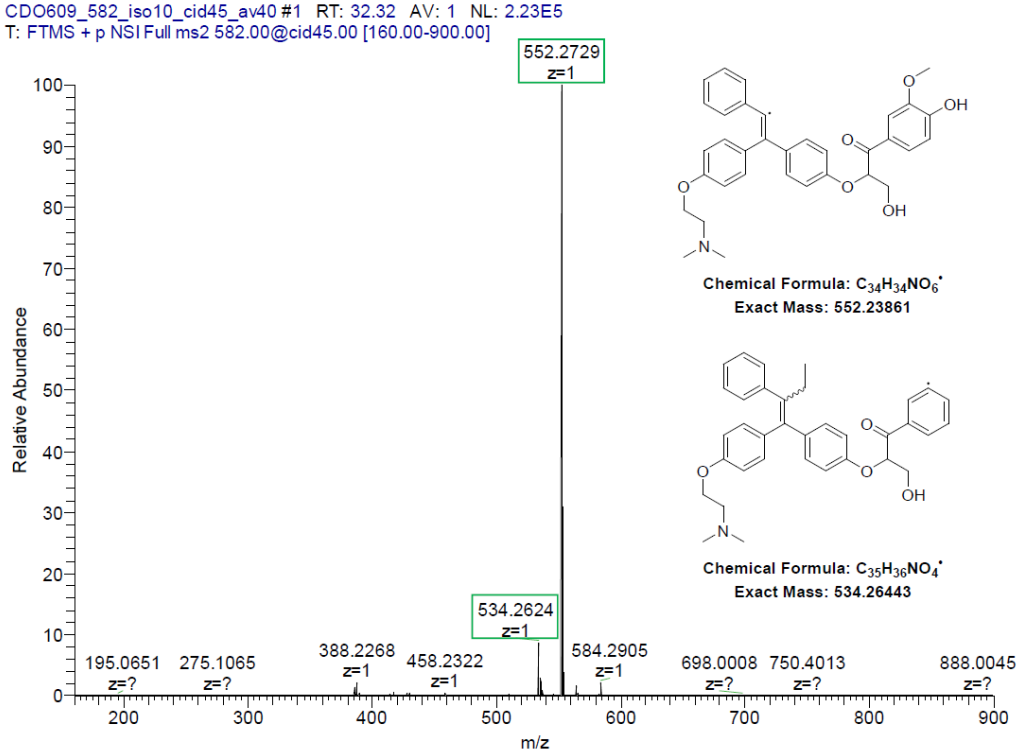

Guaymoxifen MS/MS Mass spectrum m/z 552; iso width 10, CID 45 **H_2O:ACN (50:50) + 1%FA**

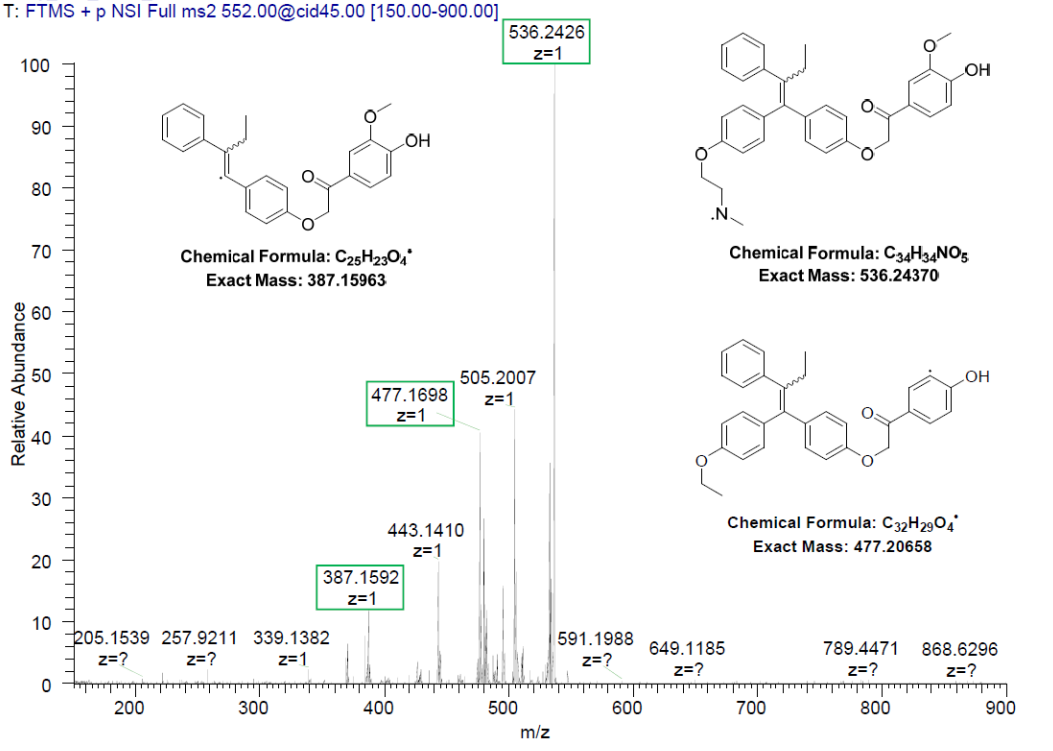

Z-TamOH MS/MS Mass spectrum m/z 388; iso width 10, CID 45 **H_2O:ACN (50:50) + 1%FA**

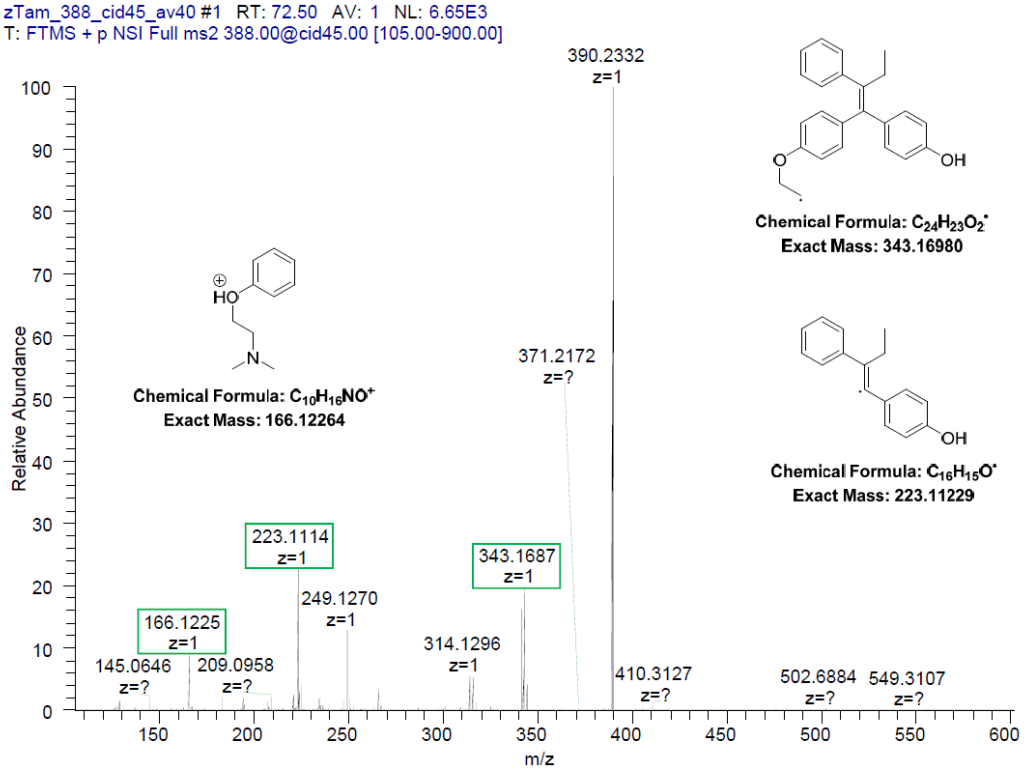

CDO608 MS/MS Mass spectrum m/z 402; iso width 10, CID 45 **H_2O:ACN (50:50) + 1%FA**

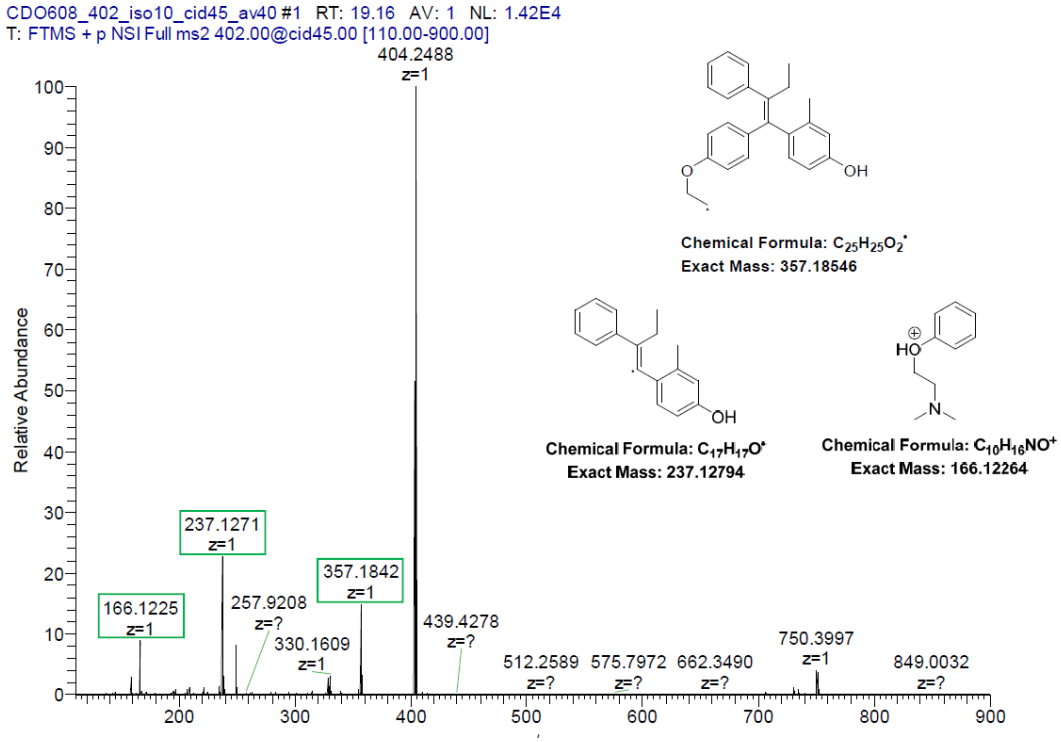

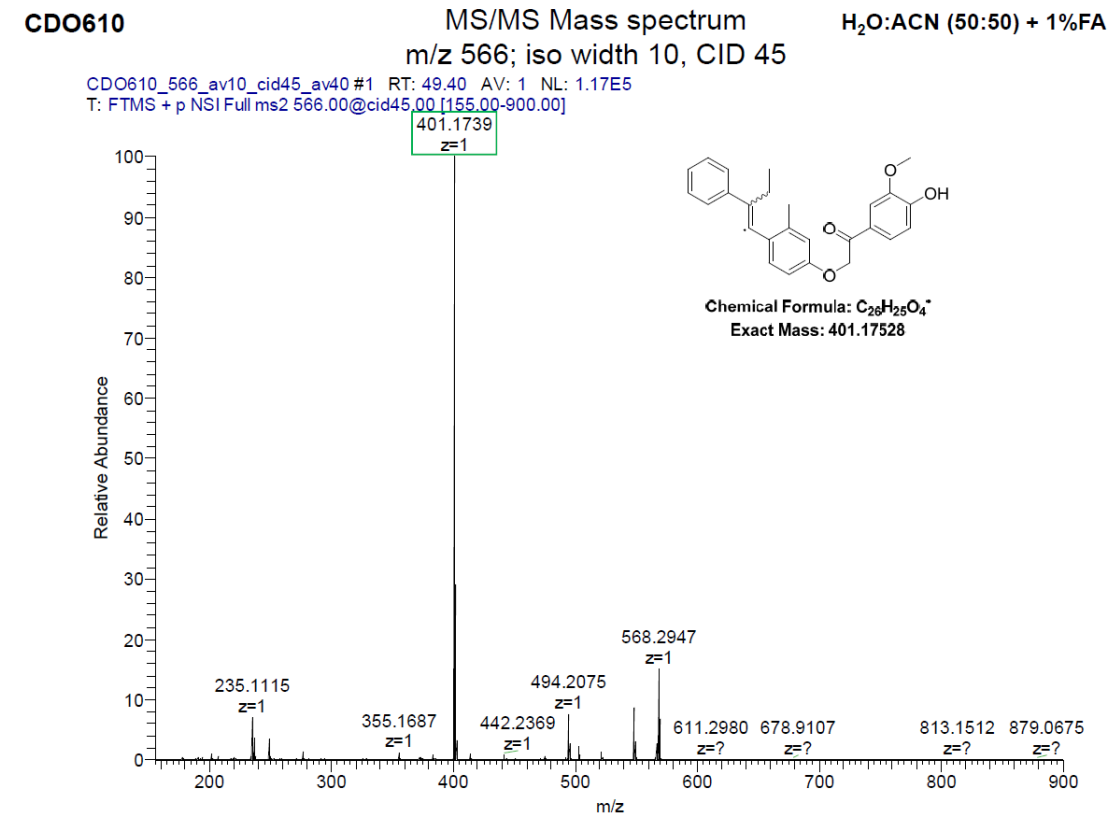

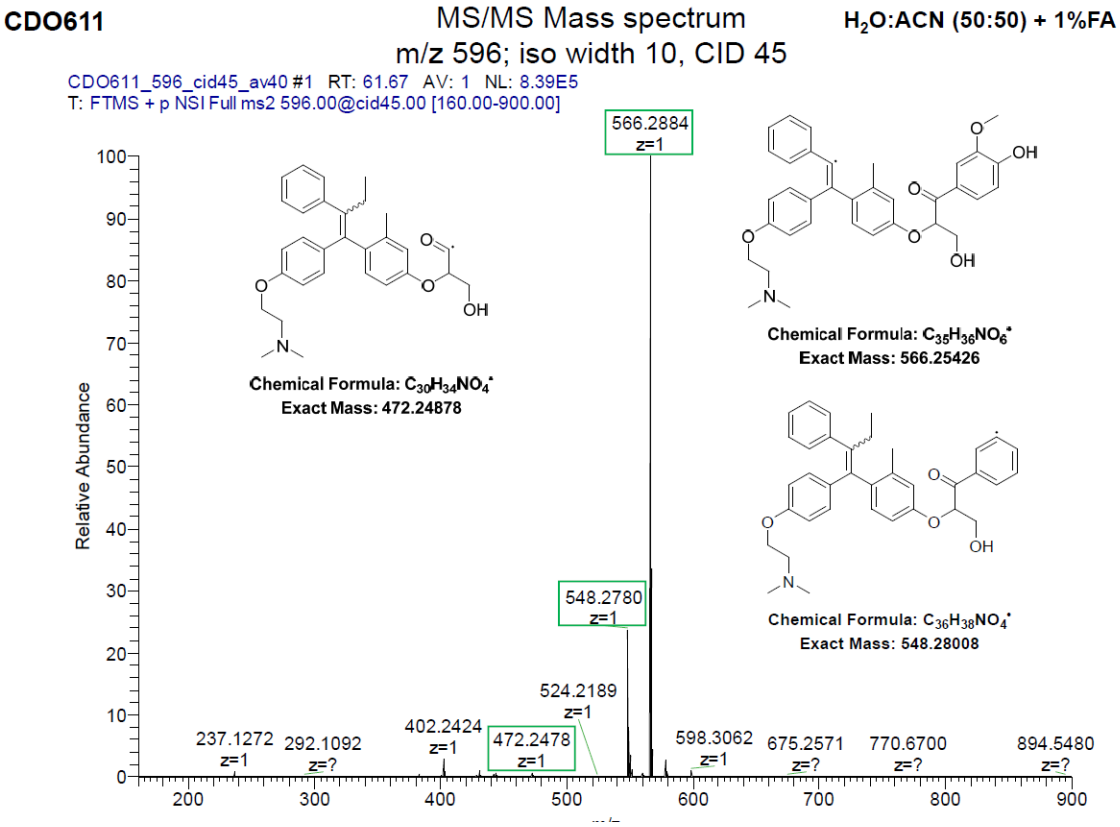

Tamoxifen calibration curve:

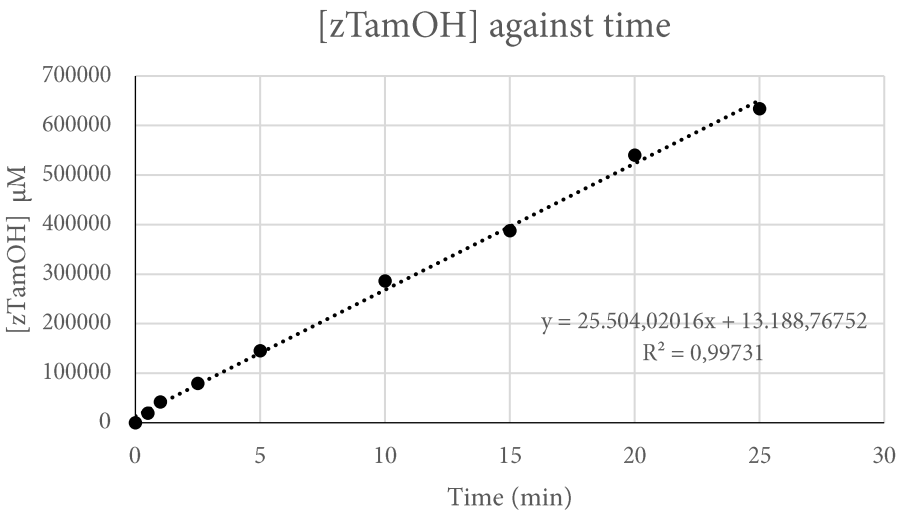

Graph 6.2.1. Calibration curve for concentration of *Z*-hydroxytamoxifen (4OHT) over time as detected by mass spec

6.3. Preparation and characterisation of compounds targeting p38α (from chapter 3)

Methyl 3-(4-hydroxy-6-methyl-2-oxopyridin-1(2*H*)-yl)-4-methylbenzoate (4-3)

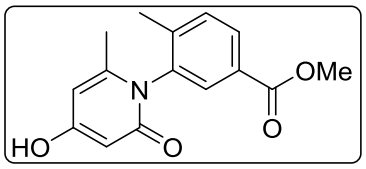

Methyl 3-amino-4-methylbenzoate (40.0 g, 242 mmol) 4-hydroxy-6-methyl-2H-pyran-2-one (45.8 g, 363 mmol) and catalytic potassium carbonate (4.0 g, 29 mmol) were mixed in trifluoroethanol (80 mL) and heated to 85 °C for 22 h. The mixture was removed from the oil bath and allowed to cool before addition of ethyl acetate. The precipitation of the product was observed and collected by filtration, washed with further ethyl acetate to afford product as a pale yellow/white solid (39.3 g, 144 mmol, **60%**).

The NMR spectra were consistent with that reported in the literature.[7]

^{1}H NMR (400 MHz, DMSO-d_6) δ 10.71 (bs, 1H), 7.92 (dd, *J* = 8, 2 Hz, 1H), 7.63 (d, *J* = 2 Hz, 1H), 7.54 (dt, *J* = 8, 1 Hz, 1H), 5.94 (dd, *J* = 3, 1 Hz, 1H), 5.58 (dd, *J* = 3, 1 Hz, 1H), 3.85 (s, 3H), 2.03 (s, 3H), 1.77 (t, *J* = 2 Hz, 3H) ppm.

Methyl 3-(5-bromo-4-hydroxy-6-methyl-2-oxopyridin-1(2*H*)-yl)-4-methylbenzoate (4-4)

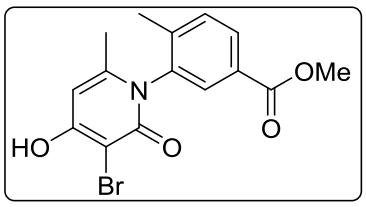

To a suspension of **4-3** (39.3 g, 144 mmol) in AcOH (160 mL) H_2O (41 mL) at 0 °C, in minimal exposure to light, was added a solution of Br_2 (7.7 mL, 150 mmol) in AcOH (40 mL) dropwise over 45 min then left another 10 minutes until no more starting material could be observed by TLC. The mixture was then diluted with water (400 mL), precipitation was observed. The product was obtained by filtration, washed with water (100 mL) and then cold acetonitrile (75 mL), and then dried in the desiccator over 48 h to afford **2** as a faint beige solid (45.7 g, 130 mmol, **90%**).

The NMR spectra were consistent with that reported in the literature.[7]

^{1}H NMR (400 MHz, DMSO-d_6) δ 11.54 (s, 1H), 7.93 (dd, *J* = 8, 2 Hz, 1H), 7.69 (d, *J* = 2 Hz, 1H), 7.54 (d, *J* = 8 Hz, 1H), 6.11 (d, *J* = 1 Hz, 1H), 3.82 (s, 3H), 2.01 (s, 3H), 1.76 (d, *J* = 1 Hz, 3H) ppm.

Methyl 3-(5-bromo-4-((2,4-difluorobenzyl)oxy)-6-methyl-2-oxopyridin-1(2*H*)-yl)-4-methylbenzoate (4-6)

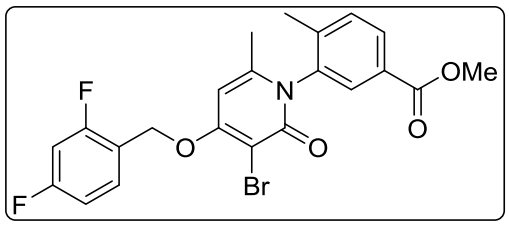

4-4 (45.7 g, 130 mmol) and K_2CO_3 (26.9 g, 195 mmol) were dissolved in DMF (116 mL) and heated to 65 °C. 2,4-Diflouorobenzyl chloride (**4-5,** 17.6 mL, 143 mmol) was then added dropwise and heating was maintained for 3.5 h. The reaction mixture was then removed from the oil bath and allowed to cool for 30 min before decanting it into stirring water (300 mL) at 0 °C causing precipitation. The precipitate was collected by filtration and washed with more water (300 mL) to afford a light orange solid. The crude solid was then triturated using methanol to afford **3** as a white solid (56.1 g, 117 mmol, **90%**).

The NMR spectra were consistent with that reported in the literature.[7]

^{1}H NMR (400 MHz, Chloroform-*d*) δ 8.03 (dd, *J* = 8, 2 Hz, 1H), 7.76 (d, *J* = 2 Hz, 1H), 7.62 (td, *J* = 8, 6 Hz, 1H), 7.44 (dt, *J* = 8, 1 Hz, 1H), 7.02 – 6.95 (m, 1H), 6.89 (ddd, *J* = 10, 9, 3 Hz, 1H), 6.13 (d, *J* = 1 Hz, 1H), 5.27 (q, *J* = 1 Hz, 2H), 3.89 (s, 3H), 2.14 (s, 3H), 1.93 (d, *J* = 1 Hz, 3H) ppm.

3-(5-Bromo-4-((2,4-difluorobenzyl)oxy)-6-methyl-2-oxopyridin-1(2*H*)-yl)-4-methylbenzoic acid (4-7)

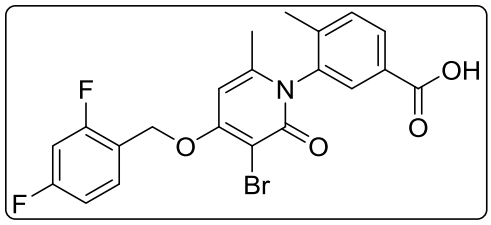

To a flask charged with **4-6** (20.0 g, 42 mmol), suspended in MeCN (70 mL) and water (50 mL), was added 2.5 M NaOH (18.4 mL, 46 mmol) and the reaction mixture was heated to 65 °C for 1 h, at which point the mixture became homogenous. After a second hour at this temperature the reaction mixture was removed from the oil bath and allowed to cool, then acidified to pH 5 using concentrated HCl under a stream of N_2 and stirred for a further hour. The yellow precipitate was then collected by filtration and washed with H_2O (100 mL) then cold MeCN (100 mL) to afford **4** as a white solid (15.9 g, 34 mmol, **82%**).

The NMR spectra were consistent with that reported in the literature.[7]

^{1}H NMR (400 MHz, DMSO-d_6) δ 13.08 (s, 1H), 7.93 (dd, *J* = 8, 2 Hz, 1H), 7.73 – 7.65 (m, 2H), 7.54 (d, *J* = 8 Hz, 1H), 7.34 (ddd, *J* = 10, 9, 3 Hz, 1H), 7.18 (td, *J* = 9, 3 Hz, 1H), 6.71 (s, 1H), 5.33 (s, 2H), 2.01 (s, 3H), 1.89 (s, 3H) ppm.

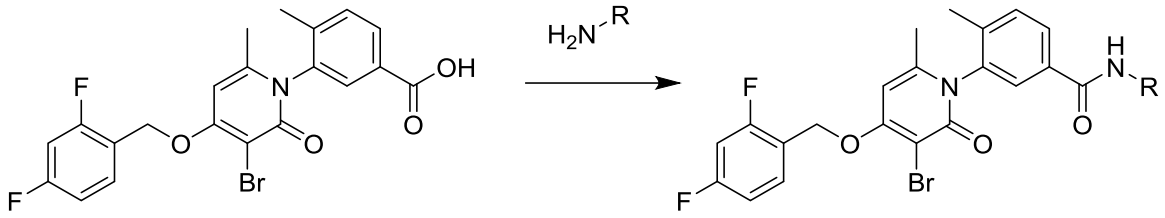

General procedure A for amide bond formation via acid chloride intermediate

To **4-7** (1 eq.) suspended in dry THF was added DMF (2 drops) then cooled to 0 °C. Oxalyl chloride (1.5 eq.) was then added dropwise. The reaction was warmed to room temperature, after 0.5 h the reaction mixture became homogenous. This solution was then added dropwise to a second vial containing a solution of the corresponding amine (1 eq.) in dry THF (water was used in the case of methylamine) under N_2 at 0 °C. The reaction mixture was then allowed to reach rt and left 1 – 3 h before the addition of water to quench the reaction. The precipitate was collected by filtration and washed with water to afford the desired product.

General procedure B for amide bond formation using coupling agent

4-7 (1 eq.) was dissolved in anhydrous DMF, cooled to 0 °C, then added oxime (1.66 eq.) and CDI (1.66 eq.). After 15 min the solution turned yellow, then NEt_3 (1.66 mL) was added, followed by the corresponding amine starting material (1.1 mL). The reaction was left 18 – 24 h before quenching with water. The mixture was separated between EtOAc and water, then the aqueous layer re-extracted using EtOAc. The combined organic layers were washed with brine, dried over $MgSO_4$, and then concentrated by rotary evaporator under reduced pressure. The corresponding crude amide was then purified by flash column chromatography.

3-(3-Bromo-4-((2,4-difluorobenzyl)oxy)-6-methyl-2-oxopyridin-1(2*H*)-yl)-*N*,4-dimethylbenzamide (PH)

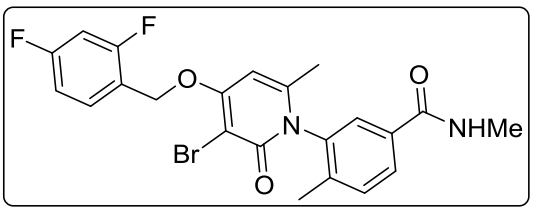

The product was prepared following general procedure A from **4-7** and a 40% aqueous solution of methylamine, the product was collected by filtration, washing with water, and dried in the desiccator, to afford a white solid (2.6 g, 3.63 mmol, **56%**).

The NMR spectra were consistent with that reported in the literature.[7]

^{1}H NMR (400 MHz, Chloroform-*d*) δ 7.83 (dd, *J* = 8, 2 Hz, 1H), 7.65 – 7.57 (m, 1H), 7.49 (d, *J* = 2 Hz, 1H), 7.39 (d, *J* = 8 Hz, 1H), 6.98 – 6.91 (m, 1H), 6.83 (ddd, *J* = 11, 9, 2 Hz, 1H), 6.53 (d, *J* = 5 Hz, 1H), 6.16 (NH, q, *J* = 1 Hz, 1H), 5.22 (s, 2H), 2.78 (d, *J* = 5 Hz, 3H), 2.11 (s, 3H), 1.92 (d, *J* = 1 Hz, 3H) ppm.

^{1}H NMR (400 MHz, MeOD-*d*$_4$) δ 8.46 (NH, q, *J* = 5 Hz, 1H), 7.86 (dd, *J* = 8, 2 Hz, 1H), 7.71 (td, *J* = 9, 7 Hz, 1H), 7.62 (d, *J* = 2 Hz, 1H), 7.52 (d, *J* = 8 Hz, 1H), 7.37 (ddd, *J* = 11, 9, 3 Hz, 1H), 7.24 – 7.17 (m, 1H), 6.74 (d, *J* = 1 Hz, 1H), 5.37 (s, 2H), 2.78 (d, *J* = 5 Hz, 3H), 2.01 (s, 3H), 1.92 (d, *J* = 1 Hz, 3H) ppm.

Methyl (3-(3-bromo-4-((2,4-difluorobenzyl)oxy)-6-methyl-2-oxopyridin-1(2*H*)-yl)-4-methylbenzoyl)glycinate (4-9a)

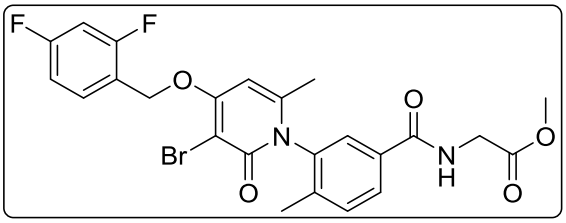

The product was prepared following general procedure A from **4-7** and methyl glycinate, the product was collected by filtration, washing with water, and dried in the desiccator, to afford a white solid (214 mg, 0.400 mmol, **95%**).

^{1}H NMR (400 MHz, Chloroform-*d*) δ 7.80 (dd, *J* = 8, 2 Hz, 1H), 7.62 (dd, *J* = 15, 8 Hz, 1H), 7.53 (t, *J* = 4 Hz, 1H), 7.43 (d, *J* = 8 Hz, 1H), 6.98 (t, *J* = 8 Hz, 1H), 6.91 – 6.84 (m, 1H), 6.73 (s, 1H), 6.13 (s, 1H), 5.27 (s, 2H), 4.19 (dd, *J* = 13, 5 Hz, 2H), 3.79 (s, 3H), 2.13 (s, 3H), 1.92 (d, *J* = 1 Hz, 3H) ppm.

^{13}C NMR (CDCl3, 101 MHz): δ 170.3 (C), 166.2 (C), 163.1 (C), 160.4 (C), 154.1 (C), 151.3 (d, J_F = 16 Hz, C)146.0 (C) , 139.5 (C), 137.8 (C), 133.4 (C), 131.6 (CH), 130.3 (dd, *J* = 10, 5 Hz, CH), 128.2

(CH), 126.8 (CH), 121.4 (dd, J_F = 49, 9 Hz, C), 112.0 (dd, J_F = 21, 4 Hz, CH), 104.0 (t, J_F = 25 Hz, CH), 97.1 (C), 96.2 (CH), 64.4 (d, J_F = 4 Hz, CH_2), 52.4 (CH_3), 41.7 (CH_2), 21.5 (CH_3), 17.4 (CH_3) ppm.

^{19}F NMR (CDCl3, 376 MHz): δ -109.10 – -109.21 (m), -114.55 (dd, *J* = 18, 9 Hz).

IR (film): 3323, 1749, 1646, 1531, 1355, 1208, 844 cm^{-1}.

HRMS (ES): *m/z* calc. C24H21BrF2N2O5Na+ [M+Na]+ 557.0498 found 557.0506.

Melting Point: 138 - 140 °C.

(3-(3-Bromo-4-((2,4-difluorobenzyl)oxy)-6-methyl-2-oxopyridin-1(2H)-yl)-4-methylbenzoyl)glycine (4-9b)

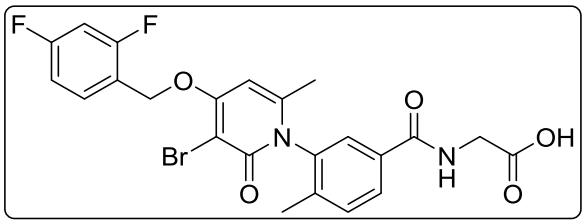

The product was prepared following the procedure for **4-7** but using **4-9a** as starting material. The product was collected by filtration, washing with water and MeCN, dried in the desiccator, to afford a white solid (60 mg, 0.115 mmol, **62%**).

^{1}H NMR (DMSO, 400 MHz): δ 12.59 (s, 1H), 8.86 (t, *J* = 6 Hz, 1H), 7.88 (dd, *J* = 8, 2 Hz, 1H), 7.68 (ddd, *J* = 12, 7, 4 Hz, 2H), 7.52 (d, *J* = 8 Hz, 1H), 7.35 (ddd, *J* = 11, 9, 3 Hz, 1H), 7.23 – 7.14 (m, 1H), 6.73 (s, 1H), 5.35 (s, 2H), 3.90 (qd, *J* = 17, 6 Hz, 2H), 2.01 (s, 3H), 1.90 (d, *J* = 6 Hz, 3H) ppm.

^{13}C NMR (101 MHz, DMSO-d_6) δ 171.3 (C), 165.4 (C), 163.3 (C), 161.9 (d, J_F = 13 Hz, C), 159.3 (C), 146.7 (C), 138.9 (C), 137.7 (C), 133.1 (C), 132.0 (dd, J_F = 10, 6 Hz, CH), 131.2 (CH), 128.0 (CH), 127.0 (CH), 119.3 (dd, *J* = 15, 4 Hz, C), 112.2 – 111.5 (m, CH), 104.3 (t, J_F = 26 Hz, CH), 96.3 (CH), 94.7 (C), 64.8 (d, J_F = 3 Hz, CH_2), 41.2 (CH_2), 20.8 (CH_3), 16.9 (CH_3) ppm.

^{19}F NMR (DMSO, 376 MHz): δ -109.12 – -109.26 (m), -113.25 (dd, *J* = 18, 9 Hz) ppm.

IR (film): 3386, 2933, 1741, 1632, 1600, 1504, 1193 cm^{-1}

HRMS (ESI): calc. for $[C_{23}H_{21}O_5N_2BrF_2]^+$: 521.0479; found: 521.0529

Melting Point: 252 - 253 °C

3-(3-Bromo-4-((2,4-difluorobenzyl)oxy)-6-methyl-2-oxopyridin-1(2*H*)-yl)-*N*-(2-hydroxyethyl)-4-methylbenzamide (4-11)

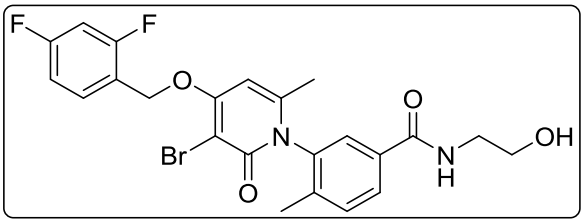

The product was prepared following general procedure A using **4-7** and 2-aminoethan-1-ol as starting materials. The product was collected by filtration, washing with water and MeCN, dried, to afford a white solid, (128 mg, 0.25 mmol, **55%**).

^{1}H NMR (400 MHz, Chloroform-*d*) δ 7.89 (dd, *J* = 8, 2 Hz, 1H), 7.62 (d, *J* = 2 Hz, 1H), 7.58 (td, *J* = 9, 6 Hz, 1H), 7.35 (d, *J* = 8 Hz, 1H), 7.29 – 7.26 (m, NH), 6.95 (tdd, *J* = 9, 3, 1 Hz, 1H), 6.79 (ddd, *J* = 10, 9, 3 Hz, 1H), 6.21 (d, *J* = 1 Hz, 1H), 5.15 (s, 2H), 3.80 (bt, *J* = 6 Hz, OH), 3.67 – 3.42 (m, 3H), 3.11 – 3.01 (m, 1H), 2.06 (s, 3H), 1.94 (s, 3H) ppm.

^{13}C NMR (101 MHz, Chloroform-*d*) δ 165.8 (C), 164.2 (d, J_F = 12 Hz, C), 163.7 (C), 161.7 (d, J_F = 12 Hz, C), 161.0 (d, J_F = 12 Hz, C), 160.8 (C), 158.5 (d, J_F = 12 Hz, C), 147.2 (C), 138.3 (C), 136.8 (C), 133.9 (C), 131.5 (CH), 129.57 – 129.36 (m, 2 X CH), 126.1 (CH), 118.3 (dd, J_F = 14, 4 Hz, C), 111.9 (dd, J_F = 21, 4 Hz, CH), 104.2 – 103.5 (m, CH), 97.2 (CH), *96.3 (C)*, 64.8 (d, J_F = 4 Hz, CH_2), 61.8 (CH_2), 43.5 (CH_2), 21.7 (CH_3), 17.2 (CH_3) ppm.

HRMS (ESI): calc. for $[C_{33}H_{39}O_5N_2BrF_2]^+$:; found:

IR (film): 3343, 2929, 1647, 1523, 1346, 1037, 727 cm^{-1}.

Melting Point: 170.2 – 171.2 °C.

3-((*Tert*-butyldiphenylsilyl)oxy)propan-1-aminium chloride

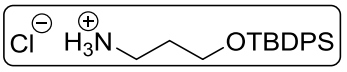

To a solution of tert-butyl (3-hydroxypropyl)carbamate (97.5 mL, 0.571 mmol) in DMF (3 mL) at rt was added dropwise imidazole (85 mg (1.26 mmol) then tert-butylchlorodiphenylsilane (163 mL, 0.628 mmol) and left to stir for 20 h. The reaction mixture was then separated between brine and EtOAc. The aqueous layer was re-extracted using EtOAc, then the combined organic layers were washed with brine, dried over $MgSO_4$ and concentrated under reduced pressure to afford a colourless oil. To the crude was then added 4N HCl in dioxane (1 mL, 4 mmol) and left to stir at rt for 2 h. The reaction mixture was then removed under reduced pressure to afford a colourless oil (84 mg, 0.240 mmol, **42%**).

Spectra consistent with that reported in the literature.[8]

^{1}H NMR (400 MHz, MeOD-*d4*) δ 7.70 – 7.64 (m, 4H), 7.48 – 7.35 (m, 6H), 3.70 (t, *J* = 6 Hz, 2H), 3.06 (t, *J* = 7 Hz, 2H), 1.86 (tt, *J* = 7, 6 Hz, 2H), 1.01 (s, 9H) ppm.

3-(3-Bromo-4-((2,4-difluorobenzyl)oxy)-6-methyl-2-oxopyridin-1(2*H*)-yl)-*N*-(3-hydroxypropyl)-4-methylbenzamide (4-12a)

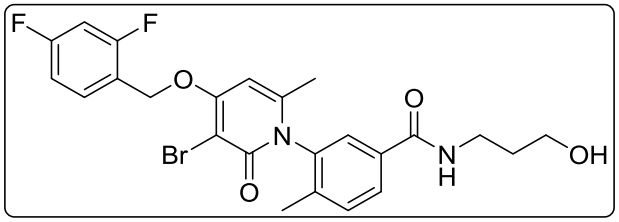

The product was prepared following general procedure A using **4-7** and 3-((*Tert*-butyldiphenylsilyl)oxy)propan-1-aminium chloride as starting materials. The product eluted from the silica column at 75% EtOAc/hexanes, as a white solid (17 mg, 0.033 mmol, **15%**).

^{1}H NMR (400 MHz, Chloroform-*d*) δ 7.81 (dd, *J* = 8, 2 Hz, 1H), 7.60 (td, *J* = 9, 6 Hz, 1H), 7.50 (d, *J* = 2 Hz, 1H), 7.35 (dd, *J* = 8, 1 Hz, 1H), 7.22 (t, *J* = 6 Hz, 1H), 6.99 – 6.93 (m, 1H), 6.83 (ddd, *J* = 10, 9, 3 Hz, 1H), 6.18 (d, *J* = 1 Hz, 1H), 5.20 (s, 2H), 3.57 (t, *J* = 6 Hz, 2H), 3.51 – 3.40 (m, 1H), 3.27 (dq, *J* = 13, 6 Hz, 1H), 2.09 (s, 3H), 1.93 (d, *J* = 1 Hz, 3H), 1.65 (q, *J* = 6 Hz, 3H) ppm.

^{13}C NMR (101 MHz, Chloroform-*d*) δ 166.3 (C), 164.2 (d, J_F = 12 Hz, C), 163.4 (C), 161.2 – 160.9 (m, C) 160.7 (C), 146.7 (C), 138.4 (C), 137.2 (C), 133.9 (C), 131.5 (CH), 129.8 (dd, J_F = 10, 5 Hz, CH), 128.8 (CH), 126.3 (CH), 118.6 – 118.2 (m, C), 111.9 (dd, J_F = 21, 4 Hz, CH), 104.2 – 103.5 (m, CH), 96.8 (CH), 96.5 (C), 64.6 (d, J_F = 4 Hz, CH_2), 59.3 (CH_2), 36.7 (CH_2), 31.8 (CH_2), 21.6 (CH_3), 17.3 (CH_3) ppm.

IR (Film): 2929, 1633, 1450, 1340, 1037 cm^{-1}.

HRMS (ESI): calc. for $[C_{24}H_{24}O_4N_2BrF_2]^+$: 521.08820; found: 521.08976.

4-((*Tert*-butyldiphenylsilyl)oxy)butan-1-aminium chloride

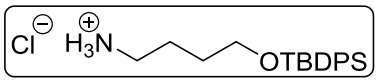

To a solution of tert-butyl (4-hydroxybutyl)carbamate (750 mg, 3.96 mmol) in DCM (5 mL) at rt was added 4-dimethylaminopyridine (24 mg, 0.20 mmol), NEt_3 (0.69 mL, 4.95 mmol), then tert-butylchlorodiphenylsilane (1.5 mL, 5.94 mmol) and left to stir for 8 h. The reaction mixture was then separated between brine and EtOAc. The aqueous layer was re-extracted using EtOAc, then the combined organic layers were washed with brine, dried over $MgSO_4$ and concentrated under reduced pressure to afford a colourless oil. To the crude was then added 4N HCl in dioxane (1 mL, 4 mmol) and left to stir at rt for 1.5 h. The reaction mixture was then removed under reduced pressure to afford a colourless oil (712 mg, 1.66 mmol, **42%**).

Spectra were consistent with that reported in the literature.[9]

^{1}H NMR (400 MHz, Chloroform-*d*) δ 7.64 – 7.60 (m, 4H), 7.42 – 7.36 (m, 6H), 3.76 – 3.71 (m, 2H), 3.07 (s, 2H), 1.85 (t, *J* = 7 Hz, 2H), 1.71 – 1.62 (m, 2H), 1.05 (s, 9H) ppm.

3-(3-Bromo-4-((2,4-difluorobenzyl)oxy)-6-methyl-2-oxopyridin-1(2*H*)-yl)-*N*-(4-hydroxybutyl)-4-methylbenzamide (4-15)

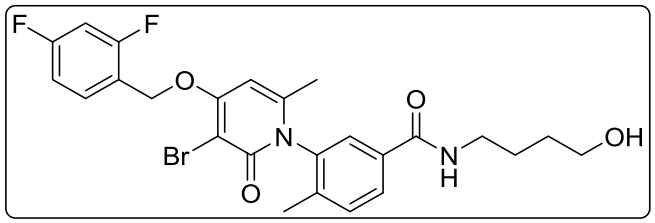

The product was prepared following general procedure A using **4-7** and 4-((*Tert*-butyldiphenylsilyl)oxy)butan-1-aminium chloride as starting materials. The product eluted from the silica column at 95% EtOAc/hexanes, as a white solid (221 mg, 0.413 mmol, **24%**).

^{1}H NMR (400 MHz, Chloroform-*d*) δ 7.74 (dd, *J* = 8, 2 Hz, 1H), 7.61 (td, *J* = 9, 6 Hz, 1H), 7.50 (d, *J* = 2 Hz, 1H), 7.32 – 7.26 (m, 2H), 7.00 – 6.94 (m, 1H), 6.85 (ddd, *J* = 10, 9, 3 Hz, 1H), 6.18 (d, *J* = 1 Hz, 1H), 5.23 (s, 2H), 3.67 – 3.53 (m, 2H), 3.43 (dd, *J* = 13, 6 Hz, 2H), 3.21 (dd, *J* = 13, 5 Hz, 1H), 2.08 (s, 3H), 1.92 (s, 3H), 1.59 – 1.51 (m, 3H) ppm.

^{13}C NMR (101 MHz, Chloroform-*d*) δ 166.1 (C), 164.26 (d, J_F = 12 Hz, C), 163.4 (C), 161.7 – 160.9 (m, C), 160.7 (C), 146.6 (C), 138.1 (C), 137.2 (C), 134.44 (C), 131.4 (CH), 130.1 (dd, J_F = 10, 5 Hz, CH), 128.4 (CH), 126.6 (CH), 118.5 (dd, J_F = 14, 4 Hz, C), 111.9 (dd, J_F = 21, 4 Hz, CH), 103.9 (t, J_F = 25 Hz, CH), 96.6 (CH), 96.6 (C), 64.5 (d, J_F = 4 Hz, CH_2), 62.5 (CH_2), 39.8 (CH_2), 30.1 (CH_2), 26.0 (CH_2), 21.6 (CH_3), 17.3 (CH_3) ppm.

IR (Film): 3331, 2929, 1786, 1647, 1219 cm^{-1}.

HRMS (ESI): calc. for $[C_{25}H_{26}O_4N_2BrF_2]^+$: 535.10385; found: 535.10370.

***Tert*-butyl (3-(3-(3-bromo-4-((2,4-difluorobenzyl)oxy)-6-methyl-2-oxopyridin-1(2*H*)-yl)-4-methylbenzamido)propyl)carbamate (4-13boc)**

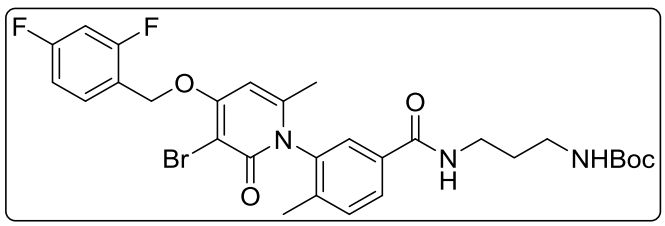

The product was prepared following general procedure A using **4-7** and tert-butyl (3-aminopropyl)carbamate as

starting materials. The product eluted from the silica column at 100% EtOAc/hexanes, as a yellow-white solid (340 mg, 0.52 mmol, **92%**).

^{1}H NMR (400 MHz, Chloroform-*d*) δ 7.86 (dd, *J* = 8, 2 Hz, 1H), 7.64 – 7.55 (m, 2H), 7.39 (d, *J* = 8 Hz, 1H), 7.30 (NH, bs, 1H), 7.01 – 6.93 (m, 1H), 6.84 (ddd, *J* = 10, 9, 2.5 Hz, 1H), 6.15 (s, 1H), 5.22 (s, 2H), 5.13 (NH, bt, *J* = 7 Hz, 1H), 3.40 (dq, *J* = 12, 6 Hz, 1H), 3.29 – 3.04 (m, 3H), 2.10 (s, 3H), 1.94 (s, 3H), 1.63 (p, *J* = 6 Hz, 2H), 1.41 (s, 9H) ppm.

^{13}C NMR (101 MHz, Chloroform-*d*) δ 165.8 (C), 164.2 (d, J_F = 12 Hz, C), 163.2 (C), 161.43 (dd, J_F = 58, 12 Hz, C), 160.5 (C), 156.6 (dd, J_F = 7, 3 Hz, C), 152.1 (C), 146.5 (C), 138.6 (C), 137.4 (C), 134.1 (C), 131.4 (CH), 130.0 (dd, J_F = 11, 6 Hz, CH), 128.4 (CH), 126.6 (CH), 118.8 – 118.5 (m, C), 112.2 – 111.5 (m, CH), 104.4 – 103.5 (m, CH), 96.4 (CH), 79.2 (C), 64.4 (d, J_F = 4 Hz, CH_2), 37.1 (CH_2), 36.3 (CH_2), 29.6 (CH_2), 28.4 (3 x CH_3), 21.6 (CH_3), 17.3 (CH_3) ppm.

IR (Film): 3342, 2920, 1636, 1523, 1340, 1179 cm^{-1}.

HRMS (ESI): calc. for $[C_{24}H_{25}O_3N_3BrF_2]^+$: 520.10419 (minus boc group) = 520.60455

3-(3-(3-Bromo-4-((2,4-difluorobenzyl)oxy)-6-methyl-2-oxopyridin-1(2*H*)-yl)-4-methylbenzamido)propan-1-aminium chloride (4-13a)

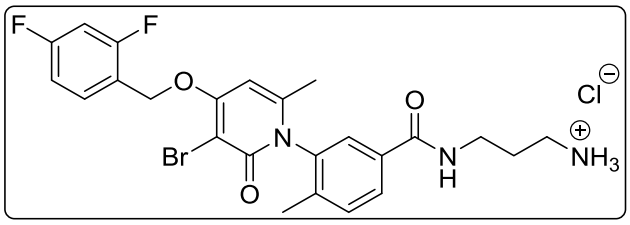

4-13boc dissolved in 4N HCl in dioxane (2 mL) and stirred at rt for 2 h. Evaporation of the product then precipitation using EtOAc and hexanes afforded the product as a white solid (148 mg, 0.266 mmol, **99%**).

^{1}H NMR (400 MHz, DMSO-d_6) δ 8.79 (bt, *J* = 6 Hz, 1H), 7.98 (s, 3H), 7.91 (dd, *J* = 8, 2 Hz, 1H), 7.75 – 7.69 (m, 1H), 7.68 (d, *J* = 2 Hz, 1H), 7.52 (d, *J* = 8 Hz, 1H), 7.36 (ddd, *J* = 11, 9, 3 Hz, 1H), 7.20 (tdd, *J* = 9, 2.6, 1 Hz, 1H), 6.76 (s, 1H), 5.36 (s, 2H), 3.30 (d, *J* = 8 Hz, 2H), 2.83 (t, *J* = 7 Hz, 2H), 2.01 (s, 3H), 1.93 (s, 3H), 1.82 (p, *J* = 7 Hz, 2H) ppm.

^{13}C NMR (101 MHz, DMSO-d_6) δ 165.3 (C), 163.8 (d, J_F = 13 Hz, C), 163.3 (C), 161.6 (dd, J_F = 50, 13 Hz, C), 159.32 (d, J_F = 12 Hz, C), 159.2 (C), 146.7 (C), 138.6 (C), 137.5 (C), 133.4 (C), 131.9 (dd, J_F = 10, 5 Hz, CH), 131.0 (CH), 127.9 (CH), 126.97 – 126.77 (m, CH), 119.3 (dd, J_F = 15, 4 Hz, C), 111.8 (dd, J_F = 21, 4 Hz, CH), 104.2 (t, J_F = 26 Hz, CH), 96.3 (CH), 94.6 (C), 64.8 (d, J_F = 3 Hz, CH_2), 36.7 (CH_2), 36.2 (CH_2), 27.2 (CH_2), 20.8 (CH_3), 16.8 (CH_3) ppm.

IR (Film): 3330, 2916, 1641, 1345, 1105, 718 cm^{-1}.

HRMS (ESI): calc. for $[C_{24}H_{25}O_3N_3BrF_2]^+$: 520.10419; found: 520.10351

4-(3-(3-Bromo-4-((2,4-difluorobenzyl)oxy)-6-methyl-2-oxopyridin-1(2*H*)-yl)-4-methylbenzamido)butan-1-aminium chloride (4-16)

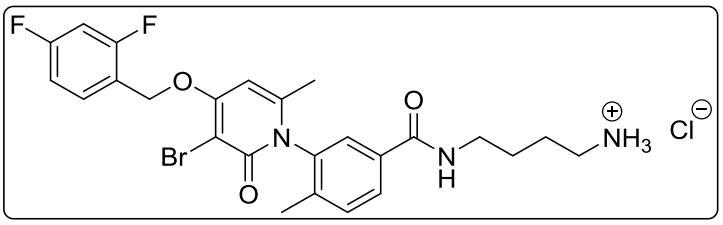

The product was prepared following general procedure A using **4-7** and *tert*-butyl (4-aminobutyl)carbamate as starting materials to afford crude *tert*-butyl (4-(3-(3-bromo-4-((2,4-difluorobenzyl)oxy)-6-methyl-2-oxopyridin-1(2*H*)-yl)-4-methylbenzamido)butyl)carbamate. This was directly dissolved in 4N HCl in dioxane (2 mL) and stirred at rt for 2 h. Evaporation of the product then precipitation using EtOAc and hexanes afforded the product as a white solid (251 mg, 0.438 mmol, **67%**).

^{1}H NMR (400 MHz, Methanol-d_4) δ 7.88 (dd, *J* = 8, 2 Hz, 1H), 7.69 – 7.62 (m, 1H), 7.60 (d, *J* = 2 Hz, 1H), 7.53 (dd, *J* = 8, 1 Hz, 1H), 7.08 – 7.02 (m, 2H), 6.68 (d, *J* = 1 Hz, 1H), 5.36 (s, 2H), 3.42 – 3.37 (m, 2H), 2.96 (t, *J* = 7 Hz, 2H), 2.09 (s, 3H), 2.00 (d, *J* = 1 Hz, 3H), 1.69 (dq, *J* = 5, 3, 2 Hz, 4H) ppm.

^{13}C NMR (101 MHz, Methanol-d_4) δ 167.3 (C), 164.5 (C), 162.1 (dd, J_F = 12, 8 Hz, C), 161.1 (C), 159.7 (d, J_F = 12 Hz, C), 147.13 (C), 139.3 (C), 137.7 (C), 133.7 (C), 131.5 – 131.1 (m, 2 x CH), 128.0 (CH), 126.6 (CH), 119.0 (dd, J_F = 15, 4 Hz, C), 111.2 (dd, J_F = 22, 4 Hz, CH), 103.5 (t, J_F = 26 Hz, CH), 97.2 (CH), 95.3 (C), 64.8 (d, J_F = 4 Hz, CH_2), 39.0 (CH_2), 38.6 (CH_2), 26.0 (CH_2), 24.5 (CH_2), 19.9 (CH_3), 15.9 (CH_3) ppm.

IR (Film): 3321, 2994, 1641, 1344, 1201, 1126, 753 cm^{-1}.

HRMS (ESI): calc. for $[C_{25}H_{27}O_3N_3BrF_2]^+$: 534.11984; found: 534.12007

***N*-(3-azidopropyl)-3-(3-bromo-4-((2,4-difluorobenzyl)oxy)-6-methyl-2-oxopyridin-1(2*H*)-yl)-4-methylbenzamide (4-14)**

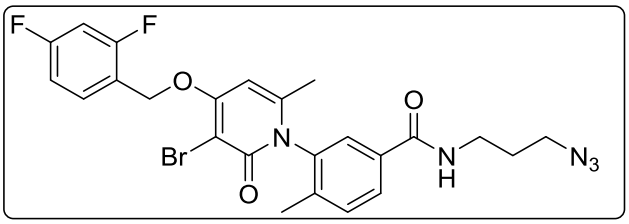

The product was prepared following general procedure A using **4-7** and 3-azidopropan-1-amine as starting materials. The crude was purified by

preparative TLC (3% MeOH/DCM) to obtain the desired product as a white solid (2.5 mg, 2.7 μmol, **3%**).

^{1}H NMR (400 MHz, Chloroform-*d*) δ 7.75 (dd, *J* = 8, 2 Hz, 1H), 7.60 – 7.50 (m, 1H), 7.46 (d, *J* = 2 Hz, 1H), 7.31 (d, *J* = 8 Hz, 1H), 6.95 – 6.87 (m, 1H), 6.84 (t, *J* = 6 Hz, 1H), 6.77 (ddd, *J* = 10, 9, 3 Hz, 1H), 6.08 (s, 1H), 5.14 (s, 2H), 3.47 – 3.10 (m, 4H), 2.03 (s, 3H), 1.86 (d, *J* = 1 Hz, 3H), 1.79 – 1.64 (m, 2H) ppm.

^{13}C NMR (101 MHz, Chloroform-*d*) δ 165.9 (C), 163.2 (C), 160.4 (C), 146.4 (C), 138.6 (C), 137.3 (C), 134.1 (CH), 131.4 (CH), 128.6 (CH), 126.4 (CH), 112.0 (m, CH), 103.9 (m, CH), 96.6 (C), 96.4 (CH), 64.5 (d, J_F = 4 Hz, CH_2), 49.3 (CH_2), 37.5 (CH_2), 28.6 (CH_2), 21.6 (CH_3), 17.3 (CH_3) ppm.

IR (Film): 3334, 2920, 2089 (azide), 1641, 1531, 1349, 1097 cm^{-1}.

HRMS (ESI): calc. for $[C_{24}H_{23}O_3N_5BrF_2]^+$: 546.09469; found: 546.09522

Methyl N^6-(3-(3-bromo-4-((2,4-difluorobenzyl)oxy)-6-methyl-2-oxopyridin-1(2*H*)-yl)-4-methylbenzoyl)-N^2-(tert-butoxycarbonyl)-*L*-lysinate (4-17a)

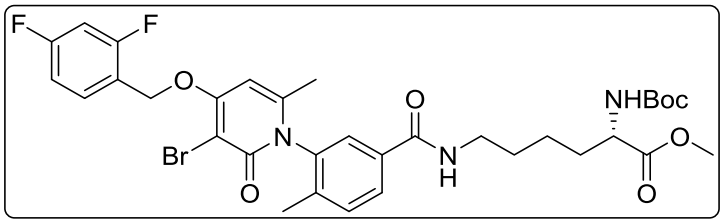

The product was prepared following general procedure A from **4-7** and methyl (tert-butoxycarbonyl)-L-lysinate. The product eluted from the silica column at 70% EtOAc/hexanes, as a white solid (48 mg, 0.068 mmol, **16%**).

^{1}H NMR (CDCl3, 400 MHz): δ 7.79 (d, *J* = 8 Hz, 1H), 7.62 (dd, *J* = 15, 8 Hz, 1H), 7.49 (s, 1H), 7.37 (d, *J* = 8 Hz, 1H), 7.03 – 6.94 (m, 1H), 6.86 (t, *J* = 10 Hz, 1H), 6.63 (s, 1H), 6.15 (s, 1H), 5.24 (s, 2H), 5.12 (s, 1H), 4.33 – 4.19 (m, 1H), 3.72 (d, *J* = 1 Hz, 3H), 3.49 – 3.46 (m, 3H), 3.32 (ddd, *J* = 20, 14, 6.5 Hz, 2H), 2.09 (s, 3H), 1.93 (s, 4H), 1.81 (s, 2H), 1.66 (td, *J* = 14, 8 Hz, 2H), 1.54 (d, *J* = 7 Hz, 3H), 1.45 – 1.35 (m, 12H) ppm.

^{13}C NMR (CDCl3, 101 MHz) δ 173.3 (C), 165.8 (C), 163.3 (C), 160.5 (C), 155.5 (C), 146.6 (C), 138.3 (C), 137.3 (C), 137.2 (C), 134.2 (C), 131.3 (CH), 128.6 (CH), 128.6 (CH), 126.5 (CH), 118.6 (dd, *J* = 15, 4 Hz, C), 111.8 (dd, J_F = 21, 4 Hz, CH), 103.9 (t, J_F = 26 Hz, CH), 96.6 (CH), 96.5 (C), 79.8 (C), 64.4 (d, J_F = 4 Hz, CH_2), 53.4 (CH), 52.2 (CH_3), 39.7 (CH_2), 32.2 (CH_2), 28.8 (CH_2), 28.3 (3 x CH_3), 22.7 (CH_2), 21.6 (CH_3), 17.3 (CH_3) ppm.

^{19}F NMR (CDCl3, 376 MHz): δ -109.11 – -109.49 (m), -114.18 – -114.57 (m) ppm.

HRMS (ESI): calc. for $[C_{33}H_{39}O_5N_2BrF_2]^+$: 706.1979; found: 706.1966.

IR (film): 3306, 2928, 1709, 1643, 1525 cm^{-1}.

Melting Point: 87 - 97 °C.

N^6-(3-(3-bromo-4-((2,4-difluorobenzyl)oxy)-6-methyl-2-oxopyridin-1(2*H*)-yl)-4-methylbenzoyl)-D-lysine (4-17b)

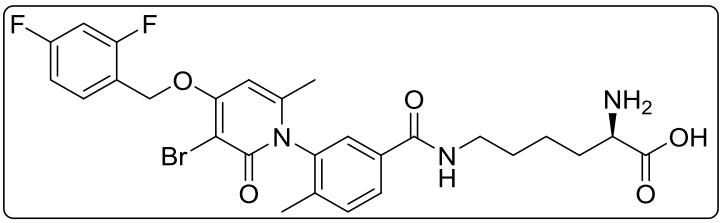

4-18a (67 mg, 0.10 mmol) dissolved in THF (1 mL) and 3M HCl (1 mL) was heated at 69 °C for 45 min. The evolution of the reaction was monitored by TLC. The mixture was concentrated then cooled to 0 °C before addition of 1M NaOH (7 mL) until a white precipitation occurred. The product was then collected by filtration as a white solid (24 mg, 0.041 mmol, **43%**).

1H NMR (DMSO, 400 MHz): δ 8.56 (t, *J* = 6 Hz, 1H), 8.34 (s, 2H), 7.90 (ddd, *J* = 22, 8, 2 Hz, 1H), 7.73 – 7.63 (m, 2H), 7.51 (dd, *J* = 20, 8 Hz, 1H), 7.34 (td, *J* = 11, 3 Hz, 1H), 7.18 (td, *J* = 9, 2 Hz, 1H), 6.73 (d, *J* = 5 Hz, 1H), 5.34 (d, *J* = 4 Hz, 2H), 3.84 (bs, 1H), *(CH_2 signal obscured by H_2O peak)* 1.95 (dd, *J* = 39, 9 Hz, 6H), 1.8 (dq, *J* = 13, 7, 7 Hz, 2H), 1.6 – 1.3 (m, 4H) ppm.

13C NMR (DMSO, 101 MHz): δ 171.4 (C), 166.9 (C), 165.4 (C), 163.7 (C), 159.7 (C), 147.2 (C), 141.0 (C), 138.8 (C), 137.9 (C), 134.2 (C), 132.5 (CH), 131.4 (CH), 129.5 (CH), 127.3 (CH), 119.1 (d, J_F = 14 Hz, CH), 112.3 (dd, J_F = 21, 4 Hz, CH), 104.7 (t, J_F = 26 Hz, CH), 96.7 (C), 95.1 (CH), 65.2 (CH_2), 52.3 (CH), 39.2 (CH_2), 30.1 (CH_2), 29.0 (CH_2), 22.2 (CH_2), 21.3 (CH_3), 17.2 (CH_3) ppm.

19F NMR (DMSO, 376 MHz): δ -109.06 – -109.28 (m), -113.23 (dd, *J* = 19, 9 Hz).

IR (film): 2924, 2843, 1634, 1505, 1345, 1099 cm^{-1}.

HRMS (ESI): calc. for $[C_{27}H_{30}O_5N_2BrF_2]^+$: 592.12532; found: 592.12609

HRMS (ES): *m/z* calc. C27H29BrF2N2O5+ [M+H]+ 592.12532 found 592.12609.

Melting Point: 153 - 160 °C.

3-(Bis(4,5-dimethoxy-2-nitrobenzyl)amino)propan-1-aminium chloride (4-21b)

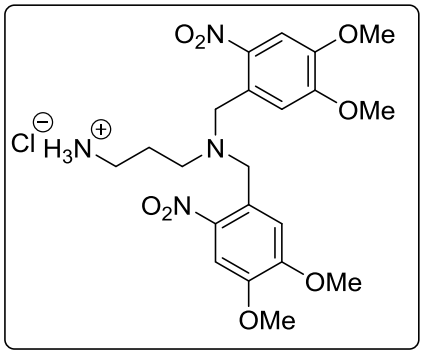

1-(Bromomethyl)-4,5-dimethoxy-2-nitrobenzene (1.1 g, 4.02 mmol) and K_2CO_3 (792 mg, 5.74 mmol) were dissolved in DMF (10 mL) then tert-butyl (3-aminopropyl)carbamate (500 mg, 2.87 mmol) was added and stirred at rt for 20 h. The solution was concentrated under reduced pressure, separated between EtOAc and H_2O. The organic layer was then washed with $CuSO_4$ and brine, then dried over $MgSO_4$, before concentration under reduced pressure to afford a brown oil. 4N HCl in dioxane (2 mL, 8 mmol) was then added at 0 °C and stirred for 2 h. The mixture was then concentrated under reduced pressure to afford a brown gum. Purification by flash column chromatography (elution at 2% MeOH/EtOAc) afforded product as a yellow oily solid (550 mg, 1.10 mmol, **38%**).

^{1}H NMR (400 MHz, Methanol-*d*$_4$) δ 7.85 (s, 2H), 7.42 (s, 2H), 4.96 (d, *J* = 13 Hz, 2H), 4.77 (d, *J* = 13 Hz, 2H), 4.04 (s, 6H), 3.95 (s, 6H), 3.57 – 3.51 (m, 2H), 3.05 (t, *J* = 8 Hz, 2H), 2.41 (s, 2H) ppm.

^{13}C NMR (101 MHz, Methanol-*d*$_4$) δ 154.2 (2 x C), 150.6 (2 x C), 141.7 (2 x C), 118.7 (2 x C), 116.8 (2 x CH), 108.8 (2 x CH), 56.2 (2 x CH_2), 56.2 (2 x CH_3), 55.6 (2 x CH_3), 51.8 (CH_2), 36.5 (CH_2), 22.4 (CH_2) ppm.

IR (Film): 3395, 2925, 1527, 1284, 1062, 748 cm^{-1}.

HRMS (ESI): calc. for $[C_{21}H_{29}O_8N_4]^+$: 465.19799; found: 465.19753

***N*-(3-(bis(4,5-dimethoxy-2-nitrobenzyl)amino)propyl)-3-(3-bromo-4-((2,4-difluorobenzyl)oxy)-6-methyl-2-oxopyridin-1(2*H*)-yl)-4-methylbenzamide (4-13b)**

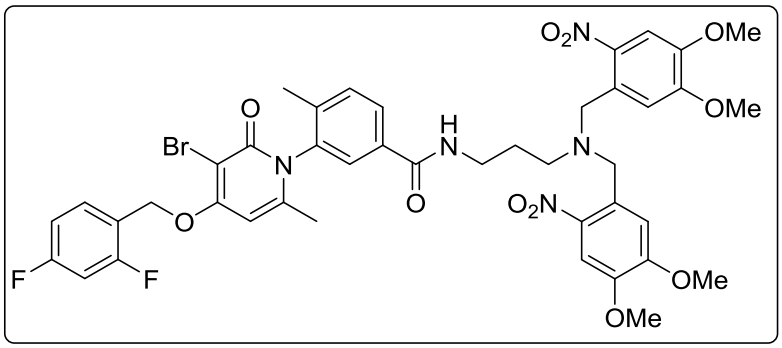

The product was prepared following general procedure A using **4-7** and **4-21b**. Product eluted at 85% EtOAc/hexanes as a yellow white solid (206 mg, 0.226 mmol, **33%**).

^{1}H NMR (400 MHz, Chloroform-*d*) δ 7.73 (dd, *J* = 8, 2 Hz, 1H), 7.58 (td, *J* = 9, 6 Hz, 1H), 7.50 (d, *J* = 2 Hz, 1H), 7.41 (s, 2H), 7.28 (dd, *J* = 8, 1 Hz, 1H), 7.06 (s, 2H), 7.04 (t, *J* = 6 Hz, 1H), 6.98 – 6.91

(m, 1H), 6.81 (ddd, *J* = 10, 9, 3 Hz, 1H), 6.13 (d, *J* = 1 Hz, 1H), 5.17 (s, 2H), 3.92 (s, 4H), 3.90 (s, 6H), 3.86 (s, 6H), 3.31 (dq, *J* = 13, 7 Hz, 1H), 3.09 (dt, *J* = 13, 7 Hz, 1H), 2.52 (td, *J* = 9, 8, 2 Hz, 2H), 2.03 (s, 3H), 1.88 (d, *J* = 1 Hz, 3H), 1.76 (q, *J* = 8 Hz, 2H) ppm.

^{13}C NMR (101 MHz, Chloroform-*d*) δ 165.5 (C), 164.2 (d, J_F = 12 Hz, C), 163.3 (C), 161.4 (dd, J_F = 59, 12 Hz, C), 160.4 (C), 158.6 (d, J_F = 12 Hz, C), 152.9 (2 x C), 147.4 (2 x C), 146.6 (C), 141.3 (2 x C), 138.2 (C), 137.2 (C), 134.1 (C), 131.2 (CH), 130.0 (C), 129.9 – 129.7 (m, CH), 128.6 (CH), 126.4 (CH), 118.5 (dd, *J* = 14, 4 Hz, C), 112.0 – 111.5 (m, 3 x CH), 108.0 (2 x CH), 103.9 (t, J_F = 25 Hz, CH), 96.5 (CH), 96.4 (C), 64.5 (d, J_F = 4 Hz, CH_2), 56.4 (2 x CH_2), 56.3 (2 x CH_3), 56.2 (2 x CH_2), 53.4 (CH_2), 38.2 (CH_2), 26.6 (CH_2), 21.6 (CH_3), 17.2 (CH_3) ppm.

IR (Film): 3334, 2933, 2250, 1654, 1510, 1340, 735 cm^{-1}.

HRMS (ESI): calc. for $[C_{45}H_{45}O_{12}N_2BrF_2]^+$: 910.21185; found: 910.21390.

3-((4,5-Dimethoxy-2-nitrobenzyl)oxy)propan-1-amine

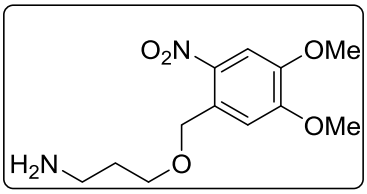

Product was prepared as for **4-13b** using 3-aminopropan-1-ol and 1-(bromomethyl)-4,5-dimethoxy-2-nitrobenzene. Product was afforded as a yellow oil (205 mg, 0.674 mmol, **24%**).

^{1}H NMR (400 MHz, Chloroform-*d*) δ 7.63 (s, 1H), 7.12 (s, 1H), 4.96 (bs, 1H), 4.04 (s, 2H), 3.99 (s, 3H), 3.94 (s, 3H), 3.24 (q, *J* = 7 Hz, 2H), 2.72 (t, *J* = 7 Hz, 2H), 1.71 (dd, *J* = 8, 5 Hz, 2H) ppm.

^{13}C NMR (101 MHz, Chloroform-*d*) δ 156.0 (C), 153.3 (C), 147.6 (C), 140.9 (C), 112.4 (CH), 108.2 (CH), 56.4 (CH_3), 56.4 (CH_3), 51.2 (CH_2), 47.3 (CH_2), 39.1 (CH_2), 30.1 (CH_2) ppm.

IR (Film): 3356, 2973, 1645, 1523, 1271, 728 cm^{-1}.

HRMS (ESI): calc. for $[C_{33}H_{33}O_8N_3BrF_2]^+$: 716.14136; found: 716.14381

3-(3-Bromo-4-((2,4-difluorobenzyl)oxy)-6-methyl-2-oxopyridin-1(2*H*)-yl)-*N*-(3-((4,5-dimethoxy-2-nitrobenzyl)oxy)propyl)-4-methylbenzamide (4-12b)

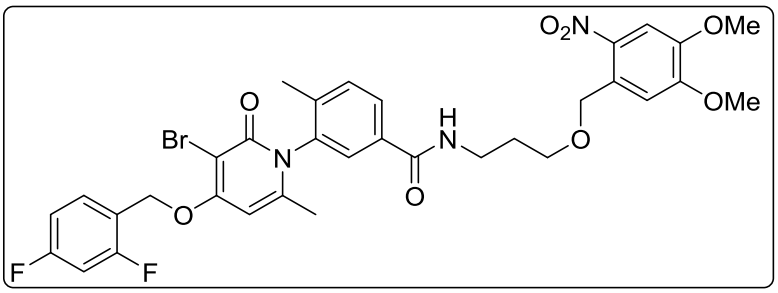

The product was prepared following general procedure A using **4-7** and **4-20c**. Product eluted at 75%

EtOAc/hexanes as a yellow white solid (107 mg, 0.150 mmol, **34%**).

^{1}H NMR (400 MHz, Chloroform-*d*) δ 7.73 (dd, *J* = 8, 2 Hz, 1H), 7.67 (s, 1H), 7.61 (td, *J* = 9, 6 Hz, 1H), 7.53 (d, *J* = 2 Hz, 1H), 7.34 – 7.29 (m, 1H), 7.23 (s, 1H), 7.00 – 6.93 (m, 2H), 6.84 (ddd, *J* = 10, 9, 3 Hz, 1H), 6.12 (d, *J* = 1 Hz, 1H), 5.22 (d, *J* = 1 Hz, 2H), 4.87 (d, *J* = 1 Hz, 2H), 3.95 (s, 3H), 3.94 (s, 3H), 3.68 (t, *J* = 6 Hz, 2H), 3.54 (dq, *J* = 13, 7 Hz, 1H), 3.41 (dq, *J* = 12, 7 Hz, 1H), 2.07 (s, 3H), 1.96 – 1.86 (m, 5H) ppm.

^{13}C NMR (101 MHz, Chloroform-d) δ 165.8 (C), 163.2 (C), 160.4 (C), 152.8 (C), 147.5 (C), 146.3 (C), 141.5 (C), 138.6 (CH), 137.5 (CH), 134.2 (CH), 131.4 (CH), 130.3 – 129.9 (m, CH), 129.8 (CH), 128.2 (CH), 126.5 (CH), 112.0 (d, J_F = 5 Hz, CH), 112.0 – 111.7 (m, CH), 108.0 (CH), 103.9 (t, J_F = 25 Hz, CH), 96.7 (CH), 96.3 (C), 64.4 (d, J_F = 4 Hz, CH_2), 56.4 (2 x CH_3), 53.3 (CH_2), 38.1 (CH_2), 26.8 (CH_2), 21.6 (CH_3), 17.3 (CH_3) ppm.

^{19}F NMR (376 MHz, Chloroform-*d*) δ -109.28 (p, *J* = 8 Hz), -114.48 (q, *J* = 8 Hz).

IR (Film): 3334, 2920, 1645, 1523, 1271, 728 cm^{-1}.

HRMS (ESI): calc. for $[C_{33}H_{33}O_8N_3BrF_2]^+$: 716.14136; found: 716.14381

2-(2-(2-(3-(3-Bromo-4-((2,4-difluorobenzyl)oxy)-6-methyl-2-oxopyridin-1(2*H*)-yl)-4-methylbenzamido)ethoxy)ethoxy)ethan-1-aminium chloride (4-19)

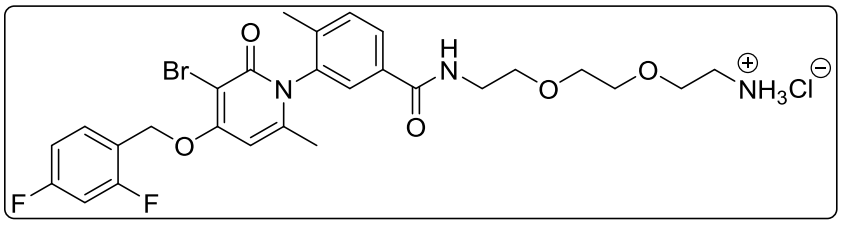

As for **4-16.**

Product as an off white powder.

3-(3-Bromo-4-((2,4-difluorobenzyl)oxy)-6-methyl-2-oxopyridin-1(2*H*)-yl)-*N*-((2,2-dimethyl-1,3-dioxolan-4-yl)methyl)-4-methylbenzamide (4-10)

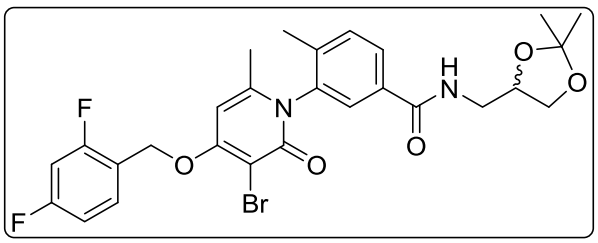

The product was prepared following general method A using **4-7** and (2,2-dimethyl-1,3-dioxolan-4-yl)methanamine. Product eluted from the column at 80% EtOAc/hexanes as a white solid (150 mg, 0.260 mmol, **40%**).

^{1}H NMR (400 MHz, Chloroform-*d*) δ 7.69 (ddd, *J* = 17.3, 7.9, 1.8 Hz, 1H), 7.54 (td, *J* = 8.5, 6.3 Hz, 1H), 7.48 (dd, *J* = 8.3, 1.9 Hz, 1H), 7.31 (dd, *J* = 10, 8 Hz, 1H), 6.95 – 6.87 (m, 1H), 6.80 (ddt, *J* = 11, 9, 2 Hz, 1H), 6.80 (ddt, *J* = 11, 9, 2 Hz, 1H), 6.72 (dt, *J* = 26, 6 Hz, 1H), 6.07 (d, *J* = 1 Hz, 1H), 5.18 (s, 2H), 4.20 (dddd, *J* = 11, 6, 6, 1 Hz, 1H), 3.99 (ddd, *J* = 9, 6, 5 Hz, 1H), 3.67 – 3.58 (m, 1H), 3.53 (ddd, *J* = 14, 6, 4 Hz, 1H), 3.31 (dddd, *J* = 37, 14, 6, 5 Hz, 1H), 2.04 (s, 3H), 1.85 (dd, *J* = 2, 1 Hz, 3H), 1.35 (d, *J* = 3 Hz, 3H), 1.27 (s, 3H) ppm.

^{13}C NMR (101 MHz, Chloroform-*d*) δ 166.3 (d, *J* = 8 Hz, C), 163.1 (d, *J* = 1 Hz, C), 160.4 (d, *J* = 5 Hz, C), 146.1 (d, *J* = 4 Hz, C), 139.0 (d, *J* = 9 Hz, C), 137.7 (d, *J* = 4 Hz, C), 133.9 (d, *J* = 10 Hz, C), 131.5 (d, *J* = 5 Hz, CH), 130.5 – 130.0 (m, CH), 128.0 (d, *J* = 25 Hz, CH), 126.7 (d, *J* = 21 Hz, CH), 118.8 – 118.3 (m, C), 111.9 (dd, *J* = 22, 4 Hz, CH), 109.4 (d, *J* = 2 Hz, C), 104.3 – 103.4 (m, CH), 96.9 (d, *J* = 2 Hz, CH), 96.2 (d, *J* = 3 Hz, C), 74.5 (d, *J* = 13 Hz, CH), 67.1 (d, *J* = 6 Hz, CH_2), 64.3 (d, *J* = 4 Hz, CH_2), 42.5 (d, *J* = 16 Hz, CH_2), 26.9 (d, *J* = 2 Hz, CH_3), 25.3 (d, *J* = 4 Hz, CH_3), 21.5 (d, *J* = 2Hz, CH_3), 17.4 (d, *J* = 1 Hz, CH_3) ppm.

IR (Film): 3325, 2985, 1640, 1527, 1336, 1036, 726 cm^{-1}.

HRMS (ESI): calc. for $[C_{27}H_{28}O_5N_2BrF_2]^+$: 577.11442; found: 577.11424

Methyl 6-(3-(3-bromo-4-((2,4-difluorobenzyl)oxy)-6-methyl-2-oxopyridin-1(2*H*)-yl)-4-methylbenzamido)hexanoate (4-18a)

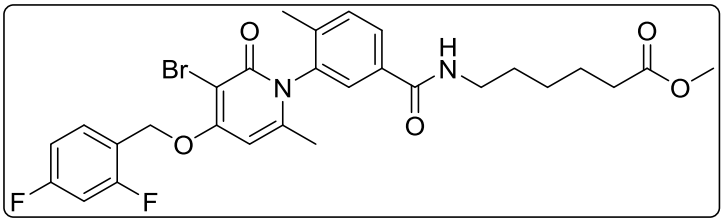

The product was prepared following general method A using **4-7** and methyl 6-aminohexanoate. Product eluted from the column at 80% EtOAc/hexanes as a white solid (174 mg, 0.294 mmol, **27%**).

^{1}H NMR (400 MHz, Chloroform-*d*) δ 7.80 (dd, *J* = 8, 2 Hz, 1H), 7.61 (td, *J* = 9, 6 Hz, 1H), 7.51 (d, *J* = 2 Hz, 1H), 7.42 – 7.31 (m, 1H), 7.01 – 6.91 (m, 1H), 6.83 (ddd, *J* = 10, 9, 3 Hz, 1H), 6.72 (t, *J* = 6 Hz, 1H), 6.14 (d, *J* = 1 Hz, 1H), 5.21 (s, 2H), 3.64 (s, 3H), 3.39 – 3.15 (m, 2H), 2.30 (t, *J* = 8 Hz, 2H), 2.08 (s, 3H), 1.92 (s, 2H), 1.63 (dt, *J* = 15, 8 Hz, 2H), 1.56 – 1.44 (m, 2H), 1.41 – 1.30 (m, 2H) ppm.

^{13}C NMR (101 MHz, Chloroform-*d*) δ 174.1 (C), 165.7 (C), 164.2 (d, J_F = 12 Hz, C), 163.2 (C), 161.4 (dd, J_F = 57, 12 Hz, C), 160.4 (C), 158.7 (d, *J* = 12 Hz, C), 146.4 (C), 138.3 (C), 137.3 (C), 134.4 (C), 131.3 (CH), 129.9 (dd, J_F = 10, 5 Hz, CH), 128.5 (CH), 126.3 (CH), 118.7 – 118.4 (m, C),

111.9 (dd, J_F = 21, 4 Hz, CH), 104.4 – 103.3 (m, CH), 96.6 (C), 96.3 (CH), 64.4 (d, J_F = 4 Hz, CH_2), 51.5 (CH_3), 39.8 (CH_2), 33.9 (CH_2), 28.9 (CH_2), 26.4 (CH_2), 24.5 (CH_2), 21.6 (CH_3), 17.3 (CH_3) ppm.

IR (Film): 3337, 2946, 1740, 1644, 1349, 1100, 727 cm^{-1}.

HRMS (ESI): calc. for $[C_{33}H_{33}O_8N_3BrF_2]^+$: ; found:

Methyl 4-(3-formyl-4-nitrophenoxy)butanoate Nv (4-42)

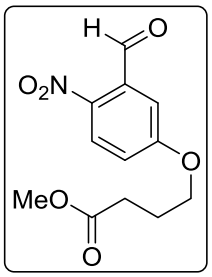

To 5-hydroxy-2-nitrobenzaldehyde (**4-40,** 1.0 g, 6.00 mmol) and K_2CO_3 (**4-41,** 0.45 g, 3.29 mmol) in DMF (8.5 mL) was added methyl 4-bromobutanoate (1.0 g, 5.68 mmol) then heated 85 °C for 5 h. Some remaining starting materials were observed by TLC. The reaction mixture was stirred at 75 °C for 18 h, then separated between EtOAc and H_2O. The organic layer was washed with H_2O (x4) then brine, dried over $MgSO_4$, then concentrated under reduced pressure to afford a brown oil (1.59 g, 6.00 mmol, **100%**).

^{1}H NMR (400 MHz, Chloroform-*d*) δ 10.48 (s, 1H), 8.15 (d, *J* = 9 Hz, 1H), 7.31 (d, *J* = 3 Hz, 1H), 7.13 (dd, *J* = 9, 3 Hz, 1H), 4.16 (t, *J* = 6 Hz, 2H), 3.71 (s, 3H), 2.54 (t, *J* = 7 Hz, 2H), 2.23 – 2.11 (m, 2H) ppm.

The NMR spectra were consistent with that reported in the literature.[10,11]

Methyl 4-(3-(((3-(3-(3-bromo-4-((2,4-difluorobenzyl)oxy)-6-methyl-2-oxopyridin-1(2*H*)-yl)-4-methylbenzamido)propyl)amino)methyl)-4-nitrophenoxy)butanoate (4-43a)

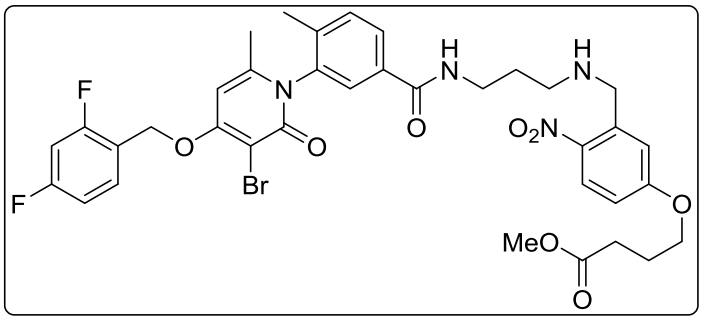

To a flask charged with molecular sieves (4Å, 500 mg), **4-42** (300 mg, 1.12 mmol), **4-13a** (656 mg, 1.18 mmol), pyrrolidine (0.87 mL, 0.11 mmol) dissolved in THF (11 mL) was heated at 60 °C for 7 h. At this point minimal remaining amine starting material remained by TLC. The reaction mixture was cooled to 0 °C then $NaBH_3$ (64 mg, 1.68 mmol) and MeOH (10 mL) were added. The mixture was allowed to warm to rt for 1 hour before quenching with $NaHCO_3$ (aq). The organics were extracted using EtOAc (x2), then washed with brine, dried over $MgSO_4$, then concentrated under reduced

pressure to afford a brown oil. The product was purified by flash column chromatography (eluting at 5% MeOH/DCM) as a beige/yellow foamy solid (509 mg, 0.66 mmol, **60%**).

^{1}H NMR (400 MHz, Chloroform-*d*) δ 7.97 (d, *J* = 9 Hz, 1H), 7.65 (dd, *J* = 8, 2 Hz, 1H), 7.55 (td, *J* = 9, 6 Hz, 1H), 7.45 (d, *J* = 2 Hz, 1H), 7.42 (t, *J* = 6 Hz, 1H), 7.27 – 7.23 (m, 1H), 6.98 (d, *J* = 3 Hz, 1H), 6.93 – 6.86 (m, 1H), 6.81 (d, *J* = 3 Hz, 1H), 6.79 – 6.74 (m, 2H), 6.07 (s, 1H), 5.17 (s, 2H), 4.03 – 3.98 (m, 4H), 3.61 (s, 3H), 3.39 (dddt, *J* = 25, 20, 13, 6 Hz, 2H), 2.69 (td, *J* = 6, 2 Hz, 2H), 2.45 (t, *J* = 7 Hz, 2H), 2.10 – 2.03 (m, 2H), 2.02 (s, 3H), 1.85 (d, *J* = 1 Hz, 3H), 1.68 (p, *J* = 6 Hz, 2H) ppm.

^{13}C NMR (101 MHz, Chloroform-*d*) δ 173.4 (C), 165.9 (C), 163.1 (C), 162.7 (C), 160.3 (C), 158.8 (d, J_F = 13 Hz, C), 146.3 (C), 141.7 (C), 138.6 (C), 137.6 (C), 134.2 (C), 131.3 (CH), 130.5 – 129.9 (m, CH), 128.0 (CH), 127.9 (CH), 126.6 (CH), 118.6 (dd, *J* = 14, 4 Hz, C), 116.6 (CH), 113.3 (CH), 112.6 – 111.3 (m, CH), 103.9 (t, J_F = 25 Hz, CH), 96.7 (C), 96.2 (CH), 67.5 (CH_2), 64.4 (d, J_F = 4 Hz, CH_2), 51.7 (CH_3), 51.5 (CH_2), 47.6 (CH_2), 38.9 (CH_2), 30.2 (CH_2), 28.8 (CH_2), 24.3 (CH_2), 21.6 (CH_3), 17.3 (CH_3) ppm. 2 C not visible

IR (Film): 3330, 2951, 1641, 1497, 1340, 1036, 744 cm^{-1}.

HRMS (ESI): calc. for $[C_{36}H_{38}O_8N_4BrF_2]^+$: 771.183560; found: 771.18326.

4-(3-(((3-(3-(3-Bromo-4-((2,4-difluorobenzyl)oxy)-6-methyl-2-oxopyridin-1(2*H*)-yl)-4-methylbenzamido)propyl)amino)methyl)-4-nitrophenoxy)butanoic acid (4-43b)

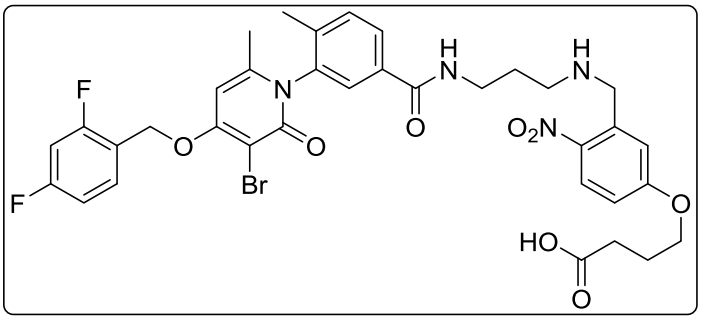

The product was prepared as for **4-7,** starting from **4-43a** Product eluted at 12% MeOH/DCM as a cream solid (260 mg, 0.343 mmol, **53%**).

^{1}H NMR (400 MHz, Methanol-d_4) δ 8.27 (d, *J* = 9 Hz, 1H), 7.85 (dd, *J* = 8, 2 Hz, 1H), 7.67 (td, *J* = 8, 6 Hz, 1H), 7.57 – 7.50 (m, 2H), 7.27 (d, *J* = 3 Hz, 1H), 7.15 (dd, *J* = 9, 3 Hz, 1H), 7.09 – 7.01 (m, 2H), 6.70 (d, *J* = 1 Hz, 1H), 5.38 (s, 2H), 4.59 – 4.43 (m, 2H), 4.19 (t, *J* = 6 Hz, 2H), 3.51 (hept, *J* = 8, 7 Hz, 2H), 3.20 (td, *J* = 7, 4 Hz, 2H), 2.45 (t, *J* = 7 Hz, 2H), 2.13 – 2.03 (m, 7H), 2.01 (d, *J* = 1 Hz, 3H) ppm.

^{13}C NMR (101 MHz, Methanol-*d*$_4$) δ 168.0 (C), 164.6 (C), 163.4 (C), 162.4 – 161.4 (m, C), 161.0 (C), 160.0 – 159.3 (m, C), 147.2 (C), 141.2 (C), 139.7 (C), 139.5 – 139.2 (m, C), 137.7 (C), 132.9 (C), 131.7 – 131.0 (m, CH), 129.2 (C), 128.3 (CH), 127.9 (CH), 126.9 (CH), 119.6 (CH), 119.2 – 118.8 (m, CH), 115.5 (CH), 111.2 (dd, J_F = 22, 4 Hz, CH), 103.5 (t, J_F = 26 Hz, CH), 97.3 (CH), 95.3 (C), 68.2 (CH_2), 64.9 – 64.7 (m, CH_2), 49.3 (CH_2), 45.3 (CH_2), 36.0 (CH_2), 26.4 (CH_2), 24.3 (CH_2), 20.0 (CH_3), 15.9 (CH_3) ppm. One CH2, and one C not observed.

IR (Film): 3325, 2933, 1632, 1504, 1340, 1196 cm^{-1}.

HRMS (ESI): calc. for $[C_{35}H_{36}O_8N_4BrF_2]^+$: 757.16791; found: 757.16825

3-(3-Bromo-4-((2,4-difluorobenzyl)oxy)-6-methyl-2-oxopyridin-1(2*H*)-yl)-*N*-(but-3-yn-1-yl)-4-methylbenzamide (4-72c)

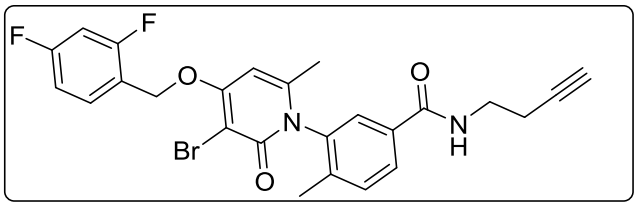

Compound synthesised using method B using **4-7** and but-3-yn-1-aminium chloride. The product eluted from the silica column at 70% EtOAc/hexanes, as a white solid (92 mg, 0.179 mmol, **50 %**).

TLC: R_f = 0.63 (80% EtOAc/hexanes)

^{1}H NMR (400 MHz, Chloroform-*d*) δ 7.73 (dd, *J* = 8, 2 Hz, 1H), 7.54 (td, *J* = 8, 6 Hz, 1H), 7.45 (d, *J* = 2 Hz, 1H), 7.31 (dd, *J* = 8, 1 Hz, 1H), 6.90 (tdd, *J* = 9, 3, 1 Hz, 1H), 6.85 (NH, t, *J* = 6 Hz, 1H), 6.78 (ddd, *J* = 10, 9, 3 Hz, 1H), 6.08 (d, *J* = 1 Hz, 1H), 5.16 (s, 2H), 3.38 (dtd, *J* = 43, 13, 7 Hz, 2H), 2.34 (td, *J* = 7, 3 Hz, 2H), 2.03 (s, 3H), 1.92 (t, *J* = 3 Hz, 1H), 1.85 (s, 3H) ppm.

^{13}C NMR (101 MHz, Chloroform-*d*) δ 165.8 (C), 164.2 (d, J_F = 12 Hz, C), 163.2 (C), 161.5 (dd, J_F = 56, 12 Hz, C), 160.4 (C), 158.7 (d, J_F = 12 Hz, C), 146.3 (C), 138.7 (C), 137.5 (C), 134.1 (C), 131.4 (CH), 130.0 (dd, J_F = 10, 5 Hz, CH), 128.4 (CH), 126.5 (CH), 118.5 (dd, J_F = 14, 4 Hz, C), 111.9 (dd, J_F = 21, 4 Hz, CH), 104.3 – 103.5 (m, CH), 96.3 (CH), 81.6 (C), 69.8 (CH), 64.4 (d, J_F = 4 Hz, CH_2), 38.8 (CH_2), 21.6 (CH_3), 19.2 (CH_2), 17.3 (CH_3) ppm.

IR (NaCl) υ_{max}: 3304, 2933, 1649, 1527, 1349, 1088 cm^{-1}.

HRMS (ESI): calc. for $[C_{25}H_{22}O_3N_2BrF_2]^+$: 515.07764, found 515.07740.

3-(3-Bromo-4-((2,4-difluorobenzyl)oxy)-6-methyl-2-oxopyridin-1(2*H*)-yl)-4-methyl-*N*-(pent-4-yn-1-yl)benzamide (4-72b)

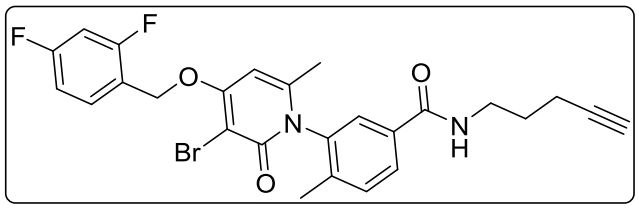

Compound synthesised using method B using **4-7** and pent-4-yn-1-aminium chloride. The product eluted from the silica column at 70% EtOAc/hexanes, as a white solid (139 mg, 262 mmol, **73%**).

TLC: R_f = 0.43 (80% EtOAc/hexanes)

^{1}H NMR (400 MHz, Chloroform-*d*) δ 7.82 (dd, *J* = 8, 2 Hz, 1H), 7.61 (td, *J* = 9, 6 Hz, 1H), 7.54 (d, *J* = 2 Hz, 1H), 7.37 (dd, *J* = 8, 1 Hz, 1H), 7.00 – 6.93 (m, 1H), 6.91 (NH, t, *J* = 6 Hz, 1H), 6.83 (ddd, *J* = 10, 9, 3 Hz, 1H), 6.14 (d, *J* = 1 Hz, 1H), 5.20 (s, 2H), 3.45 – 3.25 (m, 2H), 2.22 (td, *J* = 7, 3 Hz, 2H), 2.08 (s, 3H), 1.96 (t, *J* = 3 Hz, 1H), 1.92 (d, *J* = 1 Hz, 3H), 1.71 (p, *J* = 7 Hz, 2H) ppm.

^{13}C NMR (101 MHz, Chloroform-*d*) δ 165.8 (C), 164.2 (d, J_F = 12 Hz, C), 163.2 (C), 161.4 (dd, J_F = 60, 12 Hz, C), 160.3 (C), 158.6 (d, J_F = 12 Hz, C), 146.5 (C), 138.4 (C), 137.3 (C), 134.2 (C), 131.4 (CH), 129.8 (dd, J_F = 10, 5 Hz, CH), 128.7 (CH), 126.4 (CH), 118.5 (dd, J_F = 14, 4 Hz, C), 111.9 (dd, J_F = 21, 4 Hz, CH), 103.9 (t, J_F = 25 Hz, CH), 96.4 (CH), 83.9 (C), 68.9 (CH), 64.4 (d, J_F = 4 Hz, CH_2), 39.3 (CH_2), 27.9 (CH_2), 21.6 (CH_3), 17.3 (CH_3), 16.2 (CH_2) ppm.

IR (NaCl) υ_{max}: 3299, 2929, 1644, 1527, 1340, 1088 cm^{-1}

HRMS (ESI): calc. for $[C_{26}H_{24}O_3N_2BrF_2]^+$: 529.09329, found 529.09285

3-(5-Bromo-4-((2,4-difluorobenzyl)oxy)-6-methyl-2-oxopyridin-1(2*H*)-yl)-*N*-(hex-5-yn-1-yl)-4-methylbenzamide (4-72a)

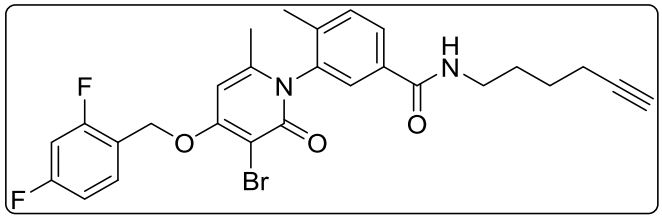

Compound synthesised using method B using **4-7** and hex-5-yn-1-aminium chloride. The product eluted from the silica column at 70% EtOAc/hexanes, as a light beige, foamy solid (631 mg, 1.16 mmol, **77%**).

TLC: R_f = 0.36 (50% EtOAc/hexanes)

^{1}H NMR (400 MHz, Chloroform-*d*) δ 7.79 (dd, *J* = 8, 2 Hz, 1H), 7.61 (td, *J* = 9, 6 Hz, 1H), 7.50 (d, *J* = 2 Hz, 1H), 7.36 (dd, *J* = 8, 1 Hz, 1H), 7.01 – 6.92 (m, 1H), 6.84 (ddd, *J* = 10, 9, 3 Hz, 1H), 6.74 (NH, t, *J* = 6 Hz, 1H), 6.14 (d, *J* = 1 Hz, 1H), 5.22 (d, *J* = 1 Hz, 2H), 3.39 – 3.21 (m, 2H), 2.21 (td, *J* = 7, 3 Hz, 2H), 2.08 (s, 3H), 1.94 (t, *J* = 3 Hz, 1H), 1.92 (d, *J* = 2 Hz, 3H), 1.66 – 1.52 (m, 3H) ppm.

^{13}C NMR (101 MHz, Chloroform-*d*) δ 165.9 (C), 164.2 (d, J_F = 12 Hz, C), 163.2 (C), 161.4 (dd, J_F = 57, 12 Hz, C), 160.4 (C), 158.7 (d, J_F = 12 Hz, C), 146.4 (C), 138.4 (C), 137.3 (C), 134.4 (C), 131.4 (CH), 130.0 (dd, J_F = 10, 5 Hz, CH), 128.5 (CH), 126.4 (CH), 118.5 (dd, J_F = 14, 4 Hz, C), 111.9 (dd, J_F = 21, 4 Hz, CH), 103.9 (t, J_F = 25 Hz, CH), 96.3 (CH), 84.2 (C), 68.6 (CH), 64.4 (d, J_F = 4 Hz, CH_2), 39.6 (CH_2), 28.4 (CH_2), 25.8 (CH_2), 21.6 (CH_3), 18.1 (CH_2), 17.3 (CH_3) ppm.

IR (NaCl) υ_{max}: 3304, 2925, 1640, 1527, 1340, 1101 cm^{-1}

HRMS (ESI): calc. for $[C_{27}H_{26}O_3N_2BrF_2]^+$: 543.10894 found 543.10700

2-(2,6-Dioxopiperidin-3-yl)-4-fluoroisoindoline-1,3-dione (4-59)

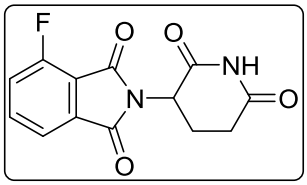

A boiling tube charged with 4-fluoroisobenzofuran-1,3-dione (**4-58,** 1.2 g, 7.22 mmol), 2,6-dioxopiperidin-3-aminium chloride (1.33 g, 8.092 mmol), KOAc (1.49 g, 15.171 mmol) and AcOH (16 mL) was sealed and heated to 110 °C for 24 h. The reaction mixture was then concentrated and the dark blue crude solid obtained was purified using flash column chromatography. The product eluted at 4% MeOH/DCM, affording a white solid, (1.75 g, 6.34 mmol, **88%**).

The NMR spectra were consistent with that reported in the literature.[12]

^{1}H NMR (400 MHz, Chloroform-*d*) δ 8.10 (s, 1H), 7.77 (ddd, *J* = 8, 7, 4 Hz, 1H), 7.71 (dt, *J* = 7, 1 Hz, 1H), 7.43 (td, *J* = 9, 1 Hz, 1H), 5.02 – 4.95 (m, 1H), 2.96 – 2.70 (m, 3H), 2.20 – 2.12 (m, 1H) ppm.

4-Fluoro-2-(1-(2-nitrobenzyl)-2,6-dioxopiperidin-3-yl)isoindoline-1,3-dione (4-59Nv)

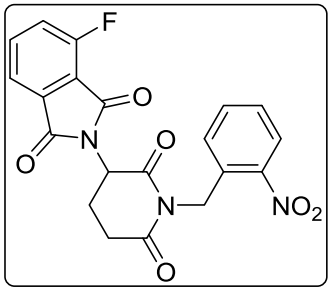

To a solution of **655** (87 mg, 0.32 mmol) in DMF (2.5 mL) was added K_2CO_3 (87 mg, 0.63 mmol) and 1-(bromomethyl)-2-nitrobenzene (102 mg, 0.47 mmol). The reaction mixture was heated at 60 °C for 20 h, then separated between EtOAc and water. The aqueous layer was re-extracted (x2) using EtOAc, then the combined organic layers

were washed with brine (x3), dried over $MgSO_4$, and then concentrated under reduced pressure. The crude was purified by flash column chromatography, product eluted at 45% EtOAc/hexanes as an off-white solid, (120 mg, 0.29 mmol, **93%**).

TLC: $\mathbf{R_f}$ = 0.39 (50% EtOAc/Hexanes)

^{1}H NMR (400 MHz, Chloroform-*d*) δ 7.97 (dd, *J* = 8, 1 Hz, 1H), 7.70 (ddd, *J* = 8, 7, 4 Hz, 1H), 7.65 – 7.62 (m, 1H), 7.57 (td, *J* = 7, 1 Hz, 1H), 7.39 – 7.32 (m, 2H), 7.25 (dd, *J* = 8, 1 Hz, 1H), 5.32 (s, 2H), 5.06 – 4.99 (m, 1H), 3.04 – 2.95 (m, 1H), 2.85 – 2.76 (m, 2H), 2.19 – 2.09 (m, 1H) ppm.

^{13}C NMR (101 MHz, Chloroform-*d*) δ 169.4 (C), 166.1 (C), 164.1 (C), 159.5 (C), 156.5 (C), 148.5 (C), 147.1 (C), 137.1 (d, J_F = 8 Hz, CH), 133.8 (CH), 131.8 (C), 128.0 (CH), 127.6 (CH), 125.0 (CH), 122.9 (d, J_F = 20 Hz, CH), 120.1 (d, J_F = 4 Hz, CH), 50.1 (CH), 41.1 (CH_2), 31.8 (CH_2), 21.8 (CH_2) ppm.

IR (NaCl) υ_{max}: 3242, 2911, 1723, 1684, 1388, 1179 cm^{-1}

HRMS (ESI): calc. for $[C_{20}H_{15}O_6N_3F]^+$: 412.09394, found 412.09416.

***Tert*-butyl (2-((2-(2,6-dioxopiperidin-3-yl)-1,3-dioxoisoindolin-4-yl)amino)ethyl)carbamate (4-61c)**

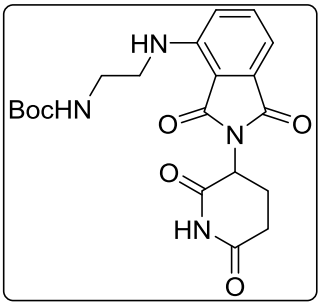

To a solution of **4-59** (200 mg, 0.724 mmol) in NMP (5 mL) in a boiling tube was added DIPEA (0.25 mL, 1.45 mmol) and *tert*-butyl (2-aminoethyl)carbamate (0.13 mL, 0.869 mmol), sealed, then heated to 110 °C for 20 h. The mixture was then separated between EtOAc and water. The aqueous layer was re-extracted using EtOAc. The combined organic layers were then washed with brine (x2), 10% $CuSO_4$, brine, dried over $MgSO_4$, then concentrated under reduced pressure. The crude was purified by flash column chromatography, product eluted at 70% EtOAc/hexanes as a fluorescent yellow solid, (180 mg, 0.432 mmol, **60%**).

The NMR spectra were consistent with that reported in the literature.[12,13]

^{1}H NMR (400 MHz, Chloroform-*d*) δ 8.17 (bs, 1H), 7.53 – 7.46 (m, 1H), 7.11 (dd, *J* = 7, 1 Hz, 1H), 6.98 (d, *J* = 8 Hz, 1H), 6.39 (t, *J* = 6 Hz, 1H), 4.92 (dd, *J* = 12, 5 Hz, 1H), 4.87 (bs, 1H), 3.49 – 3.32 (m, 4H), 2.93 – 2.67 (m, 3H), 2.16 – 2.08 (m, 1H), 1.44 (s, 9H) ppm.

***Tert*-butyl (3-((2-(2,6-dioxopiperidin-3-yl)-1,3-dioxoisoindolin-4-yl)amino)propyl)carbamate (4-61b)**

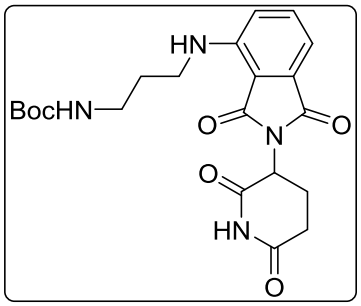

The product was afforded by employing the reaction conditions of **4-61c**, using *tert*-butyl (3-aminopropyl)carbamate. The crude was purified by flash column chromatography, product eluted at 72% EtOAc/hexanes as a fluorescent yellow solid, (220 mg, 0.513 mmol, **71%**).

The NMR spectra were consistent with that reported in the literature.[14]

^{1}H NMR (400 MHz, Chloroform-*d*) δ 8.10 (s, 1H), 7.54 – 7.43 (m, 1H), 7.10 (dd, *J* = 7, 1 Hz, 1H), 6.88 (d, *J* = 8 Hz, 1H), 6.31 (s, 1H), 4.97 – 4.85 (m, 1H), 4.64 (s, 1H), 3.39 – 3.28 (m, 2H), 3.25 (q, *J* = 7 Hz, 2H), 2.89 – 2.66 (m, 3H), 2.18 – 2.06 (m, 1H), 1.84 (p, *J* = 7 Hz, 2H), 1.44 (s, 9H) ppm.

***Tert*-butyl (4-((2-(2,6-dioxopiperidin-3-yl)-1,3-dioxoisoindolin-4-yl)amino)butyl)carbamate (4-61a)**

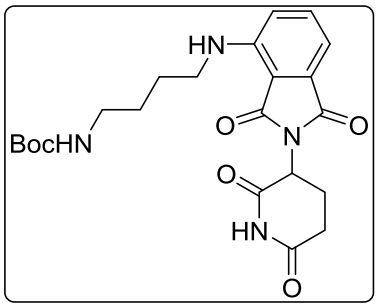

The product was afforded by employing the reaction conditions of **4-61c**, using 4-((*tert*-butoxycarbonyl)amino)butan-1-aminium chloride. The crude was purified by flash column chromatography, product eluted at 70% EtOAc/hexanes as a fluorescent yellow solid, (560 mg, 1.26 mmol, **70%**).

The NMR spectra were consistent with that reported in the literature.[14]

^{1}H NMR (400 MHz, Chloroform-*d*) δ 7.97 (s, 1H), 7.49 (dd, *J* = 9, 7 Hz, 1H), 7.09 (dd, *J* = 7, 1 Hz, 1H), 6.89 (d, *J* = 9 Hz, 1H), 6.23 (bs, 1H), 4.91 (dd, *J* = 12, 5 Hz, 1H), 4.55 (bs, 1H), 3.30 (t, *J* = 7 Hz, 2H), 3.17 (q, *J* = 6 Hz, 2H), 2.94 – 2.69 (m, 3H), 2.13 (ddd, *J* = 10, 5, 2 Hz, 1H), 1.74 – 1.65 (m, 2H), 1.64 – 1.59 (m, 2H), 1.44 (s, 9H) ppm.

***Tert*-butyl (2-(2-(2-((2-(2,6-dioxopiperidin-3-yl)-1,3-dioxoisoindolin-4-yl)amino)ethoxy)ethoxy)ethyl)carbamate (4-64a)**

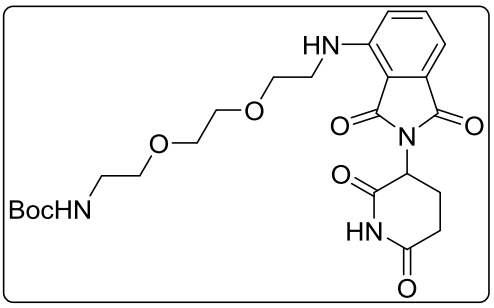

The product was afforded by employing the reaction conditions of **4-61c** using 2,2-dimethyl-4-oxo-3,8,11-trioxa-5-azatridecan-13-aminium chloride and DMF as solvent. The crude was purified by flash column chromatography, product eluted at 80% EtOAc/hexanes as a fluorescent yellow solid, (133 mg, **74%**).

TLC: R_f = 0.44 (50% EtOAc/Hexanes)

^{1}H NMR (400 MHz, Chloroform-*d*) δ 8.29 (bs, 1H), 7.49 (dd, *J* = 9, 7 Hz, 1H), 7.11 (d, *J* = 7 Hz, 1H), 6.91 (d, *J* = 9 Hz, 1H), 6.52 (NH, bs, 1H), 5.03 (NH, bs, 1H), 4.91 (m, 1H), 3.72 (t, *J* = 5 Hz, 2H), 3.65 (dq, *J* = 3, 2 Hz, 4H), 3.57 (t, *J* = 5 Hz, 2H), 3.47 (q, *J* = 5 Hz, 2H), 3.32 (dd, *J* = 10, 5 Hz, 2H), 2.92 – 2.70 (m, 3H), 2.16 – 2.09 (m, 1H), 1.43 (d, *J* = 2 Hz, 9H) ppm.

^{13}C NMR (101 MHz, Chloroform-*d*) δ 156.1 (C), 146.8 (C), 136.0 (CH), 132.5 (C), 116.7 (CH), 111.7 (C), 110.0 (CH), 88.0 (C), 70.8 – 69.3 (4 x CH_2, CH), 61.0 (CH), 48.9 (CH_2), 42.3 (CH_2), 31.4 (CH_2), 28.4 (3 x CH_3), 22.8 (CH_2) ppm. (Some quaternary C signals were not observed, due to low quantity)

IR (NaCl) υ_{max}: 3378, 2911, 1693, 1510, 1362, 1175 cm^{-1}

HRMS (ESI): calc. for $[C_{24}H_{33}O_8N_4]^+$: 505.22929, found 505.22910

4-((2-(2-(2-(2-Azidoethoxy)ethoxy)ethoxy)ethyl)amino)-2-(2,6-dioxopiperidin-3-yl)isoindoline-1,3-dione (4-74a)

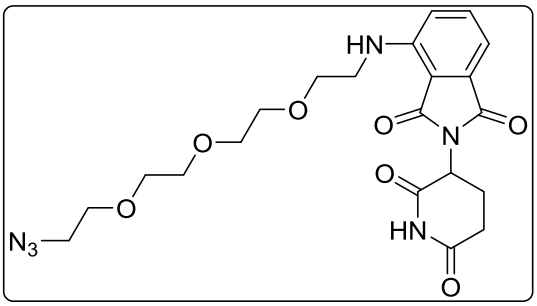

The product was afforded by employing the reaction conditions of **4-61c** using 2-(2-(2-(2-azidoethoxy)ethoxy)ethoxy)ethan-1-aminium chloride. The crude was purified by flash column chromatography. The product eluted at 80% EtOAc/hexanes as a fluorescent yellow film, (55 mg, 0.116 mmol, **33%**).

^{1}H NMR (400 MHz, $CDCl_3$) δ 8.46 (NH, bs, 1H), 7.47 (dd, *J* = 9, 7 Hz, 1H), 7.08 (d, *J* = 7 Hz, 1H), 6.91 (d, *J* = 9 Hz, 1H), 6.47 (NH, t, *J* = 6 Hz, 1H), 4.91 (dd, *J* = 12, 5 Hz, 1H), 3.71 (t, *J* = 5 Hz, 2H), 3.68 – 3.62 (m, 10H), 3.46 (q, *J* = 5 Hz, 2H), 3.36 (t, *J* = 5 Hz, 2H), 2.90 – 2.66 (m, 3H), 2.13 – 2.06 (m, 1H) ppm.

^{13}C NMR (101 MHz, $CDCl_3$) δ 171.4 (C), 169.4 (C), 168.6 (C), 167.7 (C), 146.9 (C), 136.1 (CH), 132.6 (C), 116.9 (CH), 111.7 (C), 110.3 (CH), 70.8 (CH_2), 70.8 (3 x CH_2), 70.1 (CH_2), 69.6 (CH), 50.8 (CH_2), 49.0 (CH_2), 42.5 (CH_2), 31.5 (CH_2), 22.9 (CH_2) ppm.

IR (Film): 3390, 2107 (azide), 1698, 1624, 1324, 1115 cm^{-1}.

HRMS (ESI): calc. for $[C_{21}H_{27}O_7N_6]^+$: 475.1936; found: 475.1937

4-((14-azido-3,6,9,12-tetraoxatetradecyl)amino)-2-(2,6-dioxopiperidin-3-yl)isoindoline-1,3-dione (4-74b)

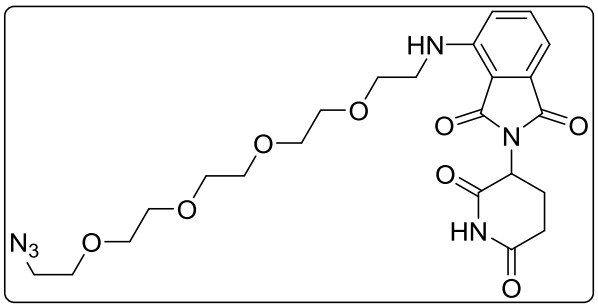

The product was afforded by employing the reaction conditions of **4-61c** using 14-azido-3,6,9,12-tetraoxatetradecan-1-aminium chloride. The crude was purified by flash column chromatography, product eluted at % EtOAc/hexanes as a fluorescent yellow solid, (47 mg, 0.091 mmol, **38%**).

^{1}H NMR (400 MHz, $CDCl_3$) δ 8.18 (NH, bs, 1H), 7.49 (dd, *J* = 9, 7 Hz, 1H), 7.10 (dd, *J* = 7, 1 Hz, 1H), 6.92 (dd, *J* = 9, 1 Hz, 1H), 6.49 (NH, t, *J* = 5 Hz, 1H), 4.91 (dd, *J* = 12, 5 Hz, 1H), 3.72 (t, *J* = 5 Hz, 2H), 3.69 – 3.64 (m, 14H), 3.47 (q, *J* = 5 Hz, 2H), 3.38 (dd, *J* = 6, 5 Hz, 2H), 2.92 – 2.67 (m, 3H), 2.18 – 2.07 (m, 1H) ppm.

^{13}C NMR (101 MHz, CD_3OD) δ 171.2 (C), 169.4 (C), 168.5 (C), 167.7 (C), 147.0 (C), 136.2 (CH), 132.6 (C), 116.9 (CH), 111.8 (C), 110.4 (CH), 70.9 (CH_2), 70.8 (3 x CH_2), 70.7 (2 x CH_2), 70.1 (CH_2), 69.6 (CH), 50.8 (CH_2), 49.0 (CH_2), 42.6 (CH_2), 31.5 (CH_2), 22.9 (CH_2) ppm.

IR (Film): 3391, 2107 (azide), 1698, 1624, 1324, 1113 cm^{-1}.

HRMS (ESI): calc. for $[C_{23}H_{31}O_8N_6]^+$: 519.2198; found: 519.2192.

***Tert*-butyl (20-((2-(2,6-dioxopiperidin-3-yl)-1,3-dioxoisoindolin-4-yl)amino)-3,6,9,12,15,18-hexaoxaicosyl)carbamate (4-64b)**

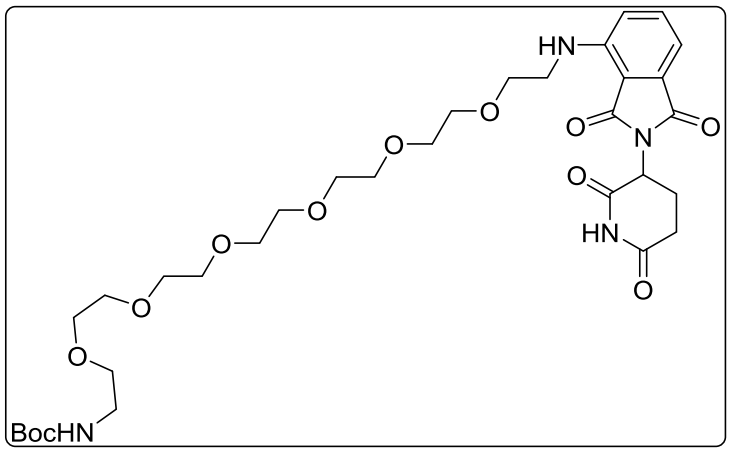

The product was afforded by employing the reaction conditions of **4-61c** using 2,2-dimethyl-4-oxo-3,8,11,14,17,20,23-heptaoxa-5-azapentacosan-25-aminium chloride. The crude was purified by flash column chromatography, product eluted at 90% EtOAc/hexanes as a yellow oil (196 mg, 0.289 mmol, 81%).

^{1}H NMR (400 MHz, $CDCl_3$) δ 8.34 (NH, bs, 1H), 7.49 (dd, *J* = 9, 7 Hz, 1H), 7.10 (dd, *J* = 7, 1 Hz, 1H), 6.92 (dd, *J* = 9, 1 Hz, 1H), 6.49 (NH, bs, 1H), 5.06 (s, 1H), 4.90 (dd, *J* = 12, 5 Hz, 1H), 3.72 (t, *J* = 5.4 Hz, 2H), 3.68 – 3.57 (m, 20H), 3.53 (t, *J* = 5 Hz, 2H), 3.47 – 3.46 (m, 2H), 3.31 – 3.29 (m, 2H), 2.93 – 2.69 (m, 3H), 2.15 – 2.08 (m, 1H), 1.44 (s, 9H) ppm.

^{13}C NMR (101 MHz, $CDCl_3$) δ 171.2 (C), 169.4 (C), 169.0 (C), 168.5 (C), 167.8 (C), 147.0 (C), 136.2 (CH), 132.7 (C), 116.9 (CH), 111.8 (C), 110.5 (CH), 70.9 – 70.6 (10 x CH_2), 70.4 (2 x CH_2), 69.6(CH), 49.0 (CH_2), 42.6 (CH_2), 31.6 (CH_2), 28.6 (3 x CH_3), 23.0 (CH_2) ppm. 1 C not observed.

IR (Film): 3387, 2870, 1698, 1625, 1325, 1112 cm^{-1}.

HRMS (ESI): calc. for $[C_{32}H_{49}O_{12}N_4]^+$: 681.3342; found: 681.3308.

***Tert*-butyl (2-(2-(2-((2-(1-(2-nitrobenzyl)-2,6-dioxopiperidin-3-yl)-1,3-dioxoisoindolin-4-yl)amino)ethoxy)ethoxy)ethyl)carbamate (4-64aNv)**

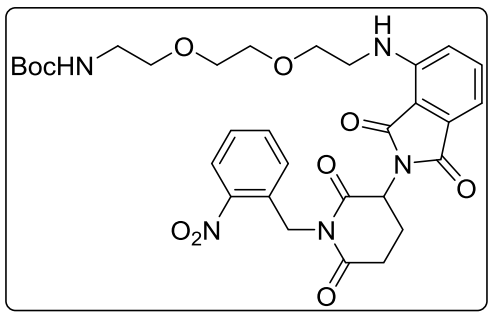

The product was afforded by employing the reaction conditions of **4-61c** using **4-59Nv** and tert-butyl (2-(2-(2-aminoethoxy)ethoxy)ethyl)carbamate. The crude was purified by flash column chromatography, product eluted at 65% EtOAc/hexanes as a fluorescent yellow solid, (60 mg, 0.094 mmol, **39%**).

TLC: R_f = 0.21 (50% EtOAc/Hexanes)

^{1}H NMR (400 MHz, Chloroform-*d*) δ 8.03 (dd, *J* = 8, 1 Hz, 1H), 7.62 (td, *J* = 8, 1 Hz, 1H), 7.48 (dd, *J* = 9, 7 Hz, 1H), 7.43 – 7.37 (m, 1H), 7.32 (dd, *J* = 8, 1 Hz, 1H), 7.09 (d, *J* = 7 Hz, 1H), 6.91 (d, *J* = 9 Hz, 1H), 6.50 (NH, bs, 1H), 5.38 (s, 2H), 5.02 (s, 2H), 3.72 (t, *J* = 5 Hz, 2H), 3.67 – 3.61 (m, 4H), 3.55 (t, *J* = 5 Hz, 2H), 3.48 (q, *J* = 6 Hz, 2H), 3.31 (q, *J* = 6 Hz, 2H), 3.03 (d, *J* = 12 Hz, 1H), 2.85 (t, *J* = 10 Hz, 2H), 2.17 (td, *J* = 5, 3 Hz, 1H), 1.42 (s, 9H) ppm.

^{13}C NMR (101 MHz, Chloroform-*d*) δ 171.0 (C), 170.8 (C), 170.4 (C), 169.3 (C), 168.9 (C), 167.7 (C), 162.3 (C), 146.8 (C), 136.0 (CH), 133.7 (CH), 132.5 (C), 127.9 (CH), 127.6 (CH), 125.0 (CH), 116.7 (CH), 111.7 (CH), 110.2 (C), 70.6 (CH_2), 70.3 – 70.1 (3 x CH_2), 69.5 (CH_2), 49.5 (CH), 42.3 (CH_2), 41.0 (CH_2), 31.9 (CH_2), 28.4 (3 x CH_3), 22.1 (CH_2) ppm.

IR (NaCl) υ_{max}: 3386, 2916, 2842, 1702, 1519, 1362, 1171 cm^{-1}

HRMS (ESI): calc. for $[C_{31}H_{38}O_{10}N_5]^+$: 640.26132, found 640.26083.

2-((2-(2,6-Dioxopiperidin-3-yl)-1,3-dioxoisoindolin-4-yl)amino)ethan-1-aminium trifluoroacetate (4-62c)

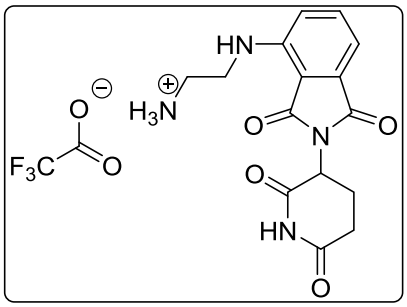

To a vial charged with **4-61c** (65 mg, 0.158 mmol) was added DCM (5 mL) followed by TFA (0.06 mL, 0.1 mmol). After 1 h the reaction was observed to be complete by TLC and the reaction mixture was concentrated under reduced pressure to afford a yellow film. The film was dissolved in DCM before concentration under reduced pressure to further remove residual TFA, affording the product as a yellow film (68 mg, 0.158, **100%**).

The NMR spectra were comparable with those reported in the literature.

^{1}H NMR (400 MHz, Methanol-d_4) δ 7.54 (dd, *J* = 9, 7 Hz, 1H), 7.09 – 7.03 (m, 2H), 5.00 (dd, *J* = 13, 5 Hz, 1H), 3.59 (t, *J* = 6 Hz, 2H), 3.11 (t, *J* = 6 Hz, 2H), 2.85 – 2.58 (m, 3H), 2.03 (dtd, *J* = 13, 5, 2 Hz, 1H) ppm.

3-((2-(2,6-Dioxopiperidin-3-yl)-1,3-dioxoisoindolin-4-yl)amino)propan-1-aminium chloride (4-62b)

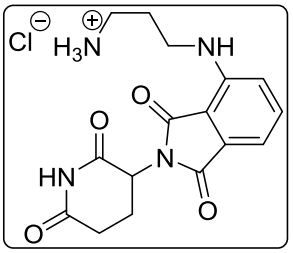

To a vial charged with **4-61b** (65 mg, 0.158 mmol) was added 4N HCl in dioxane (1 mL). After 1 h the reaction was observed to be complete by TLC and the reaction mixture was concentrated under reduced pressure to afford a yellow film. The film was dissolved in DCM before concentration under reduced pressure to further remove residual HCl, affording the product as a yellow film (44, mg, 0.10 mmol, **100%**).

The NMR spectra were consistent with that reported in the literature.

^{1}H NMR (400 MHz, Methanol-d_4) δ 7.59 (dd, *J* = 8, 7 Hz, 1H), 7.11 – 7.08 (m, 2H), 5.06 (dd, *J* = 13, 6 Hz, 1H), 3.47 (t, *J* = 7 Hz, 2H), 3.05 (t, *J* = 8 Hz, 2H), 2.91 – 2.65 (m, 3H), 2.15 – 2.06 (m, 1H), 2.04 – 1.95 (m, 2H) ppm.

4-((2-(2,6-Dioxopiperidin-3-yl)-1,3-dioxoisoindolin-4-yl)amino)butan-1-aminium chloride (4-62a)

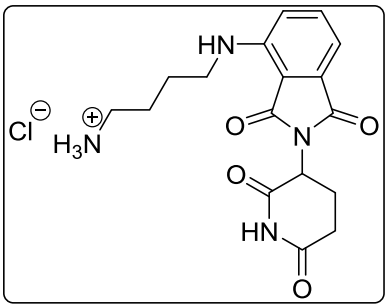

Prepared as for **4-62b** but using **4-61a** (475 mg, 1.14 mmol, **92%**).

The NMR spectra were consistent with that reported in the literature.

^{1}H NMR (400 MHz, Methanol-d_4) δ 7.56 (dd, *J* = 8, 7 Hz, 1H), 7.07 (dd, *J* = 12, 8 Hz, 2H), 5.05 (dd, *J* = 12, 6 Hz, 1H), 3.40 (t, *J* = 6 Hz, 2H), 3.01 – 2.96 (m, 2H), 2.93 – 2.64 (m, 3H), 2.14 – 2.06 (m, 1H), 1.77 (dq, *J* = 7, 4 Hz, 4H) ppm.

2-(2-(2-((2-(2,6-Dioxopiperidin-3-yl)-1,3-dioxoisoindolin-4-yl)amino)ethoxy)ethoxy)ethan-1-aminium chloride (4-65a)

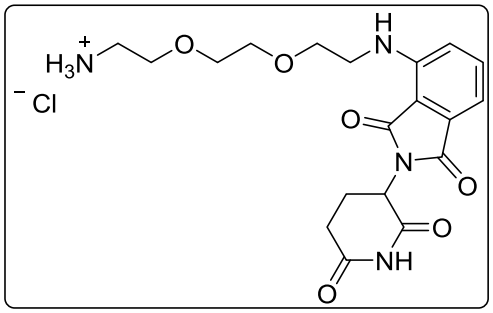

Prepared as for **4-62b** but using **4-64a.** A precipitate formed after addition of Et_2O, which upon evaporation gave the product as a fluorescent yellow solid, (61 mg, 0.138 mmol, **100%**).

^{1}H NMR (400 MHz, Methanol-d_4) δ 7.57 (dd, *J* = 9, 7 Hz, 1H), 7.13 – 7.06 (m, 2H), 5.06 (dd, *J* = 13, 6 Hz, 1H), 3.74 (dd, *J* = 6, 5 Hz, 2H), 3.72 – 3.69 (m, 6H), 3.52 (dd, *J* = 6, 5 Hz, 2H), 3.10 (t, *J* = 5 Hz, 2H), 2.88 – 2.67 (m, 3H), 2.16 – 2.07 (m, 1H) ppm.

^{13}C NMR (101 MHz, Methanol-d_4) δ 173.1 (C), 170.3 (C), 169.5 (C), 167.7 (C), 146.7 (C), 135.9 (CH), 132.5 (C), 116.8 (CH), 110.8 (CH), 110.0 (C), 70.2 (CH_2), 69.9 (CH_2), 69.0 (CH_2), 66.5 (CH_2), 48.8 (CH), 41.7 (CH_2), 39.4 (CH_2), 30.8 (CH_2), 22.4 (CH_2) ppm.

IR (NaCl) υ_{max}: 2912, 2363, 1689, 1353, 1262, 1096 cm^{-1}

HRMS (ESI): calc. for $[C_{19}H_{25}O_6N_4]^+$: 405.17686, found 405.17629.

20-((2-(2,6-Dioxopiperidin-3-yl)-1,3-dioxoisoindolin-4-yl)amino)-3,6,9,12,15,18-hexaoxaicosan-1-aminium 2,2,2-trifluoroacetate (4-65b)

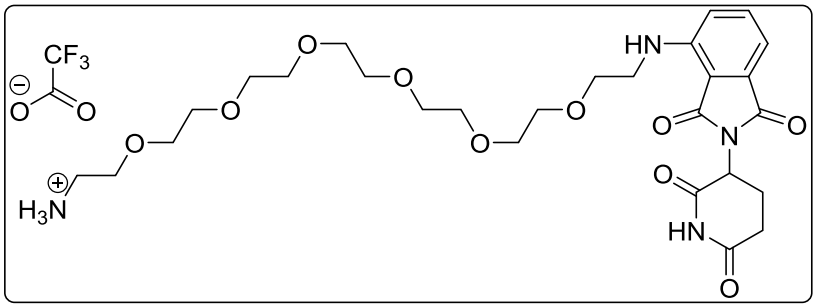

The product was obtained utilising the method described for **4-62b** but using **4-64b**. The product was isolated as a yellow/orange film and used directly without further purification (167 mg, 0.27 mmol **100%**).

^{1}H NMR (400 MHz, Methanol-d_4) δ 7.62 (dd, *J* = 9, 7 Hz, 1H), 7.13 (dd, *J* = 14, 8 Hz, 2H), 5.12 (dd, *J* = 13, 6 Hz, 1H), 3.83 – 3.63 (m, 24H), 3.57 (t, *J* = 5 Hz, 2H), 3.19 (t, *J* = 5 Hz, 3H), 2.99 – 2.69 (m, 3H), 2.23 – 2.13 (m, 1H) ppm.

^{13}C NMR (101 MHz, Methanol-d_4) δ 174.6 (C), 171.5 (C), 170.7(C), 169.2 (C), 148.1 (C), 137.3 (CH), 133.8 (C), 118.3 (C), 112.1 (CH), 111.3 (CH), 71.3 (3 x CH_2), 71.3 (CH_2), 71.3 (CH_2), 71.2

(CH_2), 71.2 (CH_2), 71.1 (CH_2), 71.0 (CH_2), 70.7 (CH_2), 70.5 (CH_2), 67.7 (CH_2), 50.2 (CH), 43.1 (CH_2), 40.4 (CH_2), 32.2 (CH_2), 23.8 (CH_2) ppm.

IR (Film): 3282, 2913, 1602, 1244, 1049, 835 cm^{-1}.

HRMS (ESI): calc. for $[C_{27}H_{41}O_{10}N_4]^+$: 581.2817; found: 581.2800.

4-Azidobutanoic acid (4-77)

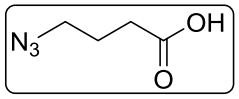

To a 10 mL microwave vial charged with methyl 4-bromobutanoate (**4-75,** 0.35 mL, 2.76 mmol) was added water (4.5 mL) followed by sodium azide (449 mg, 6.91 mmol), capped, then heated to 120 °C by microwave irradiation for 1 h. The mixture turned from Brown to colourless. The completion of the reaction was confirmed by proton NMR, then the mixture was transferred to a round bottom flask, washing with MeOH (2 mL). To the reaction mixture was then added 2M NaOH (2 mL, 4.14 mmol) and stirred at rt for 2 h. The reaction mixture was then adjusted to pH 5 using concentrated HCl and extracted using Et_2O (3 x 30 mL). The combined organic layers were washed with brine, dried over $MgSO_4$ and concentrated under reduced pressure to afford the product as a colourless oil, (357 mg, 2.76 mmol, **100%**).

The NMR spectra were consistent with that reported in the literature.[15]

^{1}H NMR (400 MHz, Chloroform-*d*) δ 3.38 (t, *J* = 7 Hz, 2H), 2.48 (t, *J* = 7 Hz, 2H), 1.97 – 1.84 (m, 2H) ppm.

Methyl 4-bromo-2-((*tert*-butoxycarbonyl)amino)butanoate (4-97)

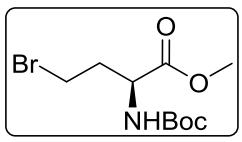

To a round bottom flask containing MeOH (7.5 mL) at 0 °C was added dropwise $SOCl_2$ and stirred for 30 min. 3-Bromo-1-carboxypropan-1-aminium bromide was then added and the mixture was stirred overnight. The crude ester was obtained upon evaporation of the reaction mixture, to which was then added Boc_2O (342 mg, 1.57 mmol) and dioxane (5 mL). The mixture was cooled before dropwise addition of $NaHCO_3$ (10%, 5 mL). The mixture was stirred at rt for 22 h before extraction using DCM (2 x 20 mL). The crude was purified by flash column chromatography, product eluted at 45% EtOAc/hexanes as a colourless oil. The crude was taken on to subsequent reaction without further purification.

^{1}H NMR (400 MHz, Chloroform-*d*) δ 5.12 (s, 1H), 4.48 – 4.37 (m, 1H), 3.42 (t, *J* = 7 Hz, 2H), 2.46 – 2.33 (m, 1H), 2.20 (dq, *J* = 15, 7 Hz, 1H), 1.44 (s, 9H) ppm.

(S)-(+)-4-Azido-2-((*tert*-butoxycarbonyl)amino)butanoic acid (4-98b)

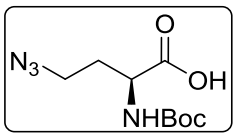

To a round bottom flask charged with **4-97** (225 mg, 0.76 mmol) was added DMF (2.5 mL) followed by sodium azide (99 mg, 1.52 mmol), then heated to 80 °C for 22 h. The completion of the reaction was confirmed by proton NMR, then 2M NaOH (0.6 mL, 1.52 mmol) and MeOH (2 mL) were added to the reaction mixture and stirred at rt for 1 h. The reaction mixture was then adjusted to pH 5 using concentrated HCl and extracted using Et_2O (3 x 30 mL). The combined organic layers were washed with brine, dried over $MgSO_4$ and concentrated under reduced pressure to afford the product as a colourless oil, (147 mg, 0.60 mmol, **79%**).

The NMR spectra compares well with that reported in the literature.[16]

^{1}H NMR (400 MHz, Chloroform-*d*) δ 6.45 (s, 2H), 5.22 (d, *J* = 13 Hz, 1H), 4.27 (bs, 1H), 3.38 (t, *J* = 7 Hz, 2H), 2.14 – 2.02 (m, 1H), 1.90 (dq, *J* = 13, 7 Hz, 1H), 1.39 (s, 9H) ppm.

4-Azido-*N*-(2-((2-(2,6-dioxopiperidin-3-yl)-1,3-dioxoisoindolin-4-yl)amino)ethyl)butanamide (4-95c)

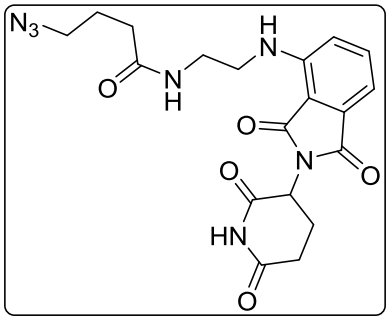

The product was prepared following method B but using **4-77** as the starting acid and **4-62c** as the starting amine. The product was eluted from the column at 80% EtOAc/hexanes as a fluorescent yellow solid, (68 mg, 0.159 mmol, **65%**).

^{1}H NMR (400 MHz, Chloroform-*d*) δ 8.43 (NH, s, 1H), 7.54 – 7.47 (m, 1H), 7.11 (d, *J* = 7 Hz, 1H), 6.97 (d, *J* = 9 Hz, 1H), 6.39 (NH, bs, 1H), 6.15 (NH, bs, 1H), 4.93 (dd, *J* = 12, 5 Hz, 1H), 3.52 – 3.42 (m, 4H), 3.33 (t, *J* = 7 Hz, 2H), 2.91 – 2.67 (m, 3H), 2.25 (t, *J* = 7 Hz, 2H), 2.15 – 2.08 (m, 1H), 1.90 (p, *J* = 7 Hz, 2H) ppm.

^{13}C NMR (101 MHz, Chloroform-*d*) δ 172.5 (C), 171.2 (C), 169.5 (C), 168.6 (C), 167.5 (C), 146.7 (C), 136.3 (CH), 132.5 (C), 116.7 (CH), 112.0 (CH), 110.4 (C), 50.7 (CH_2), 48.9 (CH), 42.1 (CH_2), 39.1 (CH_2), 33.0 (CH_2), 31.4 (CH_2), 24.7 (CH_2), 22.7 (CH_2) ppm.

IR (NaCl) υ_{max}: 3382, 2916, 2093 (azide), 1697, 1358, 1197, 748 cm^{-1}

HRMS (ESI): calc. for $[C_{19}H_{22}O_5N_7]^+$: 428.16769, found 428.16767

4-Azido-*N*-(3-((2-(2,6-dioxopiperidin-3-yl)-1,3-dioxoisoindolin-4-yl)amino)propyl)butanamide (4-95b)

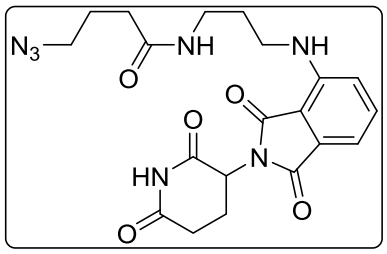

The product was prepared following general method B but using **4-77** as the starting acid and **4-62b** as the starting amine. The product was eluted from the column at 80% EtOAc/hexanes as a fluorescent yellow solid, (100 mg, 0.23 mmol, **92%**).

TLC Rf: 0.31 (10% MeOH/DCM)

^{1}H NMR (400 MHz, Chloroform-*d*) δ 8.30 (NH, s, 1H), 7.52 – 7.46 (m, 1H), 7.09 (dd, *J* = 7, 1 Hz, 1H), 6.88 (d, *J* = 9 Hz, 1H), 6.39 (NH, bs, 1H), 5.81 (NH, bs, 1H), 4.92 (dd, *J* = 12, 5 Hz, 1H), 3.41 – 3.30 (m, 6H), 2.91 – 2.67 (m, 3H), 2.27 (t, *J* = 7 Hz, 2H), 2.16 – 2.08 (m, 1H), 1.89 (dp, *J* = 27, 7 Hz, 4H) ppm.

^{13}C NMR (101 MHz, Chloroform-*d*) δ 172.2 (C), 171.1 (C), 169.4 (C), 168.4 (C), 167.5 (C), 146.6 (C), 136.2 (CH), 132.5 (C), 116.5 (CH), 111.7 (CH), 110.2 (C), 50.8 (CH_2), 48.9 (CH), 40.2 (CH_2), 37.2 (CH_2), 33.2 (CH_2), 31.4 (CH_2), 29.3 (CH_2), 24.7 (CH_2), 22.8 (CH_2) ppm.

IR (NaCl) υ_{max}: 3378, 2925, 2098 (azide), 1697, 1353, 1188 cm^{-1}

HRMS (ESI): calc. for $[C_{20}H_{24}O_5N_7]^+$: 442.18334, found 442.18341

4-Azido-*N*-(4-((2-(2,6-dioxopiperidin-3-yl)-1,3-dioxoisoindolin-4-yl)amino)butyl)butanamide 4-95a

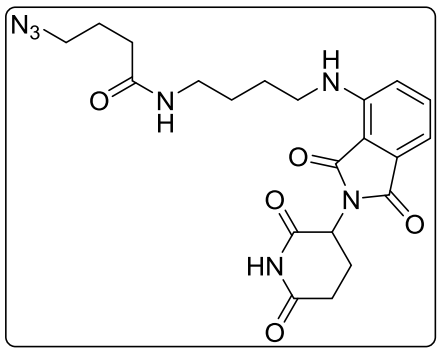

The product was afforded using method B but using **4-77** as the starting acid and **4-62a** as the starting amine. The product was eluted from the column at 80% EtOAc/hexanes as a fluorescent yellow solid, (273 mg, 0.60 mmol, **92%**).

TLC Rf: 0.39 (100% EtOAc)

^{1}H NMR (400 MHz, $CDCl_3$) δ 8.23 (NH, s, 1H), 7.49 (ddd, *J* = 9, 7, 1 Hz, 1H), 7.09 (dd, *J* = 7, 1 Hz, 1H), 6.88 (d, *J* = 8 Hz, 1H), 6.23 (NH, t, *J* = 6 Hz, 1H), 5.65 (NH, bs, 1H), 4.92 (dd, *J* = 12, 5 Hz, 1H), 3.40 – 3.25 (m, 6H), 2.93 – 2.64 (m, 3H), 2.25 (t, *J* = 7 Hz, 2H), 2.16 – 2.09 (m, 1H), 1.96 – 1.88 (m, 2H), 1.73 – 1.58 (m, 4H) ppm.

^{13}C NMR (101 MHz, $CDCl_3$) δ 172.0 (C), 171.5 (C), 169.7 (C), 168.9 (C), 167.7 (C), 146.9 (C), 136.3 (CH), 132.6 (C), 116.8 (CH), 111.7 (CH), 110.0 (C), 50.9 (CH_2), 49.0 (CH), 39.1 (CH_2), 33.3 (CH_2), 31.3 (CH_2), 29.8 (CH_2), 27.2 (CH_2), 26.6 (CH_2), 24.9 (CH_2), 22.9 (CH_2) ppm.

IR (Film): 3385, 2924, 2099 (azide), 1695, 1360, 1198 cm^{-1}.

HRMS (ESI): calc. for $[C_{21}H_{26}O_5N_7]^+$: 456.1990; found: 456.1988.

4-Azido-*N*-(2-(2-(2-((2-(2,6-dioxopiperidin-3-yl)-1,3-dioxoisoindolin-4-yl)amino)ethoxy)ethoxy)ethyl)butanamide (4-78)

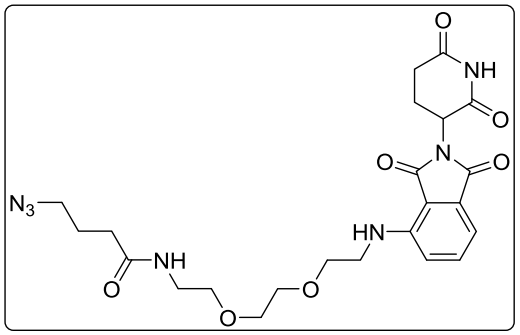

The product was prepared following general method B but using **4-77** as the starting acid and **4-65a** as the starting amine. The product eluted from the column at 80% EtOAc/hexanes as a fluorescent yellow oil, (51 mg, 0.099 mmol, **73%**).

^{1}H NMR (400 MHz, Chloroform-*d*) δ 8.55 (s, 1H), 7.50 (dd, *J* = 9, 7 Hz, 1H), 7.12 (dd, *J* = 7, 1 Hz, 1H), 6.90 (d, *J* = 8 Hz, 1H), 6.53 (t, *J* = 5 Hz, 1H), 6.10 (t, *J* = 5 Hz, 1H), 4.95 – 4.84 (m, 1H), 3.73 (t, *J* = 5 Hz, 2H), 3.66 (d, *J* = 1 Hz, 4H), 3.59 (dd, *J* = 5, 4 Hz, 2H), 3.50 – 3.41 (m, 5H), 3.32 (t, *J* = 7 Hz, 2H), 2.90 – 2.84 (m, 1H), 2.80 – 2.68 (m, 1H), 2.24 (t, *J* = 7 Hz, 2H), 2.17 – 2.10 (m, 1H), 1.90 (p, *J* = 7 Hz, 2H) ppm.

^{13}C NMR (101 MHz, Chloroform-*d*) δ 171.9 (C), 171.0 (C), 169.4 (C), 168.5 (C), 167.5 (C), 146.7 (C), 136.1 (CH), 132.5 (C), 116.7 (CH), 111.8 (CH), 110.4 (C) 77.2 (CH_2), 70.7 (CH_2), 70.1 (CH_2), 69.8 (CH_2), 50.8 (CH_2), 48.9 (CH), 42.3 (CH_2), 39.4 (CH_2), 33.1 (CH_2), 31.4 (CH_2), 24.7 (CH_2), 22.9 (CH_2) ppm.

IR (NaCl) υ_{max}: 3373, 2868, 2089 (azide), 1684, 1353, 1253, 1114 cm^{-1}

HRMS (ESI): calc. for $[C_{23}H_{30}O_9N_7]^+$: 516.22012; found 516.21879

4-Azido-*N*-(2-(2-(2-((2-(1-(2-nitrobenzyl)-2,6-dioxopiperidin-3-yl)-1,3-dioxoisoindolin-4-yl)amino)ethoxy)ethoxy)ethyl)butanamide (4-78Nv)

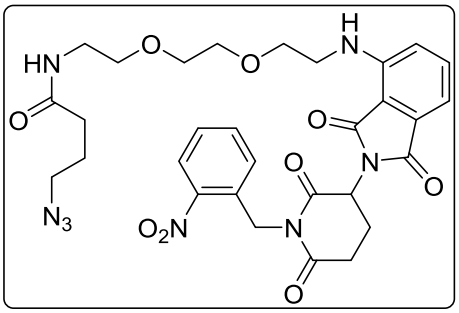

The product was prepared following method B but using **4-77** as the starting acid and **4-65aNv** as the starting amine. The product was eluted from the column at 90% EtOAc/hexanes as a fluorescent yellow solid, (39 mg, 0.073 mmol, **68%**).

^{1}H NMR (400 MHz, Chloroform-*d*) δ 8.01 (dd, *J* = 8, 1 Hz, 1H), 7.61 (td, *J* = 8, 1 Hz, 1H), 7.49 (dd, *J* = 9, 7 Hz, 1H), 7.39 (ddd, *J* = 8, 7, 1 Hz, 1H), 7.31 (dd, *J* = 8, 1 Hz, 1H), 7.09 (dd, *J* = 7, 1 Hz, 1H), 6.91 (d, *J* = 9 Hz, 1H), 6.50 (NH, t, *J* = 6 Hz, 1H), 6.06 (NH, bs, 1H), 5.36 (s, 2H), 5.04 – 4.98 (m, 1H), 3.72 (t, *J* = 5 Hz, 2H), 3.68 – 3.61 (m, 4H), 3.55 (dd, *J* = 6, 5 Hz, 2H), 3.50 – 3.40 (m, 4H), 3.29 (t, *J* = 7 Hz, 2H), 3.06 – 2.95 (m, 1H), 2.91 – 2.78 (m, 2H), 2.23 – 2.13 (m, 3H), 1.92 – 1.82 (m, 2H) ppm.

^{13}C NMR (101 MHz, Chloroform-*d*) δ 171.7 (C), 170.9 (C), 169.3 (C), 169.0 (C), 167.6 (C), 148.4 (C), 146.8 (C), 136.1 (CH), 133.7 (CH), 132.5 (C), 132.0 (C), 128.0 (CH), 127.6 (CH), 125.0 (CH), 116.8 (CH), 111.8 (CH), 110.3 (C), 70.5 (CH_2), 70.2 (CH_2), 70.29 (CH_2), 69.8 (CH_2), 69.3 (CH_2), 50.8 (CH_2), 49.5 (CH), 42.3 (CH_2), 41.0 (CH_2), 33.1 (CH_2), 31.9 (CH_2), 24.8 (CH_2), 22.1 (CH_2) ppm.

IR (NaCl) υ_{max}: 3234, 2916, 2093 (azide), 1723, 1693, 1262, 735 cm^{-1}

HRMS (ESI): calc. for $[C_{30}H_{35}O_9N_8]^+$: 651.25215; found 651.25261

General Method C "click reaction" triazole formation

To a solution of the azide component (1 eq) in tBuOH (0.05 mmol mL^{-1}) and water (0.05 mmol mL^{-1}) at 30 °C was added $CuSO_4$ (0.3 eq.), sodium ascorbate (0.1 eq.) and the alkyne component (1 eq.). The reaction mixture was then degassed using N_2 for 20 min, then left to stir at this temperature for 20 h. The reaction mixture was then separated between EtOAc and water, the aqueous layer re-extracted using EtOAc (x3). The combined organic layers were then washed with water and brine, dried over MgSO4 and concentrated under reduced pressure to afford a fluorescent yellow film. The crude was then purified by flash column chromatography, to afford the desired product.

8-Bromo-N-(2-(2,6-dioxopiperidin-3-yl)-1,3-dioxoisoindolin-4-yl)octanamide. (4-56)

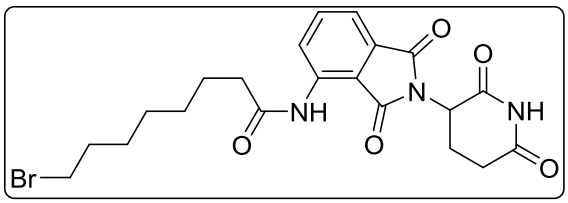

To a solution of 8-bromooctanoic acid (164 mg, 0.74 mmol) in THF (3 mL) was added DMF (2 drops) and then oxalyl chloride (63 µL, 0.74 mmol) was added dropwise under N_2 at 0 °C. After 25 min warming to rt, the reaction mixture was added dropwise to a separate flask charged with 4-amino-2-(2,6-dioxopiperidin-3-yl)isoindoline-1,3-dione (pomalidomide **(4-44c)** 100 mg, 0.37 mmol) in THF (3 mL). After 2 h the mixture was quenched with the addition of $NaHCO_3$, extracted using EtOAc (x3) then the combined organic layers were washed with brine, dried over $MgSO_4$, and concentrated under reduced pressure to afford as a brown oil.

TLC R_f: 0.66 (50% EtOAc/hexanes), (Pomalidomide R_f: 0.37)

^{1}H NMR (400 MHz, Chloroform-*d*) δ 9.41 (NH, bs, 1H), 8.83 (dd, *J* = 9, 1 Hz, 1H), 8.07 (NH, bs, 1H), 7.72 (ddd, *J* = 9, 7, 1 Hz, 1H), 7.55 (dd, *J* = 7, 1 Hz, 1H), 5.00 – 4.92 (m, 1H), 3.41 (t, *J* = 7 Hz, 2H), 2.97 – 2.70 (m, 3H), 2.46 (t, *J* = 8 Hz, 2H), 2.22 – 2.13 (m, 1H), 1.86 (dt, *J* = 14, 7 Hz, 2H), 1.76 (p, *J* = 8 Hz, 2H), 1.51 – 1.35 (m, 6H) ppm.

^{13}C NMR (101 MHz, Chloroform-*d*) δ 172.2 (C), 170.5 (C), 169.2 (C), 167.7 (C), 166.6 (C), 137.9 (C), 136.5 (CH), 131.1 (C), 125.3 (CH), 118.4 (CH), 115.2 (C), *110.0 (C),* 70.3 (CH), 65.2 (CH_2), 63.3 (CH_2), 49.3 (CH), 37.9 (CH_2), 34.1 (CH_2), 33.9 (CH_2), 32.6 (CH_2), 31.9 (CH_2), 31.4 (CH_2), 25.1 (CH_2), ppm.

IR (film): 2926, 2851, 1708, 1618, 1262, 739 cm^{-1}.

HRMS (ESI): calc. for $[C_{21}H_{25}O_5N_3Br]^+$: 478.09721; found: 478.09726.

8-Azido-N-(2-(2,6-dioxopiperidin-3-yl)-1,3-dioxoisoindolin-4-yl)octanamide (4-80)

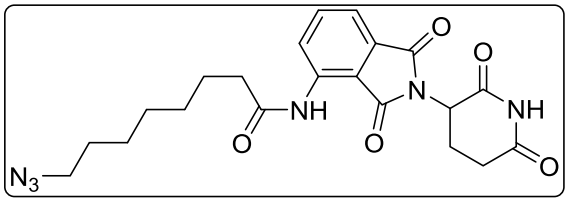

The crude compound **4-56** (31 mg, 0.065 mmol) was dissolved in DMF (0.5 mL) in a vial. NaN_3 (21 mg, 0.32 mmol) was added, the vial was sealed, placed under an atmosphere of N_2, and then subjected to heating at 36 °C for 48 h. The mixture was then separated between EtOAc and water, re-extracted using EtOAc (x2) then the combined organic layers were washed with brine (x2), $CuSO_4$, dried over $MgSO_4$, and concentrated under reduced pressure to afford a crude waxy

solid. The crude was purified by flash column chromatography. The product eluted at 35% EtOAc/hexanes as a white solid, (25 mg, 0.059 mmol, **16%**).

^{1}H NMR (400 MHz, Chloroform-*d*) δ 9.41 (NH, bs, 1H), 8.83 (dd, *J* = 8, 1 Hz, 1H), 8.16 (NH, bs, 1H), 7.71 (dd, *J* = 8, 7 Hz, 1H), 7.55 (dd, *J* = 7, 1 Hz, 1H), 4.96 (dd, *J* = 12, 6 Hz, 1H), 3.26 (t, *J* = 7 Hz, 2H), 2.96 – 2.73 (m, 3H), 2.46 (t, *J* = 7 Hz, 2H), 2.21 – 2.13 (m, 1H), 1.76 (p, *J* = 7 Hz, 2H), 1.59 (q, *J* = 7 Hz, 2H), 1.39 (q, *J* = 4 Hz, 6H) ppm.

^{13}C NMR (101 MHz, Chloroform-*d*) δ 172.2 (C), 170.6 (C), 169.2 (C), 167.7 (C), 166.6 (C), 137.9 (C), 136.5 (CH), 131.1 (C), 125.3 (CH), 118.4 (CH), 115.2 (C), 51.4 (CH_2), 49.3 (CH), 37.9 (CH_2), 31.4 (2 x CH_2), 28.9 (CH_2), 28.8 (CH_2), 28.7 (CH_2), 26.5 (CH_2), 25.1 (CH_2) ppm.

tert-Butyl hex-5-yn-1-ylcarbamate (4-83a)

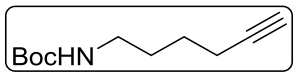

To hex-5-yn-1-aminium chloride (174 mg, 1.30 mmol) and Boc_2O (284 mg, 1.30 mmol) in MeCN (5 mL) was added NEt_3 (0.36 mL, 2.60 mmol) then stirred at rt for 22 h. The reaction mixture was then separated between EtOAc and NH_4Cl, the organics were washed with H_2O, then dried with $MgSO_4$ then concentrated under reduced pressure to afford an off white powder (252 mg, **98%**).

Characterisation is consistent with that reported in the literature.[14]

tert-Butyl pent-4-yn-1-ylcarbamate (4-83b)

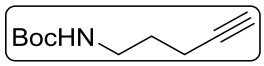

To pent-4-yn-1-aminium chloride (174 mg, 1.30 mmol) and Boc_2O (284 mg, 1.30 mmol) in MeCN (5 mL) was added NEt_3 (0.36 mL, 2.60 mmol) then stirred at rt for 22 h. The reaction mixture was then separated between EtOAc and NH_4Cl, the organics were washed with H_2O, then dried with $MgSO_4$ then concentrated under reduced pressure to afford an off white powder (252 mg, **98%**).

Characterisation is consistent with that reported in the literature.[14]

4-Bromo-2-(2,6-dioxopiperidin-3-yl)isoindoline-1,3-dione (4-82)

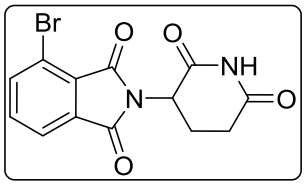

2,6-Dioxopiperidin-3-aminium chloride (**4-52,** 159 mg, 0.96 mmol), 4-bromoisobenzofuran-1,3-dione (200 mg, 0.88 mmol) and NaOAc (86 mg, 1.05 mmol) were suspended in AcOH (3 mL) then heated to 140 for 5 h then rt for18 h. The reaction mixture was concentrated under reduced pressure to afford a brown gum, then purified by column chromatography. Product eluted at 12% MeOH/DCM as a white solid (239 mg, **81%**).

Characterisation is consistent with that reported in the literature.[14]

Methyl 3-bromo-2-(bromomethyl)benzoate (4-88)

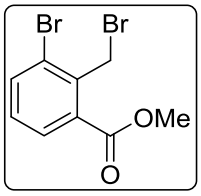

Methyl 3-bromo-2-methylbenzoate (**4-87,** 200 mg, 0.87 mmol) NBS (185 mg, 1.04 mmol) and VAZO™ 88 (1,1'-(diazene-1,2-diyl)bis(cyclohexane-1-carbonitrile), 21 mg, 0.09 mmol) in benzene (2 mL) was heated to 90 °C for 6 h. The solvent was removed under reduced pressure then the crude was purified by column chromatography. Product eluted at 7% EtOAc/hexane as an off white solid (256 mg, **96%**).

Characterisation is consistent with that reported in the literature.[14]

3-(4-Bromo-1-oxoisoindolin-2-yl)piperidine-2,6-dione (4-88)

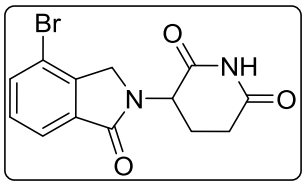

To a solution of **4-88** (288 mg, 0.94 mmol) in MeCN (10 mL) was added NEt_3 and 2,6-dioxopiperidin-3-aminium chloride (**4-52,** 188 mg, 1.41 mmol) then heated in a sealed pressure tube at 85 °C for 22 h. The solvent was evaportated under reduced pressure and the residue was purified by column chromatography. Product eluted at 7% MeOH/DCM as a white solid (290, **96%**).

Characterisation is consistent with that reported in the literature.[14]

tert-Butyl (5-(2-(2,6-dioxopiperidin-3-yl)-1,3-dioxoisoindolin-4-yl)hex-5-yn-1-yl)carbamate (4-84a)

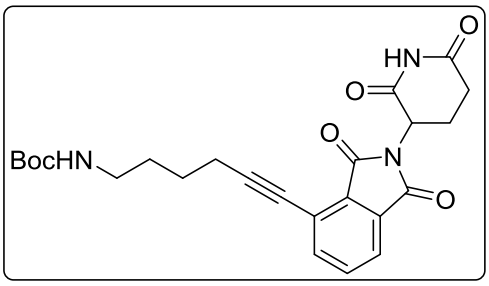

A vial charged with **4-82** (100 mg, 0.30 mmol), **4-83a** (117 mg, 0.59 mmol), CuI (11 mg, 0.06 mmol), $Pd(PPh_3)_2Cl_2$ (42 mg, 0.06 mmol), NEt_3 (0.72 mL, 5.2 mmol) in DMF (2 mL) was heated to 70 °C for 20 h. The mixture was then cooled to rt, filtered through celite, washed with DCM and then concentrated under reduced pressure. The crude was purified by column chromatography, product eluted at 8% MeOH/DCM as a white solid (125 mg, **93%**).

Characterisation is consistent with that reported in the literature.[14]

5-(2-(2,6-Dioxopiperidin-3-yl)-1,3-dioxoisoindolin-4-yl)hexan-1-aminium trifluoroacetate

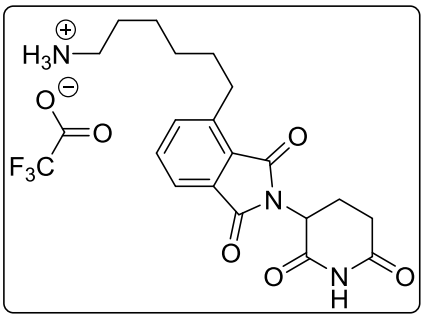

To **4-84a** (47 mg, 0.10 mmol) in EtOH (2 mL) was added Pd/C (10%, 4.4 mg), purged with N_2/H_2 then left under a positive pressure of H_2 stirring at rt for 22 h.The mixture was filtered through celite and concentrated under reduced pressure to afford an off white

solid. The solid was dissolved in DCM (1 mL) and added TFA (0.2 mL), stirring for 2 h at rt. The solvents were then removed under reduced pressure to afford a colourless wax (50 mg, **100%**). The crude was used directly in the subsequent reaction without further purification.

Characterisation is consistent with that reported in the literature.[14]

4-Azido-N-(6-(2-(2,6-dioxopiperidin-3-yl)-1,3-dioxoisoindolin-4-yl)hexyl)butanamide (4-86a)

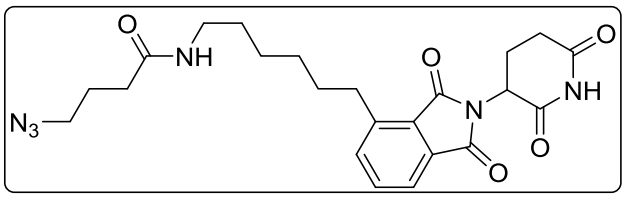

Method B followed, using **4-77** as acid and **4-85a** as amine. Product as a white wax (43 mg, **68%**).

^{1}H NMR (400 MHz, $CDCl_3$) δ 8.45 (s, 1H), 7.71 (dd, *J* = 7, 1 Hz, 1H), 7.62 (t, *J* = 8 Hz, 1H), 7.51 (dd, *J* = 8, 1 Hz, 1H), 5.64 (s, 1H), 4.97 (dd, *J* = 12, 5 Hz, 1H), 3.34 (t, *J* = 7 Hz, 2H), 3.22 (q, *J* = 7 Hz, 2H), 3.13 – 2.99 (m, 2H), 2.93 – 2.68 (m, 3H), 2.24 (t, *J* = 7 Hz, 2H), 2.18 – 2.12 (m, 1H), 1.91 (p, *J* = 7 Hz, 2H), 1.65 (p, *J* = 7 Hz, 2H), 1.48 (p, *J* = 7 Hz, 2H), 1.45 – 1.28 (m, 4H) ppm.

^{13}C NMR (101 MHz, CD_3OD) δ 171.9 (C), 171.2 (C), 168.4 (C), 168.0 (C), 167.4 (C), 143.7 (C), 136.1 (C), 134.3 (C), 132.4 (CH), 128.2 (CH), 121.7 (CH), 51.0 (CH_2), 49.3 (CH), 39.7 (CH_2), 33.4 (CH_2), 31.5 (CH_2), 31.2 (CH_2), 30.7 (CH_2), 29.5 (CH_2), 28.9 (CH_2), 26.5 (CH_2), 25.0 (CH_2), 22.8 (CH_2) ppm.

IR (Film): 3385, 2931, 2099 (azide), 1655, 1354, 1198 cm^{-1}

HRMS (ESI): calc. for $[C_{23}H_{29}O_5N_6BrF_2]^+$: 469.2194; found 469.2205.

tert-butyl (5-(2-(2,6-dioxopiperidin-3-yl)-1,3-dioxoisoindolin-4-yl)pent-4-yn-1-yl)carbamate

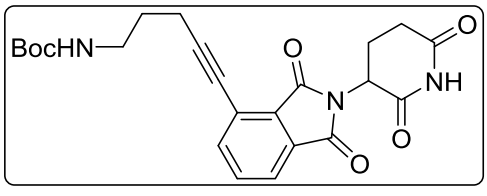

As for **4-84a,** starting from **4-83b** and **4-82.** Product afforded as an off white powder, (129 mg, **94%**).

Characterisation is consistent with that reported in the literature.[14]

5-(2-(2,6-Dioxopiperidin-3-yl)-1,3-dioxoisoindolin-4-yl)pentan-1-aminium trifluoroacetate (4-84b)

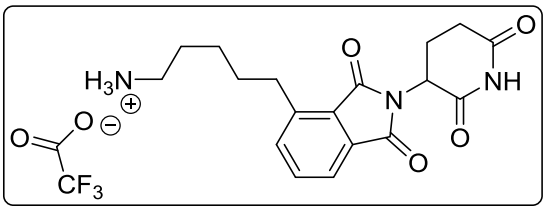

Product was prepared as for **4-85a**, starting from **4-84b** (109 mg, **81%**).

Characterisation is consistent with that reported in the literature.[14]

4-Azido-N-(5-(2-(2,6-dioxopiperidin-3-yl)-1,3-dioxoisoindolin-4-yl)pentyl)butanamide (4-86b)

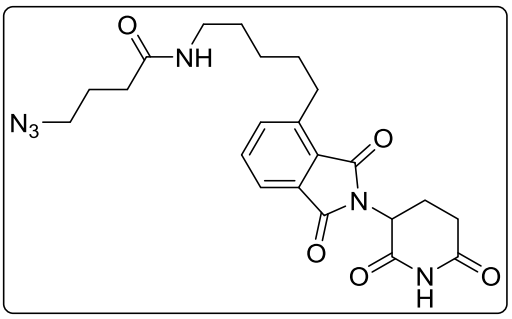

The product was synthesised following general coupling procedure B, starting from **4-77** and **4-85b** (57 mg, **49%**). Product used directly in subsequent reaction without further purification.

tert-butyl (6-(2-(2,6-dioxopiperidin-3-yl)-1-oxoisoindolin-4-yl)hex-5-yn-1-yl)carbamate (4-90a)

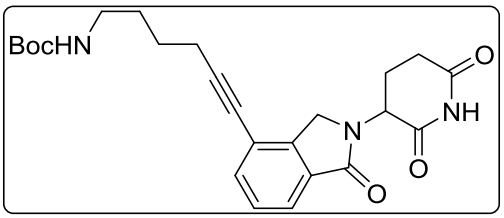

As for **4-84a**, starting from **4-89** and **4-83a,** to afford a off-white solid (105 mg, **71%**).

Characterisation was consistent with that reported in the literature.[14]

6-(2-(2,6-Dioxopiperidin-3-yl)-1-oxoisoindolin-4-yl)hexan-1-aminium chloride (4-91a)

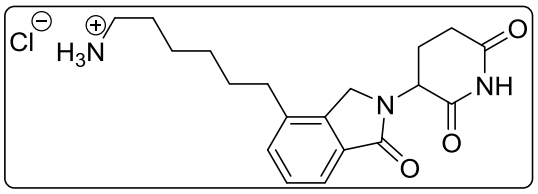

As for **4-86a**, starting from **4-90a,** to afford product as an off-white compound (70 mg, **75%**).

Characterisation is consistent with that reported in the literature.[14]

4-Azido-*N*-(6-(2-(2,6-dioxopiperidin-3-yl)-1-oxoisoindolin-4-yl)hexyl)butanamide (4-92a)

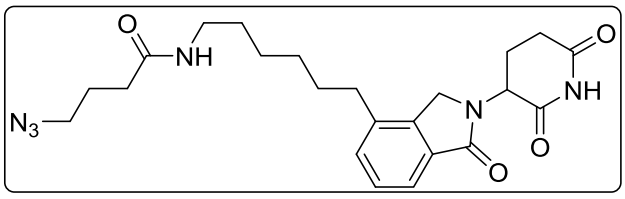

As for **4-86a**, using **4-77** and **4-91a,** to afford product as an off-white solid (56 mg, **68%**).

^{1}H NMR (400 MHz, $CDCl_3$) δ 8.42 (s, 1H), 7.72 (dd, *J* = 7, 1 Hz, 1H), 7.42 (t, *J* = 8 Hz, 1H), 7.37 (dd, *J* = 8, 1 Hz, 1H), 5.60 (s, 1H), 5.26 (dd, *J* = 13, 5 Hz, 1H), 4.44 (d, *J* = 16 Hz, 1H), 4.29 (d, *J* = 16 Hz, 1H), 3.38 – 3.33 (m, 2H), 3.23 (q, *J* = 7 Hz, 2H), 2.96 – 2.78 (m, 2H), 2.65 – 2.56 (m, 2H), 2.48 – 2.30 (m, 1H), 2.31 – 2.16 (m, 3H), 1.96 – 1.87 (m, 3H), 1.64 (p, *J* = 8 Hz, 2H), 1.49 (p, *J* = 7 Hz, 2H), 1.43 – 1.29 (m, 3H) ppm.

^{13}C NMR (101 MHz, CD_3OD) δ 171.9, 171.4, 169.9, 169.9, 140.0, 137.4, 132.1, 131.4, 128.8, 121.9, 52.0, 50.9, 50.7, 46.4, 39.6, 33.4, 32.1, 31.7, 30.8, 29.8, 29.7, 29.1, 26.8, 24.99, 24.24, 23.61 ppm.

3312, 2097 (azide), 1708, 1336, 1185

IR (Film): 3312, 2097 (azide), 1708, 1336, 1185 cm^{-1}.

HRMS (ESI): calc. for $[C_{23}H_{31}O_4N_6]^+$: 455.2401; found: 455.2406.

M_P: 154 °C.

tert-butyl (5-(2-(2,6-dioxopiperidin-3-yl)-1-oxoisoindolin-4-yl)pent-4-yn-1-yl)carbamate (4-90b)

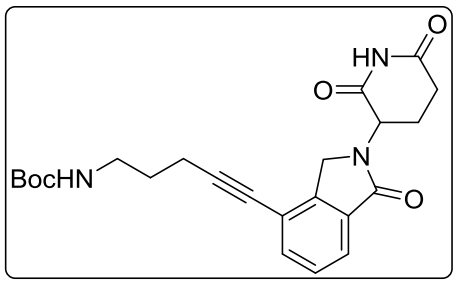

As for **4-84a**, starting from **4-89** and **4-83b,** to afford an off-white solid (85 mg, **61%**).

Characterisation is consistent with that reported in the literature.[14]

5-(2-(2,6-dioxopiperidin-3-yl)-1-oxoisoindolin-4-yl)pentan-1-aminium trifluoroacetate (4-91b)

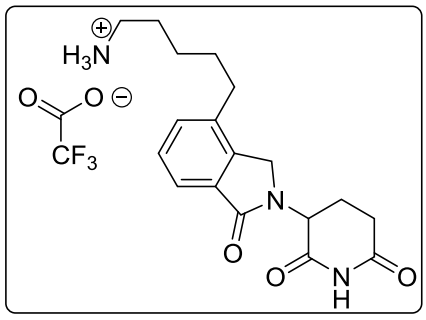

As for **4-85a**, starting from **4-90b,** to afford an off-white solid, (67 mg, **79%**).

Characterisation is consistent with that reported in the literature.[14]

4-Azido-*N*-(5-(2-(2,6-dioxopiperidin-3-yl)-1-oxoisoindolin-4-yl)pentyl)butanamide (4-92b)

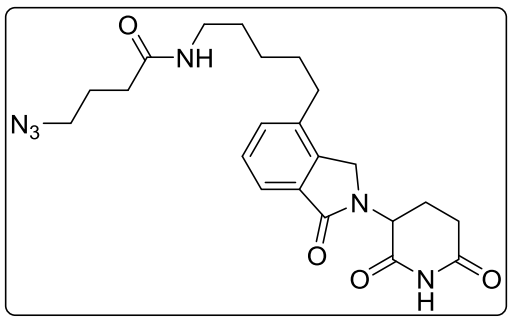

The product was prepared following general method B but using **4-77** as the starting acid and **4-91b** as the starting amine. The product was eluted from the column at 85% EtOAc/hexanes as a white solid, (43 mg, 0.095 mmol, **62%**).

TLC Rf: 0.31 (10% MeOH/DCM)

^{1}H NMR (400 MHz, $CDCl_3$) δ 8.26 (NH, s, 1H), 7.73 (dd, *J* = 7, 1 Hz, 1H), 7.43 (t, *J* = 8 Hz, 1H), 7.37 (dd, *J* = 8, 1 Hz, 1H), 5.57 (NH, s, 1H), 5.26 (dd, *J* = 13, 5 Hz, 1H), 4.45 (d, *J* = 16 Hz, 1H), 4.31 (d, *J* = 16 Hz, 1H), 3.33 (t, *J* = 7 Hz, 2H), 3.28 – 3.19 (m, 2H), 2.93 – 2.78 (m, 2H), 2.63 (td, *J* = 7, 2 Hz, 1H), 2.50 – 2.34 (m, 1H), 2.28 – 2.20 (m, 2H), 1.95 – 1.84 (m, 2H), 1.67 (p, *J* = 8 Hz, 2H), 1.53 (p, *J* = 7 Hz, 2H), 1.43 – 1.30 (m, 2H) ppm.

^{13}C NMR (101 MHz, CD_3OD) δ 171.9 (C), 171.3 (C), 169.9 (C), 169.8 (C), 140.1 (C), 137.2 (C), 132.1 (C), 131.4 (CH), 128.8 (CH), 122.0 (CH), 52.0 (CH_2), 50.9 (CH_2), 50.7 (CH), 46.3 (CH_2), 39.5 (CH_2), 33.4 (CH_2), 32.0 (CH_2), 31.7 (CH_2), 29.6 (CH_2), 26.7 (CH_2), 25.0 (CH_2), 23.6 (CH_2) ppm.

M_P: 136 °C.

2-(2,6-Dioxopiperidin-3-yl)-1,3-dioxoisoindoline-5-carboxylic acid (4-45)

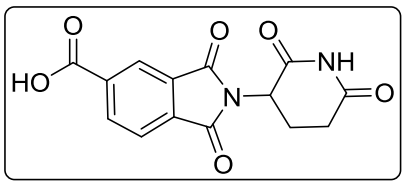

To a pressure tube charged with 1,3-dioxo-1,3-dihydroisobenzofuran-5-carboxylic acid (**4-66,** 300 mg, 1.56 mmol) in AcOH (3 mL) was added KOAc (368 mg, 3.75 mmol) and 3-aminopiperidine-2,6-dione (**4-52,** 308 mg, 1.87 mmol) then sealed and heated to 120 °C for 24 h. The reaction mixture was separated between EtOAc and water, then further organics were extracted using EtOAc. The combined organic layers were washed with brine, dried with $MgSO_4$, and then concentrated under reduced pressure to afford a beige solid, which upon recrystalisation using hot methanol afforded a white solid (364 mg, 1.20 mmol, **34%**).

The NMR spectra were consistent with that reported in the literature.[17]

TLC: R_f = 0.21 (10% MeOH/EtOAc)

^{1}H NMR (400 MHz, DMSO-d_6) δ 11.15 (s, 1H), 8.40 (dd, *J* = 8, 1 Hz, 1H), 8.27 (d, *J* = 1 Hz, 1H), 8.05 (d, *J* = 8 Hz, 1H), 5.20 (dd, *J* = 13, 5 Hz, 1H), 2.90 (ddd, *J* = 17, 14, 5 Hz, 1H), 2.66 – 2.51 (m, 2H), 2.08 (ddd, *J* = 13, 6, 3 Hz, 1H) ppm.

tert-butyl (4-(2-(2,6-dioxopiperidin-3-yl)-1,3-dioxoisoindoline-5-carboxamido)butyl)carbamate (4-67)

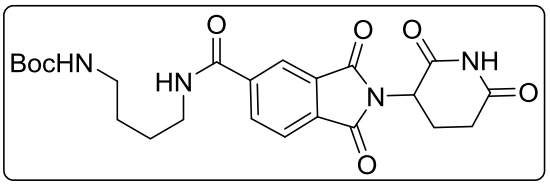

To **4-45** (350 mg, 1.16 mmol) in DMF (15 mL) at 0 °C, was added DIPEA (423 mL, 2.43 mmol), propylphosphonic anhydride solution (**T3P,** 50% in EtOAc, 379 mL, 1.27 mmol), then tert-butyl (4-aminobutyl)carbamate (**4-60a,** 244 mg, 1.27 mmol). The reaction mixture was heated at 35 °C for 22 h, before separation between EtOAc and water. The organic layer was washed with water and then brine (x 2), dried with $MgSO_4$, then concentrated under reduced pressure. To afford a yellow waxy solid (72 mg, 0.15 mmol, **13%**).

TLC: R_f = 0.27 (50% EtOAc/Hexanes)

^{1}H NMR (400 MHz, Chloroform-*d*) δ 8.52 (s, 1H), 8.28 (s, 2H), 7.91 (s, 1H), 7.39 (s, 1H), 5.00 (s, 1H), 4.74 (s, 1H), 3.51 (d, *J* = 18 Hz, 2H), 3.17 (d, *J* = 19 Hz, 2H), 2.91 (d, *J* = 17 Hz, 1H), 2.80 (d, *J* = 42 Hz, 2H), 2.16 (d, *J* = 15 Hz, 1H), 1.76 – 1.50 (m, 4H), 1.44 (s, 9H) ppm.

^{13}C NMR (101 MHz, Methanol-d_4) δ 171.6 (C), 168.3 (C), 165.1 (C), 165.0 (C), 139.0 (C), 132.2 (C), 131.8 (C), 130.5 (CH), 121.7 (CH), 120.1 (CH), 87.3 (C), 77.0 (CH_2), 56.9 (CH), 47.9 (CH_2), 38.0 (CH_2), 29.2 (CH_2), 25.8 (3 x CH_3), 24.6 (CH_2), 20.6 (CH_2) ppm.

4-(2-(2,6-Dioxopiperidin-3-yl)-1,3-dioxoisoindoline-5-carboxamido)butan-1-aminium trifluoroacetate (4-68).

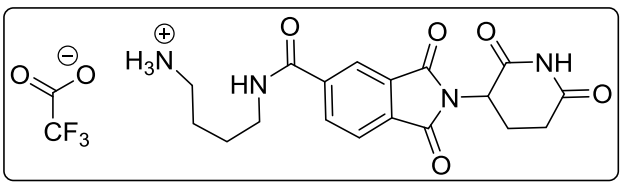

The product was obtained utilising the method described for **4-62c,** but using **4-68**. The product was isolated as a yellow/orange film and used directly without further purification (134 mg, 0.28 mmol, **94%**).

TLC: R_f = 0.05 (100% EtOAc/Hexanes)

^{1}H NMR (400 MHz, Methanol-d_4) δ 8.30 – 8.25 (m, 2H), 7.98 (dq, J = 8, 1 Hz, 1H), 5.18 (ddd, J = 13, 5, 1 Hz, 1H), 3.49 – 3.44 (m, 2H), 2.99 (q, J = 5, 3 Hz, 2H), 2.94 – 2.68 (m, 3H), 2.16 (dddd, J = 13, 8, 5, 2 Hz, 1H), 1.74 (tt, J = 5, 2 Hz, 5H) ppm.

^{13}C NMR (101 MHz, Methanol-d_4) δ 173.1 , 170.0 , 166.7 , 158.8 , 158.5 , 133.3 , 123.3 (CH), 121.6 (CH), 116.7 , 113.8 , 113.2 , 64.2 (CH), 38.9 (CH_2), 30.7 (CH_2), 29.3 (CH_2), 26.0 (CH_2), 24.5 (CH_2), 22.2 (CH_2) ppm.

tert-Butyl (2-(2-(2-(2-(2,6-dioxopiperidin-3-yl)-1,3-dioxoisoindoline-5-carboxamido)ethoxy)ethoxy)ethyl)carbamate (4-69)

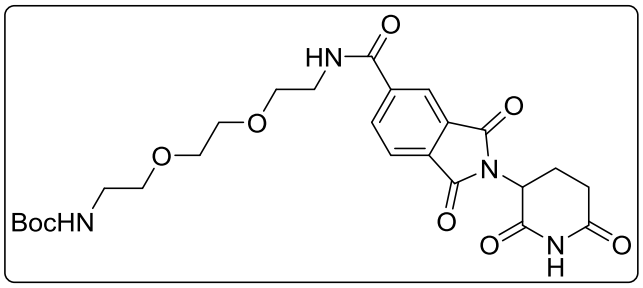

The product was prepared following general method B using tert-butyl (2-(2-(2-aminoethoxy)ethoxy)ethyl)carbamate (**4-63a)** and 2-(2,6-dioxopiperidin-3-yl)-1,3-dioxoisoindoline-5-carboxylic acid (**4-66**). The crude was purified by flash column chromatography, product eluted at 80% EtOAc/hexanes as a white solid, (739 mg, 1.56 mmol, **92%**).

TLC: R_f = 0.38 (100% EtOAc)

^{1}H NMR (400 MHz, Chloroform-*d*) δ 9.25 (s, 2H), 8.27 (d, *J* = 7.9 Hz, 2H), 7.90 (d, *J* = 7.7 Hz, 2H), 7.52 (s, 1H), 5.15 (s, 1H), 5.03 (ddd, *J* = 9.9, 5.4, 2.3 Hz, 1H), 3.75 – 3.63 (m, 12H), 3.56 (td, *J* = 5.3, 2.1 Hz, 3H), 3.35 – 3.24 (m, 3H), 2.94 – 2.75 (m, 3H), 2.21 – 2.13 (m, 1H), 1.41 (s, 9H).

^{13}C NMR (101 MHz, Chloroform-*d*) δ 171.9 , 168.8 , 166.6 , 165.5 , 156.1 , 140.5 , 137.8 , 134.0 , 131.8 , 129.0 , 128.2 , 125.3 , 79.2 , 70.1 , 49.5 , 40.2 (CH_2), 40.1 (CH_2), 31.3 (CH_2), 28.4 (3 x CH_3), 22.5 (CH_2), 21.4 (CH_2).

IR (NaCl) υ_{max}: 3303, 2921, 1723, 1643, 1349, 1192 cm^{-1}

HRMS (ESI): calc. for $[C_{25}H_{33}O_9N_4]^+$: 878.18563; found 878.18526.

2-(2-(2-(2-(2,6-Dioxopiperidin-3-yl)-1,3-dioxoisoindoline-5-carboxamido)ethoxy)ethoxy)ethan-1-aminium 2,2,2-trifluoroacetate (4-70)

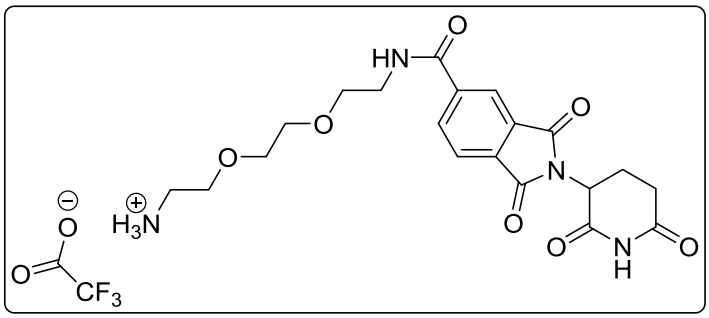

The product was obtained utilising the method described for **4-62c,** but using **4-69**. The product was isolated as a yellow/orange film and used directly without further purification (167 mg, 0.27 mmol **100%**).

TLC: R_f = 0.07 (100% EtOAc/Hexanes)

^{1}H NMR (400 MHz, Methanol-d_4) δ 8.25 (td, J = 4.0, 1.5 Hz, 2H), 7.92 (d, J = 8.2 Hz, 1H), 5.15 (dd, J = 12.7, 5.4 Hz, 1H), 3.74 – 3.60 (m, 11H), 3.15 (t, J = 5.1 Hz, 2H), 2.96 – 2.66 (m, 3H), 2.17 (ddq, J = 10.3, 5.4, 2.7 Hz, 1H).

^{13}C NMR (101 MHz, Methanol-d_4) δ 173.30 , 169.93 , 166.69 , 140.23 , 133.65 , 133.50 , 131.86 , 123.41 , 121.93 , 115.97 , 113.15 , 69.85 (d, J = 6.4 Hz), 69.02 , 66.42 , 39.60 , 39.27 , 30.76 , 26.28 , 22.09 .

N-(2-(2-(2-(4-azidobutanamido)ethoxy)ethoxy)ethyl)-2-(2,6-dioxopiperidin-3-yl)-1,3-dioxoisoindoline-5-carboxamide (4-79)

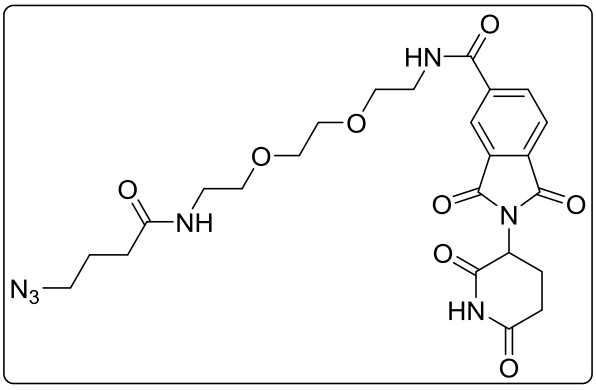

The product was prepared following general method B using **4-70** and **4-77**. The crude was purified by flash column chromatography, product eluted at 80% EtOAc/hexanes as an off-white waxy solid, (84 mg, 0.15 mmol, **37%**).

TLC: R_f = 0.10 (50% EtOAc/Hexanes)

^{1}H NMR (400 MHz, Chloroform-*d*) δ 8.64 (s, 1H), 8.29 (dd, *J* = 8, 2 Hz, 1H), 8.25 (dd, *J* = 2, 1 Hz, 1H), 7.92 (dd, *J* = 8, 1 Hz, 1H), 7.34 (s, 1H), 6.22 (t, *J* = 5 Hz, 1H), 5.01 (dd, *J* = 12, 5 Hz, 1H), 3.75 – 3.63 (m, 8H), 3.58 (t, *J* = 6 Hz, 2H), 3.44 (q, *J* = 6 Hz, 2H), 3.33 (t, *J* = 7 Hz, 2H), 2.97 – 2.72 (m, 3H), 2.26 (t, *J* = 7 Hz, 2H), 1.89 (p, *J* = 7 Hz, 2H) ppm.

^{13}C NMR (101 MHz, Chloroform-*d*) δ 172.0 (C), 170.9 (C), 168.2 (C), 166.7 (C), 166.4 (C), 165.3 (C), 140.6 (C), 134.2 (CH), 133.6 (C), 131.8 (C), 124.1 (CH), 121.9 (CH), 70.2 (CH_2), 70.1 (CH_2), 69.8 (CH_2), 69.5 (CH_2), 50.8 (CH_2), 49.6 (CH), 40.1 (CH_2), 39.1 (CH_2), 33.1 (CH_2), 31.4 (CH_2), 24.8 (CH_2), 22.6 (CH_2) ppm.

IR (NaCl) υ_{max}: 2928, 2099 (azide), 1693, 1359, 1192 cm^{-1}

HRMS (ESI): calc. for $[C_{24}H_{30}O_8N_7]^+$: 544.21504; found 544.21.

3-(3-Bromo-4-((2,4-difluorobenzyl)oxy)-6-methyl-2-oxopyridin-1(2*H*)-yl)-*N*-(4-((2-(2,6-dioxopiperidin-3-yl)-1,3-dioxoisoindolin-4-yl)amino)butyl)-4-methylbenzamide (*NR-1a*)

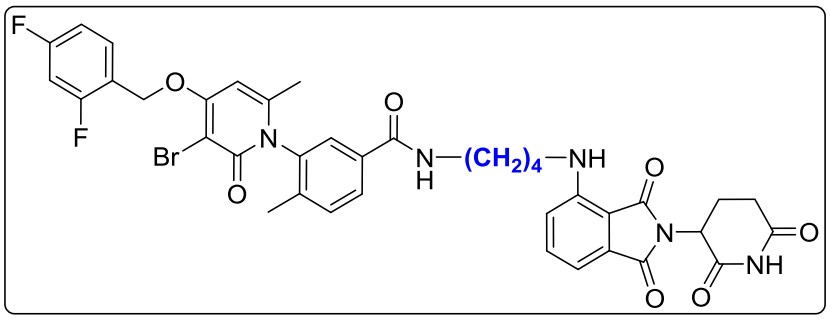

The product was prepared using general method A described previously, using **4-62a.** The product was purified using preparative TLC using 5% MeOH/DCM as eluent, to afford a fluorescent yellow solid (3 g, 3.8 μmol, **6%**).

mp =108.1 – 108.6 °C

^{1}H NMR (400 MHz, $CDCl_3$) δ 8.07 (d, *J* = 43 Hz, 1H), 7.75 (d, *J* = 8 Hz, 1H), 7.65 – 7.57 (m, 1H), 7.52 – 7.37 (m, 3H), 7.08 (dd, *J* = 7, 1 Hz, 1H), 7.01 – 6.95 (m, 1H), 6.92 – 6.84 (m, 2H), 6.51 (s, 1H), 6.24 (s, 1H), 6.15 (d, *J* = 1 Hz, 1H), 5.25 (s, 2H), 4.90 (dd, *J* = 11, 6 Hz, 1H), 3.43 (s, 2H), 3.32 (t, *J* = 6 Hz, 2H), 2.92 – 2.70 (m, 3H), 2.10 (s, 4H), 1.91 (d, *J* = 1 Hz, 3H), 1.76 – 1.66 (m, 4H) ppm.

HPLC MS: RT: 5.02 min, *m/z*: 791.2

3-(3-Bromo-4-((2,4-difluorobenzyl)oxy)-6-methyl-2-oxopyridin-1(2*H*)-yl)-*N*-(2-(2-(2-((2-(2,6-dioxopiperidin-3-yl)-1,3-dioxoisoindolin-4-yl)amino)ethoxy)ethoxy)ethyl)-4-methylbenzamide (*NR-1b*)

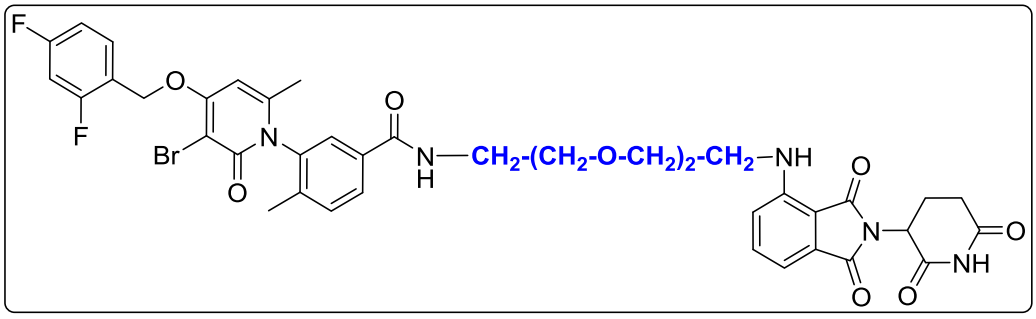

The product was prepared using general method A described previously, but using **4-65a.** The product was purified using preparative TLC using 5% MeOH/DCM as eluent, to afford a fluorescent yellow solid (2.8 g, 3.3 μmol, **3%**).

mp =112 °C

^{1}H NMR (400 MHz, $CDCl_3$) δ 8.80 (d, *J* = 73 Hz, 1H), 7.78 (dt, *J* = 8, 2 Hz, 1H), 7.59 (tdd, *J* = 9, 6, 3 Hz, 1H), 7.50 (dd, *J* = 10, 2 Hz, 1H), 7.45 (ddd, *J* = 8, 7, 1 Hz, 1H), 7.33 (dd, *J* = 8, 5 Hz, 1H), 7.11 – 7.03 (m, 2H), 6.99 – 6.94 (m, 1H), 6.90 – 6.83 (m, 2H), 6.52 (d, *J* = 15 Hz, 1H), 6.09 (d, *J* = 5 Hz, 1H), 5.20 (d, *J* = 7 Hz, 2H), 4.86 (ddd, *J* = 12, 5, 4 Hz, 1H), 3.73 – 3.50 (m, 10H), 3.41 (s, 3H), 2.85 – 2.64 (m, 2H), 2.12 – 2.02 (m, 4H), 1.87 (d, *J* = 5 Hz, 3H) ppm.

^{13}C NMR (101 MHz, $CDCl_3$) δ 171.3 (C), 169.4 (d, *J* = 4 Hz, C), 168.7 (C), 167.5 (C), 166.4 (d, *J* = 6 Hz, C), 164.2 (d, *J* = 12 Hz, C), 163.1 (d, *J* = 2 Hz, C), 161.9 – 161.2 (m, C), 160.4 (d, *J* = 4 Hz, C), 146.7 (d, *J* = 3 Hz, C), 146.2 (d, *J* = 4 Hz, C), 138.8 (d, *J* = 7 Hz, C), 137.5 (d, *J* = 7 Hz, C), 136.0 (CH), 134.2 (d, *J* = 4 Hz, C), 132.4 (d, *J* = 2 Hz, C), 131.4 (CH), 130.3 (dd, J_F = 10, 5 Hz, CH), 128.3 (CH), 126.6 (d, J_F = 11 Hz, CH), 118.6 (ddd, J_F = 14, 4, 1 Hz, C), 116.9 (d, *J* = 3 Hz, CH), 111.9 (dt, J_F = 22, 4 Hz, CH), 111.6 (CH), 110.2 (C), 103.9 (t, J_F = 25 Hz, CH), 96.8 (d, *J* = 4 Hz, C), 96.0 (d, *J* = 3 Hz, CH), 70.4* , 70.4 (CH_2), 70.1 (CH_2), 69.6* , 69.6 (CH_2), 69.1* , 69.1 (CH_2), 64.3 (d, J_F = 4 Hz, CH_2), 48.9 (CH), 42.1 (CH_2), 39.9 (CH_2), 39.8* , 31.4 (CH_2), 22.8* , 22.7 (CH_2), 21.5* , 21.4 (CH_3), 17.3 (CH_3) ppm. (Extra signals* due to rotational isomers, some quaternary carbon signals were not observed).

IR (NaCl) υ_{max}: 3307, 2929, 1693, 1641, 1353, 1196, 731 cm^{-1}

HRMS (ESI): calc. for $[C_{40}H_{39}O_9N_5BrF_2]^+$: 850.18937, found 850.18834.

HPLC MS RT: 4.89 min, *m/z*: 850.2.

3-(3-Bromo-4-((2,4-difluorobenzyl)oxy)-6-methyl-2-oxopyridin-1(2*H*)-yl)-*N*-(20-((2-(2,6-dioxopiperidin-3-yl)-1,3-dioxoisoindolin-4-yl)amino)-3,6,9,12,15,18-hexaoxaicosyl)-4-methylbenzamide (*NR-1c*)

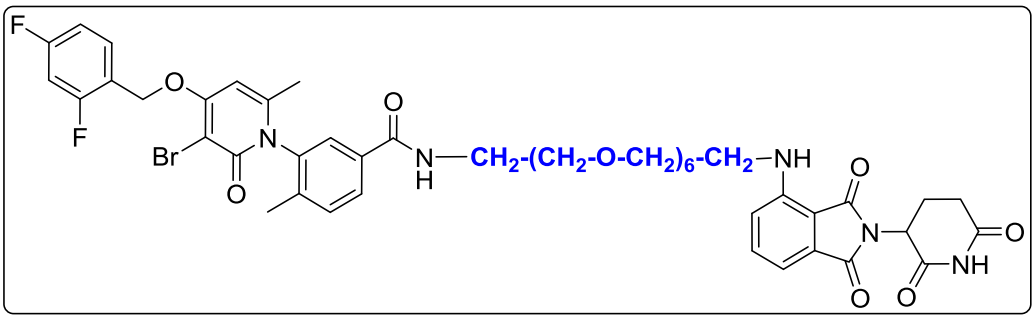

The product was prepared using general method B described previously, starting from **4-65b.** Product eluted at 4% MeOH/DCM as a yellow oil (95 mg, 0.093 mmol, **77%**).

^{1}H NMR (400 MHz, $CDCl_3$) δ 8.66 (NH, bs, 1H), 7.81 (dd, *J* = 8, 2 Hz, 1H), 7.60 (td, *J* = 9, 6 Hz, 1H), 7.54 (s, 1H), 7.47 (dd, *J* = 9, 7 Hz, 1H), 7.39 (d, *J* = 7 Hz, 1H), 7.27 (NH, s, 1H), 7.08 (d, *J* = 7 Hz, 1H), 6.99 – 6.94 (m, 1H), 6.92 – 6.84 (m, 2H), 6.48 (NH, t, *J* = 6 Hz, 1H), 6.13 (s, 1H), 5.25 (s, 2H), 4.89 (dd, *J* = 12, 6 Hz, 1H), 4.11 (d, *J* = 5 Hz, 1H), 3.69 (t, *J* = 5 Hz, 2H), 3.66 – 3.53 (m, 22H), 3.44 (q, *J* = 5 Hz, 2H), 2.89 – 2.65 (m, 2H), 2.12 – 2.08 (m, 4H), 2.05 – 2.01 (m, 2H), 1.90 (s, 3H) ppm.

^{13}C NMR (101 MHz, $CDCl_3$) δ 171.4 (C), 169.4 (C), 168.6 (C), 167.8 (C), 166.6 (C), 163.2 (C), 160.5 (C), 146.9 (C), 146.3 (C), 139.0 (C), 137.8 (C), 136.2 (CH), 134.5 (C), 132.6 (C), 131.5 (CH), 130.6 (dd, J_F = 10, 5 Hz, CH), 128.3 (CH), 127.1 (d, J_F = 2 Hz, CH), 118.8 (dd, J_F = 14, 4 Hz, C), 116.9 (CH), 112.1 (dd, *J* = 21, 4 Hz, CH), 111.7 (CH), 110.4 (C), 104.1 (t, J_F = 25 Hz, CH), 97.0 (C), 96.1 (CH), 70.9 (CH_2), 70.8 (CH_2), 70.7 (CH_2), 70.7 (CH_2), 70.6 (CH_2), 70.6 (CH_2), 70.6 (CH_2), 70.5 (CH_2), 69.9 (CH_2), 69.5 (CH_2), 64.5 (d, J_F = 4 Hz, CH_2) 49.0 (CH), 42.5 (CH_2), 42.3 (CH_2), 40.0 (CH_2), 31.6 (CH_2), 23.6 (CH_2), 22.9 (CH_2), 21.6 (CH_3), 17.5 (CH_3) ppm. (Some quaternary carbon signals were not observed).

IR (NaCl) υ_{max}: 3386, 3080, 2871, 1698, 1527, 1352, 1199 cm^{-1}.

HRMS (ESI): calc. for $[C_{48}H_{55}O_{13}N_5BrF_2]^+$: 1026.2942; found: 1026.2940.

***N*-(4-(3-(3-Bromo-4-((2,4-difluorobenzyl)oxy)-6-methyl-2-oxopyridin-1(2*H*)-yl)-4-methylbenzamido)butyl)-2-(2,6-dioxopiperidin-3-yl)-1,3-dioxoisoindoline-5-carboxamide (*NR-2a*)**

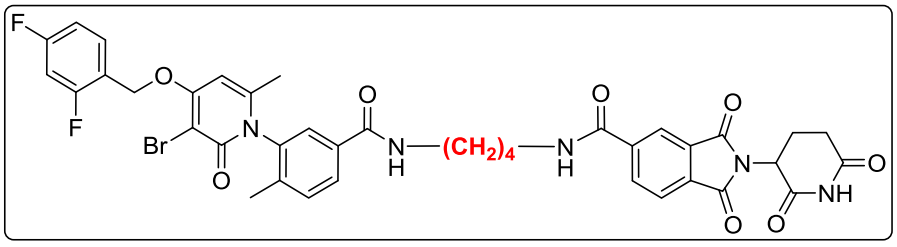

The product was prepared following general method A using **4-68** and **4-7**. The crude was purified by flash column chromatography, product eluted at 80% EtOAc/hexanes as a white waxy solid, (19 mg, 0.023 mmol, **8%**).

^{1}H NMR (400 MHz, $CDCl_3$) δ 8.51 – 8.40 (m, 2H), 8.39 – 8.32 (m, 1H), 7.84 (d, *J* = 8 Hz, 1H), 7.67 – 7.56 (m, 2H), 7.33 (d, *J* = 14 Hz, 1H), 7.13 (dd, *J* = 13, 8 Hz, 1H), 7.00 (t, *J* = 9 Hz, 1H), 6.92 – 6.83 (m, 1H), 6.21 (s, 1H), 5.25 (s, 2H), 4.99 (dd, *J* = 12, 5 Hz, 1H), 3.54 (s, 1H), 3.41 (s, 2H), 3.22

(s, 1H), 2.94 – 2.72 (m, 3H), 2.15 (dd, *J* = 15, 8 Hz, 1H), 2.05 (d, *J* = 3 Hz, 4H), 1.76 (d, *J* = 7 Hz, 3H), 1.50 (s, 2H), 1.44 – 1.32 (m, 2H) ppm.

IR (NaCl) υ_{max}: 3426, 1716, 1644, 1385, 1198 cm^{-1}.

***N*-(2-(2-(2-(3-(3-Bromo-4-((2,4-difluorobenzyl)oxy)-6-methyl-2-oxopyridin-1(2*H*)-yl)-4-methylbenzamido)ethoxy)ethoxy)ethyl)-2-(2,6-dioxopiperidin-3-yl)-1,3-dioxoisoindoline-5-carboxamide (*NR-2b*)**

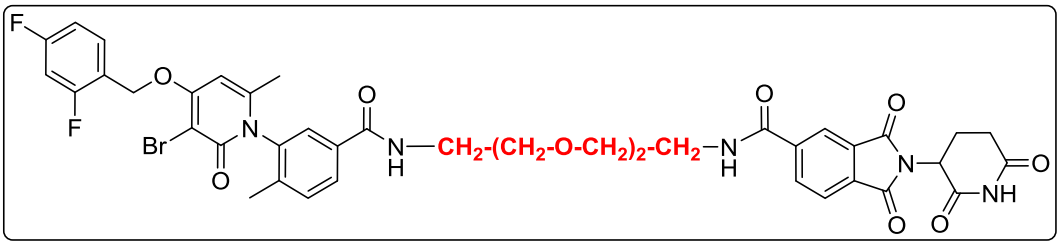

The product was prepared following general method B using **4-70** and **4-7**. The crude was purified by flash column chromatography, product eluted at 80% EtOAc/hexanes as a off-white waxy solid, (78 mg, 0.11 mmol, **12%**).

^{1}H NMR (400 MHz, $CDCl_3$) δ 9.26 (d, *J* = 14 Hz, 1H), 8.16 – 8.11 (m, 2H), 8.04 – 7.97 (m, 1H), 7.73 – 7.69 (m, 1H), 7.60 (td, *J* = 8, 2 Hz, 1H), 7.52 (td, *J* = 9, 6 Hz, 1H), 7.35 (t, *J* = 2 Hz, 1H), 7.28 – 7.18 (m, 2H), 6.93 – 6.86 (m, 1H), 6.80 (ddd, *J* = 10, 9, 3 Hz, 1H), 6.17 (s, 1H), 5.17 (s, 2H), 4.95 (q, *J* = 8, 6 Hz, 1H), 3.63 – 3.32 (m, 12H), 2.80 – 2.65 (m, 3H), 2.07 (q, *J* = 4, 3 Hz, 1H), 1.95 (s, 3H), 1.82 – 1.78 (m, 3H) ppm.

^{13}C NMR (101 MHz, $CDCl_3$) δ 171.7 (d, J_F = 3 Hz, C), 168.6 (d, *J* = 2 Hz, C), 166.5 (d, *J* = 5 Hz, C), 166.0 (d, *J* = 4 Hz, C), 165.4 (C), 164.2 (d, *J* = 12 Hz, C), 163.5 (C), 161.7 (d, *J* = 12 Hz, C), 161.3 (d, J_F = 12 Hz, C), 160.5 (d, J_F = 2 Hz, C), 158.9 (d, J_F = 12 Hz, C), 146.6 (d, J_F = 2 Hz, C), 140.4 (d, J_F = 2 Hz, C), 138.7 (d, J_F = 4 Hz, C), 137.2 (C), 133.9 (C), 133.9 (C), 133.2 (C), 131.7 – 131.3 (m, CH), 130.4 (dd, J_F = 10, 5 Hz, CH), 128.5 (d, J_F = 5 Hz, CH), 125.9 (CH), 123.6 (CH), 122.3 (d, *J* = 4 Hz, CH), 118.4 (dd, J_F = 14, 4 Hz, CH), 111.8 (dd, J_F = 21, 4 Hz, CH), 103.9 (t, J_F = 25 Hz, CH), 96.5 (CH), 96.4 (CH), 70.1 (CH_2), 69.7 (CH_2), 69.5 (CH_2), 69.4 (CH_2), 68.8 (CH_2), 64.5 (d, J_F = 4 Hz, CH_2), 49.4 (CH), 39.5 (d, *J* = 5 Hz, CH_2), 31.3 (CH_2), 22.5 (CH_2), 21.3 (d, *J* = 2 Hz, CH_3), 17.1 (d, *J* = 2 Hz, CH_3) ppm.

IR (NaCl) υ_{max}: 3317, 2919, 1723, 1643, 1349, 1198, 731 cm^{-1}.

HRMS (ESI): calc. for $[C_{43}H_{41}O_{11}N_2BrF_2]^+$: 878.18563; found 878.18526.

HPLC: rt = 4.52 min, *m/z* = 878.

3-(3-Bromo-4-((2,4-difluorobenzyl)oxy)-6-methyl-2-oxopyridin-1(2*H*)-yl)-*N*-(4-(1-(2-(2-(2-(2-((2-(2,6-dioxopiperidin-3-yl)-1,3-dioxoisoindolin-4-yl)amino)ethoxy)ethoxy)ethoxy)ethyl)-1*H*-1,2,3-triazol-4-yl)butyl)-4-methylbenzamide (*NR-3a*)

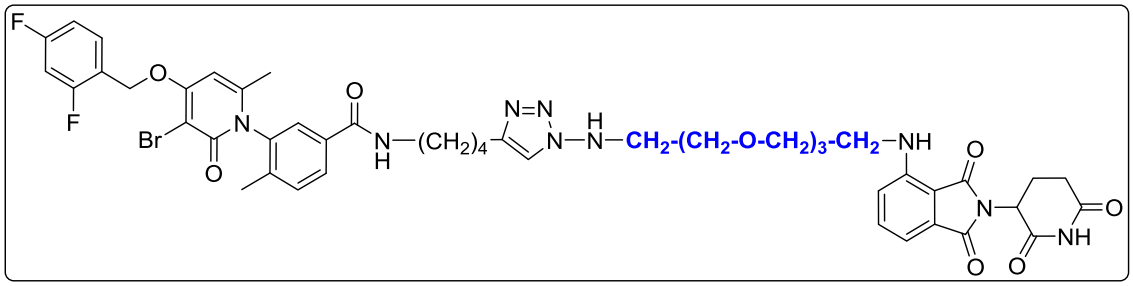

The product was prepared following method C, using **4-72a** and **4-74a,** and eluted from the column at 7% MeOH/DCM as a fluorescent yellow solid, (56 mg, 0.055 mmol, **89%**).

^{1}H NMR (400 MHz, $CDCl_3$) δ 8.76 (d, *J* = 17 Hz, 1H), 7.80 (d, *J* = 8 Hz, 1H), 7.60 (td, *J* = 9, 6 Hz, 1H), 7.52 (d, *J* = 5 Hz, 1H), 7.46 (dd, *J* = 9, 7 Hz, 1H), 7.32 (d, *J* = 8 Hz, 1H), 7.06 (d, *J* = 7 Hz, 1H), 7.01 (s, 1H), 6.98 – 6.93 (m, 1H), 6.89 (d, *J* = 9 Hz, 1H), 6.86 – 6.81 (m, 1H), 6.46 (t, *J* = 6 Hz, 1H), 6.14 (s, 1H), 5.21 (s, 2H), 4.93 – 4.87 (m, 1H), 4.45 (t, *J* = 5 Hz, 2H), 3.83 (t, *J* = 5 Hz, 2H), 3.69 (t, *J* = 5 Hz, 2H), 3.64 – 3.54 (m, 8H), 3.43 (q, *J* = 5 Hz, 2H), 3.37 – 3.18 (m, 3H), 2.89 – 2.58 (m, 5H), 2.10 – 2.05 (m, 4H), 1.89 (s, 3H), 1.75 – 1.60 (m, 2H), 1.61 – 1.46 (m, 2H) ppm.

^{13}C NMR (101 MHz, $CDCl_3$) δ 171.6 (C), 169.4 (C), 168.8 (d, J_F = 6 Hz, C), 167.7 (d, J_F = 3 Hz, C), 166.1 (d, J_F = 2 Hz, C), 164.3 (d, J_F = 12 Hz, C), 163.3 (C), 161.8 (d, J_F = 12 Hz, C), 161.3 (d, J_F = 12 Hz, C), 160.5 (C), 158.8 (d, J_F = 11 Hz, C), 146.8 (C), 146.7 (C), 138.5 (C), 137.4 (C), 136.1 (CH), 134.4 (d, J_F = 3 Hz, C), 132.5 (C), 131.4 (CH), 130.2 (dd, J_F = 9, 5 Hz, CH), 128.7 (CH), 126.6 (CH), 118.7 (dd, J_F = 14, 3 Hz, C), 116.9 (CH), 112.0 (dd, J_F = 21, 3 Hz, CH), 111.7 (CH), 110.3 (C), 104.0 (t, J_F = 25 Hz, CH), 96.6 (CH), 96.4 (CH), 70.8 (CH_2), 70.6 (CH_2), 69.6 (CH), 69.6 (CH_2), 64.5 (d, J_F = 4 Hz, CH_2), 53.6 (CH_2), 50.2 (CH_2), 49.0 (CH_2), 42.4 (CH_2), 39.9 (CH_2), 31.5 (CH_2), 29.8 (CH_2), 28.7 (CH_2), 26.7 (CH_2), 25.3 (CH_2), 22.9 (CH_2), 21.7 (CH_3), 17.4 (CH_3) ppm.

IR (NaCl) υ_{max}: 3392, 2920, 1698, 1643, 1353, 1101cm^{-1}.

HRMS (ESI): calc. for $[C_{48}H_{52}O_{10}N_8BrF_2]^+$: 1017.2952; found 1017.2981.

3-(3-Bromo-4-((2,4-difluorobenzyl)oxy)-6-methyl-2-oxopyridin-1(2*H*)-yl)-*N*-(4-(1-(14-((2-(2,6-dioxopiperidin-3-yl)-1,3-dioxoisoindolin-4-yl)amino)-3,6,9,12-tetraoxatetradecyl)-1*H*-1,2,3-triazol-4-yl)butyl)-4-methylbenzamide (*NR-3b*)

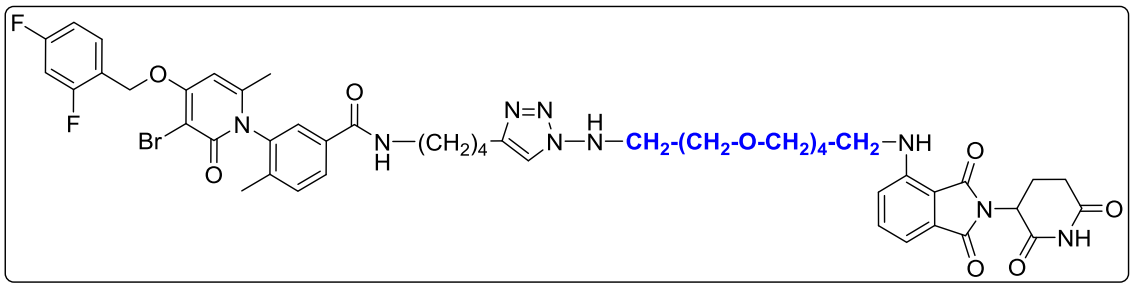

The product was prepared following method C, using **4-72a** and **4-74b,** and eluted from the column at 7% MeOH/DCM as a fluorescent yellow solid, (41 mg, 0.039 mmol, **78%**).

^{1}H NMR (400 MHz, $CDCl_3$) δ 8.60 (d, *J* = 15 Hz, 1H), 7.81 (d, *J* = 8 Hz, 1H), 7.61 (td, *J* = 9, 6 Hz, 1H), 7.51 (s, 1H), 7.47 (dd, *J* = 9, 7 Hz, 1H), 7.36 (d, *J* = 8 Hz, 1H), 7.08 (d, *J* = 7 Hz, 1H), 7.02 – 6.94 (m, 1H), 6.92 – 6.82 (m, 2H), 6.48 (t, *J* = 6 Hz, 1H), 6.13 (s, 1H), 5.23 (s, 2H), 4.89 (dd, *J* = 12, 5 Hz, 1H), 4.47 (t, *J* = 5 Hz, 2H), 3.84 (t, *J* = 5 Hz, 2H), 3.69 (t, *J* = 5 Hz, 2H), 3.66 – 3.56 (m, 16H), 3.43 (q, *J* = 5 Hz, 2H), 3.32 (td, *J* = 14, 13, 6 Hz, 2H), 2.88 – 2.64 (m, 3H), 2.07 (s, 3H), 1.91 (s, 3H), 1.81 – 1.68 (m, 3H), 1.59 (s, 2H) ppm.

^{13}C NMR (101 MHz, $CDCl_3$) δ 171.5 (C), 169.4 (C), 168.7 (C), 167.7 (d, J_F = 3 Hz, C), 166.2 (d, J_F = 2 Hz, C), 164.3 (d, J_F = 12 Hz, C), 163.3 (C), 161.8 (d, J_F = 12 Hz, C), 161.3 (d, J_F = 12 Hz, C), 160.5 (C), 158.9 (d, J_F = 12 Hz, C), 146.9 (C), 146.6 (C),138.6 (C), 137.5 (C), 136.2 (CH), 134.5 (d, J_F = 2 Hz, C), 132.6 (C), 131.5 (CH), 130.3 (dd, J_F = 10, 5 Hz, CH), 128.6 (CH), 126.6 (CH), 118.7 (dd, J_F = 14, 4 Hz, C), 116.9 (CH), 112.0 (dd, J_F = 22, 4 Hz, CH), 111.7 (CH), 110.4 (C), 104.3 – 103.7 (m, CH), 96.7 (CH), 96.4 (CH), 70.8 (CH_2), 70.7 (CH_2), 70.7 (2 x CH_2) , 70.5 (CH_2), 69.6 (CH_2), 69.6 (CH_2), 64.5 (d, J_F = 4 Hz, CH_2), 53.6 (CH_2), 50.2 (CH_2), 49.0 (CH), 42.5 (CH_2), 40.0 (CH_2), 31.6 (CH_2), 28.7 (CH_2), 26.8 (CH_2), 25.3 (CH_2), 22.9 (CH_2), 21.7 (CH_3), 17.4 (CH_3) ppm.

IR (NaCl) υ_{max}: 3361, 2941, 1697, 1644, 1355, 1130 cm^{-1}

HRMS (ESI): calc. for $[C_{50}H_{56}O_{11}N_8BrF_2]^+$:; found.

3-(3-Bromo-4-((2,4-difluorobenzyl)oxy)-6-methyl-2-oxopyridin-1(2*H*)-yl)-*N*-(4-(1-(4-((2-(2-(2-((2-(2,6-dioxopiperidin-3-yl)-1,3-dioxoisoindolin-4-yl)amino)ethoxy)ethoxy)ethyl)amino)-4-oxobutyl)-1*H*-1,2,3-triazol-4-yl)butyl)-4 methylbenzamide (*NR-3c*)

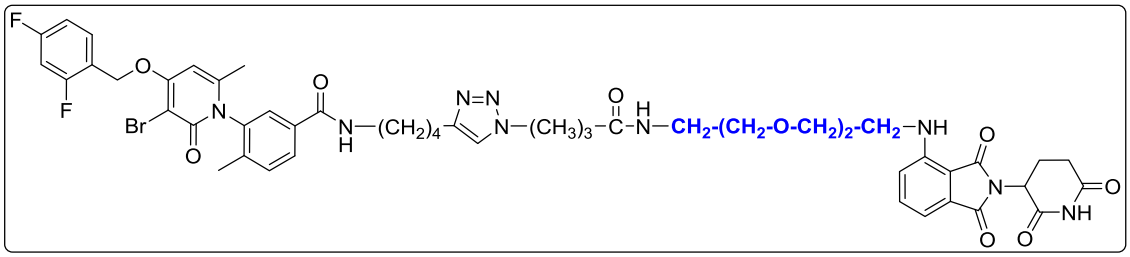

The product was prepared following method C, using **4-72a** and **4-78,** and eluted from the column at 95% EtOAc as a fluorescent yellow solid, (61 mg, 0.057 mmol, **57%**).

DSC = 218.2 °C (peak), 178.5 °C (onset)

^{1}H NMR (400 MHz, $CDCl_3$) δ 9.40 (bs, 1H), 7.74 (d, *J* = 8 Hz, 1H), 7.57 – 7.46 (m, 2H), 7.40 (dd, *J* = 9, 7 Hz, 1H), 7.25 (d, *J* = 8 Hz, 1H), 6.99 (d, *J* = 7 Hz, 1H), 6.89 (td, *J* = 9, 3 Hz, 1H), 6.81 (d, *J* = 9 Hz, 1H), 6.76 (ddd, *J* = 11, 9, 3 Hz, 1H), 6.61 (bs, 1H), 6.43 (t, *J* = 5 Hz, 1H), 6.10 (s, 1H), 5.14 (s, 2H), 4.85 (q, *J* = 6, 5 Hz, 1H), 4.24 (s, 2H), 3.62 (t, *J* = 5 Hz, 2H), 3.55 (s, 4H), 3.47 (t, *J* = 5 Hz, 2H), 3.34 (dt, *J* = 18, 5 Hz, 4H), 3.22 (s, 1H), 3.14 (s, 1H), 2.66 (td, *J* = 21, 11 Hz, 6H), 2.09 – 2.00 (m, 6H), 1.97 (s, 3H), 1.83 (s, 3H), 1.58 (s, 2H), 1.44 (s, 2H) ppm.

^{13}C NMR (101 MHz, $CDCl_3$) δ 172.0 (C), 171.8 (C), 169.4 (C), 169.1 (C), 169.0 (C), 167.6 (d, J_F = 1 Hz, C), 165.9 (d, J_F = 2 Hz, C), 164.2 (d, J_F = 12 Hz, C), 163.3 (C), 161.7 (d, J_F = 12 Hz, C), 161.2 (d, J_F = 12 Hz, C), 160.4 (C), 158.7 (d, J_F = 12 Hz, C), 146.7 (d, J_F = 7 Hz, C), 138.4 (C), 137.3 (C), 136.1 (CH), 134.2 (d, *J* = 3 Hz, C), 132.5 (C), 131.3 (CH), 130.1 (dd, J_F = 10, 5 Hz, CH), 128.6 (CH), 126.5 (CH), 118.6 (dd, J_F = 14, 4 Hz, C), 116.8 (CH), 111.8 (dd, J_F = 21, 4 Hz, CH), 111.6 (CH), 110.2 (C), 103.9 (t, J_F = 25 Hz, CH), 96.4 (CH), 96.4 (CH), 70.6 (CH_2), 70.3 (CH_2), 69.7 (CH_2), 69.1 (CH_2), 64.5 (d, J_F = 4 Hz, CH_2), 49.2 (CH_2), 48.9 (CH), 42.2 (CH_2), 39.8 (CH_2), 39.3 (CH_2), 32.5 (CH_2), 31.4 (CH_2), 28.5 (CH_2), 26.5 (CH_2), 26.0 (CH_2), 25.0 (CH_2), 22.8 (CH_2), 21.6 (CH_3), 17.3 (CH_3) ppm.

IR (NaCl) υ_{max}: 3373, 2934, 2246, 1693, 1645, 1349, 730 cm^{-1}

HRMS (ESI): calc. for $[C_{50}H_{55}O_{10}N_9BrF_2]^+$: 1058.32178; found 1058.31966.

3-(3-Bromo-4-((2,4-difluorobenzyl)oxy)-6-methyl-2-oxopyridin-1(2*H*)-yl)-4-methyl-*N*-(4-(1-(4-((2-(2-(2-((2-(1-(2-nitrobenzyl)-2,6-dioxopiperidin-3-yl)-1,3-dioxoisoindolin-4-yl)amino)ethoxy)ethoxy)ethyl)amino)-4-oxobutyl)-1*H*-1,2,3-triazol-4-yl)butyl)benzamide (*NR-3d*)

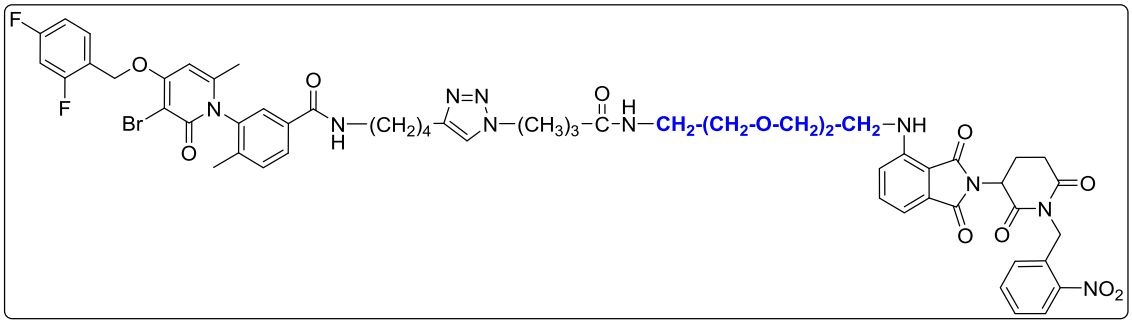

Prepared using general method C starting from alkyne **4-72a** and azide **4-78ONB**. Yellow waxy solid (62 mg, **98%**).

^{1}H NMR (400 MHz, Chloroform-*d*) δ 7.99 (dd, *J* = 8, 1 Hz, 1H), 7.78 (ddd, *J* = 8, 3, 2 Hz, 1H), 7.63 – 7.55 (m, 2H), 7.52 (d, *J* = 2 Hz, 1H), 7.47 (dd, *J* = 9, 7 Hz, 1H), 7.38 (ddd, *J* = 8, 8, 1 Hz, 1H), 7.35 – 7.29 (m, 4H), 7.08 – 7.01 (m, 2H), 6.99 – 6.93 (m, 1H), 6.89 (d, *J* = 9 Hz, 1H), 6.84 (ddd, *J* = 10, 9, 3 Hz, 1H), 6.49 – 6.45 (m, 2H), 6.15 (s, 1H), 5.33 (s, 2H), 5.21 (s, 2H), 5.06 (ddd, *J* = 13, 6, 2 Hz, 1H), 4.30 (t, *J* = 6 Hz, 2H), 3.69 (t, *J* = 5 Hz, 2H), 3.65 – 3.58 (m, 5H), 3.52 (t, *J* = 5 Hz, 2H), 3.44 (q, *J* = 5 Hz, 2H), 3.38 (tq, *J* = 5, 2 Hz, 2H), 3.27 (dh, *J* = 20, 6 Hz, 2H), 3.03 – 2.77 (m, 3H), 2.67 (t, *J* = 7 Hz, 2H), 2.19 – 2.08 (m, 4H), 2.05 (s, 3H), 1.90 (s, 2H), 1.67 (p, *J* = 7 Hz, 2H), 1.53 (p, *J* = 7 Hz, 2H) ppm.

^{13}C NMR (101 MHz, Chloroform-*d*) δ 171.6 (C), 171.1 (C), 169.4 – 169.1 (m, C), 167.6 (d, J_F = 2 Hz, C), 166.0 (d, J_F = 3 Hz, C), 163.2 (C), 161.5 (dd, J_F = 50, 12 Hz, C), 160.4 (C), 158.8 (d, J_F = 12 Hz, C), 148.4 (d, J_F = 2 Hz, C), 147.7 (C), 146.8 (C), 146.5 (C), 138.5 (C), 137.4 (d, J_F = 2 Hz, C), 136.1 (CH), 134.3 (d, J_F = 4 Hz, C), 133.7 (d, J_F = 2 Hz, CH), 132.4 (C), 132.0 (C), 131.4 (CH), 130.1 (dd, J_F = 10, 5 Hz, CH), 128.4 (CH), 127.9 (CH), 127.7 (d, J_F = 3 Hz, CH), 126.4 (CH), 124.9 (CH), 121.3 (CH), 118.6 (dd, J_F = 14, 4 Hz, C), 116.8 (CH), 112.1 – 111.7 (m, CH), 111.7 (CH), 110.2 (C), 103.9 (t, J_F = 25 Hz, CH), 96.6 (C), 96.3 (CH), 70.5 (CH_2), 70.2 (CH_2), 69.7 (CH_2), 69.3 (CH_2), 64.4 (d, J_F = 4 Hz, CH_2), 49.5 (CH), 49.1 (CH_2), 42.3 (CH_2), 41.0 (CH_2), 39.8 (CH_2), 39.2

(CH_2), 32.5 (CH_2), 31.8 (CH_2), 28.4 (d, J = 2 Hz, CH_2), 26.5 (CH_2), 26.0 (CH_2), 25.0 (CH_2), 22.1 (CH_2), 21.6 (CH_3), 17.3 (CH_3) ppm.

IR (NaCl) υ_{max}: 3326, 2938, 2864, 2241, 1697, 914, 731 cm^{-1}

HRMS (ESI): calc. for $[C_{57}H_{60}O_{12}N_{10}BrF_2]^+$: 1193.35381; found 1193.35022.

_N_-(2-(2-(2-(4-(4-(4-(3-(3-Bromo-4-((2,4-difluorobenzyl)oxy)-6-methyl-2-oxopyridin-1(2_H_)-yl)-4-methylbenzamido)butyl)-1_H_-1,2,3-triazol-1-yl)butanamido)ethoxy)ethoxy)ethyl)-2-(2,6-dioxopiperidin-3-yl)-1,3-dioxoisoindoline-5-carboxamide (_NR-4_)

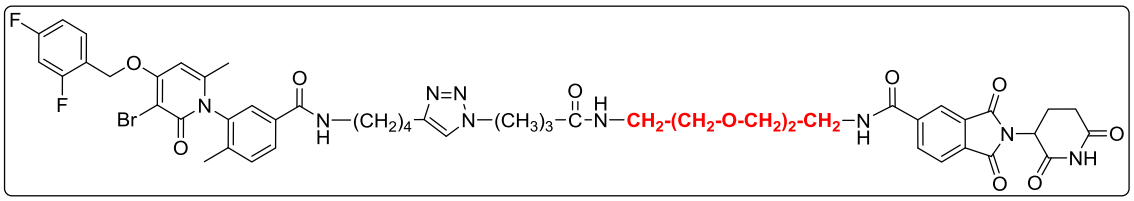

The product was prepared following method C, using **4-72a** and **4-79.** It eluted from the column at 7% MeOH/DCM as a white waxy solid, (32 mg, 0.032 mmol, **26%**).

^{1}H NMR (400 MHz, $CDCl_3$) δ 9.17 (d, J = 49 Hz, 1H), 8.30 (d, J = 8 Hz, 1H), 8.26 (s, 1H), 8.19 (s, 1H), 7.87 (d, J = 8 Hz, 1H), 7.77 (s, 1H), 7.60 (q, J = 8 Hz, 1H), 7.51 (d, J = 5 Hz, 1H), 7.33 (d, J = 7 Hz, 1H), 7.20 – 7.12 (m, 1H), 6.97 (t, J = 8 Hz, 1H), 6.91 – 6.78 (m, 1H), 6.16 (s, 1H), 5.24 (s, 2H), 4.99 (s, 1H), 4.34 (s, 2H), 3.65 (d, J = 20 Hz, 10H), 3.53 (s, 1H), 3.30 (d, J = 62 Hz, 4H), 2.80 (t, J = 16 Hz, 3H), 2.63 (s, 1H), 2.14 (t, J = 13 Hz, 6H), 2.05 (s, 3H), 1.90 (s, 4H), 1.57 (d, J = 46 Hz, 3H) ppm.

^{13}C NMR (101 MHz, $CDCl_3$) δ 172.1 (C), 171.6 (C), 168.8 (C), 167.0 – 166.6 (m, C), 166.5 (d, J_F = 9 Hz, C), 165.8 (C), 163.5 (C), 162.2 – 161.2 (m, C), 160.7 (C), 146.7 (C), 141.0 (C), 138.6 (C), 137.5 (C), 134.5 (CH), 133.5 (C), 131.8 (C), 131.5 (CH), 130.4 (dd, J_F = 10, 5 Hz, CH), 128.6 (CH), 126.7 (CH), 124.0 (CH), 122.4 (CH), 118.6 (dd, J_F = 14, 4 Hz, CH), 112.1 (dd, J_F = 22, 4 Hz, CH), 104.1 (t, J_F = 25 Hz, CH), 96.7 (C), 96.6 (CH), 70.3 (CH_2), 70.2 (CH_2), 69.8 (CH_2), 69.6 (CH_2), 64.6 (CH_2), 49.7 (CH), 49.7 (CH_2), 40.2 (CH_2), 39.9 (CH_2), 39.2 (CH_2), 32.7 (CH_2), 31.6 (CH_2), 29.8 (CH_2), 28.5 (CH_2), 26.1 (CH_2), 22.7 (CH_2), 21.7 (CH_3), 17.4 (CH_3) ppm. (some quaternary carbon signals not observed).

IR (NaCl) υ_{max}: 3373, 2934, 2246, 1693, 1645, 1349, 730 cm^{-1}

HRMS (ESI): calc. for $[C_{51}H_{54}O_{11}N_9BrF_2]^+$: 1086.31670; found 1086.31293.

3-(3-Bromo-4-((2,4-difluorobenzyl)oxy)-6-methyl-2-oxopyridin-1(2*H*)-yl)-*N*-(4-(1-(4-((6-(2-(2,6-dioxopiperidin-3-yl)-1,3-dioxoisoindolin-4-yl)hexyl)amino)-4-oxobutyl)-1*H*-1,2,3-triazol-4-yl)butyl)-4-methylbenzamide (*NR-5a)*

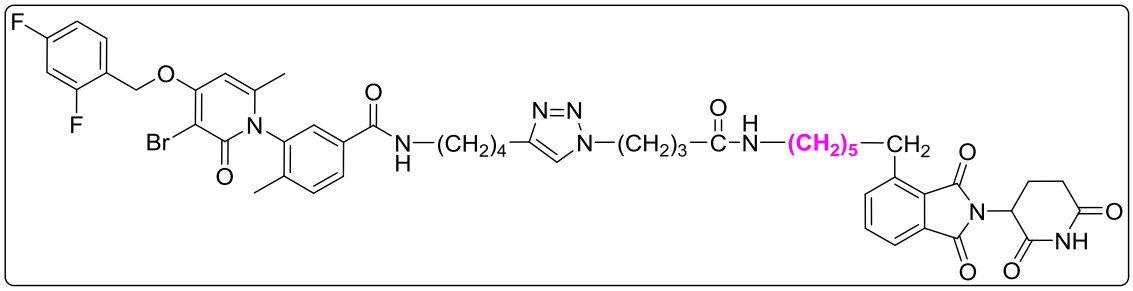

The product was prepared following method C, using **4-86a** and **4-72a.** It eluted from the column at 7% MeOH/DCM as a white solid, (32 mg, **59%**).

M_P: 138 °C.

^{1}H NMR (400 MHz, $CDCl_3$) δ 9.11 (s, 1H), 7.78 (dt, *J* = 8, 1.7 Hz, 1H), 7.69 (dd, *J* = 7, 0.9 Hz, 1H), 7.59 (q, *J* = 8 Hz, 2H), 7.55 – 7.47 (m, 2H), 7.36 – 7.32 (m, 2H), 7.23 (s, 1H), 7.01 – 6.92 (m, 1H), 6.84 (ddd, *J* = 11, 9, 3 Hz, 1H), 6.51 (s, 1H), 6.16 (s, 1H), 5.22 (s, 2H), 4.96 (dd, *J* = 12, 5 Hz, 1H), 4.32 (t, *J* = 6 Hz, 2H), 3.38 – 2.93 (m, 5H), 2.89 – 2.71 (m, 3H), 2.67 (t, *J* = 7 Hz, 2H), 2.18 – 2.02 (m, 8H), 1.92 – 1.88 (m, 3H), 1.73 – 1.56 (m, 4H), 1.57 – 1.47 (m, 2H), 1.48 – 1.36 (m, 2H), 1.39 – 1.21 (m, 5H). ppm.

^{13}C NMR (101 MHz, CD_3OD) δ 171.8 (C), 171.6 (C), 168.7 (C), 168.0 (C), 167.4 (C), 166.3 (d, J_F = 4 Hz, C), 164.4(d, J_F = 12 Hz, C), 163.4 (C), 161.50 – 161.24 (m, C), 161.9 (d, J_F = 12 Hz, C), 160.6 (C), 158.9 (d, J_F = 12 Hz, C), 147.8 (C), 146.7 (C), 143.7 (C), 138.6 (C), 137.5 (C), 136.1 (CH), 134.4 (d, J_F = 5 Hz, C), 134.2 (C), 132.4 (C), 131.6 (CH), 130.5 – 129.9 (m, CH), 128.7 (CH), 128.2 (CH), 126.6 (d, J_F = 2 Hz, CH), 121.6 (CH), 118.7 (dd, J_F = 14, 4 Hz, C), 112.0 (dd, J_F = 21, 4 Hz, CH), 104.3 (t, J_F = 25 Hz, CH), 96.7 (CH), 96.5 (CH), 64.6 (d, J_F = 4 Hz, CH_2), 49.3 (CH), 39.9 (CH_2), 39.6 (CH_2), 32.7 (CH_2), 31.6 (CH_2), 31.1 (CH_2), 31.1 (CH_2), 30.6 (CH_2), 29.3 (CH_2), 28.8 (CH_2), 28.5 (CH_2), 26.6 (CH_2), 26.5 (CH_2), 26.2 (CH_2), 25.1 (CH_2), 22.8 (CH_2), 21.7 (CH_3), 17.4 (CH_3) ppm.

IR (NaCl) υ_{max}: 3385, 2926, 1710, 1642, 1350, 1199 cm^{-1}.

HRMS (ESI): calc. for $[C_{50}H_{54}O_8N_8BrF_2]^+$: 1011.3211; found: 1011.3215.

3-(3-Bromo-4-((2,4-difluorobenzyl)oxy)-6-methyl-2-oxopyridin-1(2*H*)-yl)-*N*-(4-(1-(4-((5-(2-(2,6-dioxopiperidin-3-yl)-1,3-dioxoisoindolin-4-yl)pentyl)amino)-4-oxobutyl)-1*H*-1,2,3-triazol-4-yl)butyl)-4-methylbenzamide (*NR-5b*)

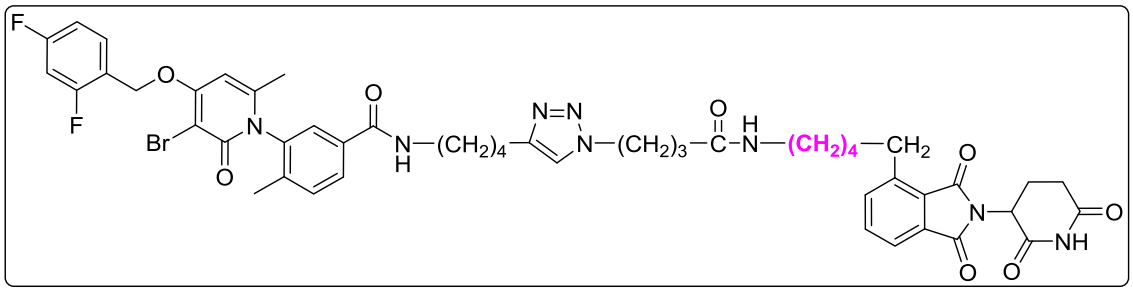

The product was prepared following method C, using **4-86b** and **4-72a.** It eluted from the column at 7% MeOH/DCM as a white solid, (32 mg, 0.032 mmol, **26%**).

M_P: 114 °C.

^{1}H NMR (400 MHz, $CDCl_3$) δ 9.01 (s, 1H), 7.79 (dt, *J* = 8, 1 Hz, 1H), 7.68 (dt, *J* = 7, 1 Hz, 1H), 7.64 – 7.56 (m, 2H), 7.55 – 7.47 (m, 2H), 7.35 (d, *J* = 9 Hz, 2H), 7.15 (s, 1H), 7.00 – 6.93 (m, 1H), 6.84 (ddd, *J* = 10, 9, 3 Hz, 1H), 6.48 (s, 1H), 6.16 (s, 1H), 5.22 (s, 2H), 5.03 – 4.92 (m, 1H), 4.32 (t, *J* = 6 Hz, 2H), 3.37 – 3.20 (m, 2H), 3.20 – 2.96 (m, 4H), 2.88 – 2.73 (m, 3H), 2.69 (t, *J* = 7 Hz, 2H), 2.17 – 2.03 (m, 8H), 1.91 (s, 3H), 1.74 – 1.57 (m, 4H), 1.60 – 1.41 (m, 4H), 1.38 – 1.27 (m, 2H) ppm.

^{13}C NMR (101 MHz, $CDCl_3$) δ 171.7 (C), 171.5 (C), 168.6 (C), 167.9 (C), 167.3 (C), 166.0 (C), 164.2 (d, J_F = 12 Hz, C), 163.3 (C), 161.5 (dd, J_F = 51, 12 Hz, C), 160.4 (C), 147.7 (C), 146.6 (C), 143.3 (C), 138.4 (C), 137.3 (C), 136.0 (C), 134.2 (d, J_F = 2 Hz, CH), 134.1 (C), 132.2 (C), 131.4 (C), 130.1 (dd, J_F = 10, 5 Hz, CH), 128.6 (CH), 128.1 (CH), 126.5 (CH), 121.5 (CH), 121.4 (CH), 118.5 (dd, J_F = 14, 4 Hz, CH), 111.9 (dd, *J* = 21, 4 Hz, CH), 103.9 (t, J_F = 25 Hz, CH), 96.5 (CH), 96.4 (C), 64.5 (d, J_F = 4 Hz, CH_2), 49.2 (CH_2), 49.2 (CH), 39.8 (CH_2), 39.3 (CH_2), 32.5 (CH_2), 31.4 (CH_2), 30.9 (CH_2), 30.4 (CH_2), 29.7 (CH_2), 29.0 (CH_2), 28.3 (CH_2), 26.4 (d, J_F = 2 Hz, CH_2), 26.1 (CH_2), 24.9 (CH_2), 22.7 (CH_2), 21.6 (CH_3), 17.3 (CH_3) ppm.

IR (NaCl) υ_{max}: 3318, 2930, 1713, 1645, 1350, 120, 1102 cm^{-1}.

HRMS (ESI): calc. for $[C_{49}H_{52}O_8N_8BrF_2]^+$: 997.3054; found: 997.3046.

3-(3-Bromo-4-((2,4-difluorobenzyl)oxy)-6-methyl-2-oxopyridin-1(2*H*)-yl)-*N*-(4-(1-(4-((6-(2-(2,6-dioxopiperidin-3-yl)-1-oxoisoindolin-4-yl)hexyl)amino)-4-oxobutyl)-1*H*-1,2,3-triazol-4-yl)butyl)-4-methylbenzamide (*NR-6a*)

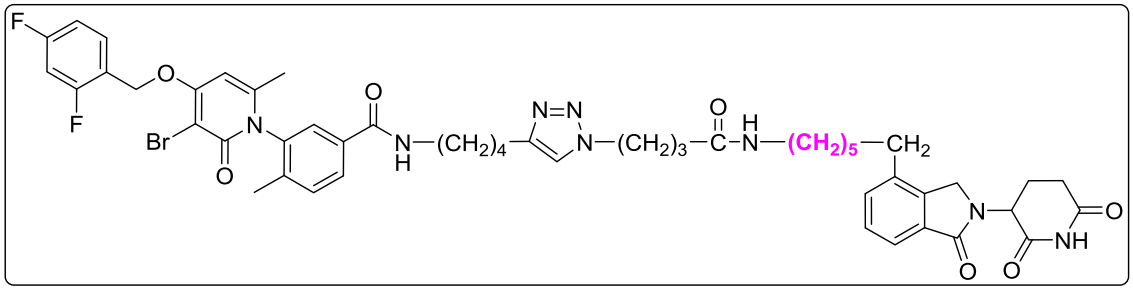

The product was prepared following method C, using **4-72a** and **4-92a.** It eluted from the column at 7% MeOH/DCM as a white solid, (21 mg, **56%**).

M_P: 148 °C.

^{1}H NMR (400 MHz, $CDCl_3$) δ 9.06 (d, *J* = 15 Hz, 1H), 7.83 (d, *J* = 8 Hz, 1H), 7.69 (d, *J* = 7 Hz, 1H), 7.65 – 7.54 (m, 2H), 7.45 – 7.31 (m, 5H), 7.02 – 6.92 (m, 1H), 6.90 – 6.82 (m, 1H), 6.60 (s, 1H), 6.17 (s, 1H), 5.27 – 5.16 (m, 3H), 4.46 – 4.23 (m, 4H), 3.37 – 3.22 (m, 2H), 3.22 – 3.04 (m, 2H), 2.89 – 2.75 (m, 2H), 2.72 – 2.64 (m, 2H), 2.60 (t, *J* = 8 Hz, 2H), 2.48 – 2.35 (m, 1H), 2.24 – 2.01 (m, 7H), 1.92 (s, 3H), 1.73 – 1.49 (m, 6H), 1.48 – 1.38 (m, 2H), 1.37 – 1.23 (m, 5H) ppm.

^{13}C NMR (101 MHz, CD_3OD) δ 171.8 (C), 170.2 (C), 169.8 (C), 166.4 (C), 164.4 (d, J_F = 12 Hz, C)163.5 (C), 161.8 (d, J_F = 14 Hz, C), 160.6 (C), 159.0 (d, J_F = 12 Hz, C), 147.8 (C), 146.7 (C), 140.1 (C), 138.7 (C), 137.7 (C), 137.6 (CH), 134.4 (d, J_F = 5 Hz, C), 132.0 (C), 131.6 (CH), 131.4 (CH), 130.5 – 129.9 (m, CH), 128.7 (CH), 128.6 (CH), 126.7 (d, J_F = 2 Hz, CH), 121.9 – 121.4 (m, CH), 118.7 (dd, J_F = 14, 4 Hz, C), 112.1 (dd, J_F = 21, 4 Hz, CH), 104.3 (t, J_F = 25 Hz, CH), 96.7 (CH), 96.5 (C), 64.6 (d, J_F = 4 Hz, CH_2), 51.9 (CH_2), 49.3 (CH), 46.5 (CH_2), 40.0 (CH_2), 39.5 (CH_2), 32.7 (CH_2), 32.1 (CH_2), 30.6 (CH_2), 29.8 (CH_2), 29.4 (CH_2), 29.0 (CH_2), 28.4 (CH_2), 26.7 (CH_2), 26.6 (CH_2), 26.2 (CH_2), 25.1 (CH_2), 23.5 (CH_2), 21.7 (CH_3), 17.4 (CH_3) ppm.

IR (NaCl) υ_{max}: 3408, 2931, 1644, 1349, 1201, 1101 cm^{-1}.

HRMS (ESI): calc. for $[C_{50}H_{56}O_7N_8BrF_2]^+$: 997.3418; found: 997.3426.

3-(3-Bromo-4-((2,4-difluorobenzyl)oxy)-6-methyl-2-oxopyridin-1(2*H*)-yl)-*N*-(4-(1-(4-((5-(2-(2,6-dioxopiperidin-3-yl)-1-oxoisoindolin-4-yl)pentyl)amino)-4-oxobutyl)-1*H*-1,2,3-triazol-4-yl)butyl)-4-methylbenzamide (*NR-6b*)

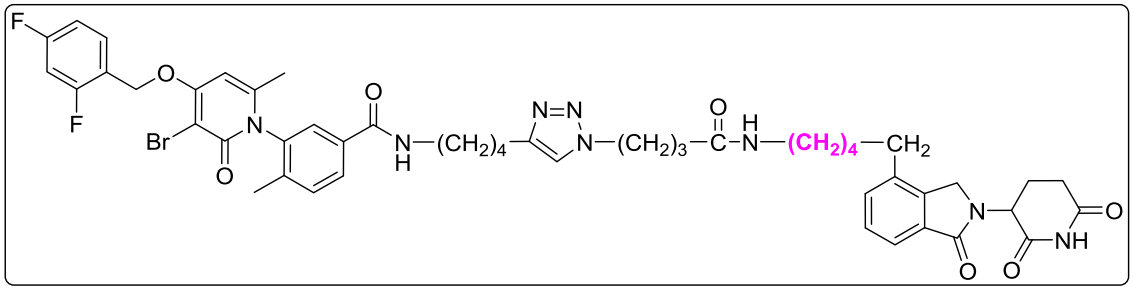

The product was prepared following method C, using **4-92b** and **4-72a.** It eluted from the column at 7% MeOH/DCM as a white solid, (32 mg, 0.032 mmol, **26%**).

M_P: 136 °C.

^{1}H NMR (400 MHz, $CDCl_3$) δ 8.99 (s, 1H), 7.79 (ddd, *J* = 8, 3, 2 Hz, 1H), 7.69 (dt, *J* = 7, 2 Hz, 1H), 7.60 (td, *J* = 9, 6 Hz, 1H), 7.54 (s, 1H), 7.40 (t, *J* = 8 Hz, 1H), 7.37 – 7.31 (m, 3H), 7.26 – 7.16 (m, 1H), 7.01 – 6.93 (m, 1H), 6.86 (ddd, *J* = 10, 9, 3 Hz, 1H), 6.46 (t, *J* = 6 Hz, 1H), 6.15 (dd, *J* = 2, 1 Hz, 1H), 5.25 – 5.17 (m, 3H), 4.42 (dd, *J* = 16, 5 Hz, 1H), 4.35 – 4.26 (m, 3H), 3.37 – 3.25 (m, 2H), 3.23 – 3.05 (m, 2H), 2.88 – 2.79 (m, 1H), 2.69 (t, *J* = 7 Hz, 2H), 2.65 – 2.55 (m, 2H), 2.49 – 2.36 (m, 1H), 2.25 – 2.01 (m, 8H), 1.91 (s, 3H), 1.81 – 1.52 (m, 7H), 1.53 – 1.38 (m, 2H), 1.37 – 1.26 (m, 2H) ppm.

^{13}C NMR (101 MHz, CD_3OD) δ 171.8 (C), 170.2 (C), 169.8 (C), 167.7 (C), 166.4 (C), 163.5 (C), 162.0 (C), 160.6 (C), 159.1 (C), 148.7 – 147.7 (m, C), 146.7 (C), 143.1 (C), 140.3 (d, J_F = 2 Hz, C), 138.7 (C), 137.6 (C), 137.4 (CH), 134.4 (m, C), 132.0 (C), 131.6 (CH), 131.4 (CH), 130.4 (m, CH), 128.7 (CH), 126.7 (CH), 121.8 (CH), 118.6 (d, J_F = 4 Hz, C), 118.1 – 117.2 (m, CH), 112.08 (dd, J_F = 21, 4 Hz, CH), 104.6 – 103.3 (m, CH), 96.7 (C), 96.5 (CH), 64.7 (d, J_F = 3 Hz, CH_2), 52.0 (CH_2), 49.3 (CH), 46.5 (CH_2), 40.0 (CH_2), 39.4 (CH_2), 32.7 (CH_2), 31.9 (CH_2), 31.8 (CH_2), 29.8 (CH_2), 29.6 (CH_2), 29.3 (CH_2), 28.4 (CH_2), 26.5 (CH_2), 26.2 (CH_2), 25.1 (CH_2), 23.5 (CH_2), 21.7 (CH_3), 17.4 (CH_3) ppm.

IR (NaCl) υ_{max}: 3385, 2929, 1642, 1528, 1349, 1141, 1101 cm^{-1}.

HRMS (ESI): calc. for $[C_{49}H_{54}O_7N_8BrF_2]^+$: 983.3261; found 983.3238.

3-(3-Bromo-4-((2,4-difluorobenzyl)oxy)-6-methyl-2-oxopyridin-1(2*H*)-yl)-*N*-(2-(1-(4-((2-((2-(2,6-dioxopiperidin-3-yl)-1,3-dioxoisoindolin-4-yl)amino)ethyl)amino)-4-oxobutyl)-1*H*-1,2,3-triazol-4-yl)ethyl)-4-methylbenzamide (*NR-7a*)

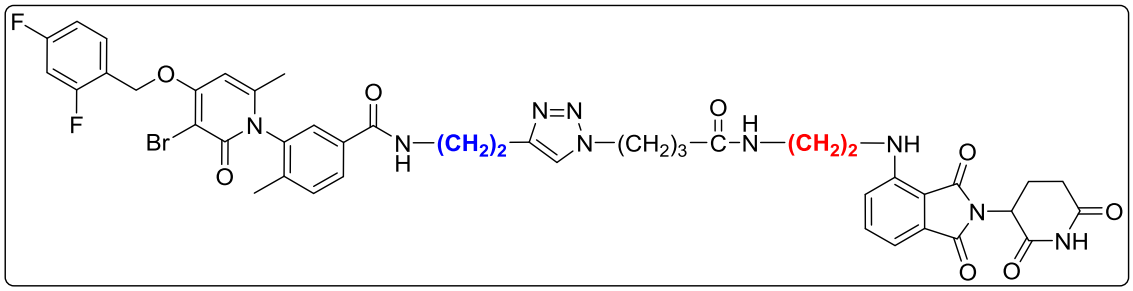

The product was prepared following method C, using **4-72c** and **4-95c,** and eluted from the column at 7% MeOH/DCM as a fluorescent yellow solid, (28 mg, 0.029 mmol, **96%**).

^{1}H NMR (400 MHz, $CDCl_3$) δ 9.13 (d, *J* = 23 Hz, 1H), 7.69 (t, *J* = 6 Hz, 1H), 7.57 – 7.49 (m, 1H), 7.45 (s, 1H), 7.38 (ddd, *J* = 9, 7, 1 Hz, 2H), 7.31 (s, 1H), 7.24 (t, *J* = 8 Hz, 2H), 6.98 (dd, *J* = 7, 2 Hz, 1H), 6.94 – 6.84 (m, 2H), 6.80 (ddd, *J* = 10, 9, 3 Hz, 1H), 6.36 (s, 1H), 6.09 (d, *J* = 3 Hz, 1H), 5.16 (s, 2H), 4.87 – 4.80 (m, 1H), 4.21 (s, 2H), 3.61 – 3.44 (m, 2H), 3.32 (s, 4H), 2.83 – 2.61 (m, 5H), 1.98 (d, *J* = 14 Hz, 6H), 1.89 – 1.80 (m, 5H) ppm.

^{13}C NMR (101 MHz, $CDCl_3$) δ 172.6 (C), 171.9 (C), 171.7 (C), 169.2 (C), 169.1 (C), 167.6 (C), 166.2 (d, J_F = 8 Hz, C), 164.5 – 164.1 (m, C), 163.3 (C), 162.0 (C), 161.7 (C), 160.5 (d, *J* = 2 Hz, C), 158.9 (d, J_F = 12 Hz, C), 146.7 (C), 146.4 (C), 138.8 (C), 137.5 (C), 136.2 (CH), 134.0 (d, J_F = 6.3 Hz, C), 132.4 (C), 131.4 (d, J_F = 5 Hz, CH), 130.3 (dd, J_F = 10, 6 Hz, CH), 128.3 (CH), 126.7 (CH), 118.5 (d, J_F = 3 Hz, CH), 116.8 (CH), 111.9 (dd, J_F = 21, 3 Hz, CH), 111.6 (CH), 110.1 (C) , 104.4 – 103.5 (m, CH), 96.4 (CH), 64.5 (d, J_F = 4 Hz, CH_2), 49.1 (CH_2), 48.9 (CH), 42.2 (CH_2), 39.2 (CH_2), 38.6 (CH_2), 31.9 (CH_2), 31.4 (CH_2), 25.7 (CH_2), 25.5 (CH_2), 22.7 (CH_2), 21.5 (CH_3), 17.3 (CH_3) ppm.

IR (NaCl) υ_{max}: 3338, 2938, 1702, 1641, 1501, 1340, 1040 cm^{-1}.

HRMS (ESI): calc. for $[C_{44}H_{43}O_8N_9BrF_2]^+$: 942.23805, found 942.23882.

3-(3-Bromo-4-((2,4-difluorobenzyl)oxy)-6-methyl-2-oxopyridin-1(2*H*)-yl)-*N*-(2-(1-(4-((3-((2-(2,6-dioxopiperidin-3-yl)-1,3-dioxoisoindolin-4-yl)amino)propyl)amino)-4-oxobutyl)-1*H*-1,2,3-triazol-4-yl)ethyl)-4-methylbenzamide (*NR-7b*)

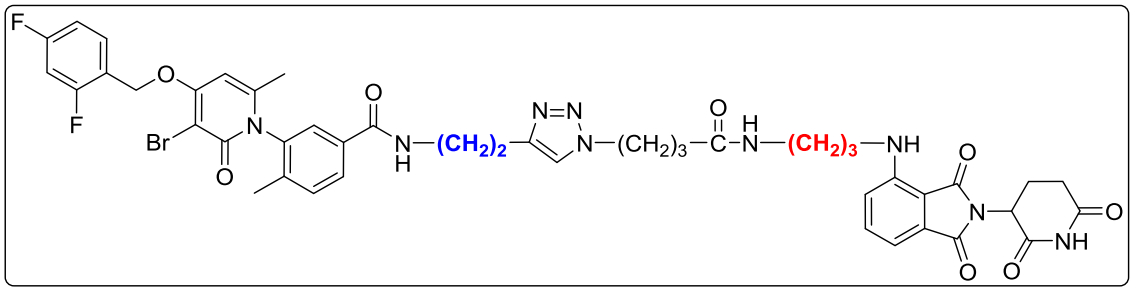

The product was prepared following method C, using **4-72c** and 4-**95b,** and eluted from the column at 7% MeOH/DCM as a fluorescent yellow solid, (41 mg, 0.039 mmol, **78%**).

^{1}H NMR (400 MHz, $CDCl_3$) δ 8.71 (d, *J* = 28.6 Hz, 1H), 7.69 (d, *J* = 8.1 Hz, 1H), 7.53 (q, *J* = 8.1 Hz, 1H), 7.42 (s, 1H), 7.38 (t, *J* = 7.9 Hz, 1H), 7.34 (s, 1H), 7.26 (dd, *J* = 8.1, 3.8 Hz, 1H), 7.21 (s, 1H), 6.98 (d, *J* = 7.0 Hz, 1H), 6.91 (t, *J* = 8.1 Hz, 1H), 6.85 – 6.77 (m, 3H), 6.32 (s, 1H), 6.09 (s, 1H), 5.17 (s, 2H), 4.85 (dd, *J* = 11.6, 5.5 Hz, 1H), 4.27 (d, *J* = 7.2 Hz, 2H), 3.59 (d, *J* = 13.1 Hz, 2H), 3.21 (d, *J* = 6.2 Hz, 4H), 2.86 (s, 2H), 2.76 (t, *J* = 11.6 Hz, 1H), 2.68 (t, *J* = 10.9 Hz, 2H), 2.00 (d, *J* = 27.0 Hz, 7H), 1.90 – 1.80 (m, 4H), 1.70 (t, *J* = 6.6 Hz, 2H) ppm.

^{13}C NMR (101 MHz, $CDCl_3$) δ 172.1 (2 x C), 171.4 (C), 169.3 (C), 168.7 (C), 167.6 (C), 166.2 (d, J_F = 6 Hz, C), 164.3 (dd, J_F = 13, 3 Hz, C), 163.3 (C), 162.0 (C), 160.7 (C), 160.5 (C), 157.8 (C), 146.7 (C), 146.3 (C), 138.9 (C), 137.5 (C), 136.1 (CH), 134.0 (C), 132.5 (C), 131.5 (CH), 130.4 (CH), 128.2 (CH), 126.5 (CH), 122.5 – 122.0 (m, CH), 118.5 (m, C), 116.7 (CH), 112.0 (dd, J_F = 21, 3 Hz, CH), 111.4 (CH), 110.0 (C), 104.4 – 103.6 (m, CH), 96.4 (CH), 64.4 (d, J_F = 4 Hz, CH_2), 49.3 (CH_2), 48.9 (CH), 40.2 (CH_2), 39.0 (CH_2), 37.0 (CH_2), 31.9 (CH_2), 31.4 (CH_2), 29.0 (CH_2), 25.8 (CH_2), 25.5 (CH_2), 22.8 (CH_2), 21.5 (CH_3), 17.3 (CH_3) ppm.

IR (NaCl) υ_{max}: 3303, 2925, 1697, 1641, 1501, 1358, 1192 cm^{-1}.

HRMS (ESI): calc. for $[C_{45}H_{45}O_8N_9BrF_2]^+$: 956.25370, found 956.25392.

3-(3-Bromo-4-((2,4-difluorobenzyl)oxy)-6-methyl-2-oxopyridin-1(2*H*)-yl)-*N*-(3-(1-(4-((3-((2-(2,6-dioxopiperidin-3-yl)-1,3-dioxoisoindolin-4-yl)amino)propyl)amino)-4-oxobutyl)-1*H*-1,2,3-triazol-4-yl)propyl)-4-methylbenzamide (*NR-7c*)

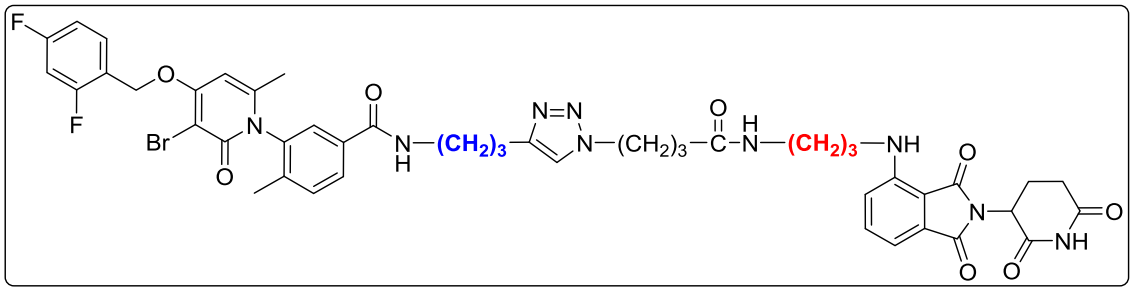

The product was prepared following method C, using **4-72b** and **4-95b** and eluted from the column at 7% MeOH/DCM as a fluorescent yellow solid, (22 mg, 0.023 mmol, **99%**).

^{1}H NMR (400 MHz, $CDCl_3$) δ 8.90 (d, *J* = 6 Hz, 1H), 7.74 – 7.69 (m, 1H), 7.63 – 7.59 (m, 2H), 7.46 – 7.38 (m, 3H), 7.32 (dd, *J* = 8, 2 Hz, 1H), 7.18 (q, *J* = 5 Hz, 1H), 7.03 (dd, *J* = 7, 2 Hz, 1H), 7.00 – 6.93 (m, 1H), 6.89 – 6.82 (m, 2H), 6.35 (t, *J* = 6 Hz, 1H), 6.18 (t, *J* = 1 Hz, 1H), 5.22 (s, 2H), 4.94 – 4.87 (m, 1H), 4.31 (h, *J* = 8 Hz, 2H), 3.42 (dt, *J* = 12, 6 Hz, 1H), 3.33 – 3.15 (m, 5H), 2.87 – 2.65 (m, 5H), 2.15 – 1.98 (m, 8H), 1.97 – 1.81 (m, 5H), 1.74 (q, *J* = 6 Hz, 2H) ppm.

^{13}C NMR (101 MHz, $CDCl_3$) δ 172.3 (2 x C), 171.5 (2 x C), 169.3 (C), 168.8 (2 x C), 167.6 (C), 165.7 (C), 165.6 (C), 163.4 (C), 161.6 (dd, J_F = 47, 12 Hz, C), 160.5 (C), 146.7 (C), 146.6 (C), 138.7 (C), 137.5 (C), 136.1 (CH), 133.9 (d, J_F = 8 Hz, C), 132.5 (C), 131.4 (CH), 130.3 (CH), 128.2 (CH), 126.6 (CH), 122.0 (CH), 118.5 (dd, J_F = 15, 5 Hz, C), 116.7 (CH), 111.9 (d, J_F = 25 Hz, CH), 111.3 (CH), 110.0 (d, J_F = 9 Hz, C), 104.0 (t, J_F = 25 Hz, CH), 96.5 (CH), 64.5 (d, J_F = 4 Hz, CH_2), 49.3 (CH_2), 48.9 (CH), 40.1 (CH_2), 39.6 (CH_2), 36.8 (CH_2), 32.0 (CH_2), 31.4 (CH_2), 29.0 (CH_2), 28.2 (CH_2), 25.9 (CH_2), 23.3 (CH_2), 22.8 (CH_2), 21.6 (CH_3), 17.3 (CH_3) ppm.

IR (NaCl) υ_{max}: 3308, 3082, 2942, 1693, 1641, 1358, 1192, 726 cm^{-1}.

HRMS (ESI): calc. for $[C_{46}H_{47}O_8N_9BrF_2]^+$: 970.26935, found 970.26913.

3-(3-Bromo-4-((2,4-difluorobenzyl)oxy)-6-methyl-2-oxopyridin-1(2*H*)-yl)-*N*-(2-(1-(4-((4-((2-(2,6-dioxopiperidin-3-yl)-1,3-dioxoisoindolin-4-yl)amino)butyl)amino)-4-oxobutyl)-1*H*-1,2,3-triazol-4-yl)ethyl)-4-methylbenzamide (*NR-7d*)

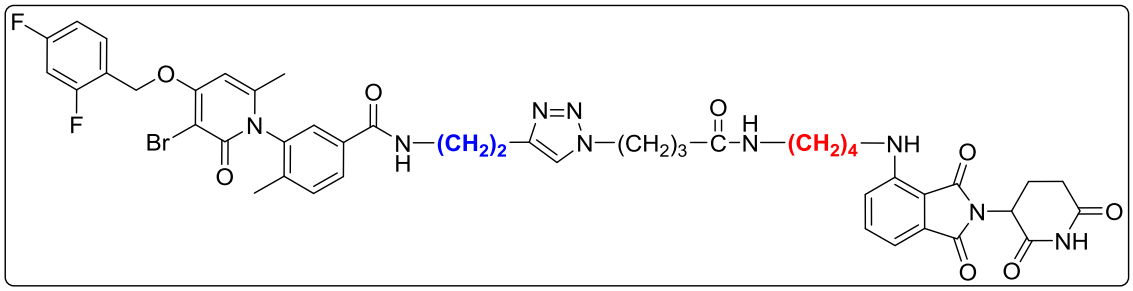

The product was prepared following method C, using **4-72c** and **4-95a** and eluted from the column at 7% MeOH/DCM as a fluorescent yellow solid, (11 mg, 0.012 mmol, **52%**).

^{1}H NMR (400 MHz, $CDCl_3$) δ 8.93 (d, *J* = 24 Hz, 1H), 7.76 (d, *J* = 8 Hz, 1H), 7.60 (q, *J* = 8 Hz, 1H), 7.51 (s, 1H), 7.48 – 7.31 (m, 4H), 7.06 – 7.02 (m, 1H), 7.01 – 6.93 (m, 1H), 6.90 – 6.81 (m, 2H), 6.78 (s, 1H), 6.21 (s, 1H), 6.16 (s, 1H), 5.23 (s, 2H), 4.91 (dd, *J* = 12, 6 Hz, 1H), 4.33 (s, 2H), 3.62 (d, *J* = 30 Hz, 2H), 3.22 (d, *J* = 18 Hz, 4H), 2.95 – 2.68 (m, 5H), 2.10 (s, 3H), 2.07 – 2.01 (m, 3H), 1.97 – 1.90 (m, 2H), 1.90 – 1.87 (m, 3H), 1.69 – 1.53 (m, 4H) ppm.

^{13}C NMR (101 MHz, $CDCl_3$) δ 171.8 (C), 171.4 (2 x C), 169.4 (2 x C), 168.8 (C), 167.6 (C), 166.2 (d, J_F = 16 Hz, C), 164.3 (C), 163.3 (C), 161.5 (dd, J_F = 48, 12 Hz, C), 160.4 (d, J_F = 5 Hz, C), 158.8 (d, J_F = 12 Hz, C), 146.8 (C), 146.4 (C), 138.9 (d, J_F = 2 Hz, C), 137.5 (d, J_F = 2 Hz, C), 136.1 (CH), 134.0 (d, J_F = 9 Hz, C), 132.4 (C), 131.6 – 131.3 (m, CH), 130.4 – 130.0 (m, CH), 128.5 – 128.2 (m, CH), 126.6 (CH), 122.3 (CH), 118.5 (dd, J_F = 14, 4 Hz, C), 116.7 (CH), 112.1 – 111.7 (m, CH), 111.4 (CH), 109.8 (d, J_F = 3 Hz, C), 104.0 (t, *J* = 25 Hz, CH), 96.7 – 96.3 (m, CH), 64.5 (d, J_F = 4 Hz, CH_2), 49.2 (CH_2), 48.9 (CH), 42.2 (CH_2), 39.1 (CH_2), 38.9 (CH_2), 32.0 (d, J_F = 8 Hz, CH_2), 31.4 (CH_2), 26.8 (CH_2), 26.5 (CH_2), 25.9 (CH_2), 25.5 (CH_2), 22.8 (CH_2), 21.5 (CH_3), 17.3 (CH_3) ppm.

IR (NaCl) υ_{max}: 3299, 2929, 1702, 1641, 1349, 1349, 1044 cm^{-1}.

HRMS (ESI): calc. for $[C_{46}H_{47}O_8N_9BrF_2]^+$: 970.26935, found 970.26984.

3-(3-Bromo-4-((2,4-difluorobenzyl)oxy)-6-methyl-2-oxopyridin-1(2*H*)-yl)-*N*-(4-(1-(4-((2-((2-(2,6-dioxopiperidin-3-yl)-1,3-dioxoisoindolin-4-yl)amino)ethyl)amino)-4-oxobutyl)-1*H*-1,2,3-triazol-4-yl)butyl)-4-methylbenzamide (*NR-7e*)

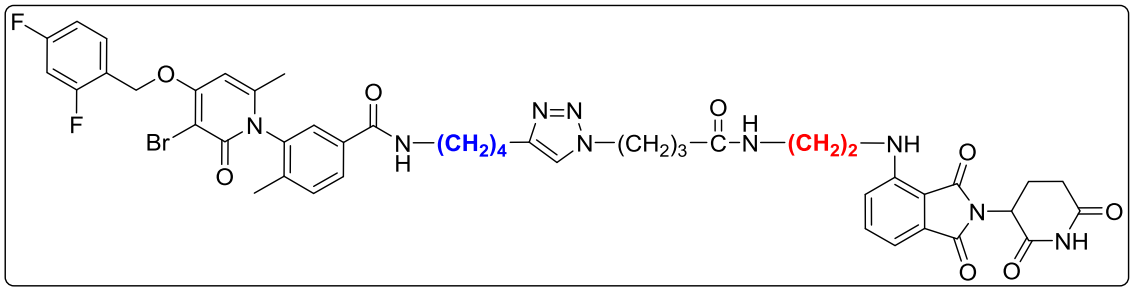

The product was prepared following method C, using **4-72a** and **4-95c,** and eluted from the column at 7% MeOH/DCM as a fluorescent yellow solid, (28 mg, 0.029 mmol, **96%**).

^{1}H NMR (400 MHz, $CDCl_3$) δ 9.07 (d, *J* = 53 Hz, 1H), 7.81 – 7.75 (m, 1H), 7.60 (td, *J* = 8, 6 Hz, 1H), 7.51 (dd, *J* = 4, 2 Hz, 1H), 7.45 (dd, *J* = 9, 7 Hz, 1H), 7.34 (dd, *J* = 15, 7 Hz, 4H), 7.04 (dd, *J* = 7, 3 Hz, 1H), 7.00 – 6.90 (m, 2H), 6.86 (ddd, *J* = 11, 9, 3 Hz, 1H), 6.40 (t, *J* = 5 Hz, 1H), 6.17 (dd, *J* = 2, 1 Hz, 1H), 5.22 (s, 2H), 4.92 – 4.84 (m, 1H), 4.36 – 4.26 (m, 2H), 3.52 – 3.41 (m, 1H), 3.41 – 3.29 (m, 3H), 3.16 (ddd, *J* = 30, 14, 7 Hz, 2H), 2.83 – 2.59 (m, 5H), 2.18 – 2.01 (m, 8H), 1.93 – 1.88 (m, 3H), 1.60 (dt, *J* = 16, 7 Hz, 2H), 1.48 (t, *J* = 7 Hz, 2H) ppm.

^{13}C NMR (101 MHz, $CDCl_3$) δ 172.6 (C), 171.6 (2 x C), 169.2 (d, J_F = 5 Hz, C), 169.0 (C), 167.5 (2 x C), 166.5 (C), 166.2 (C), 163.3 (C), 161.7 (C), 160.5 (d, J_F = 7 Hz, C), 146.7 (C), 146.5 (d, J_F = 3 Hz, C), 138.6 (d, J_F = 5 Hz, C), 137.4 (d, J_F = 2 Hz, C), 136.1 (d, J_F = 2 Hz, CH), 134.2 (d, J_F = 20 Hz, C), 132.4 (C), 131.4 (CH), 130.3 (CH), 128.5 (CH), 126.6 (d, *J* = 10 Hz, CH), 121.7 (CH), 118.5 (d, J_F = 14 Hz, C), 116.8 (CH), 111.9 (dd, J_F = 22, 4 Hz, CH), 111.6 (CH), 110.0 (d, J_F = 4 Hz, C), 104.0 (t, J_F = 25 Hz, CH), 96.6 (d, J_F = 5 Hz, C), 96.4 (CH), 64.5 (d, J_F = 4 Hz, CH_2), 49.2 (d, *J* = 8 Hz, CH_2), 48.8 (d, *J* = 3 Hz, CH), 42.20 (d, *J* = 10 Hz, CH_2), 39.8 (CH_2), 38.8 (d, *J* = 6 Hz, CH_2), 32.2 (d, *J* = 20 Hz, CH_2), 31.4 (CH_2), 28.1 (CH_2), 26.3 (CH_2), 25.7 (d, *J* = 11 Hz, CH_2), 24.8 (CH_2), 22.7 (CH_2), 21.5 (CH_3), 17.3 (CH_3) ppm.

IR (NaCl) υ_{max}: 3307, 2929, 1693, 1641, 1353, 1196, 731 cm^{-1}

HRMS (ESI): calc. for $[C_{46}H_{47}O_8N_9BrF_2]^+$: 970.26935, found 970.26872

3-(3-Bromo-4-((2,4-difluorobenzyl)oxy)-6-methyl-2-oxopyridin-1(2*H*)-yl)-*N*-(3-(1-(4-((4-((2-(2,6-dioxopiperidin-3-yl)-1,3-dioxoisoindolin-4-yl)amino)butyl)amino)-4-oxobutyl)-1*H*-1,2,3-triazol-4-yl)propyl)-4-methylbenzamide (*NR-7f*)

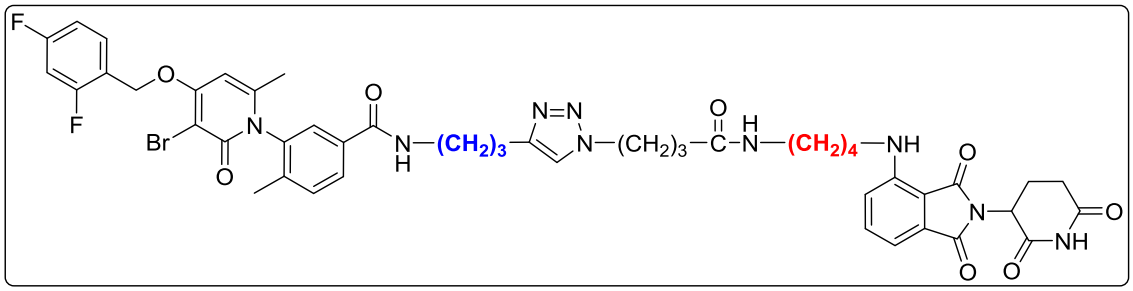

The product was prepared following method C, using **4-72b** and **4-95a** and eluted from the column at 7% MeOH/DCM as a fluorescent yellow solid, (12 mg, 0.012 mmol, **53%**).

^{1}H NMR (400 MHz, $CDCl_3$) δ 8.78 (d, *J* = 11 Hz, 1H), 7.71 (d, *J* = 8 Hz, 1H), 7.63 – 7.53 (m, 2H), 7.44 (ddd, *J* = 9, 7, 5 Hz, 1H), 7.40 – 7.31 (m, 2H), 7.07 – 6.93 (m, 2H), 6.90 – 6.82 (m, 2H), 6.17 (s, 2H), 5.22 (s, 2H), 4.90 (dd, *J* = 12, 6 Hz, 1H), 4.33 (dt, *J* = 11, 7 Hz, 2H), 3.42 (dd, *J* = 13, 6 Hz, 1H), 3.34 – 3.17 (m, 4H), 3.09 (td, *J* = 14, 13, 6 Hz, 1H), 2.88 – 2.66 (m, 6H), 2.09 (d, *J* = 7 Hz, 3H), 2.06 (d, *J* = 2 Hz, 3H), 1.99 (q, *J* = 7 Hz, 1H), 1.95 – 1.85 (m, 6H), 1.63 – 1.47 (m, 5H) ppm.

^{13}C NMR (101 MHz, $CDCl_3$) δ 172.0 (d, *J* = 4 Hz, C), 171.3 (2 x C), 169.4 (C), 168.8 (d, *J* = 4 Hz, C), 167.6 (2 x C), 165.8 (2 x C), 163.4 (d, *J* = 3 Hz, C), 160.5 (d, *J* = 9 Hz, C), 146.8 (C), 146.5 (d, *J* = 5 Hz, C), 138.7 (d, *J* = 6 Hz, C), 137.6 (C), 136.1 (CH), 134.0 (C), 132.4 (C), 131.4 (CH), 130.5 – 130.0 (m, CH), 128.1 (CH), 126.7 (CH), 122.0 (d, *J* = 6 Hz, CH), 118.4 (C), 116.7 (CH), 112.2 – 111.6 (m, CH), 111.3 (d, *J* = 3 Hz, CH), 109.7 (C), 104.46 – 103.41 (m, CH), 96.6 (CH), 96.4 (C), 64.5 (d, J_F = 4 Hz, CH_2), 49.3 (d, *J* = 9 Hz, CH_2), 48.9 (d, *J* = 2 Hz CH), 42.1 (CH_2), 39.7 (CH_2), 39.5 (CH_2), 38.8 (CH_2), 31.9 (d, *J* = 10 Hz, CH_2), 31.4 (CH_2), 28.3 (CH_2), 26.7 (d, *J* = 30 Hz, CH_2), 25.9 (CH_2), 23.2 (CH_2), 22.8 (CH_2), 21.5 (CH_3), 17.3 (CH_3) ppm. (1 C not observed in spectrum)

IR (NaCl) υ_{max}: 3308, 3090, 2920, 1697, 1640, 1353, 726 cm^{-1}

HRMS (ESI): calc. for $[C_{47}H_{49}O_8N_9BrF_2]^+$: 984.28500, found 984.28549

3-(3-Bromo-4-((2,4-difluorobenzyl)oxy)-6-methyl-2-oxopyridin-1(2*H*)-yl)-*N*-(4-(1-(4-((3-((2-(2,6-dioxopiperidin-3-yl)-1,3-dioxoisoindolin-4-yl)amino)propyl)amino)-4-oxobutyl)-1*H*-1,2,3-triazol-4-yl)butyl)-4-methylbenzamide (*NR-7g*)

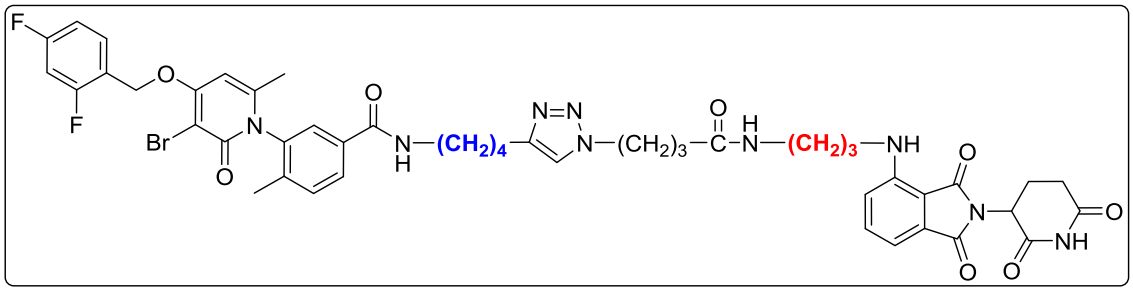

The product was prepared following method C, using **4-72a** and **4-95b,** and eluted from the column at 7% MeOH/DCM as a fluorescent yellow solid, (28 mg, 0.029 mmol, **96%**).

^{1}H NMR (400 MHz, $CDCl_3$) δ 8.93 (d, *J* = 11 Hz, 1H), 7.71 (d, *J* = 8 Hz, 1H), 7.53 (td, *J* = 9, 6 Hz, 1H), 7.48 (s, 1H), 7.37 (t, *J* = 8 Hz, 1H), 7.26 (d, *J* = 8 Hz, 1H), 7.00 – 6.86 (m, 3H), 6.82 – 6.75 (m, 2H), 6.30 (s, 1H), 6.10 (s, 1H), 5.15 (s, 2H), 4.89 – 4.81 (m, 1H), 4.26 (s, 2H), 3.20 (s, 7H), 2.78 – 2.51 (m, 5H), 2.06 (d, *J* = 30 Hz, 6H), 1.97 (d, *J* = 1 Hz, 3H), 1.83 (s, 3H), 1.69 (t, *J* = 6 Hz, 2H), 1.58 (s, 2H), 1.44 (s, 2H) ppm.

^{13}C NMR (101 MHz, $CDCl_3$) δ 172.2 (C), 171.6 (d, *J* = 4 Hz, C), 169.3 (C), 168.9 (d, *J* = 4 Hz, C), 167.6 (C), 166.2 (d, *J* = 8 Hz, C), 164.2 (C), 163.3 (C), 161.8 (d, *J* = 12 Hz, C), 161.3 (d, *J* = 12 Hz, C), 160.5 (C), 158.8 (d, *J* = 12 Hz, C), 146.6 (d, *J* = 7 Hz, C), 138.5 (C), 137.4 (C), 136.1 (CH), 134.2 (d, *J* = 7 Hz, C), 132.5 (C), 131.4 (CH), 130.2 (dd, *J* = 10, 5 Hz, CH), 128.5 (CH), 126.5 (CH), 118.5 (dd, *J* = 14, 4 Hz, C), 116.7 (CH), 111.9 (dd, *J* = 21, 4 Hz, CH), 111.3 (CH), 109.9 (C), 103.9 (t, *J* = 25 Hz, CH), 96.5 (d, *J* = 9 Hz, CH), 64.5 (d, *J* = 4 Hz, CH_2), 49.3 (CH_2), 48.9 (CH), 40.1 (CH_2), 39.8 (CH_2), 36.9 (CH_2), 32.4 (CH_2), 31.4 (CH_2), 29.0 (CH_2), 28.2 (CH_2), 26.3 (CH_2), 25.8 (CH_2), 24.9 (CH_2), 22.8 (CH_2), 21.6 (CH_3), 17.3 (CH_3) ppm.

IR (NaCl) υ_{max}: 3282, 2929, 1702, 1644, 1349, 1192, 1031 cm^{-1}.

HRMS (ESI): calc. for $[C_{47}H_{49}O_8N_9BrF_2]^+$: 984.28531, found 984.28505.

3-(3-Bromo-4-((2,4-difluorobenzyl)oxy)-6-methyl-2-oxopyridin-1(2H)-yl)-N-(4-(1-(4-((4-((2-(2,6-dioxopiperidin-3-yl)-1,3-dioxoisoindolin-4-yl)amino)butyl)amino)-4-oxobutyl)-1H-1,2,3-triazol-4-yl)butyl)-4-methylbenzamide (*NR-7h*)

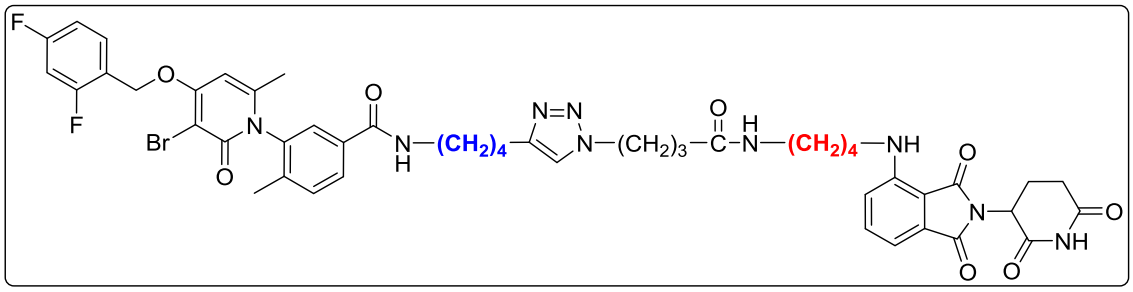

The product was prepared following method C, using **4-72a** and **4-95a,** and eluted from the column at 7% MeOH/DCM as a fluorescent yellow solid, (61 mg, 0.039 mmol, **78%**).

DSC = 231.6 °C (peak), 188.7 °C (onset)

^{1}H NMR (400 MHz, $CDCl_3$) δ 8.84 (d, *J* = 15 Hz, 1H), 7.78 (d, *J* = 8 Hz, 1H), 7.60 (td, *J* = 9, 6 Hz, 1H), 7.53 (s, 1H), 7.45 (dd, *J* = 9, 7 Hz, 1H), 7.34 (d, *J* = 8 Hz, 2H), 7.21 (s, 1H), 7.04 (dd, *J* = 7, 1 Hz, 1H), 7.00 – 6.92 (m, 1H), 6.88 – 6.72 (m, 3H), 6.20 (dd, *J* = 9, 5 Hz, 1H), 6.16 (s, 1H), 5.22 (s, 2H), 4.95 – 4.85 (m, 1H), 4.32 (s, 2H), 3.34 – 3.08 (m, 6H), 2.91 – 2.59 (m, 6H), 2.19 – 2.02 (m, 6H), 1.90 (s, 3H), 1.80 (s, 1H), 1.73 – 1.47 (m, 8H) ppm.

^{13}C NMR (101 MHz, $CDCl_3$) δ 172.0 (C), 171.8 (C), 171.7 (C), 169.6 (C), 169.1 (C), 167.7 (2 x C), 166.1 (d, J_F = 7 Hz, C), 164.4 (C), 163.5 (C), 161.9 (C), 161.8 (C), 160.6 (d, J_F = 3 Hz, C), 146.9 (C), 146.8 (C), 138.6 (d, J_F = 2 Hz, C), 137.5 (C), 136.3 (CH), 134.3 (d, *J* = 4 Hz, C), 132.5 (C), 131.5 (CH), 130.3 (dd, *J* = 10, 4 Hz, CH), 128.7 (CH), 126.7 (CH), 121.9 – 121.2 (m, CH), 118.9 – 118.3 (m, C), 116.9 (CH), 112.0 (dd, J_F = 22, 4 Hz, CH), 111.4 (CH), 109.9 (d, J_F = 3 Hz, C), 104.1 (t, *J* = 25 Hz, CH), 96.6 (CH), 64.7 (d, J_F = 4 Hz, CH_2), 49.4 (CH_2), 49.0 (CH), 42.3 (CH_2), 39.9 (CH_2), 39.0 (CH_2), 32.6 (CH_2), 32.5 (CH_2), 31.6 (CH_2), 27.0 (CH_2), 26.7 (CH_2), 26.6 (CH_2), 26.1 (CH_2), 25.1 (CH_2), 22.9 (CH_2), 21.7 (CH_3), 17.4 (CH_3) ppm.

IR (NaCl) υ_{max}: 3388, 2925, 1697, 1641, 1354, 1198, 1101 cm^{-1}.

HRMS (ESI): calc. for $[C_{48}H_{51}O_8N_9BrF_2]^+$: 998.3007, found 998.2978.

tert-Butyl(4-(4-(4-(3-(3-bromo-4-((2,4-difluorobenzyl)oxy)-6-methyl-2-oxopyridin-1(2*H*)-yl)-4-methylbenzamido)butyl)-1*H*-1,2,3-triazol-1-yl)-1-((4-((2-(2,6-dioxopiperidin-3-yl)-1,3-dioxoisoindolin-4-yl)amino)butyl)amino)-1-oxobutan-2-yl)carbamate (*NR-7i*)

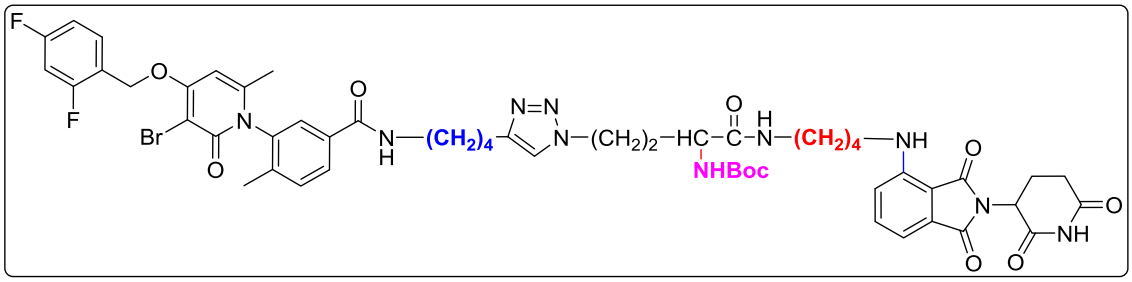

Prepared using general method C starting from alkyne **4-72a** and azide **4-99**, to afford a yellow solid (20 mg, **46%**).

^{1}H NMR (400 MHz, $CDCl_3$) δ 8.72 (s, 1H), 7.71 (dd, *J* = 8, 2 Hz, 1H), 7.58 – 7.50 (m, 1H), 7.46 (dd, *J* = 6, 2 Hz, 1H), 7.42 – 7.36 (m, 1H), 7.35 (s, 1H), 7.28 (dd, *J* = 8, 4 Hz, 1H), 7.18 – 7.08 (m, 1H), 7.06 – 6.98 (m, 1H), 6.98 (d, *J* = 7 Hz, 1H), 6.90 (td, *J* = 9, 2 Hz, 1H), 6.83 – 6.75 (m, 2H), 6.16 – 6.05 (m, 2H), 5.56 (d, *J* = 8 Hz, 1H), 5.17 (s, 2H), 4.84 (dd, *J* = 12, 6 Hz, 1H), 4.35 – 4.20 (m, 2H), 3.96 (s, 1H), 3.28 – 3.10 (m, 5H), 2.82 – 2.71 (m, 1H), 2.72 – 2.57 (m, 4H), 2.21 (s, 1H), 2.11 – 2.01 (m, 2H), 1.98 (dd, *J* = 8, 2 Hz, 3H), 1.88 – 1.81 (m, 3H), 1.62 (q, *J* = 7 Hz, 3H), 1.51 (dd, *J* = 11, 6 Hz, 6H), 1.33 (d, *J* = 3 Hz, 9H) ppm.

^{13}C NMR (101 MHz, $CDCl_3$) δ 199.3 (C), 197.6 (C), 171.0 (C), 169.5 (C), 168.8 (C), 167.6 (C), 166.5 – 165.9 (m, C), 163.3 (C), 160.5 (C), 157.2 (C), 147.7 (C), 146.8 (C), 146.4 (C), 138.5 (C), 137.4 (C), 136.1 (CH), 134.4 (C), 132.4 (C), 131.4 (CH), 130.2 (d, J_F = 11 Hz, CH), 128.4 (CH), 126.7 – 126.3 (m, CH) 122.0 (CH), 118.4 (C), 116.8 (CH), 111.9 (d, J_F = 18 Hz, CH), 111.4 (CH), 109.9 (C), 104.1 (d, J_F = 25 Hz, CH), 96.7 (C), 96.3 (CH) 64.4 (d, J_F = 5 Hz, CH_2), 60.4 (CH_2), 51.7 (CH), 48.9 (CH), 46.7 (CH_2), 42.1 (CH_2), 39.7 (CH_2), 39.0 (CH_2), 33.8 (CH_2), 31.4 (CH_2), 28.3 (3 x CH_3), 28.1 (CH_2), 26.5 (CH_2), 26.3 (CH_2), 24.9 (CH_2), 22.8 (CH_2), 21.5 (CH_3), 21.0 (CH_2), 17.3 (CH_3), 14.2 (C) ppm. Some quaternary carbons not observed.

IR (NaCl) υ_{max}: 3388, 2925, 1697, 1641, 1354, 1198, 1101 cm^{-1}

HRMS (ESI): calc. for $[C_{53}H_{60}O_{10}N_{10}BrF_2]^+$: 1113.3640; found 1115.3638

HPLC/ms, RT: 5.15 min, m/z: 1115.6, 558.3 (z = 2)

4-(4-(4-(3-(3-Bromo-4-((2,4-difluorobenzyl)oxy)-6-methyl-2-oxopyridin-1(2*H*)-yl)-4-methylbenzamido)butyl)-1*H*-1,2,3-triazol-1-yl)-1-((4-((2-(2,6-dioxopiperidin-3-yl)-1,3-dioxoisoindolin-4-yl)amino)butyl)amino)-1-oxobutan-2-aminium chloride (*NR-7j*)

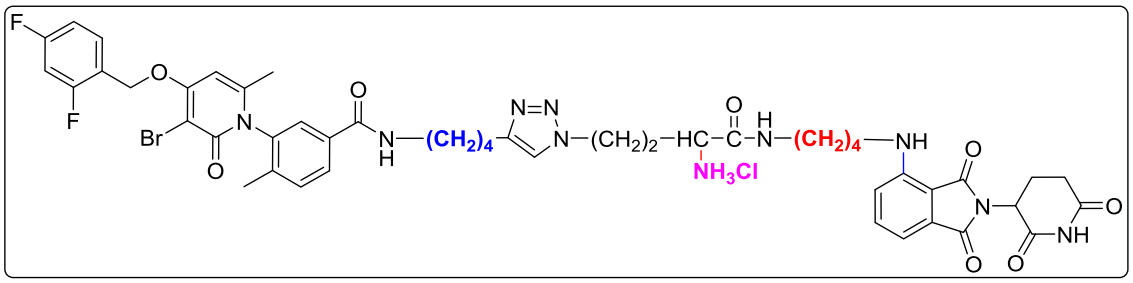

Product prepared as for **4-13a,** using **NR-7i** as starting material to afford a yellow waxy solid (10 mg, **91%**).

^{1}H NMR (400 MHz, Methanol-d_4) δ 8.04 (s, 1H), 7.77 (d, *J* = 8 Hz, 1H), 7.60 – 7.50 (m, 2H), 7.42 (t, *J* = 8 Hz, 2H), 7.00 – 6.90 (m, 5H), 6.58 (s, 1H), 5.26 (s, 2H), 4.94 (dd, *J* = 13, 5 Hz, 1H), 4.47 (d, *J* = 7 Hz, 2H), 3.92 – 3.81 (m, 1H), 3.30 (t, *J* = 7 Hz, 2H), 3.24 (d, *J* = 6 Hz, 2H), 3.16 (s, 4H), 2.78 – 2.53 (m, 6H), 2.38 (d, *J* = 9 Hz, 2H), 1.98 (s, 5H), 1.90 (t, *J* = 2 Hz, 4H), 1.68 (d, *J* = 8 Hz, 2H), 1.57 (s, 8H) ppm.

^{19}F NMR (376 MHz, Methanol-d_4) δ -111.02 (p, *J* = 8 Hz), -115.46 (q, *J* = 9 Hz).

HRMS (ESI): calc. for $[C_{48}H_{53}O_8N_{10}BrF_2]^+$: 1013.3116; found 1013.3112

HPLC/ms, RT: 4.65 min, m/z: 1013.3, 507.3 (z = 2)

3-(3-Bromo-4-((2,4-difluorobenzyl)oxy)-6-methyl-2-oxopyridin-1(2H)-yl)-N-(4-(1-(8-((2-(2,6-dioxopiperidin-3-yl)-1,3-dioxoisoindolin-4-yl)amino)-8-oxooctyl)-1H-1,2,3-triazol-4-yl)butyl)-4-methylbenzamide (NR-8)

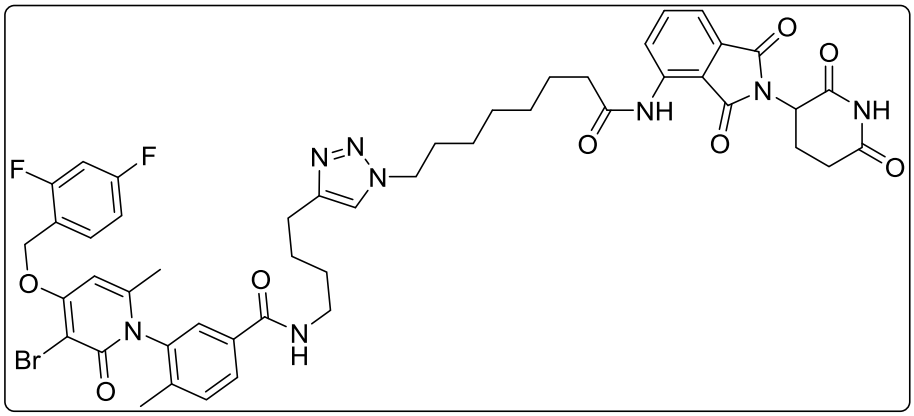

The product was prepared following general method C, using **4-72a** and **4-80** as starting materials. The product eluted from the column at 9% MeOH/DCM, as a white solid, (10 mg, 8.7 μmol, **21**%).

TLC R_f: 0.31 (10% MeOH/DCM)

^{1}H NMR (400 MHz, Chloroform-*d*) δ 9.42 (s, 1H), 8.80 (d, *J* = 8.5 Hz, 1H), 8.58 (s, 1H), 7.82 (s, 1H), 7.70 (dd, *J* = 8.5, 7.3 Hz, 1H), 7.61 (q, *J* = 8.3 Hz, 1H), 7.53 (dd, *J* = 7.4, 0.7 Hz, 1H), 7.36 (d, *J* = 7.1 Hz, 1H), 6.97 (td, *J* = 8.2, 2.1 Hz, 1H), 6.85 (ddd, *J* = 10.9, 8.7, 2.4 Hz, 1H), 6.13 (s, 1H), 5.23 (s, 2H), 4.97 (s, 1H), 4.29 (s, 2H), 3.36 (s, 2H), 2.87 (t, *J* = 12.7 Hz, 1H), 2.76 (q, *J* = 12.7, 10.9 Hz, 3H), 2.43 (t, *J* = 7.3 Hz, 2H), 2.16 (s, 1H), 2.07 (s, 3H), 1.91 (s, 3H), 1.70 (s, 5H), 1.60 (s, 0H), 1.35 (d, *J* = 15.0 Hz, 4H), 0.84 (q, *J* = 9.9, 9.1 Hz, 1H) ppm.

^{13}C NMR (101 MHz, Chloroform-*d*) δ 172.2 (C), 170.9 (C), 169.1 (C), 168.0 (C), 166.7 (C), 166.2 (C), 163.1 (C), 160.4 (C), 146.4 (C), 138.6 (C), 137.8 (C), 137.4 (C), 136.4 (CH), 134.4 (C), **131.4 (C),** 131.1 (CH), 130.2 (dd, J_F = 10, 5 Hz CH), 128.5 (CH), 126.6 (CH), 125.2 (CH), 118.6 (dd, J_F = 14, 4 Hz, CH), 118.4 (CH), 115.3 (C), 111.90 (dd, J_F = 21, 4 Hz, CH), 103.9 (t, *J* = 25 Hz, CH) 96.7 (C), 96.2 (CH), 64.4 (d, J_F = 4 Hz, CH_2), 50.2 (CH_2), 49.3 (CH), 39.8 (CH_2), 37.8 (CH_2), 31.4 (2 x CH_2), 29.7 (CH_2), 28.7 (CH_2), 28.6 (CH_2), 28.5 (CH_2), 26.3 (CH_2), 25.0 (CH_2), 22.7 (CH_2), 22.6 (CH_2), 21.6 (CH_3), 17.3 (CH_3) ppm. Some carbon signals not observed.

General buffers and solutions

Buffers and solutions used in this thesis are specified below, or in the corresponding sections.

PBS 10X
1.37 M NaCl
27 mM KCl
100 mM Na2HPO4
17.5 mM KH2PO4
pH 7.4

Running Buffer 10X
0.25 M Tris base
2 M glycine
1% SDS
pH 8.3

Transfer Buffer 10X
0.2 M Tris base
1.5 M glycine

Protein Loading buffer 5X
250 mM Tris pH 6.8
50% glycerol
250 mM DTT
10% SDS
0.1% bromophenol blue

Ponceau Red
0.1% Ponceau Red powder
5% acetic acid
HBS buffer (2X)
50 mM HEPES
280 mM NaCl
1.5 mM Na2HPO4
pH 7.12

IP buffer
50 mM Tris-HCl (pH 7.5)
150 mM NaCl
5 mM EGTA
5 mM EDTA
1% NP-40
20 mM NaF
1 mM Na orthovanadate
1 mM PMSF
2.5 mM benzamidine
10 µg/mL pepstatin A
1 µM mycrocystin
10 µg/mL leupeptin
10 µg/mL aprotinin

Coomassie staining solution
0.5% Coomassie Blue R250
10% acetic acid
45% methanol

Coomassie distaining solution
25% methanol
7% acetic acid

TBS 1X
0.1 M Trizma base
1.5 NaCl

Cell culture

For standard culture, cells were maintained in Dulbecco's Modified Eagle´s Medium (DMEM) supplemented with 10% heat inactivated foetal bovine serum (FBS), 1% L-Glutamine and 1% penicillin-streptomycin at 37 °C and 5% CO_2.

Cell maintenance

For sub-culturing, cells were washed once in PBS and incubated in 1 mL trypsin at 37 °C until detached. Then, complete media was added and the cells were diluted as desired depending on

the confluence and re-plated in a new culture dish. In the case of differentiated BMDM, cells were harvested by using cell scrappers and plated with the same media until they attached. The media was changed 18 h before treatment to render the cells quiescent.

Cell collection

For harvesting, cell cultures were washed with PBS and digested using trypsin. Cells were re-suspended in 5 mL of complete fresh media and the suspension was transferred to a 15 mL conical tube and centrifuged at 1000 rpm for 5 min. Afterwards, the media was removed under vacuum, then the pellet was washed in 3 mL of PBS. The cell suspension was centrifuged again in the same conditions and supernatant was discarded. The cell pellet was re-suspended according to the following procedures:

Cell counting

Cells were harvested and placed in a 15 mL tube with 5 mL of DMEM. Cells were re-suspended carefully up and down until a homogeneous suspension was obtained. 10 mL of cell solution were added to counting slides and the cell number was determined using a TC10 automated cell counter.

Cell freezing and thawing

Cells from a 70-85% confluent p10 cm culture dish were collected as above and re-suspended in freezing media (90% FBS and 10% DMSO) then transferred to 1.5 mL cryo-tubes. Cryo-tubes were stored in a Mr. Frosty container at -80 °C for up to one week and then transferred to liquid nitrogen for long term storage.
Frozen cells were quickly placed in a 37 °C water bath until completely thawed. Then cells were transferred to a p10 cm plate with 10 mL of media. The media was replaced the following day by 10 mL of fresh DMEM to remove remaining DMSO in culture.

p38 MAPK pathway stimulation

Several agents were used to activate the p38a pathway. In all cases, cells were plated at 60-70% confluence and attached in a p10 cm plate. Incubation times for the different treatments are indicated in each experiment.

- *UV radiation*: cell media was removed and placed into 15 mL tubes, and plates were introduced into a UV crosslinker apparatus. UV radiation intensities were determined according to the experiment. After stimulation, the media was added back to the cells.
- *NaCl*: 200 mM NaCl was used to induce osmotic stress.
- *H_2O_2*: 100 mM H_2O_2 was used to generate oxidative stress.
- *Anisomycin*: This is an antibiotic produced by *Streptomyces griseolus* that inhibits protein synthesis, and it was used at 20 mM.

Inhibitors were added and incubated for at least 1 h before p38 stimulation.

Protein detection by western blotting

Protein extraction: Samples were lysed in IP buffer. Tissue samples were homogenised using the Percellys instrument whereas cells were washed twice with PBS and scrapped. Samples were incubated for 15 min on ice and then centrifuged at 16000 ×g at 4 °C for 15 min. Then the supernatants were placed in new Eppendorf tubes. Cell lysates were processed by western blotting or frozen at -80 °C.

Protein quantification: Total protein was quantified using RC DC protein assay kit according to manufacturer's instructions. Protein concentration was measured at 750 nm using a spectrophotometer (BioTek, #FLx800) and a BSA standard curved as a reference.

Western blot: 50 mg of protein was re-suspended in loading buffer 1X and boiled for 5 min at 95 °C. Then, samples were loaded onto SDS-polyacrylamide gel: H_2O Milli-Q (6.3 mL), 1.5 M Tris (5.0 mL), 30% Acrylamide (8.3 mL), 10% SDS (100 µL), APS (100 µL), TEMED (100 µL).

Proteins were separated by SDS-PAGE at 100 V for 2 h. After electrophoresis, proteins were transferred from polyacrylamide gels to a nitrocellulose membrane using a wet-transfer system (BioRad). Ponceau red was used to determine transfer quality and efficiency. After washing out the Ponceau red with PBS, membrane was blocked for 1 h in 5% non-fat dry milk in PBS at rt. Then, primary antibody was added to the membrane and incubated for 20 h at 4 °C. The next day, the membrane was washed three times with TBS-0.05% Tween and incubated with the secondary antibody diluted in 1% non-fat milk in TBS-0.05% Tween for 1 h at rt. Finally, membranes were washed as previously mentioned and protein fluorescence was detected using an Odyssey Infrared Imaging System. (Antibodies are indicated in **Table X**).

Protein detection by Immunofluorescence

293T cells grown in coverslips were washed with PBS and fixed for 20 min in ice-cold methanol (-20 °C). After fixation, cells were placed in a petri dish covered with aluminium foil with a strip of wetted Whattman paper around the inside wall of the plate to avoid coverslips from drying out. Then, coverslips were washed again with PBS and blocked for 1 h with PBS-BT solution (3% BSA, 0.1% Triton X-100, 0.02% Azide in PBS) at rt. Primary antibodies were incubated for 18-22 h at 4 °C. Coverslips were then washed with PBS-BT buffer and secondary antibodies were incubated for 1 h at rt. Coverslips were placed into superfrost glass slides with ProLong Gold anti-fade DAPI mounting. Primary and secondary antibodies were diluted with PBS-BT and are indicated in Table 5.3.1.

Antibodies for western blotting				
Antibody	**Dilution**	**Buffer**	**Company**	**Reference**
Hsp27	1:1000	5% BSA (TBS-T)	Santa-Cruz	Sc-1049
Hsp27phospho-S82	1:1000	5% BSA (TBS-T)	Cell Signalling	2401
MK2	1:500	5% BSA (TBS-T)	Cell Signalling	3042
MK2 phospho-T334	1:500	5% BSA (TBS-T)	Cell Signalling	3007
MKK6	1:500	1% BSA (PBS)	Nebreda lab (in house synthesis)	Ambrosino *et al., 2003*
P38α	1:1000	1% BSA (PBS)	Santa-Cruz	Sc81621
P38α phospho-T180/Y182	1:1000	5% BSA (TBS-T)	Cell Signalling	9211
Tubulin	1:10 000	1% BSA (PBS)	Sigma Aldrich	T9026
Secondary antibodies				
Rabbit IgG (Alexa Fluor 488)	1:400		Invitrogen	A-21441
Mouse IgG (Alexa Fluor 555)	1:400		Invitrogen	A-21422

References

(1) Masai, E.; Katayama, Y.; Kubota, S.; Kawai, S.; Yamasaki, M.; Morohoshi, N. A Bacterial Enzyme Degrading the Model Lignin Compound β-Etherase Is a Member of the Glutathione-S-Transferase Superfamily. *FEBS Lett.* **1993**, *323* (1–2), 135–140.

(2) Byrom, D. Synthesis of TGF-Beta Inhibitors and Compounds for Spatiotemporal Drug Release Daniel Byrom, Universitat de Barcelona, 2018.

(3) Zhang, Q.; Peng, X.; Grilley, M.; Takemoto, J. Y.; Chang, C. T. Using Fluorogenic Probes for the Investigation of Selective Biomass Degradation by Fungi. *Green Chem.* **2015**, *17*, 1918–1925.

(4) Gao, W.; Li, Q.; Chen, J.; Wang, Z.; Hua, C. Total Synthesis of Six 3,4-Unsubstituted Coumarins. *Molecules* **2013**, *18* (12), 15613–15623.

(5) Speicher, A.; Groh, M.; Hennrich, M.; Huynh, A. Syntheses of Macrocyclic Bis (Bibenzyl) Compounds Derived from Perrottetin E. *European J. Org. Chem.* **2010**, 6760–6778.

(6) Yasuma, T.; Kitamura, S.; Negoro, N. 3-(4-Benzyloxyphenyl)Propanoic Acid Derivatives. WO 2005/063729 A1, 2005.

(7) Selness, S. R.; Devraj, R. V.; Devadas, B.; Walker, J. K.; Boehm, T. L.; Durley, R. C.; Shieh, H.; Xing, L.; Rucker, P. V.; Jerome, K. D.; et al. Discovery of PH-797804, a Highly Selective and Potent Inhibitor of P38 MAP Kinase. *Bioorganic Med. Chem. Lett.* **2011**, *21* (13), 4066–4071.

(8) Turočkin, A.; Honeker, R.; Raven, W.; Selig, P. Synthesis of Chiral Bicyclic Guanidinium Salts Using Di(Imidazole-1-Yl)Methanimine. *J. Org. Chem.* **2016**, *81* (11), 4516–4529.

(9) Zajdel, P.; Subra, G.; Pawłowski, M.; Martinez, J. Solid-Phase Synthesis of Aryl-Alkylamine Derivatives Using Protected Aminoalcohol Building Blocks on SynPhase™ Lanterns. *QSAR Comb. Sci.* **2007**, *26* (2), 215–219.

(10) Meanwell, N. A.; Pearce, B. C.; Roth, H. R.; Smith, E. C. R.; Wedding, D. L.; Wright, J. J. K.; Buchanan, J. O.; Baryla, U. M.; Gamberdella, M. Inhibitors of Blood Platelet CAMP Phosphodiesterase. 2. Structure-Activity Relationships Associated with 1,3-Dihydro-2H-Imidazo[4,5-b]Quinolin-2-Ones Substituted with Functionalized Side Chains. *J. Med. Chem.* **1992**, *35* (14), 2672–2687.

(11) Jones, G. H.; Venuti, C.; Alvarez, R.; Bruno, J. J.; Berks, A. H.; Prince, A. Inhibitors of Cyclic AMP Phosphodiesterase . Analogues of Cilostamide and I-6 v7 X . Q-N. *J. Med. Chem.* **1987**, No. 3, 295–303.

(12) Crew, A. P.; Crews, C.; Dong, H.; Qian, Y.; Wang, J.; Qian, Y.; Siu, K.; Ferraro, C.; Jin, M.; Chen, X. IMIDE-BASED MODULATORS OF PROTEOLYSIS AND ASSOCIATED METHODS OF USE. US 2015/0291562, 2015.

(13) BRADNER, J.; BUCKLEY, D.; WINTER, G. Methods To Induce Targeted Protein Degradation Through Bifunctional Molecules. WO/2017/024317, 2017.

(14) Zhou, B.; Hu, J.; Xu, F.; Chen, Z.; Bai, L.; Fernandez-Salas, E.; Lin, M.; Liu, L.; Yang, C. Y.; Zhao, Y.; et al. Discovery of a Small-Molecule Degrader of Bromodomain and Extra-Terminal (BET) Proteins with Picomolar Cellular Potencies and Capable of Achieving Tumor Regression. *J. Med. Chem.* **2018**, *61* (2), 462–481.

(15) Tang, K.; Coward, J. K. Synthesis of Acyl Phosphonate Analogues of Biologically Important Acyl Phosphates: N-(2-Amino-10-Methylpteroyl)-5-Amino-2-Oxopentanephosphonic Acid. *J. Org. Chem* **1983**, *48* (25), 5001–5006.

(16) Bernardes, G. J. L.; Linderoth, L.; Doores, K. J.; Boutureira, O.; Davis, B. G. Site-Selective Traceless Staudinger Ligation for Glycoprotein Synthesis Reveals Scope and Limitations. *ChemBioChem* **2011**, *12* (9), 1383–1386.

(17) Burslem, G. M.; Ottis, P.; Jaime-Figueroa, S.; Morgan, A.; Cromm, P. M.; Toure, M.; Crews, C. M. Efficient Synthesis of Immunomodulatory Drug Analogues Enables Exploration of Structure–Degradation Relationships. *ChemMedChem* **2018**, *13* (15), 1508–1512.

6.4. Selected Spectra

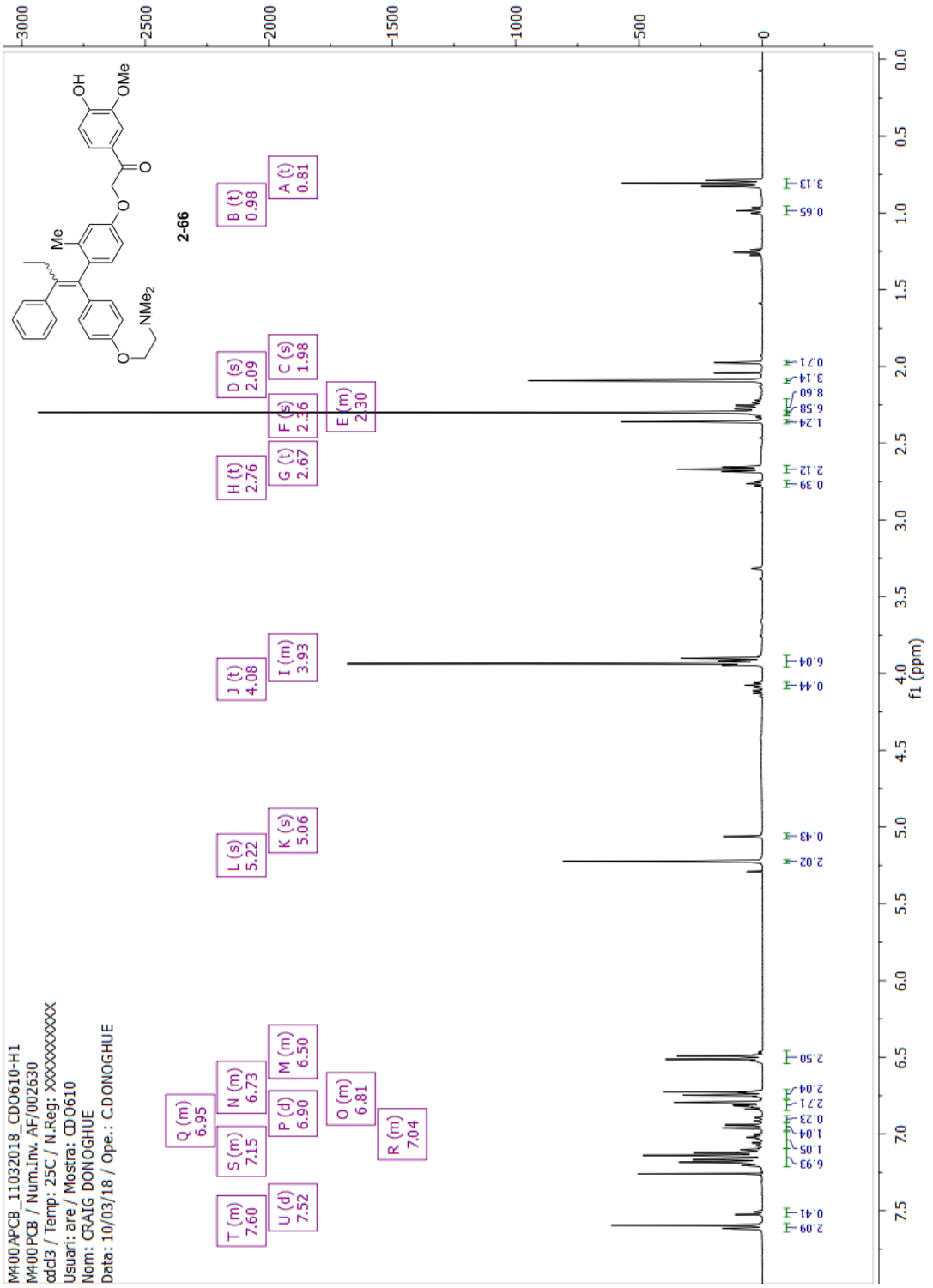

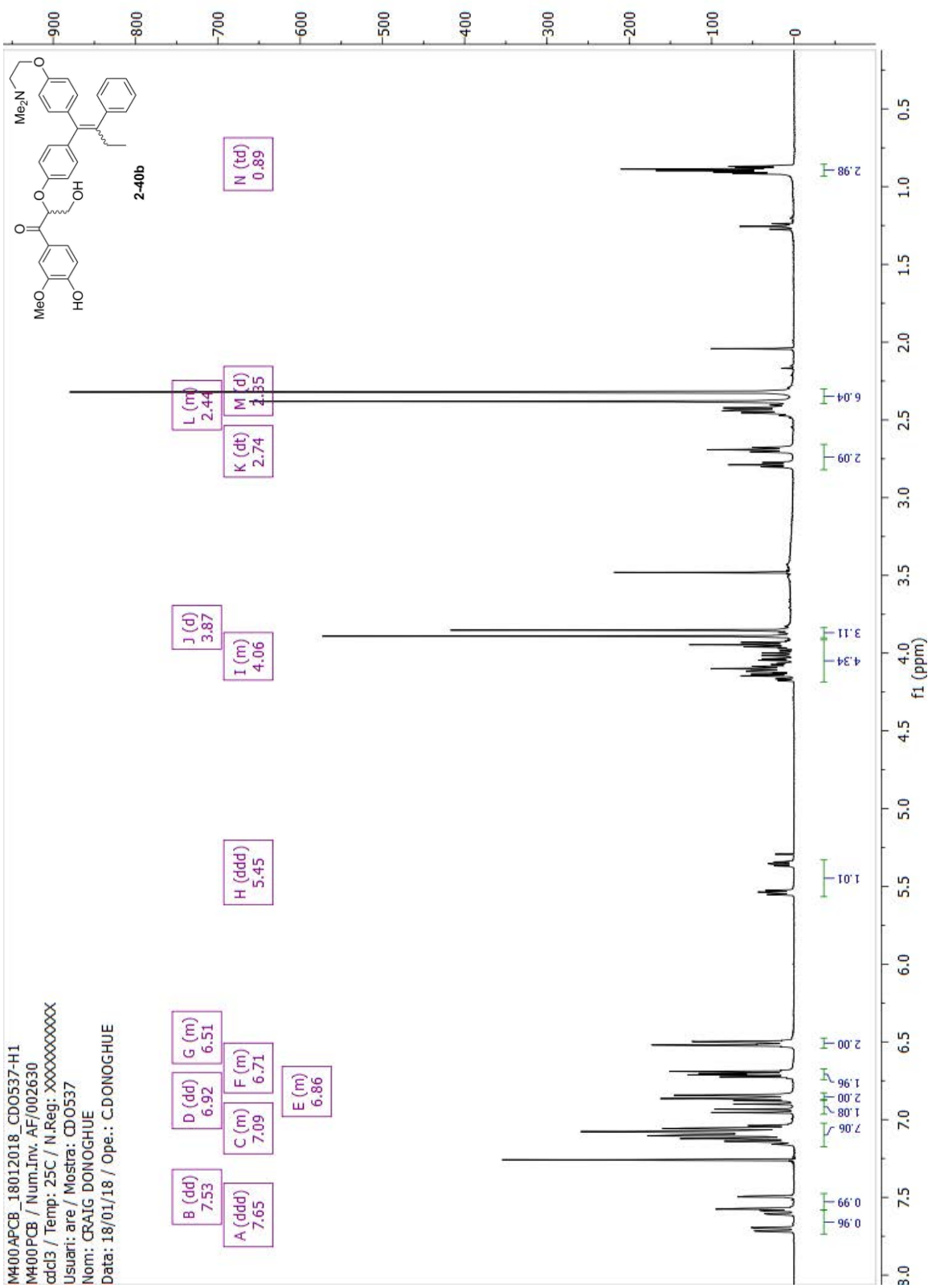
M400APCB_18012018_CDO537-H1
M400PCB / Num.Inv. AF/002630
cdcl3 / Temp: 25C / N.Reg: XXXXXXXXXX
Usuari: are / Mostra: CDO537
Nom: CRAIG DONOGHUE
Data: 18/01/18 / Ope.: C.DONOGHUE
2-40b
A (ddd) 7.65
B (dd) 7.53
C (m) 7.09
D (dd) 6.92
E (m) 6.86
F (m) 6.71
G (m) 6.51
H (ddd) 5.45
I (m) 4.06
J (d) 3.87
K (dt) 2.74
L (m) 2.44
M (d) 4.35
N (td) 0.89
f1 (ppm)

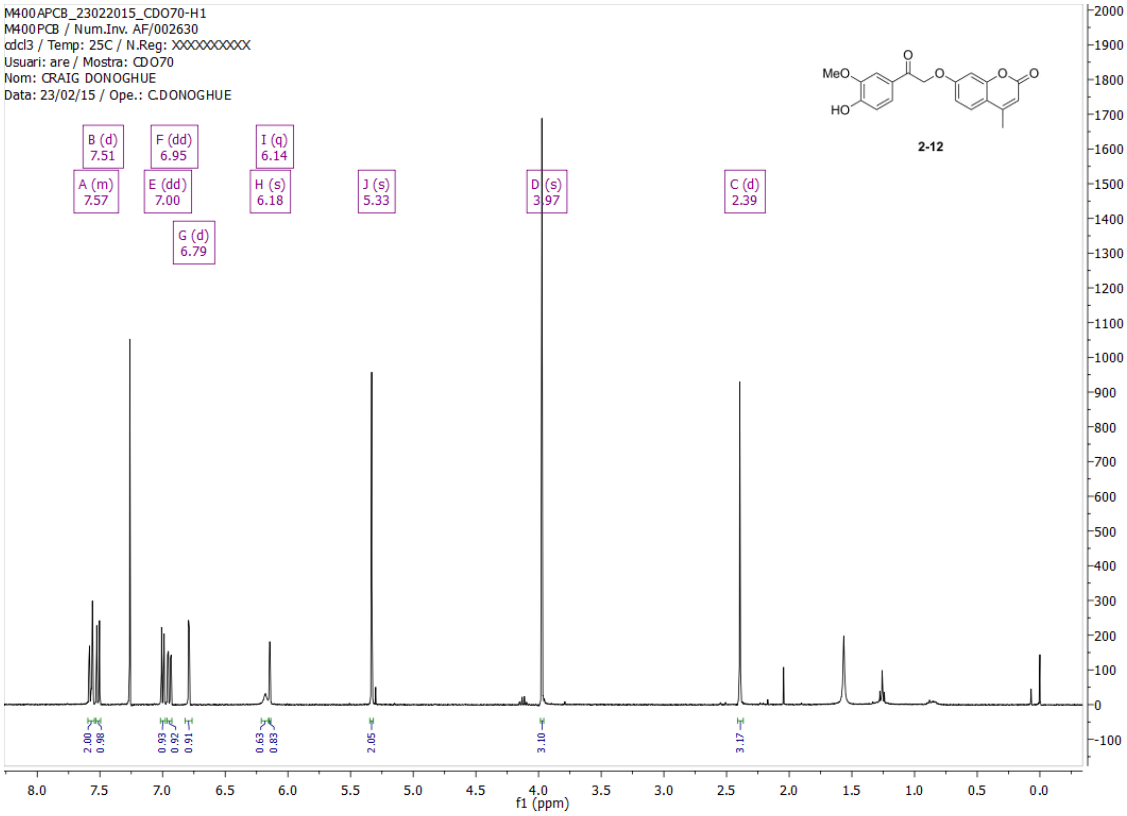
M400APCB_23022015_CDO70-H1
M400PCB / Num.Inv. AF/002630
cdcl3 / Temp: 25C / N.Reg: XXXXXXXXX
Usuari: are / Mostra: CDO70
Nom: CRAIG DONOGHUE
Data: 23/02/15 / Ope.: C.DONOGHUE
MeO
HO
2-12
B (d) 7.51
F (dd) 6.95
I (q) 6.14
A (m) 7.57
E (dd) 7.00
H (s) 6.18
J (s) 5.33
D (s) 3.97
C (d) 2.39
G (d) 6.79
f1 (ppm)

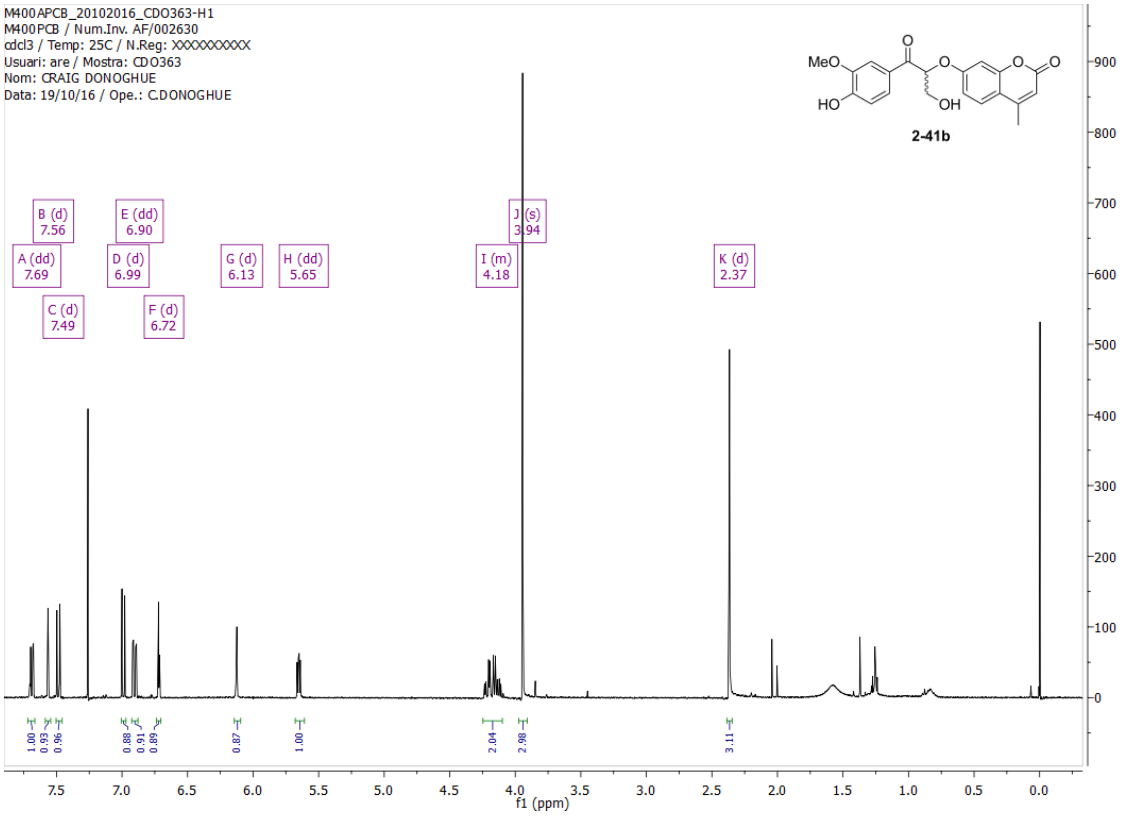
M400APCB_20102016_CDO363-H1
M400PCB / Num.Inv. AF/002630
cdcl3 / Temp: 25C / N.Reg: XXXXXXXXX
Usuari: are / Mostra: CDO363
Nom: CRAIG DONOGHUE
Data: 19/10/16 / Ope.: C.DONOGHUE
MeO
HO
OH
2-41b
B (d) 7.56
E (dd) 6.90
J (s) 3.94
A (dd) 7.69
D (d) 6.99
G (d) 6.13
H (dd) 5.65
I (m) 4.18
K (d) 2.37
C (d) 7.49
F (d) 6.72
f1 (ppm)

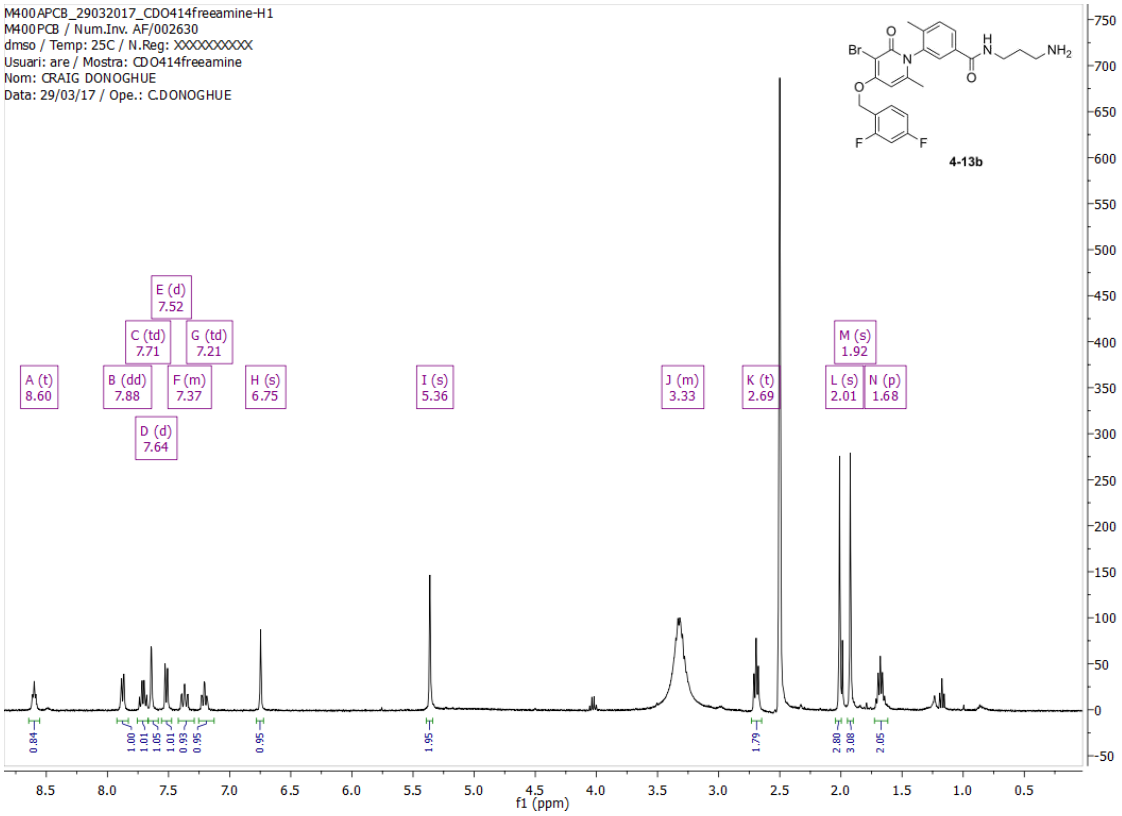
M400APCB_29032017_CDO414freeamine-H1
M400PCB / Num.Inv. AF/002630
dmso / Temp: 25C / N.Reg: XXXXXXXXX
Usuari: are / Mostra: CDO414freeamine
Nom: CRAIG DONOGHUE
Data: 29/03/17 / Ope.: C.DONOGHUE
4-13b
A (t) 8.60
B (dd) 7.88
C (td) 7.71
D (d) 7.64
E (d) 7.52
F (m) 7.37
G (td) 7.21
H (s) 6.75
I (s) 5.36
J (m) 3.33
K (t) 2.69
L (s) 2.01
M (s) 1.92
N (p) 1.68
f1 (ppm)

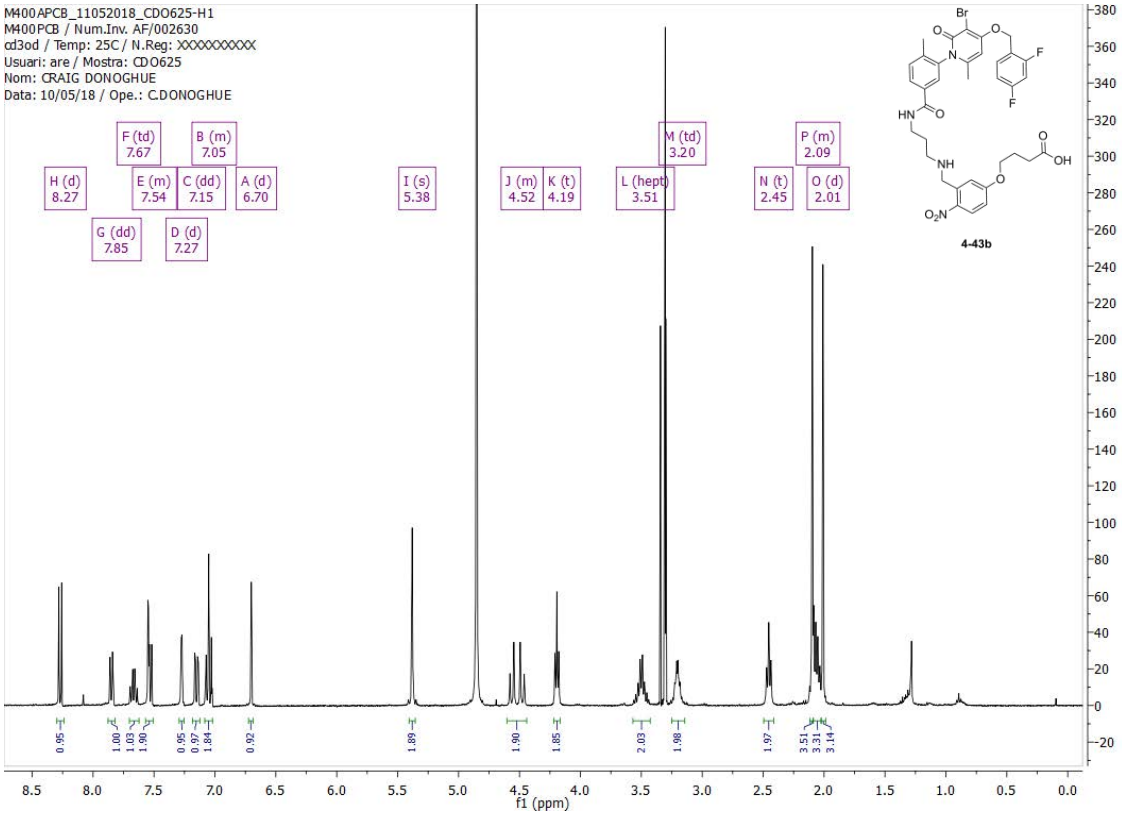
M400APCB_11052018_CDO625-H1
M400PCB / Num.Inv. AF/002630
cd3od / Temp: 25C / N.Reg: XXXXXXXXX
Usuari: are / Mostra: CDO625
Nom: CRAIG DONOGHUE
Data: 10/05/18 / Ope.: C.DONOGHUE
4-43b
H (d) 8.27
G (dd) 7.85
F (td) 7.67
E (m) 7.54
D (d) 7.27
C (dd) 7.15
B (m) 7.05
A (d) 6.70
I (s) 5.38
J (m) 4.52
K (t) 4.19
L (hept) 3.51
M (td) 3.20
N (t) 2.45
O (d) 2.01
P (m) 2.09
f1 (ppm)

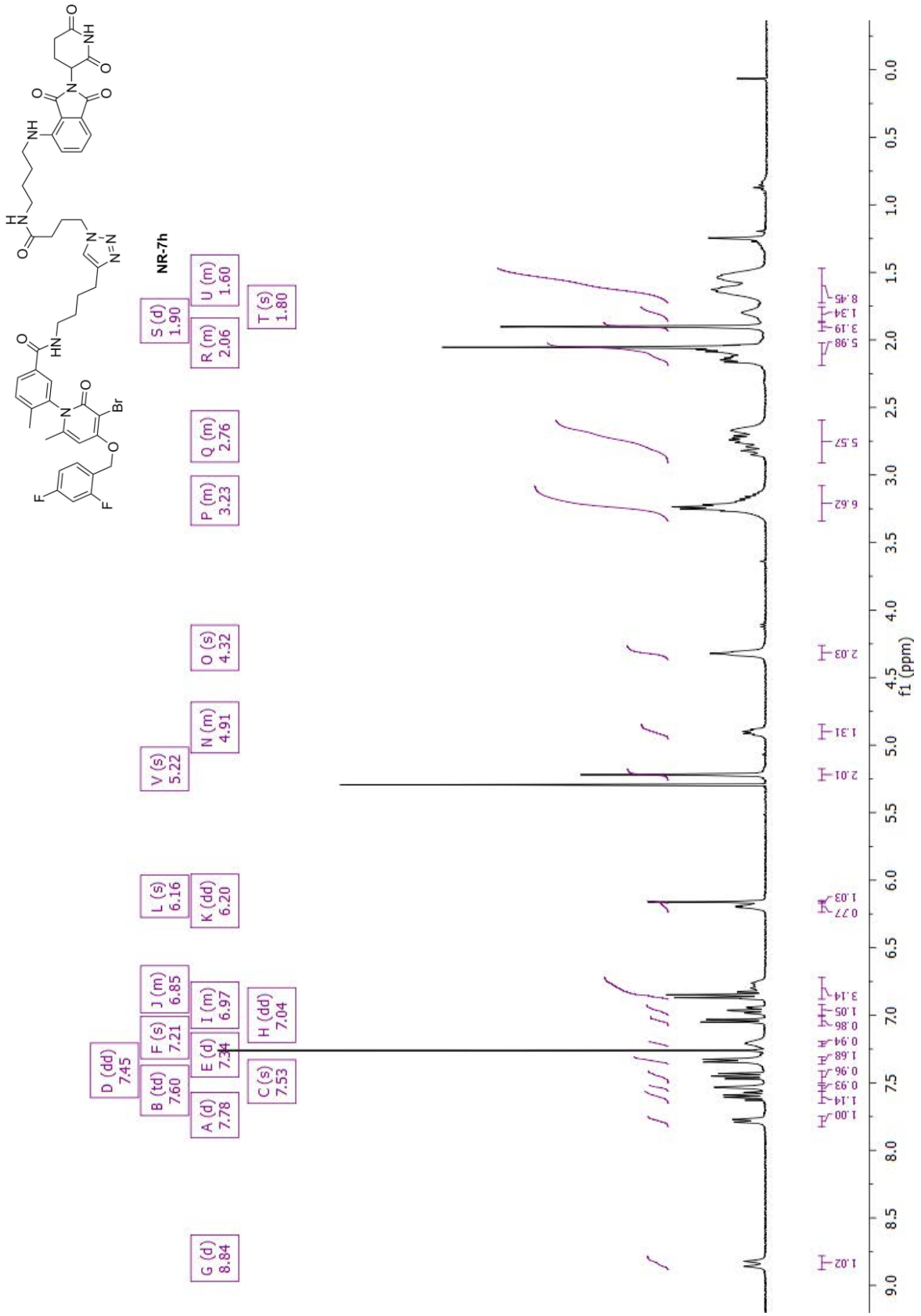
NR-7h
G (d) 8.84
D (dd) 7.45
B (td) 7.60
A (d) 7.78
F (s) 7.21
E (d) 7.34
J (m) 6.85
I (m) 6.97
C (s) 7.53
H (dd) 7.04
L (s) 6.16
K (dd) 6.20
V (s) 5.22
N (m) 4.91
O (s) 4.32
P (m) 3.23
Q (m) 2.76
S (d) 1.90
R (m) 2.06
U (m) 1.60
T (s) 1.80
f1 (ppm)

6.5. List of Structures

From chapter 1

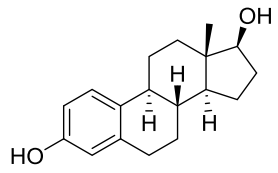

17β-oestradiol, (**1-1**)

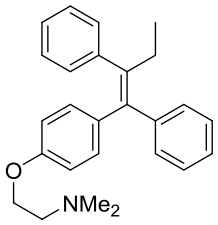

Tamoxifen (**1-2**)

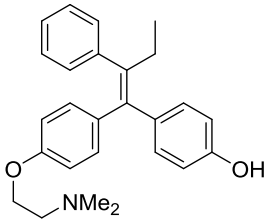

4-hydroxytamoxifen (4OHT, **1-3**)

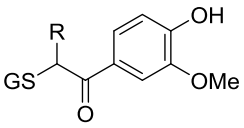

1-5a, R = H
1-5b, R = CH_2OH

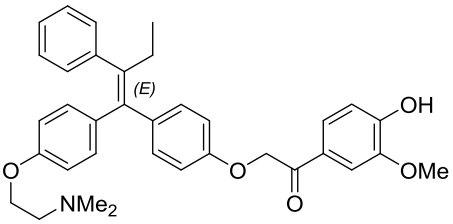

Guaymoxifen (**1-4**)

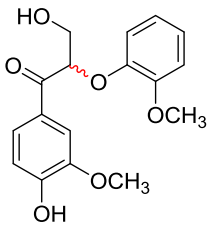

1-6

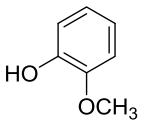

Guaiacol

1-7

GSH =

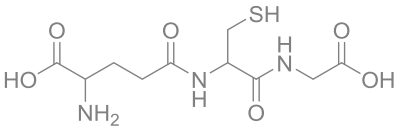

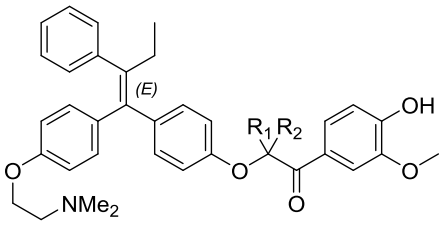

1-8

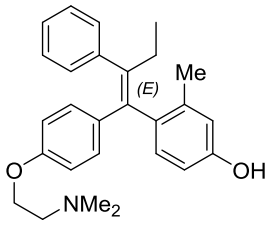

(***E***)-**1-9**

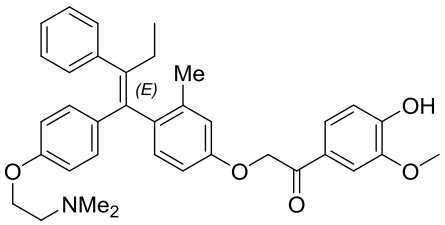

(***E***)-**1-10**

From chapter 2

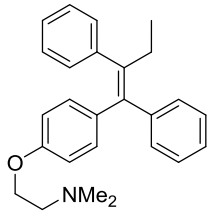

2-1, Tamoxifen

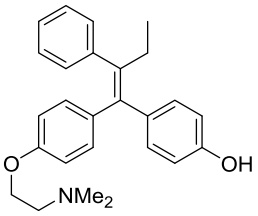

2-2, 4OHT

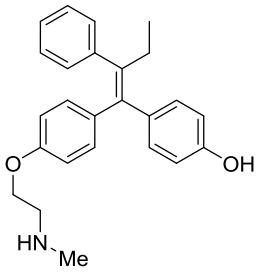

2-3, Endoxifen

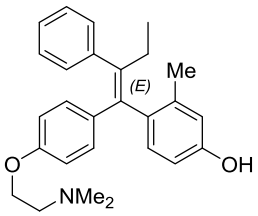

2-4

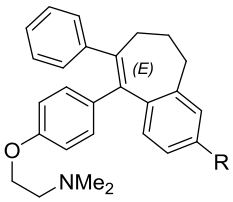

2-5a, R = H
2-5b, R = OH

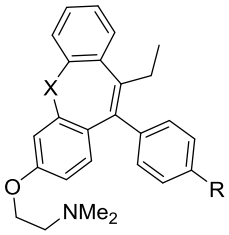

2-6a, R = H
2-6b, R = OH

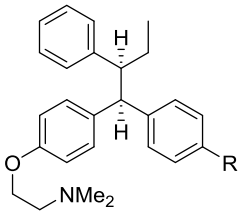

2-7a, R = H
2-7b, R = OH

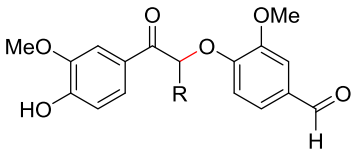

2-8a, R = H
2-8b, R = CH_2OH

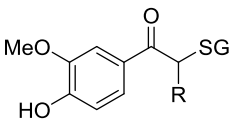

2-9a, R = H
2-9b, R = CH_2OH

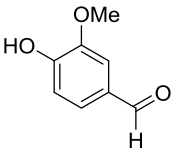

2-10

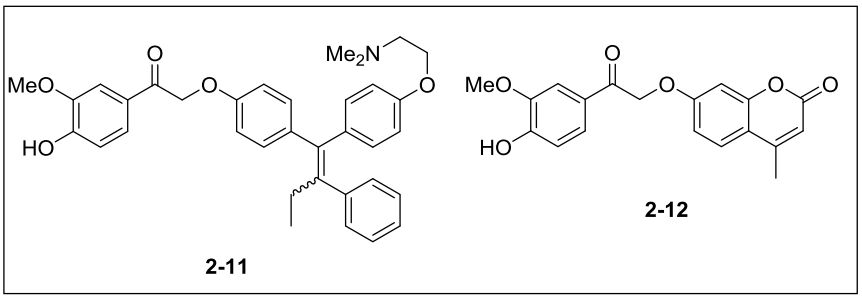

2-11

2-12

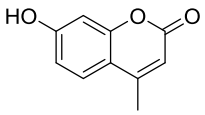

2-13

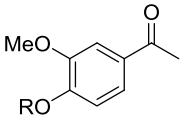

2-14a, R = H
2-14b, R = Bn
2-14c, R = Piv
2-14d, R = PMB
2-14e, R = Bnz

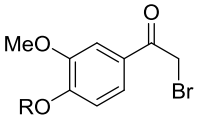

2-15a, R = Bn
2-15b, R = Piv
2-15c, R = Me
2-15d, R = PMB
2-15e, R = Bnz

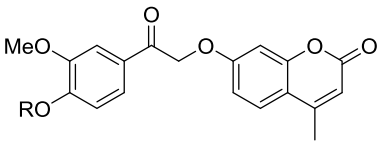

2-16a, R = Bn
2-16b, R = Piv
2-16c, R = Bnz

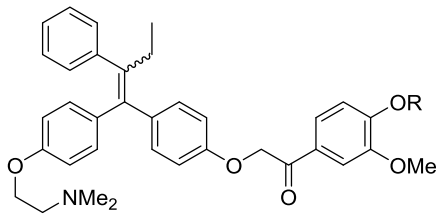

2-17a, R = Bn
2-17b, R = Piv

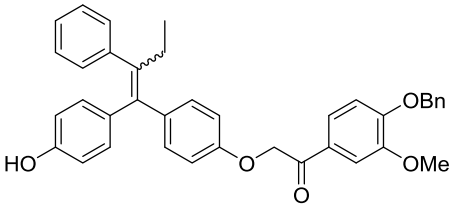

2-18

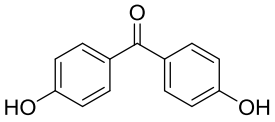

2-19

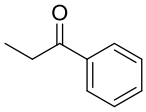

2-20

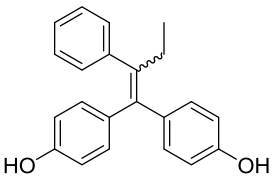

2-21

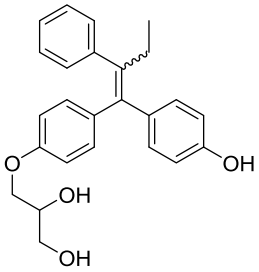

2-22

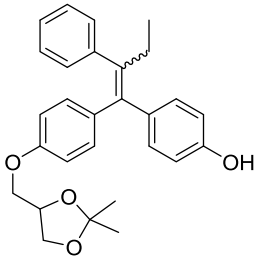

2-23

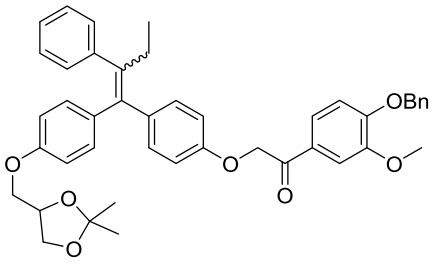

2-24

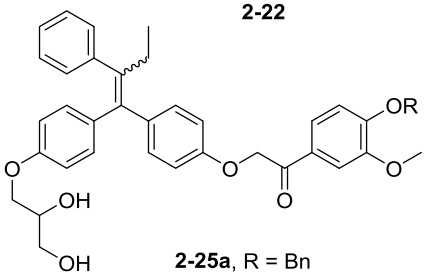

2-25a, R = Bn
2-25b, R = Piv

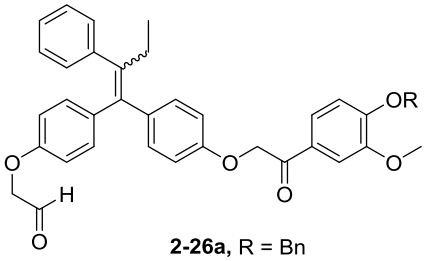

2-26a, R = Bn
2-26b, R = Piv

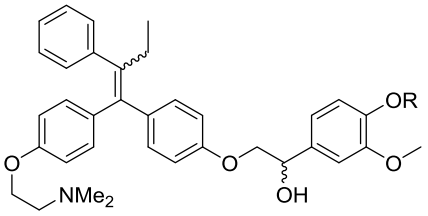

2-27a, R = Bn
2-27b, R = H

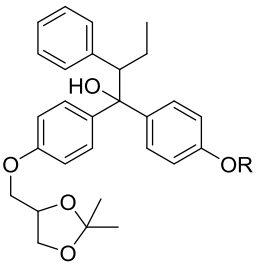

2-28a, R = Me
2-28b, R = allyl

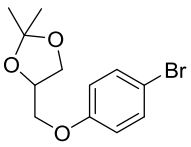

2-29a, X = Br
2-29b, X = I

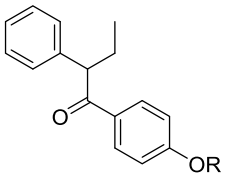

2-30a, R = Me
2-30b, R = H
2-30c, R = allyl

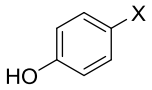

2-31aa, X = Br, R = H
2-31ba, X = I, R = H
2-31ab, X = Br, R = THP

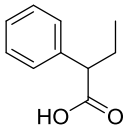

2-32

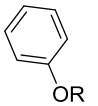

2-33a, R = Me
2-33b, R = allyl

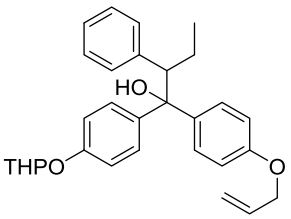

2-34

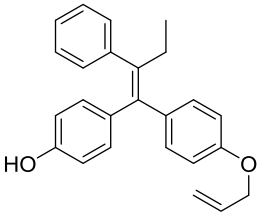

2-35

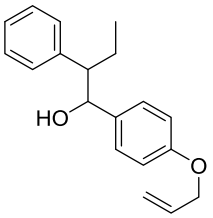

2-36

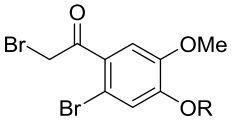

2-37

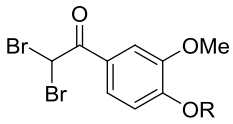

2-38

2-39a, R = tBu
2-39b, R = Bn

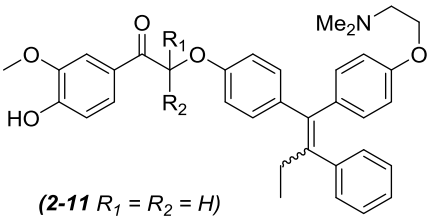

*(**2-11** $R_1 = R_2 = H$)*
2-40a $R_1 = CH_3$, $R_2 = H$
2-40b $R_1 = CH_2OH$, $R_2 = H$
2-40c $R_1 = CH_2OH$, $R_2 = CH_3$
2-40d $R_1 = F$, $R_2 = H$
2-40e $R_1 = CH_2OH$, $R_2 = F$
2-40f $R_1 = R_2 = F$

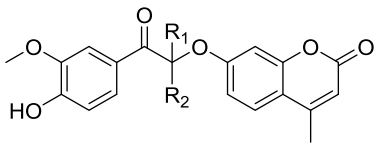

*(**2-12** $R_1 = R_2 = H$)*
2-41a $R_1 = CH_3$, $R_2 = H$
2-41b $R_1 = CH_2OH$, $R_2 = H$
2-41c $R_1 = CH_2OH$, $R_2 = CH_3$
2-41d $R_1 = F$, $R_2 = H$
2-41e $R_1 = CH_2OH$, $R_2 = F$
2-41f $R_1 = R_2 = F$
2-41g $R_1 = D$, $R_2 = H$
2-41h $R_1 = R_2 = D$

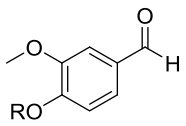

2-42a, R = H
2-42b, R = Bn
2-42c, R = Piv

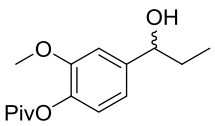

2-43

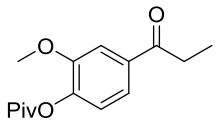

2-44

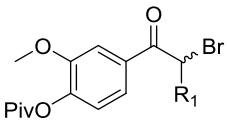

2-45

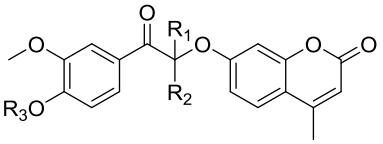

2-46ba $R_1 = CH_3$, $R_2 = H$ $R_3 = Piv$
2-46bb $R_1 = CH_2OH$, $R_2 = H$ $R_3 = Piv$
2-46bc $R_1 = CH_2OH$, $R_2 = CH_3$ $R_3 = Piv$
2-46ad $R_1 = F$, $R_2 = H$ $R_3 = Bn$
2-46ae $R_1 = CH_2OH$, $R_2 = F$ $R_3 = Bn$
2-46af $R_1 = R_2 = F$ $R_3 = Bn$
2-46ag $R_1 = D$ $R_2 = H$ $R_3 = Bn$
2-46ah $R_1 = D = H$, $R_3 = Bn$
2-46bi $R_1 = R_2 = CH_2OH$, $R_3 = Piv$

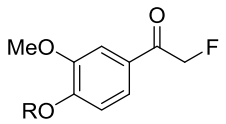

2-47a, R = Bn
2-47b, R = Piv

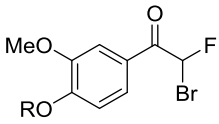

2-48a, R = Bn
2-48b, R = Piv

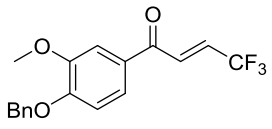

2-49

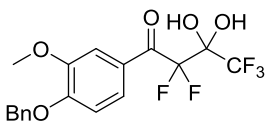

2-50

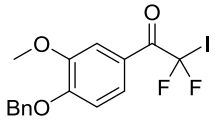

2-51

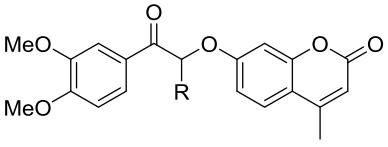

2-52a, R = H
2-52b, R =CH_2OH

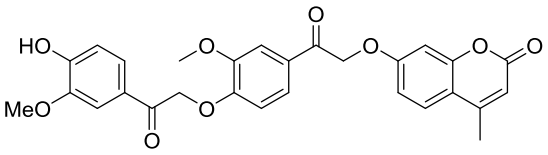

2-53

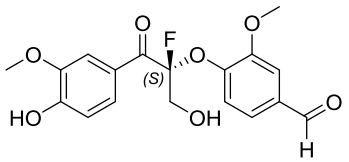

(*S*)-2-54

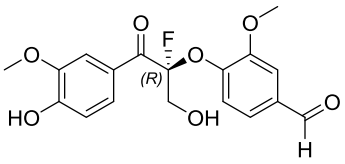

(*R*)-2-54

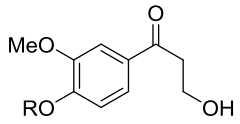

2-56

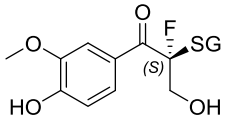

(*S*)-2-55

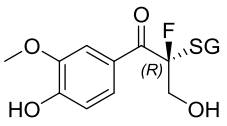

(*R*)-2-55

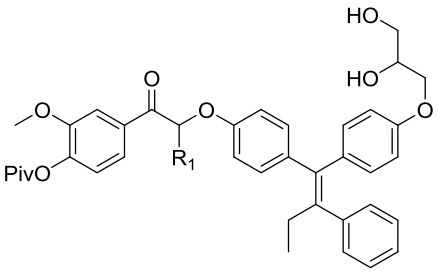

(2-25b, *R_1 = H)*
2-57a, R_1 = Me
2-57d, R_1 = F

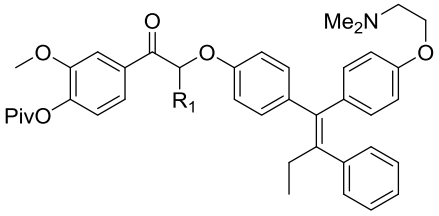

(2-17b, *R_1 = H)*
2-58a, R_1 = Me
2-58b, R1 = CH2OH
2-58d, R_1 = F

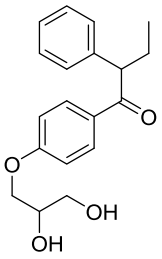

2-59

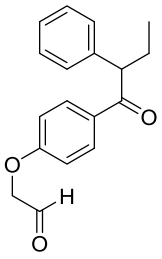

2-60

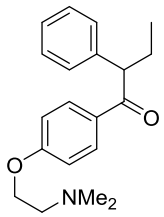

2-61

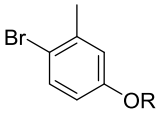

2-62a, R = H
2-62b, R = THP

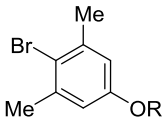

2-63a, R = H
2-63b, R = THP

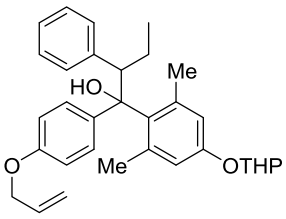

2-64

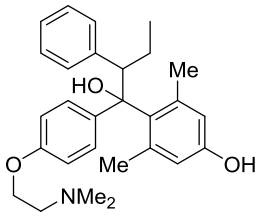

2-65

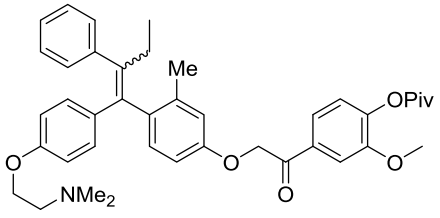

2-66

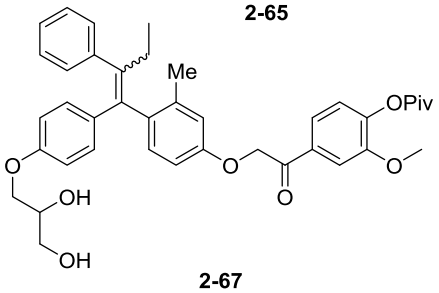

2-67

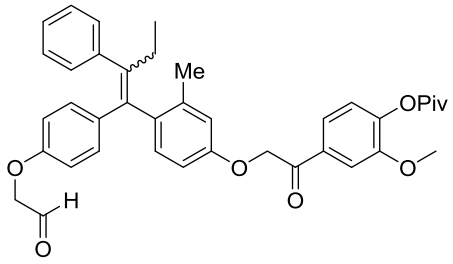

2-68

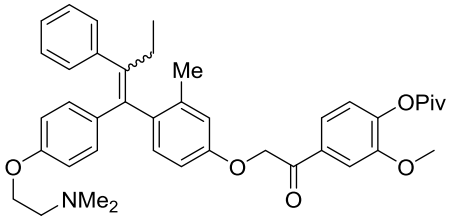

2-69

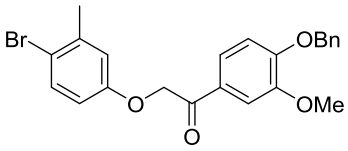

2-70

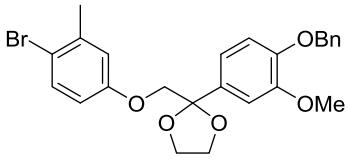

2-71

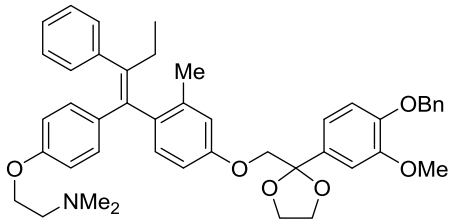

2-72

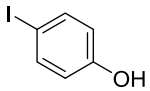

2-73

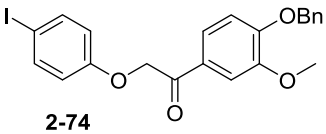

2-74

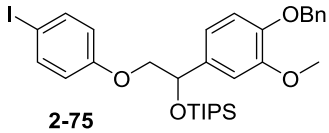

2-75

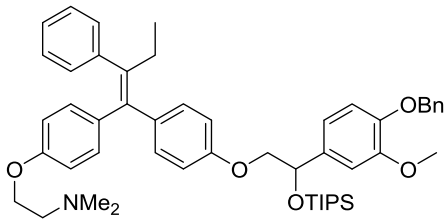

2-76

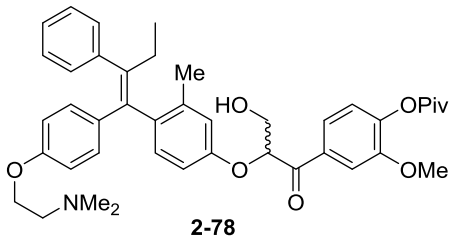

2-78

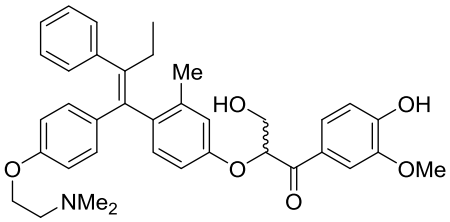

2-79

From chapter 3

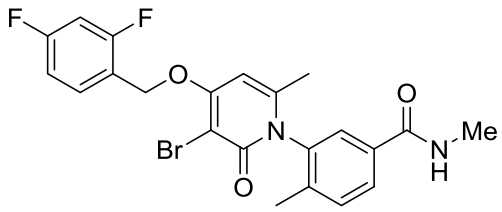

PH

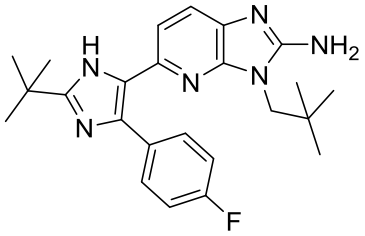

LY

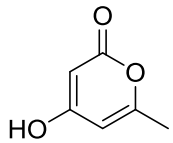

3-1

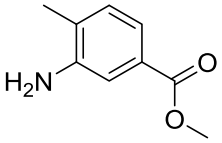

3-2

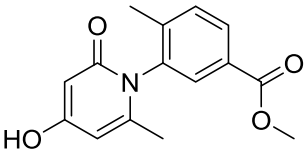

3-3

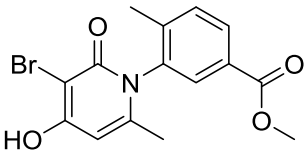

3-4

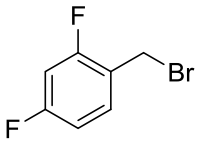

3-5

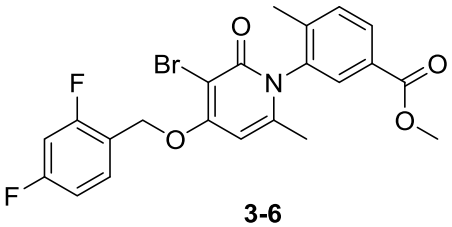

3-6

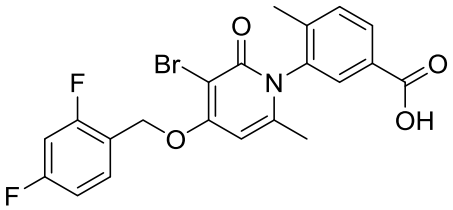

3-7

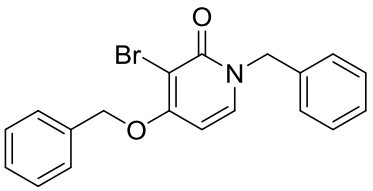

SC-25028 (1)

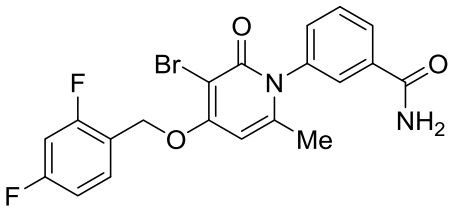

3-8

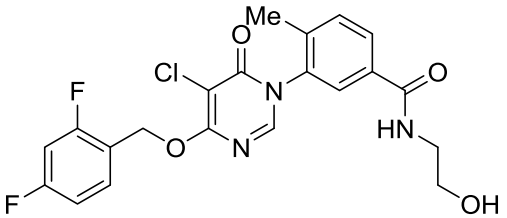

3-9

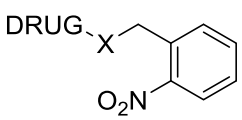

3-10

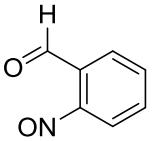

3-11

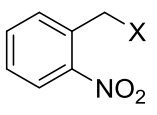

3-12

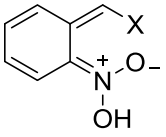

3-13

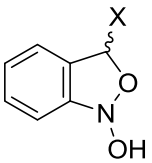

3-14

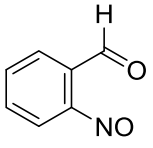

3-15

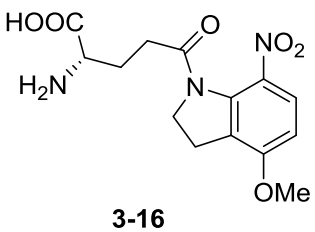

3-16

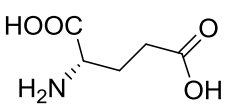

Glutamate

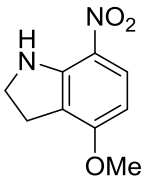

3-17

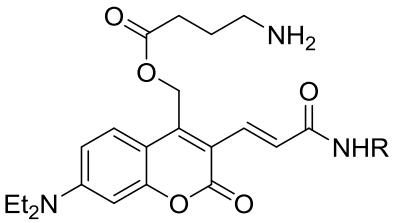

3-18

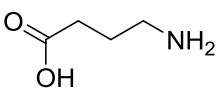

GABA

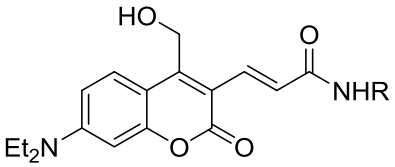

3-19

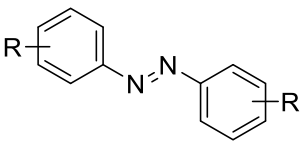

Azobenzenes

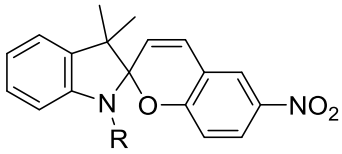

Spiropyrans

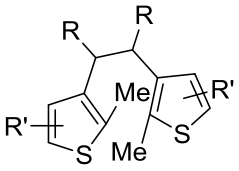

Diarylethenes

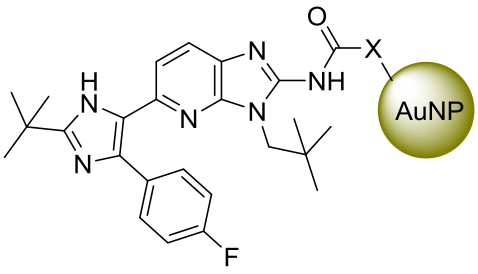

LY-NP

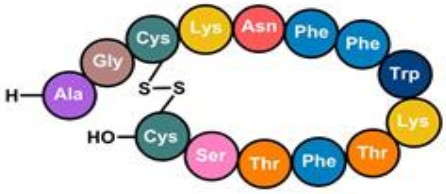

Somatostatin

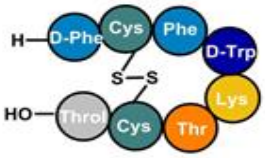

Octreotide

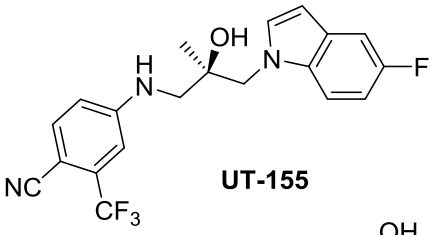

UT-155

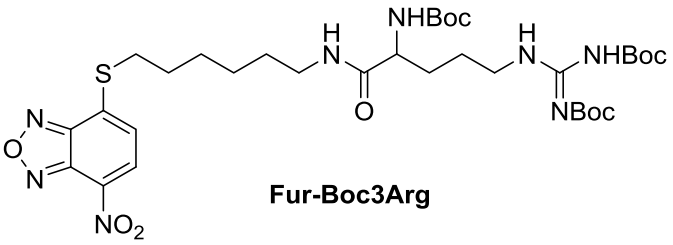

Fur-Boc3Arg

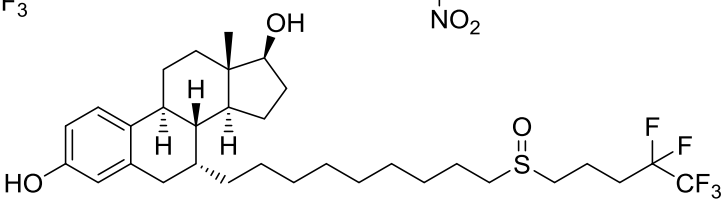

Fulvestrant

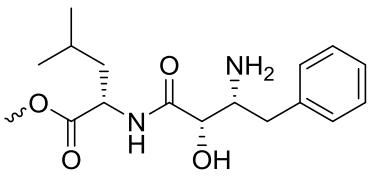

cIAP ligand

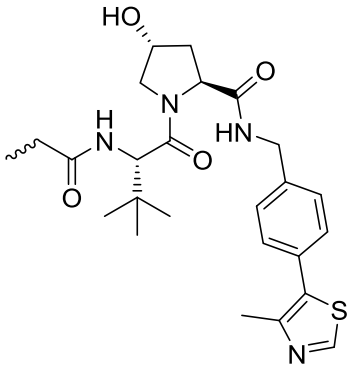

VHL ligand

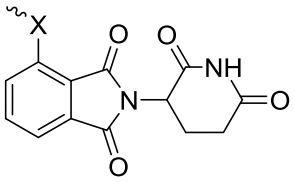

CRBN ligand
X = NH or O

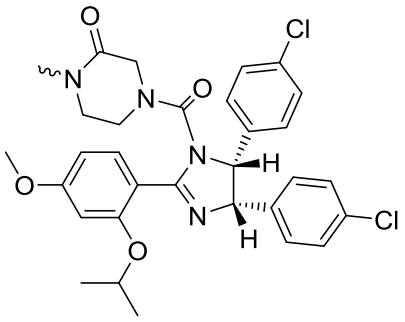

MDM2 ligand

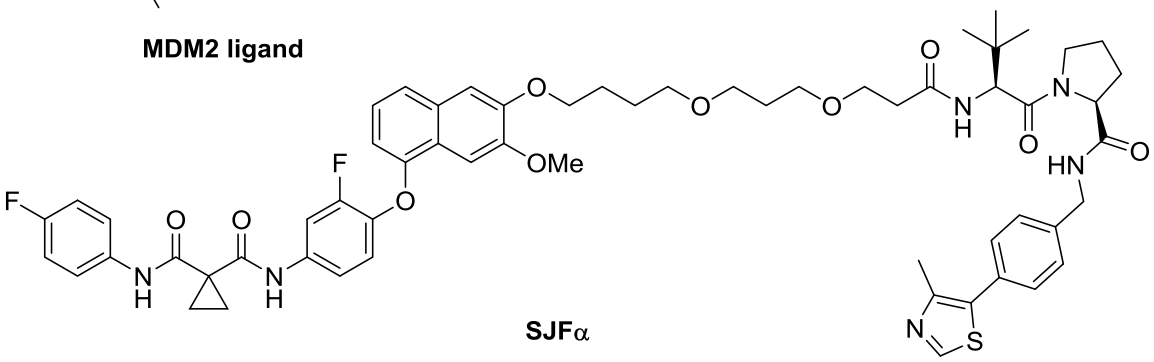

SJFα

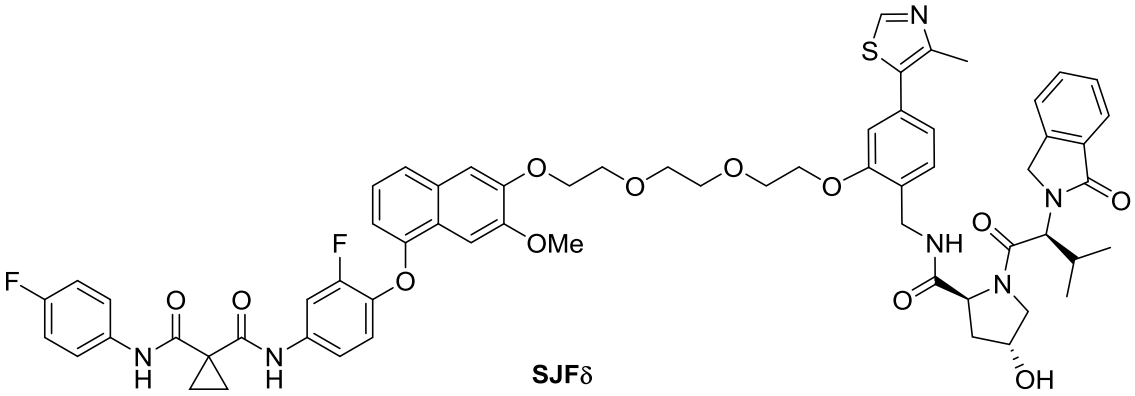

SJFδ

From chapter 4

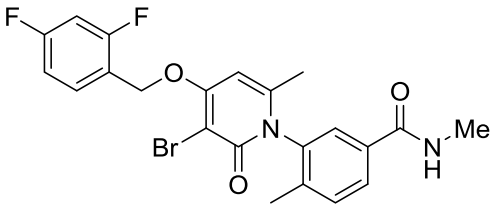

PH

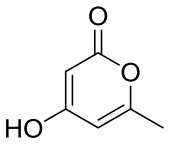

4-1

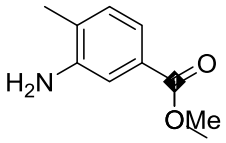

4-2

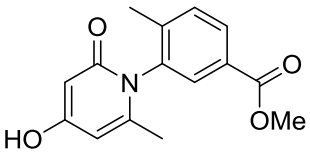

4-3

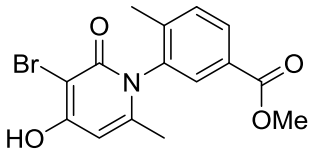

4-4

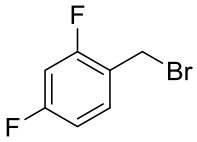

4-5

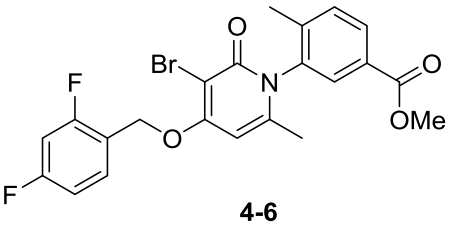

4-6

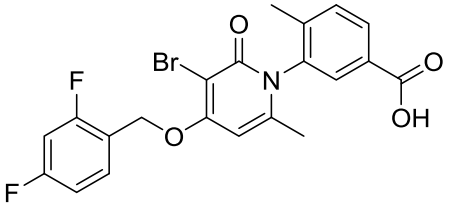

4-7

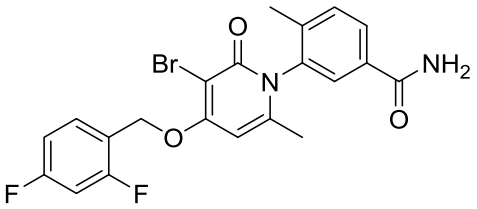

4-8

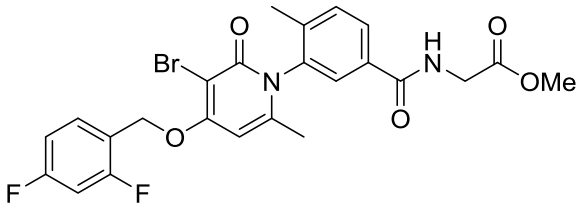

4-9a, R = Me
4-9b, R = H

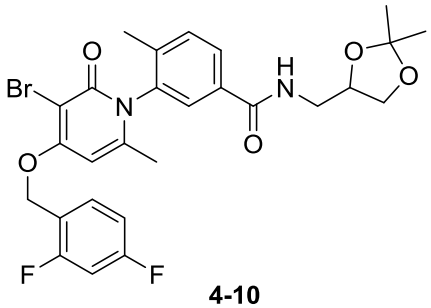

4-10

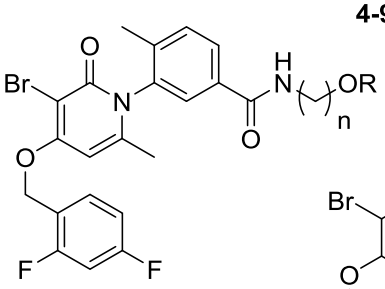

4-11, n = 2, R = H
4-12a, n = 3, R = H
4-12b, n = 3, R = Nv
4-15, n = 4, R = H

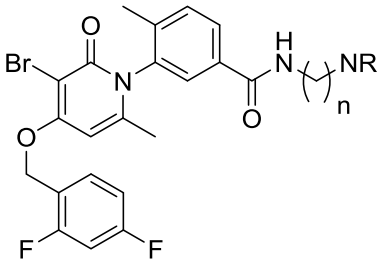

4-13a, n = 3, R = H_2
4-13b, n = 3, R = Nv_2
4-16, n = 4, R = H_2

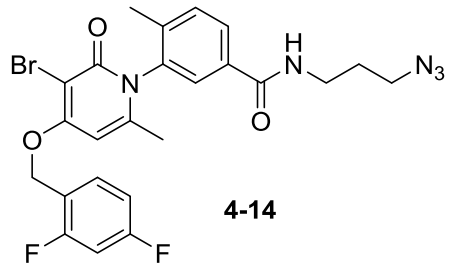

4-14

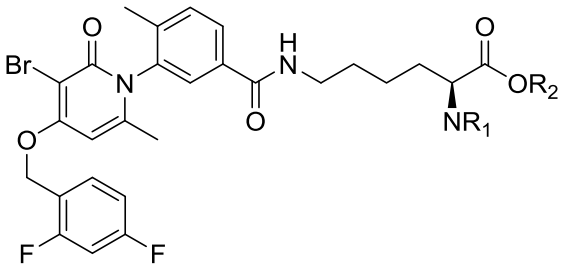

4-17a, R_1 = HBoc, R_2 = Me
4-17b, R_1 = H_2, R_2 = H

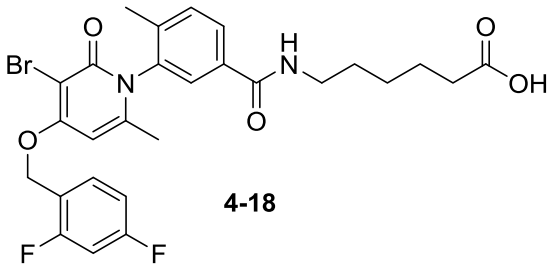

4-18

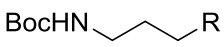

4-20a, R = OH
4-20b, R = NH_2

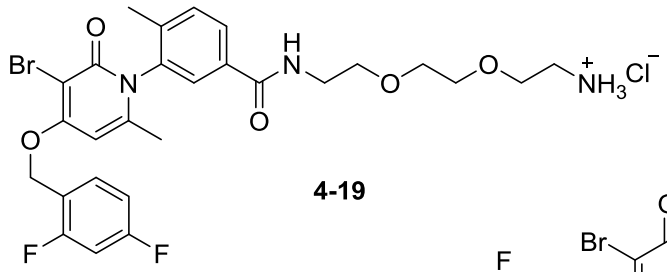

4-19

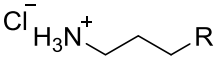

4-21a, R = ONv
4-21b, R = NNv_2

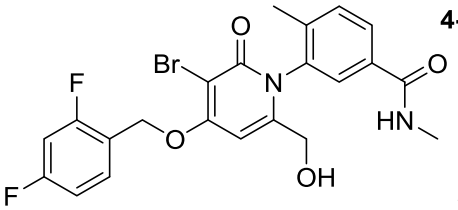

4-23

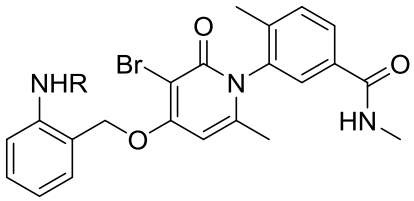

4-22, R = H
4-28, R = Nv

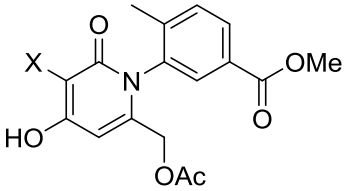

4-26, X = H
4-27, X = Br

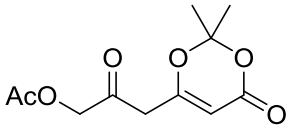

4-25

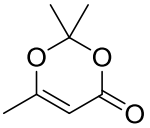

4-24

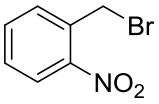

4-29

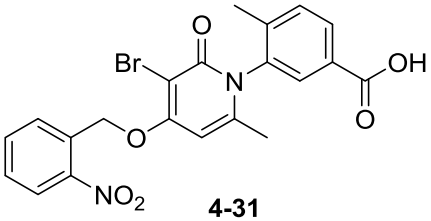

4-31

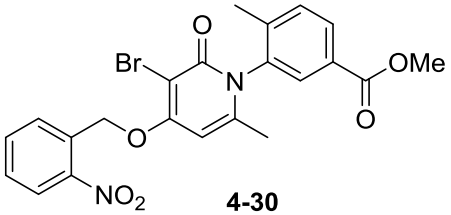

4-30

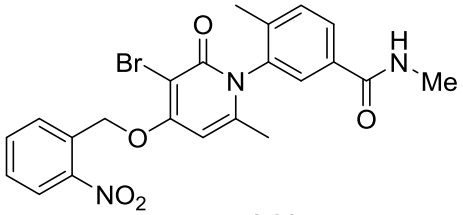

4-32

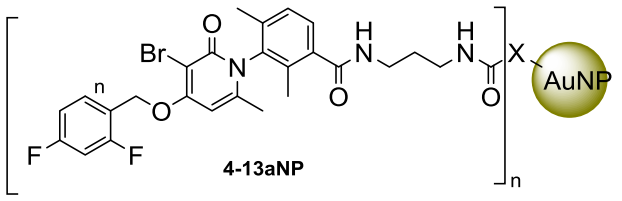

4-13aNP

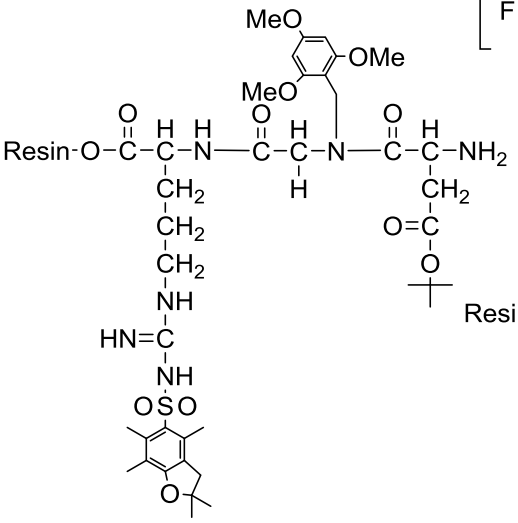

4-33

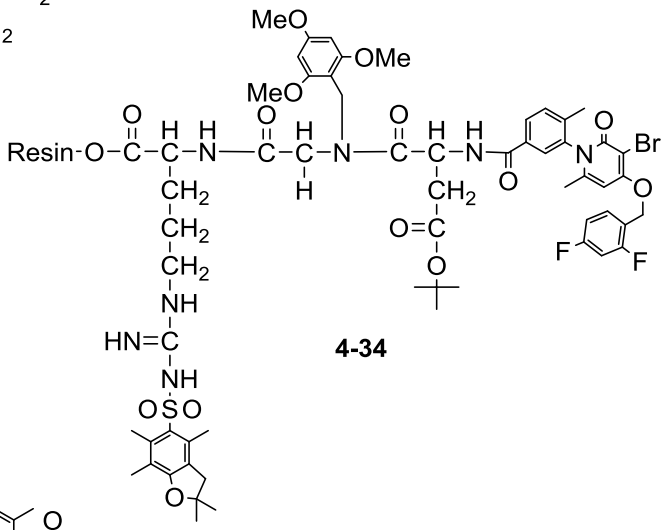

4-34

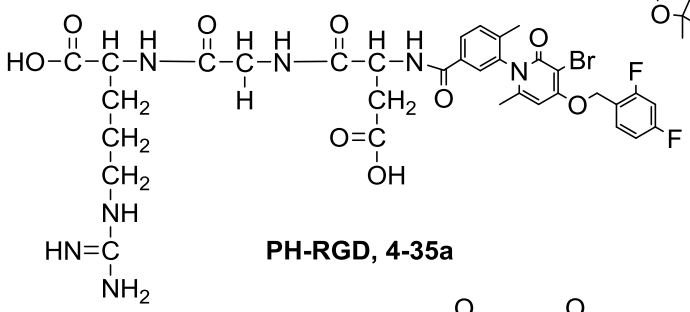

PH-RGD, 4-35a

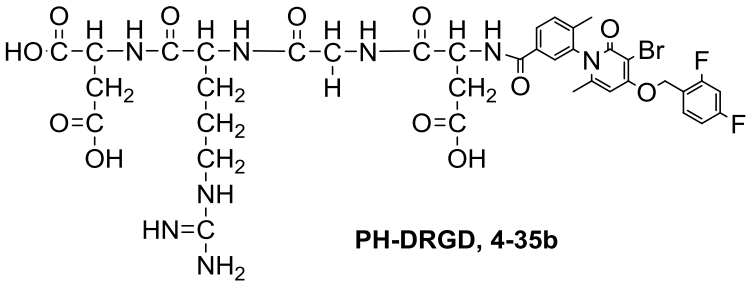

PH-DRGD, 4-35b

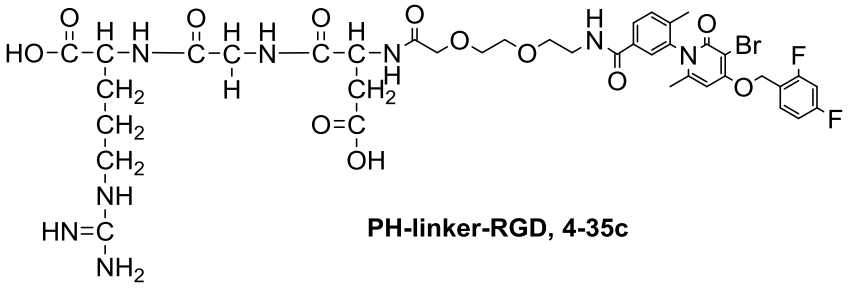

PH-linker-RGD, 4-35c

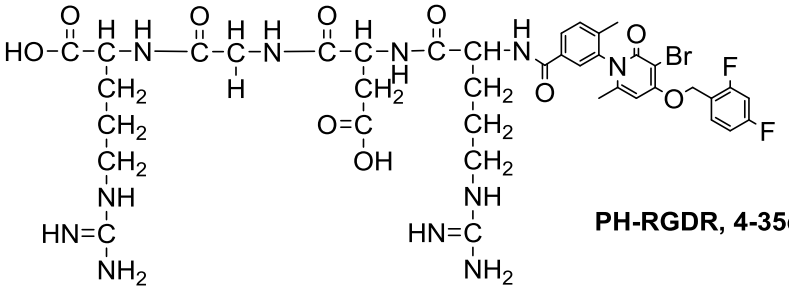

PH-RGDR, 4-35d

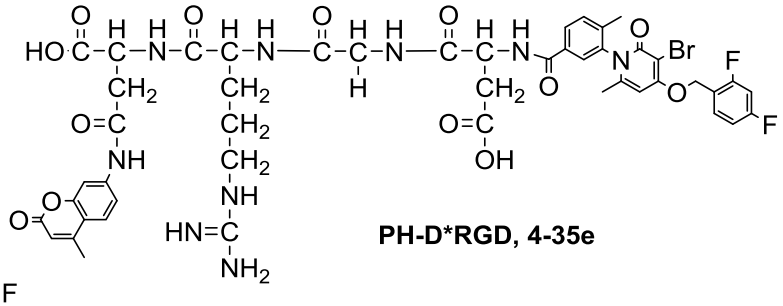

PH-D*RGD, 4-35e

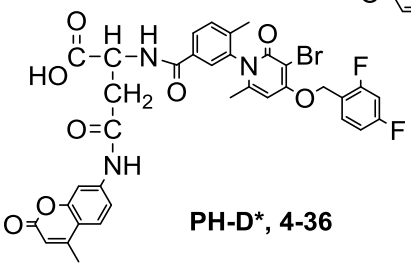

PH-D*, 4-36

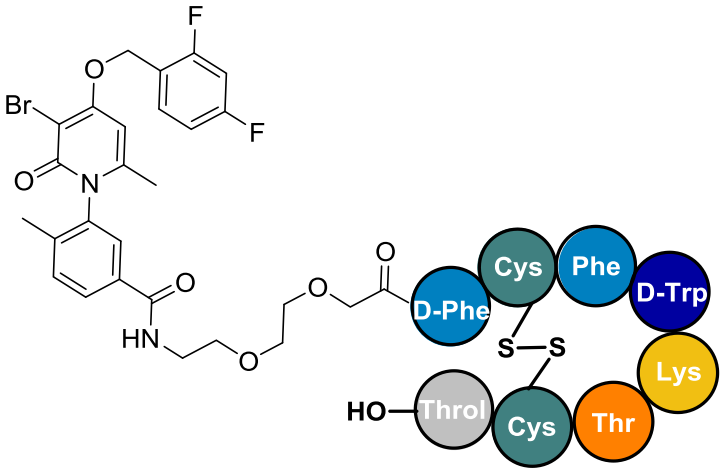

PH-peg-Oct, (**4-37**)

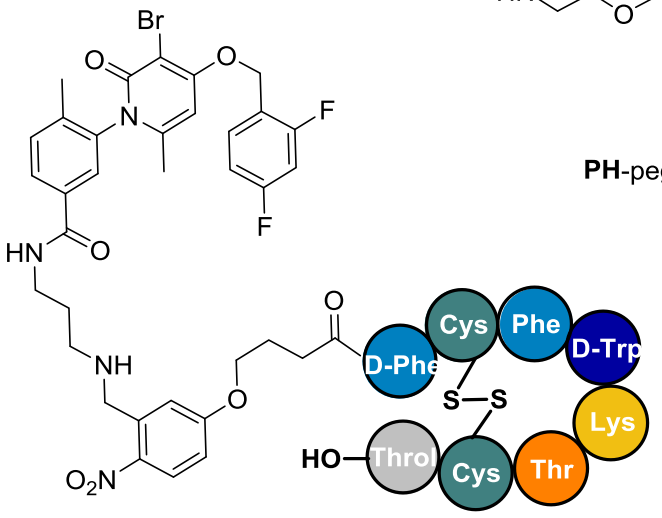

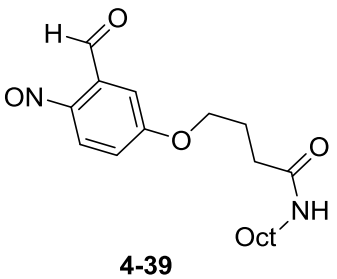

4-39

4-13a-UVlink-Oct, (**4-38**)

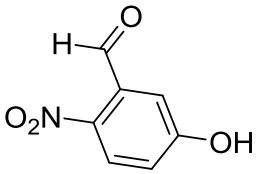

4-40

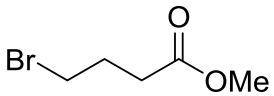

4-41

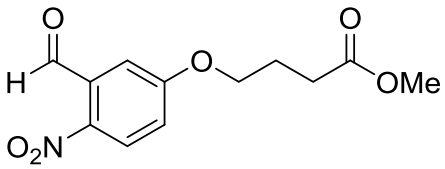

4-42

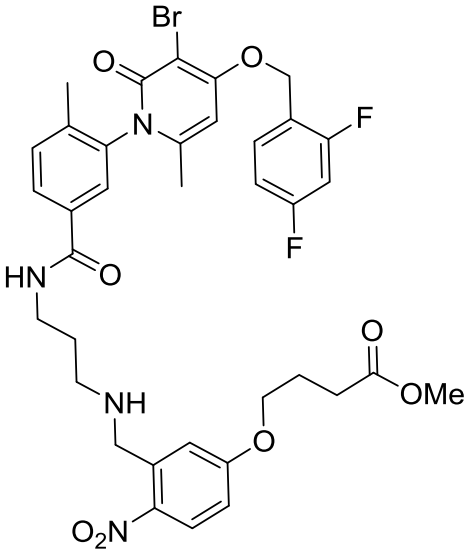

4-43a

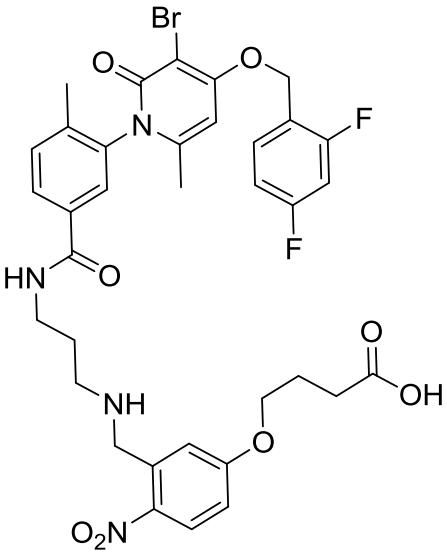

4-43b

PROTACs

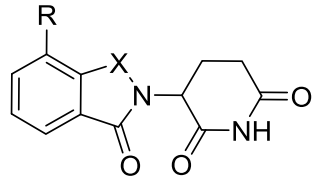

4-44a, R = H, X = CO
4-44b, R = OH, X = CO
4-44c, R = NH_2, X = CO Pomalidomide
4-44d, R = NH_2, X = CH_2 Lenalidomide

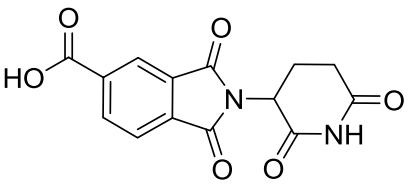

4-45

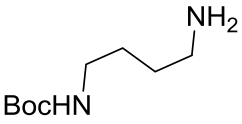

4-46

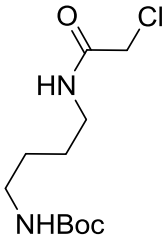

4-47

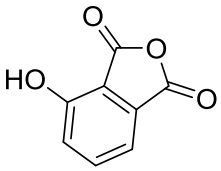

4-48

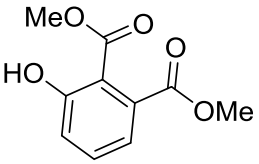

4-49

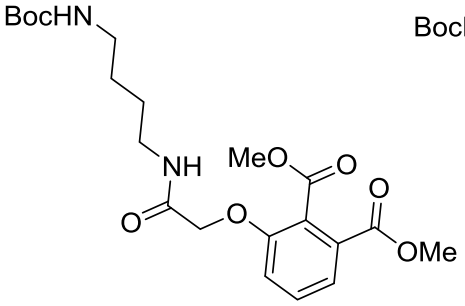

4-50

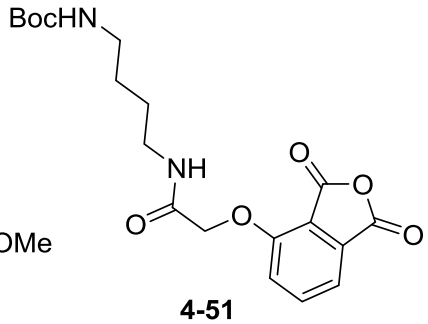

4-51

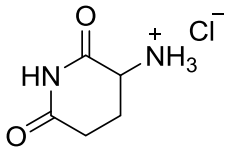

4-52

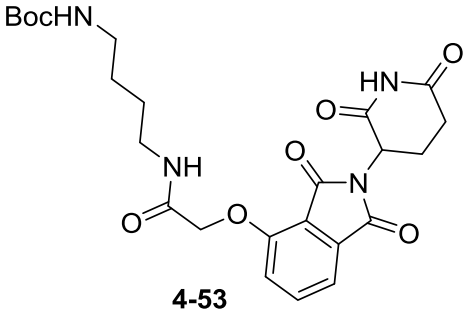

4-53

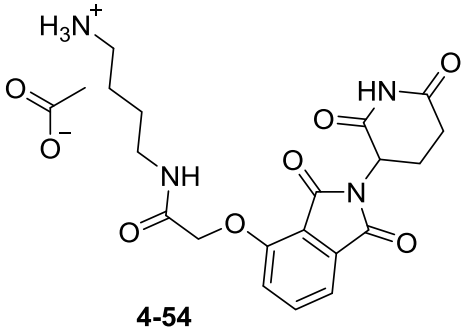

4-54

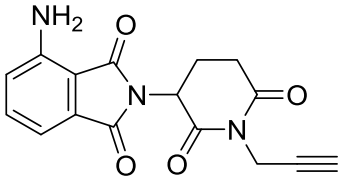

4-55

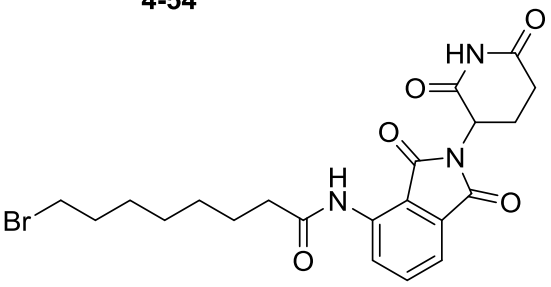

4-56

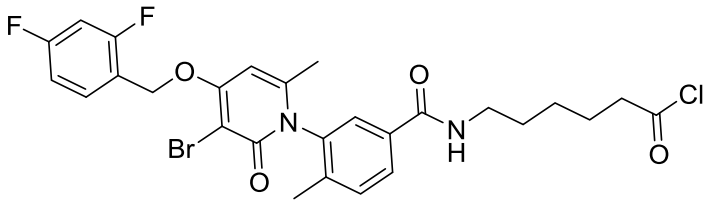

4-57

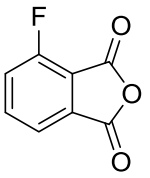

4-58

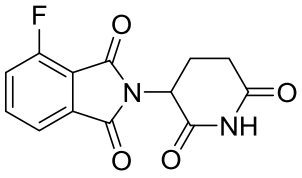

4-59

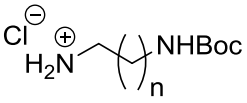

4-60a, n = 3
4-60b, n = 2
4-60c, n = 1

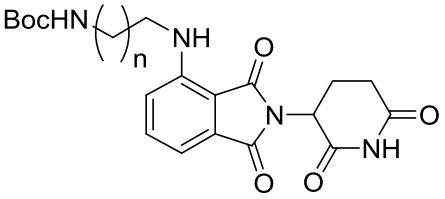

4-61a, n = 3
4-61b, n = 2
4-61c, n = 1

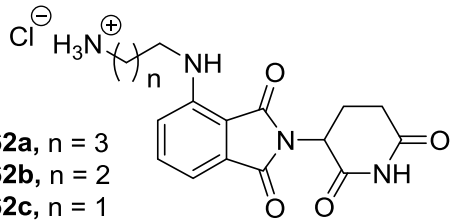

4-62a, n = 3
4-62b, n = 2
4-62c, n = 1

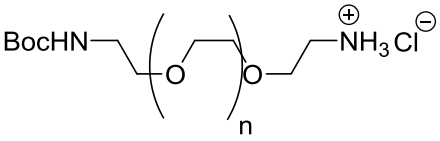

4-63a, n = 1
4-63b, n = 5

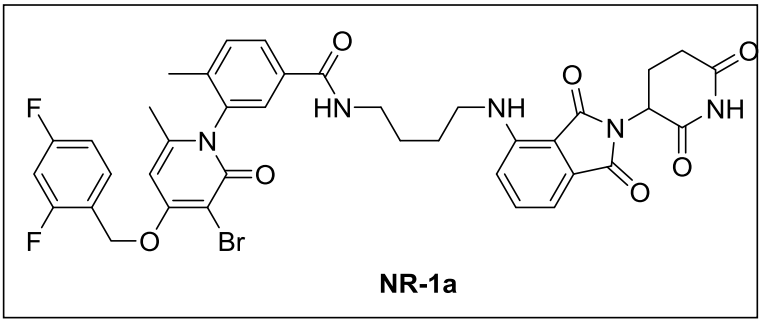

NR-1a

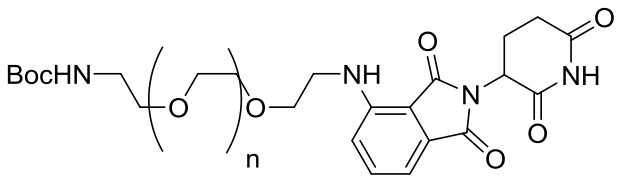

4-64a, n = 1
4-64b, n = 5

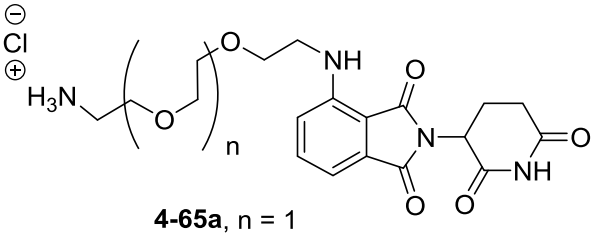

4-65a, n = 1
4-65b, n = 5

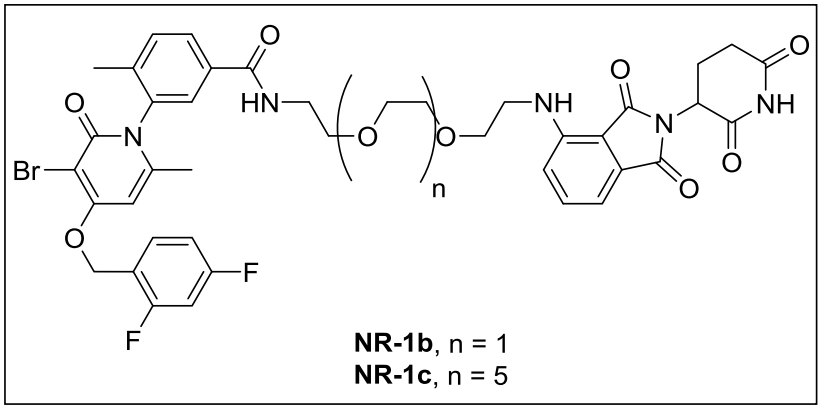

NR-1b, n = 1
NR-1c, n = 5

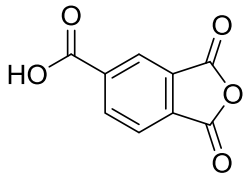

4-66

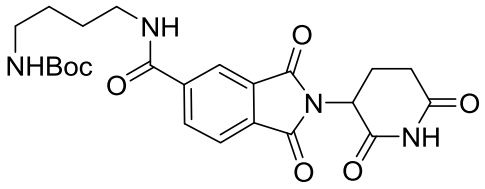

4-67

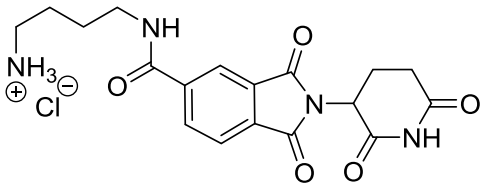

4-68

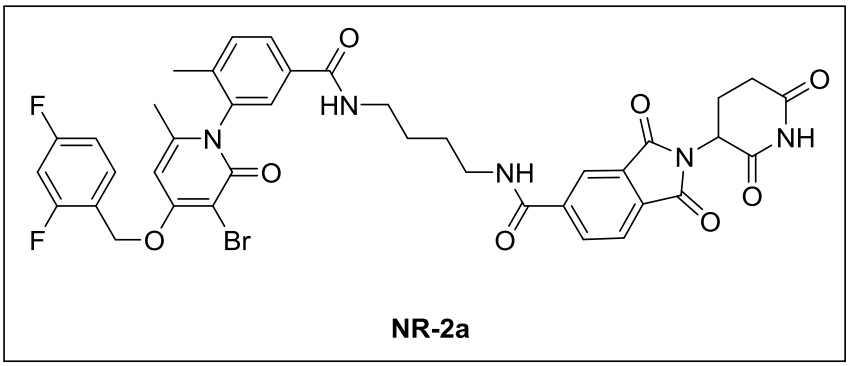

NR-2a

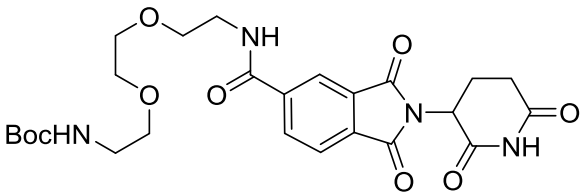

4-69

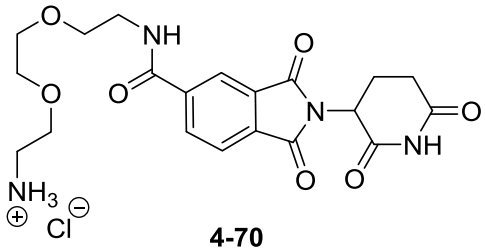

4-70

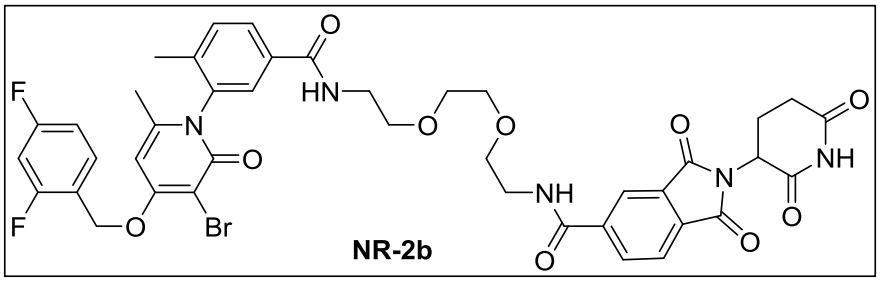

NR-2b

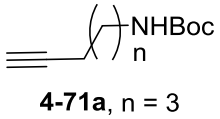

4-71a, n = 3
4-71b, n = 2
4-71c, n = 1

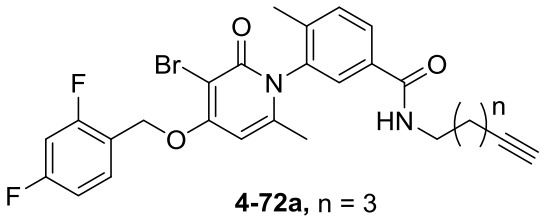

4-72a, n = 3
4-72b, n = 2
4-72c, n = 1

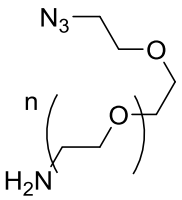

4-73a n = 2
4-73b n = 3

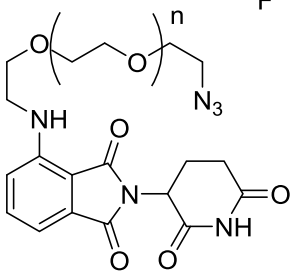

4-74a n = 2
4-74b n = 3

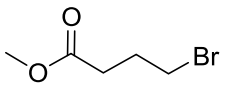

4-75

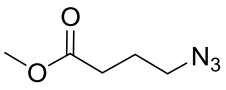

4-76

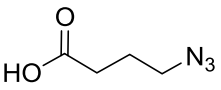

4-77

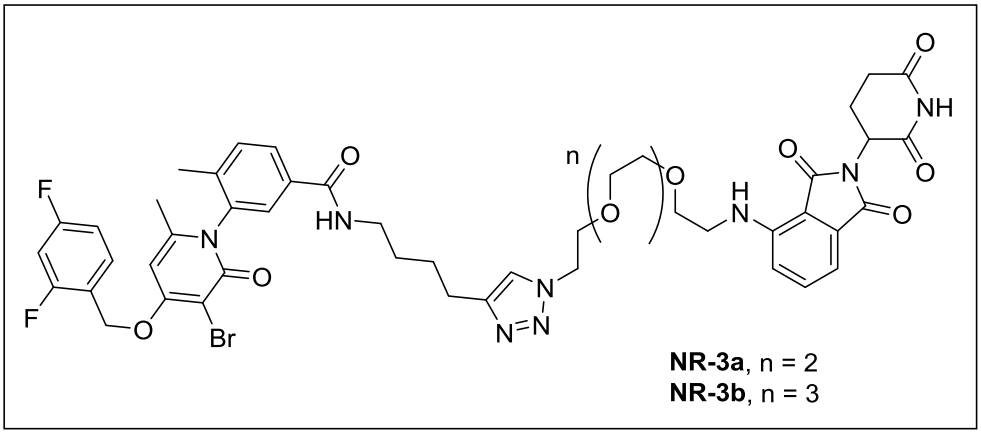

NR-3a, n = 2
NR-3b, n = 3

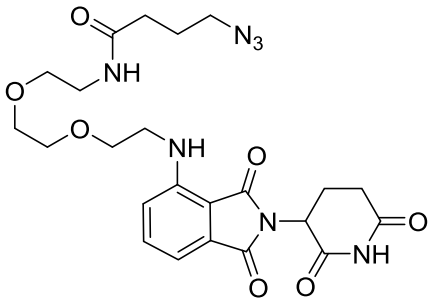

4-78

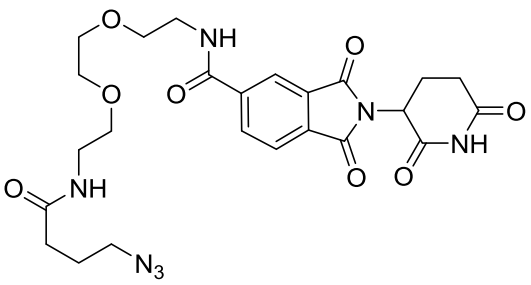

4-79

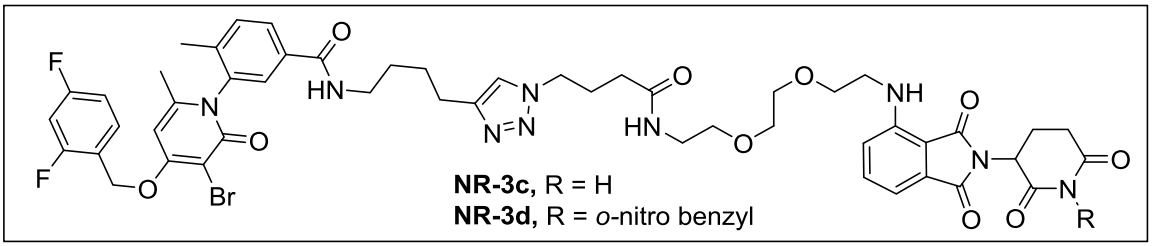

NR-3c, R = H
NR-3d, R = *o*-nitro benzyl

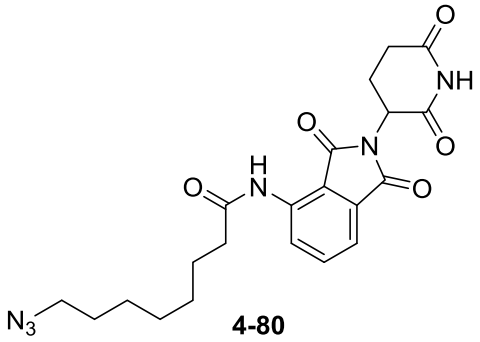

4-80

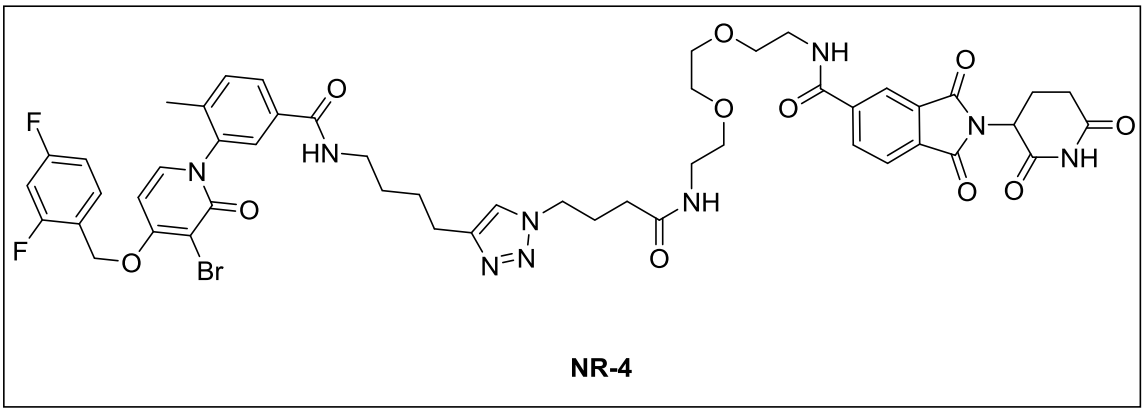

NR-4

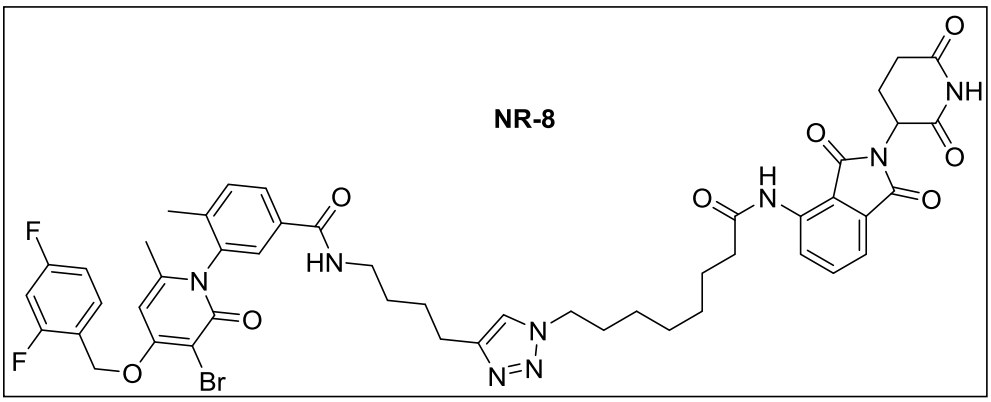

NR-8

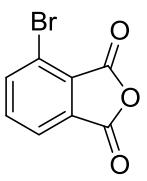

4-81

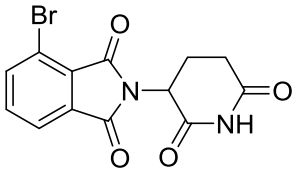

4-82

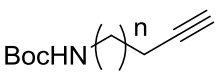

4-83a, n = 3
4-83b, n = 2

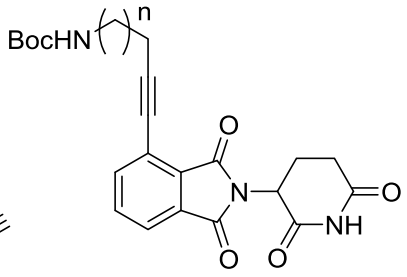

4-84a, n = 3
4-84b, n = 2

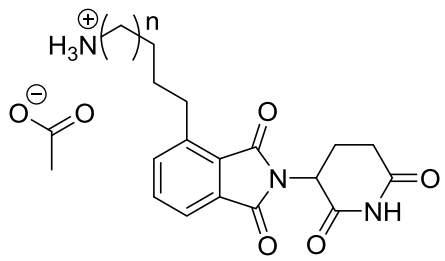

4-85a, n = 3
4-85b, n = 2

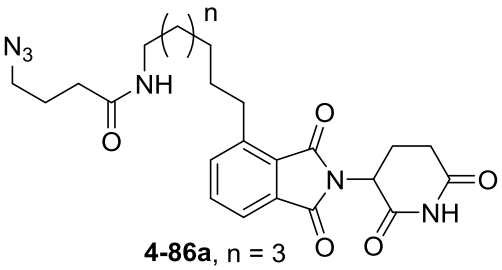

4-86a, n = 3
4-86b, n = 2

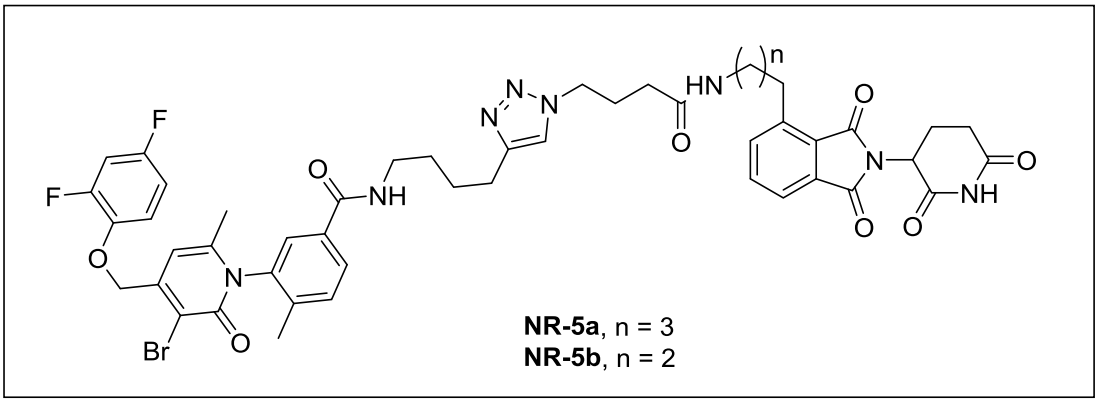

NR-5a, n = 3
NR-5b, n = 2

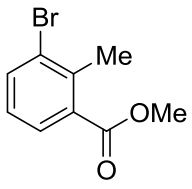

4-87

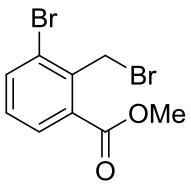

4-88

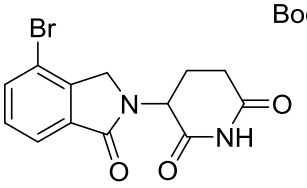

4-89

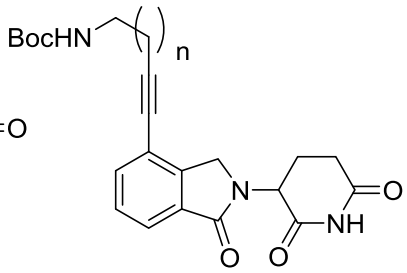

4-90a, n = 3
4-90b, n = 2

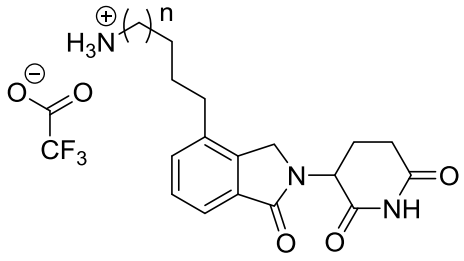

4-91a, n = 3
4-91b, n = 2

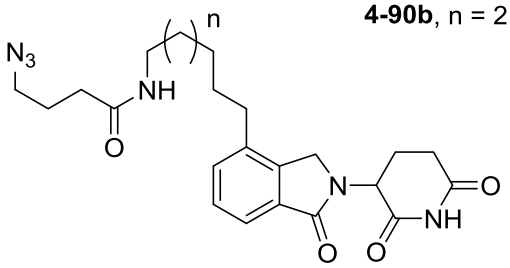

4-92a, n = 3
4-92b, n = 2

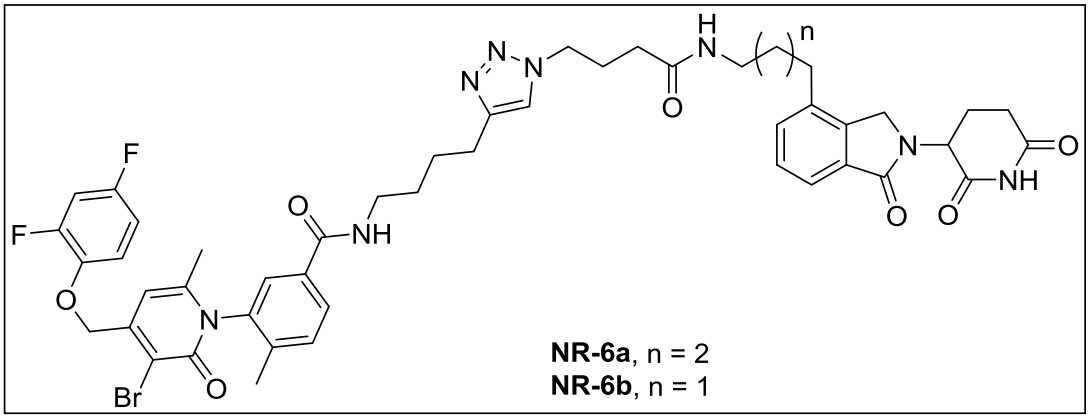

NR-6a, n = 2
NR-6b, n = 1

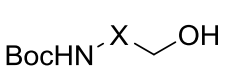

4-93a, X = $(CH_2)_3$
4-93b, X = PEG2

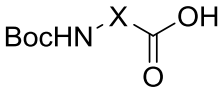

4-94a, X = $(CH_2)_3$
4-94b, X = PEG2

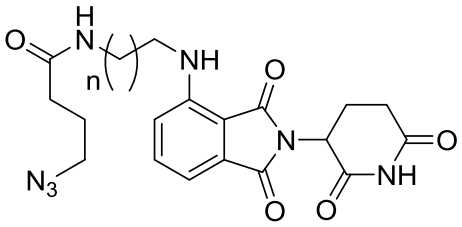

4-95a, n = 3
4-95b, n = 2
4-95c, n = 1

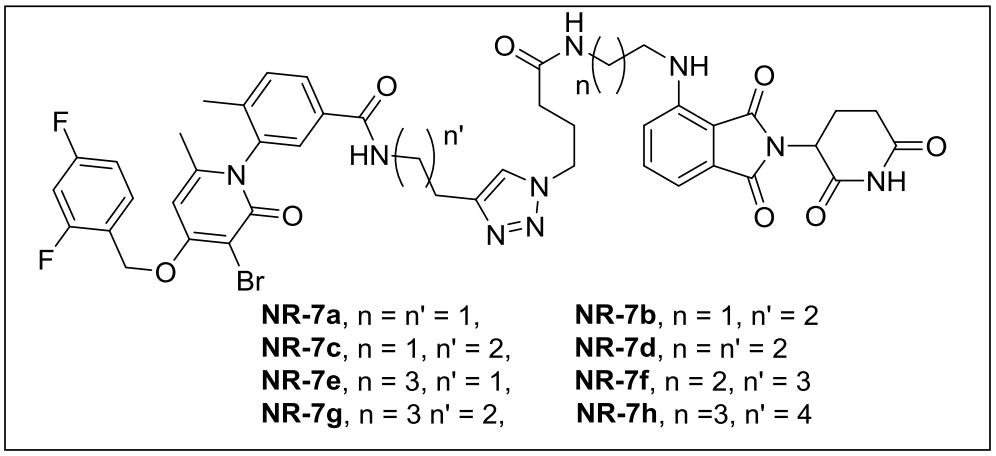

NR-7a, n = n' = 1,
NR-7b, n = 1, n' = 2
NR-7c, n = 1, n' = 2,
NR-7d, n = n' = 2
NR-7e, n = 3, n' = 1,
NR-7f, n = 2, n' = 3
NR-7g, n = 3 n' = 2,
NR-7h, n =3, n' = 4

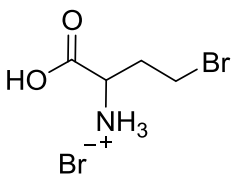

4-96

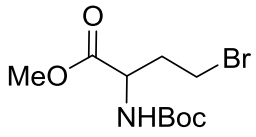

4-97

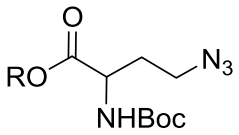

4-98a, R = Me
4-98b, R = H

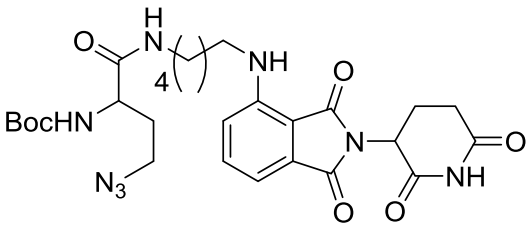

4-99

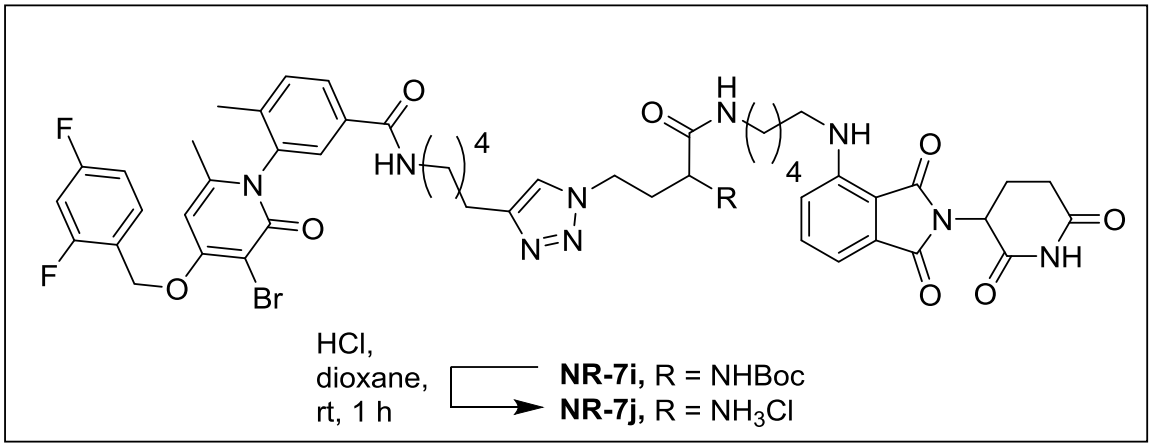
F
F
O
Br
N
O
O
HN
4
N
N=N
O
H
N
R
4
NH
O
N
O
NH
O
O
HCl,
dioxane,
rt, 1 h
NR-7i, R = NHBoc
NR-7j, R = NH3Cl

INDEX